The Use of Pluripotent Stem Cells (PSCs) and CRISPR Genome Editing to Study the Roles of TRPV4 Ion Channels in Skeletal Malformation

Yudha Nur Patria

ORCID: https://orcid.org/0000-0002-4802-2685

Submitted in total fulfilment of the requirements of the degree of Doctor of Philosophy

Supervisors:

A/Prof. Shireen Lamandé

Prof. John Bateman

Prof. Andrew Elefanty

October 2019

Department of Paediatrics

Faculty of Medicine, Dentistry and Health Sciences

The University of Melbourne

Abstract

Transient Receptor Potential Vanilloid 4 (TRPV4) is a non-selective calcium channel that plays an important role in the mechanotransduction system in chondrocytes. Heterozygous TRPV4 mutations cause skeletal disorders with varying severity. Heterologous cells such as fibroblasts and HEK-293 cells are commonly used to model TRPV4-inherited skeletal diseases *in vitro*. Studies using human chondrocytes are limited because cartilage is rarely available from patients and controls. Although heterologous cells cannot completely recapitulate the biological processes occurring in human chondrocytes, the studies show that two distinct disease phenotypes, TRPV4 skeletal dysplasia and arthropathy, might be caused by differences in the way the mutations change TRPV4 channel behaviour. TRPV4 skeletal dysplasia causing mutations show channel over-activity whereas arthropathy causing mutations show reduced channel activity upon channel stimulation. However, the downstream pathogenic mechanisms responsible for the distinct skeletal phenotypes remain undefined.

Recognising the limitations of previous studies, human-induced pluripotent stem cells (hiPSCs) offer a new approach for inherited disease modeling. Their ability to differentiate into disease-relevant cells such as chondrocytes creates new opportunities for TRPV4-inherited skeletal disease modelling. Therefore, this PhD project aims to model the disorders caused by two TRPV4 mutations using hiPSCs and identify the pathogenic mechanisms underlying the two distinct TRPV4-inherited skeletal disease phenotypes.

To obtain disease-relevant cells, establishing a robust and reproducible chondrocyte differentiation protocol is required. To do this, a reporter hiPSC line, SOX9-T2A-tdTom, was generated from MCRIi001-A (PB001.1) (1) using CRISPR/Cas9 genome editing. Thus *in vitro* chondrocyte differentiation could be monitored in real-time. The T2A linker and tdTomato fluorescent reporter gene were inserted downstream of the SOX9 coding sequence through homology-directed repair. The targeted allele was designed to produce SOX9 with the T2A sequence at the C-terminal end and a separate tdTom fluorescent protein.

Genomic DNA sequencing of the SOX9-T2A-tdTom hiPSC line confirmed that the hiPSC line had one SOX9 allele with the T2A tdTom gene fusion and one wild type allele. Pluripotency was maintained as indicated by expression of pluripotency markers OCT4 and NANOG (immunostaining); CD9, CD326, and SSEA-4 (flowcytometry); and the

ability to form tissues derived from three germ layers. SNP array showed there were no aneuploidies. The SOX9-T2A-tdTom hiPSC line had a similar capability to the parental line, MCRIi001-A, to form sclerotome. Western blotting showed that SOX9 protein expression was similar between SOX9-2A-tdTom and its parental line suggesting that adding tdTom gene sequence downstream of SOX9 gene did not disrupt the SOX9 expression and stability.

The chondrocyte differentiation protocol was established using the SOX9-T2A-tdTom hiPSC line. Two stages of differentiation were performed. First, sclerotome induction was achieved by culturing hiPSCs in a 6-day multiple-step chemically defined culture mimicking embryonic development with pellet culture format was established on day 4. Secondly, chondrocyte differentiation was performed by transferring day-6 pellets into chondrogenic media in swirling culture format up to 10 weeks. A 4-week course of FGF2 treatment followed by an optional TGFβ3 and GDF5 treatment until week 10 was performed during chondrocyte differentiation. RNA was collected every day during a 6-day sclerotome induction and at different time points during chondrocyte differentiation. The optimised protocol that involved a multiple-step chemically-defined 3-dimensional (3D) culture with swirling in an extended culture that included a 4-week FGF2 supplementation and optional subsequent TGFβ3 and GDF5 treatment was able to generate cartilage that closely resembles fetal cartilage.

CRISPR/Cas9 genome editing was also used to introduce two human TRPV4 mutations, a TRPV4 c.819C>G (p.F273L) mutation causing familial digital arthropathy with brachydactyly (FDAB) and a TRPV4 c.2396C>T (p.P799L) mutation causing metatropic dysplasia, into the SOX9-T2A-tdTom hiPSC line. For *in vitro* disease modelling, the mutant and their isogenic wild-type control (SOX9-T2A-tdTom) hiPSC lines were differentiated towards chondrocytes using optimised chondrocyte differentiation. The phenotypic differences between mutants and wild-type were assessed using various techniques including gene (RNA sequencing) and protein expression analysis.

The two mutant cell lines and their isogenic wild-type control (SOX9-T2A-tdTom) were able to form cartilage. The pellet cartilage histology did not show any striking differences between the two mutants and their isogenic control. COL2A1 and TRPV4 protein expression was similar between mutants and control and this was consistent with the RNA sequencing data. RNA sequencing suggested that the pathogenic mechanisms underlying the two distinct TRPV4-inherited skeletal diseases were different. Compared

to the isogenic control, F273L mutant cartilage had 263 differentially expressed genes. F273L cartilage showed a slight reduction in cartilage related gene expression including *COL2A1*, *CSPG4*, *BGN*, and *CILP2*. The F273L cartilage tissue was also less mature than the wild-type as indicated by increased *SHH* expression. On the other hand, P799L cartilage had more differentially expressed genes (655 genes) than F273L. *MEF2C*, the main regulator of chondrocyte hypertrophy, was upregulated in P799L. The hypertrophic chondrocyte markers such as *RUNX2*, *SPP1* or osteopontin, and *PTH1R*, were also upregulated in P799L suggesting increased chondrocyte hypertrophy of P799L chondrocytes. The other characteristics of hypertrophic chondrocytes such as a reduction in cell proliferation and increased apoptosis were also observed in P799L cartilage.

In conclusion, this study is the first study that conducts global gene expression analysis using RNA sequencing to characterise gene expression changes downstream of *TRPV4* mutations in hiPSC-derived chondrocytes. The pathogenic mechanisms underlying the two distinct TRPV4-inherited skeletal diseases are different. The fewer differentially expressed genes in the F273L cartilage than in P799L suggests a milder disease phenotype. The slight reduction in cartilage marker expression in F273L cartilage might cause the cartilage tissues less resilient to physical forces thus leading to FDAB. In contrast, accelerated chondrocyte hypertrophic maturation can be the pathogenic mechanism underlying TRPV4 skeletal dysplasia phenotype. Accelerated chondrocyte hypertrophic maturation can disrupt growth plate development and cause systemic skeletal defects seen in patients. This thesis demonstrates that hiPSCs are a powerful tool to model inherited skeletal disease *in vitro*.

Declaration

This is to certify that:

1. the thesis comprises only my original work towards the PhD except where acknowledged,
2. due acknowledgment has been made in the text to all other material used,
3. the thesis is fewer than 100, 000 words in length, exclusive of tables, maps, bibliographies and appendices

Signed: _____ Date: 15 November 2019

Yudha Nur Patria

Preface

My contribution to this thesis project is greater than 85% which involved designing and conducting the experiments, collecting the data, statistical analysis and interpretation, writing and reporting. This thesis consists of seven chapters including introduction (chapter 1), materials and methods (chapter 2), four result chapters (chapter 3 to 6), and general discussion (chapter 7).

Chapter 3 describes and discuss the generation of SOX9-T2A-tdTom hiPSC lines, an hiPSC line with heterozygous tdTom reporter gene inserted downstream of SOX9 gene hence tagging the expression of SOX9 gene, the master regulator of chondrocyte development. Chapter 3 of this thesis has been prepared for journal article submission to Stem Cell Research. I independently carried out all the experiments described, analysed the data and wrote the initial manuscript draft. A/Prof Shireen Lamande, my primary supervisor, Prof John Bateman, and Prof. Andrew Elefanty; coordinated and supervised all of the experiments conducted and involved in the interpretation of the data. I acknowledge the significant contributions from others to this chapter:

- Prof. Andrew Elefanty assisted me in designing the gRNA used for CRISPR mediated reporter gene knock in to generate SOX9-T2A-tdTom hiPSC reporter lines
- Tanya Labonne for her generosity in providing the tdTom expressing plasmid
- Jinia Lilianty performed teratoma immunostaining for the manuscript

Chapter 4 describes and discusses the chondrocyte differentiation protocol optimisation using SOX9-T2A-tdTom hiPSC lines.

Chapter 5 describes the generation of two mutant hiPSC lines. The two heterozygous TRPV4 mutations, c.819C>G (p.F273L) TRPV4 mutation causing familial digital arthropathy with brachydactyly (FDAB) and c.2396C>T (p.P799L) TRPV4 mutation causing metatropic dysplasia, were introduced into SOX9-T2A-tdTom hiPSC reporter lines using CRISPR/Cas9 genome editing.

Chapter 6 describes and discuss the TRPV4-inherited disease modelling using mutant TRPV4 hiPSC lines and their isogenic wild-type control. I acknowledge the significant contributions from others to this chapter:

- Lynn Rowley and A/Prof. Shireen Lamandé extracted the RNA from the pellets
- RNA sequencing was performed by Genomics Centre, Murdoch Children's Research Institute
- A/Prof. Shireen Lamandé performed RNA sequencing data processing and differential gene expression analysis.

Acknowledgments

This PhD project would not have been possible without the support of many people. I would like to take this opportunity to thank my supervisors, A/Prof. Shireen Lamande, Prof. John Bateman and Prof. Andrew Elefanty for the guidance, inspiration, and support they offered throughout my PhD.

Thanks to Dr. Trevor Cameron, who helped me in the first year of PhD candidature before his move and also Lynn Rowley who has been very helpful to train and teach many laboratory techniques.

I must also thank my colleagues in the Musculoskeletal Research at MCRI, again Lynn Rowley, Lisa Sampurno, Dr. Louise Kung, Jinia Lilianty and Hani Hosseini for their encouragement and supports during my PhD.

I would like to extend my gratitude to Prof. Ed Stanley and Tanya Labonne for their scientific advice.

I would like to thank my committee members, Prof. Ed Stanley and Dr. Alex Combes who offered guidance and supports.

My thanks also go to person/organisation I had the opportunity to work with during this project:

a. Dr. Katherina Vlahos, Penelope McDonald, Koula Souris, Robbyn Murberry (iPS Core Facility, MCRI) for providing the PB001.1 hiPSC lines and MEFs
b. Dr. Matt Burton, Paul, Eleanor (Flowcytometry and Microscopy Core Facility, MCRI) for assisting me in performing flowcytometry, FACS and confocal microscopy
c. Dr. Sara Howden (Kidney Development and Diseases, MCRI) for her scientific advice on CRISPR/Cas9 gene editing
d. Tanya Labonne (Stem Cell Technology, MCRI) for scientific advice and assistance in generating the SOX9-reporter hiPSC line.

e. Dr. Katrina Bell (Bioinformatics unit, MCRI) and A/Professor Shireen Lamande (Musculoskeletal Research, MCRI) for their contributions in performing and analysing RNA sequencing data
f. Dr. Stephanie Eagers and her team (Translational Genomic Unit, MCRI) for conducting Sanger sequencing
g. VCGS for their contribution in performing SNP array and SNPduo analysis

I would also like to acknowledge Melbourne International Research Scholarships and Melbourne International Fee Remission Scholarships (now is called Melbourne Scholarships) for providing funding for my PhD. Also, the Department of Paediatrics' Graduate Research Officers who has been very helpful for assisting the administrative works regarding my PhD candidature.

Thanks to 'Orange Laboratory' members; Dr. Peter Howling, Dr. Jane Seto, Crystal, Harry, Kelly, Lyra (from Neuromuscular research, MCRI); Sue Golub, Karena (from Arthritis research, MCRI); Lab members of Neurogenetics, MCRI for being very supportive lab mates.

Thank you to my brothers; dr. Abdul Hadi and Sultan Al Amri for their supports and brotherhood. My writing buddy; Hidaya Noor Suaini, Yichao Wang, Suffian, Azri, Razi and Thy Nguyen; thanks for your encouragement and supports. Also, my Indonesian PhD "warriors" who have been very supportive throughout my PhD candidature.

Special thanks for my colleagues at Department of Child Health, Faculty of Medicine, Public Health and Nursing, Universitas Gadjah Mada for their supports. Looking forward to working with you very soon.

Special thanks also go to my family and friends for all their support, especially Mum, Dad and sister for always calling my names in their prayers and encouraging me to pursue my dreams.

Conference Abstracts

1. **Patria, Y.N**., Labonne, T., Cameron, T.L., Stanley, E.G., Elefanty, A. G., Bateman, J. F., Lamandé., S. R., An human iPS cell SOX9 reporter line for monitoring chondrocyte differentiation. *Matrix Biology Society of Australia and New Zealand Melbourne Meeting*, Melbourne, Australia, 2017.

2. **Patria, Y.N.**, Labonne, T., Cameron, T. L., Vlahos, K., Stanley, E.G., Elefanty, A. G., Bateman, J. F., Lamandé., S. R., A Human IPSC SOX9 Reporter Line for Monitoring Chondrocyte Differentiation. *International Society for Stem Cell Research Annual Meeting*, Melbourne, Australia, 2018.

3. **Patria, Y.N**., Labonne, T., Cameron, T. L., Vlahos, K., Stanley, E.G., Elefanty, A. G., Bateman, J. F., Lamandé., S. R., Newly Optimised Protocol for Generating Cartilage Tissues from hiPSCs. *The 14th World Advanced Therapies and Regenerative Medicine*, London, England, 2019

Publications

1. Hosseini, F. H., **Patria, Y. N.**, Motazedian, A., Elefanty, A. G., Stanley, E. G., Lamandé, S. R., Bateman, J. F., 2019, Generation of a heterozygous COL1A1 (c.3969_3970insT) osteogenesis imperfecta mutation human iPSC line, MCRIi001-A-1, using CRISPR/Cas9 editing. *Stem Cell Research*. DOI:10.1016/j.scr.2019.101449.

2. **Patria, Y. N**., Lilianty, J., Elefanty, A. G., Stanley, E. G., Labonne, T., Bateman, J. F., Lamandé, S. R., 2019, Generation of a SOX9-tdTomato reporter human iPSC line, MCRIi001-A-2, using CRISPR/Cas9 editing. *Stem Cell Research*. **(manuscript in preparation)**

Scholarships and Awards

1. Melbourne International Research Scholarship awarded by The University of Melbourne to undertake my PhD (November 2015 – November 2019).
2. Melbourne International Fee Remission Scholarship awarded by The University of Melbourne to undertake my PhD (November 2015 – May 2019).
3. The Henry and Rachel Ackman Travelling Scholarship awarded by the Department of Paediatrics, The University of Melbourne (2018) to attend Croucher Summer School on Stem Cell Biology and Regenerative Medicine, Chinese University of Hong Kong, Hong Kong.
4. Erasmus Summer Program Fellowship awarded by National Institute of Health Sciences (NIHES) (2018) to attend Genetic Epidemiology Courses, Erasmus University Rotterdam, The Netherland.
5. Student Conference Support Scholarship awarded by Murdoch Children's Research Institute (MCRI) (2019) to attend The 14th World Advanced Therapies and Regenerative Medicine, London, England.

Table of contents

List of Tables

List of Figures

Chapter 1

Introduction

1.1 General overview

Transient Receptor Potential Vanilloid 4 (TRPV4) is a non-selective calcium channel that is expressed in many tissues including cartilage (2). Although TRPV4 is widely expressed, heterozygous mutations in TRPV4 cause skeletal disorders with varying degrees of severity (3, 4) suggesting that TRPV4 mutant channels cause tissue-specific phenotypes. This also suggests the essential roles of TRPV4 in skeletal development. Since the pathogenic mechanism of the TRPV4 mutations in causing skeletal defects is largely undescribed, this study aims to model TRPV4-inherited skeletal diseases to find pathogenic mechanisms underlying the diseases.

Given that cartilage provides a template for bone formation (5, 6), the differentiation of cartilage forming cells, chondrocytes, is absolutely critical for normal skeletal system development. Therefore, being able to study patients' chondrocytes could provide a better understanding of the roles of mutant TRPV4 channels in causing the disease phenotypes. However, obtaining patients' cartilage requires invasive procedures and very often the amount of tissue obtained is very limited. Therefore, instead of using chondrocytes, a number of studies have been carried out using heterologous cells such as fibroblasts and HEK-293 cells to model TRPV4-inherited skeletal diseases *in vitro* (7-10). However, since the mutations cause tissue-specific phenotypes, using heterologous cells adds complexity in translating the results into human chondrocytes as they do not completely recapitulate the true biological processes occurring in human chondrocytes.

Transgenic mouse models have also been generated to provide a better understanding of the pathogenesis of TRPV4-inherited skeletal diseases (11-14). However, the way they have been generated resulted in a *TRPV4* over-expression as well as inappropriate timing and location of *TRPV4* expression due to *COL2A1* promoter-targeted *TRPV4* expression thus it does not work the same way as the *TRPV4* promoter-targeted expression. More importantly, the potential genetic background differences between mouse and human may cause differences in the observed phenotypes. Given all of the drawbacks from previous studies, human-induced pluripotent stem cells (hiPSCs) provide a new promising approach for inherited disease modelling (15). Therefore, the hiPSC-disease model approach is used in this PhD project to model TRPV4-inherited skeletal diseases.

The possibility of generating patient hiPSCs from somatic cells through reprogramming techniques (16) and the ability of hiPSCs to differentiate into disease-relevant cells such as chondrocytes in defined culture conditions (17-20), the *in vitro*

development of cartilage diseases could be examined. In addition, the capabilities of the PSCs to be maintained in an *in vitro* culture for an extended period (16) would provide more flexibility on when and how many disease-relevant cells would be generated for downstream experiments. However, developing a robust and reproducible chondrocyte differentiation protocols remains the biggest challenge for hiPSC-based disease model. To optimise the protocol, we generated a SOX9-T2A-tdTom hiPSC line. This hiPSC line contains a fluorescent reporter, tdTomato, that tags the expression of SOX9 transcription factor, the master regulator of chondrogenesis. This allows *in vitro* chondrocyte differentiation to be monitored in real-time. The description of how this SOX9-T2A-tdTom hiPSC line is generated is available in Chapter 3 and the strategies to optimise a chondrocyte differentiation protocol using the SOX9-T2A-tdTom hiPSC line are presented in Chapter 4.

The potential use of hiPSC for TRPV4-inherited skeletal disease modelling has been shown in a study conducted by Saitta, Passarini (21). However, the potential pathogenic mechanisms responsible for the disease phenotypes were not identified and some improvements are needed including the use of a more optimised chondrocyte differentiation protocol and isogenic control cell lines. Therefore, to improve the experimental design, we generated two mutant TRPV4 hiPSC lines, one with a p.F273L TRPV4 mutation (causing familial digital arthropathy with brachydactyly (FDAB)) and one with p.P799L TRPV4 mutation (causing metatropic dysplasia) in the SOX9-T2A-tdTom hiPSC line using CRISPR/Cas9 genome editing (Chapter 5). Both mutant lines and the control are isogenic, they have the same genetic background. Finally, we generated cartilage from these TRPV4 mutant hiPSC lines to model the diseases and the data are presented in Chapter 6.

To provide a contextual framework for this study, in this introduction chapter, we provide reviews on TRPV4 ion channel and its essential roles in chondrocyte mechanotransduction (section 1.2). The discussion on current *in vivo* and *in vitro* TRPV4-inherited disease modelling studies are presented in section 1.3. For providing a basis on the developing pluripotent stem cell disease model, a review on skeletal system development and current updates on hiPSC disease model for skeletal diseases are presented in section 1.4.

1.2 TRPV4 and the skeletal system

1.2.1 TRPV4 ion channel

Transient Receptor Potential Vanilloid 4 (TRPV4) is a non-selective cation channel and a member of the TRP-Vanilloid ion channel subfamily (22). The TRPV4 gene is located on chromosome 12q23-q24.1. It has 16 exons encoding 871 amino acids and its mRNA consists of 3229 bases (2). The functional TRPV4 ion channel shows homotetramer or heterotetramer formation. The heterotetramer formation is formed with other TRP family isoforms (23). The channel pore is located at the centre of the formation (Figure 1-1) (24). Each subunit consists of 3 domains: 6 transmembrane segments (S1-S6) segments, intracellular N-terminal tails and intracellular C-terminal tails (Figure 1-1) (24). The channel pore is formed between transmembrane segments 5 and 6 of four subunits.

TRPV4 is more permeable to Ca^{2+} and Mg^{2+} than Na^{+} ion thus its activation results in Ca^{2+} influx from outside the cell into the intracellular compartment (25). The channel is activated by physical/mechanical stimuli such as hypotonicity (26-32) and biochemical stimuli (reviewed in (2)) such as the lipid metabolite arachidonic acid (33) and synthetic agonists (GSK1016790A and 4α-PDD) (34). Temperature >25^{o}C (30, 35, 36) and electrical stimuli (35) can also activate the channel.

TRPV4 is expressed in many different tissues and organs including cartilage, bone, brain, nerve, kidney, lung, heart, blood vessels, liver, spleen, testis, bladder, cochlea, skin and skeletal muscle (reviewed by White, Cibelli (2)). In the skeletal system, *TRPV4* is highly expressed in chondrocytes (37, 38) located in the growth-plate (39, 40) and articular cartilage (41-43). TRPV4 is also expressed in osteoblasts (44, 45) and osteoclasts (13, 46).

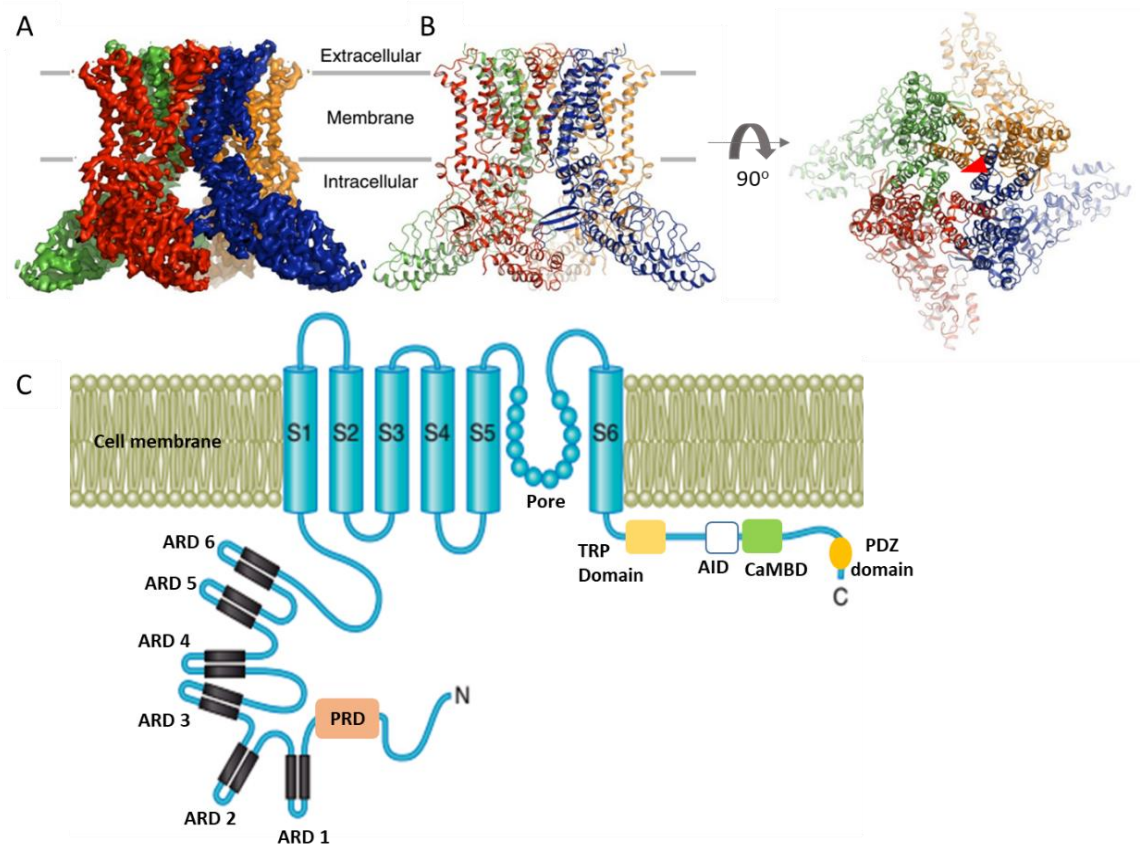

Figure 1-1. The structure of the TRPV4 channel. Cryo-electron microscopy reconstruction of tetrameric TRPV4 (A) with each subunit in a different colour. Orthogonal views of the TRPV4 structure with pore (red arrow) is located in the centre of the tetrameric structure (after 90° rotation) (B) (adapted from (24)). The schematic figure of a single TRPV4 subunit shows the N-terminal region, transmembrane region and C-terminal region (C) (adapted from (White et al., 2016)). S5 and S6 form the pore. S1-S6: transmembrane segment 1 to 6, ARD: ankyrin repeat domains, PRD: proline-rich domain, TRP: Transient receptor potential, AID: autoinhibitory domain, CaMBD: Calmodulin binding domain, PDZ domain: Post-synaptic density protein, Drosophila disc large tumour suppressor and Zonula occludens-1 protein domain

Growth-plate is specialised cartilage structure that is responsible for providing template for bone formation during skeletal development and for longitudinal bone growth during childhood (47, 48). Histologically, the fully developed growth plate consists of 4 distinctive zones: the resting zone, proliferating zone, pre-hypertrophic and hypertrophic zone which are distinguished based on the differences in morphology and gene expression profiles of cartilage-forming cells, chondrocyte (Figure 1-2) (5, 6). Trpv4 is primarily found in the proliferative zone, is downregulated in the pre-hypertrophic zone and is undetectable in the hypertrophic zone (39) suggesting the importance in skeletal development.

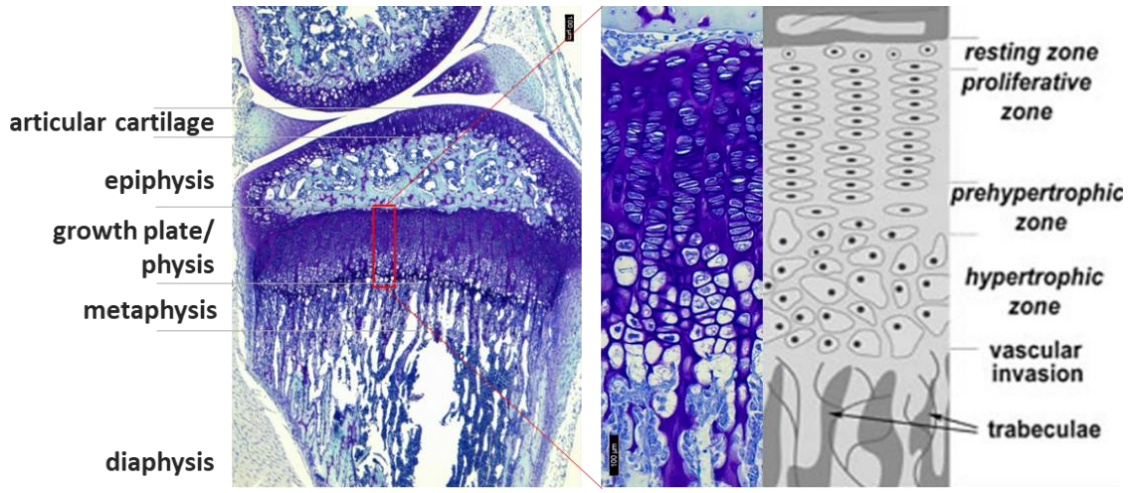

Figure 1-2. The structure of fully developed growth plate in 4-week old mouse proximal tibia. The figure also shows the general structure of long bones, including articular cartilage, epiphysis, growth plate, metaphysis, and diaphysis.

1.2.2 TRPV4 ion channel as a mechanosensor in chondrocytes

1.1.1.1 The structure and components of cartilage tissue

Cartilage can be found in many organs including growth-plate, joints, intervertebral discs, ribs, trachea, bronchus, larynx, epiglottis, external ears and nose (49). Cartilage tissue is very important in providing anatomical structure for these organs. Cartilage found in the joints, intervertebral discs and growth plates also absorbs physical forces generated from skeletal movements and body weight (50).

Cartilage tissue is composed of chondrocytes and a highly organised extracellular matrix (ECM) (49) which contains proteoglycans, water and ions, collagens and non-collagenous matrix proteins (51-53). It is an avascular and aneural tissue with water comprising 80% of the total cartilage volume (47). Thus, the nutrients for chondrocytes are primarily delivered via passive diffusion through water (54). To adapt to this

condition, chondrocytes have a very low metabolic rate which means they have a limited repair capacity when cartilage injury occurs especially injury involving the articular cartilage (47). The ECM provides a suitable microenvironment for the chondrocytes to survive and grow as well as providing mechanical properties to support tissue function (55).

Aggrecan (ACAN) is the most common proteoglycan found in cartilage and embryonic bone template cartilage (56). The molecular weight of the aggrecan core protein is about 250 kDa with around 150 glycosaminoglycans (GAGs) side chains of keratan sulfate and chondroitin sulfate attached to it (49, 57). Link protein links aggrecan to hyaluronic acid to form proteoglycan aggregates. Other proteoglycans found in cartilage include perlecan, versican, bikunin and small leucine-rich proteoglycans (SLRPs) such as decorin and lumican (56, 57). Since proteoglycans are negatively charged, they attract positively charged ions such as sodium which eventually attracts water into the tissue. Hence, water makes up 70-80% of articular cartilage weight (49).

The composition of collagens determines the mechanical properties and the shape of tissues. Collagen type II is the most abundant collagen in cartilage (47, 58). Collagen type II is a fibrillar collagen that is a homotrimer of α1(II) polypeptide chains encoded by the *COL2A1* gene (59). *COL2A1* has 4 different variants that are derived from alternative splicing of the mRNA: IIA, IIB, IIC, and IID (60, 61). The IIA, IIC and IID isoform mRNAs retain exon 2 but the IIB isoform has exon 2 spliced out. Collagen IIA is the major isoform in early embryonic cartilage whereas the IIB isoform is highly expressed in mature cartilage (60, 62, 63). The molecular process that triggers the switching of *COL2A1* from the IIA to IIB isoform in mature cartilage remains unclear (61).

Other types of collagens including collagen type VI, IX, X, XI, XII, XIV (47, 58, 64) XVI, XXII. XXV and XXVII (40, 64) are also found in cartilage. Collagen type VI is found in both pericellular and territorial matrix surrounding the chondrocytes while collagen type X is abundantly expressed in the growth plate. Other important cartilage ECM proteins include COMP or thrombospondin-5, matrilin-1 (MATN1) and matrilin-3 (MATN3), fibronectin, and laminin (65).

1.1.1.2 TRPV4 mechanotransduction in chondrocytes

Cartilage tissues (especially in the growth plate and joint) are exposed to repetitive mechanical stresses including compression, tension and shear forces which are generated from skeletal movements and weight-bearing. Studies on the effect of mechanical forces on cartilage tissues have shown intriguing results (66). Applying various types of

mechanical forces onto different forms of chondrocyte culture formats including monolayer chondrocyte culture (27, 30, 67), 3-dimensional culture (26, 68-70), and cartilage explants (32, 71, 72) results in changes in cartilage marker expressions as well as ECM composition and organisation. These findings indicate the importance of mechanotransduction in chondrocytes to maintain cartilage integrity (66, 73). Mechanotransduction has also been shown to regulate skeletal system development (74) and *in vitro* mesenchymal stem cell differentiation towards chondrocytes (68, 75-82).

Mechanical forces generated from skeletal movement cause water to come in and out of the articular and growth plate cartilage changing tissue osmolarity to be relatively more hypo- or hypertonic (66). Hypotonicity causes water influx into the cell resulting in cell swelling (31, 83-85). Cell swelling physically stretches the cell membrane which eventually induces phospholipase 2 (PLA2) mediated TRPV4 activation allowing Ca^{2+} influx into the cells (26, 30, 31, 86). The C-terminal tail of TRPV4 interacts with cytoskeletal components (87) actin and tubulin (88-91) to facilitate cellular volume changes following external stimuli exposure (89, 92). This stretch-activated process indicates that TRPV4 functions as an osmo-mechanosensor.

TRPV4 mechanosensing has also been demonstrated in a study involving three different mechanical stimuli: stretching, indentation and culture-substrate deflection onto single chondrocyte to stimulate TRPV4. The study found that TRPV4 was activated by culture-substrate deflection at the contact point between substrate and chondrocyte indicating that TRPV4 can be activated through direct physical stimulus (93). This finding also mimics the direct interaction between chondrocytes and ECMs where chondrocytes directly interact with ECM molecules through membrane proteins/focal adhesion molecules such as integrins (94) (Figure 1-3). The interaction between chondrocytes and the ECM allows the transduction of mechanical forces which eventually leads to TRPV4 activation. This complex interaction is essential for maintaining the structural integrity of the cartilage tissues (55, 95, 96). Additionally, TRPV4 has also been reported to play essential roles in collagen matrix assembly (97) and extracellular matrix deposition (82) in mesenchymal stem cells which again indicates its essential role in maintaining cartilage homeostasis.

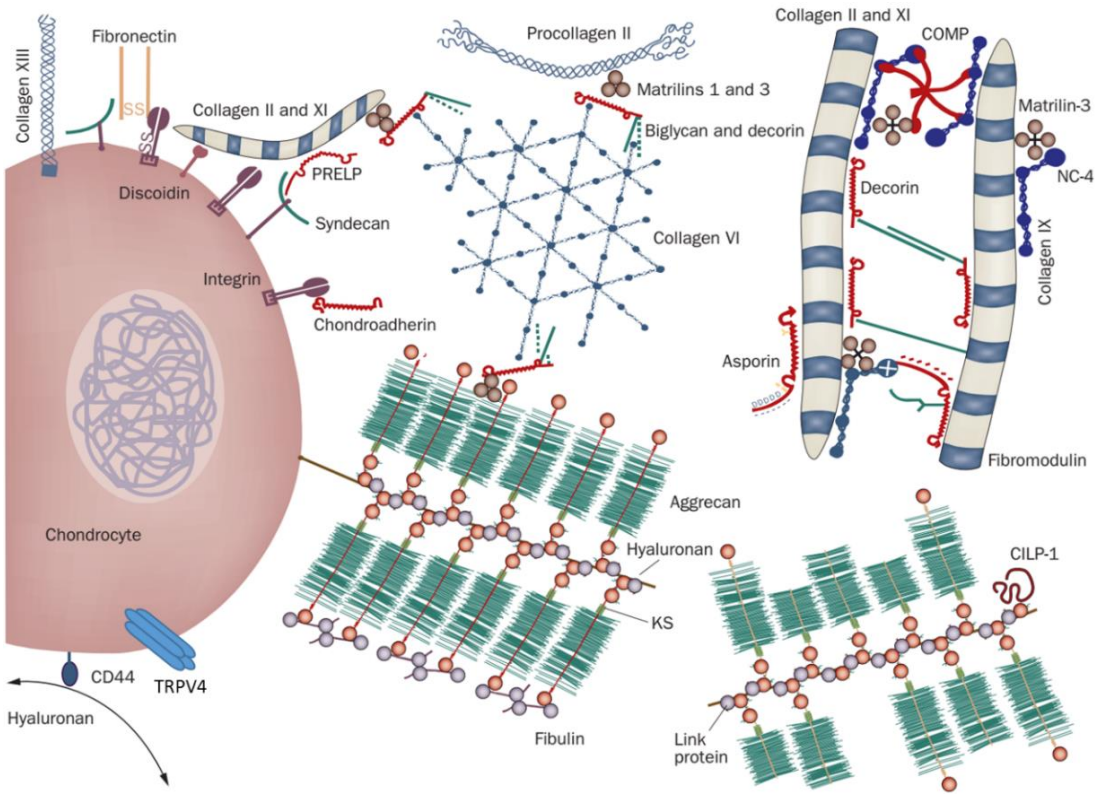

Figure 1-3 The complex interaction between chondrocytes and cartilage extracellular matrixes. Taken from (95)

Oscillatory intracellular calcium influx is the key molecular response of the TRPV4 mechanotransduction system in chondrocytes (98-100). Since many essential cellular processes such as metabolism and proliferation are regulated through calcium signaling (101) and the fact that a 20,000-fold gradient of Ca^{2+} concentration between the inside and outside of the cell at rest has to be maintained (102), TRPV4 could be the main ion channel responsible for maintaining calcium homeostasis. Given the importance of TRPV4 in maintaining cartilage structure integrity, it is not surprising that mutations in TRPV4 could cause significant skeletal diseases in human as described in section 1.3 of this chapter.

1.3 Current disease models for TRPV4-inherited skeletal diseases

1.3.1 TRPV4-allelic variants causing inherited diseases

More than 40 TRPV4 allelic variants have been reported to cause human diseases (Figure 1-4) (4, 103). Skeletal dysplasia, arthropathy, familial osteonecrosis, and neuropathy are four different disease phenotypes found in the clinic (104). Spinal muscular atrophy (SMA) is the most common neuropathy phenotype and the combination of skeletal dysplasia and neuropathy phenotypes is also seen (105-108). The two main

skeletal phenotypes caused by TRPV4 mutations are skeletal dysplasias and arthropathy. For the purpose of this study, we will focus the discussion on skeletal phenotypes and the review of neuropathy phenotypes can be found elsewhere (4).

Four categories of skeletal dysplasia that share similar clinical manifestations are caused by TRPV4 mutations: Metatropic dysplasia (MD, OMIM #156530), Spondylometaphyseal dysplasia, Kozlowski type (SMDK, OMIM #184252), Spondyloepimetaphyseal dysplasia of Maroteaux, Pseudo-Morquio Type II Syndrome (SEDM-PM2, OMIM #184095) and brachyolmia type 3 (OMIM #113500). Rather than representing distinct disease entities; these disease categories are part of a spectrum of disease severity ranging from lethal skeletal dysplasia at the most severe to the autosomal dominant brachyolmia at the mild end (3). TRPV4 skeletal dysplasias are characterised by dwarfism, short appendicular bones, platyspondyly of the vertebrae and halberd-shaped pelvis (Figure 1-5).

Metatropic dysplasia is an autosomal dominant skeletal dysplasia. It is characterised by short stature, short appendicular bones, progressive kyphoscoliosis, joint contracture, squared-off the jaw and prominent forehead. Radiological features include platyspondyly of the vertebrae, halberd-shaped pelvis, and brachydactyly with delayed ossification of the carpal bones. The lethal form of the disease causes perinatal death due to severe cardiopulmonary compromise (109). Mutations occurred at TRPV4 codon number 89, 278, 280, 331, 324, 471, 604, 618, 799 have been reported to cause MD (110-112).

The clinical features of SMDK overlap with MD. The only sign found in MD but not in SMDK are dumbbell-shaped femora (110) and in overall assessment, SMDK is milder than MD. However, the clinical diagnosis is not based on a single sign but rather a combination of many clinical features. On the other hand, the clinical features that differentiate SEDM from other TRPV4 skeletal dysplasias are marked brachydactyly and the absence of progressive childhood kyphoscoliosis (113). However, other clinical features are shared between SEDM and other skeletal dysplasia phenotypes. At the mild end of the TRPV4 skeletal dysplasia spectrum, brachyolmia has clinical symptoms being apparent by school age (114). Patients usually suffer from chronic pain in the spine and extremities. Patients with brachyolmia show normal growth during childhood and then start to deteriorate throughout adulthood.

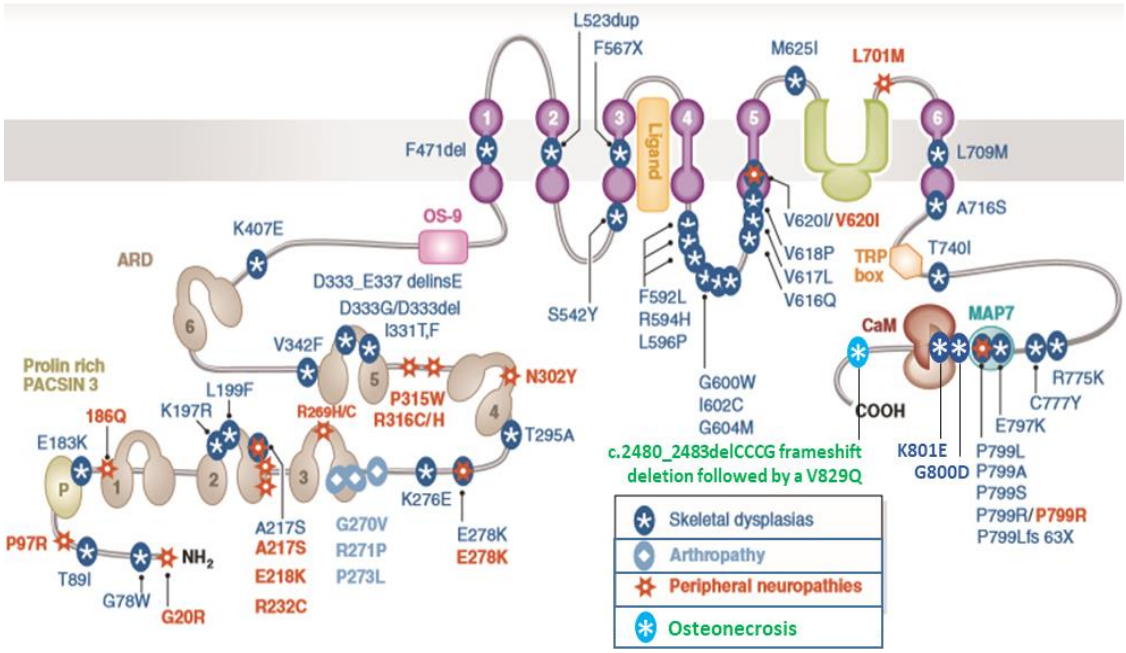

Figure 1-4. The location of TRPV4-allelic variants causing inherited skeletal diseases relative to TRPV4 structural domains. Adapted from (4). Notice that the same mutations cause different disease phenotypes. The skeletal phenotypes show a spectrum of disease severity ranging from mild, intermediate, severe and lethal form. OS-9 indicates putative interaction site of OS-9 protein. Ligand indicates the putative binding site of 4α-PDD and MAP7 indicates the putative interaction site of MAP7 protein.

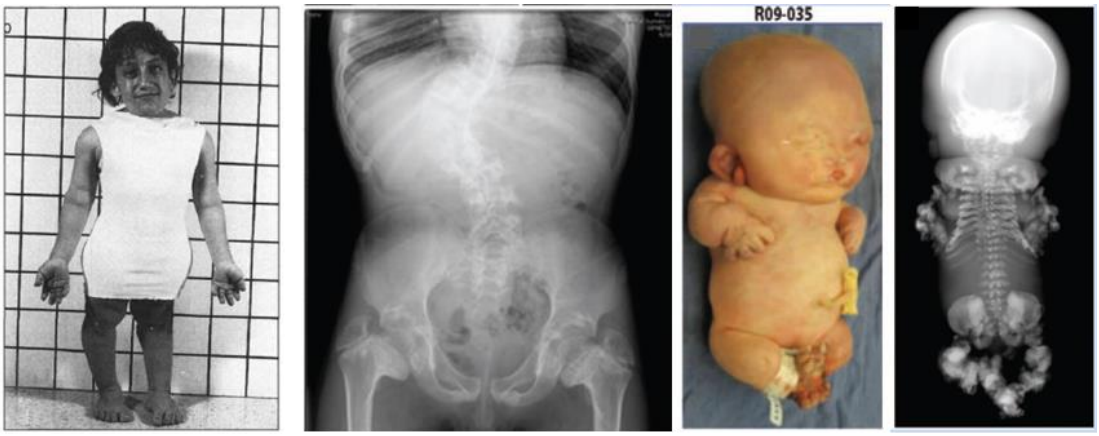

Figure 1-5. Clinical phenotype of skeletal dysplasia. The first two images from left show the classical clinical feature of skeletal dysplasia phenotypes: short stature, short appendicular bone (long bone), brachydactyly, platyspondyly and scoliosis of the vertebrae, halberd-shaped pelvis (reprinted from (115) and (3). The last two images from the left show the lethal phenotype (reprinted from (116). The patients die due to respiratory distress caused by the malformed respiratory tract.

On the other hand, familial digital arthropathy with brachydactyly (FDAB) caused by TRPV4 mutation is classified as a distinct disorder as the patients are clinically normal at birth but then develop skeletal abnormalities during childhood which are limited to the small joints of the hands and feet (interphalangeal, metacarpophalangeal and metatarsophalangeal joints) (39). The skeletal abnormalities show an osteoarthritis-like appearance; however, the cardinal features of other TRPV4 skeletal disorders including spine abnormalities and short stature are absent (Figure 1-6). A study conducted by Lamande, Yuan (39) found three allelic TRPV4 variants, p.G270V, p.R271P, and p.F273L, in three independent families with FDAB. A recent study reported the clinical similarity between Thiemann's disease and FDAB. The study found that one of the FDAB variants, p.G270V, caused Thiemann's disease suggesting that both diseases are a single disease entity (117).

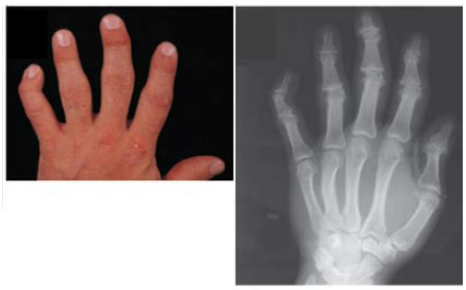

Figure 1-6. Clinical phenotype of Familial digital arthropathy with brachydactyly (FDAB). Adapted from (39). The patient shows osteoarthritis-like appearances limited to the interphalangeal, metacarpophalangeal, and metatarsophalangeal joints. The clinical features of skeletal dysplasia phenotype are absent.

TRPV4 mutation also cause a disease called osteonecrosis of the femoral head. A genetic test revealed that the patients had heterozygous *TRPV4* mutation, a c.2480_2483delCCCG frameshift deletion followed by a c.2486T>A substitution (118). The clinical characteristics of TRPV4 skeletal dysplasia were absent in all of the patients. Radiology examination shows detrimental changes in the femoral head caused by an impaired blood supply.

1.3.2 Cellular models for TRPV4 inherited skeletal disease modelling

Given that many skeletal elements are affected in the TRPV4 inherited skeletal diseases, it is clear that TRPV4 is very important in skeletal development. Both *in vivo* and *in vitro* disease modelling studies have been carried out to elucidate the molecular mechanisms responsible for skeletal disease phenotypes. No less than 27 different TRPV4 mutations have been studied (Table 1-1) and 5 different transgenic animals with 4 different genotypes have been generated (8, 11, 12, 14, 119).

Cellular modellings of TRPV4 mutations have mostly performed in heterologous cells such as HEK-293, *Xenopus* oocytes, and dermal fibroblasts (Table 1-1). The main driver of using these heterologous cells is the simplicity since the cells are readily available. Isolating primary chondrocytes from transgenic mice requires transgenic animal generation and animal breeding. In addition, obtaining cartilage tissues from patients and healthy control is difficult due to the rarity of the patients and invasive surgery is required. Moreover, chondrocytes cannot be expanded in culture because they lose the chondrocyte phenotypes (de-differentiation) after subsequent passaging (120).

Transfecting mutant TRPV4 variant causing SMDK (p.D333G) (10) and metatropic dysplasia (p.P799L) (116) into HEK-293 cells resulted in a higher basal intracellular calcium level measured using fluorescence-based assay. This finding was confirmed by electrophysiological measurements of the whole-cell membrane current showing robust basal currents. Following TRPV4 agonist (4α-PDD) administration and hypotonic stimulation, both $TRPV4^{D333G}$ (10) and $TRPV4^{P799L}$ (116) HEK-293 showed a significant increase in intracellular calcium levels. $TRPV4^{P799L}$ channel also showed channel over-activity which might be a result of constitutive channel opening caused by a defect in autoinhibition of channel closure (121). Similar finding to $TRPV4^{P799L}$ channel was observed in HEK-293 cells (7) and *Xenopus* oocytes (9) expressing TRPV4 variant causing brachyolmia (p.V620I). These findings suggest that skeletal dysplasia causing mutations cause a gain of function mutation (8, 9, 103) which might responsible for the clinical phenotypes.

Only two studies have used chondrocytes to study skeletal dysplasia causing mutations. The first study used humanised-porcine chondrocytes which were generated by transfecting plasmids containing mutant or wild type human TRPV4 gene sequence into porcine chondrocytes showed that $TRPV4^{V620I}$ had a significantly higher basal intracellular calcium level than wild-type TRPV4 (8). The peak intracellular calcium level after hypotonic stimulation in $TRPV4^{V620I}$ was higher than the wild type TRPV4 which was consistent with the increased membrane cell current in the transfected HEK-293 cells (7) and *Xenopus* oocytes (122). In addition, the study concluded that follistatin (FST), a BMP inhibitor; mediated the pathogenesis of TRPV4 mutations. The TRPV4 channel over-activity upregulated follistatin (*FST*) expression which inhibited BMP signaling, a signaling pathway essential for maintaining cartilage homeostasis and normal chondrocyte development (8).

Table 1-1. Cellular modelling studies of TRPV4 mutant variants

No.	TRPV4 mutations	Phenotypes	Cellular models	References
1.	T89I	MD, lethal	*Xenopus* oocytes	(9)
		MD, lethal	Porcine chondrocytes	(8)
2.	G270V	FDAB	HEK293	(39)
3.	R271P	FDAB	HEK293	(39)
4.	F273L	FDAB	HEK293	(39)
		FDAB	Porcine chondrocytes	(8)
5.	E278K	SMDK, MD	*Escherichia coli*	(123)
6.	I331F	MD	HEK293	(116)
		MD, severe	*Xenopus* oocytes	(9)
7.	I331T	MD	*Escherichia coli*	(123)
8.	V342F	MD	*Escherichia coli*	(123)
9.	D333G	SMDK	HEK293	(10)
		SMDK	*Xenopus* oocytes	(9)
10.	Del333-7	MD	*Xenopus* oocytes	(9)
11.	F471del	MD, lethal	*Xenopus* oocytes	(9)
12.	R594H	SMDK	HEK293	(10)
		SMDK	*Xenopus* oocytes	(9)
13.	I604M	MD, lethal	*Xenopus* oocytes	(9)
		SMDK	hiPSC-derived chondrocytes	(124)
14.	R616Q	Brachyolmia, AD	HEK293	(7)
		Brachyolmia, AD	*Xenopus* oocytes	(122)
		Brachyolmia, AD	*Xenopus* oocytes	(9)
15.	F617L	MD, mild	*Xenopus* oocytes	(9)
		SMDK	HEK293	(125)
16.	L618P	MD, lethal	*Xenopus* oocytes	(9)
17.	L619F	MD	Dental pulp stem cells	(126)
18.	V620I	Brachyolmia, AD	HEK293	(7)
		SMDK	*Xenopus* oocytes	(9)
		Brachyolmia, AD	Porcine chondrocytes	(8)
19.	F621L	None	HEK293	(125)
20.	F624L	None	HEK293	(125)
21.	Y702L	None	HEK293, yeasts	(125, 127, 128)
22.	F707L	None	HEK293	(125)
23.	A716S	SMDK	HEK293	(10)
		SMDK	*Xenopus* oocytes	(9)
		SMDK	HEK293	(8)
24.	E797K	MD, mild	*Xenopus* oocytes	(9)
25.	P799L	MD	HEK293	(116)
		MD	Chondrocytes	(86)
		MD, moderate	*Xenopus* oocytes	(9)
26.	G800D	MD, severe	Chondrocytes	(86)
27.	c.2480_2483delCCCG frameshift deletion followed by a V829Q	Osteonecrosis	Dermal fibroblast	(118)
			HEK293	(118)

The second study reported TRPV4 channel overactivity in other skeletal dysplasia causing mutations ($TRPV4^{P799L}$ and $TRPV4^{G800D}$) (86). Similar to $TRPV4^{V620I}$, the patient $TRPV4^{P799L}$ and $TRPV4^{G800D}$ chondrocytes had significantly higher basal intracellular calcium level than non-isogenic wild-type chondrocytes. Following channel stimulations (hypotonic exposure and TRPV4 agonist (GSK101) administration), both mutant peak intracellular calcium level was significantly higher than the non-isogenic wild-type control which is consistent with the previous study on HEK293 (116) and Xenopus oocytes (9).

In vitro modelling of TRPV4 mutations causing Familial digital arthropathy with brachydactyly (FDAB) showed a distinct channel behaviour to TRPV4 skeletal dysplasia mutant channel. FDAB causing mutations (p.G270V, p.R271P, p.F273L) expressed in HEK-293 cells also resulted in higher basal intracellular calcium than the wild-type. However, the mutant channels had a weaker response to TRPV4 agonists (4α-PDD and GSK101) than wild type TRPV4 expressing cells and did not respond to hypo-osmotic conditions (39). These findings were reproduced in humanised-porcine chondrocytes (8). The less efficient transportation of TRPV4 protein from the ER to the Golgi during protein maturation and resultant decreased cell surface expressions of TRPV4 could be the main cause of the reduced channel responses to activating stimuli (39). Collectively, these findings highlighted the difference between FDAB and skeletal dysplasia mutations (8, 9, 103).

With regards to *in vitro* disease modelling, most studies transfected the mutant TRPV4 gene variants into heterologous cells to create the disease model (8, 39, 129). This results in non-physiological *TRPV4* over-expression and often the mutant TRPV4 is expressed on top of the endogenous *TRPV4*. Over-expression of TRPV4 could result in increased intracellular calcium mimicking the mutant channels (122) hence it would be ideal if human chondrocytes expressing endogenous levels of wild-type and mutant alleles are used. Moreover, since TRPV4 mutations cause tissue-specific phenotypes the observed changes in heterologous cells might be different from the ones in human chondrocytes. In addition, most TRPV4-inherited skeletal diseases are caused by heterozygous mutations, however only one study that has used heterozygous TRPV4 mutation for *in vitro* disease modelling study (86). Hence, modelling other heterozygous TRPV4 mutations is needed to explore the potential differences in TRPV4 channel behaviour caused by different types of mutations. Most importantly, the question of how the mutant TRPV4 channels contribute to skeletal defects remains unanswered.

1.3.3 Animal models for TRPV4 inherited skeletal diseases

Animal models for TRPV4 mutations have been extensively studied. There are three transgenic mice with human TRPV4 mutations (8, 11, 12), two TRPV4 knock out mice (14, 119) and one cat with a naturally occurring TRPV4 mutation (130). Knock out *Trpv4* (*Trpv4*$^{-/-}$) mice look phenotypically normal and no significant developmental skeletal abnormality is apparent (131, 132). Interestingly, the *Trpv4*$^{-/-}$ mice were significantly heavier than *Trpv4*$^{+/+}$ mice (131) and the male *Trpv4*$^{-/-}$ mice were heavier than the female mice (132). At age 12 months there were significant osteoarthritic changes in the hips and knee joints of the *Trpv4*$^{-/-}$ mice. Intriguingly, male *Trpv4*$^{-/-}$ mice have more severe osteoarthritic changes than female mice suggesting that there might be sex-specific regulation of *Trpv4* expression and function (131).

Histology of the bone and growth-plate of 12 week-old *Trpv4*$^{-/-}$ mice showed an increase in bone mass and bone calcification that is caused by reduced bone resorption suggesting that the osteoclast activity is decreased (13). Given that osteoclast differentiation is regulated by calcium signaling, the total ablation of TRPV4 channels in the *Trpv4*$^{-/-}$ mice could have disrupted the calcium signaling which eventually led to impaired osteoclast differentiation (13).

In addition, notable abnormal findings in organ systems other than the skeletal systems have been well documented. *Trpv4*$^{-/-}$ mice have abnormal vascular endothelial cell physiology, reduced water intake (14), reduced tactile and nociception stimuli response (133), impaired hearing (134), decreased/increased blood osmolality, decreased circulating anti-diuretic hormone (14), higher urine osmolality (119), urinary incontinence and abnormal respiratory physiology (Mouse Genome Database (MGD), Mouse Genome Informatics, The Jackson Laboratory, Bar Harbor, Maine. World Wide Web (URL: http://www.informatics.jax.org).

On the other hand, a naturally occurring *Trpv4*^{V342F} mutation in Scottish fold cats causes dominantly inherited folded ears and osteochondrodysplasia (130, 135). This mutation caused metatropic dysplasia in humans (110). Cellular modelling of the mutation in HEK-293 cells showed a significant lower membrane expression of TRPV4 ion channel in the mutant cells even though the expression of total TRPV4 is similar between mutant and wild-type cells. The basal level of free intracellular calcium was higher in the mutant cells however the channel response following hypotonic stress exposure was also lower in the mutant cells than the wild-type (130).

Three transgenic mice have been generated; *TRPV4*^{R594H}, *TRPV4*^{V620I}, and *Trpv4*$^{R616Q/V620I}$ transgenic mice, with all of them expressing the mutant TRPV4 in addition to expression of normal level of endogenous wild-type TRPV4. *TRPV4*^{R594H} was generated by fusing human mutant TRPV4 cDNA downstream of a *Col2a1* promoter sequence (11) whereas *TRPV4*^{V620I} transgenic mice were generated by using bacterial artificial chromosomes (BAC) containing the human mutant *TRPV4* gene (8). On the other hand, the *Trpv4*$^{R616Q/V620I}$ was generated to obtain mice expressing Trpv4 mutants restricted to osteoclasts (12). It was achieved by injecting the Trpv4 transgenes (the mouse mutant *Trpv4* cDNA) containing the 1.8-kb tartrate-resistant acid phosphatase (Trap) gene into fertilised mouse egg. In these three cases, the human mutant *TRPV4* gene sequence integrated randomly into the mice genome.

Phenotypic assessment of the *TRPV4*^{R594H} mice showed significant skeletal defects including dumbbell-shaped long bones, platyspondyly, and hypoplasia of the face. Histology of the growth plate shows a disruption in growth-plate architecture where no clear boundaries between growth-plate zones are observed. The reserve zone widens but the hypertrophic zone narrows suggesting a delay in chondrocyte hypertrophic maturation leading to a delay in bone mineralisation (11). On the other hand, the *TRPV4*^{V620I} transgenic mice show a significant reduction in long bone length and a significant increase in the width of the tibial plateau and femoral head. However, no significant change in the growth-plate structure was observed (8). The *Trpv4*$^{R616Q/V620I}$ showed a reduction in bone mass due to increased osteoclast activity (12).

Although transgenic mice are useful for examining the impact of mutations on skeletal development, the number of mutations that can be modelled is limited by the complexity of generating heterozygous mutant mice and the cost and time for breeding and maintaining colonies. Furthermore, the genetic, physiological and biomechanical differences between humans and mice could also influence the observed disease phenotypes. Therefore, a different experiment design is needed.

Given that pluripotent stem cells (PSCs) can self-renew and form tissues derived from the three germ layers including cartilage, it can be used as a cell source to generate skeletal disease-relevant cells including chondrocytes. When this PSC system is combined with CRISPR genome editing technology, engineered PSCs harbouring heterozygous mutations could be used to model TRPV4-inherited skeletal diseases (described in more detail in section 1.4.3 to 1.4.5).

1.4 hiPSCs for inherited skeletal disease modelling

1.4.1 The skeletal system development

To provide contextual background on hiPSC-based disease model, this section will describe reviews on skeletal embryogenesis and cartilage development. The skeletal system is derived from the ectoderm and mesoderm of embryonic layers (136, 137). The ectoderm forms craniofacial cartilages and bones whereas mesoderm develops into axial and appendicular (limb) skeletons (Figure 1-7). During embryogenesis, mesoderm develops into paraxial, intermediate and lateral plate mesoderm. Paraxial mesoderm develops into somites, a segmented paraxial mesoderm, which further develops into three distinct parts: dermatome, myotome, and sclerotome. Dermatome, myotome, and sclerotome develop into dermis, skeletal muscle and vertebra (axial skeleton) respectively (137-139). On the other hand, the lateral plate mesoderm develops into somatic and splanchnic parts which later develop into limbs and internal organs respectively (138). The growth of the limb bud in humans is initiated at about the 4^{th} week of gestation compared to day 11.5 of embryonic development in mice (48, 49).

Bone is the main component of the skeletal system. During embryonic development, bone formation is divided into two types, intramembranous ossification and endochondral ossification (137). Intramembranous ossification mainly occurs in craniofacial bones such as the skull. The bones are formed by direct calcification of connective tissues. On the other hand, endochondral ossification mainly occurs in appendicular bones such as the limbs. Bones that are formed through endochondral ossification require cartilage tissues as a template for calcification (140-142), thus chondrocyte differentiation plays significant roles in determining the outcome of bone formation. For the purpose of this review, we will focus on endochondral ossification as TRPV4-inherited skeletal diseases affect bones formed by endochondral ossification.

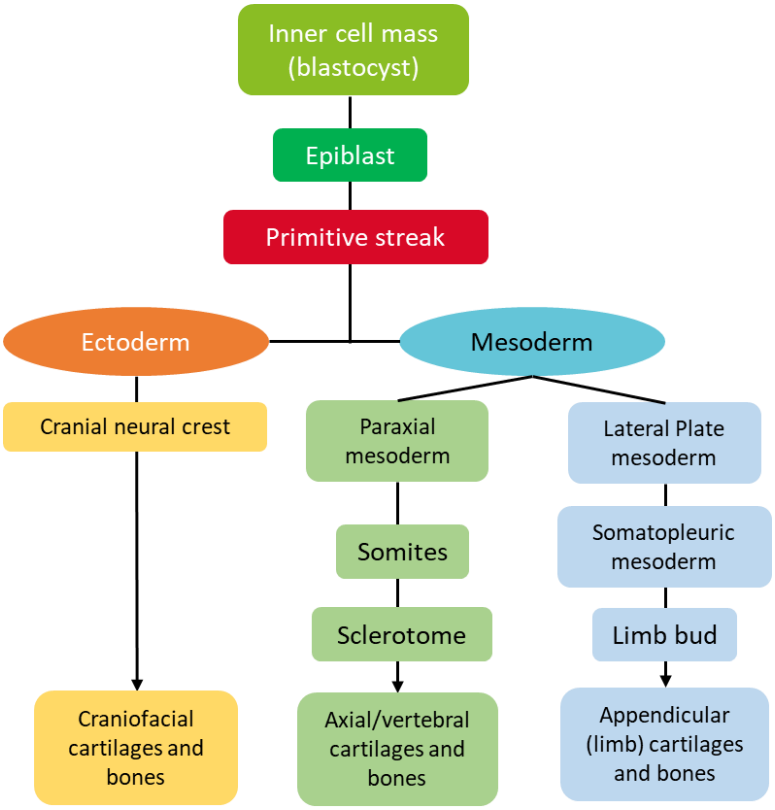

Figure 1-7. The embryology of the skeletal system. Inner cell mass in the blastocyst develops into epiblast then primitive streak. Primitive streak develops into three germ layers: ectoderm, mesoderm, and endoderm. The skeletal system is derived from ectoderm and mesoderm with ectoderm differentiates into cranial neural crest which further forms craniofacial cartilages and bones. Whereas mesoderm develops into three mesodermal derivatives: paraxial, intermediate and lateral plate mesoderm but only paraxial and lateral plate mesoderm develops into skeletal systems. Paraxial mesoderm forms axial and vertebral cartilages and bones whereas lateral plate mesoderm develops into appendicular (limb) cartilages and bones.

The complex molecular pathways of chondrocyte development and endochondral ossification in mouse have been reviewed by Yeung Tsang, Wa Tsang (5), Kozhemyakina, Lassar (6). These processes are illustrated in Figure 1-8. At day 11 of mouse embryonic development, an aggregate of mesenchymal progenitor cells in the hindlimb form primordial cartilage (Figure 1-8a). The cells in the aggregate proliferate and recruit more mesenchymal progenitor cells (Figure 1-8b). The proliferative cells are characterised by flattened cells with upregulation of the sex-determining region (SRY)-box-9 (*Sox9*) transcription factor, the master regulator of chondrogenesis (143, 144). *Sox9* expression is positively correlated with *Trpv4* expression (38) which is consistent with the finding of an *in vitro* study showing that *TRPV4* can modulate *SOX9* expression in chondrogenic cell lines (145).

At day 12.5 of embryonic development, mesenchymal progenitor cells differentiate into chondrocytes by the action of complex molecular pathways involving the sex-determining region (SRY)-box-5 (SOX5), SOX6, SOX9, and bone morphogenetic protein (BMP) signaling. As the chondrocytes differentiate and mature, the cartilage template which is rich in COL2A1 and ACAN, is surrounded by a perichondrium, a structure that later develops into periosteum. Cells in the perichondrium later differentiate into bone-forming cells, osteoblasts (48, 146).

At day 14.5 of embryonic development, the cartilage template is maturing and the chondrocytes begin to form a unique arrangement resulting in 3 distinctive zones: proliferating, pre-hypertrophic and hypertrophic zones (Figure 1-8c). This structure is called an epiphyseal growth plate. The proliferating zone is characterised by flat actively dividing chondrocytes arranged in longitudinal columns. This zone is where the longitudinal bone growth mainly occurs. The proliferating zone chondrocytes express *Sox5, Sox6, Sox9, Col2a1,* and *Acan* and they show increased activity of the BMP signaling pathway (5, 6). The pre-hypertrophic zone is characterised by enlarged chondrocytes and the hypertrophic zone contains pre-hypertrophic chondrocytes undergoing further maturation in preparation for endochondral ossification. Chondrocytes in the pre-hypertrophic zone show a decrease in expression of *Sox5, Sox6, Sox9, Col2a1*. The parathyroid hormone (*Pth1r*) receptor and Indian Hedgehog (*Ihh*) are upregulated in these enlarged chondrocytes suggesting their significant roles in ossification regulation (5, 6). The hypertrophic chondrocytes express *Runx2*, *Col10a1* (encoding collagen type X), *Vegfa, Mmp13* and secrete osteopontin (5, 6, 147). *Vegfa* and *Mmp13* facilitate vascular invasion which eventually promotes the formation of trabecular bone, the marrow cavity and the deposition of osteoclasts, monocyte derivatives responsible for matrix resorption (47, 148).

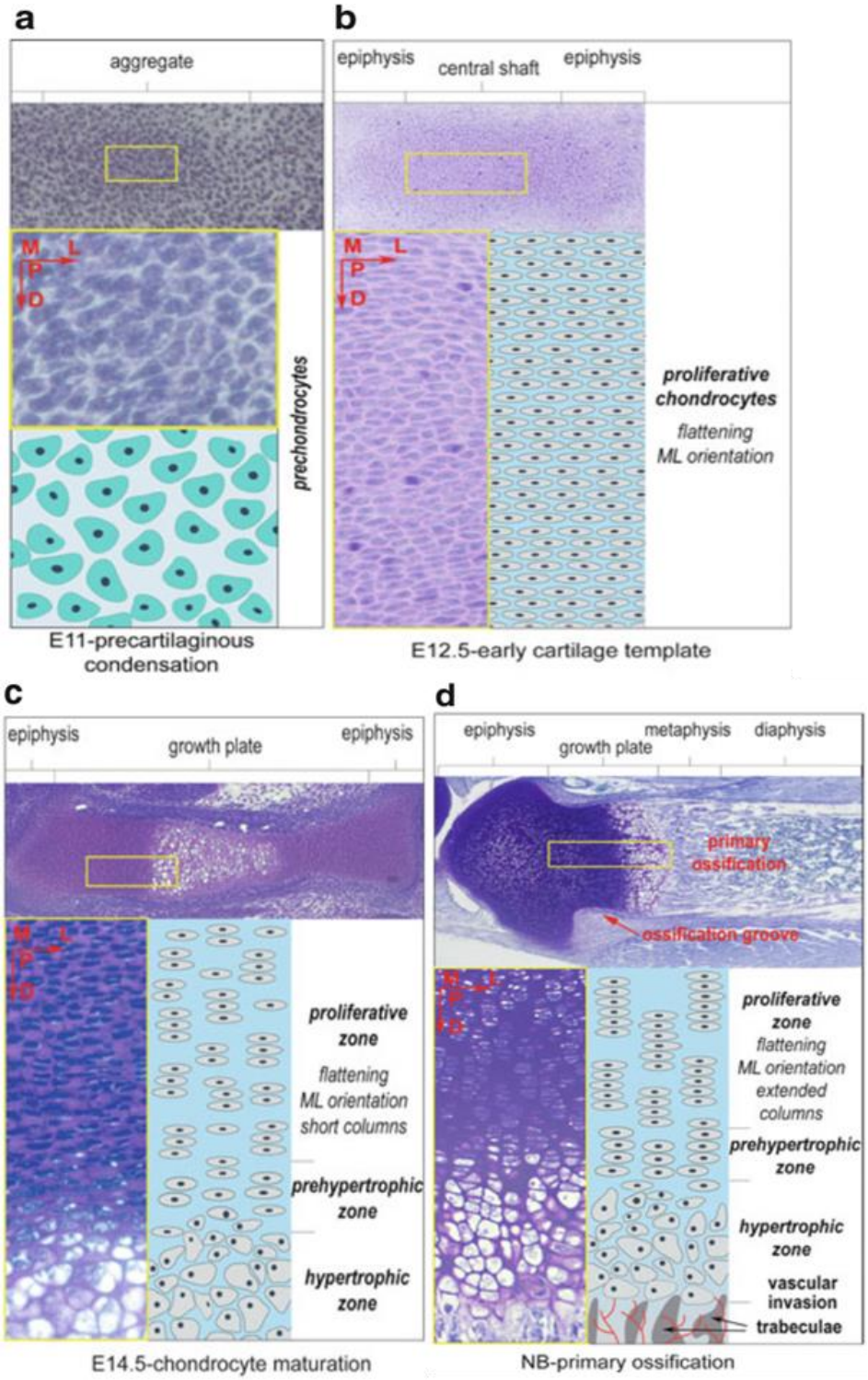

Figure 1-8. The endochondral ossification process of the long bone in mice. Modified from (149)). The endochondral ossification is started with the differentiation of mesenchymal progenitor cells towards chondrocytes. The differentiation is initiated by the formation of aggregates of mesenchymal progenitor cells at E11 (a). The cells proliferate and change their morphology into flat cells at E12.5 (b). Early growth plate structure is apparent at E14.5 where the chondrocytes form 3 distinctive zones: proliferative, pre-hypertrophic, and hypertrophic zone (c). Primary ossification occurs in the hypertrophic zone and vascular invasion is also observed (d). M: medial, L: lateral, P: proximal, D: distal.

The endochondral ossification process begins from the hypertrophic zone where the primary ossification centre starts to form (Figure 1-8d). At this stage, the distinctive bone structure: epiphysis, metaphysis, and diaphysis becomes more apparent. The initiation of calcification in the hypertrophic region is still poorly understood. The proposed theory explains that the hypertrophic chondrocytes undergo programmed cell death (5, 150) and the matrix vesicles that extrude from their membrane are substrate for calcification. These matrix vesicles contain mineral crystals such as calcium and phosphates. The ATPase in the matrix vesicles facilitates the transport of calcium ions into the vesicles against the concentration gradient. As the mineral crystal accumulates, it spreads beyond the vesicle wall and the apatite crystals start to grow and to integrate with the extracellular matrix (47).

As the ossification continues, the lacunae left by the dead hypertrophic chondrocytes provide a path for blood vessels to invade the calcified cartilage. Osteoclasts gain access to the lacunae and resorb the calcified cartilage. Eventually, the osteoblasts which are mostly differentiated from perichondrium cells, lay down bone matrices such as collagen type I on top of the calcified cartilage. Tissue remodeling continues to occur to convert the calcified cartilage into bone (47).

The anabolic and catabolic processes occurring in the growth plate are regulated in such a way that there is a balance between the two to control the growth plate length. A delay in chondrocyte proliferation or a delay in ossification shortens the growth plate length (47). Mutations in patterning molecules important during embryo development, transcription factors, ECM molecules, enzymes and intracellular trafficking molecules important for ECM synthesis and secretion (151) can disrupt growth plate development during embryogenesis and cause various types of inherited-skeletal abnormalities.

1.4.2 The SOX9 transcription factor and molecular signaling involved in chondrogenesis

SOX9 is the master regulator of cartilage development. Mutations in SOX9 gene cause campomelic dysplasia (152) and its milder phenotype, acampomelic variants of campomelic dysplasia (153). Campomelic dysplasia is characterised by severe skeletal malformation showing bowed long bones, hip dislocation, tracheolaryngomalacia, cleft palate, and ambiguous genitalia (144, 154). Most campomelic dysplasia patients die during the newborn period due to respiratory distress caused by abnormal respiratory tract structures where cartilage plays a vital role in providing tube-like structure.

Animal studies show that knocking out the *Sox9* gene results in significant skeletal defects in mice and the absence of *Col2a1* expression (155-157). These indicate that the Sox9 transcription factor is important in chondrogenesis. The roles of *SOX9* in chondrogenesis have been reviewed by Akiyama and Lefebvre (158). *Sox9* up-regulates the expression of *Col2a1* (159, 160) and *Acan* (161, 162). Sox9 works synergistically with other transcription factors, Long-Sox5 (L-Sox5) and Sox6, to regulate the expression of *Col2a1* (163-165) and other cartilage markers (166-168).

Signaling pathways that control chondrogenesis are summarised in Figure 1-9. In general, positive regulators of chondrogenesis simultaneously increase and maintain SOX9 activity but reduce the activity of the RUNX2 transcription factor (169). These positive regulators of chondrogenesis include BMP, fibroblast growth factors (FGFs), hypoxia-inducible factor-1α (HIF1α) and Protein Kinase A (PKA) (170, 171) and the Sonic Hedgehog (SHH) signaling pathway.

Wnt signaling is essential in limb patterning during embryogenesis. Wnt signaling controls *SOX9* expression by promoting methylation of the *SOX9* promoter thus downregulating SOX9 expression (172). IHH signaling promotes the maturation of chondrocytes towards hypertrophic chondrocytes by upregulating *RUNX2*.

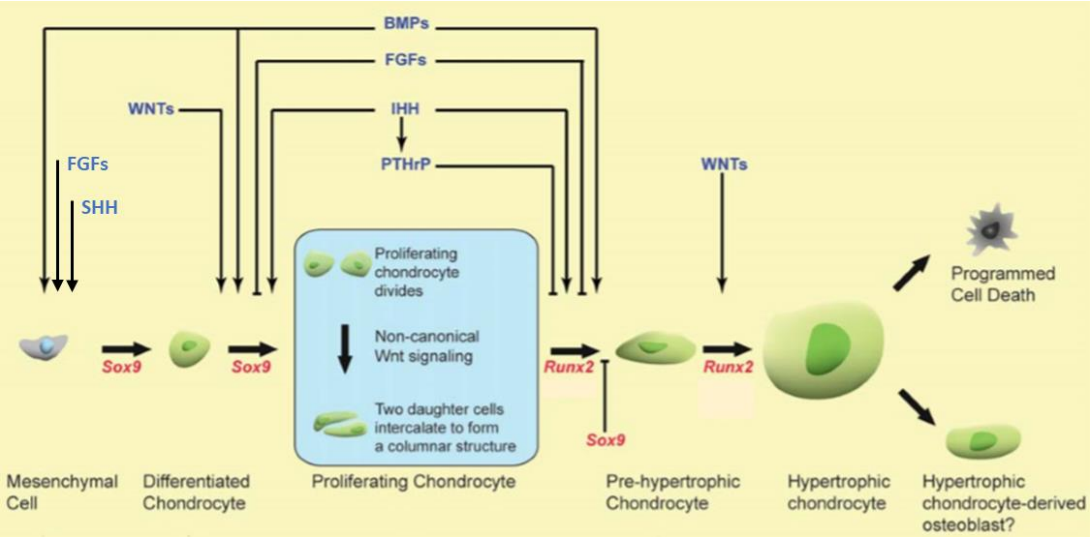

Figure 1-9. Multiple signalling pathways regulating *Sox9* and *Runx2* expression . Adapted from (5). FGF: fibroblast-growth factor, SHH: Sonic-Hedgehog, Wnt: Wingless-integrated, BMP: bone morphogenetic, IHH: Indian-Hedgehog, PTHrP: Parathyroid hormone-related protein.

1.4.2.1 Bone Morphogenetic Protein (BMP) signaling pathway

BMP signaling is essential in chondrogenesis. During sclerotome formation, Bmp2, Bmp4, and Bmp7 are abundantly expressed in mouse 10.5-day post-coitus (dpc) limb bud, just before mesenchymal cell aggregation occurs (173). In addition, BMP also plays a crucial role in promoting the maturation of chondrocyte progenitors into chondrocytes (174). In vitro administration of BMP2 into C3H10T1/2 chondrogenic cell lines (175) and human mesenchymal stem cells (176) increases the expression of *SOX9*, *COL2A1*, and *ACAN*. However, in another study using the ATDC5 chondrogenic cell line, BMP2 promotes maturation of the cells into hypertrophic chondrocytes (177) whereas BMP7 suppresses the differentiation towards hypertrophic chondrocytes (178).

Mice deficient in both bone morphogenetic protein receptor-1a (*Bmpr1a*) and bone morphogenetic protein receptor-1b (*Bmpr1b*) show severe chondrodysplasia phenotypes (179) with a significant decrease in the expression of *L-Sox5, Sox6,* and *Sox9* (180). Another member of the BMP protein family, growth and differentiation factor-5 (GDF5) or BMP14, has a unique property to promote chondrocytes differentiation toward articular cartilage (19, 181, 182).

The chondrogenic properties of BMPs are mediated through two main pathways: 1) through SMADs family signal transduction (183) and 2) through the downregulation of β-catenin/Wnt7a signaling which is responsible for SOX9 degradation via the ubiquitin-proteasome degradation pathway (184). On the other hand, BMP signaling is inhibited by Noggin (173). Noggin is upregulated by BMP signaling at the beginning of chondrogenesis which eventually promotes negative feedback to the BMP signaling. Ventroptin is another BMP inhibitor that is expressed earlier than Noggin (185).

1.4.2.2 Transforming Growth Factor- β (TGFβ) signaling pathway

TGFβ has an important role in promoting chondrogenesis (186-188). It promotes mesenchymal cell aggregation/condensation to initiate chondrogenesis (189) and it increases mesenchymal cell responsiveness to the chondrogenic activity of BMP signaling (190). TGFβ is also essential in promoting chondrocytes differentiation towards articular chondrocytes (19, 191) by preventing the differentiation of resting chondrocytes into hypertrophic chondrocytes (188).

The administration of TGFβ in synovial mesenchymal stem cell culture increases the expression of chondrogenic markers *SOX9, ACAN,* and *COL2A1* which is mediated by the SMAD pathway (192). TGFβ in combination with FGF2 (193) or BMP4 (191, 194) has a synergistic effect in enhancing chondrogenic marker expression in cultured

human mesenchymal stem cells. TGFβ actions are mediated by activating SMAD pathway and by inhibiting WNT signaling (195).

1.4.2.3 Fibroblast Growth Factor (FGF) signaling pathway

Three FGF proteins are relevant in chondrogenesis: FGF2, FGF9, and FGF18 (Figure 1-10). FGF2 promotes mesenchymal cell proliferation and priming the cells to differentiate towards chondrocytes at the early stage of chondrogenesis (193). *FGF9* is expressed in the perichondrium cells and it regulates chondrocyte maturation and hypertrophy. *FGF18* is expressed in the perichondrium cells and chondrocytes, and it shows a biphasic action during the early and late stage of chondrocyte development. In the early stage of chondrocyte development (E14-15 dpc), FGF18 promotes chondrocyte proliferation and initiates chondrocyte hypertrophy whereas in the later stage (E16-18 dpc), it blocks chondrocyte proliferation and delays the initiation of hypertrophy. The regulation by which FGF18 shows biphasic action remains unclear but it has been reported that FGFR3 mediates the action of FGF18 in inhibiting chondrocyte proliferation and hypertrophy (5, 6, 193).

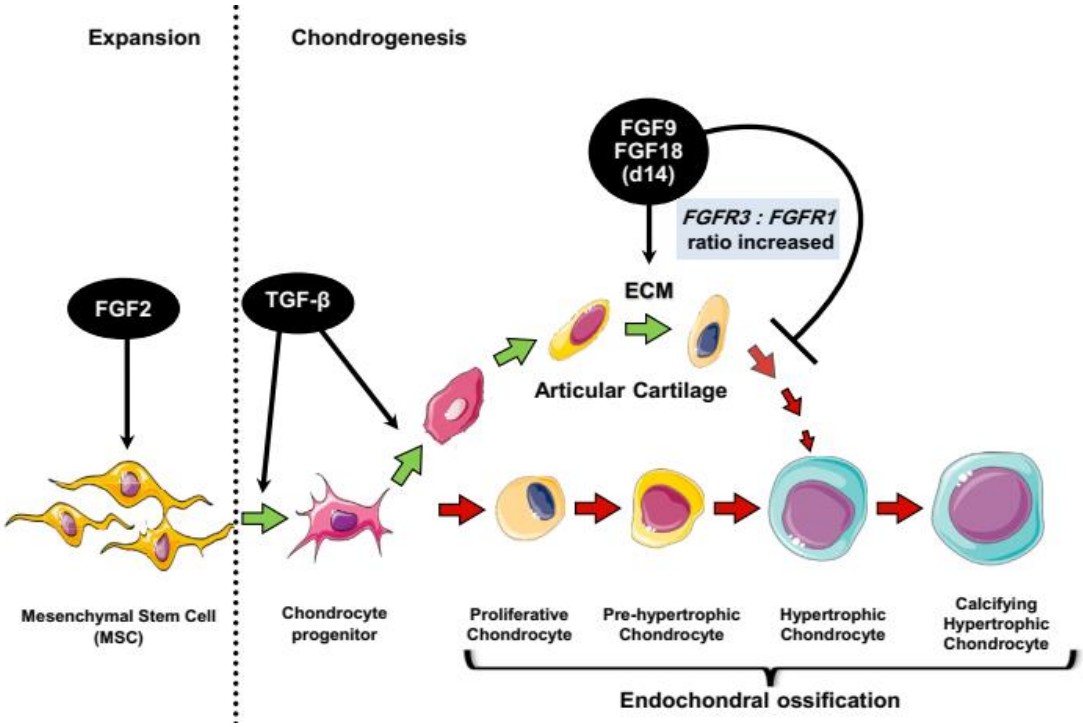

Figure 1-10. The roles of FGF signalling in chondrogenesis. Adapted from (193)

Three out of 4 FGF receptors play important roles in chondrogenesis (5). *FGFR1* is expressed in pre-hypertrophic and hypertrophic chondrocytes and may have a role in maintaining hypertrophic chondrocyte (196). *FGFR2* is initially expressed in mesenchymal stem cell condensations but then it is exclusively expressed in the peripheral mineralised zone of hypertrophic chondrocytes, in the adjacent osteoblast and perichondrium cells. Hence, it seems that FGFR2 has an essential role in regulating chondrocyte hypertrophy and osteoblast differentiation (6). On the other hand, *FGFR3* is mainly expressed in proliferating chondrocytes and is downregulated in hypertrophic chondrocytes(197). In achondroplasia where mutations in *FGFR3* cause the receptor to be constitutively active (198), patients have dwarfism (199, 200) indicating that over-activity of the receptor inhibits chondrocyte proliferation which eventually reduced the number of hypertrophic chondrocytes. However, Fgfr3-null mice have elongated bones suggesting that there is an increase in chondrocyte proliferation. FGFR3 thus plays an important role in inhibiting both chondrocyte proliferation and hypertrophic initiation (6).

FGF signaling promotes chondrogenesis by increasing the expression of SOX9 via a mitogen-activated protein kinase (MAPK) pathway (201, 202) in *in vitro* cultured human mesenchymal stem cells (193), primary cultured chondrocytes (201) and chicken limb bud cells (203). FGF abrogates the epigenetic silencing of SOX9 by inducing the phosphorylation of DNA methyl-transferase 3A (Dnmt3a) resulting in the upregulation of *Sox9* expression (172).

1.4.2.4 Sonic HedgeHog (SHH) signaling pathway

Sonic Hedgehog (SHH) signaling plays a critical role in cell fate determination during embryogenesis (204). It is secreted by the notochord and floor plate of the developing embryo. SHH signaling facilitates subsequent BMP signaling to promote chondrogenesis. Administration of SHH into presomitic mesoderm of chicken explant culture induces the expression of *Sox9, Col2a1, Acan* (205).

1.4.2.5 Hypoxia-inducible factor-1α (Hif1α) signaling pathway

HIF1α deficient mice show defects in cartilage and joint formation, suggesting the essential role of HIF1α signaling in chondrogenesis. *In vitro* micromass culture of mesenchymal cells derived from day 11-11.5 HIF1α-deficient mouse embryos also shows a significant reduction in chondrogenic marker expressions (206). Chromatin immunoprecipitation (ChIP) analysis shows a putative hypoxia response element located upstream of the *Sox9* promoter where HIF1α might bind to regulate SOX9 expression (206). Hypoxic condition is the main trigger of HIF1α activity. Primary human

chondrocytes (207, 208) and rat bone marrow isolated mesenchymal stem cells (209) cultured in hypoxic condition show increased expression of *HIF1α, SOX9,* and *COL2A1*.

1.4.2.6 Notch signaling pathway

Both overexpression and inactivation of Notch signaling cause skeletal defects in mice suggesting an essential role in skeletal development and chondrocyte differentiation (210). The interaction between Notch signaling and SOX9 expression contribute to chondrocyte maturation towards hypertrophic chondrocyte (211). However, the exact pathway by which Notch signaling regulates skeletal development and chondrocyte differentiation remains unclear.

1.4.2.7 WNT/ β-catenin signaling pathway

The interaction of WNT signaling and FGF has been demonstrated in chicken limb bud development (203). The administration of WNT3A into *in vitro* culture of limb bud mesenchymal stem cells significantly decreases *Sox9, Col2a1,* and *Acan* expression suggesting that WNT signaling inhibits chondrogenesis (172). However, the interaction of WNT and FGF signaling secreted by the apical ectodermal ridge (AER) at the apical region of the limb bud is essential to promote its normal limb bud patterning (203) (Figure 1-11). WNT/β-catenin signaling pathway during chondrogenesis initiation is inhibited by the TGFβ mediated increase in histone deacetylase 1 (HDAC1) activity. The increased HDAC1 activity promotes deacetylation of the β-catenin promoter resulting in the downregulation of β-catenin, the main effector of WNT signalling (195).

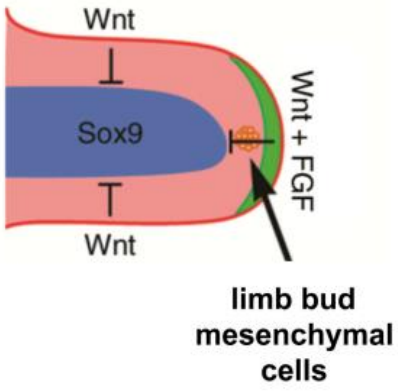

Figure 1-11. Schematic figure of the limb bud. Adapted from (172). WNT signalling from the ectodermal tissues (pink) located at the peripheral region of the limb bud inhibits chondrogenesis in the chondrogenic core of the limb bud (blue). The FGF signal from the apical ectodermal ridge (AER) (green) maintains chondrogenesis and the viability of the limb bud mesenchymal cells allowing proximodistal growth of the limb bud.

1.4.2.8 Indian Hedgehog (IHH) signaling pathway

IHH promotes the maturation of chondrocytes (212, 213) by upregulating *Runx2* and *Col10a1* expression (212, 214). Ihh promotes the differentiation of resting chondrocytes towards proliferating chondrocytes via Gli3 (215). As negative feedback on increased IHH activity, parathyroid hormone-related protein (PTHrP) is upregulated (215, 216). PTHrP enhances cyclic adenosine monophosphate (cAMP) signaling resulting in increased protein kinase A (PKA) activity that promotes SOX9 phosphorylation hence increases SOX9 activity (171). Therefore, it might be plausible that PTHrP plays an important role in maintaining the non-hypertrophic chondrocytes in the growth plate by increasing Sox9 activity (171, 217, 218) and by repressing Runx2 activity (219, 220).

1.4.3 PSCs differentiation towards chondrocytes

There are two types of PSCs, human embryonic stem cells (hESCs) and human-induced pluripotent stem cells (hiPSCs) (16, 221, 222). These cells can be maintained indefinitely in stem cell culture conditions without losing their pluripotency (221, 222). The potential uses of PSCs have been shown in many studies including for regenerative cell therapy (223, 224), studying human development (17, 225), disease modeling studies (223, 226-229) and drug screening and discovery (223, 226, 227).

The hESCs are isolated from the inner cell mass of blastocysts (222) thus raising ethical concerns over the destruction of embryos (230). These concerns can be overcome by using hiPSCs as they are generated from adult somatic cells using reprogramming techniques. The reprogramming involves the transduction of four stem cell factors OCT3/4, SOX2, KLF4 and c-MYC (OSKM) into human adult somatic cells (16). With this technique in place, in theory, almost all adult somatic cells could be reprogramed into hiPSCs. Like hESCs, hiPSCs are able to self-renew and to differentiate into tissues originated from three embryonic layers including cartilage. The other advantage of hiPSCs over hESCs is that because hiPSCs are generated from adult somatic cells, they are relatively easy to obtain.

In developing hiPSC disease model, the appropriate use of disease-relevant cells is the key for accurate disease modelling study. Given that chondrocytes provide cartilage templates for endochondral ossification, chondrocytes would be the appropriate disease-relevant cells for TRPV4-inherited skeletal disease modelling. Therefore, generating chondrocytes from hiPSCs becomes the first priority of this present study to perform hiPSC disease model for TRPV4-inherited skeletal diseases. To obtain hiPSC-derived

chondrocytes, establishing a robust and reproducible chondrocyte differentiation protocol is required and it remains the biggest challenge for hiPSC-skeletal disease modelling. Many chondrocyte differentiation protocols have been developed with a huge range of approaches. Table 1-2 summarises the advantages and disadvantages of various approaches used to generate chondrocyte-like cells from PSCs. The approaches include using embryoid body formation, conditioned culture medium, intermediate mesenchymal cell generation and directed differentiation (231-233).

Table 1-2. Different approaches to generate chondrocytes from PSC. Adapted from (234)

Approaches	**Advantages**	**Disadvantages**
Embryoid body formation	Easy culture Mimics embryonic development	Low efficiency Heterogeneous cell population
Co-culture with chondrocytes/ Conditioned medium culture	Helps target differentiation Use fewer growth factors	Low efficiency Complicated culture system Depends on primary cells
PSC to MSC to Chondrocytes	Higher expansion capacity than adult mesenchymal stem cells	Long process Batch variation Heterogeneous cell population
Directed differentiation:		
1. Single step	Easy culture	Massive cell death Heterogeneous cell population
2. Multiple steps/chemically defined	Mimics embryonic development High yield/scalable Homogenous cells	Complicated culture More growth factor required

The multiple steps and chemically defined approach became popular after being pioneered by Oldershaw, Baxter (20). The study showed that PSCs could be directed into chondrogenic lineages using growth factors through a process that mimics embryonic development (section 1.4.1). Since then, several chondrocyte differentiation protocols that used a similar approach have been reported (17-19, 235, 236). Table 1-3 summarises the comparison of four chondrocyte differentiation protocols that use a multi-step chemically defined approach.

In general, multiple steps and chemically defined chondrocyte differentiation directs the differentiation of PSCs into four different stages; the primitive streak stage, paraxial or lateral mesoderm stage, chondroprogenitor stages, and chondrocyte differentiation and maintenance stage. The differentiation of PSCs towards primitive streak is achieved by upregulating TGFβ signaling (237) through the administration of Activin-A. FGF2 is used to promote the survival of the differentiating hiPSCs (20). Increasing BMP (BMP4) and WNT signalling (by administering WNT3A or WNT signalling agonist, CHIR99021) upregulates primitive streak markers T and MIXL1 (17,

236, 238). The primitive streak is able to develop into mesoderm and endoderm lineages (138, 238).

Table 1-3. Chondrocyte differentiation protocols using multiple steps and chemically defined approach

	Oldershaw, Baxter (20)	**Craft, Rockel (19)**	**Yamashita, Morioka (18)**	**Loh, Chen (17)**
PSCs	hES cells	hES and hiPS cells	hES and hiPS cells	hES and hiPS cells
Duration	2 weeks	12 weeks	8 weeks	<2 weeks
Embryoid body formation	Yes and No	Yes	No	No
Primitive streak (mesendoderm) induction (duration)	Activin-A BMP4 FGF2 WNT3A (3x24 hours)	Activin-A BMP4 FGF2 (3x24 hours)	Activin-A WNT3A (3x24 hours)	Activin-A CHIR99021 FGF2 PIK90 (1x24 hours)
Mesoderm (paraxial) induction (duration)	BMP4 Follistatin FGF2 NT4 (5x24 hours)	Dorsomorphin FGF2 (15x24 hours)	BMP2 FGF2 GDF5 TGFβ (12 x 24 hours)	A-83-01 FGF2 CHIR99021 LDN193189 (1x24 hours)
Somite (ventral) induction/ chondroprogenitor (duration)	BMP4 FGF2 GDF5 NT4 (1 week)	FGF2 TGF-β3 (10x24 hours)		A-83-01 LDN193189 PD0325901 C59 (1x24 hours)
Sclerotome induction/ chondroprogenitor (duration)				21K C59 (3x24 hours)
Cartilage differentiation (duration)		BMP4 or TGF-β3 (4-12 weeks)	BMP2 GDF5 TGFβ (6-10 weeks)	BMP4 (1 week)

As mentioned in section 1.4.1, mesoderm is divided into paraxial, intermediate and lateral plate mesoderm. Paraxial mesoderm gives rise to somites whereas lateral plate mesoderm develops into limb bud and internal organs (138). To direct the differentiation of primitive streak into mesoderm, blocking endoderm specification is required. This can be achieved by inhibiting TGFβ signaling (238, 239) with the TGFβ signalling blocker, A-83-01, and stopping the Activin-A treatment. Differentiation towards paraxial mesoderm is preferable for generating chondroprogenitor cells as differentiation towards lateral plate mesoderm requires extra steps to block signalling essential for internal organ development. Blocking BMP signalling directs mesoderm differentiation towards paraxial mesoderm indicated by the upregulation of paraxial mesoderm markers such as *CDX2*, *DLL1*, *TBX6*, and *MSGN1* (17). This can be achieved by administration of dorsomorphin, the BMPR1 inhibitor (19), or other BMP signalling inhibitors such as

follistatin (20) and the small molecule LDN193189 (17, 236). Upregulating WNT signalling by CHIR99021 increases paraxial mesoderm markers and downregulates lateral plate mesoderm markers (*HAND1* and *FOXF1*) and cardiac markers (internal organ) such as *NKX2*.5 and *ISL1* (17). FGF2 and NT4 administration promote the survival of the differentiated cells (20).

The chondroprogenitor stage involves somite and sclerotome induction. Most chondrocyte differentiation protocols do not specify the differentiation towards somites and sclerotome (18-20). The segmented somites are divided into ventral and dorsal parts with ventral somites giving rise to sclerotome, the precursor of vertebrae, whereas the dorsal somites develop into dermo-myotome that generates soft tissues including adipose tissues, skeletal muscle, and dermis (137). With the enormous potential of somites to give rise to many different tissues, directed differentiation towards sclerotome is required to get a more homogenous cell population. Blocking TGFβ and BMP4 signalling (through the administration of small molecules A-83-01 or SB and LDN193189 or dosomorphine) upregulates somite markers such as *MEOX1* and *FOXC2* (17, 236). The efficiency of somite induction is increased by blocking WNT and FGF signalling using small molecules C59 and PD0325901 (17). Sclerotome specification is achieved by upregulating SHH signalling (small molecules 21K/ SAG/ purmorphamine treatment) (17, 236) and preserving the WNT signalling blockage (C59 treatment) (17). This upregulates sclerotome markers such as *PAX1*, *SOX9*, and *TWIST1*.

The chondrocyte differentiation and maintenance stage vary a lot. Several growth factors such as BMP2 (18, 240-243), BMP4 (19, 20, 235, 244-248), BMP7 (249-251), FGF2 (19, 246, 247, 252, 253), PDGF (235, 251, 254), TGFβ1 (18, 240, 241, 249, 250, 253, 255-257), TGFβ3 (19, 235, 244, 254, 258-262) and GDF5 (18, 20, 246) have been reported to enhance chondrocyte development and differentiation. The standard culture formats for primary chondrocytes, micromass and pellet, are widely applied in PSC-derived chondrocyte culture and maintenance protocols.

1.4.4 hiPSC disease model

The pipeline of disease modeling using hiPSCs is illustrated in Figure 1-12. Patient-derived hiPSC lines can be generated from somatic cells such as skin fibroblasts via reprogramming (16). Before being used for further study, the generated hiPSCs are characterised to confirm that the cells maintain their pluripotency. The patient-derived hiPSCs are then differentiated into disease-relevant cell types such as chondrocytes. By comparing the patient-derived hiPSCs with independent healthy-control hiPSCs,

molecular and cellular phenotypic changes can be observed and measured. This approach provides an opportunity to discover novel pathogenic pathways underlying the disease.

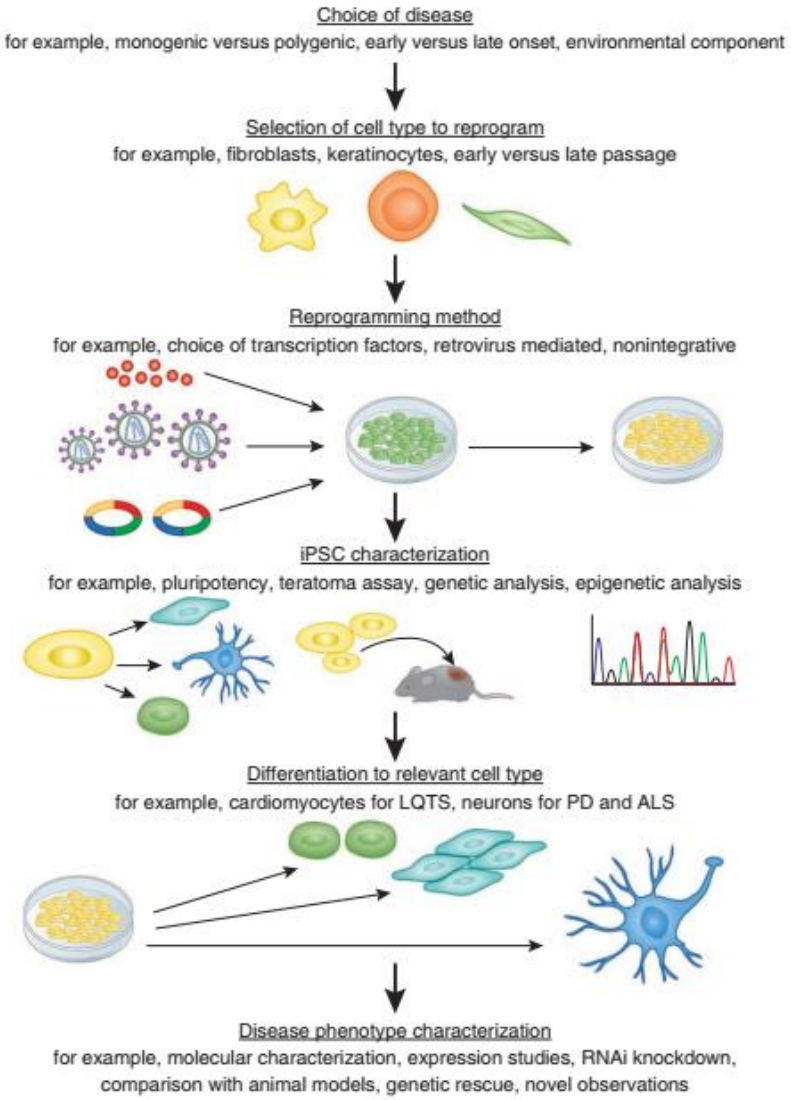

Figure 1-12. The pipeline of disease modeling study using hiPSCs. Adapted from (229).

The utility of this hiPSC approach has been demonstrated in studies that have modelled several monogenic skeletal diseases (Table 1-4). The findings from the studies show promising results in which they could demonstrate abnormal molecular and phenotypic changes in the mutant hiPSC-derived chondrocyte-like cells compared to the control.

Table 1-4. Current cartilage disease modelling studies using hiPSCs

Disease	Gene	Mutation	Isogenic control	Chondrocyte differentiation approach	Chondrogenic factors	Results	References
Fibrodysplasia ossificans progressive (FOP), AD	*ACVR1**	p.R206H, heterozygous	No	Multiple steps and chemically defined	TGFβ3	The mutants show increased mineralisation and cartilage formation	(263)
Lethal metatropic dysplasia, AD	*TRPV4*	p.I604M, heterozygous	No	Single-step	BMP2 or TGFβ1	Lower expression of cartilage markers in the mutant TRPV4	(21)
Thanatophoric dysplasia type 1 (TD1), AD	*FGFR3*	p.R248C, heterozygous	No	Multiple steps and chemically defined	BMP2, TGFβ1, GDF5	Significant defect in cartilage tissue formation in the mutant FGFR3. The defects rescued by FGFR3 inhibition and administration of statins	(264)
Achondrodysplasia (ACH), AD	*FGFR3*	p.G380R, heterozygous	No				
Achondrodysplasia (ACH), AD	*FGFR3*	p.G380R, homozygous	No				
Fibrodysplasia ossificans progressive (FOP), AD	*ACVR1**	p.R206H, heterozygous	Yes	PSC to MSC to chondrocytes through neural crest lineages	TGFβ3	The mutants show increased mineralisation and cartilage formation	(265)
Achondrogenesis type 2 (ACGII), AD	*COL2A1*	p.G1182A, heterozygous	No	Multiple steps and chemically defined	BMP2, TGFβ1, GDF5	Significant defect in cartilage tissue formation in the mutant COL2A1. Upregulation of ER stress markers and increased apoptosis in the mutant cartilage.	(266)
Hypochondrogenesis (HCG), AD	*COL2A1*	p.G450R, heterozygous	No				
Spondyloperipheral dysplasia (SPD), AD	*COL2A1*	p.K1447CInfsX 18heterozygous	No				
Familial osteochondritis dissecans (FOCD), AD	*ACAN*	p.V2303M, heterozygous	No	Teratoma formation	N/A	The mutants exhibit an endoplasmic reticulum stress response and defective matrix assembly	(267)
Oculodentodigital dysplasia (ODDD), AD	*Cx43 or GJA1*	p.V216L, heterozygous	No	PSC to MSC to chondrocytes	StemPro Chondrogenesis kit (ThermoFisher)	The mutant Cx43 showed reduced Cx43 mRNA and protein abundance as well as an altered subcellular localisation of the Cx43 protein.	(268)
Fibrodysplasia ossificans progressive (FOP), AD	*ACVR1**	p.R206H, heterozygous	Yes	Multiple steps and chemically defined & PSC to MSC to chondrocytes	BMP7, TGFβ3	The mutants show increased mineralisation and cartilage formation	(269)
Andersen's Syndrome with skeletal manifestations	*KCNJ2*	p.C154Y' heterozygous	No	PSC to MSC to chondrocytes	StemPro Chondrogenesis kit (ThermoFisher)	Downregulation of SOX9 and RUNX2 in the mutant lines. Impairment in chondrocyte and osteoblast differentiation.	(270)

AD: autosomal dominant, *using the same hiPSC lines

Patient fibroblasts with FGFR3 mutations (p.R248C, p.G380R) were reprogrammed into hiPSCs and differentiated into chondrocytes (264). The mutations cause a constitutively active FGFR3 resulting in dwarfism and defects in endochondral ossification. Chondrocyte differentiation was performed according to Oldershaw, Baxter (20) with some modifications including performing 3D-culture and extending the culture period. The wild-type hiPSC line was able to form cartilage and showed upregulation of chondrogenic markers *SOX9, COL2A1*, and *ACAN*. However, the mutant FGFR3 hiPSC failed to form cartilage tissues. The expression of cartilage markers: *SOX9, COL2A1*, and *ACAN* were similar in wild type and mutant up until differentiation day 21 but at differentiation day 28, their expression in the FGFR3 mutant line was significantly lower than in the wild-type. Mutant FGFR3 cells expressed high levels of COL1A1 instead of COL2A1 and practically no Safranin O staining was visible indicating a significant decrease in proteoglycan expression. Decreased cell proliferation and increased apoptosis were the main pathways that contributed to the failure of cartilage tissue formation in the FGFR3 mutant line. Interestingly, the defects were rescued by inhibiting FGFR3 activity using an anti-FGFR3 antibody and administration of statins, lipid lowering agents.

In another study, hiPSC from patients with *COL2A1* mutations (p.G1182A and p.G450R) were differentiated into chondrocytes (266). A similar chondrocyte differentiation protocol to the one used in the FGFR3 disease modeling was used. After 42 days of chondrocyte differentiation culture, the wild-type hiPSC line was able to form cartilage tissues indicated by positive proteoglycan staining (Safranin O) and the upregulation of *COL2A1* and *ACAN*. On the other hand, the mutant hiPSC lines showed defects in cartilage formation indicated by negative Safranin O staining on day 42 pellets. Mutant cartilage also showed lower *COL2A1* and *ACAN* expression than the wild-type. Increased apoptosis was identified in the mutant COL2A1 pellet shown by increased TUNEL staining and upregulation of the apoptosis marker caspase-3 (CASP3) compared to the wild type control. Upregulation of ER stress markers such as *BIP* and *CHOP* were found in the mutant pellets.

Teratomas were generated in this study. Teratoma is an embryonic tumour that contains various types of tissues originated from three embryonic layers including cartilage. Due to their pluripotent characteristics, hiPSCs are able to generate teratomas after subcutaneous injection into immunocompromised mice. Therefore, teratoma cartilage can be used as a source of cartilage tissues for cartilage disease modeling. From cartilage teratoma histology, the study found that the COL2A1 mutant teratoma cartilage

had a significantly higher intracellular retention of collagen type II protein than the wild type control. Electron microscopic analysis identified distended rough endoplasmic reticulum indicating the increase in ER stress.

Only one study has used hiPSCs to model TRPV4 inherited skeletal dysplasias (21). The study modelled the p.I604M TRPV4 mutant variant causing lethal metatopic dysplasia. Chondrocyte differentiation was performed in a single-step chemically-defined micromass culture which was different from the two previous studies. The chondrocyte differentiation resulted in only a small amount of cartilage-like tissue structure positive for proteoglycan staining (Alcian blue). A significant amount of non-cartilage tissue was also present in the micromass culture. Moreover, collagen type II immunostaining showed sporadic expression with no clear organisation. These findings indicated that the chondrocyte differentiation was not optimal. Despite the suboptimal chondrocyte differentiation, the mutant TRPV4 line showed marked reduction in chondrogenic marker expression: *SOX9*, *ACAN*, and *COL2A1* compared to the non-isogenic wild-type control. However, since the TRPV4 expression data were not available, it was difficult to be certain that heterozygous TRPV4 mutation contributed to the phenotypes.

These three studies and many others have demonstrated the feasibility using hiPSCs to study inherited skeletal disease. However, most of the studies used non-isogenic controls (independent and unrelated hiPSCs) to compare the effect of genetic mutation in hiPSC-derived cartilage tissues. Comparing patient-derived hiPSCs with independent healthy-control hiPSCs generated from different individuals raises a concern that the cellular and molecular phenotypic differences might be simply due to clonal differences between the hiPSCs and not the disease-causing mutation. Therefore, isogenic controls are crucial in disease modeling studies to minimise the confounding effects of genetic background differences between independent hiPSC clones particularly for a disease that is partly heritable or phenotypically heterogeneous (271).

1.4.5 The importance of isogenic control hiPSCs for hiPSC disease model

Correcting the mutation in the patient-derived hiPSCs is one strategy to generate isogenic control hiPSCs. However, when patient-derived hiPSCs are not available, introducing known pathogenic mutations into wild-type hiPSC to generate engineered-mutant-hiPSCs is an alternative strategy that results in isogenic control and mutant hiPSCs (Figure 1-13). Currently, isogenic control hiPSC lines can be obtained using improved gene editing techniques such as CRISPR/Cas9.

Clustered regularly interspaced short palindromic repeat (CRISPR) was first discovered in the early 1990s by Mojica, Juez (272). CRISPR refers to the element of sequence which consists of series of 29-nucleotide repeats separated by 32-nucleotide spacer sequences in the *E.coli*. It is a part of adaptive bacterial immunity and it works similar to the action of RNA interference in eukaryotes (reviewed by Lander (273)). The CRISPR-Cas9 system has proven to be a powerful tool for genome editing in eukaryotic cells (274) superseding its predecessors of genomic editing tools such as transcription activator-like effector nucleases (TALEN) and Zinc finger (ZF) protein.

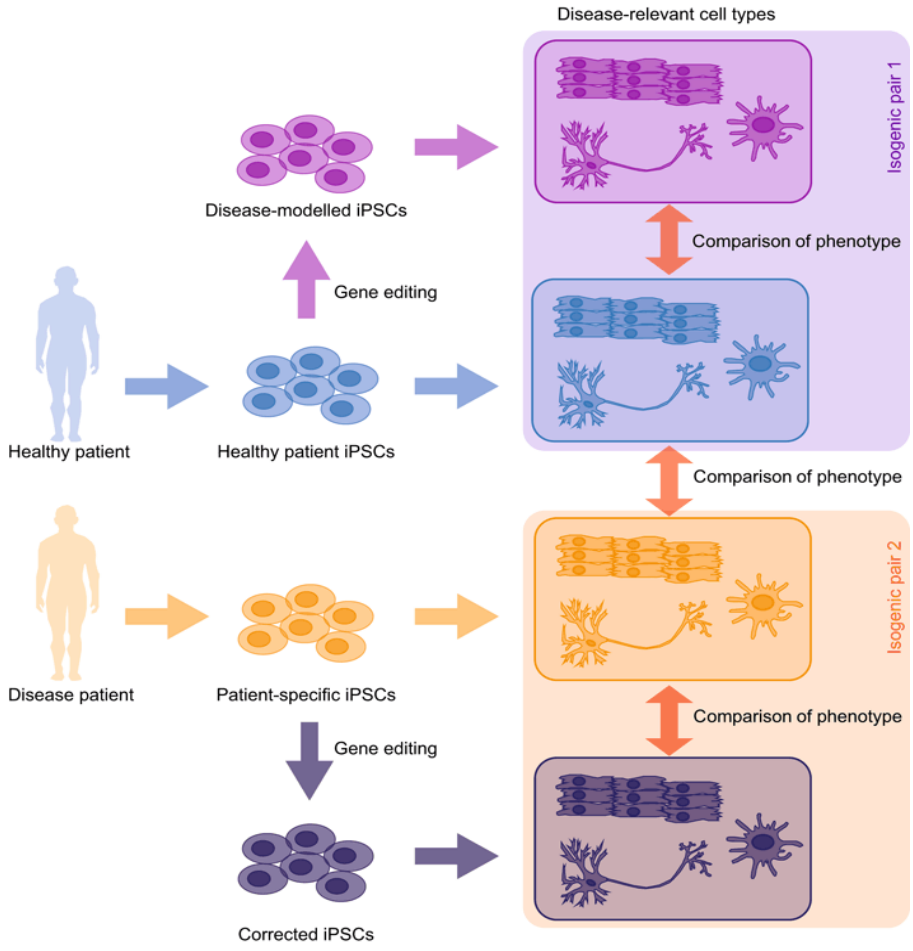

Figure 1-13. Approaches to generating isogenic control for monogenic disease modelling study. Adapted from (275).

The CRISPR system consists of CRISPR-associated (Cas9) nuclease and the single guide RNA (gRNA). Cas9 has six domains: recognition lobe I (REC I), REC II, Bridge Helix, protospacer adjacent motif (PAM) interacting (Topo-homology and C-terminal domain), HNH and RuvC nuclease (276) (Figure 1-14). Cas9 protein plays an important role in cleaving target DNA.

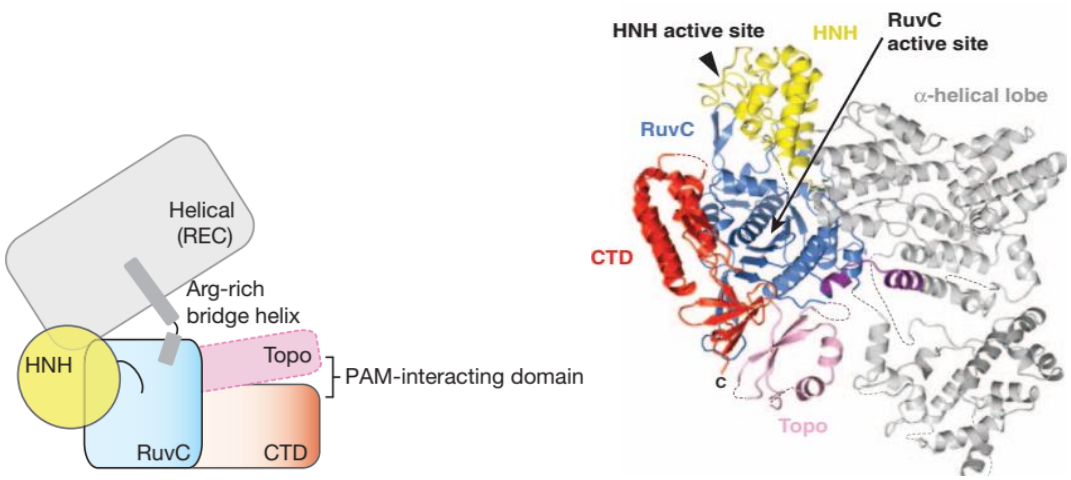

Figure 1-14. The schematic and crystal protein structure of *Streptococcus pyogens*' Cas9 protein. Adapted from(277) and (278). REC: recognition lobe, Topo: Topo homology domain, CTD: C-terminal domain, HNH: HNH nuclease, RuvC: RuvC nuclease.

Guide RNA (gRNA) encodes target specific CRISPR-RNA (crRNA) array and trans-activating crRNA (tracrRNA) which is important for crRNA processing (274). The target-specific crRNA recognises and binds to the DNA target through Watson and Crick base pairing and directs the Cas9 nuclease to induce double-strand break via RuvC and HNH nuclease domain. The CRISPR/Cas9 system derived from *S. pyogenes* requires that the DNA target precedes a 5'-NGG protospacer adjacent motif (PAM). Cas9 nuclease mediates the double-strand DNA break 3 bases upstream of the PAM site (274). By changing the target-specific crRNA sequence (usually called as gRNA for simplicity), it can precisely target a DNA sequence for genomic alterations.

The repair of DNA double-strand breaks can be through non-homologous end joining (NHEJ), microhomology-mediated end joining (MMEJ) or homologous recombination (279) (Figure 1-15). NHEJ causes unintended insertions or deletions in the DNA sequence as the broken DNA is randomly rejoined. This repair mechanism is very useful in generating knock out cell lines since the unintended insertions and/or deletions often generate early stop codons in the codon reading frame resulting in unstable mRNA that is prone to degradation by non-sense mediated mRNA decay (280), or less commonly, a non-functional truncated protein (281, 282). MMEJ is an alternative of NHEJ where 5–25 base pair microhomologous sequences are used to align the broken ends before joining, thus resulting in deletions flanking the original break (279).

On the other hand, homologous recombination uses an homologous DNA sequence to repair the break resulting in a high-fidelity repair of the DNA sequence (274, 283). In CRISPR/Cas9 genome editing, homologous recombination is enhanced by

providing a donor homology-directed repair (HDR) DNA template. The DNA donor can be single-stranded DNA oligonucleotides (ssODNs) or double-stranded DNA (274). By introducing modified sequences into the donor DNA, the target DNA sequence can be manipulated precisely. A ssODN is preferable for generating or correcting single point mutations whereas double-stranded DNA (usually in the form of a plasmid) is preferable for inserting long DNA sequences such as fluorescent reporter DNA sequence (274).

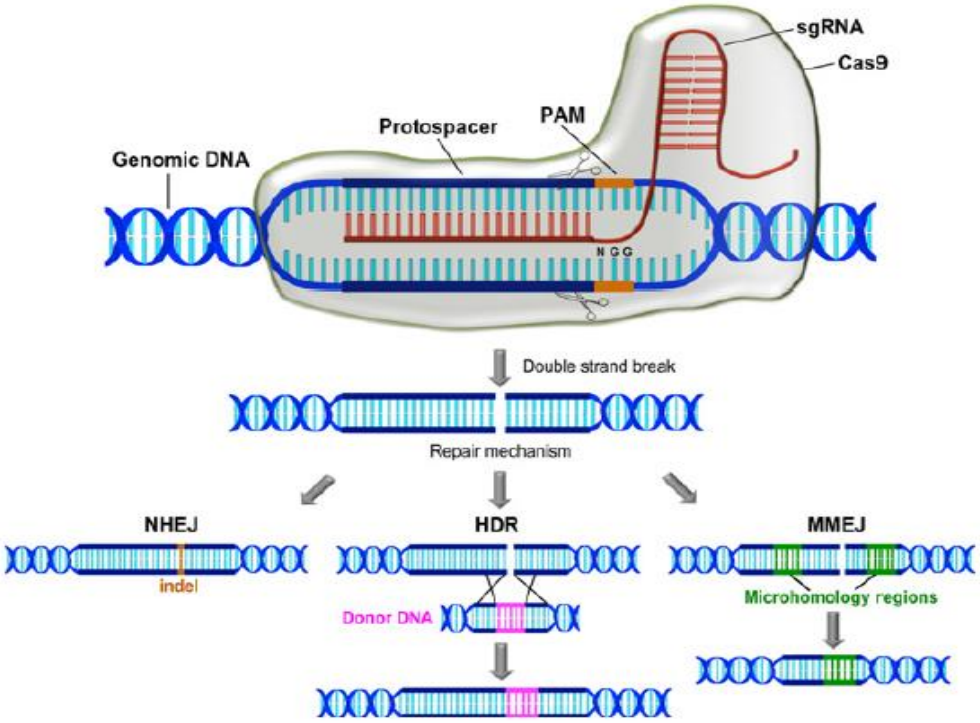

Figure 1-15. The double-strand break repair mechanisms. Adapted from (279). NHEJ: non-homologous end joining, HDR: Homology-directed repair, MMEJ: microhomology-mediated end joining.

1.5 Problem statement and study aim

Transient Receptor Potential Vanilloid 4 (TRPV4) is a non-selective calcium channel that plays an important role in the mechanotransduction system in chondrocytes. Given the importance of TRPV4 in maintaining cartilage structure integrity, it is not surprising that mutations in TRPV4 could cause significant skeletal diseases in human. More than 40 TRPV4 allelic variants have been reported to cause skeletal diseases with varying severity. However, the pathogenic mechanism of the TRPV4 mutations in causing skeletal defects is largely undescribed.

Heterologous cells such as fibroblasts and HEK-293 cells are commonly used to model TRPV4-inherited skeletal diseases *in vitro*. However, this system cannot completely recapitulate the biological processes occurring in human chondrocytes. Studies using human chondrocytes are limited because cartilage is rarely available from patients and controls. Transgenic animal study is complex, costly, and time consuming. Recognising the limitations of previous studies, human-induced pluripotent stem cells (hiPSCs) offer a new approach for inherited disease modeling. Their ability to differentiate into disease-relevant cells such as chondrocytes creates new opportunities for TRPV4-inherited skeletal disease modelling. Therefore, this PhD project aims to model TRPV4-inherited skeletal diseases using hiPSCs and to identify pathogenic mechanisms underlying the diseases. To achieve this aim, the following measures are undertaken:

1. Generating SOX9 gene reporter hiPSC line (Chapter 3),
2. Optimising the chondrocyte differentiation protocol using SOX9 gene reporter hiPSC line (Chapter 4),
3. Generating mutant TRPV4 hiPSC lines using CRISPR/Cas9 system by introducing two TRPV4 mutations causing distinct TRPV4-inherited skeletal diseases, a p.F273L TRPV4 mutation causing familial digital arthropathy with brachydactyly (FDAB) and a p.P799L mutation causing metatropic dysplasia, into SOX9 gene reporter hiPSC line (Chapter 5),
4. Comparing the gene expression profile between the mutant TRPV4 and wild-type cartilage using global gene expression analysis (RNA sequencing) (Chapter 6).

Chapter 2

Materials and Methods

2.1 Cell culture

2.1.1 Irradiated-mouse embryonic fibroblasts (MEFs) culture

The irradiated mouse embryonic fibroblasts (MEFs) were purchased from the IPSC core, MCRI. We cultured the MEFs in T25 or T75 flask (Falcon) containing 4mL feeder media (440mL DMEM 1X with high glucose (4.5g/L), without glutamine and sodium pyruvate (Life Technologies/Gibco); 50mL of Fetal Bovine Serum (FBS) (GE Health Care); 5mL of 200mM GlutaMAX^{TM}I, 5mL of Penicillin-Streptomycin solution (Gibco) containing 5,000U/mL Penicillin and 5,000µg streptomycin in 100mL 0.85% saline). Culture flasks were coated with feeder media at least 2 hours before MEF plating and the MEFs were plated at $2x10^4$ cells/cm^2.

2.1.2 Human-induced Pluripotent Stem Cells (hiPSCs) culture

IPSC core, Stem Cell Technology Laboratory, Murdoch Children's Research Institute (MCRI) generously provided the hiPSC line, MCRIi001-A (PB001.1) (1). Ethical approval for this cell to be used in this study has been granted by the Royal Children Hospital Human Research Ethics Committee (RCH HREC) with HREC reference number 35121A. The cells were maintained in feeder-dependent culture medium (284). In feeder dependent culture, at least 2 hours after MEF plating, the feeder media was replaced with hiPSC media which consisted of 400mL of DMEM/F12 (1X) + L-glutamine + sodium bicarbonate, 100mL of Knock Out Serum Replacer (KOSR) (Gibco/Invitrogen), 5mL of 100X non-essential amino acid (NEAA) (Gibco/Invitrogen), 5mL of 200mM (100X) GlutaMAX^{TM}I (Gibco/Invitrogen), 1mL of 55mM 2-Mercaptoethanol (Gibco/Invitrogen) and 100ng/µl of basic-fibroblast growth factor (bFGF/FGF2) (PeproTech).

When the cells reached 70-80% confluence, which was usually after 3-4 days of culture, we passaged the hiPSCs using 0.5mM EDTA (Thermo Scientific) in DPBS (Life Technologies) with 1:4 split ratio. In brief, we removed the culture medium and washed the cells with 2.5mL DPBS. After the DPBS was discarded, 1.5mL of 0.5mM EDTA in DPBS was added followed by a 4-minute incubation at 37^{o}C, 5%CO_2 incubator. The 0.5mM EDTA in DPBS was carefully aspirated and the cells were dislodged by putting 2mL of hiPSC or E8 medium directly to the cells followed by gentle tapping of the flask. Cell suspension (500µL) was transferred to the new flask/disk containing culture medium.

2.2 Characterisation and validation of hiPSC lines

Characterisation of the hiPSC line was performed using several methods involving colony morphology assessment, mycoplasma testing, pluripotency marker assessment, SNP array, and teratoma formation (1, 285, 286) . The colony morphology was captured using an Olympus IX70 fluorescence inverted microscope and was processed using QCapture Pro software version 5.0.0.26. For mycoplasma testing, culture medium (1mL) of 70% confluent hiPSC culture was collected. The mycoplasma testing was performed to all the hiPSC lines by Cerberus Sciences, Adelaide, South Australia using PCR based method. The mycoplasma test results are available in Appendix 2. SNP array, pluripotency marker assessment and teratoma assay will be described in sections 2.12, 2.17, and 2.27 respectively.

2.3 Sclerotome differentiation of hiPSCs

Multistep-chemically defined sclerotome differentiation approach was performed to direct the differentiation of hiPSCs towards sclerotome via mesodermal lineages (17). A day before administering the differentiation medium, 1.5-2.0 x10^5 cells of hiPSCs were cultured in each well of feeder-coated 6 well-plate with hiPSC medium. The following day, APEL2 medium (Stemcell Technologies) supplemented with, 30ng/mL Activin A (R&D systems), 4µM CHIR (Tocris), 20ng/mL FGF2 (Peprotech), 100nM PIK90 (Merck Millipore) and 5% protein-free hybridoma media II (PFHM II) (Gibco) that induces the differentiation of PSC into anterior primitive streak was added and after 24 hours, the cells were called as day 1 cells. Medium which was supplemented with 1µM A8301 (Tocris), 3µM CHIR, 20ng/mL FGF2, 0.25µM LDN193189 (Sapphire) and 5% PFHM II was added for paraxial mesoderm induction. Twenty-four hours later, medium which was supplemented with 1µM A8301, 3µM C59 (Tocris), 0.25µM LDN193189, 0.50µM PD0325901 (Sapphire) and 5% PFHM II was added to induce early somites/somitomere precursor formation. The sclerotome was induced by adding medium which contained 2µM purmorphamine (Sigma Aldrich), 1µM C59 and with or without 5% PFHM II for 3x24 hours. In total, 6 days were needed for sclerotome induction (Figure 2-1) and RNA was extracted (see section 2.13) at each day of sclerotome induction.

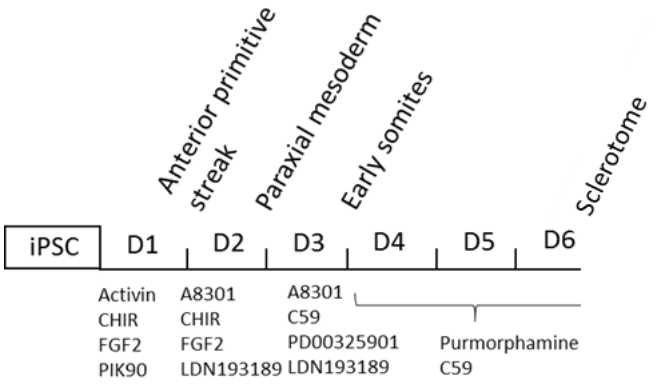

Figure 2-1. Sclerotome induction protocol.

2.4 Freezing and thawing of cells

To freeze hiPSCs, the culture medium was removed from a 70-80% confluent T75 flask (Falcon) and the cells were washed with DPBS. We added 2.5mL of TryPLE (Life Technologies) into the flask and incubated it for 3 minutes at 37ºC, 5% CO_2. The TryPLE was carefully aspirated and the cells were dislodged by putting 5mL of DPBS directly to the cells followed by gentle tapping of the flask. The cells were pelleted by centrifugation at 450g for 3 minutes. Ice cold 1X freezing mix (5ml; table 2-1) + 10% DMSO was added to resuspend the pellet and 1mL aliquots transferred to 1mL Nunc Cryo Tubes (Sigma Aldrich). Cells were frozen in a Mr. Frosty (Nalgene) pre-filled with isopropanol overnight at -80ºC or by using controlled rate freezer EF600 (Grant-Asymptote), then transferred to liquid nitrogen tank for long term storage.

Table 2-1. The reagents required to make a 100X freezing mix.

Reagent	Source	Molecular weight	100X freezing mix (mg/100mL)	Final concentration (mM)
$C_5H_{14}NOCl$ (choline chloride)	Sigma	139.62	19,150.00	136.82
CJ2				
$CaCl_2.2H_2O$	Sigma	147.02	1.47	0.01
KCl	Sigma	74.55	200.00	2.68
KH_2PO_4	Sigma	136.09	200.00	1.47
$K_2HPO_4.3H_2O$	Sigma	228.23	1490.00	6.54
$MgCl_2.6H_2O$	Sigma	203.30	100.00	0.50
D-glucose	Sigma	180.16	1000.00	5.50
dH_2O	Invitrogen		add to 100mL	

Cryovials were thawed in a 37ºC water bath. When almost thawed, the cryovial was removed from the water bath and the hiPSC suspension was transferred into a hiPSC medium-filled 15mL Falcon tube (E8 medium if the hiPSCs were cultured in feeder-free

culture). We pelleted the cells by centrifugation at 450g for 3 minutes at room temperature and the supernatant was removed. We resuspended the pellet with 1mL of appropriate culture medium and transferred the cells into feeder-coated T25 flasks for feeder-dependent culture.

2.5 Cloning and bacterial culture

2.5.1 Plasmid restriction enzyme digestion

Restriction enzyme digestions were performed to linearise plasmid vectors and to screen plasmids for correct inserts following cloning. Restriction enzymes used in this study are available in each relevant chapter. In general, 100ng to 5µg plasmid was incubated with a mixture of restriction enzyme and its appropriate buffer and was incubated for 1 hour to overnight at appropriate incubation temperature depending on the restriction enzyme being used.

To check for complete plasmid linearisation/digestion, gel electrophoresis of the digested plasmids was performed. Two µL of the digested plasmid mixed with 1µL of 6X Orange G loading dye were run in 1% agarose gels in 0.5X TBE buffer (5.4gr Tris base, 2.75gr boric acid, 2mL of 0.5M EDTA and H_2O up to 1L) together with the undigested plasmid and 6µL of 1:6 dilutions of 10.0kb 2-Log DNA ladder (New England BioLabs) at 120 Volts for 60 minutes. The bands were visualised using GBox (Syngene). For cloning purposes, in-gel DNA purification (see section 7) was performed to purify the digested plasmids.

2.5.2 Ligation of insert into plasmid vector

Inserts were ligated into plasmid vectors using Quick ligase (New England Biolabs) according to the manufacturer's instructions. In brief, a ligation mixture which consisted of 50ng of plasmid vector, 1µL of ligase, 10µL of 2X ligase buffer, DNA insert with a concentration of 3 times molarity of the plasmid vector and H_2O added up to 20µL was incubated for 5 minutes at room temperature.

2.5.3 Transformation

Ligation mixture (3µl) was added to 50-100µL of DH5α competent cells (Invitrogen), then incubated on ice for 30 minutes followed by a 45-second incubation in 42^{o}C water bath with gentle shaking. The mixture was immediately incubated on ice for 2 minutes. Luria-Bertani (LB) broth (250µL) (4g tryptone, 4g NaCl, 2g yeast extract and water added up to 400mL) was added and the mixture was incubated for one hour at 37^{o}C with shaking (250rpm). We plated 100-150µL of the transformation mixture onto

appropriate antibiotic-containing LB agarose plates (400mL LB broth + 6g agarose) and incubated overnight at 37^{o}C (16-21 hours).

2.5.4 Liquid-based bacterial culture

Bacterial colonies (usually 8-10 colonies) were picked and each of them was transferred into a 14mL round-bottom falcon tube (Corning) containing 3mL of LB broth for miniprep or into 250mL Erlenmeyer containing 150mL LB broth with appropriate antibiotic for colony selection. The bacteria were incubated at 37^{o}C on shaker (250rpm) overnight.

2.5.5 Plasmid isolation

2.5.5.1 Miniprep plasmid isolation

The plasmids were isolated using the PureYield Miniprep Plasmid DNA Extraction kit (Promega) according to the manufacturer's instructions. In brief, the bacterial cultures were harvested and pelleted by centrifugation at 10,000g for 30 seconds. We resuspended the pellets with 600µL of 1X TE buffer (10mM Tris-Cl (pH 8.0), 1mM EDTA) and lysed the bacteria by adding 100µL cell lysis buffer and inverting the tubes 6 times. The lysis reaction was stopped by adding 350µL of iced cold neutralisation solution. The lysates were pelleted by centrifugation at 10,000g for 3 minutes and the supernatant was transferred into the membrane column and centrifuged at 10,000g for 30 seconds to capture the plasmids. The captured plasmids were washed with a 200µL endotoxin removal wash buffer followed by a 400µL Column wash solution. The plasmids were eluted with 30µL of nuclease-free water and centrifugation at 10,000g for 1-2 minutes. The plasmid yield was determined using a Nanodrop (Thermo Scientific).

2.5.5.2 Midiprep plasmid isolation

The plasmids were isolated using PureYield Midiprep plasmid DNA extraction (Promega) according to manufacturer instruction. In brief, the bacterial cultures were pelleted by centrifugation at 3000g for 15 minutes, resuspended with 3mL of cell resuspension solution and lysed by adding 3mL of cell lysis solution followed by inverting the tubes 3-5 times and incubating at room temperature for 3 minutes. The lysis reaction was stopped by adding 5mL of neutralisation solution and inverting the tubes 5-10 times. The lysates were transferred into Blue clearing membrane column tubes, centrifuged at 3000g for 15 minutes and the supernatant transferred into a White binding membrane column. Plasmids were captured on the membrane by centrifuging at 1500g for 5 minutes, then washed with 5mL Endotoxin removal wash buffer followed by a 20mL Column wash solution. The plasmids were eluted with 400µL nuclease-free water and

centrifugation at 10,000g for 5 minutes. A second elution was performed by adding 400µL followed by centrifugation at 10,000g for 5 minutes.

2.6 CRISPR/Cas9 construct design

2.6.1 Single-guide RNA (gRNA) designing

The gRNAs targeting specific region of the DNA was designed through the http://crispr.mit.edu/ or www.benchling.com website. The gRNA which has the highest score and induces double-strand break (DSB) as close as possible to the target region was selected. The CACC base sequence was added at the 5' end of the gRNA sequence (gRNA TOP) and AAAC base sequence was added at the 5' end of the gRNA complementary sequence (gRNA BOTTOM). The annealing of gRNA to its complementary sequence was performed by phosphorylating each gRNA (1µL) using a mixture of 1µL of T4 Polynucleotide Kinase (PNK) (NEB), 2µL of 10X T4 PNK buffer, 2µL of 10mM ATP and distilled water added up to 20µL in room temperature followed by incubation at 95^{o}C for 10 minutes and then room temperature for 10 minutes for annealing (274). The annealed gRNA was diluted to 500nM/µL.

2.6.2 Generating pSpCas9-2A-GFP-gRNA construct

We used *Streptococcus pyogenes* Cas9 variant expressing plasmid, pSpCas9-2A-GFP (Addgene, PX458) (274). The pSpCas9-2A-GFP vector was linearised with the BbSI restriction enzyme and was dephosphorylated using Antarctic Phosphatase (NEB).

2.6.2.1 BbsI restriction enzyme digestion

BbsI restriction enzyme digestion was done by treating 5µg of pSpCas9-2A-GFP with a mixture of 2µL of 10,000U/µL BbsI restriction enzyme, 10µL of 10X 2.1 NEB buffer and distilled water added up to 100µL followed by incubation at 37^{o}C for at least 4 hours. To check the complete digestion of the plasmid, 1µL of the digest was run in gel electrophoresis together with 6µL of 1:6 dilutions of 10.0kb 2-Log DNA ladder and un-digested plasmid as a control.

2.6.2.2 pSpCas9-2A-GFP vector dephosphorylation

Dephosphorylation of the pSpCas9-2A-GFP vector was done by treating 45µL of the linearised pSpCas9-2A-GFP vector with a mixture of 1µL Antarctic Phosphatase, 10µL of 10X Antarctic Phosphatase buffer and distilled water added up to 100µL (274). Incubation at 37^{o}C for 30 minutes was performed, followed by another incubation at 65^{o}C for 10 minutes to inactivate the enzyme. In-gel purification was performed to purify the linearised- dephosphorylated plasmid.

2.6.2.3 gRNA cloning into pSpCas9-2A-GFP

The gRNA was cloned into the linearised-dephosphorylated pSpCas9-2A-GFP plasmid vector using T4 ligase (NEB). The linearised-dephosphorylated pSpCas9-2A-GFP plasmid vector (50ng) was mixed with ligation reaction which consisted of 1µL of T4 ligase, 1µL of 10X T4 ligase buffer, 1µL of 500nM/µL gRNA and distilled water added up to 10µL. The ligation mixture was incubated at room temperature for 24 hours.

The pSpCas9-2A-GFP-gRNA was transformed into Alfa Select competent cells (Bioline). Eight colonies were picked for miniprep plasmid DNA extraction (Promega) and were screened through double digestion with NotI (NEB) and BbSI restriction enzyme. The plasmid DNA which had the gRNA insert was cut once by the NotI producing clear single band as the BbsI cutting sites have been removed. Afterward, sequencing using U6 primer (5'-GGGCAGGAAGAGGGCCTAT-3') was done to confirm the correct ligation of the insert. The correct plasmid was expanded by transforming it into competent cells (see 2.5.3) followed by plasmid extraction using PureYield Plasmid Midiprep.

2.7 In-gel DNA purification

Plasmid DNA or PCR products were mixed with 6X Orange G loading dye (10mM Tris-HCL (pH 8.0, 0.15% Orange G, 60% glycerol and 60mM EDTA) and run in 1% agarose gels at 120 Volts for 60 minutes. The appropriate DNA band in the gel was excised and purified using a QIAprep Spin Miniprep kit (Qiagen) according to the manufacturer's instructions. Buffer QG was used to dissolve the gel slice (1w/3v). Once the gel dissolved completely, 1 gel volume of isopropanol was added. The suspension was transferred into a QIAquick spin column and centrifugation was performed at 10,000g for 1 minute. Another 500µL of Buffer QG was added and the centrifugation was repeated. The columns were washed with 750µL of Buffer PE and the DNA was eluted by adding 50µL EB buffer followed by 1-minute centrifugation at 10,000g.

2.8 Electroporation of hiPSCs

Cells were electroporated using an Invitrogen Neon™ System VXMPK5000S according to manufacturer's instructions. The 100µL Neon Electroporation Kit (Invitrogen) was used for electroporation reaction. In brief, 70-80% confluent hiPSCs were harvested and were resuspended with buffer R at $1x10^7$ cells/1mL. hiPSC suspension (100µL) was added into 10µL electroporation mixture which contained 2µg of pSpCas9-2A-GFP-gRNA plasmid construct and 10µM of HDR template of each mutant TRPV4. The electroporation was performed in Invitrogen Neon™ System VXMPK5000S with 2

times of 30ms pulses of 1050 Volt. The electroporated hiPSCs were plated on a 6cm dish and maintained in feeder dependent culture and three days after, Flowcytometry Assisted Cell Sorting (FACS) was performed (see section 2.17).

2.9 DNA extraction from adherent cell culture

2.9.1 DNA extraction by centrifugation

The culture media was removed and the cells were rinsed with DPBS. Cells were lysed with 250µL of lysis buffer (100mM Tris pH 8.0, 200mM NaCl, 5mM EDTA pH 8.0, 0.2% SDS, water, 200µg/mL proteinase K) per well of 24-well plate or cell pellet derived from a confluent 6-well plate, then incubated at 37ºC overnight or 55ºC for 3 hours. The samples were transferred into Eppendorf tubes and 100µL of 5M NaCl was added. We centrifuged the samples at 10,000g for 10 minutes at room temperature. Supernatants were transferred into new Eppendorf tubes and 1 volume of ice-cold 100% isopropanol was added followed by centrifugation at 10,000g for 10 minutes at room temperature. The supernatant was discarded and 750µL of 70% ethanol was added to the pellet. Five-minute centrifugation was done at 10,000g at room temperature and the supernatant was discarded. The pellet was spun down again by 10,000g centrifugation for 30 seconds and the remaining ethanol was removed using a 10µL pipette. We left the Eppendorf cap open for 30-60 minutes at room temperature to remove remaining ethanol and 30-50µL sterile water was added to resuspend the DNA pellet. Incubation at 37ºC for at least 2 hours was done to dissolve the DNA completely. The DNA concentration was calculated using a Nanodrop (Thermo Scientific).

2.9.2 Manifold DNA extraction

Cells growing on 48-well plates were rinsed with DPBS and the cells lysed with 100µL of lysis buffer and incubation at 37ºC overnight or 55ºC for 3 hours. Buffer PB (500µl; Qiagen, #19066) was added to the cell lysate and the suspension transferred into 96-well Unifilter plates (Whatman). The liquid was filtered using a vacuum manifold and the filter washed with 400µL of Buffer PE (Qiagen). To elute the DNA, 70µL of pre-warmed (70ºC) 1X TE buffer was added directly to the filter and vacuum was applied to elute the DNA into a collection plate (PS-Microplate 96-well v-shape).

2.10 Polymerase chain reaction (PCR)

In general, PCR was performed using the GoTaq enzyme (Promega) unless otherwise specified. In brief, 20ng of human genomic DNA was mixed with a PCR mixture which consisted of 0.05µL of GoTaq DNA polymerase, 2µL of 5X GoTaq buffer, 0.6µL of 25mM $MgCl_2$, 1µL of 2.5mM dNTPs, 25ng each of forward and reverse primer

and nuclease-free water added up to 10µL. The PCR was conducted using touchdown PCR with denaturation at 95ºC for 40 seconds, annealing at 65ºC for 30 seconds, decreasing in steps of 1-2ºC/cycle until 55ºC, and elongation at 72ºC for 45 seconds. Two µL of the PCR products mixed with 1µL of 6X Orange G loading dye were run in 1% agarose gels in 0.5X TBE buffer (5.4gr Tris base, 2.75gr boric acid, 2mL of 0.5M EDTA and H2O up to 1L) together with 6µL of 1:6 dilutions of 10.0kb 2-Log DNA ladder at 120 Volts for 60 minutes and were visualised using GBox (Syngene).

PCR using CloneAmp HiFi^{TM} PCR Premix (Clonetech) was performed by mixing 20ng of the genomic DNA with 12.5 µL of CloneAmp HiFi^{TM} PCR Premix, 50ng each of forward and reverse primer and adding nuclease-free water up to 25µL final volume. PCR was performed in a standard PCR reaction with thermocycling protocol involving 35 cycles of denaturation at 95°C for 20 seconds, annealing at 55°C for 15 seconds, and amplification at 72°C for 60 seconds.

PCR using AccuPrime Taq DNA polymerase (ThermoFisher Scientific) was performed by adding 20ng of human genomic DNA into PCR mixture which consisted of 0.2µL of AccuPrime Taq DNA polymerase, 2µL of 10X AccuPrime buffer II, 50ng each of forward and reverse infusion cloning primer and nuclease-free water added up to 20µL. PCR was performed in Touchdown PCR reaction.

2.11 Sequencing

Plasmids were sequenced using a BigDye^{TM} Terminator v3.1 cycle sequencing kit (ThermoFisher Scientific). In brief, the 100ng DNA sample was mixed with 3µL sequencing buffer, 2µL BigDye mix, 0.5ng of sequencing primer and water was added up to 20µL. The sequencing reaction was 40 cycles of denaturation at 95ºC for 2 minutes, annealing at 60ºC for 15 seconds and amplification at 72ºC for 50 seconds. Unincorporated nucleotides were removed using a DyeEx 96 Kit (Qiagen) according to the manufacturer's instructions. The sequencing products were dried in an 80ºC heat block for 20-30 minutes. The dried samples were submitted to the sequencing centre, Translational Genomics Unit, MCRI, for sequencing.

2.12 SNP array and SNPduo analysis

Victorian Clinical Genetics Services (VCGS), MCRI performed the SNP array. Illumina Infinium GSA-24 v1.0 array with 0.50Mb resolution was used to generate the microarray data. SNPduo comparative analysis of the microarray genotyping data was performed to assess the similarity of the SNP patterns between different samples in order to validate the cell identity.

2.13 RNA extraction

Cell culture medium was removed and the cells were washed using DPBS. TRIzol reagent (500µl; Life Technologies) was added and the cells lysed and homogenised by repetitive pipetting. Further homogenisation using a disposable syringe was sometimes necessary, especially for micromass and pellet culture samples. Chloroform (200µl; Merck) was added into the mixture followed by vigorous shaking for 15 seconds and room temperature incubation for 5 minutes. We centrifuged the samples at 12,000g for 10 minutes at 4^{o}C, transferred the aqueous phase into clean Eppendorf tubes containing 10ng of glycogen and added 450µL of isopropanol followed by vigorous shaking for 15 seconds and room temperature incubation for 10 minutes to precipitate the RNA. RNA was pelleted by centrifugation at 12,000g for 10 minutes. The pellets were washed with 750uL of 75% ethanol twice and to remove the remaining ethanol; the pellets were heated at 70^{o}C for 2 minutes. To elute the RNA, 20µL of nuclease-free water was added into the pellets. For RNA sequencing, RNA was extracted using DirectZol^{TM} RNA MiniPrep kits (Zymo Research) according to the manufacturer's instructions. RNA integrity was assessed using Agilent 2200 TapeStation (Integrated Sciences).

2.14 cDNA synthesis

RNA (200ng-1000ng) was used for cDNA synthesis using Transcriptor High Fidelity cDNA kits (Roche) according to the manufacturer's instructions. In brief, water was added to RNA and 2µL of random hexamer primer to a final volume of 11.4µL and incubated for 10 minutes at 65^{o}C. A mixture of 4µL buffer, 0.5µL RNase inhibitor, 2.0µL dNTPs, 1µL 100nM DTT, and 1.1µL reverse transcriptase was added to the denatured RNA and incubated for 30 minutes at 55^{o}C followed by a 5-minute incubation at 85^{o}C to inactivate the reverse transcriptase. The cDNA was stored at -20^{o}C.

2.15 Quantitative Polymerase Chain Reaction (qPCR)

For each sample, the qPCR was performed in triplicate using Brilliant III UltraFast Sybr Green qPCR Master Mix (Agilent Technologies) according to the manufacturer's instructions. In brief, 1µL of cDNA, 5µL of qPCR Master Mix and 400nM (4µL) of primers (Table 2-2) were mixed and placed into 384 well-qPCR plates (Integrated Sciences). A Light Cycler 480 II qPCR machine (Roche Life Sciences) was used for qPCR with the thermocycling protocol involving 40 cycles of denaturation at 95°C for 20 seconds, annealing at 55°C for 20 seconds, and amplification at 72°C for 20 seconds. The qPCR data were analysed using LightCycler 480 Software (release 1.5.1.62) and β-actin (ACTB) was used as the reference gene.

The qPCR data were presented in mean normalised expression (MNE) which is calculated by a formula: MNE = 2CT reference gene/ 2CT gene of interest; with 2 = ideal primer efficiency. The data were analysed using GraphPad Prism 7.

Table 2-2. Primers used for qPCR

Gene name	Primer name	Primer sequence
OCT4	Sybr.hOCT4.F	GAAGTGGGTGGAGGAAGCTG
	Sybr.hOCT4.R	TAGTCGCTGCTTGATCGCTT
MIXL1	Sybr.hMIXL1.F	GGTACCCCGACATCCACTTG
	Sybr.hMIXL1.R	GGGCAGGCAGTTCACATCTA
TBX6	Sybr.hTBX6F	AGATTGCAGCCAATCCCTTTG
	Sybr.hTBX6R	CTCCTGGTGGGAAGGTGACTG
MSGN1	Sybr.hMSGN1F	GGCCTGGTAGAGGTGGACTA
	Sybr.hMSGN1R	ACAGGTGGCAGGTAATTCCG
MEOX1	Sybr.hMEOX2F	CCAGACTGAGGCGATACGAG
	Sybr.hMEOX2R	CCAATTCCCGACAGCTCTGA
PAX1	Sybr.hPAX1F	CAACCAGCACGGCGTGTA
	Sybr.hPAX1R	CTTCCTGTCAGCCACTTCTCG
PAX3	Sybr.hPAX3F	CGCTTCCTCCAAGCACTGTA
	Sybr.hPAX3R	AGAGCGCGTAATCAGTCTGG
FOXC2	Sybr.hFOXC2F	TGGTATCTCAACCACAGCGG
	Sybr.hFOXC2R	CCCGGGACACGTCAGTATTT
HAND1	Sybr.hHAND1F	AGGCTGAACTCAAGAAGGCG
	Sybr.hHAND1R	TCGGCTCACTGGTTTAACTCC
PDGFRα	PDGFRa-F	AGTGAGCCGGAGAAGAGACC
	PDGFRa-R	GGCAGAGGAATGATGTAGCCA
COL2A1	Sybr.hCOL10A1.F2	GATACCAAATGCCCACAGGC
	Sybr.hCOL10A1.R2	TCCCTACAGCTGATGGTCCC
TRPV4	hTRPV4 qRT-PCR F	GACGGGGACCTATAGCATCA
	hTRPV4 qRT-PCR R	AACAGGTCCAGGAGGAAGGT
SOX9	Sybr.hSOX9.F2	AAGTCGGTGAAGAACGGGC
	Sybr.hSOX9.R2	TCTCGCTTCAGGTCAGCCTT
RUNX2	Sybr.hRUNX2.F	CCCAGGCAGTTCCCAAGCATTTC
	Sybr.hRUNX2.R	GGTAGTGAGTGGTGGCGGACATAC
ACTB	UPL.hActb.1545.L	AAGTCCCTTGCCATCCTAAAA
	UPL.hActb.1545.R	ATGCTATCACCTCCCCTGTG
ACAN	Sybr.hAGC1.F	TGGAGAGGACTGTGTGGTGA
	Sybr.hAGC1.R	AAGCTCTTCTCAGTGGGCTG

2.16 RNA sequencing experiment

Triplicate RNA samples were extracted from iPSC-derived cartilage pellets at day 6+14 and 6+70 of differentiation using Trizol and Direct-zol™ RNA MiniPrep (see section 2.13). RNA quality control, sequencing library preparation, and sequencing were done at the Genomics Centre, Murdoch Children's Research Institute. RNA integrity was assessed using a TapeStation 2200 (Agilent Technologies) then sequencing libraries prepared using Illumina's TruSeq stranded total RNA protocol. Samples were sequenced using an Illumina NextSeq 500 sequencer. Transcript level abundances were quantified from the 75 bp paired-end reads using Salmon v0.12.0 and the ENSEMBL GRCh38 version of the human transcriptome. Gene level counts were obtained using the tximport R package (287). Genes that had expression levels of at least 1 count per million in at least three samples in the comparison were kept for further statistical analysis. The data were TMM normalised (288) and Voom transformed (289). Differentially expressed genes were identified using the R Bioconductor limma package (290). Heatmaps were generated using the gplots and RColorBrewer packages.

2.17 Gene ontology annotation and pathway analysis

Gene ontology annotation was performed in CytoScape (291) using Biological Network Gene Ontology (BiNGO) (292) and ClueGO plugin (293).

2.18 Flowcytometry and Flowcytometry-assisted cell sorting (FACS)

Flow cytometry was performed as described previously (294). Single cells were isolated using TryPLE (Gibco). The cells were incubated for 3 minutes in TryPLE and to dislodge the cells and to neutralise the TryPLE, 2 times TryPLE volume of hiPSC media were added directly to the cells. The gentle tapping of the plate might be required to dislodge the cells further. The cell suspension was pelleted by centrifugation at 450g for 3 minutes and the supernatant was discarded. The cell pellet was resuspended with 4mL iced-cold FACS buffer then filtered by passing the cells through the FACS tube strainer cap (Falcon) to remove any clumping cells. Centrifugation at 450g for 3 minutes was done to pellet the cells and staining were performed by incubating the samples with fluorescence-conjugated primary antibodies (Table 2-3) in FACS buffer for 15-30 minutes on ice in the dark. Cells were washed twice with FACS buffer then stained with secondary antibody when a non-fluorescence-conjugated primary antibody was used. Two washes with FACS buffer removed excess antibody. We then resuspended the cell pellet with 300µL of 1ng Propidium Iodide (Sigma-Aldrich) in 10mL FACS buffer. The

flowcytometry was done using an X-20 Fortesa analyser (BD) and the FACS using an Influx cell sorter (BD) at the Flowcytometry core facility, MCRI.

For pluripotency marker expression measurement, hiPSCs were cultured onto well of 6-well plate in feeder dependent condition with hiPSC media and low-density MEFs (40,000-50,000 cells /well for 6-well plate) to reach 80% confluence. The cells were stained with pluripotency marker primary antibodies: anti-CD9, anti-SSEA-4, anti-TRA1-81 and their isotype control (Table 2-3).

For SOX9 expression measurement; day 0 to 6 cells were dissociated with TryPLE as mentioned in section 2.1.3. The cells were stained with PDGFRα-fluorescent conjugated primary antibody (Table 2-3). Flowcytometry analysis of tdTom expression was visualised against PDGFRα expression.

Table 2-3. Antibodies used for flowcytometry and FACS.

Antibody	Dilution	Company and RRID
Brilliant Violet 421 anti-human CD326 (EpCAM)	1:50	BioLegend and AB_2563847
FITC anti-human CD9	1:20	BD Biosciences and AB_395773
Alexa Fluor 647 anti-human SSEA-4	1:40	BioLegend and AB_1089200
APC anti-human TRA1-81	1:100	R and D system and AB_2687608
Brilliant Violet 421 Mouse IgG1 κ Isotype Control	1:100	BioLegend and AB_10897939
FITC Mouse IgG1 κ Isotype Control	1:100	BD Biosciences and AB_396090
Alexa Fluor 647 Mouse IgM κ Isotype Control	1:100	BioLegend and N/A
Alexa Fluor 488 anti-human PDGFRα	1:50	R and D system and N/A

For FACS of electroporated hiPSCs, the cells were stained with Brilliant-violet fluorescent conjugated Ep-CAM (CD326) antibody. FACS was performed to single sort the cells based on the Ep-CAM (hiPSC markers) and GFP positivity (Cas9 expressing plasmid, pSpCas92AGFP-gRNA). The single sorted cells were plated on 96-well plate supplemented with ROCK inhibitor (Stemcell Technologies) and penicillin/streptomycin antibiotic. The following day, the medium was replaced with hiPSC medium without 10μM ROCK inhibitor and 5U/mL penicillin-5μg/mL streptomycin antibiotic supplementation. The medium was changed every three days and 10.000 MEFs/well were added every week. The cell colonies were observed after 1-2 weeks in culture. The confluent wells were passaged and the cells were transferred into two plates of MEF coated 48-well plate for clone maintenance and PCR screening.

2.19 Histology section preparation

2.19.1 Paraffin-embedded tissues

Tissues were cut into 5mm x 5mm x 5mm volume size and were fixed in 10% paraformaldehyde (PFA) (Millipore) or 4% Confix Green (Australian Biostain P/L) overnight followed by hydration in 70% ethanol for overnight. The tissues were transferred to paraffin embedding cassettes (Technoplast) for tissue processing which was performed using Excelsior AS Tissue Processor (ThermoFisher Scientific). The tissue processing involves dehydration (incubating the tissue in 70% ethanol for 60 minutes, 90% ethanol for 45 minutes, 100% ethanol for 2 x 45 minutes, and 100% ethanol for 60 minutes), clearing (xylene incubation for 3 x 60 minutes) and infiltration (incubation in paraffin wax for 30 minutes, 60 minutes and 90 minutes). Once the tissue processing was finished, the tissues were embedded in paraffin using Paraffin Embedding Equipment (Thermo Scientific). Tissue sections with 5µm thickness were obtained by sectioning using Microm HM 325 microtome (ThermoFisher Scientific) and were attached to Superfrost Ultra Plus glass slides (LabServe).

2.19.2 Optimum Cutting Temperature (OCT)-embedded tissues

Tissues were embedded into the Tissue-Tek OCT compound (Sakura Finetek). The tissues were cut into 5mm x 5mm x 5mm volume size and were transferred into OCT compound filled Tissue-Tek Cryomold (Sakura Finetek). The cryomold/OCT was then frozen in liquid nitrogen-cooled isopentane, transferred to dry ice then stored in a -80^{o}C freezer. Cryostat sections (10µm; Leica CM3050S) were mounted onto Superfrost Plus histology slides.

2.20 Histology staining

2.20.1 Haematoxylin Eosin staining

Haematoxylin Eosin staining was performed as described elsewhere (295). The paraffin-embedded sections were deparaffinised using xylene solution twice and hydrated with gradually decreasing concentrations of ethanol (absolute ethanol, 90%, 70% ethanol) and finally were washed with running tap water. The sections were stained with Harris haematoxylin working solution (2.5g Hematoxylin, 25mL 100% ethanol, 50g aluminum ammonium sulphate, 0.5g sodium iodate, 20mL glacial acetic acid and distilled water added up to 500mL) for 8 minutes and were washed with running tap water for 3 minutes. A differentiation step was undertaken by applying 1% acid alcohol (1mL hydrochloride acid pH 1.0 in 100mL of 70% ethanol) for 1 minute and the bluing step was done by applying 0.2% ammonium hydroxide for 1 minute followed by washing in running tap

water for 3 minutes. We put the slides in pre-eosin 95% ethanol followed by Eosin staining (250mL Eosin Y stock (10g Eosin, 800mL 95% ethanol and distilled water added up to 1L), 750mL 80% ethanol, 5mL glacial acetic acid) for 30 seconds each. The slides then were transferred into post-eosin 95% ethanol for 30 seconds then 100% ethanol for 3 x 1 minute followed by xylene solution for 1 x 2 minutes and 1 x 5 minutes.

2.20.2 Toluidine blue staining

The paraffin-embedded histology sections were deparaffinised using xylene solution and hydrated with a gradually decreased concentration of ethanol (absolute ethanol, 90%, 70%). Toluidine blue stain (80mg Toluidine blue, 0.1M NaOAc pH 4.0 and distilled water added up to 200mL) was applied for 10 minutes followed by washing with running tap water for 3 minutes (296). Counterstaining with Fast Green (FCF) (200mg Fast Green in 200mL distilled water) stain was for 5 minutes followed by rinsing with running tap water for 3 minutes. The slides then were put into 100% isopropanol twice for 2 minutes each followed by xylene solution twice for 5 minutes each.

2.21 Immunostaining

Immunostaining was performed as described previously (1). Monolayer cell culture and histology sections were fixed with 4% Confix for 10 minutes then washed with tap water for 3 x 1 minute. For monolayer cell culture, it can be directly processed to antigen retrieval step or primary antibody staining. For histology sections, dewaxing was done by putting the sections into the xylene solution for 5 minutes. The sections were rehydrated using gradually decreasing concentrations of ethanol (100%, 100%, 70%, 50%) for 1 minute each followed by washing with running tap water for 5 minutes and 1X PBS for 5 minutes. The sections were incubated in an antigen retrieval solution depending on the antibody used (Table 2-4) and then washed for 3 x 1 minute with 1X PBS. Blocking of the sections was done by adding 50µL of filtered 3-5% bovine serum albumin (BSA, Sigma-Aldrich) in PBS onto each section for 1 hour at room temperature followed by 3 x 1-minute washing with 1X PBS. The histology sections and monolayer cell culture then were incubated with primary antibody (Table 2-4) for 1 hour at room temperature or overnight at 4^{o}C. The secondary antibody was added and the incubation was done in the dark for an hour at room temperature. The sections were washed for 3 x 1 minute in 1X PBS and DAPI (1:50000 in 1X PBS) was applied onto the section. FluorSafe (Calbiochem) mounting agent was applied to the sections with coverslip was put on top of the mounting agent. The mounting and coverslip were allowed to sit overnight before viewing under the fluorescence microscope.

Table 2-4. Primary antibodies for immunostaining

Antibody	Dilution	Company and RRID	Antigen retrieval and additional steps
Mouse anti-human NANOG primary antibody	1:200	eBiosience and AB_467573	N/A
Rabbit anti-human OCT-4A primary antibody	1:400	Cell Signalling Technology and AB_2167691	N/A
Rabbit anti-human SOX9 primary antibody	1:1000	Millipore and AB_2239761	0.2% Triton X-100 in 1XPBS for 10 minutes at room temperature
Rabbit anti-human TRPV4 primary antibody	1:100	Santacruz and N/A	Chondroitinase digestion (0.1U/mL chondroitinase in 0.1M Tris-acetate (pH 7.0), 0.01M EDTA for 1 hour at 37^{o}C
Mouse anti-human COL2A1 primary antibody	1:150	Millipore and AB_2260779	Pepsin digestion (2mg/mL Pepsin in 50mM Tris-HCl pH 2.0 for 30 minutes at 37^{o}C followed by hyaluronidase digestion (0.2% hyaluronidase in 1X PBS) for 30 minutes at 37^{o}C
TUNEL		Roche and N/A	0.1% Triton X-100, 0.1% sodium citrate in 1XPBS for 8-10 minutes at 4^{o}C
AlexaFluor Donkey anti-Mouse 594 secondary antibody	1:200	Life Technologies and AB_2535789	N/A
AlexaFluor Goat anti-Rabbit 488 secondary antibody	1:200	Life Technologies and AB_143165	N/A

2.22 Microscopy

2.22.1 Bright-field microscopy

The images of histology slides were captured using the Leica DM 2000 LED microscope and were processed using Leica Application Suite (LAS) software version 4.9.0. For cell culture imaging, the Olympus IX70 fluorescence microscope was used and the images were processed using QCapture Pro (version 5.0.1.26) or ImageJ Fiji (version 1.51s).

2.22.2 Fluorescence and confocal microscopy

The Leica fluorescence dissecting microscope (Leica M205 FA) was used to capture images of pellet culture. The images were processed using Leica Application Suite (LAS) software version 4.9.0. The fluorescence images of the fluorochrome-stained histology slides were captured using a Leica fluorescent microscope and processed using ImageJ Fiji (version 1.51s). Fluorescence images of monolayer cell culture were captured using an Olympus IX70 fluorescence microscope and were processed using QCapture Pro (version 5.0.1.26) or ImageJ Fiji (version 1.51s). A Zeiss LSM 780 Confocal

microscope (Zeiss) was used to capture images with high magnification and resolution. Confocal microscopy images were processed using ZEN software.

2.22.3 Fluorescence image quantification

Quantification of the fluorescence images included fluorescence intensity, fluorescence area, and the number of fluorescent expressing cells. For pellet cartilage histology, randomly selected multiple images of a histology section from 4 independent pellets were used for quantification. Quantification was performed using ImageJ Fiji (version 1.51s). Statistical analyses were performed in GraphPad Prism 7.

2.23 Protein extraction from adherent cells

An 80-90% confluent well of a 6-well plate was rinsed with 1mL PBS. The cells were dissociated using TryPLE for hiPSCs and differentiated cells during sclerotome induction. Three volumes of FBS-containing medium were added to the well to neutralise the trypsin or collagenase and to dislodge the cells. Cells were lysed with 75-150uL of cell lysis buffer (50mM Tris-HCl pH 8.0, 150mM NaCl, 10mM EDTA, 1% (v/v) Triton-X 100 (Sigma) containing protease inhibitors (20mM NEM (Sigma) and 1mM AEBSF (Roche) stock). Dissociating any clumps formed using a 21G needle was crucial to achieving complete lysis and centrifugation at 10,000g at 4^{o}C for 10 minutes was performed to spin down undissolved materials. The supernatant which contained soluble proteins was transferred into a clean Eppendorf tube and was stored in a -80^{o}C freezer.

2.24 SDS-Polyacrylamide gel electrophoresis (SDS-PAGE)

The protein samples were prepared under reducing conditions by treating the samples with 10mM DTT and 1X Bolt^{TM} LDS sample buffer (ThermoFisher Scientific) followed by heating at 65^{o}C for 10 minutes. We ran the protein samples in Bolt^{TM} 4-12% Bis-Tris Plus Gels (ThermoFisher Scientific) in 1X Bolt™ MES SDS Running Buffer (ThermoFisher Scientific) using Mini Gel Tank (ThermoFisher Scientific) for 60 minutes at 160V.

2.25 Coomassie blue staining

Gels were stained with 0.1% Coomassie brilliant blue stain (100mg Coomassie brilliant blue stain (BioRad), 45mL methanol, 10mL Acetic acid, and distilled water added to 100mL) for at least 2 hours at room temperature, then destained with destaining solution (10% methanol in 7% acetic acid) at room temperature with gentle shaking. The destaining solution was changed 2-3 times during the destaining process. The protein dynamic range was visualised using ImageQuant LAS 4000 (GE Health Care).

2.26 Western blotting

Western blotting was performed as described previously (39). In brief, Hybond-LFP membranes (GE Healthcare) were incubated in methanol for 20 seconds then H_2O for 20 seconds followed by cold transfer buffer (12g Tris base, 57.7g glycine, 20% methanol, H_2O up to 4.0L) until being used. The separated proteins in polyacrylamide gels (SDS-PAGE gel) were transferred to the Hybond-LFP membrane using Mini Bolt Module (ThermoFisher Scientific) at 20V for 60 minutes. The membrane was blocked with 5% BSA (Sigma-Aldrich) in 1XPBS for 1 hour at room temperature or overnight at 4^{o}C. The membrane was rinsed twice with PBS-T (1X PBS + 0.1% Tween20 (ThermoFisher Scientific). Primary antibody (Table 2-5) diluted in PBS-T 0.2% BSA was added into the membrane and incubated for 1 hour at RT or overnight at 4^{o}C. The membrane was rinsed with PBS-T twice followed by 2 x 5-minute washes. Incubation with secondary antibody diluted in PBS-T 0.2% BSA was for 1 hour at room temperature. The membrane was then rinsed with PBS-T twice followed by 2 x 5-minute washes. The membrane was dried at 37^{o}C for 30 minutes in the dark. Protein expression was captured using Amersham Typhoon Gel and Blot Imaging (GE Healthcare).

Table 2-5. Primary antibodies for Western blotting

Antibody	Dilution	Company and RRID
Rabbit anti-human SOX9 primary antibody	1:1000	Millipore and AB_2239761
Rabbit anti-human β-actin primary antibody	1:2500	Santacruz and AB_630836

2.27 Teratoma assay

Teratoma assay was performed as described previously (285, 286). To generate teratomas (IPSC Core Facility, MCRI), a 90% T75 confluent hiPSC culture was harvested using 0.5mM EDTA/DPBS, pelleted by centrifugation at 450g for 3 minutes and washed with DPBS. The final cell pellet was resuspended with a 200µL mixture of DPBS+35% Matrigel and transferred into a pre-cooled sterile capped FACS tube. A 1 mL syringe with a 27G size needle was used to aspirate 200µL of the cell mixture and subcutaneous injection into NOD/SCID mice was performed by trained animal house staff. Teratoma formation was monitored for up to 12 weeks and was harvested when the teratoma diameter reached 2cm. Teratoma tissues were washed with DPBS and cysts which formed the majority of the teratoma mass were removed. Half of the teratoma tissues were processed for paraffin embedding and the other half for OCT embedding (frozen section) for future use.

Chapter 3

The generation of SOX9-reporter hiPSC line (SOX9-T2A-tdTom)

3.1 Introduction

A recent paper developed a method to differentiate pluripotent stem cells into chondrocyte-like cells via intermediate embryonic development stages (17). Although this method is promising and chondrogenic markers were upregulated by day 6, they were downregulated during further chondrogenesis in defined culture media supplemented with BMP4. Hence, the chondrocyte differentiation protocol requires further optimisation before it can be used to generate accurate disease models.

Given its essential role as the master regulator of chondrogenesis (see Chapter 1, section 1.4.1 to 1.4.2), it might be very useful to tag SOX9 expression for real-time monitoring of chondrocyte differentiation *in vitro.* Therefore, as part of the chondrocyte differentiation protocol optimisation, we have developed a hiPSC reporter line where the cartilage phenotype can be monitored in real-time using SOX9-driven fluorescence. The SOX9-T2A-tdTom hiPSC line was generated using CRISPR-Cas9 genome editing to insert a T2A sequence and a tandem-tomato reporter (tdTom) downstream of SOX9. The experimental workflow is shown in Figure 3-1.

To test the fidelity of SOX9-reporter expression, differentiation towards sclerotome was compared in the SOX9-T2A-tdTom hiPSC line and its parental hiPSC line. The tdTom fluorescent signal which tags SOX9 expression started to emerge on day 3 (early somites) of differentiation and gradually increased until day 6 (sclerotome) of differentiation in monolayer culture. The increase in fluorescent signal intensity was in line with the upregulation of chondrocyte markers such as *COL2A1*. Western blotting analysis showed that the expression of SOX9 protein in SOX9-T2A-tdTom was similar to its parental line. Our data suggest that the SOX9-T2A-tdTom hiPSC line will be useful for monitoring chondrogenic differentiation and adding T2A sequence and expressing tdTom did not disturb SOX9 expression or stability.

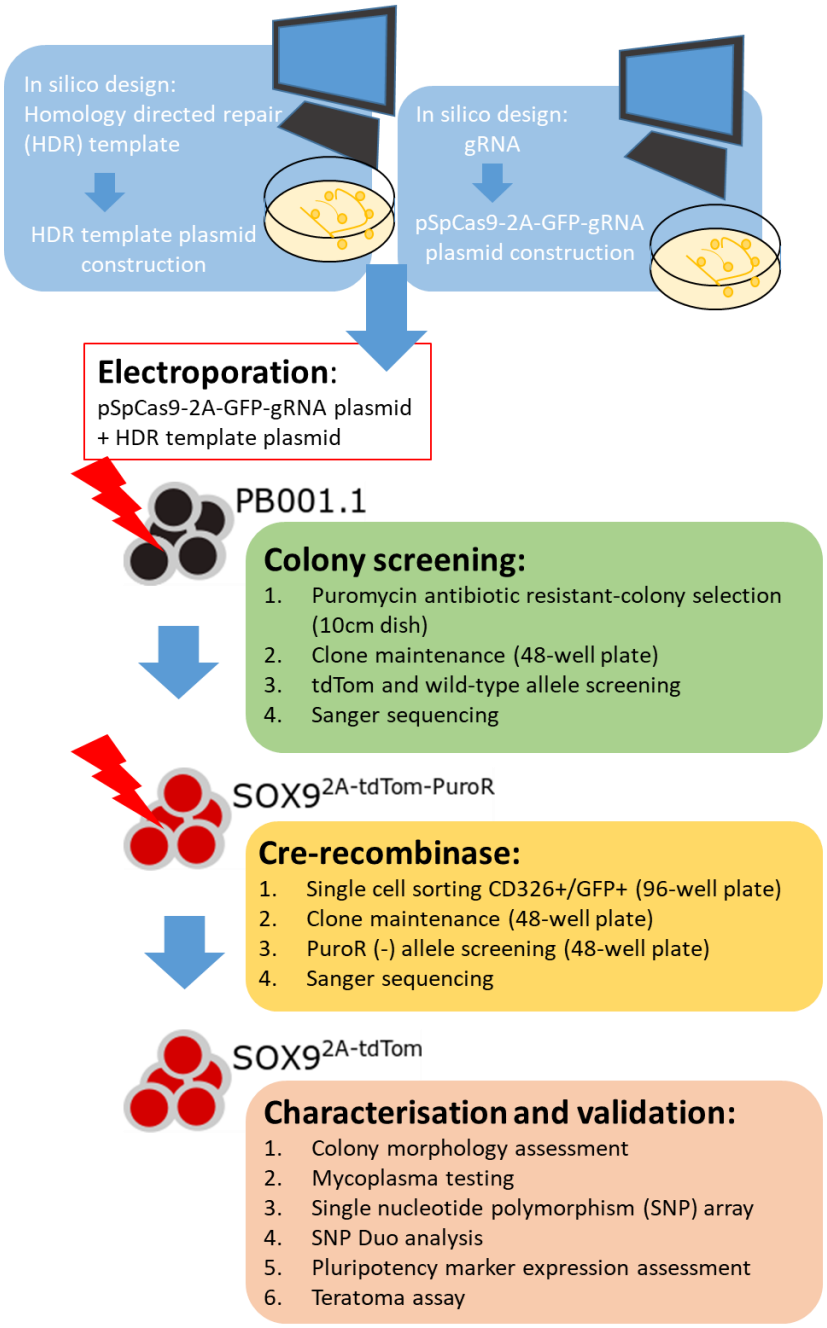

Figure 3-1. The experiment workflow to generate SOX9-reporter (SOX9-T2A-tdTom) hiPSC line.

3.2 Materials and Methods

3.2.1 Single-guide RNA (gRNA) design and generating pSpCas9-2A-GFP-gRNA construct

The single-guide RNA (gRNA) was designed to target SOX9 exon 3 using the http://crispr.mit.edu/ website(Figure 3-2). We chose the gRNA with the highest score, fewer predicted off-target sites and as close as possible to the SOX9 stop codon. The 5'-GCCATCTTCGCCCTTCGT-3' gRNA sequence was chosen and the CACC base sequence was added at the 5' end of the gRNA sequence (gRNA TOP) and AAAC base sequence was added at the 5' end of the gRNA complementary sequence (gRNA BOTTOM) (Table 3-1). The gRNA oligonucleotides were purchased from Sigma Aldrich and were resuspended at 200µM. The gRNAs were phosphorylated, annealed to the complementary sequence and ligated into pSpCas9-2A-GFP (the detailed procedures are available in Chapter 2 sections 2.6.1 and 2.6.2).

3.2.2 Homology-directed repair (HDR) template construction using infusion cloning

To allow homology-directed repair following the Cas9-induced DNA double-strand break, an HDR template was constructed (Figure 3-3A). The targeted allele was designed to produce SOX9 protein with a T2A sequence at the C-terminal end and a separate tdTom fluorescent protein (Figure 3-3B). Thus, in the HDR template, the SOX9 stop codon was replaced with amino acid serine and an additional amino acid arginine in order to insert the T2A and tdTom DNA sequence downstream of SOX9 exon 3. A plasmid encoding tdTom (pT2A-tdTom-PuroR) was used to generate the HDR template (provided by Stem Cell Technology Laboratory, MCRI). The HDR template was constructed by inserting 1000bp of homologous SOX9 DNA upstream (left SOX9 DNA homologous arm) and downstream (right SOX9 DNA homologous arm) of the SOX9 stop codon into the pT2A-tdTom-PuroR using infusion cloning techniques (Clonetech).

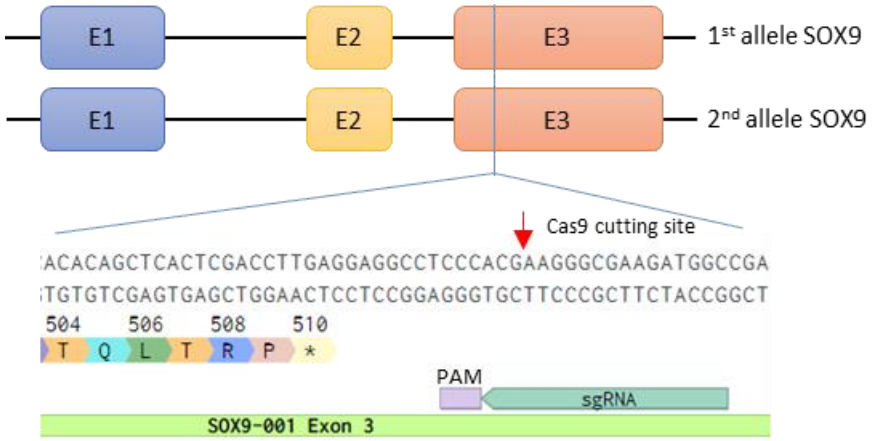

Figure 3-2. The location of gRNA in relation to the SOX9 stop codon. The gRNA is shown in the green box and the PAM sequence in the purple box. The Cas9 cutting site is located 3 bases upstream of the PAM sequence.

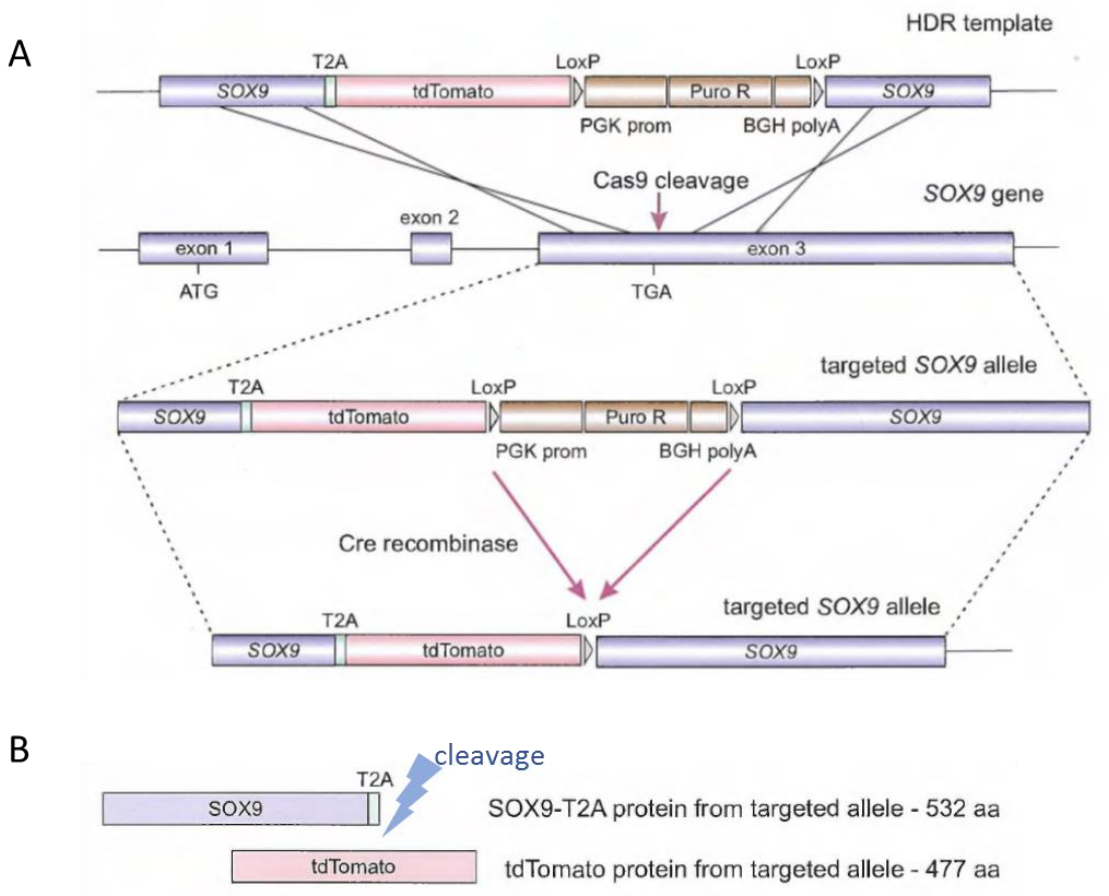

Figure 3-3. Generation of the SOX9-reporter hiPSC line. An HDR template was used to direct homologous repair following Cas9-induced DNA double-strand break (A). The SOX9 stop codon (TGA) was deleted and two extra amino acid codons (for serine and arginine) were added to insert the T2A-tdTom sequence downstream of SOX9. The peptide bond between the Glycine and Proline residues found on the C-terminus of T2A peptide does not form during protein synthesis resulting in a SOX9 protein with 20 additional amino acids in its C-terminal and a separate tdTom fluorescence protein (B). HDR: homology-directed repair, PuroR: puromycin resistance gene, T2A: Thosea asigna virus 2A, PGK: phosphoglycerine kinase, bGH poly (A): bovine growth hormone polyadenylation.

3.2.2.1 In silico infusion cloning and infusion cloning primer designing

To generate the HDR template construct, we did *in silico* infusion cloning of the left and right SOX9 DNA homologous arm into the pT2A-tdTom-PuroR using Snapgene software. The infusion cloning primers generated from *in silico* infusion cloning are available in Table 3-1.

3.2.2.2 Left and right SOX9 DNA homologous arm amplification using PCR

DNA from a healthy subject was used as a template to generate the SOX9 DNA homologous arm. To amplify the left SOX9 DNA homologous arm, PCR was performed with an infusion SOX9 L-F + R primer set using CloneAmp HiFi^{TM} PCR Premix (see Chapter 2 section 2.10) while the right SOX9 DNA homologous arm was amplified with an infusion SOX9 R-F + R primer set using AccuPrime Taq DNA polymerase with touchdown PCR (see Chapter 2 section 2.10). The PCR product was gel purified before being used for infusion cloning (Chapter 2, section 2.7).

3.2.2.3 Infusion cloning

The infusion cloning was performed in two steps using an Infusion Cloning Kit (Clonetech). The first step was to clone the right SOX9 DNA homologous arm into pT2A-tdTom-PuroR to generate pT2A-tdTom-PuroR-Right arm SOX9 and the second step was to clone the left SOX9 DNA homologous arm into pT2A-tdTom-PuroR-Right arm SOX9 to generate pT2A-tdTom-PuroR-Left-arm SOX9-Right arm SOX9 (Figure 3-4).

To clone the right SOX9 DNA homologous arm into pT2A-tdTom-PuroR, 100ng of gel-purified right SOX9 DNA homologous arm was mixed with 100ng of AscI restriction enzyme-linearised pT2A-tdTom-PuroR, 4µL of 5X infusion HD enzyme premix (Clonetech) and nuclease-free water to 20µL followed by incubation at 50^{o}C for 15 minutes. The cloning mixture was transformed into Stellar competent cells (provided in the kit) and miniprep plasmid DNA extraction was done to isolate the pT2A-tdTom-PuroR-Right arm SOX9. Correct insertion was screened by restriction enzyme digestion with AscI + AgeI combined and EcoNI and it was validated by sequencing using Seq3 and Seq4 primer (Table 3-1).

A similar cloning procedure was used to insert the left SOX9 DNA homologous arm into the pT2A-tdTom-PuroR-Right arm SOX9 plasmid. Correct insertion was screened by restriction enzyme digestion with MluI + BspMI combined and it was validated by sequencing using Seq1 and Seq2 primer (Table 3-1).

Table 3-1. The list of primers used for PCR

Oligo name	Sequence	Description
SOX9 gRNA TOP	CACCGCCATCTTCGCCCTTCGT	
SOX9 gRNA BOTTOM	AAACACGAAGGGCGAAGATGGC	
Infusion SOX9 L-F	TATCGAATTTACGCGCATTGGGCGACTTATCTCCGGT	
Infusion SOX9 L-R	CTCCGGACCCACGCGAAGGTCGAGTGAGCTGTGTGTAG	
Infusion SOX9 R-F	AAGTTATCCGGCGCGGGGCGAAGATGGCCGAGATGAT	
Infusion SOX9 R-R	AGCCTCGATGGCGCGCAGTGTGCTCGGGCACTTATTGG	
M13 Reverse	CAGGAAACAGCTATGAC	Seq1
TT sequencing Rev 2	ACTCTTTGATGACCTCCTCGCC	Seq2
BGH Forward	GATTGGGAAGACAATAGCAGGCATG	Seq3
M13 Forward	GTAAAACGACGGCCAGT	Seq4
SOX9 tdTom F	GCAGGAGGGAAGATGGAGTTGT	Primer 1F-2
L-arm SOX9 screen R	ACTCTTTGATGACCTCCTCGCC	Primer 1R
R-arm SOX9 screen F	CAACCTCCCCTTCTACGAGCG	Primer 2F
R-arm SOX9 screen R	TTCTGAGAGGCACAGGTGACAG	Primer 2R
CRE PuroR F	CCCACAACGAGGACTACACCAT	Primer 3F
CRE PuroR R	AGGATCATCTCGGCCATCTTCG	Primer 3R
SOX9 cut site F	CCACCAGAACTCCAGCTCCTAC	Primer 4F

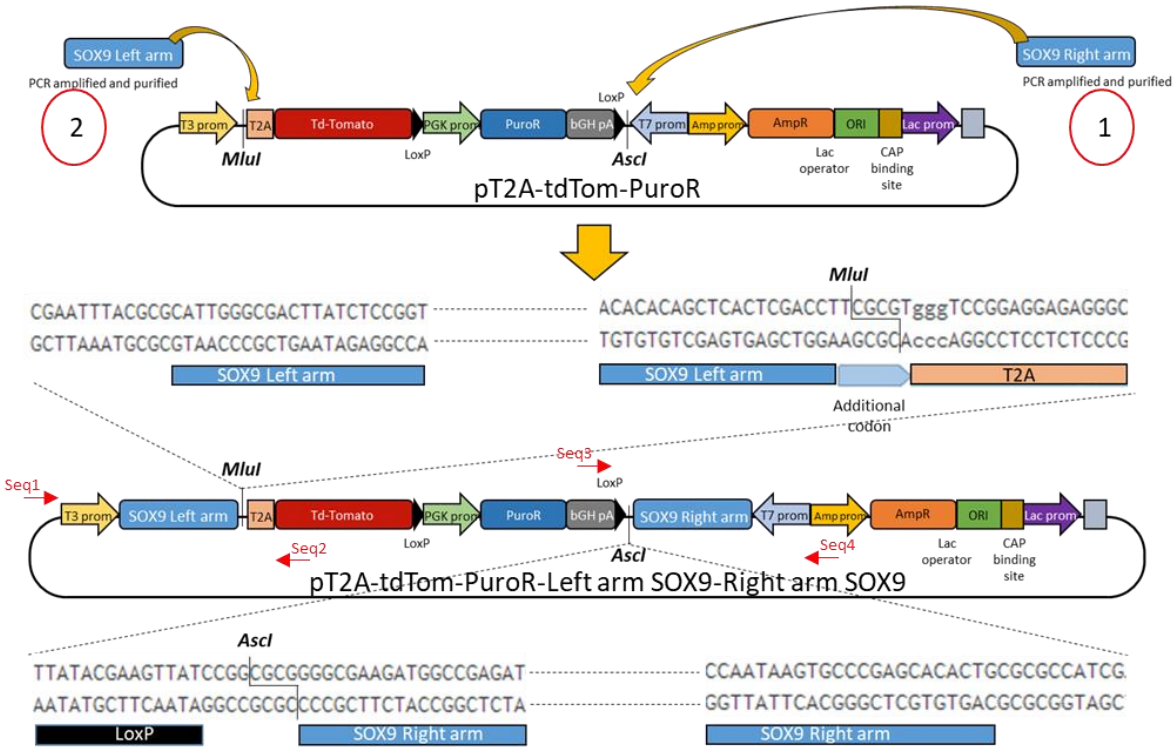

Figure 3-4. Homology directed repair (HDR) (pT2A-tdTom-PuroR-Left arm SOX9-Right arm SOX9) template construction using pT2A-tdTom-PuroR plasmid vector. Restriction enzymes used for screening are shown: BspMI (the cutting site is uniquely present in SOX9-Left-arm insert), EcoNI (the cutting site is uniquely present in SOX9-Right arm insert), and AgeI. Primers used for sequencing are shown in red arrow (Seq1 to Seq4). PuroR: puromycin resistance gene, T2A: Thosea asigna virus 2A, PGK: phosphoglycerine kinase, bGH poly (A): bovine growth hormone polyadenylation, AmpR: ampicillin resistance gene, ORI: original of replication

3.2.3 Insertion of tdTom reporter DNA sequence into the PB001.1 hiPSC line

To insert the tdTom fluorescent reporter gene, MCRIi001-A (PB001.1) hiPSCs (1) ($1x10^6$/100µL in buffer R) were electroporated with gRNA-ligated CRISPR-Cas9 expressing plasmid (pSpCas9-2A-GFP-gRNA) and HDR template plasmid (pT2A-tdTom-PuroR-Left arm SOX9-Right arm SOX9). The cas9 will induce DNA-double strand break on the targeted DNA and the tdTom gene will be inserted through homology-directed repair using HDR template. For the electroporation procedure, see section 2.9.

3.2.3.1 Puromycin selection of the electroporated cells

The HDR template plasmids had a puromycin resistance gene downstream of SOX9 making the transfected cells resistant to puromycin hence can be used for clonal selection. One week after electroporation, puromycin selection was performed by adding 1µg/mL of puromycin (Gibco) into the culture. Puromycin resistant colonies were manually picked after 3 days and transferred into MEF-coated 48-well plates for clone maintenance and PCR screening. The medium was changed every 3 days and 20,000 MEFs/well were added every week.

3.2.3.2 tdTom insertion PCR screening

Two sets of primers were used for PCR screening, tdTom specific and puromycin specific primer sets. The tdTom specific primer set (1F-2 + 1R) amplified the left-SOX9 DNA homologous arm and a part of the tdTom reporter gene sequence (1913bp) while the puromycin specific primer set (2F+2R) amplified the right-SOX9 DNA homologous arm and a part of the puromycin resistance gene (1559bp). Sequencing was performed on the PCR product from tdTom specific primer to validate the correct insertion of tdTom gene using 4F primer.

3.2.3.3 Wild type allele PCR screening

The wild type allele PCR screening was performed to check for any unintended insertions and deletions in the non-edited allele following CRISPR/Cas9 genomic manipulation which meant that heterozygous allele was preferable in this study. A 4F+2R primer set (Table 3-1) was used for PCR screening. In case of homozygous tdTom allele, the primer set would produce a single 4342bp PCR band whereas heterozygous tdTom allele would produce 2 bands: the wild type allele (1280bp) and the tdTom allele (4342bp). Sequencing using a 4F primer was performed in the heterozygous lines to confirm the heterozygosity. Confirmed heterozygous tdTom reporter hiPSC lines were selected for SNP array.

3.2.4 CRE-recombinase to remove the puromycin resistance gene

A hiPSC clone that had a heterozygous insertion of tdTom and did not show chromosomal abnormalities was selected for Cre-recombinase treatment to remove the puromycin resistance gene. The hiPSCs were electroporated with 3µg of Cre-recombinase expressing plasmid (pCRE-IRES-PURO) and 0.2µg GFP expressing plasmid (pEFBOS-GFP) in 100µL electroporation reaction (Invitrogen). The electroporation procedure is described in more detail in Chapter 2, section 2.9. Three-day post electroporation, FACS was performed based on GFP positivity to sort hiPSCs in which PuroR gene has potentially been removed by CRE-recombinase. PCR using two sets of primers (tdTom specific (3F+3R) and puromycin specific (2F+3R) primer sets) was performed to quickly identify puromycin resistance gene removal from the heterozygous tdTom reporter hiPSC lines.

3.3 Results

3.3.1 pSpCas9-2A-GFP-gRNA construct

To generate pSpCas9-2A-GFP-gRNA construct, the annealed-phosphorylated gRNA was inserted into BbsI digested-dephosphorylated-pSpCas9-2A-GFP (Figure 3-5A). gRNA insertion was screened by double restriction enzyme digestion using BbsI and NotI restriction enzyme. Successful insertion produced only a single band (10kb), a result of NotI cutting of the backbone plasmid since the BbsI cutting site has been removed upon gRNA insertion. Gel electrophoresis showed that all the plasmid clones had gRNA insertion (Figure 3-5B). Sequencing confirmed the insertion of the gRNA (blue box, Figure 3-5C).

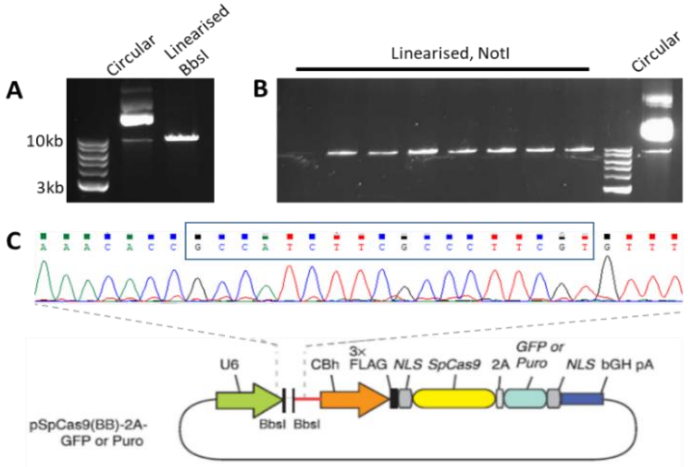

Figure 3-5. pSpCas9-2A-GFP-gRNA construct for tdTom reporter gene insertion downstream of SOX9 gene. gRNA was inserted into pSpCas9-2A-GFP (A) and the insertion was screened by NotI restriction enzyme digestion (B) and confirmed by sequencing (C). The blue box in panel C indicates the gRNA sequence insertion in the pSpCas9-2A-GFP plasmid vector.

3.3.2 pT2A-tdTom-PuroR-Left arm SOX9-Right arm SOX9 (HDR template) construction using infusion cloning

While the pSpCas9-2A-GFP-gRNA construct being generated, the HDR template was constructed by ligating the right and left SOX9 DNA homologous arm into tdTom expressing plasmid (pT2A-tdTom-PuroR). The PCR amplified-gel purified right SOX9 DNA homologous arm (Figure 3-6A) was ligated into AscI linearised-gel-purified pT2A-tdTom-PuroR (Figure 3-6B). Successful ligation was screened by restriction enzyme digestion: AscI+AgeI and EcoNI. In EcoNI digestion, successful ligation should produce a 7094bp band from the single EcoNI cuts within the right SOX9 DNA homologous arm whereas in the AscI+AgeI digestion, successful ligation should also produce single band as AgeI cuts only once and the AscI cutting site was disrupted. However, the digestion was not complete in all four plasmid clones (Figure 3-6C), so all of them were sequenced to confirm correct insertion of the right-SOX9 DNA homologous arm. The complete sequencing results of plasmid 4 are available in Appendix 1. Plasmid 4 (p4) had the correct insertion and it was selected for left-SOX9 DNA homologous arm ligation.

PCR-amplified gel-purified left-SOX9 DNA homologous arm (Figure 3-6D) was ligated into pT2A-tdTom-PuroR-Right arm SOX9 linearised with MluI restriction enzyme (Figure 3-6E). MluI+BspMI restriction enzyme digestion was used to screen for successful ligation. The successful ligation should produce a single band at 8094bp since the MluI cutting site was removed and BspMI only cuts once. From four different plasmids, only one plasmid (p2) showed complete digestion (Figure 3-6F), so all the plasmids were sequenced, confirming that all four had the correct insertion of the left-SOX9 DNA homologous arm. The complete sequencing results of p4 are available in Appendix 1. Plasmid 4 (p4) was selected for the HDR template.

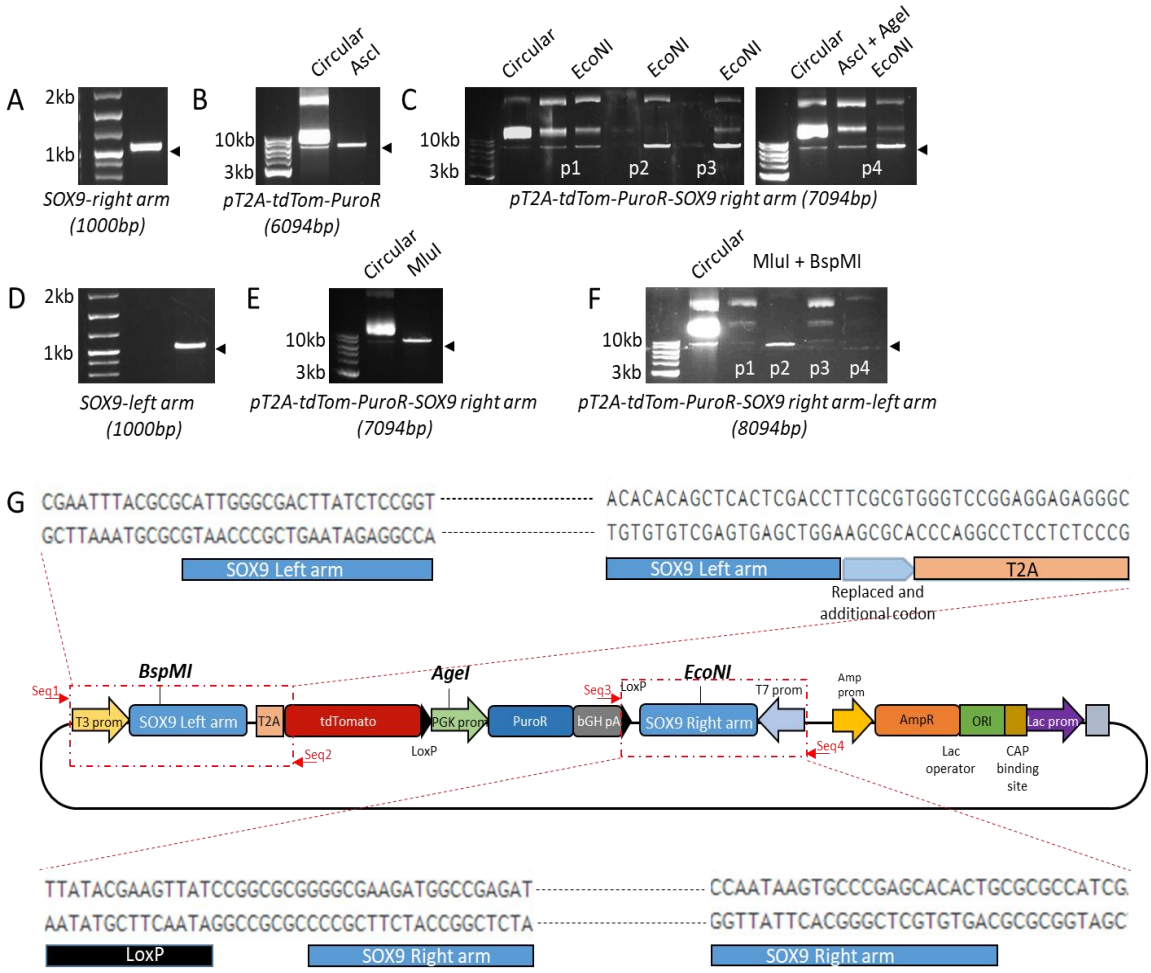

Figure 3-6. Homology Directed Repair (HDR) template construct. Screening of the successful insertion is performed by restriction enzyme digestion. Both SOX9-right arm (A) and SOX9-left arm (D) are amplified using infusion cloning primer sets (Table 3.1) which then are inserted into tdTom expressing plasmid (pT2A-tdTom-PuroR) in sequential steps (SOX9-right arm into pT2A-tdTom-PuroR (B) then SOX9-left arm into pT2A-tdTom-PuroR-SOX9 right arm (E)). For SOX9-right arm insertion screening, AscI+AgeI and AgeI restriction enzymes were used and both enzyme digestion reactions should result in a single band (7094bp) (C). For SOX9-left arm insertion screening, restriction enzyme digestion was performed using MluI+BspMI which should result in a single band (8094bp) (F). The location of restriction enzymes was shown in G. Sequencings of the whole inserts were performed using Seq1 and Seq2 for SOX9-left arm insertion and Seq3 and Seq4 for SOX9-right arm insertion (G). P1-4: plasmid isolated from bacterial colony 1-4. The black arrow indicates the expected correct band.

3.3.3 Puromycin selection and PCR screening of tdTom gene integration downstream to SOX9 gene

Once the pSpCas9-2A-GFP-gRNA and HDR template were ready, they were electroporated into PB001.1 hiPSC lines to insert the tdTom gene sequence downstream of the SOX9 gene (for electroporation procedure see section 2.8). The electroporated hiPSCs were plated on 6cm-dish and maintained in feeder dependent culture and three days after, puromycin antibiotic selection was done. Thirty-two hiPSC clones survived following puromycin selection and were screened for tdTom reporter gene insertion. Two sets of PCR primers were used (Figure 3-7A): tdTom specific (primer set#1: 1F-2 + 1R) and puromycin specific (primer set#2: 2F + 2R). From PCR screening, 13 colonies (1, 2, 4, 9, 10, 11, 12, 19, 29, 33, 35, 36, 38) showed insertion of the tdTom reporter gene (Figure 3-7B). Sequencing using a 4F primer confirmed no unwanted insertions and/or deletions around the Cas9 cutting site in the SOX9-T2A-tdTom allele (Figure 3-7C).

3.3.4 Wild type allele PCR screening

As having heterozygous tdTom allele was preferable, the wild type allele PCR screening was performed in 4 hiPSC clones confirmed to have the tdTom reporter gene insertion (clone #9, #11, #12 and #33). This PCR also aimed to check unwanted insertions and/or deletions in the other allele following CRISPR/Cas9 genomic manipulation. Primer 4F+2R (Figure 3-8A) was used for PCR screening which technically could amplify the wild type allele (1280bp) and the tdTom allele (4342bp). Interestingly, the PCR could only amplify the shorter amplicon which was the wild type allele as shown in the gel electrophoresis with the expected wild type 1280bp PCR product (Figure 3-8B). The possible explanation of this phenomenon could be the higher efficiency of the PCR reaction towards the shorter amplicon. Nonetheless, this result confirmed that the 4 clones contained a heterozygous SOX9-T2A-tdTom allele. Sequencing of the PCR products using a 4F primer revealed no unintended insertions and/or deletions around the Cas9 cutting site in the wild type allele (Figure 3-8C). Three clones: #9, #11, and #33, were selected for SNP array and the results showed no major duplications or deletions.

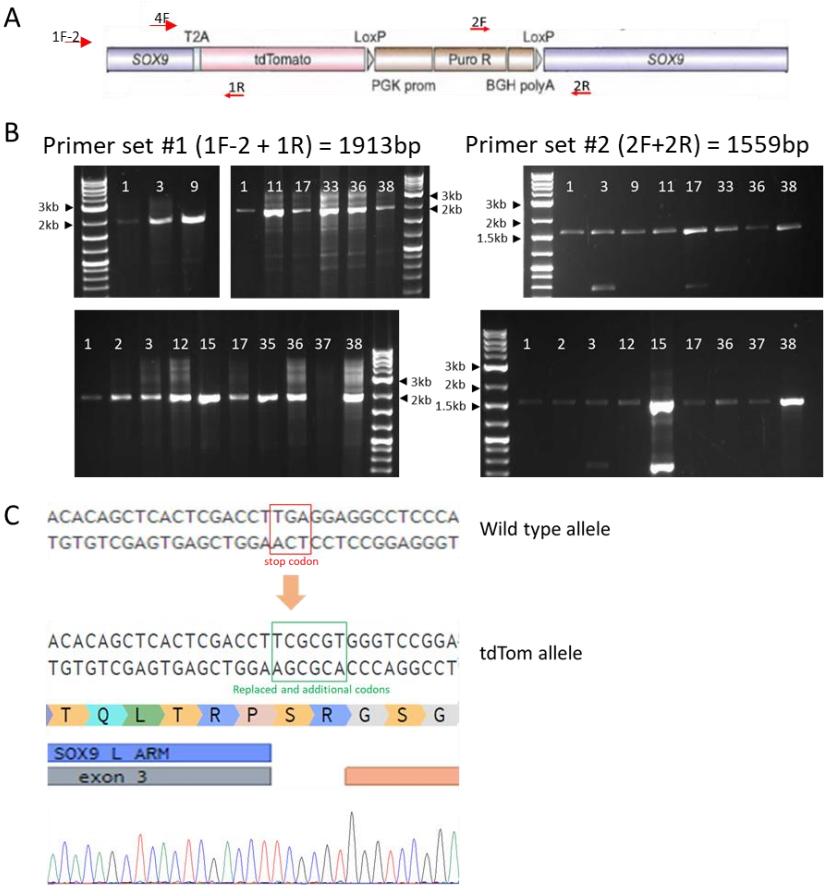

Figure 3-7. PCR screening for tdTom reporter gene insertion. The hiPSC clone of interest must have bands for both primer set #1 (Primer 1F-2+1R) and #2 (Primer 2F+2R) (A). Clone number 1, 2, 9, 11, 12, 33, 36, and 38 are clones of interest as they have correct sized bands from both primer sets and are very likely to have a correct insertion of tdTom reporter gene (B). Sequencing using a 4F primer of clone #9 showed that the stop codon has been replaced with two amino acids: serine and arginine which are followed by the T2A DNA sequence that links the tdTom gene sequence to the exon 3 of SOX9 gene (C).

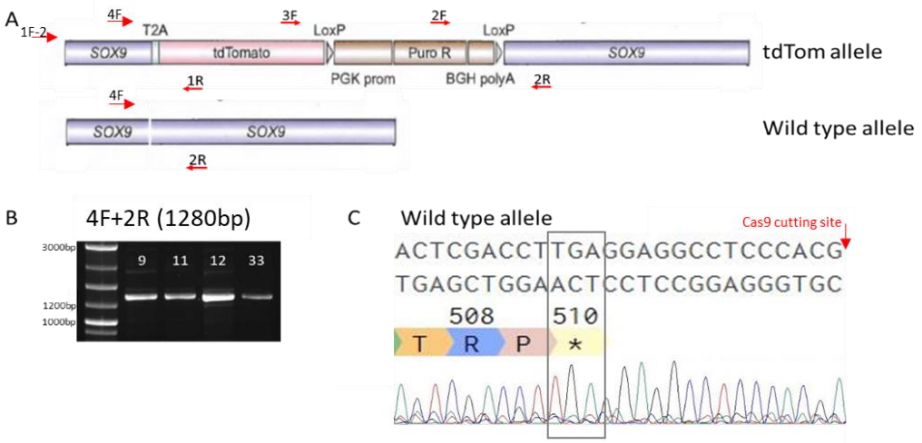

Figure 3-8. Wild type allele screening. The schematic diagram of the heterozygous allele of the SOX9 gene with tdTom reporter gene (A). Gel electrophoresis result of PCR product of primer 4F+2R indicates no tdTom insertion and unintended insertions and/or deletions (B). The sequencing result of clone #9 shows that the SOX9 stop codon remains intact (black box) and no unintended insertions and/or deletions are found (C).

3.3.5 Cre-recombinase to delete the puromycin resistance gene

After obtaining the correct clone, the puromycin resistance gene was deleted from the genome using Cre-recombinase (Figure 3-9A). hiPSC clone #9 was selected for Cre-recombinase. PCR screening confirmed puromycin gene removal. Two sets of primers were used: tdTom specific (3F+3R) and puromycin specific (2F+3R) primer sets. Clones with successful deletion of the puromycin resistance gene only had the expected 902bp and 177bp PCR products with 3F+3R primer set (Figure 3-9B, green box) and no PCR product for 2F+3R primer set. These two bands occurred because the tdTom gene has two copies of the 3F primer binding site (3Fa and 3Fb) while clones with the puromycin gene still present had the expected 2419bp and 1693bp PCR products with 3F+3R primer set and 519bp PCR product with 2F+3R primer set. However, PCR with a 3F+3R primer set showed only the shorter amplicon (1693bp) indicating that the efficiency of the PCR reaction to amplify the shorter amplicon was higher than the longer (2419) amplicon. Clone #13 (Figure 3-9B, green box) which then is called a **SOX9-T2A-tdTom hiPSC line** was selected for further characterisation and validation including SNP array, sequencing, pluripotency marker assessment, and teratoma formation.

3.3.6 PCR and sequencing of SOX9-T2A-tdTom and PB001.1 hiPSC line

PCR was performed to compare the SOX9-T2A-tdTom and its parental line, PB001.1; using primer sets shown in Figure 3-10A. PCR using a 4F+2R primer set confirmed that the SOX9-T2A-tdTom had a heterozygous tdTom reporter allele as it showed the expected 1280bp band for the wild type allele and 2826bp band for the tdTom reporter allele (Figure 3-10B). PCR using the tdTom specific primer set (3F+3R) confirmed that the tdTom reporter was present in the SOX9-T2A-tdTom line but not in PB001.1 (Figure 3-10B).

PCR products from the 4F+2R primer set for PB001.1 and from the 4F+1R primer set for SOX9-T2A-tdTom were sequenced. Sequencing using 4F primer in both lines showed that the SOX9 stop codon in the PB001.1 had been replaced with amino acid serine and arginine followed by the T2A gene sequence in the SOX9-T2A-tdTom line (Figure 3-10C).

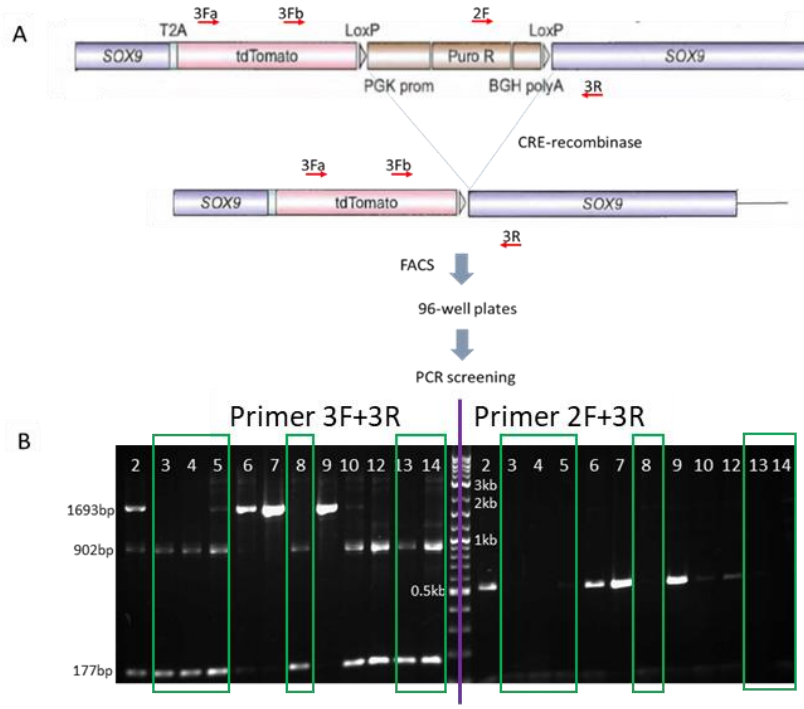

Figure 3-9. CRE-recombinase experiment to remove the puromycin resistance gene. Two sets of primers, tdTom (3F+3R) and puromycin specific (2F+3R) primer sets, were used to check the complete deletion of the puromycin resistance gene (A). hiPSC clones in which the puromycin resistance gene has been removed had 2 bands (902bp and 177bp band) for primer 3F+3R primer and no band for primer 2F+3R (green box) (B). Retained puromycin resistance gene resulted in both 1693bp (3Fb+3R primer) and 519bp (2F+3R primer) bands. The band from 3Fa+3R primer (2419bp) is not produced possibly due to low PCR efficiency.

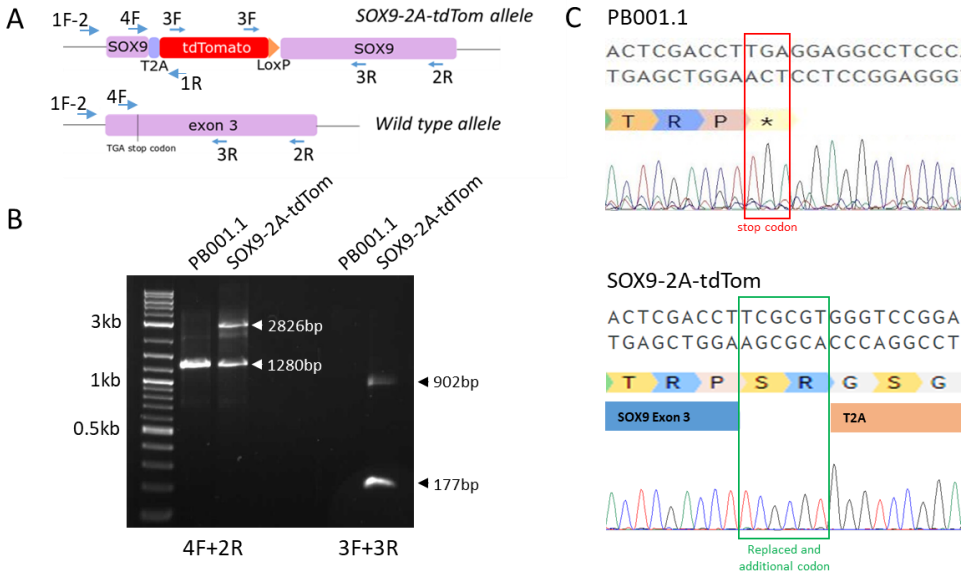

Figure 3-10. PCR and sequencing results of SOX9-T2A-tdTom and PB001.1. The location of the primers is shown (A). Gel electrophoresis of the PCR with 4F+2R and 3F+3R primer sets in PB001.1 and SOX9-T2A-tdTom indicates that the SOX9-T2A-tdTom contains heterozygous tdTom allele (B). The integration of T2A-tdTom insert in SOX9-T2A-tdTom is confirmed with sequencing using 4F primer (C).

3.3.7 Characterisation and validation of SOX9-T2A-tdTom hiPSC line

Characterisation of the SOX9-T2A-tdTom hiPSC line included mycoplasma testing, colony morphology assessment, pluripotency marker assessment, teratoma formation, and SNP array. Mycoplasma testing was confirmed negative (Appendix 2). SOX9-T2A-tdTom hiPSC lines formed tightly packed colonies with homogenous cells and clear peripheral colony edges (Figure 3-11).

To confirm the pluripotency of the SOX9-T2A-tdTom line, pluripotency markers were assessed using immunostaining and flowcytometry. Immunostaining of pluripotency marker NANOG and OCT4 protein in SOX9-T2A-tdTom hiPSC lines showed that these pluripotency markers were co-localised in most of the cells cultured in monolayer (Figure 3-11). Pluripotency marker CD9, Ep-CAM (CD326) and SSEA-4 were measured using flowcytometry. More than 99% of cells expressed both CD9 and CD326 and 95% of cells expressed SSEA-4 (Figure 3-12). Teratoma assay confirmed the pluripotency of SOX9-T2A-tdTom hiPSC line. Tissues from three germ layers were found in teratoma tissue stained with hematoxylin & eosin. The histology showed ectodermal derived neuroectoderm, mesodermal derived chondrocytes, and endodermal derived gut epithelium (Figure 3-13).

SNP array found no duplications and deletions and SNPduo analysis showed that SOX9-T2A-tdTom had 99.9% identical genotypes to the SOX9-T2A-tdTom hiPSC line indicating that both lines were from the same individual (Appendix 3).

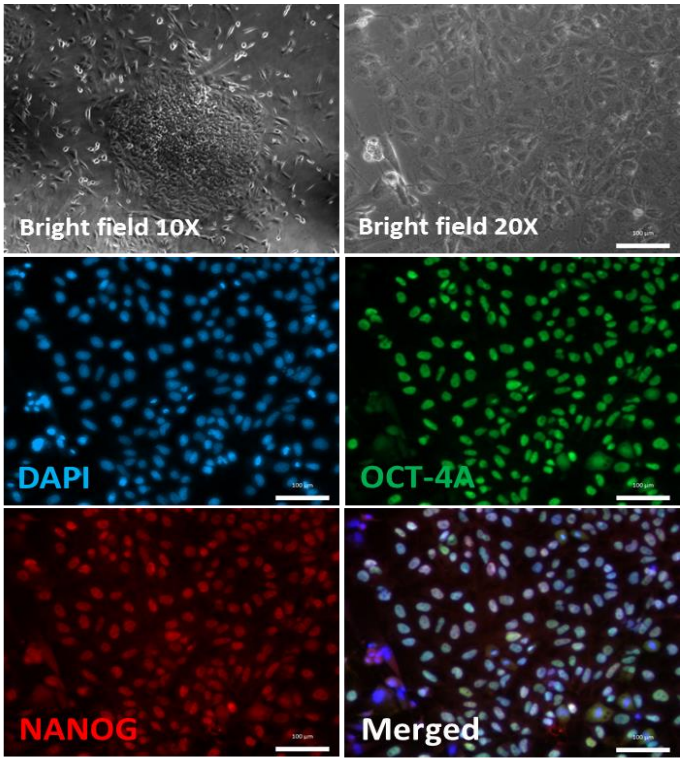

Figure 3-11. OCT4 and NANOG protein expression in SOX9-T2A-tdTom hiPSC line.

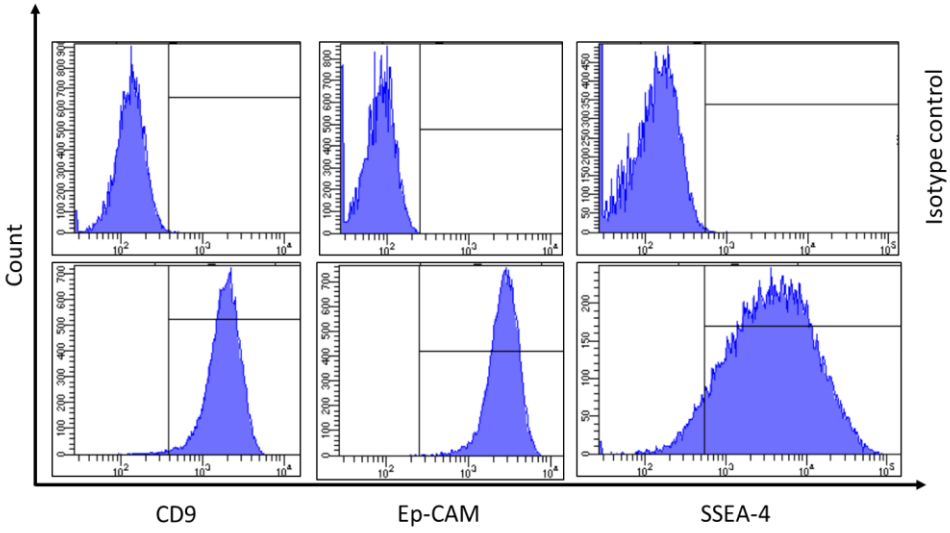

Figure 3-12. Pluripotency marker CD9, Ep-CAM (CD326) and SSEA-4 expression assessed using flowcytometry.

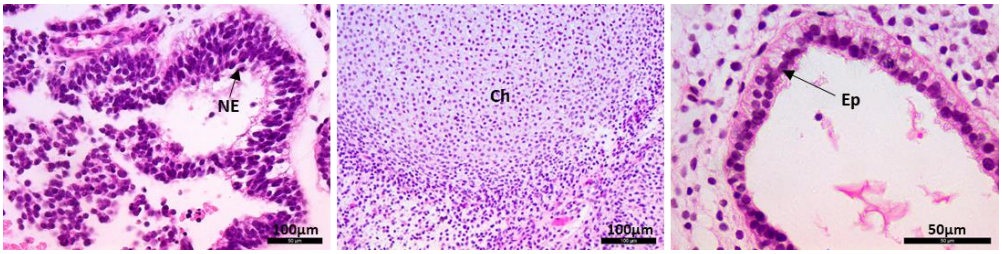

Figure 3-13. Three germ layer formation in teratoma generated from SOX9-T2A-tdTom hiPSC line. Neuroectoderm (NE) as an ectodermal tissue, Chondrocytes (Ch) as a mesodermal tissue and gut epithelium (Ep) as an endodermal tissue.

3.3.8 tdTom fluorescence was expressed during sclerotome induction

To test the fidelity of the SOX9 fluorescent reporter, we induced sclerotome formation of SOX9-T2A-tdTom hiPSC lines according to a protocol developed by Loh, Chen (17). The tdTom fluorescent signal, which tagged SOX9 expression, was detected at differentiation day 3 (Figure 3-14) and gradually increased during sclerotome induction in monolayer culture. From the images, we noticed the changes in the morphology of the cells following sclerotome induction.

The proportion of cells that expressed tdTom fluorescence gradually increased during sclerotome induction in flowcytometry analysis (Figure 3-15). The SOX9 started to be expressed at differentiation day 2 (paraxial mesoderm) and reached a peak at differentiation day 3 (somites). Two distinct cell populations, SOX9-negative ($SOX9^-$) and SOX9-positive ($SOX9^+$) cells, emerged at differentiation day 4 and they became more segregated following sclerotome differentiation. The proportion of SOX9-negative cells increased following 3-day sclerotome differentiation with only 10% at day 4 to more than 25% on day 6 thus leaving 73.5% of SOX9-positive cells on day 6.

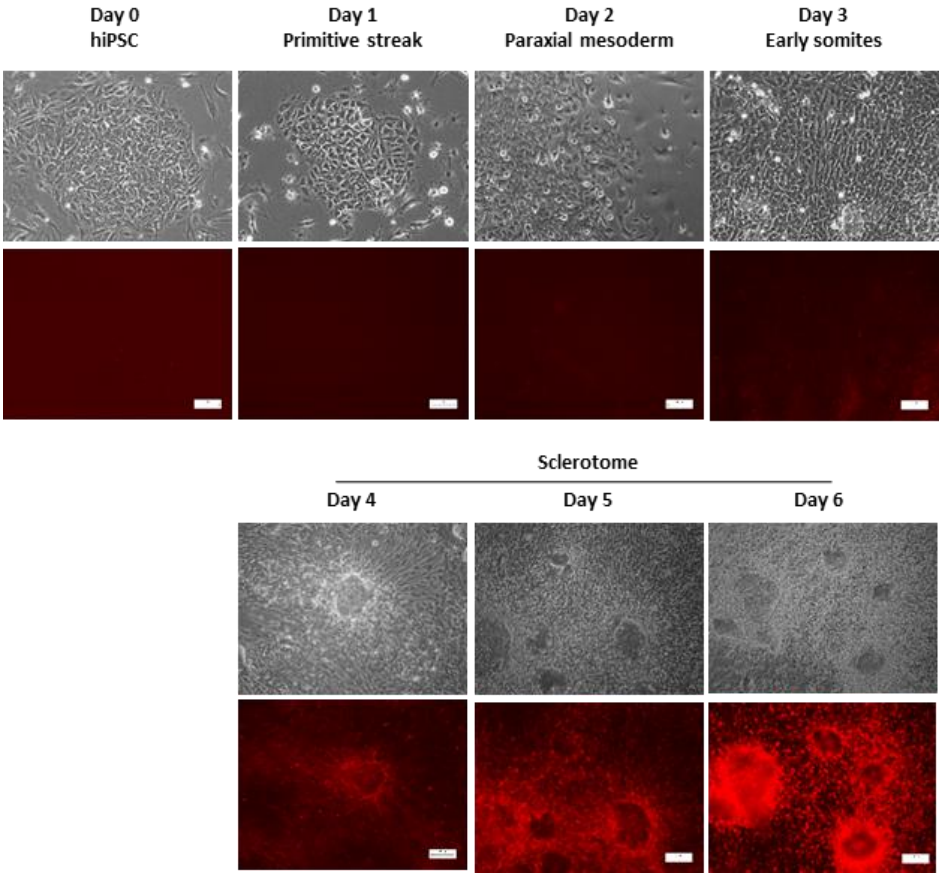

Figure 3-14. tdTom fluorescence expression (red) during sclerotome induction. The images were taken at 20X objective magnification. Scale bar: 100µm.

3.3.9 The expression of SOX9 protein in Western blotting

Western blotting was performed to confirm the level of SOX9 protein expression during sclerotome induction in both SOX9-T2A-tdTom and PB001.1 hiPSC lines. The immunoblotting results showed that the level of SOX9 expression was similar in the SOX9-T2A-tdTom and PB001.1 lines indicating that adding the reporter did not alter the SOX9 protein expression (Figure 3-16). The expressed SOX9 protein from the tdTom allele would have 20 additional amino acids derived from the T2A peptide sequence at its C-terminal which was equal to 1.9kDa additional molecular weight to SOX9 protein. However, we could not see a substantial size difference of SOX9 protein in SOX9-T2A-tdTom compared to the PB001.1 (Figure 3-16).

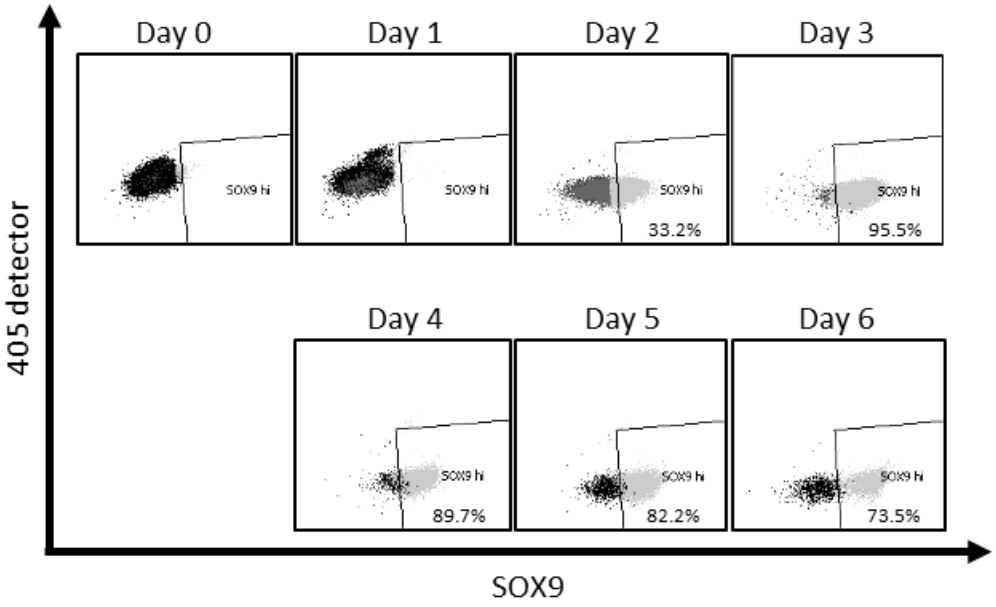

Figure 3-15. Flow cytometry analysis of tdTom fluorescence expression which tagged SOX9 expression. tdTom fluorescent signal was assessed on day 0 to day 6 of sclerotome induction.

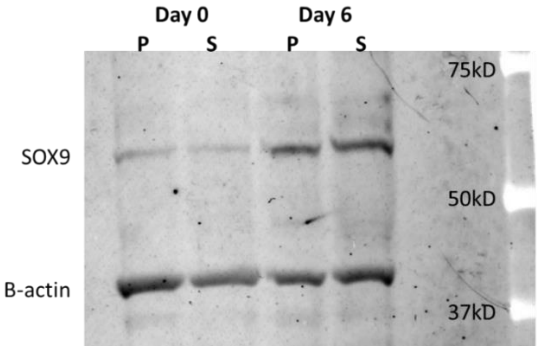

Figure 3-16. Western blotting result of SOX9 protein expression. Western blotting shows that SOX9 protein expression is similar between SOX9-T2A-tdTom (S) and its parental line, PB001.1 (P).

3.3.10 Embryonic stage-specific marker expression during sclerotome induction

To further validate that tdTom fluorescence gene insertion downstream of the SOX9 gene did not disrupt the SOX9 expression and the capacity of the SOX9-T2A-tdTom hiPSC lines to differentiate into sclerotome, we compared the SOX9 expression and the embryonic stage-specific marker expression between SOX9-T2A-tdTom and PB001.1 hiPSC lines during sclerotome induction (Figure 3-17).

The formation of the primitive streak, the initiation of mesoderm development, from pluripotent stem cells was achieved by promoting TGFβ and WNT signaling for 24 hours. It was indicated by the upregulation of transcription factor *MIXL1* at day 1 of differentiation. To direct the differentiation of primitive streak into paraxial mesoderm, WNT signaling was promoted and TGFβ and BMP signaling were inhibited. These resulted in the upregulation of *TBX6* and *MSGN1*, markers of paraxial mesoderm lineage, and downregulation of *HAND1*, a marker of lateral plate mesoderm (day 2). Early somite formation from paraxial mesoderm was induced by inhibiting BMP, WNT, TGFβ and ERK signaling pathways. This was characterised by the upregulation of early somite markers, *FOXC2, MEOX1* and *PAX3,* and the reduction of the paraxial mesoderm markers, *TBX6,* and *MSGN1* (day 3). Sclerotome formation was achieved by promoting SHH and WNT signaling simultaneously for three days. It was indicated by the upregulation of sclerotome marker *PAX1* and gradual downregulation of *PAX3*, a marker of dermomyotome patterning (Figure 3-17).

We also found that *PDGFRA* was upregulated during sclerotome induction (Figure 3-17). *PDGFRA* was highly expressed in the ventral somites which developed into sclerotome during zebrafish embryonic development (297). SOX9 was also upregulated during sclerotome induction. *RUNX2*, the regulator of osteogenesis and chondrocyte hypertrophy, was upregulated at day 1 but then downregulated following early somite induction (day 2 to 3) however, its expression gradually increased following sclerotome induction at day 4 to 6 (Figure 3-17).

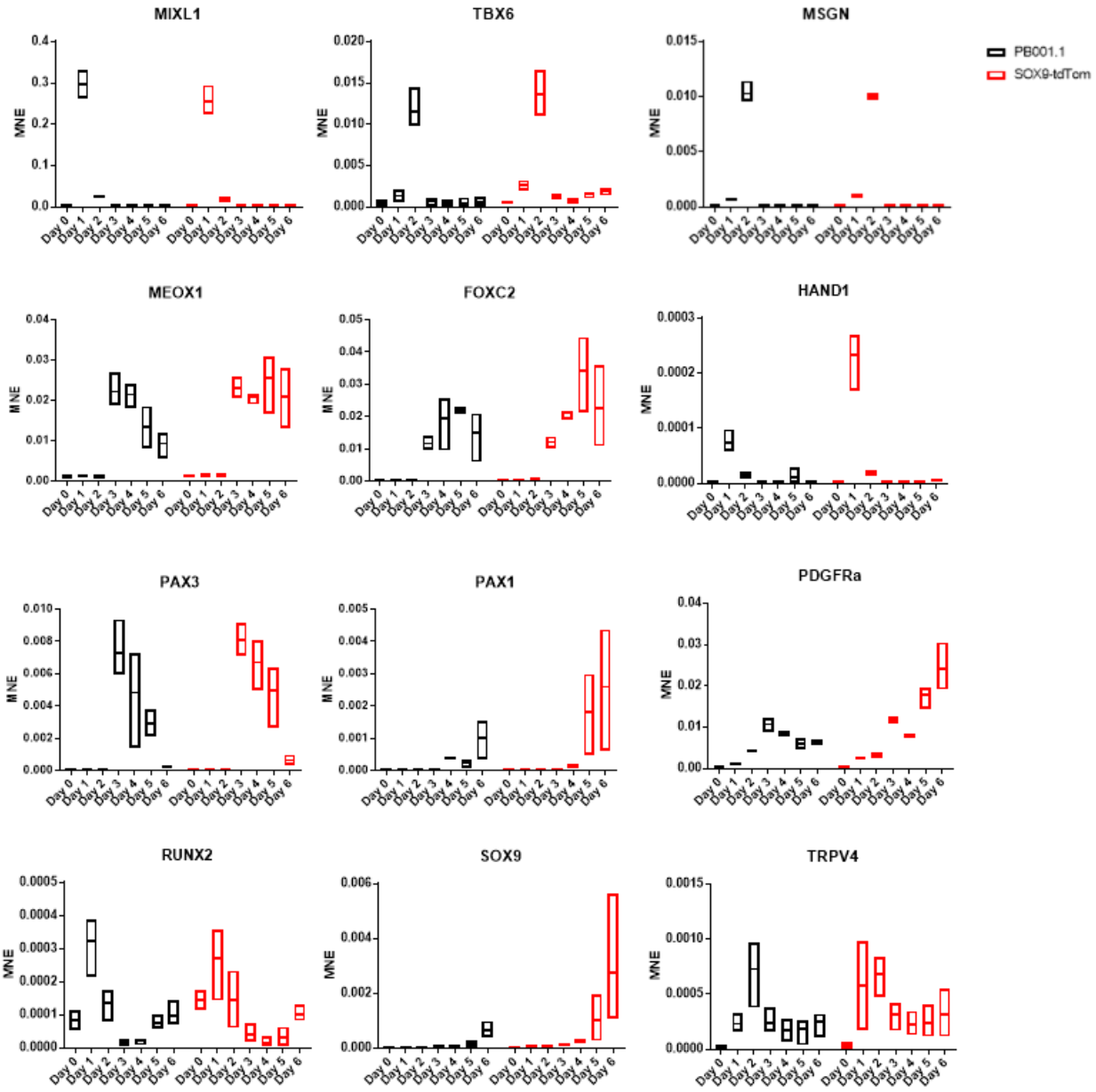

Figure 3-17. The expression of embryonic stage-specific markers during sclerotome induction. The graphs show three different technical replicates. The average mean normalised expression (MNE) value indicated by the horizontal line in each bar. The top and bottom of each bar show the minimum and maximum MNE value. MNE is calculated by the formula: MNE = $2^{\text{CT reference gene}} / 2^{\text{CT gene of interest}}$; with 2 = ideal primer efficiency).

During sclerotome induction, *OCT4* expression gradually decreased, suggesting that the cells lost their pluripotency and committed to differentiation (Figure 3-18). The increase in fluorescent signal intensity and sclerotome marker *PAX1* was positively correlated with the increase in chondrogenic marker expression such as *COL2A1*, *ACAN*, and *SOX9* (Figure 3-18). Both PB001.1 and SOX9-T2A-tdTom hiPSC lines showed a similar pattern of chondrogenic marker expression during sclerotome induction (Figure 3-18). These findings suggested that the insertion of the tdTom fluorescence gene downstream of *SOX9* did not disrupt the physiological function of SOX9 during sclerotome induction.

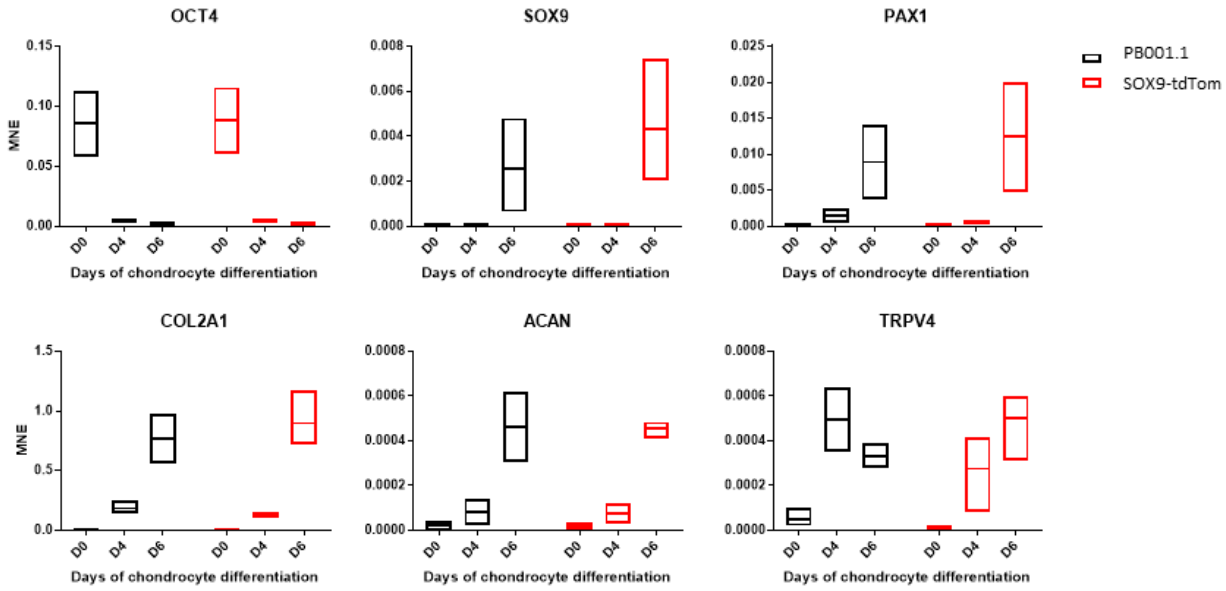

Figure 3-18. The expression of pluripotency (*OCT4*), sclerotome marker (*PAX1*), chondrogenic markers (*SOX9*, *COL2A1*, *ACAN*) and *TRPV4* mRNAs following monolayer sclerotome induction. The graphs show qPCR of three technical replicates with a mean of mean normalised expression (MNE) value is shown as a middle horizontal line in each bar. The top and bottom horizontal lines of each bar represent the minimal and maximal MNE value.

3.4 Discussions

Reporter cell lines allow real-time monitoring of changes in protein expression and provide tools for single-cell sorting and downstream analysis of the cell properties. In this study, we generated SOX9-T2A-tdTom, a hiPSC line that tags SOX9 protein expression with a tdTom fluorescent protein. As SOX9 is the primary regulator of chondrogenesis, this reporter line would be used to optimise a chondrocyte differentiation protocol. Additionally, this reporter hiPSC lines might also be useful to study gonad development since SOX9 plays an important role in regulating male gonad development (298).

In this chapter, we have shown that adding the tdTom reporter gene downstream of the SOX9 gene did not disrupt its function in regulating chondrogenesis at least up to the sclerotome stage. This is also supported by the fact that the SOX9-T2A-tdTom hiPSC line is capable of forming cartilage tissues in the teratoma. The expression patterns of key genes during sclerotome differentiation are similar between SOX9-T2A-tdTom and its parental line, PB001.1. Moreover, immunoblotting shows that SOX9 protein expression is also very similar in both lines.

A reporter hiPSC line which tags COL11A2 expression has been developed as part of chondrocyte differentiation protocol optimisation (18). Flowcytometry analysis shows that on day 14 chondrocyte differentiation, about 30% of cells express green fluorescence EGFP that tags COL11A2 expression. Another reporter hiPSC line which tags COL2A1 expression is developed after SOX9-T2A-tdTom hiPSC line has been generated (248). Using similar sclerotome induction to the one we used, the study detects the expression of green fluorescence that tags COL2A1 expression at differentiation day 3, comparable to the tdTom fluorescence in SOX9-2A-tdTom. Using flowcytometry, the tdTom fluorescence can be detected as early as day 2 of sclerotome induction; and by day 6, more than 70% cells express SOX9. Therefore, the SOX9-T2A-tdTom hiPSC line could be used as an alternative tool to rapidly assess the efficiency of the chondrocyte differentiation protocol.

3.5 Conclusions

We have demonstrated that the SOX9-T2A-tdTom hiPSC line showed similar capability to differentiate towards sclerotome as well as similar SOX9 expression level compared to its parental hiPSC line, PB001.1. Therefore, we could conclude that the insertion of tdTom fluorescence gene downstream to the SOX9 gene did not impair the SOX9 function in regulating chondrogenesis. This hiPSC lines would be used to optimise

the chondrocyte differentiation protocol (Chapter 4) and to model TRPV4-inherited skeletal diseases (Chapter 5 and 6). Chapter 4 also provides more data on a similar capacity in chondrocyte differentiation between the reporter line and PB001.1.

Chapter 4

Chondrocyte differentiation protocol optimisation

4.1 Introduction

Loh, Chen (17) differentiated pluripotent stem cells into chondrocyte-like cells via sclerotome embryonic development stages. Sclerotome was induced with a 6-day protocol followed by chondrocyte differentiation with BMP4 supplementation for another week. However; in their protocol, chondrogenic markers *SOX9, COL2A1*, and *ACAN* were downregulated during the chondrogenic culture with BMP4 treatment (Figure 4-1). Hence, this chapter focuses on optimising the chondrocyte differentiation protocol by 1) administering different types of chondrogenic growth factors, 2) manipulating culture formats (micromass, pellet and swirl culture format), 3) extending the culture length, 4) cell sorting.

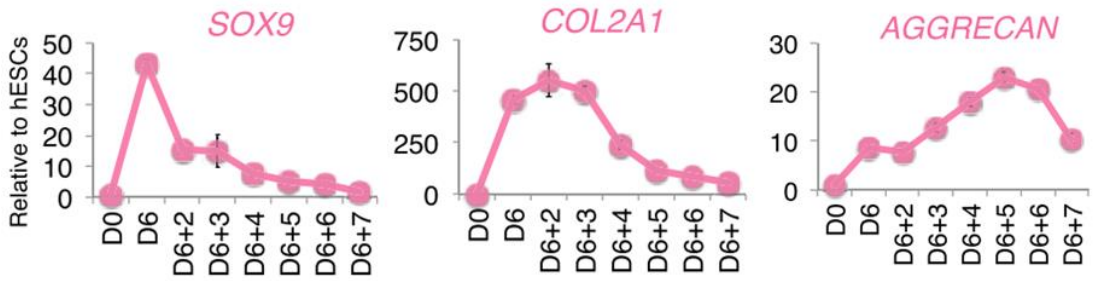

Figure 4-1. Chondrogenic markers are downregulated following BMP4 supplementation during chondrocyte differentiation (17).

4.2 Materials and Methods

4.2.1 Chondrocyte differentiation

The Loh et al. (2016) protocol involved two differentiation stages: 1) sclerotome induction over 6 days and 2) chondrocyte differentiation. We used a similar protocol for sclerotome induction, but for chondrocyte differentiation stage, the culture was extended to 3-10 weeks. The sclerotome induction protocol is described in Chapter 2, section 2.3.

After a 6-day sclerotome induction protocol, chondrocyte differentiation was performed in APEL2 medium + 50U/mL penicillin and 50µg/mL streptomycin + 5% PFHM II with one of the following chondrogenic growth factors: 20ng/mL FGF2, 10ng/mL TGFβ3 (Sigma Aldrich), 50ng/mL BMP4 (R&D systems) or 50ng/mL GDF5 for 3-10 weeks. The medium was changed every other day.

4.2.2 Micromass, pellet and swirl culture

Monolayer cultures were confluent by day 4 of sclerotome induction in 6-well plates. The day 4 sclerotome cells were harvested using TryPLE. In brief, 1mL of TryPLE (ThermoFisher Scientific) was added into the cells and incubated for 3 minutes at 37ºC, 5% CO_2. The TryPLE was carefully aspirated and the cells were dislodged by putting

2mL of DPBS directly to the cells followed by gentle tapping of the plate. The cells were pelleted by centrifugation at 450g for 3 minutes.

For micromass culture, the cells were resuspended in APEL2 medium at 20 x 10^6 cells/mL. A 10uL droplet of cell suspension was plated onto a 48-well plate (Nunclon™ Delta Surface, Thermo-Scientific) and incubated for 30 minutes at 37ºC, 5% CO_2 before 400µL of sclerotome induction medium was added. After 2 days, the medium was replaced with 400µL of chondrocyte differentiation medium. The medium was changed every other day.

For pellet culture, 2 x 10^5 cells/well were transferred into round-bottomed, low attachment 96-well plates (Corning). Plates were centrifuged at 450g for 3 minutes. After sclerotome induction was complete, the medium was replaced with 300µL of chondrocyte differentiation medium. The medium was changed every other day.

Swirl culture was performed by transferring pellets that had completed sclerotome induction into 6 cm low-attachment dishes (Corning). A maximum of 20 pellets per dish was grown in 5-6 ml of chondrocyte differentiation medium. Dishes were rotated at 60rpm at 37ºC, 5% CO_2 and the medium was changed every other day. RNA was extracted from the pellets at different time points.

4.2.3 FACS of SOX9$^+$/PDGFRα$^+$ cells

The day 5 sclerotome cells were harvested using TryPLE as described above. Cell preparation for FACS is described in Chapter 2, section 2.18. The Alexa Fluor 488 anti-PDGFRα primary antibody diluted 1:50 in FACS buffer was added to the cell suspension and incubated for 30-minutes on ice in the dark. Two washes with FACS buffer removed excess antibody. Cell pellets were resuspended in 10mL FACS buffer with 300µL of 1ng Propidium Iodide (Sigma-Aldrich). SOX9 $^+$/PDGFRα$^+$ cells were sorted using Influx cell sorter (BD) at the flowcytometry core facility, MCRI.

4.2.4 Trypsin digestion for non-cartilage tissue removal

Pellets with at least 50% cartilage tissue (assessed by Toluidine blue staining of the pellet histology sections) were treated with trypsin to remove non-cartilage tissues. Pellets were rinsed with DPBS then transferred into 1.5mL Eppendorf tube containing 1mL of 0.025% trypsin-EDTA. Incubation was for 7.5 minutes at 37ºC with shaking at 800rpm. Trypsin was removed and the pellets were transferred back to swirl culture. To assess the removal of non-cartilage tissues, at least a week after the digestion, pellets were harvested and formalin fixed. Histology sections were collected and Toluidine blue staining and immunostaining were performed.

4.3 Results

4.3.1 The administration of different types of chondrogenic growth factors

Primary chondrocytes tend to lose their differentiated phenotype in monolayer culture (120, 299) and following continuous passaging (299). Hence, a micromass 3-dimensional culture, a widely accepted culture format for chondrogenic cells was performed to increase the differentiation efficiency. To begin the chondrocyte differentiation protocol optimisation, we compared 4 growth factors, FGF2 (18, 224), BMP4 (19), TGFβ3 (19, 300), and GDF5 (18, 224) that have been described as chondrogenic. These growth factors were added after sclerotome differentiation (Figure 4-2).

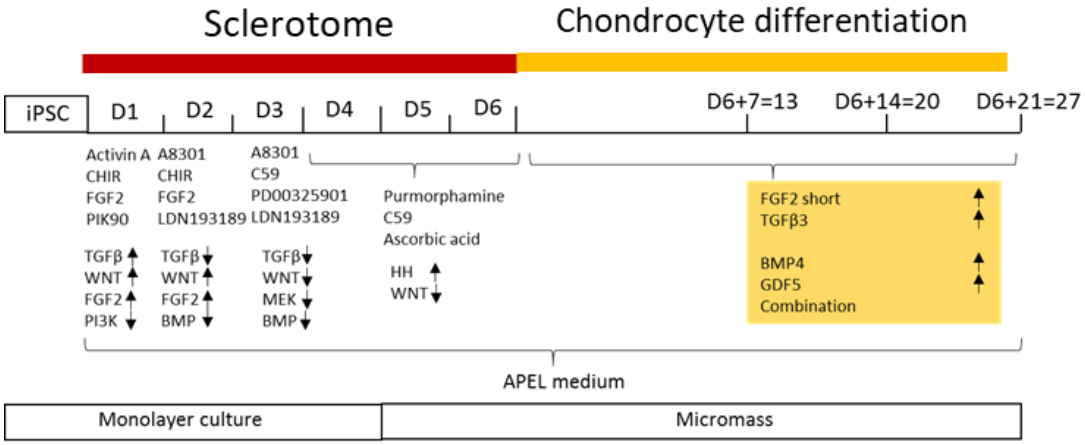

Figure 4-2. Experiment design: administration of different types of chondrogenic growth factors (yellow box).

To know the expression of chondrogenic markers after growth factor treatment, qPCR was performed at day 6+21 pellets. qPCR data showed that the FGF2 treated cultures had the highest chondrogenic marker expression when compared to other growth factors (Figure 4-3). FGF2 upregulated the expression of the key chondrogenic markers *SOX9*, *ACAN*, *COL2A1*, and *COL9A1*. The expression of our gene of interest, *TRPV4*, was also upregulated in FGF2 treated culture.

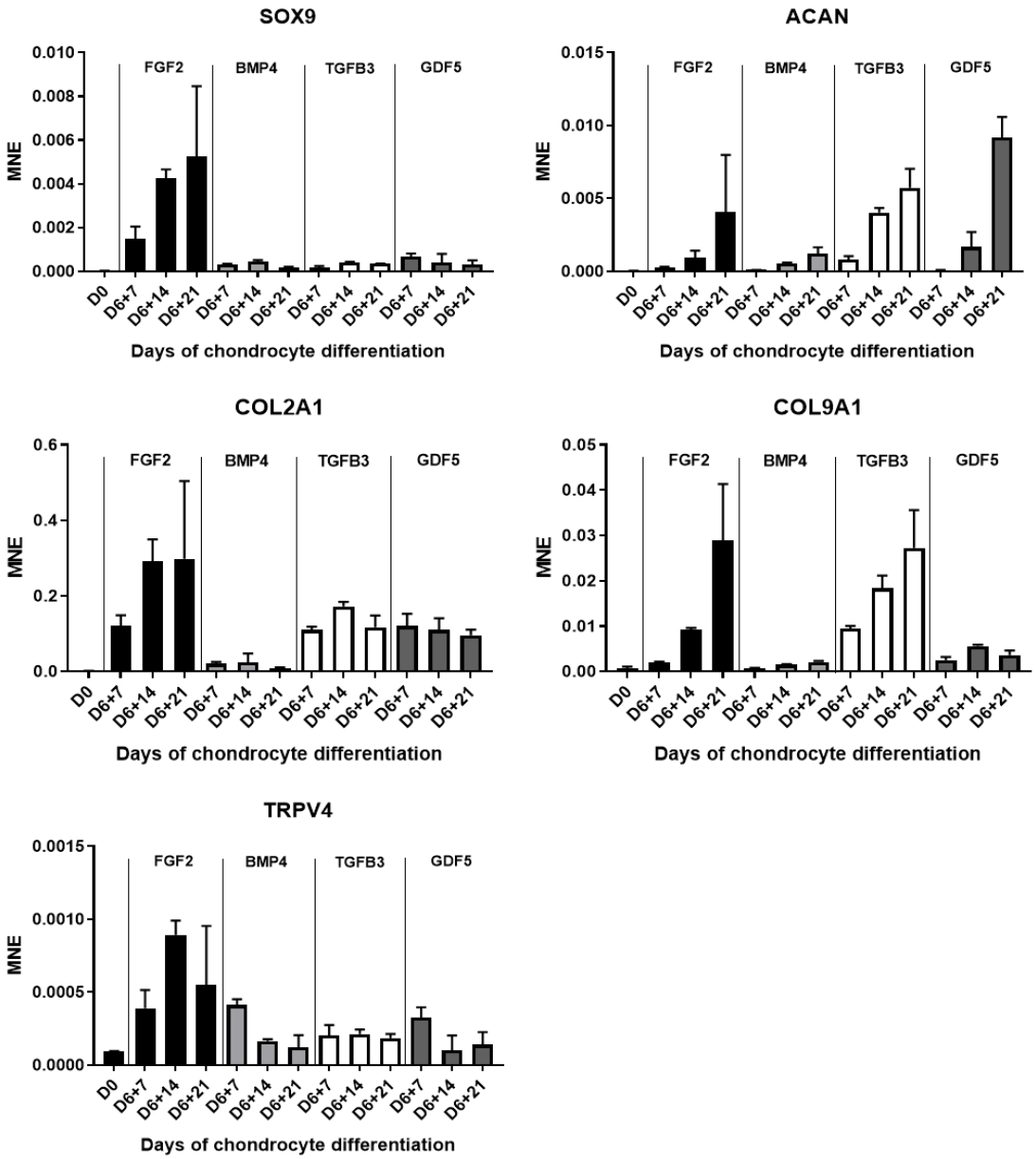

Figure 4-3. qPCR of chondrogenic marker expression following chondrocyte differentiation with different growth factor treatments. The data are based on three technical replicates and are presented as MNE. Error bars: SD.

TGFβ3 showed an interesting phenomenon in which it significantly upregulated *ACAN*, *COL2A1*, and *COL9A1* but not *SOX9* indicating that TGFβ3 might promote *ACAN*, *COL2A1*, *COL9A1* expressions through *SOX9*-independent manner. GDF5 also showed interesting phenomenon in which it only upregulated *ACAN*. On the other hand, BMP4 showed a weak chondrogenic activity as it failed to upregulated chondrogenic markers. Based on these results, FGF2 treatment will be used in chondrocyte differentiation.

4.3.2 Culture format manipulation

Since pellet format is also widely used in chondrogenic cell culture, micromass and pellet culture were compared. The design of the experiment is shown in Figure 4-4.

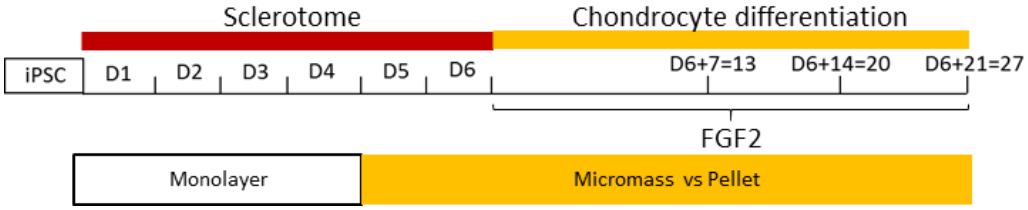

Figure 4-4. Experiment design: culture format manipulation

4.3.2.1 Chondrogenic marker expression was similar between micromass and pellet culture

To assess the difference in chondrogenic marker expression between pellet and micromass culture, qPCR was performed. The chondrogenic markers *SOX9*, *ACAN* and *COL2A1* were upregulated during chondrocyte differentiation in the two culture formats (Figure 4-5). In both culture formats, *SOX9* expression was at the highest at differentiation day 6 (sclerotome stage) and decreased at differentiation day 6+7 however pellet culture had higher *SOX9* expression in each time point. *ACAN* expression gradually increased and reached the highest level at day 6+21 in both culture formats. On the other hand, *COL2A1* expression peaked on day 6, then gradually decreased during a 3-week culture. However, *COL2A1* expression at day 6+21 was still higher than day 0. *TRPV4* expression was upregulated during a 3-week culture, with peak expression at day 6+7 in both culture formats. These results concluded that the key chondrogenic marker expression was similar between micromass and pellet culture format. Since pellet culture was easier to set up, pellet culture was used in this study.

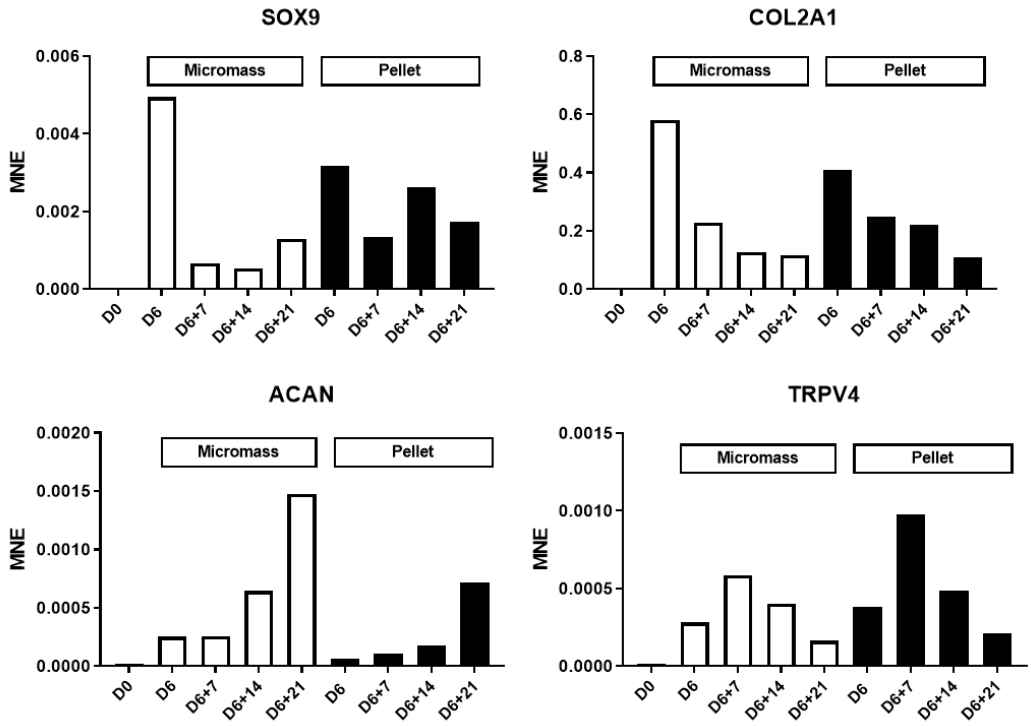

Figure 4-5. The expression of *SOX9*, *ACAN*, *COL2A1*, and *TRPV4* during chondrocyte differentiation in micromass and pellet culture. The data are from three technical replicates and are presented as MNE.

4.3.2.2 RNA sequencing data obtained from day 6+14 pellet showed characteristics of immature cartilage

To get an overall picture of the cartilage gene expression of the pellet cartilage, RNA sequencing was performed in day 6+14 pellets generated from PB001.1 and SOX9-T2A-tdTom. The RNA sequencing data were compared to the publicly available RNA sequencing data generated from 5 independent healthy human fetal cartilage (40) and cartilage selective gene expression was assessed. The list of cartilage selective genes was previously generated by Li, Balasubramanian (40) and it consists of 332 cartilage genes. RNA sequencing data analysis found that the chondrogenic markers such as *COL2A1* (Figure 4-6A), *ACAN* (Figure 4-6B), *SOX9*, *SOX5* and *SOX6* (Figure 4-6B) were expressed in the pellets. Other cartilage collagens such as collagen type VI, IX, X, and XI were also expressed (Figure 4-6A). However, the expression of these genes in day 6+14 pellets was lower than in fetal cartilage. Cartilage selective genes expression such as *TRPV4, ELN, CILP2, HAPLN1,* and *MATN2* were low and the expression of *COMP, PRG4, MATN1, MMP3,* and *MMP13* were extremely low when compared to fetal cartilage (Figure 4-6B). The day 6+14 pellets also expressed chondrogenic growth factors including *FGF2, TGFB1, TGFB3, BMP2, BMP4. FGF18, BMP6,* and *GDF5* were very lowly expressed (Figure 4-6C). Interestingly, *SHH* expression in day 6+14 pellets was higher than in fetal cartilage consistent with its significant roles in early chondrogenesis (Figure 4-6C). Collectively, these results suggest that the pellets expressed lower cartilage selective genes than fetal cartilage hence immature cartilage was generated.

To compare the overall cartilage selective gene expression between day 6+14 pellets and fetal cartilage, heatmap was generated. The heatmap showed that the expression of cartilage selective genes in day 6+14 pellets was lower than the fetal cartilage confirming the formation of less mature cartilage tissues in the pellets (Figure 4-7). The heatmap also showed that the cartilage selective gene expression was similar between PB001.1 and SOX9-T2A-tdTom confirming that the SOX9 function in SOX9-T2A-tdTom hiPSC line was intact after reporter gene insertion.

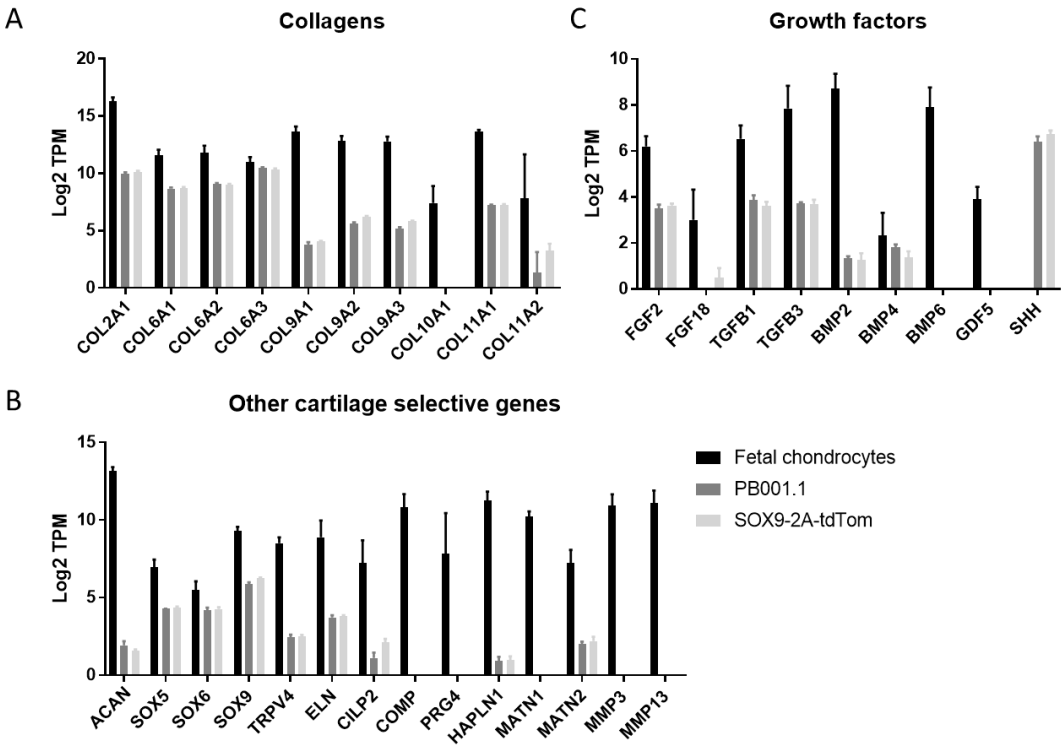

Figure 4-6. The expression of collagens (A), cartilage selective genes (B) and chondrogenic growth factors (C) in day 6+14 pellets and fetal cartilage. The pellet cartilage data were based on three technical replicates. Y-axis shows the log2 TPM (transcripts per million).

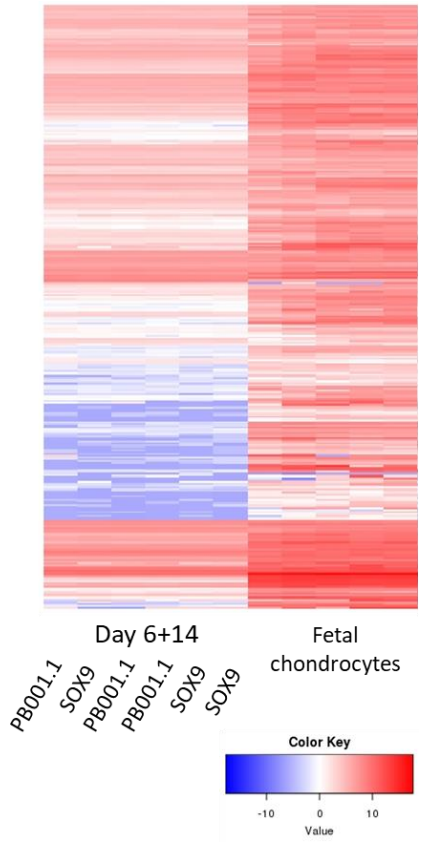

Figure 4-7. Heatmap analysis of the 332 cartilage selective genes in PB001.1 and SOX9-T2A-tdTom. Three replicates from each cell line were used to generate the data.

To confirm the maturity of the day 6+14 pellet cartilage, collagen type II isoform A (IIA) and isoform B (IIB) expression were measured. The IIA isoform mRNA retains exon 2 and is highly expressed by chondroprogenitor cells whereas IIB has exon 2 spliced out and is highly expressed by mature chondrocytes (60-63). Since the switching of IIA to IIB uniquely occurs in chondrogenesis, it can be used as a marker for chondrocyte maturity. Thus, to confirm the maturity of the pellet cartilage, PCR of the cDNA targeting the splicing site of *COL2A1* was performed. The PCR showed that the majority of *COL2A1* isoform expressed in day 6+14 SOX9-T2A-tdTom pellet was IIA isoform whereas in 2-year old human articular cartilage, IIB isoform dominated the *COL2A1* expression (Figure 4-8). Taken together, the lower expression of cartilage selective genes and the higher expression of IIA isoform of *COL2A1* in the pellet than in the fetal cartilage confirmed that the cartilage-like tissues in day 6+14 pellet was immature. Therefore, to obtain more mature cartilage-like tissue, the culture period was extended out to 10 weeks.

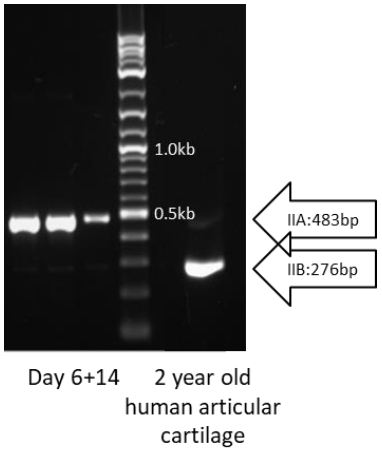

Figure 4-8. The expression of *COL2A1* isoforms in day 6+14 SOX9-T2A-tdTom pellet and human articular cartilage. The IIA isoform in which exon 2 is retained; comprised the major proportion of *COL2A1* being expressed in day 6+14 SOX9-T2A-tdTom pellet.

4.3.3 Extended culture increased chondrogenic marker expressions

To obtain more mature cartilage tissue, SOX9-T2A-tdTom pellets were cultured for 70 days (10 weeks) after sclerotome induction (Figure 4-9). PCR on the cDNA which targeted the splicing site of *COL2A1* was performed to assess the maturation of pellet cartilage. The switching of *COL2A1* isoform from IIA to IIB was observed at week 5 (day 6+35) of culture (Figure 4-10). The proportion of the IIB isoform gradually increased during extended culture indicating that chondrocyte maturation was occurring.

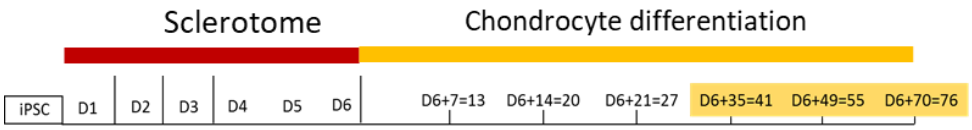

Figure 4-9. Experimental design: long-term culture

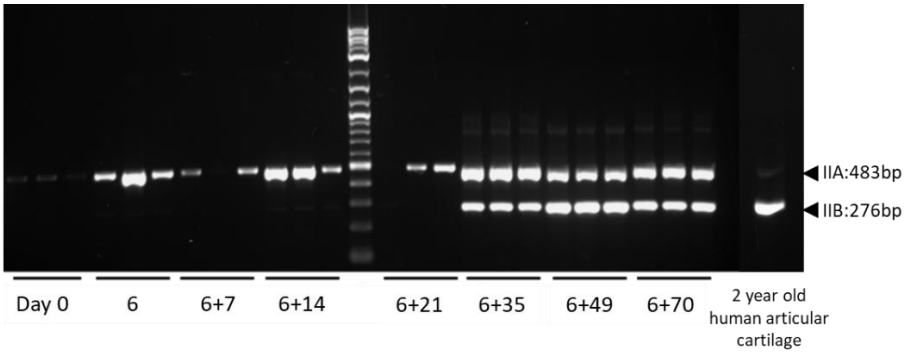

Figure 4-10. PCR of COL2A1 isoform IIA and IIB using cDNA extracted from pellet culture in different time points of chondrocyte differentiation.

Extended culture also resulted in significant upregulation of chondrogenic marker expression (Figure 4-11). *SOX9*, *COL2A1*, *COL9A1*, and *ACAN* expression increased by 2-3, 10, 20-35, and 300 fold respectively compared to day 0. *TRPV4* expression also steadily increased during extended culture and by the end of the culture, it was increased by 30 fold as compared to day 0 (Figure 4-11). Therefore, in the subsequent chondrocyte differentiation experiment, FGF2 treatment and extended culture were applied.

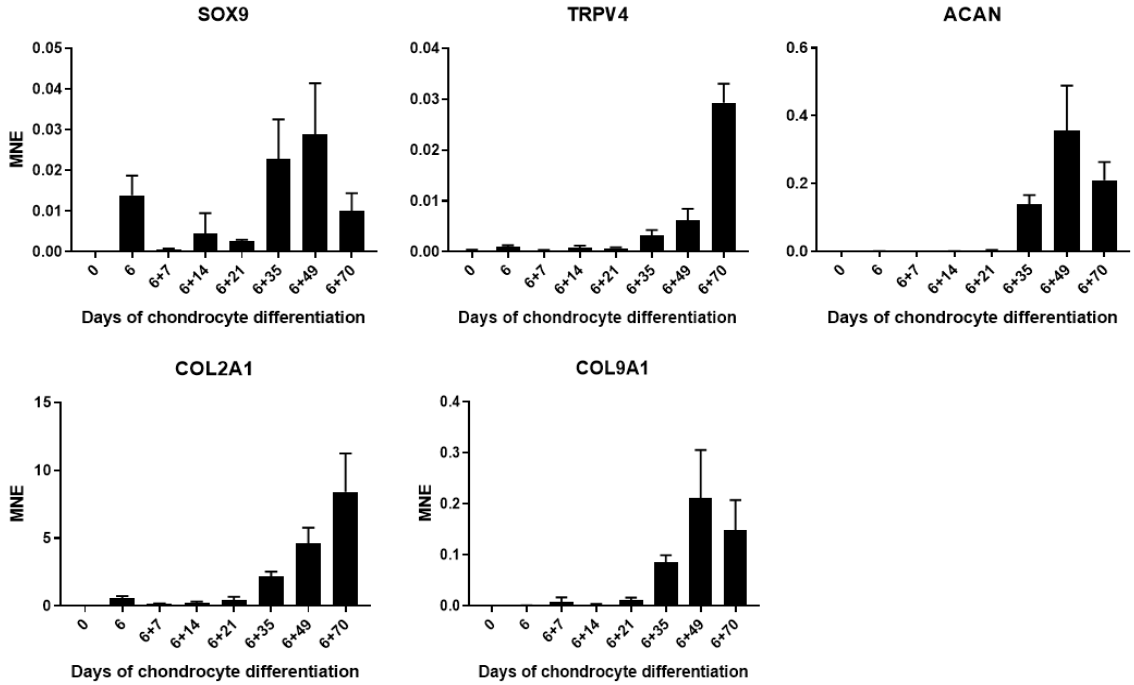

Figure 4-11. The expression of chondrogenic markers in long-term culture. Pellet cultures were grown for up to 10 weeks. The data were obtained from at least two technical replicates and presented as MNE. Error bars: SD

4.3.4 Swirl culture pellets had higher chondrogenic marker expressions

To further optimise the culture conditions, swirl culture was performed after sclerotome induction. The swirl culture had been adopted in certain types of bioreactors (301) for chondrocyte culture which resulted in higher chondrogenic marker expression (302, 303). In the swirl culture, pellets were cultured in 6cm-dishes on a rotating platform. Pellets were established from day 4 sclerotome cells and allowed to complete sclerotome induction in 96-well plates for 2 days before being transferred to 6cm-dishes for swirl culture (Figure 4-12). After 5 weeks in culture, the swirled pellets were significantly larger than static pellets (Figure 4-13A). The expression of SOX9 protein, tagged by tdTom fluorescence, was also higher in pellets grown in swirl culture indicated by the more intense red fluorescence.

To compare the chondrogenic marker expression between swirled and static pellets, qPCR was performed. qPCR showed that swirled pellets had higher chondrogenic marker expression than the static ones (Figure 4-13B). *SOX9* and *COL2A1* expression were doubled and *ACAN* expression was 5 fold higher in swirled pellets compared to the static pellet.

To assess the microscopic structure of the pellets, histology was performed. The histology sections were stained with Toluidine Blue, a specific stain for proteoglycans. Cartilage tissue positive with Toluidine blue staining indicated by intense purple colour. The staining showed that day 6+35 pellets in swirl culture had a larger Toluidine blue-stained area than the static ones (Figure 4-14). However, non-cartilage tissues were observed, hence the culture was stopped and further optimisation was undertaken.

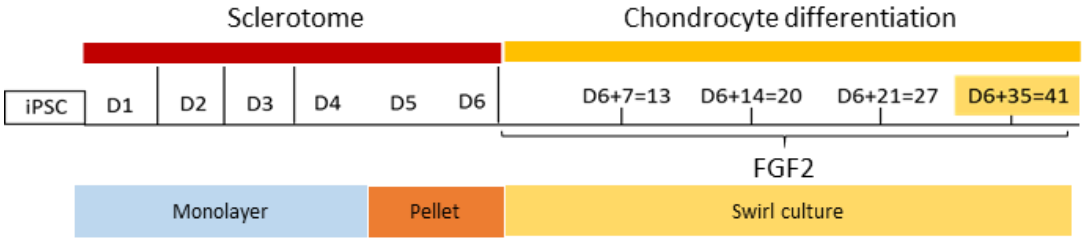

Figure 4-12. Experiment design: swirl culture

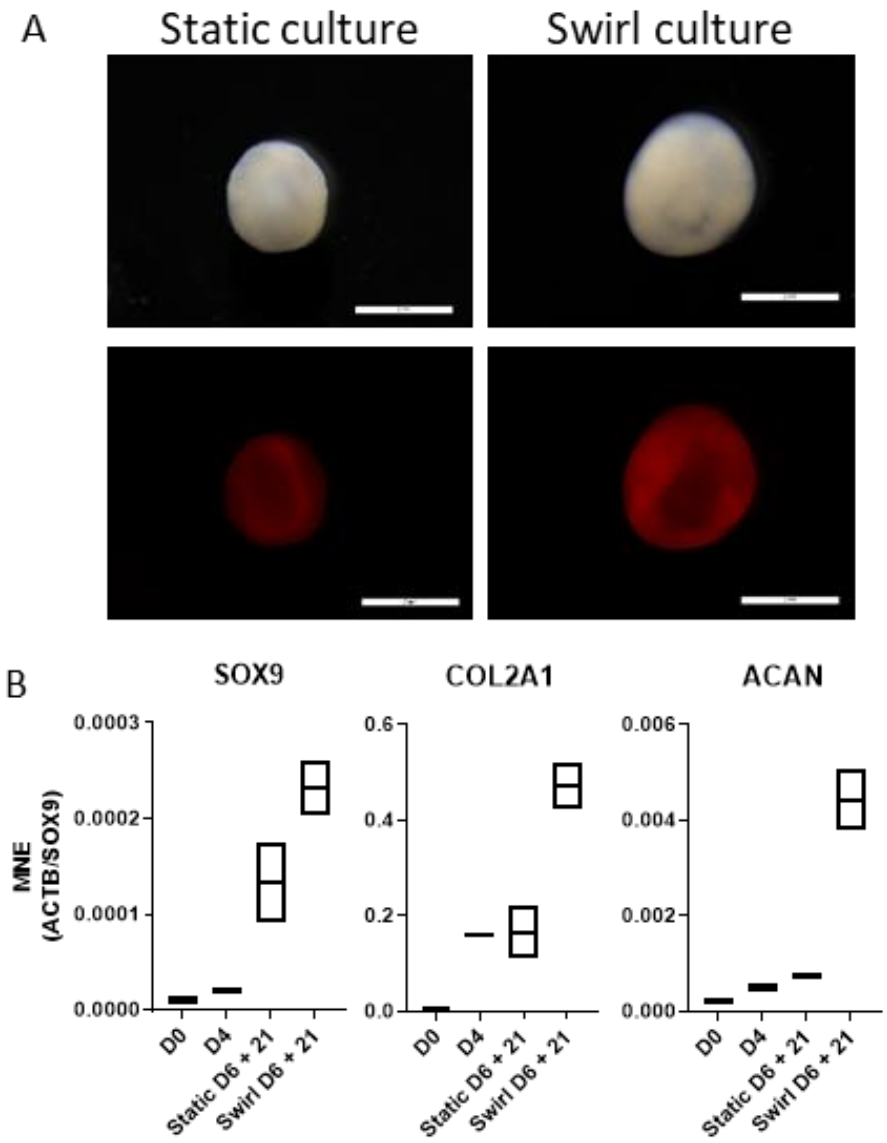

Figure 4-13. The comparison of pellet size and chondrogenic marker expression between static and swirl pellet culture. The chondrogenic marker expression is generated from 2 technical replicates and are presented in MNE.

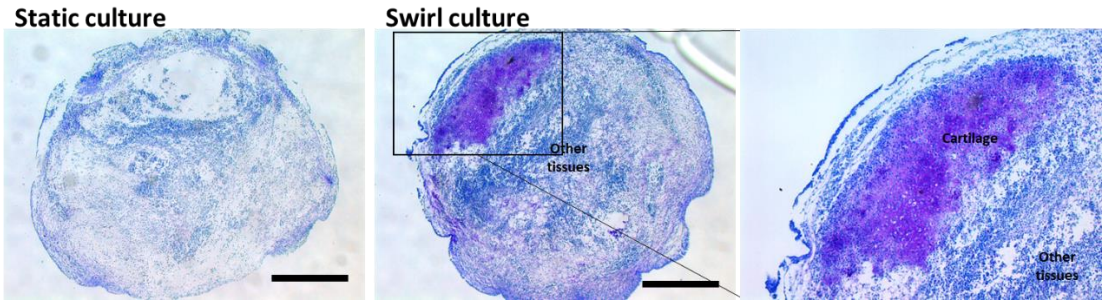

Figure 4-14. Toluidine blue staining of day 6+35 pellets in a swirl and static cultures. Cartilage tissues are positive with Toluidine blue staining indicated by intense purple colour. The faint purple colour found in some other areas likely indicates less mature cartilage tissues as the pellet is only 6+35 day-old. Some other areas negative to Toluidine blue staining suggests non-cartilage tissues.

4.3.5 Chondrogenic cell population enrichment using FACS

Since the histology showed the presence of non-cartilage tissues in the pellets; it might be plausible that these non-cartilage tissues were derived from the SOX9-negative cell population (see Chapter 3, section 3.3.8). Therefore, to further optimise the chondrocyte differentiation, flowcytometry assisted cell sorting (FACS) was performed during sclerotome induction in order to remove the SOX9-negative cell population thus enriching the SOX9-positive cell for chondrocyte differentiation.

Studies show that PDGFRα expressing cells are able to form cartilage-like tissue in micromass cultures (19, 235). Moreover, in a single-cell RNA sequencing analysis; the proportion of PDGFRα-expressing cells that expressed both SOX9 and COL2A1 is high (17). Therefore, collecting cells that express both PDGFRα and SOX9 could be a promising strategy to enrich the chondrogenic cell population.

To check the expression of PDGFRα, flowcytometry was performed. Flowcytometry analysis on day 4 cells showed two distinct cell populations, PDGFRα^{+}/SOX9^{+} and PDGFRα^{-}/SOX9^{-}. The separation of these two cell populations was more apparent on day 5 and 6 (Figure 4-15A). The proportion of non-chondrogenic cells, PDGFRα^{-}/SOX9^{-} cells, gradually increased starting from 10.3% on day 4 to 28.2% on day 6. Hence, to remove these non-chondrogenic cells, we FACS sorted PDGFRα^{+}/SOX9^{+} cell population from differentiation day 5 cells (Figure 4-15B, green box). This time point was chosen because the day 5 cells were easier to be dissociated than day 6 cells.

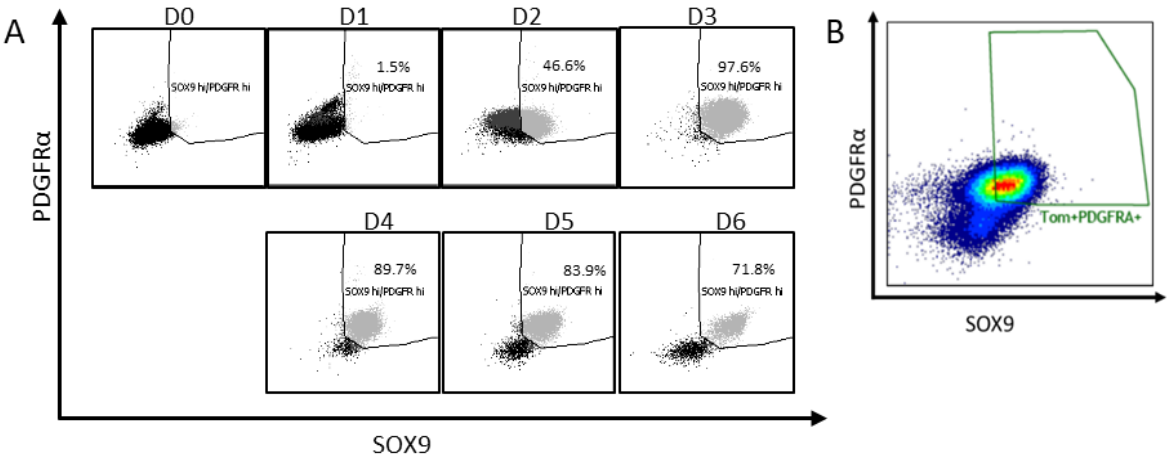

Figure 4-15. PDGFRα and SOX9 expression during sclerotome induction. Two cell population was observed in flowcytometry analysis based on PDGFRα and SOX9 expression (A). PDGFRα^{+}/SOX9^{+} cell population (green box) is collected from day 5 sclerotome (B).

The pellet cultures (200,000 cells/pellet) were set up soon after the cell sorting and they were cultured in sclerotome induction medium for 24 hours. At day 7, the pellets were transferred into swirl culture and the medium was replaced with chondrocyte differentiation medium with FGF2 supplementation. Extended culture was performed at 37ºC, 5% CO2 (Figure 4-16) and histology with Toluidine blue staining was undertaken in different time points to check the presence of non-cartilage tissues. Toluidine blue staining of day 6+28 and 6+44 showed that non-cartilage tissues were still present in the pellets (Figure 4-17A) suggesting that sorting PDGFRα^{+}/SOX9^{+} cell population at day 5 was not able to remove the non-chondrogenic cells. Immunostaining of pellet histology sections showed that SOX9, COL2A1, and TRPV4 protein were highly expressed in cartilage tissue areas of day 6+44 pellets (Figure 4-17B).

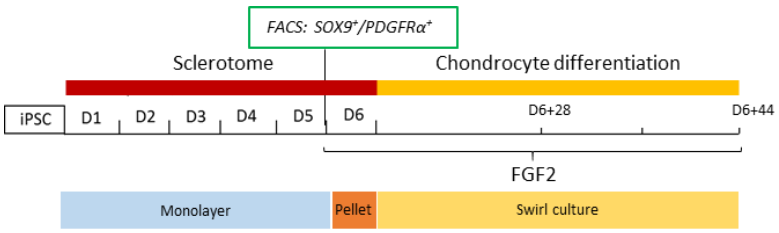

Figure 4-16. Experimental design: Swirl culture of PDGFRα^{+}/SOX9^{+} cells

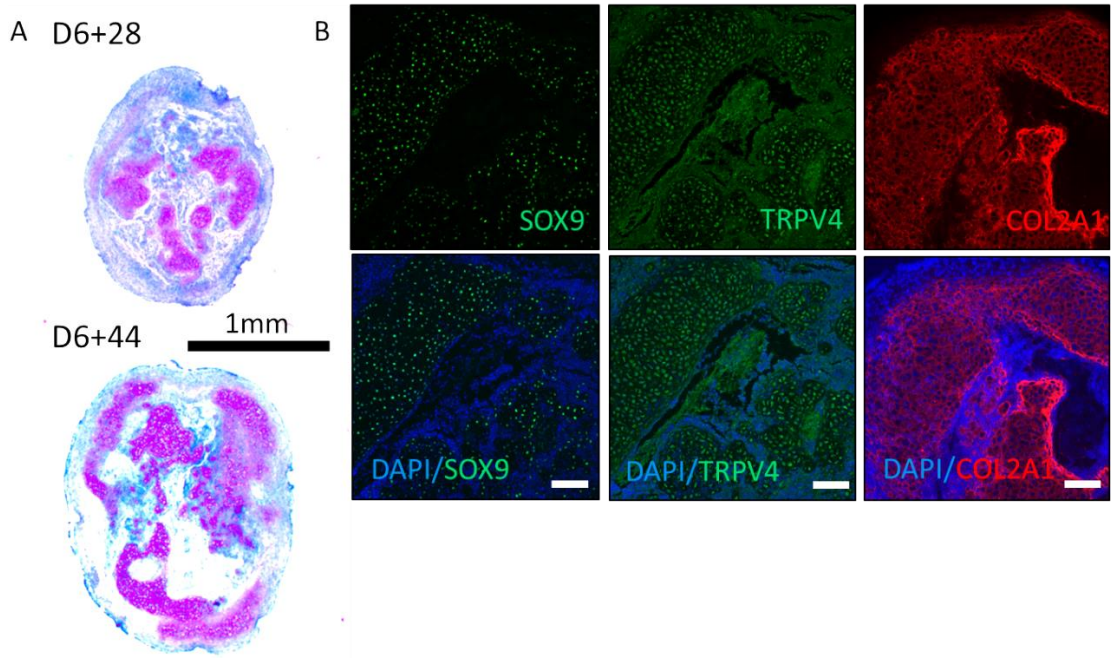

Figure 4-17. Histology of day 6+28 and day 6+44 pellets. Toluidine blue stains cartilage proteoglycan in deep purple colour (A). Immunostaining of SOX9 (B), COL2A1 (C) and TRPV4 (D) on day 6+44 pellets shows that these proteins are highly expressed in cartilage tissue area. The Toluidine blue staining and immunostaining images are representative of three technical replicates. Scale bar: 100µm.

4.3.6 Non-cartilage tissue removal using trypsin digestion

The presence of non-cartilage tissues would confound the cartilage gene expression profiling when the RNA or proteins are extracted from the whole pellets. Therefore, it is very important to remove the non-cartilage tissues before performing gene expression profiling. Since the chondrogenic cell enrichment during sclerotome induction using FACS was unsuccessful, instead of performing another cell sorting with different markers, trypsin digestion was performed on to the pellet to remove non-cartilage tissues. We found that by incubating the pellets in trypsin solution for 7.5 minutes with agitation, it could efficiently remove the non-cartilage tissues. Due to the large amount collagen type II and its triple-helical and fibrillary structure, pellet cartilage was relatively more resistant to prolonged-trypsin digestion and physical agitation than the non-cartilage tissues. By re-culturing the post-trypsin digested pellets into the chondrocyte differentiation medium for 7-10 days, it helped the chondrocytes to recover from the enzymatic digestion. The trypsin digestion resulted in pellets rich in cartilage tissues with minimal non-cartilage tissues (Figure 4-18).

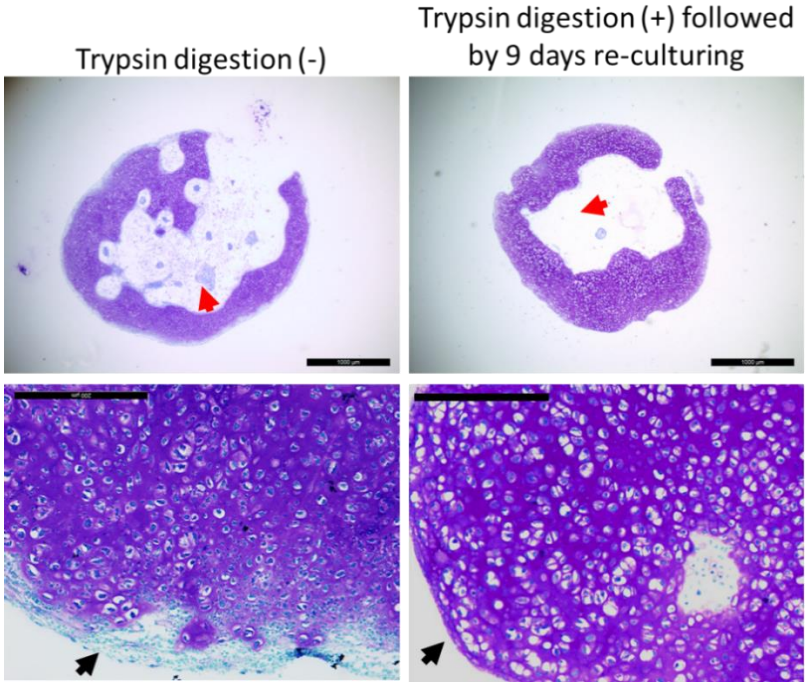

Figure 4-18. The comparison of pellets before and after trypsin digestion. The non-cartilage tissues in the centre (red arrow) and superficial surface (black arrow) of pellets were removed after trypsin digestion.

4.3.7 RNA sequencing of day 6+70 pellets revealed that the pellet cartilage was maturing

Trypsin digestion was performed in day 6+61 pellets to remove non-cartilage tissues and to enrich the cartilage tissue mass in the pellets. Re-culturing the post-digested pellets was performed for 9 days and day 6+70 pellets were harvested and RNA was extracted. To get an overall picture of the cartilage gene expression of the pellet cartilage cultured in extended-swirled culture, RNA sequencing was performed in day 6+70 pellets obtained from another batch of chondrocyte differentiation.

RNA sequencing data analysis compared the cartilage selective gene expressions between day 6+14, day 6+70, and publicly available human fetal cartilage RNA sequencing data (40). The collagens that are abundantly present in cartilage such as collagen type II, VI, IX, X, and XI were upregulated in day 6+70 pellets and their level of expression reached the expression level of fetal cartilage (Figure 4-19A). Similar findings were found for other cartilage selective genes such as *ACAN*, *SOX9*, *HAPLN1*, *MATN1*, *MATN3*, and *MATN4* (Figure 4-19B). Other cartilage selective markers such as *TRPV4*, *ELN*, *CILP2*, *COMP*, and *MMP13* were upregulated in day 6+70 pellets but their level of expression still lower than the fetal cartilage (Figure 4-19B). On the other hand, the expression of *PRG4* and *MATN3* were still very low in day 6+70 pellets (Figure 4-19B).

The known chondrogenic growth factors such as *FGF2, TGFβ1, TGFβ3, BMP2, BMP4*, *BMP6* and *GDF5* were upregulated in day 6+70 pellets, but the level of expression was lower than fetal cartilage. *FGF18* expression was not increased in day 6+70 pellets but the *SHH* expression was downregulated in day 6+70 pellets as compared to day 6+14 pellets (Figure 4-19C). To obtain the overall picture of the difference in cartilage selective gene expression between day 6+14 pellets, day 6+70 pellets and fetal cartilage, a heatmap was generated (Figure 4-20). The heatmap concluded that the pellets in an extended culture were maturing indicated by the upregulation of cartilage selective gene expression as compared to day 6+14 pellets (Figure 4-20). The heatmap once again demonstrated the similarity of chondrocyte differentiation capacity between SOX9-T2A-tdTom and its parental line, PB001.1.

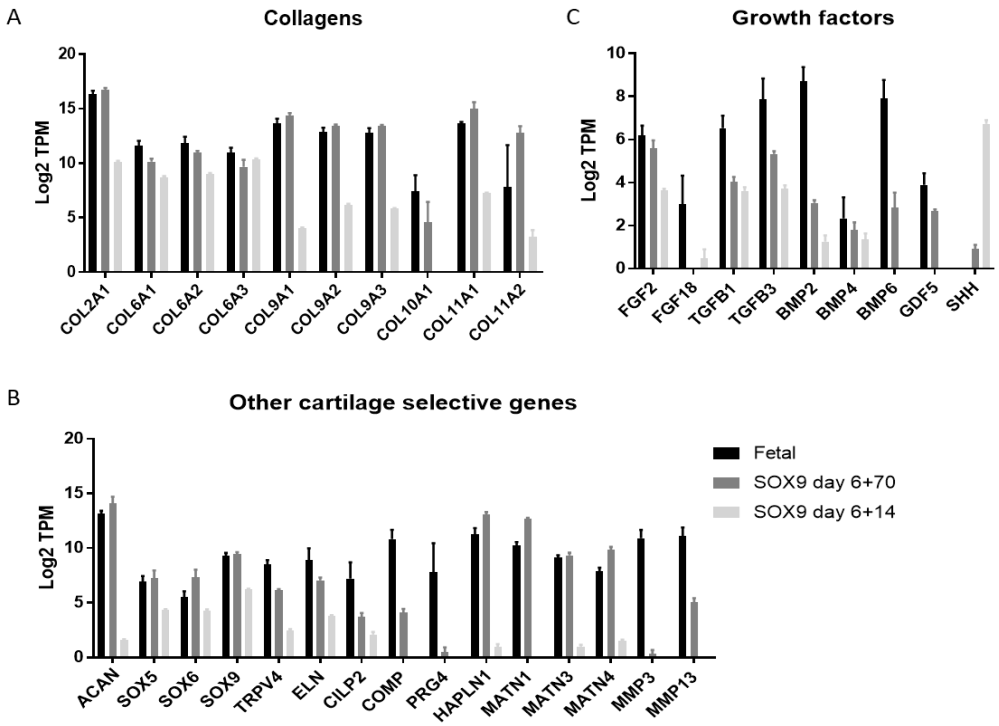

Figure 4-19. The comparison of cartilage associated gene expressions between human fetal cartilage, day 6+14 pellets, and day 6+70 pellets. The pellets were cultured in swirl format. The transcript level of each group is presented in the actual log2 transcript per million (log2TPM) value from 3 technical replicates. Error bars: SD.

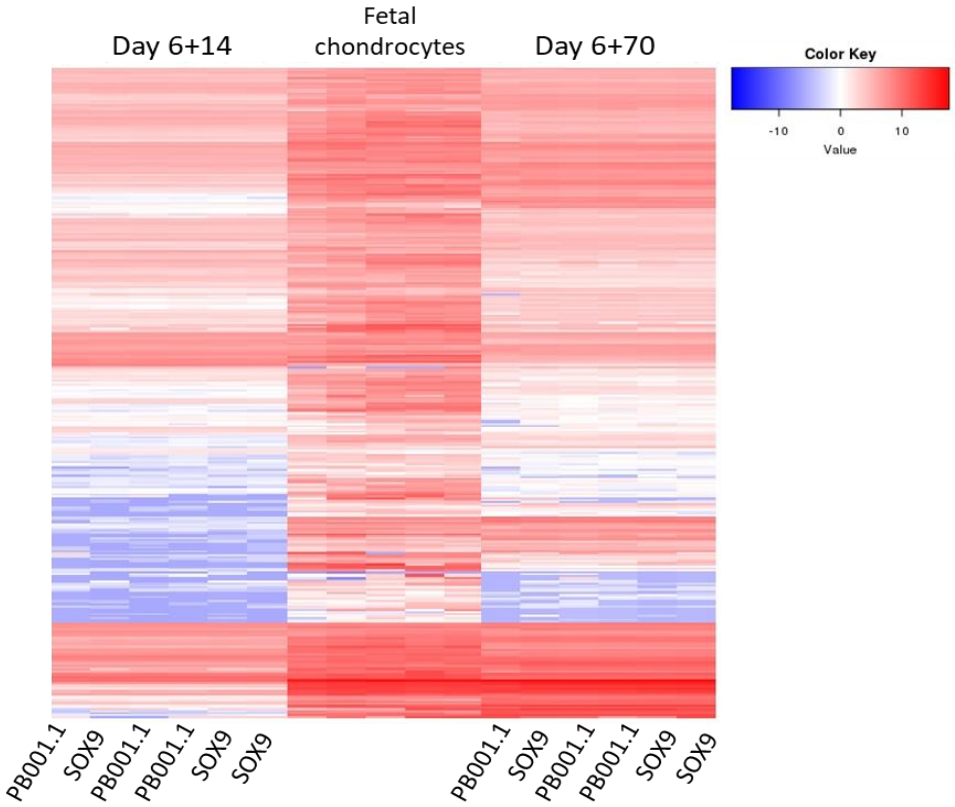

Figure 4-20. The heatmap of cartilage selective gene expression in human fetal cartilage, day 6+14 pellets, and day 6+70 pellets. The pellets were cultured in swirl format. The transcript level of each sample is presented in actual log2 transcript per million (log2TPM) value without scaling across the samples.

4.3.8 TGFβ3 and GDF5 supplementation for chondrocyte differentiation

Another strategy to improve the chondrocyte differentiation further was the administration of TGFβ3 and GDF5. The combination of TGFβ3 and GDF5 treatment was selected since in the earlier experiment (see section 4.3.1), TGFβ3 upregulated the expression of *ACAN*, *COL2A1*, and *COL9A1* while GDF5 upregulated the expression of *ACAN* (Figure 4-3). TGFβ3 and GDF5 were administered after a 4-week course of FGF2 treatment (Figure 4-21).

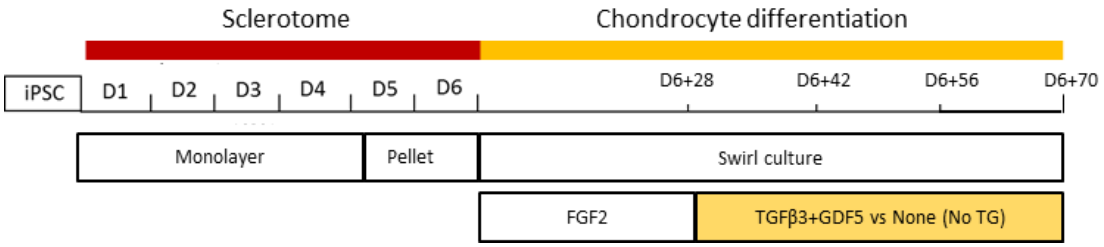

Figure 4-21. Experimental design: TGFβ3 and GDF5 treatment (TG) vs. None (No-TG). The protocol modifications are highlighted in yellow.

4.3.8.1 TGFβ3 and GDF5 supplementation resulted in distinct cartilage tissue phenotype

Histology was performed to assess the microscopic structure of the pellet cartilage. The pellets with TGFβ3 and GDF5 treatment (TG protocol) were larger than pellets without TGFβ3 and GDF5 treatment (No-TG protocol) (Figure 4-22A). Toluidine blue staining showed different histological characteristics between pellets cultured in TG vs. No-TG. The extracellular matrix in the TG protocol was more abundant than in the No-TG protocol (Figure 4-22B-C) which might explain the larger pellet size in the TG than No-TG protocol. This finding suggested that TGFβ3 and GDF5 promoted cartilage matrix production. Interestingly, the chondrocytes in the No-TG protocol looked larger than the ones in the TG suggesting that TGFβ3 and GDF5 could potentially inhibit chondrocyte development towards hypertrophic chondrocytes.

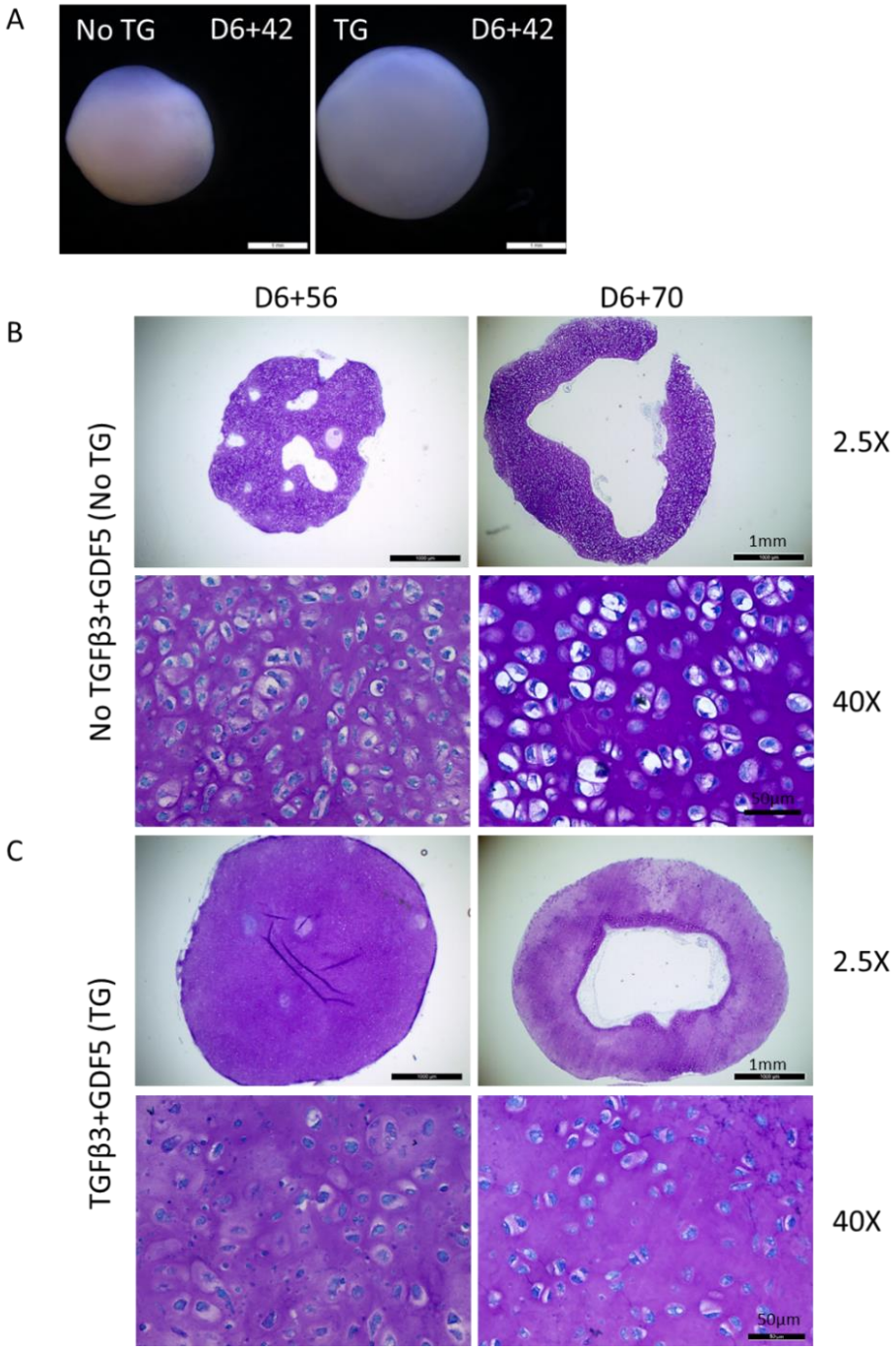

Figure 4-22. The comparison of pellets cultured with and without TGFβ3+GDF5 treatment (TG vs. No-TG). The day 6+42 pellet size and SOX9 expression (tagged with tdTom fluorescence protein) (A) were representative of at least 6 different pellets. Toluidine blue staining was performed in two different time points (day 6+42 and 6+70).

COL2A1 immunostaining showed that the TG had greater areas of collagen type II than the No-TG protocol (mean of area = 73741.14μm^2 vs. 41095.66μm^2, $p<0.0001$) (Figure 4-23A and B). The COL2A1 fluorescence intensity was not statistically different between TG and No-TG protocol (Figure 4-23C). TRPV4 protein expression was also higher in TG than No-TG cartilage (mean fluorescent intensity =28.05 vs 17.88, $p<0.01$)

(Figure 4-23D, E). Confirming the Toluidine blue staining results, the chondrocytes in No-TG protocol looked larger than the ones in TG protocol indicated by the bigger lacuna size (dark area) (Figure 4-23A). This could suggest that the No-TG chondrocytes were more hypertrophic than TG chondrocytes.

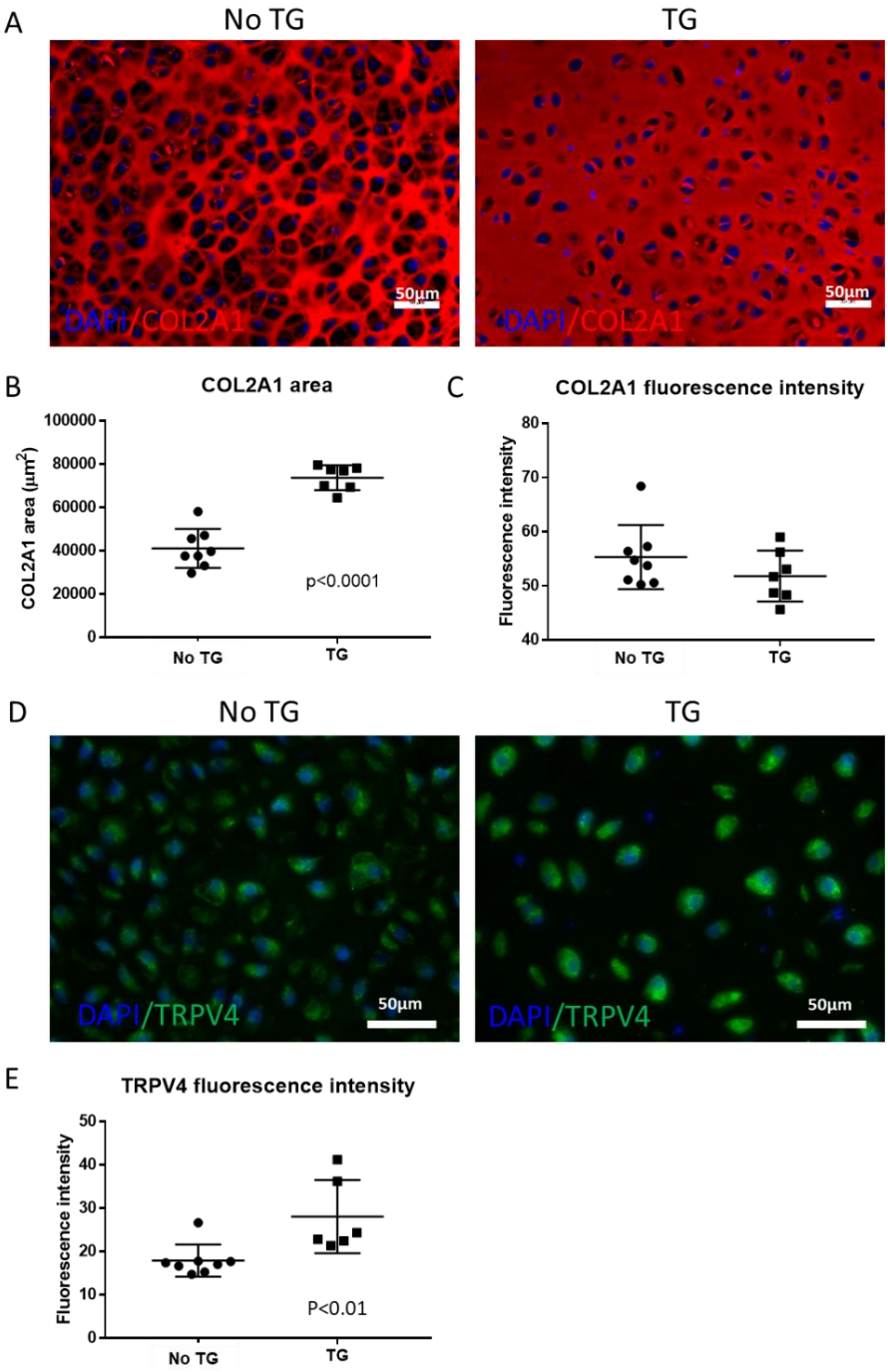

Figure 4-23. Immunostaining of COL2A1 and TRPV4 of day 6+56 SOX9-2A-tdTom pellets. Quantification of fluorescence area and intensity are obtained from at least 6 images per section (n=1 pellet) captured from randomly selected areas with objective magnification X20 (COL2A1) and X40 (TRPV4). Each dot in the graph represents one image. T-test statistics is used to compare the mean between two groups with error bars represent the SD of the mean.

4.3.8.2 RNA sequencing data showed differences in overall gene expression pattern between TG and No-TG cartilage

4.3.8.2.1 Gene ontology (GO) annotation of the differentially expressed genes between TG and No-TG cartilage showed the over-representation of skeletal development-related GO terms in TG protocol.

To compare the overall gene expression between TG and No-TG protocol, RNA sequencing was performed. PCA plot using the first and second principal components highlighted the differences in overall gene expression between fetal, TG, and No-TG cartilage with the first principal component explained 55% of the variance (Figure 4-24A). Heatmap of 332 cartilage selective gene expression showed that both TG and No-TG cartilage closely resembled human fetal cartilage (Figure 4-24B).

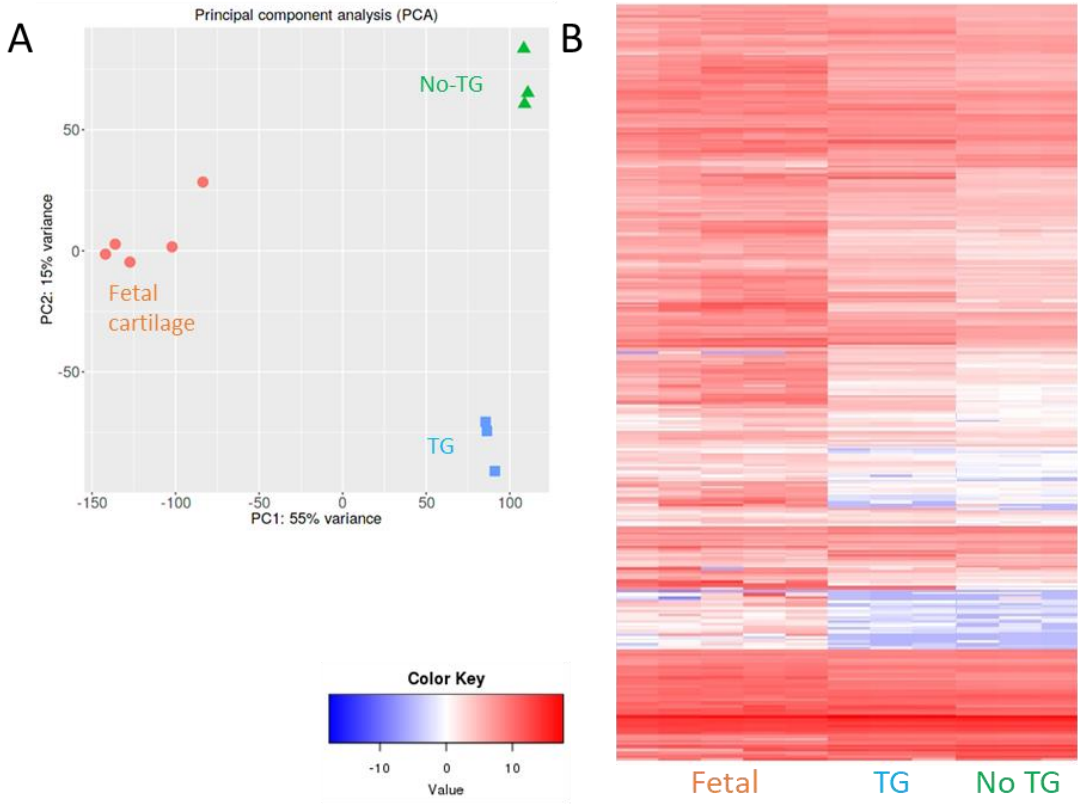

Figure 4-24. The PCA plot and heatmap of cartilage selective gene expression in human fetal cartilage, day 6+70 pellet cultured in TG and No TG chondrocyte differentiation protocol.

Differential gene expression analysis was performed in the RNA sequencing data to compare gene expression levels between TG and No-TG cartilage. The transcripts with fold change > or < 1 and adjusted p-value (adj.p-value) <0.05 were considered differentially expressed genes. The analysis found 549 differentially expressed genes with

376 genes were upregulated and 173 genes were down regulated in TG. The full list of the differentially expressed genes is available in Appendix 4.

Gene ontology (GO) annotations for the biological processes were performed separately between upregulated and downregulated differentially expressed genes using ClueGO bioinformatics tool. Only GO terms with adjusted p-value <0.01 were included in the analysis. The GO-terms for biological processes were clustered based on the similarity of genes contributing to the corresponding GOs. The number of genes contributing to the overrepresented GO terms was shown in Figure 4-25 and the cluster was indicated in different colours.

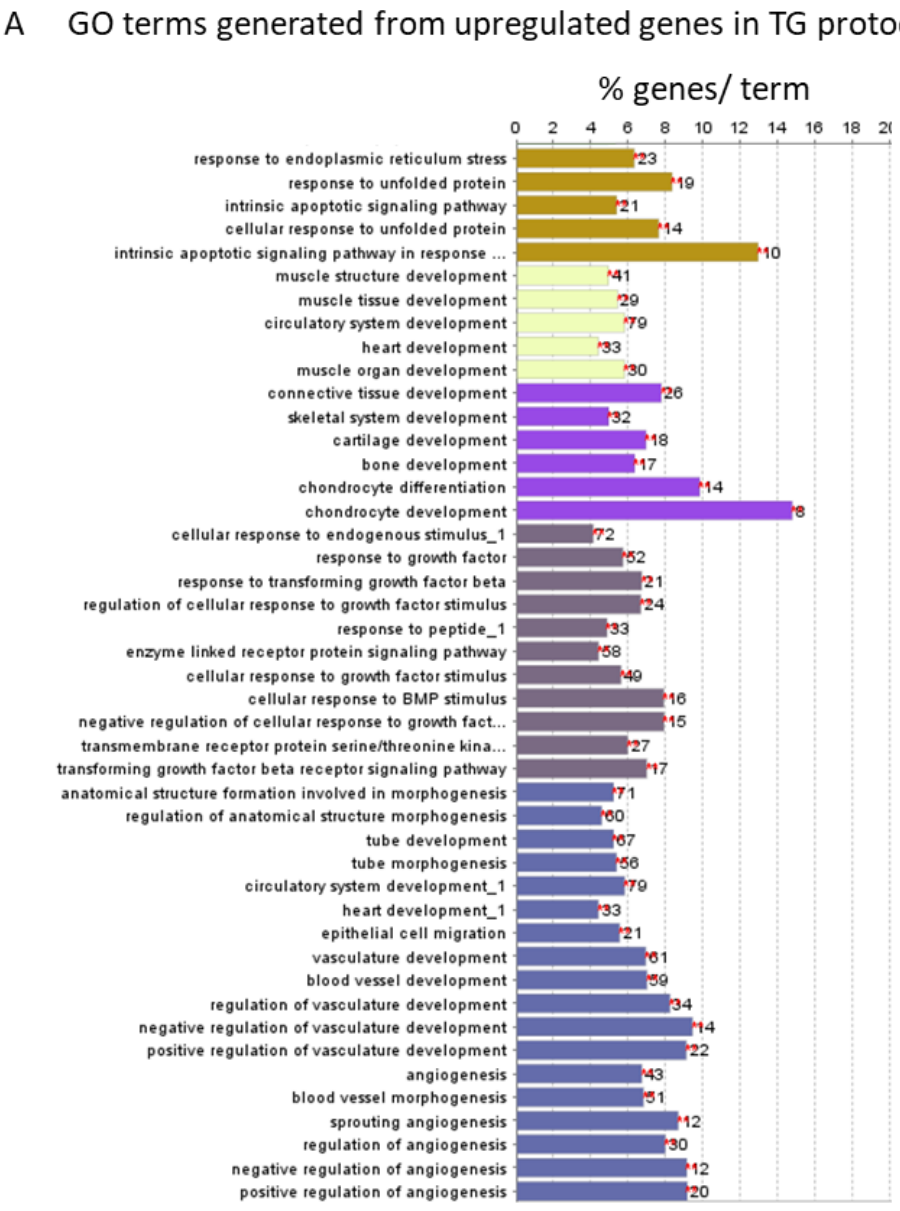

Figure 4-25. The enriched GO term for biological process generated using ClueGO. Bars represent the percentage of genes representing each term and the number represents the absolute number of differentially expressed genes in each term.

A GO terms generated from upregulated genes in TG protocol (cont.)

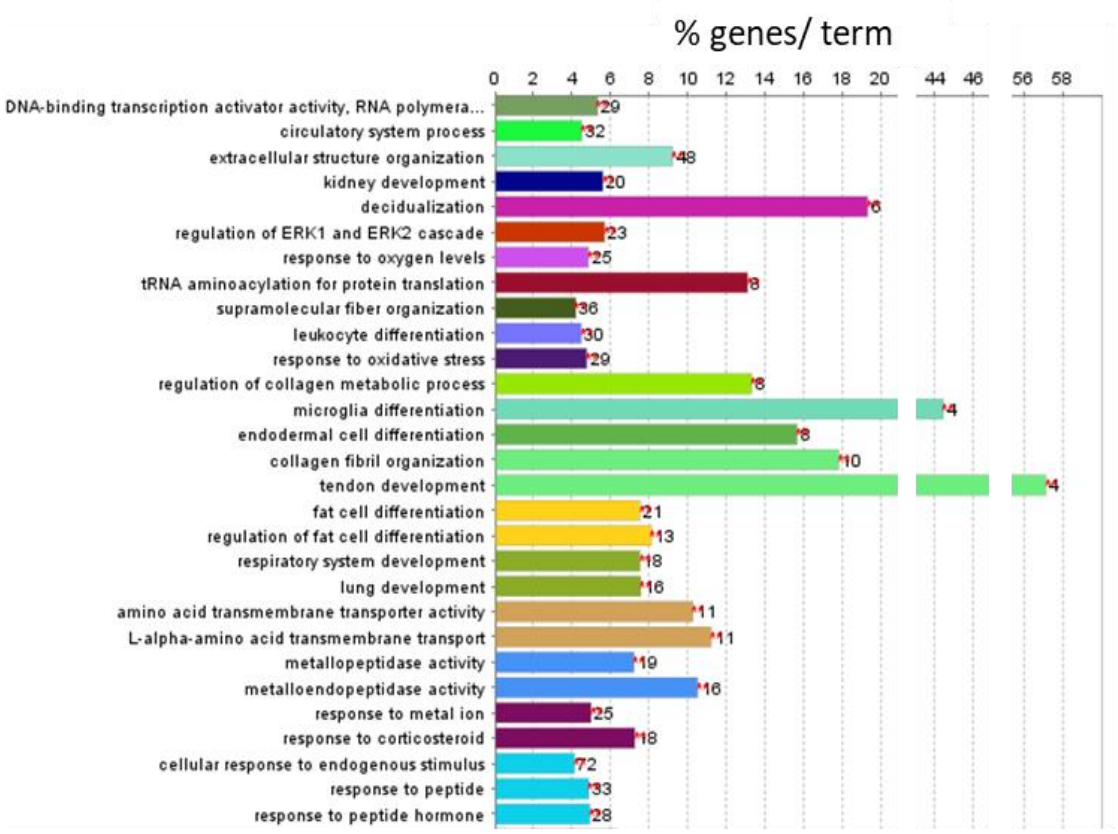

B GO terms generated from downregulated genes in TG protocol

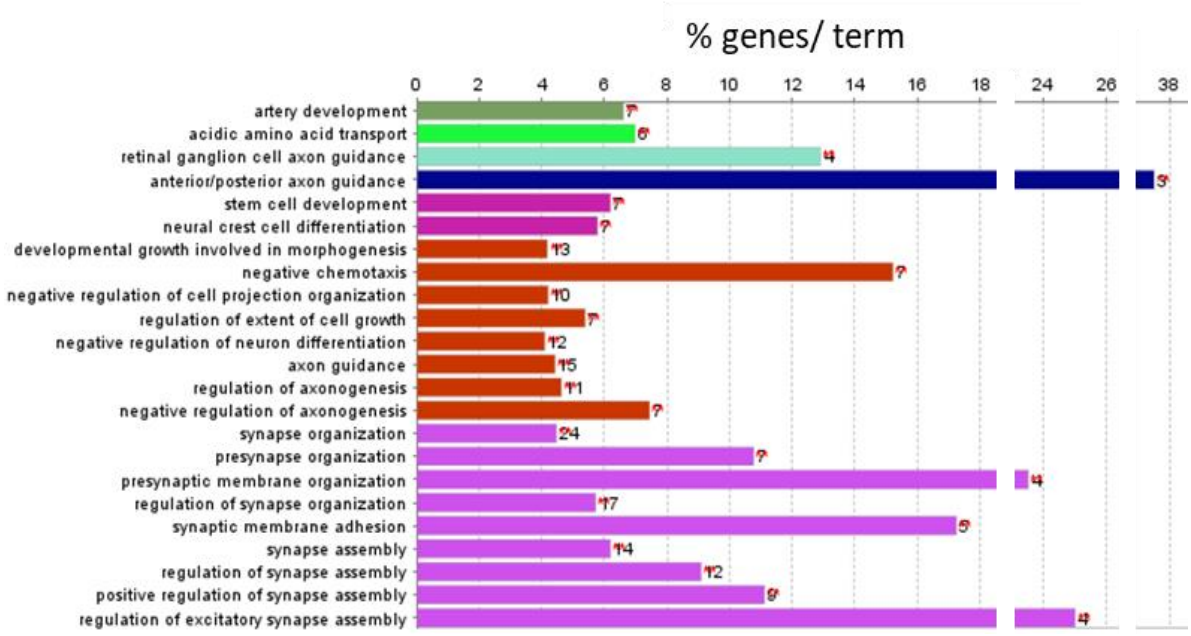

Figure 4-25. The enriched GO term for biological process generated using ClueGO. Bars represent the percentage of genes representing each term and the number represents the absolute number of differentially expressed genes in each term.

To know what kind of signalling pathways were involved in chondrocyte differentiation, pathway analysis was performed on the differentially expressed genes. Pathway analysis was performed using ClueGO with the enriched pathways were searched against the KEGG pathway database (Figure 4-26). Only pathways with adjusted p-value <0.05 were included in the analysis. Extracellular matrix (ECM) organisation was the most enriched GO. PI3K-Akt signalling pathway was identified and it was associated with focal adhesion and ECM-receptor interaction GO terms. The over-representation of extracellular matrix organisation and elastic fibre formation suggested the effect of TGFβ3 and GDF5 treatment on modulating cartilage matrix production and organisation.

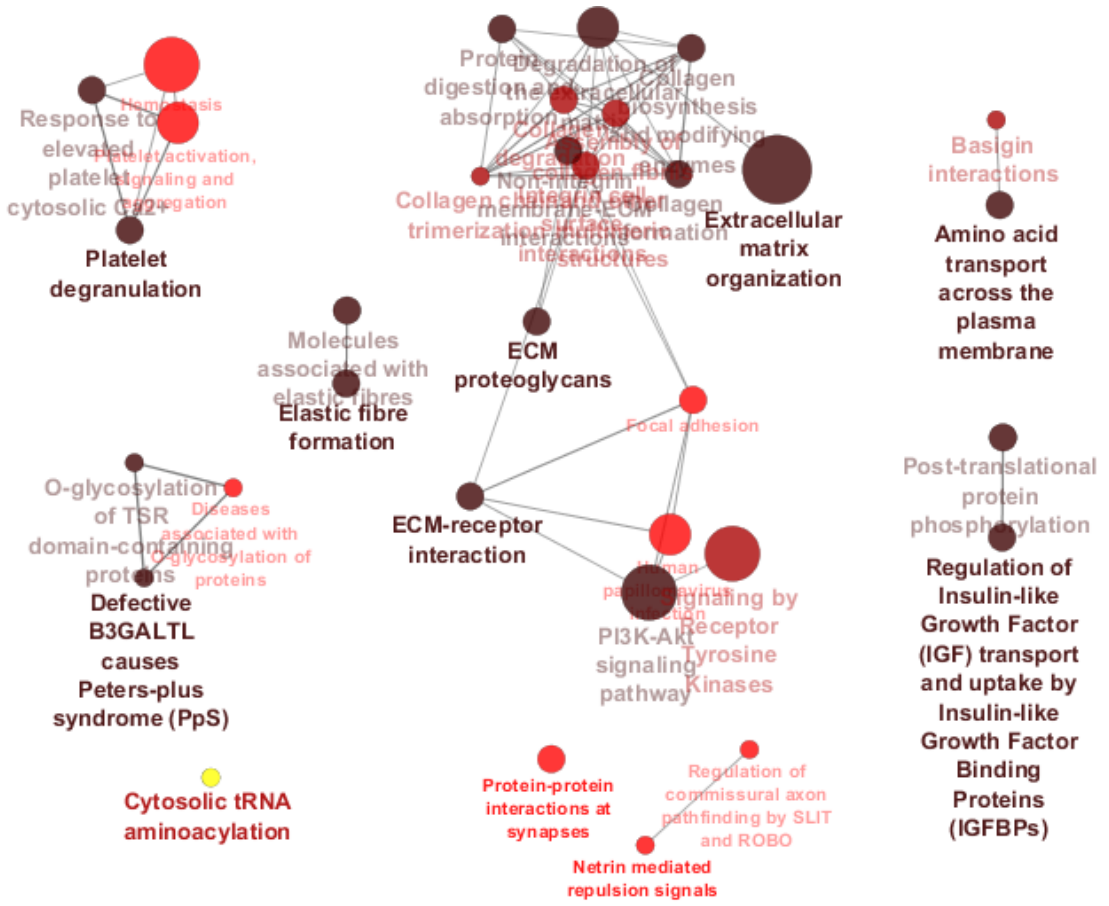

Figure 4-26. KEGG pathway analysis of the differentially expressed genes using ClueGO. Only pathways with p-value < 0.05 are included in the analysis. The colour represents the significance; the darker the colour, the more significant the GO term. The size of the nodes represents the number of genes, the bigger the size the more genes are used to generate the cluster. The line/edge represents the closeness between GO term clusters.

4.3.8.2.2 Cartilage in TG protocol showed increased articular cartilage gene expression

Skeletal system development, extracellular matrix organisation, BMP/TGFβ signalling, and tendon development-related GO terms were enriched in the upregulated genes in TG protocol (Figure 4-25A, page 107-108). Cartilage selective genes such as *TRPV4, ELN, COMP, CILP2, PRG4, ZNF385A* and *ZNF385D* were upregulated in TG cartilage. *TRPV4, COMP, ELN* (elastin) were increased by 3.6, 271, and 18 fold respectively (Figure 4-27B). The chondrogenic growth factors upregulated in TG protocol included *FGF18* and *TGFβ1* (Figure 4-27C). Cartilage collagen expression was similar between TG and No-TG protocol (Figure 4-27A).

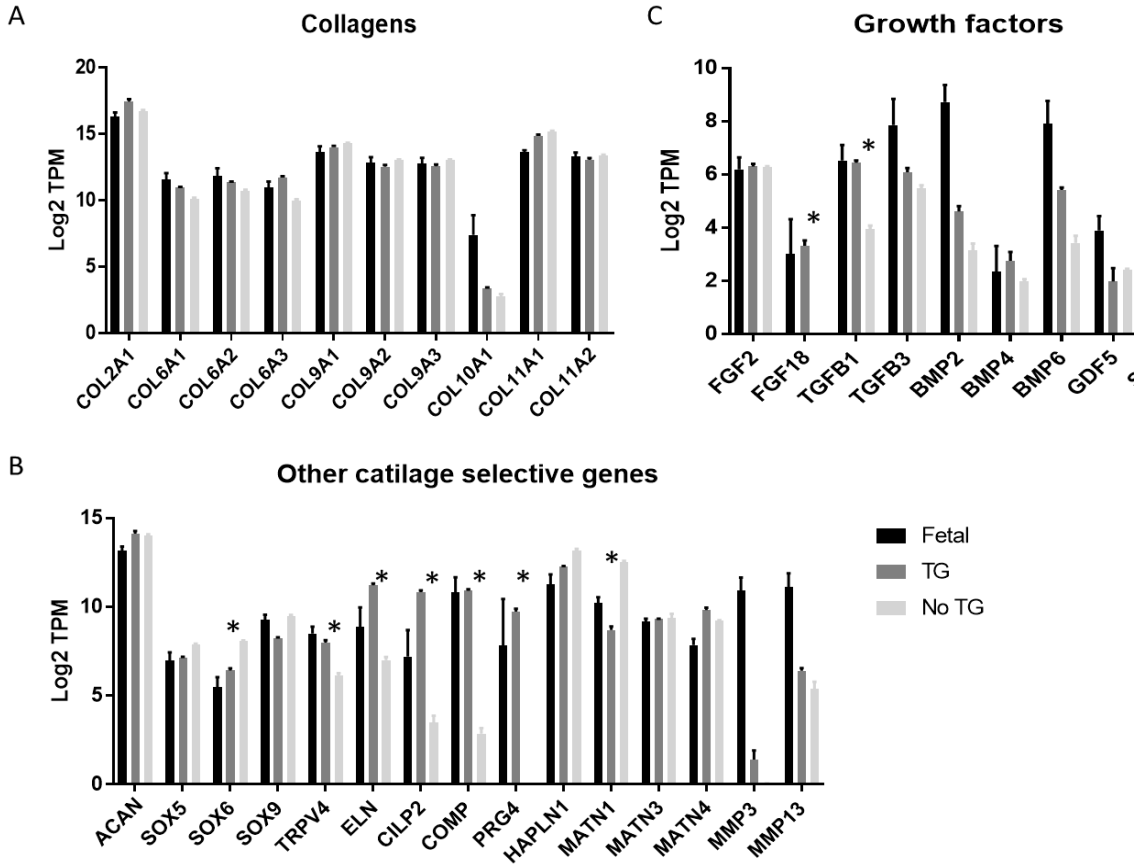

Figure 4-27. The expression of cartilage genes in human fetal cartilage and day 6+70 pellets cultured in TG and No-TG protocol. The transcript level of each group is presented in the actual log2 transcript per million (log2TPM) value from 3 technical replicates. Error bars: SD. *: adjusted p-value <0.05 (obtained from differential gene expression analysis)

Genes that are more abundantly expressed in articular cartilage including *PRG4, CILP2, EGR1, ITIH5, MATN2* (304-307) were upregulated in TG cartilage (Figure 4-28A). *PRG4* and *CILP2* were upregulated by more than 1250 and 162 fold respectively. In contrast, genes more abundantly expressed in the growth plate including *MATN1,*

BMP3, *UNC5C*, *FRZB*, *EBF1*, *LRPZ*, *POU3F3*, and *EFEMP1* (304, 305) were upregulated in No-TG cartilage. Hence, these suggested that TG cartilage had articular cartilage characteristics whereas No-TG cartilage showed characteristics of growth plate cartilage.

Since the histology showed that the No-TG chondrocytes looked more hypertrophic than TG chondrocytes, the expression of hypertrophic chondrocyte markers including *COL10A1*, *MMP13*, *PTH1R*, *MEF2C*, *RUNX2* and *ALPL* (308, 309) were assessed. However, their expression levels were similar between No-TG and TG cartilage indicating that hypertrophic maturation did not occur in the No-TG chondrocytes.

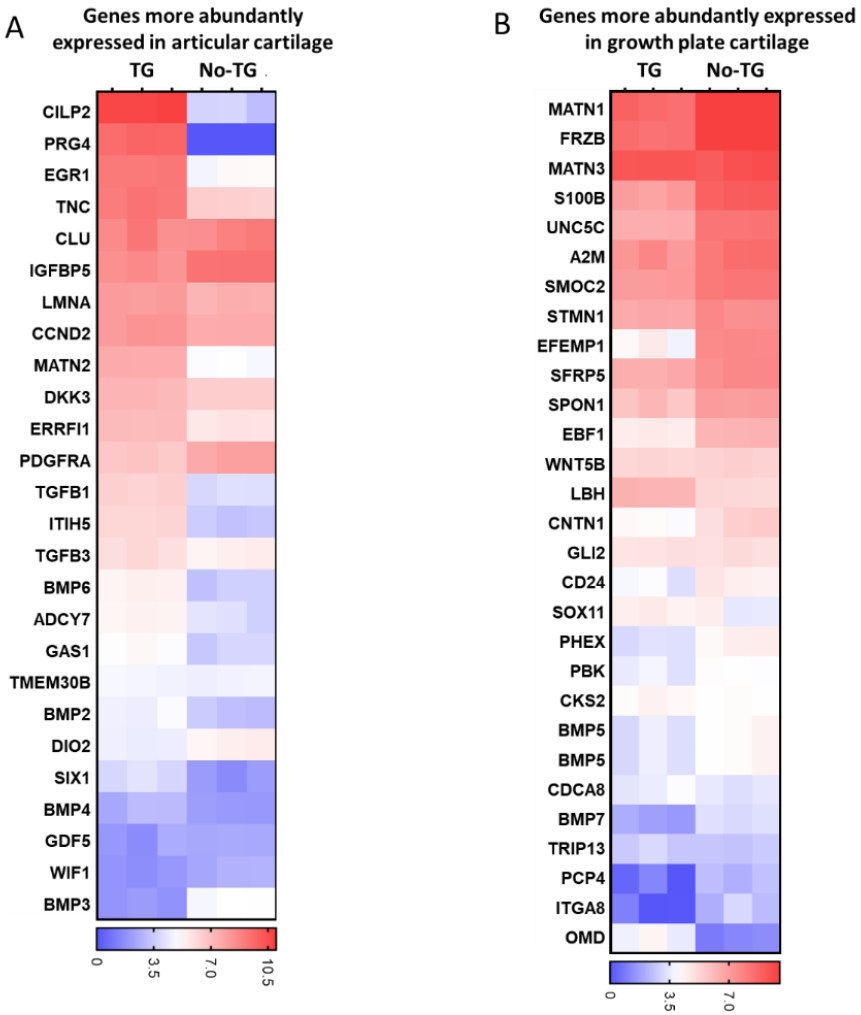

Figure 4-28. The gene expression comparison of genes more abundantly expressed in articular and growth plate cartilage between TG and No-TG cartilage. The transcript level is presented in colour which represents the actual log2 transcript per million (log2TPM) value from 3 technical replicates.

4.3.8.2.3 TG cartilage had increased metalloproteinase and cellular stress-related gene expression

GO term related to unfolded protein response (UPR) was enriched and the differentially expressed genes listed in this GO term were plotted in heatmaps (Figure 4-29). In TG cartilage, ER stress-related markers including *FGF21*, *XBP1, ATF3* were upregulated by 171, 3.5, and 11 fold respectively. Apoptosis, as one of the downstream pathways of UPR was also enriched with apoptosis-related genes such as *TNFRSF10B, TNFRSF12A, UNC5B* were upregulated by 4, 5.5 and 13 fold respectively. These findings might indicate that TG treatment promoted cartilage tissue remodelling.

4.3.8.2.4 Downregulation of neuron development-related genes and upregulation of muscle development-related genes in TG protocol

Interestingly, neuron development-related GO terms were enriched in the TG downregulated genes (upregulated in the No-TG protocol). The genes related to neuron development including *SHH, NTN1, SNAP25, BEX1, NRXN1, NPTX1, APOE, NCAM2, DCC,* and *UNC5C* were significantly downregulated in TG protocol. This is supported by the downregulation of genes related to Slit-Robo signalling, *SLIT1* and *ROBO2,* which is essential for nerve development (310-312). The *SLIT1* and *ROBO2* were downregulated by 11 and 4 fold respectively. Therefore, these findings indicated that TGFβ3 and GDF5 treatment was able to block the neuro-development pathway during chondrocyte differentiation. On the other hand, muscle development-related GO terms were upregulated in TG protocol which was indicated by the upregulation of genes related to muscle development including *MSC, MYBPC2, MYH9, MYOM3, MYO10, TPM1*.

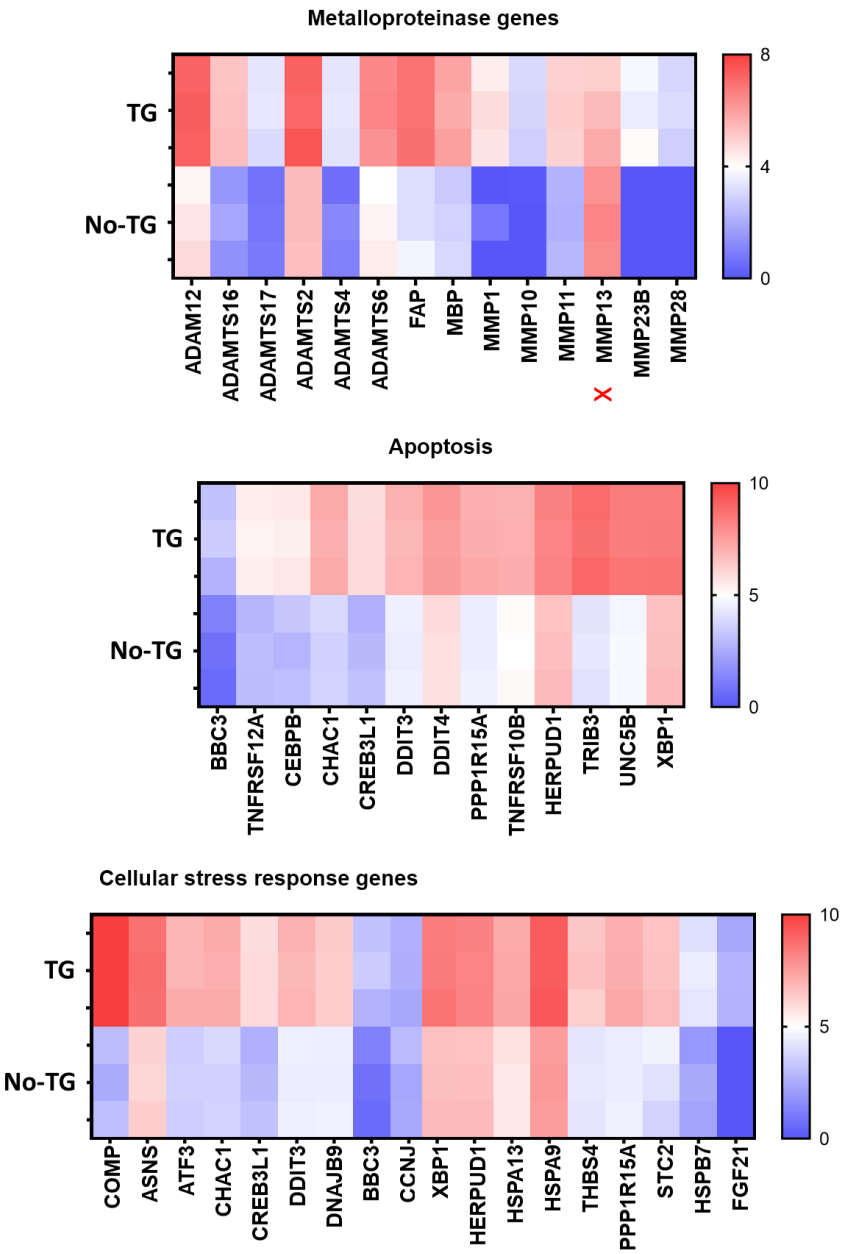

Figure 4-29. The comparison of the metalloproteinase, cellular stress response and apoptosis-related gene expressions between TG and No-TG cartilage. The transcript level is presented in colour which represents the actual log2 transcript per million (log2TPM) value from 3 technical replicates.

4.4 Discussions

In this chapter, I have established an improved chondrocyte differentiation protocol by performing a multiple-step chemically-defined 3-dimensional (3D) culture with swirling in an extended culture that included FGF2 supplementation and optional subsequent TGFβ3 and GDF5 treatment. This optimised protocol is able to produce cartilage tissues that resemble human fetal cartilage.

Our study shows that performing 3D pellet culture with swirling increases chondrogenic marker expression. The 3D culture has been a standard of chondrogenic cell culture to avoid chondrocytes de-differentiation (120, 313). It mimics pre-chondrogenic mesenchymal cell condensation during *in vivo* chondrogenesis and provides a suitable microenvironment for the chondrogenic cells to differentiate into more mature chondrocytes (241). Culture in 3D, particularly in a pellet format; also offers several practical benefits. The 3D shape makes the pellet relatively easy to harvest and process for histology. For cartilage tissue engineering, the biomechanical properties of pellet cartilage can be mechanically manipulated and assessed thus providing a platform for the advancement of cartilage tissue engineering. Moreover, pellet culture set up is less complicated than micromass culture and scaffold-based-3D culture systems; and it is easily scalable for large scale study.

In addition, swirling adds benefits by distributing nutrients, oxygen, and growth factors more evenly (314) through the continuous flow of the culture medium. Mechanical stimuli produced by the flow of culture medium might also have an important role in promoting more efficient chondrocyte differentiation (66, 81). Thus, these might explain the improved chondrogenic marker expression of hiPSC-derived cartilage tissues cultured in swirl culture than in static culture.

Given that the human skeletal development *in vivo* takes much longer than the *in vitro* cartilage differentiation protocol (48), it is not surprising that immature cartilage-like tissues are obtained in day 6 +14 pellets as indicated by a dominant presentation of isoform IIA of collagen type II. Therefore, by extending the duration of chondrocyte differentiation culture up to 10 weeks, cartilage tissues became more mature as indicated by the gradual increase in the expression of isoform IIB of collagen type II. By day 6+70, the expression of cartilage markers is significantly increased compared to day 0. In line with this finding, several studies on pluripotent stem cells conduct chondrocyte differentiation culture for at least 6 weeks to obtain consistent results (18, 19, 247, 248). Therefore, our study has shown that extended culture could drive cartilage maturation and

the switching of collagen type II isoform from IIA to IIB can be used to monitor cartilage maturation.

In the present study, to optimise the chondrocyte differentiation further, known chondrogenic growth factors: FGF2, BMP4, TGFβ3, and GDF5 are tested. Only FGF2, TGFβ3, and GDF5 show chondrogenic activity indicated by the upregulation of chondrogenic marker expression. BMP4 does not upregulate any of the chondrogenic markers consistent with the previous study conducted by Loh, Chen (17). A recently published study that uses a similar 6-day sclerotome induction approach to our induction protocol treats post-sclerotome cells with BMP4 for 6-15 days in monolayer culture to generate chondroprogenitor cells (248). Similar to our finding, the BMP4 treated post-sclerotome cells show *SOX9* downregulation as compared to day-6 sclerotome cells; however, *COL2A1* and *ACAN* expression were not changed.

BMPs are essential for mesenchymal cell condensation (173, 174, 315) during chondrogenesis initiation. BMP4 also promotes chondrocyte terminal development towards hypertrophic chondrocytes in mice (316) and during *in vitro* mesenchymal (317) and hiPSC (19) differentiation towards chondrocytes. The dual actions of BMP4 during early chondrocyte differentiation and chondrocyte maturation might suggest that the cellular response to BMP4 is cell type-dependent. Thus, exploring the role of BMP signaling in a specific stage of chondrocyte differentiation would be useful for further *in vitro* chondrocyte differentiation protocol optimisation.

Our study shows that FGF2 treatment is the most chondrogenic compared to the other growth factors being tested. FGF2 is essential for mesenchymal condensation and chondrogenesis initiation while other types of FGFs, FGF9 and FGF18, play roles at the later stage of chondrocyte differentiation (193). To elicit their effect, FGFs need to bind to FGF receptors. Three out of 4 FGF receptors are important during chondrogenesis (5). FGFR1 and FGFR2 are highly expressed in hypertrophic chondrocytes suggesting that they may have a role in chondrocyte hypertrophy (6, 196). On the other hand, FGFR3 is mainly expressed in the proliferating chondrocytes and it is downregulated in hypertrophic chondrocytes indicating its important roles in regulating chondrocyte proliferation and hypertrophy.

FGF2 supplementation has been performed in two chondrocyte differentiation protocol optimisation studies (18, 252). A 12-day course of FGF2 treatment after mesendodermal induction followed by a combined administration of BMP2, TGFβ3, and GDF5 is able to produce pellets with predominantly cartilage (18). FGF2 supplementation

is also used to maintain hiPSC-derived ectomesenchymal cells and the administration of FGF2 for the whole duration of chondrocyte differentiation promotes the differentiation of hiPSC-derived ectomesenchymal cells into chondrocytes (252). Therefore, considering the importance of FGF during chondrocyte differentiation, a 4-week course of FGF2 treatment is performed during chondrocyte differentiation in extended swirling culture. Cartilage tissues obtained from this protocol have similar gene expression pattern to human fetal cartilage.

Additionally, our study demonstrates the ability of TGFβ3 and GDF5 in upregulating chondrogenic marker expression. Hence a combined TGFβ3 and GDF5 treatment (TG protocol) is added following a 4-week FGF2 treatment to further optimise the chondrocyte differentiation. TGFβ3 and TGFβ1 are routinely used in many PSC-derived chondrocyte differentiation protocols (18, 19, 248, 250, 252, 254, 262, 318) as TGFβ signaling is essential in extracellular matrix production (187) and cartilage development (188, 319). TGFβ3 treatment upregulates chondrogenic marker expressions during mesenchymal stem cell (MSC) (186, 187, 191, 320, 321) and PSC differentiation towards chondrocytes (19, 235, 254). TGFβ3 inhibits hypertrophic maturation of PSC-derived chondrocytes indicated by a smaller cell size and a higher expression of cartilage-related genes compared to BMP4 treated cells (19, 322). On the other hand, GDF5 is important in joint development (181, 182, 323). GDF5 treatment upregulates joint development-related markers such as *Wnt9a* and *Dcx* (Doublecortin) in mouse ESC-derived chondrocytes (246). It also promotes the expression of *Prg4*, a gene more abundantly expressed in the articular cartilage, in mouse ESC-derived chondrocytes (246) and human PSC-derived chondrocytes (18).

Consistent with the findings from previous studies, our data shows that TGFβ3 and GDF5 supplementation (TG protocol) upregulates genes more abundantly expressed in articular cartilage including *PRG4, CILP2, EGR1, ITIH5, MATN2* (304-307). This suggests that TGFβ3 and GDF5 supplementation favours articular chondrocyte differentiation. In contrast, chondrocytes without TGFβ3 and GDF5 treatment (No-TG protocol) look larger than chondrocytes with TGFβ3 and GDF5 treatment and have higher expression of genes more abundantly expressed in the growth plate including *MATN1, BMP3, UNC5C, FRZB, EBF1, LRPZ, POU3F3,* and *EFEMP1* (304, 305). This suggests that chondrocytes generated without TGFβ3 and GDF5 treatment (No-TG protocol) show characteristics of growth-plate chondrocytes.

Not only that TGFβ3 and GDF5 combination treatment promotes articular cartilage phenotype, it also increases other cartilage-selective genes expression including *TRPV4*, *ELN*, and *COMP*. The expression of genes related to unfolded protein response (UPR) and metallopeptidase are also upregulated with TGFβ3 and GDF5 treatment suggesting the increase in cartilage remodelling process (324). Nonetheless, both chondrocyte differentiation protocols, with and without TGFβ3 and GDF5 treatment, are able to generate large amount of cartilage tissues that can be used for downstream study including cartilage disease modelling.

Although a fetal-looking cartilage is obtained from the optimised chondrocyte differentiation protocol, substantial amount of non-cartilage tissues is still present in the pellet cartilage generated by our two chondrocyte differentiation protocols. This might be caused by the incomplete induction of hiPSCs during sclerotome induction. The sclerotome induction involves a multiple-step differentiation approach via intermediate mesendoderm lineages that mimics *in vivo* embryonic development. Thus, incomplete induction could have resulted in mixed cell populations as shown by the appearance of two distinct cell populations, PDGFRα^{+}/SOX9^{+} and PDGFRα^{-}/SOX9^{-}; by the end of differentiation day 6. The proportion of non-chondrogenic cell population, PDGFRα^{-}/SOX9^{-}; increases from differentiation day 4 to day 6 thus flowcytometry beyond this time point is need to assess the increasing trend of this cell proportion. A chondrogenic cell sorting can then be performed once the proportion of this cell population is stable. This cell sorting is aimed at minimising non-chondrogenic cell contamination during extended chondrocyte differentiation culture.

In addition, SOX9 is also expressed in mesodermal lineages including Sertoli cell progenitors of the developing gonads, ectodermal cranial neural crest cells (298, 325) and endodermal lineages including gut epithelial progenitors (325). Therefore, it is plausible that sorting cells based on PDGFRα and SOX9 expression during sclerotome induction cannot completely remove the non-chondrogenic cell populations as we might still be collecting high SOX9 expressing cells which are not chondrogenic. In that vein, identifying the two distinct cell populations could be very useful in defining the important signalling pathways that contribute to the non-chondrogenic cell differentiation. In doing so, we can then block the signalling pathways and further refine the sclerotome and chondrocyte differentiation protocol. Interestingly, the Slit-Robo signalling, an essential signalling pathway for nerve development (310-312); is suppressed in TG protocol but the muscle-related genes were upregulated. These suggest that the non-chondrogenic

tissues might be derived from either neuron or muscle progenitor cells. Consequently, blocking the muscle differentiation pathway might be needed when TG protocol is performed while blocking Slit-Robo signaling might be necessary when performing No-TG protocol.

Recently, these optimised protocols have been applied in two other hiPSC lines in our laboratory (unpublished data obtained by Kung, Sampurno, Lamandé, Bateman (2019)). The protocols were able to produce pellets with predominantly cartilage without blocking the muscle or neuron development pathways. Several factors including 1) the original cell type for hiPSC generation, 2) the reprogramming method for hiPSC generation, 3) single nucleotide polymorphisms, mutations and copy number variations in the original cells and hiPSC, 4) epigenetic status of the original cells and hiPSCs and 5) culture conditions have been reported can influence the capacity of pluripotent stem cells to differentiate (326). Interestingly, the other two hiPSC lines that are able to generate pellets with predominantly cartilage are derived from fibroblast, generated using slightly different reprogramming methods and are maintained in feeder-free Matrigel-based culture format. On the other hand, PB001.1 and SOX9-T2A-tdTom hiPSC lines used in the present study are derived from peripheral blood mononuclear cells and maintained in a feeder-dependent culture format. Such differences could partly explain the different chondrogenic differentiation capacity between the SOX9-2A-tdTom and the other two hiPSC lines.

Furthermore, the presence of irradiated mouse embryonic fibroblast (feeder cells) during sclerotome induction in PB001.1 and SOX9-2A-tdTom might also contribute to the less efficient hiPSC differentiation as they might secrete unknown bio-active molecules that could inhibit hiPSC differentiation (20). Hence, feeder-free differentiation culture is often performed preferentially in several chondrocyte differentiation protocols (18, 20). Therefore, transferring PB001.1 and SOX9-T2A-tdTom hiPSC line from feeder-dependent culture into feeder-free Matrigel-based culture could be the first step to further optimise the chondrocyte differentiation protocol before performing cell sorting.

Since our attempt in enriching chondrogenic cells during sclerotome induction using FACS is unsuccessful in generating pellets with predominantly cartilage, trypsin digestion is undertaken to remove the non-cartilage tissues present in the pellets. Pellet cartilage is relatively more resistant to trypsin digestion than the non-cartilage tissues and by re-culturing the post-trypsin digested pellets in the chondrocyte differentiation medium for 7-10 days, the chondrocyte ECM recovered. With trypsin digestion, non-

cartilage tissues which mainly reside in the core of the pellets and in the outer layer of the pellets were removed from the pellets. The trypsin digestion step allows us to quickly obtain relatively pure cartilage while chondrocyte differentiation protocol is being optimised further. Having the non-cartilage tissues removed from the pellets is very critical for our study in order to avoid the confounding effects of non-cartilage tissues on cartilage gene expression analyses performed in TRPV4-inherited skeletal disease modeling presented in Chapter 6.

4.5 Conclusions

Herein, we have established an improved protocol for differentiating hiPSCs into chondrocytes using multiple-step chemically-defined 3-dimensional (3D) culture with swirling in an extended culture that included FGF2 supplementation and optional subsequent TGFβ3 and GDF5 treatment. By using this protocol, the cartilage that closely resembles fetal cartilage could be generated. The optimised chondrocyte differentiation protocol without TGFβ3 and GDF5 treatment is used for TRPV4-inherited skeletal disease modelling study presented in Chapter 6 as it generates growth plate-like cartilage which is very likely to be affected in the pathogenesis of TRPV4-inherited skeletal diseases.

Chapter 5

The generation of TRPV4 mutant hiPSC lines using the CRISPR/Cas9 genome editing

5.1 Introduction

In this chapter, we introduced two skeletal disease-causing TRPV4 mutations into the SOX9-T2A-tdTom hiPSC line to model TRPV4-inherited skeletal disease. The first mutation was the heterozygous TRPV4 c.2396C>T (p.P799L) mutation causing metatropic dysplasia (86) and the second mutation was heterozygous TRPV4 c.819C>G (p.F273L) mutation causing familial digital arthropathy with brachydactyly (FDAB) (39). The mutagenesis was performed by using Clustered Regularly Interspaced Short Palindromic Repeats/Cas9 (CRISPR/Cas9) genomic editing technology (Figure 5-1).

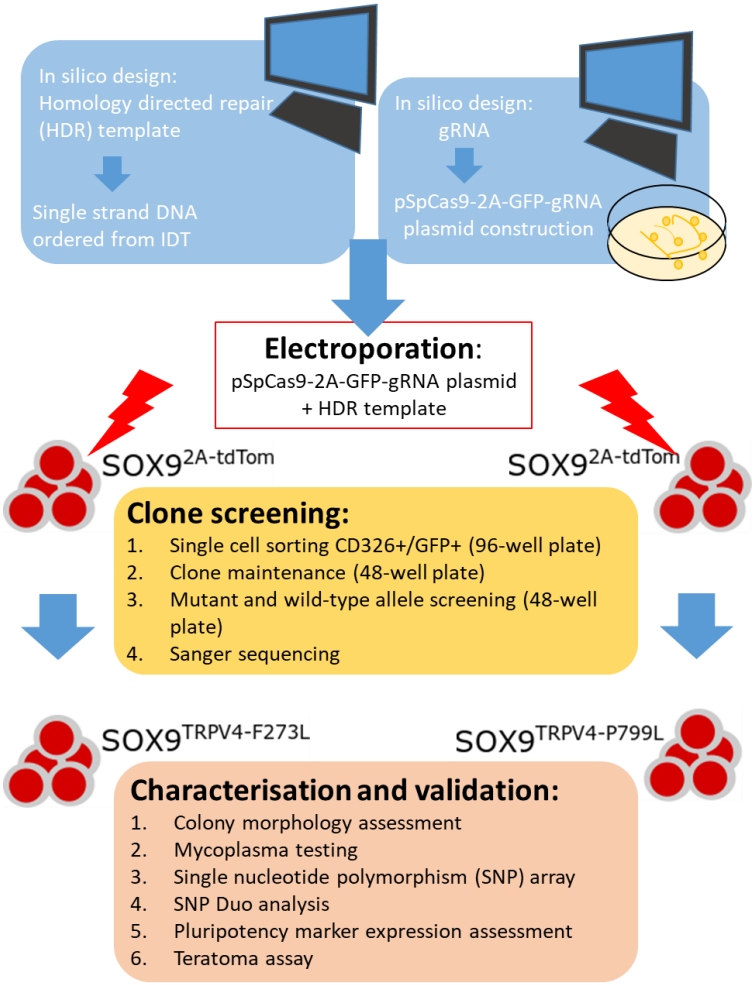

Figure 5-1. The experiment workflow to generate mutant TRPV4 hiPSC lines. Two mutant TRPV4 hiPSC lines are generated from SOX9-T2A-tdTom using CRISPR/Cas9 genomic editing.

5.2 Materials and Methods

5.2.1 CRISPR/Cas9 construct for TRPV4 c.819C>G (p.F273L) and TRPV4 c.2396C>T (p.P799L) mutation introduction

The gRNAs specifically targeting *TRPV4* exons 5 and 15 were designed using the www.benchling.com website. The position of the gRNAs relative to the point mutation introduction sites is shown in Figure 5-2. The gRNA having the highest score and making double-strand break (DSB) as close as possible to the point mutation introduction site of each TRPV4 mutant variant was selected. The 5'-GTCCACGCCAGGCCCGT-3' and 5'-GAGAAGCCATAATACTGGT-3' gRNA were selected for TRPV4 c.819C>G (p.F273L) and TRPV4 c.2396C>T (p.P799L) mutation introduction, respectively. The gRNA oligonucleotides were purchased from Sigma Aldrich and ligated into pSpCas9-2A-GFP as described in Chapter 2 section 2.6.

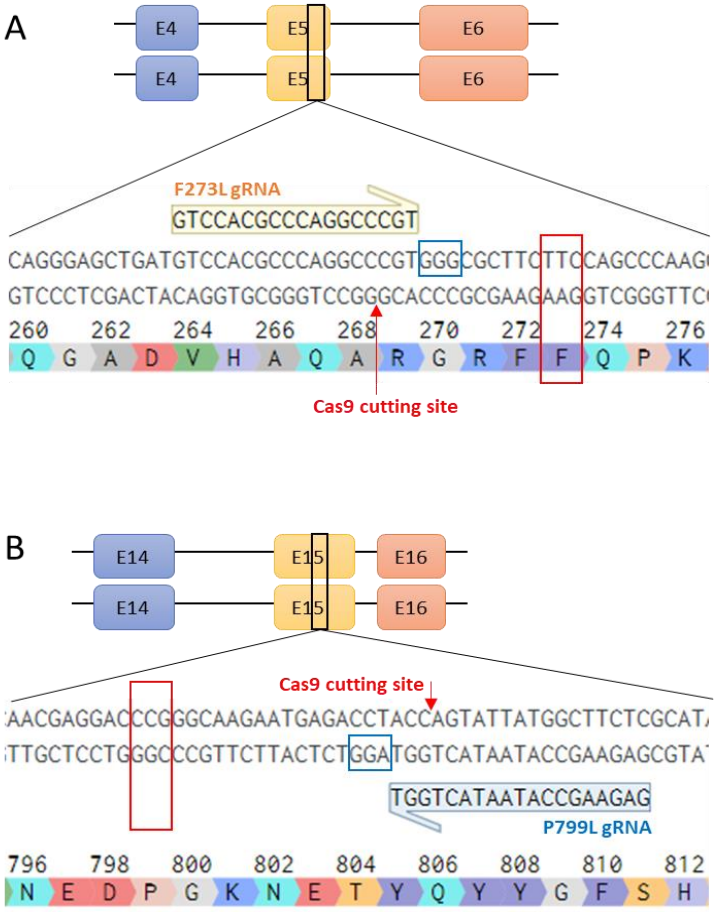

Figure 5-2. CRISPR/Cas9 target in the *TRPV4* gene. Single guide RNA (gRNA) targeting exon 5 (A) and exon 15 (B) are shown in yellow (F273L gRNA) and blue (P799L gRNA) respectively with the 5'-NGG-3' protospacer adjacent motif (PAM) for the *Streptococcus pyogenes* Cas9 variant is shown in blue box. The red arrow shows the Cas9 cutting site of each gRNA target located 3 bases upstream of the PAM sequence. The red box shows the target codon for mutation introduction.

5.2.2 Homology-directed repair (HDR) templates for p.F273L and p.P799L TRPV4 mutation introduction

The HDR templates for 32756C>G (p.F273L) and 49030C>T (p.P799L) TRPV4 mutation introduction were designed using www.benchling.com. The HDR templates were single strand DNAs containing the disease-causing point mutation and additional synonymous base changes to facilitate downstream PCR screening for clones containing the mutation and to disrupt the 5'-NGG-3' PAM sequence (Figure 5-3). The complete sequence of the HDR templates for both TRPV4 mutations are available in appendix 5.

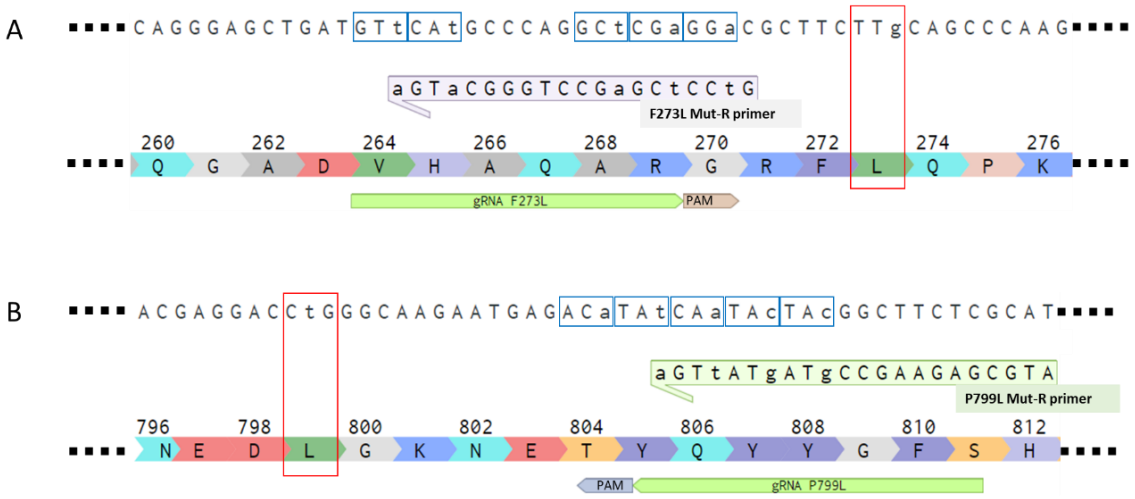

Figure 5-3. Homology-directed repair (HDR) template for TRPV4 c.819C>G (p.F273L) (A) and TRPV4 c.2396C>T (p.P799L) (B) mutation introduction. The HDR templates have 250 bases and contain a single base change (indicated in lowercase) for the target point mutation (red box). Other base changes (indicated in lowercase) are also introduced to produce synonymous codon changes (blue box) for mutation screening and to remove the 5'-NGG-3' PAM sequence to prevent re-editing the allele. Mutant specific primers (F273L Mut-R for p.F273L mutation introduction, and F799L Mut-R for P799L mutation introduction) are generated for mutation screening using PCR.

5.2.3 Generating mutant TRPV4 hiPSC lines

To generate mutant hiPSC lines, SOX9-T2A-tdTom hiPSCs were electroporated with the gRNA plasmid and the HDR template for each TRPV4 mutation. The detailed procedure for electroporation and expanding clones are available in Chapter 2 section 2.9. PCR screening for heterozygous mutant clones was performed in two steps. The first step was to screen using mutant specific primers (Table 5-1) and the second step was to screen mutant-positive clones to identify those that also had a wild type allele. TRPV4 sequences in selected clones were confirmed using Sanger sequencing. The primer sets used for PCR and sequencing are listed in Table 5-1 and the location of the primers are shown in Figure

5-5 (for F273L) and Figure 5-14 (for P799L). Heterozygous mutant hiPSC clones were selected for SNP array analysis (detailed procedure available in Chapter 2 section 2.12).

Table 5-1. List of primers used in this study

Primer name	Sequence	Description
p.F273L mutation introduction		
F273L Mut-F	ATCCCAGGGAATATCCAAGGAC	Mutant allele specific primer set (271bp)
F273L Mut-R	GtCCtCGaGCCTGGGCaTGa	
F273L Mut-F	ATCCCAGGGAATATCCAAGGAC	Amplify a region for sequencing (768bp)
F273L WT-R	TTGAACTCTTGACCTCAGGTGA	
F273L Mut-F	ATCCCAGGGAATATCCAAGGAC	Sequencing primer
p.P799L mutation introduction		
P799L Mut-F3	TCCTGACCTCAAATGACCCACC	Mutant allele specific primer set (286bp)
P799L Mut-R	ATGCGAGAAGCCgTAgTAtTGa	
P799L Mut-F3	TCCTGACCTCAAATGACCCACC	Amplify a region for sequencing (678bp)
P799L WT-R	TCCCCAGGAGAGAATGGAGGAA	
P799L Mut-F3	TCCTGACCTCAAATGACCCACC	Sequencing primer

5.3 Results and Discussions

5.3.1 TRPV4 c.819C>G (p.F273L) mutant hiPSC line

5.3.1.1 pSpCas9-2A-GFP-gRNA constructs

The pSpCas9-2A-GFP-gRNA construct for TRPV4 c.819C>G (p.F273L) mutant was generated by inserting the annealed-phosphorylated gRNA oligonucleotides into BbsI digested-dephosphorylated-pSpCas9-2A-GFP. gRNA insertion was screened by double restriction enzyme digestion using BbsI and NotI restriction enzyme. Successful insertion produced only a single band (10kb), a result of NotI cutting of the backbone plasmid since the BbsI cutting site has been removed upon gRNA insertion. Plasmid #1, #3, #5 and #8 had only a single band following NotI digestion indicating successful gRNA insertion (Figure 5-4A). These 4 clones were sequenced confirming the insertion of the gRNA in all of the clones. The sequencing result of plasmid #8 is presented in Figure 5-4B.

5.3.1.2 PCR screening for the TRPV4 c.819C>G (p.F273L) mutant allele

The SOX9-T2A-tdTom hiPSC lines were electroporated with the pSpCas9-2A-GFP-gRNA construct and single-strand DNA HDR template. The electroporated hiPSCs were plated on a 6cm-dish and maintained in feeder dependent culture. Three-day post-transfection, single GFP-positive transfected cells were sorted into 96 well plates using FACS. From 960 single sorted cells, 461 grew and formed confluent colonies after 2 weeks. All 461 clones were screened with the mutant specific primer set (F273L Mut-F and F273L Mut-R) which is shown schematically in Figure 5-5. The F273L Mut-F primer was located outside the HDR template and Mut-R was located in the HDR template. Hence, the PCR should only work if the base changes were introduced by homology-directed DNA repair following DNA double-strand breaks induced by Cas9. This PCR can be used as a proxy for mutation introduction at the targeted site (TRPV4 32756C>G) as the synonymous base changes were close to the point mutation. Of the 461 clones, 207 had the 271bp mutant-specific band (F273L Mut-F + F273L Mut-R) (Figure 5-6) and so were very likely to have a mutant TRPV4 c.819C>G (p.F273L) allele.

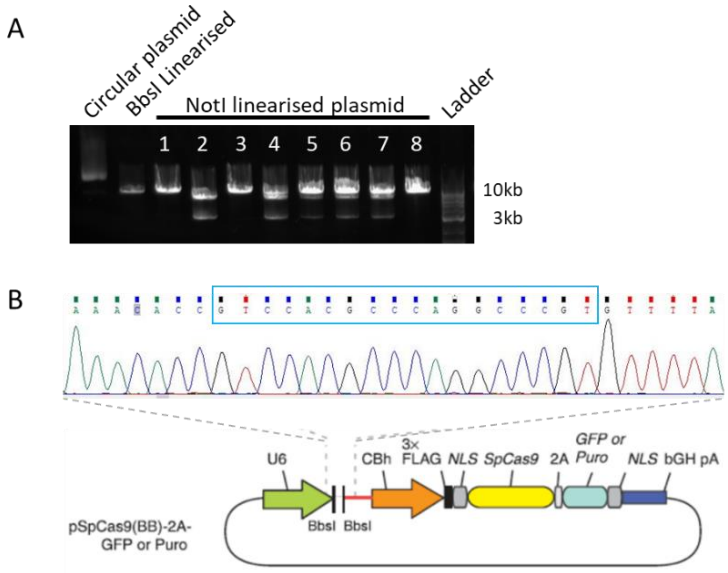

Figure 5-4. pSpCas9-2A-GFP-gRNA construct for c.819C>G (p.F273L) TRPV4 mutation introduction. Screening of the gRNA insertion was performed by NotI restriction enzyme digestion (A) and sequencing result of plasmid #8 is shown in B with a blue box indicates the gRNA insertion in the pSpCas9-2A-GFP plasmid vector.

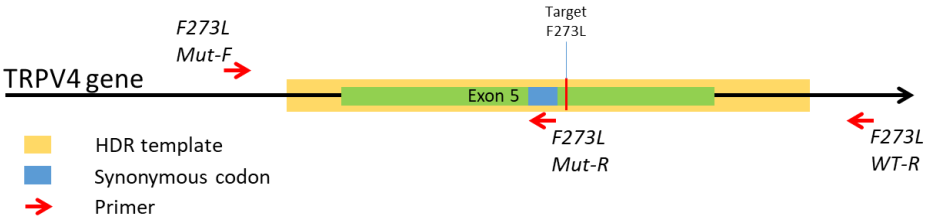

Figure 5-5. The location of the primer for TRPV4 c.819C>G (p.F273L) heterozygous mutation screening and sequencing.

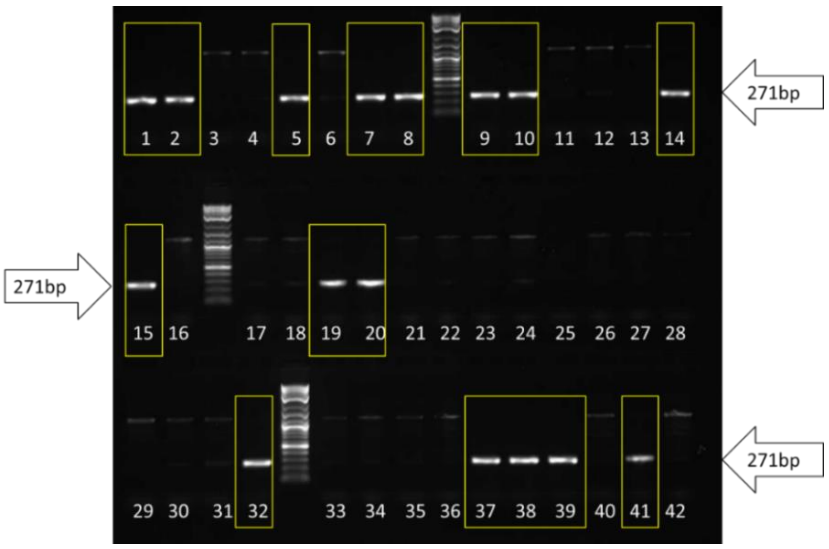

Figure 5-6. Gel electrophoresis of the mutant TRPV4 c.819C>G (p.F273L) allele PCR screening. Only the first 42 clones (indicated by the numbers) are shown here. The yellow boxes indicate bands that were amplified with mutant specific primer set. These clones are very likely to have a mutant TRPV4 c.819C>G (p.F273L) allele.

To identify clones with a heterozygous *TRPV4* c.819C>G (p.F273L) mutation and without small insertions or deletions, 52 clones were sequenced. PCR products from F273L Mut-F + F273L WT-R primer set (768bp) were sequenced using the F273L Mut-F primer. Five of the 52 clones were heterozygous mutant, 12 clones were homozygous mutant, and the remainder had insertions and/or deletions in one or both alleles. All the heterozygous mutant clones have the same sequencing results as the TRPV4-F273L-2 hiPSC clone (Figure 5-7). The heterozygous mutant clones had a heterozygous single base change from TTC to TTG at base number 819 resulting in amino acid change from phenylalanine to leucine at amino acid number 273. They also had 5 other base changes, 2 heterozygous (base number 792 and 795) and 3 homozygous (base number 804, 807, and 810). These 5 base changes were introduced into the hiPSC lines for clone screening purposes and they did not result in amino acid changes (synonymous codon).

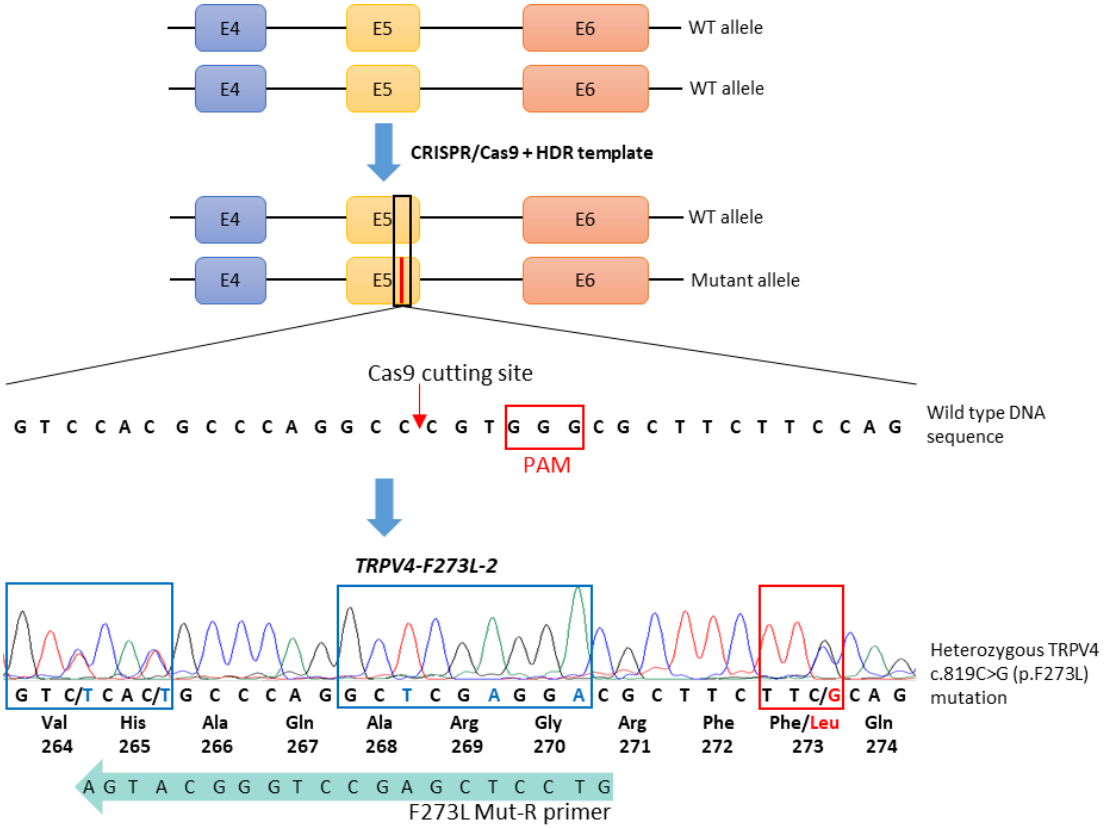

Figure 5-7. Sequencing result of TRPV4-F273L-2. The heterozygous *TRPV4* mutation c.819C>G (p.F273L) is shown in the red box & red letters and introduced base changes resulted in synonymous codons are shown in blue letter and blue boxes. Mut-R (a mutant specific reverse primer) sequence is shown in blue arrow. Notice that the protospacer adjacent motif (PAM) site was removed by introducing a base change in the PAM site to avoid a repeated cutting by Cas9.

The mechanisms of homology-directed repair DNA are complex but the simplified process is illustrated in Figure 5-8. Following a Cas9-induced double-strand break, 5' to 3' base resection occurs by the action of exonuclease resulting in 3' overhangs (usually 30-40 bases) (327). The donor HDR templates anneal to the resected strand and DNA polymerases extend the strand using the donor HDR as a template. The newly polymerised strand corresponding to the 5' end of the donor HDR template anneals to the target DNA (strand invasion). Finally, the junctions are repaired by endonucleases which trim the strand excess, repair polymerases that fill the base gaps and ligase to seal the gaps (327). Since the efficiency of the homology-directed repair also depends on the donor HDR template design and base contents, the outcome of DNA repair after Cas9-induced double-strand break is difficult to predict (283, 327-329).

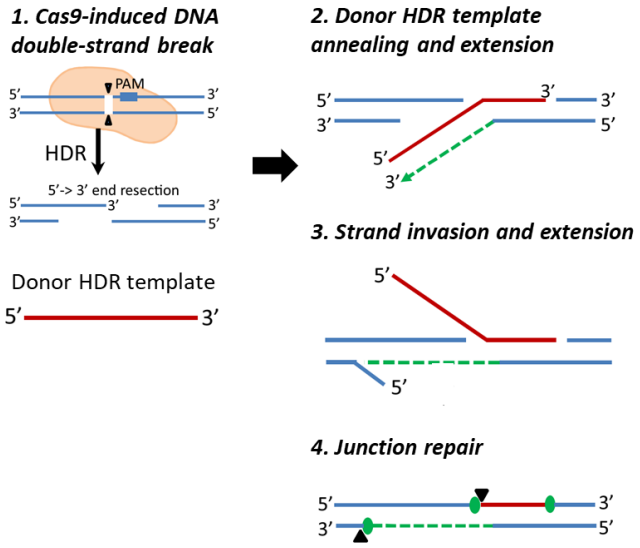

Figure 5-8. The schematic process of homology-directed repair mechanism in the presence of donor HDR template (single strand oligo deoxyribonucleic (ssODN)). Adapted from (327).

Given that 6 base changes derived from the HDR template was observed in the heterozygous mutant clones (Figure 5-7, blue letters), the donor HDR templates were used as a repair template. Interestingly, 3 out of 5 synonymous codons encoding amino acid alanine, arginine and glycine were homozygous and the 2 other synonymous codons (valine and histidine) and the targeted mutation were heterozygous. These suggested that the Cas9 induced double-strand breaks in both alleles. The difference in 5' to 3' resection of the targeted DNA and strand invasion of the repaired DNA between the two alleles could have resulted in 3 synonymous codons being homozygous and the other 2 synonymous codons and the targeted mutation being heterozygous. The schematic repair process is illustrated in Figure 5-9.

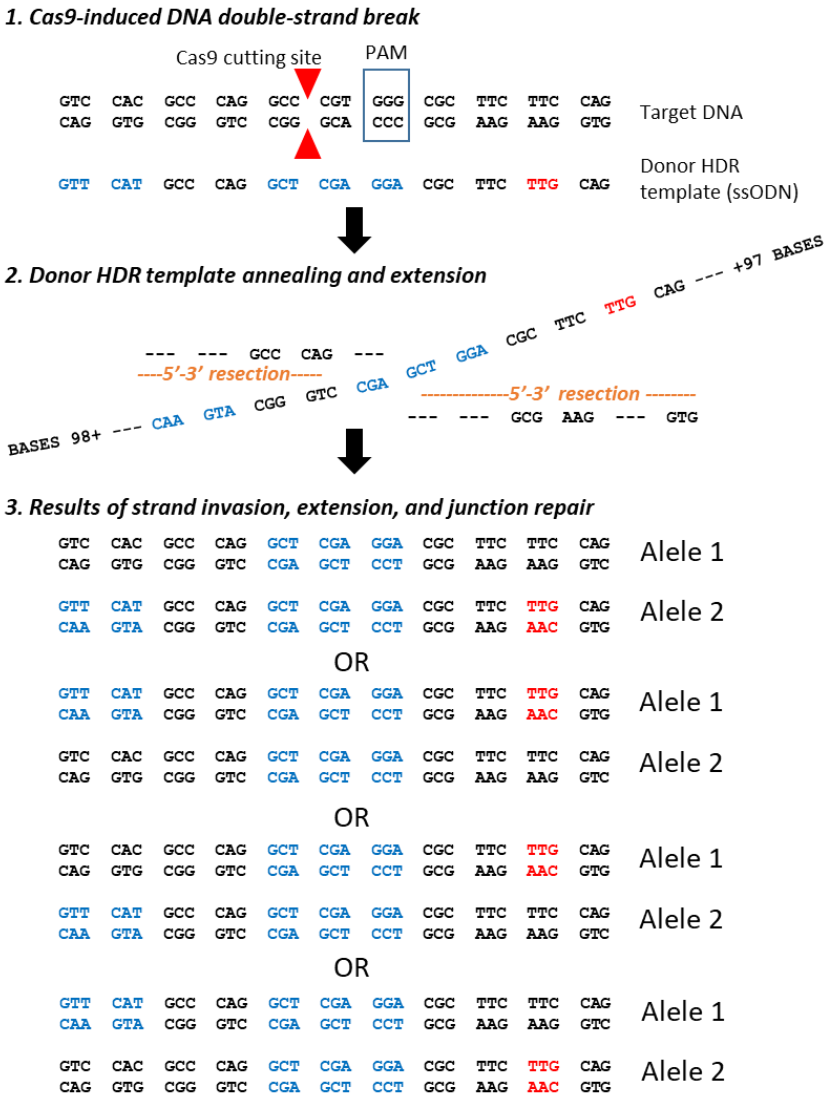

Figure 5-9. The schematic homology-directed repair process in F273L.

5.3.1.3 Characterisation of the TRPV4 F273L hiPSC line

The TRPV4-F273L-2 hiPSC clone was selected for pluripotent stem cell characterisation and validation. The TRPV4-F273L-2 hiPSC line was characterised using several methods including colony morphology assessment, pluripotency marker assessment, mycoplasma testing, SNP array, and teratoma formation. The TRPV4-F273L-2 hiPSC line formed tightly packed colonies with homogeneous cells and clear peripheral colony edges (Figure 5-10). Immunostaining of NANOG and OCT4 protein in TRPV4-F273L-2 hiPSC lines showed that these pluripotency markers were co-localised in almost all of the cells (Figure 5-10).

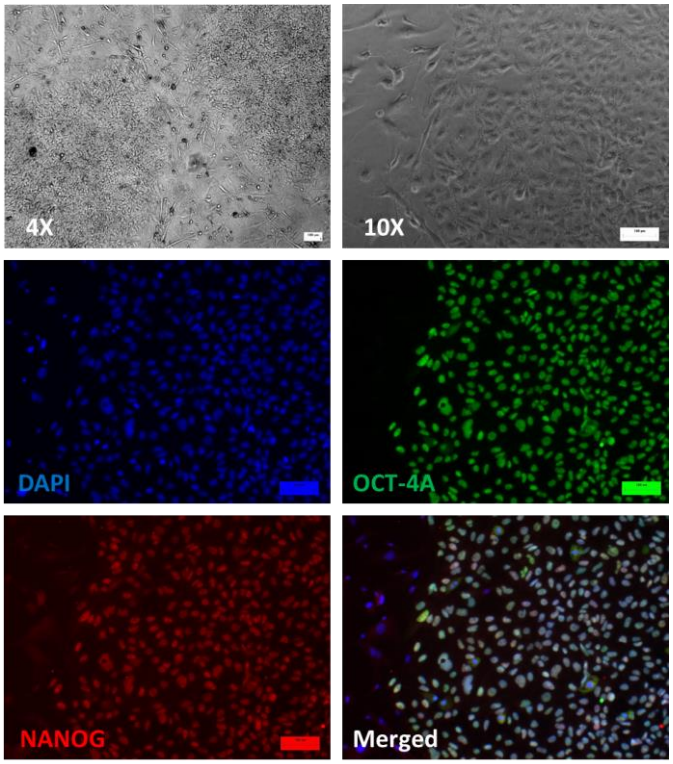

Figure 5-10. Colony morphology and pluripotency marker immunostaining of TRPV4-F273L-2 hiPSC line. Scale bar: 100µm.

Other pluripotency markers, including CD9, Ep-CAM (CD326), TRA1-81 and SSEA-4, were measured using flowcytometry. More than 99% of cells expressed CD326, TRA1-81 and SSEA-4 and around 95% of cells expressed CD9 (Figure 5-11). These results indicated that the pluripotency of the mutant hiPSCs was maintained following genomic manipulation. No chromosomal abnormalities were detected by SNP array and SNPduo analysis showed that TRPV4-F273L-2 had 99.9% identical genotypes to the SOX9-T2A-tdTom hiPSC line indicating that both lines were from the same individual (Appendix 6).

Teratoma assays confirmed that the TRPV4-F273L-2 hiPSC line could form tissues from three germ layers. The histology showed endodermal gut epithelium, mesodermal adipocytes tissues, and neuroectodermal cells as an ectodermal tissue of origin (Figure 5-12).

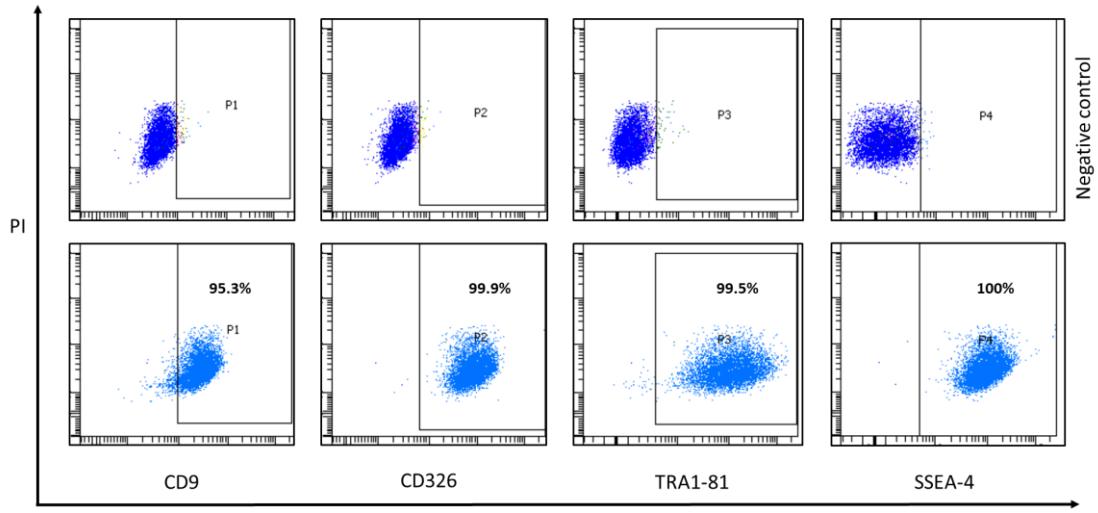

Figure 5-11. The expression of pluripotency markers assessed using flowcytometry.

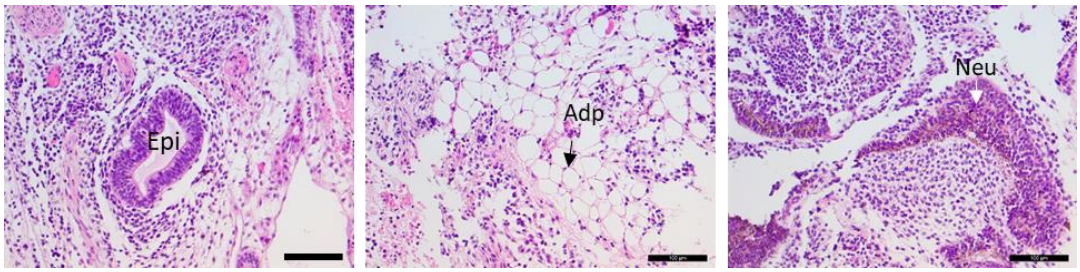

Figure 5-12. Three germ layer formation in teratoma generated from TRPV4-F273L-2 hiPSC line. Epi: gut epithelium (endoderm), Adp: adipocytes (mesoderm), Neu: Neuroectoderm (ectoderm). Scale bar: 100µm.

5.3.2 TRPV4 c.2396C>T (p.P799L) mutant hiPSC line

5.3.2.1 pSpCas9-2A-GFP-gRNA constructs

The annealed-phosphorylated gRNA oligonucleotides were cloned into BbsI digested-dephosphorylated-pSpCas9-2A-GFP. gRNA insertion screening was performed by restriction enzyme digestion using BbsI and NotI. Except plasmid #10, all of the plasmids seemed to have a gRNA insertion indicated by a single band at 10kb following restriction enzyme digestion (Figure 5-13A). These plasmid clones were sequenced to confirm the gRNA insertion. The sequencing result of plasmid #5 is presented in Figure 5-13B.

5.3.2.2 PCR screening of TRPV4 c.2396C>T (p.P799L) mutant and wild-type allele

A similar screening strategy was used to identify heterozygous edited clones for the P799L mutation. The primers used for mutation screening are available in Table 5.1 and are shown schematically in Figure 5-14.

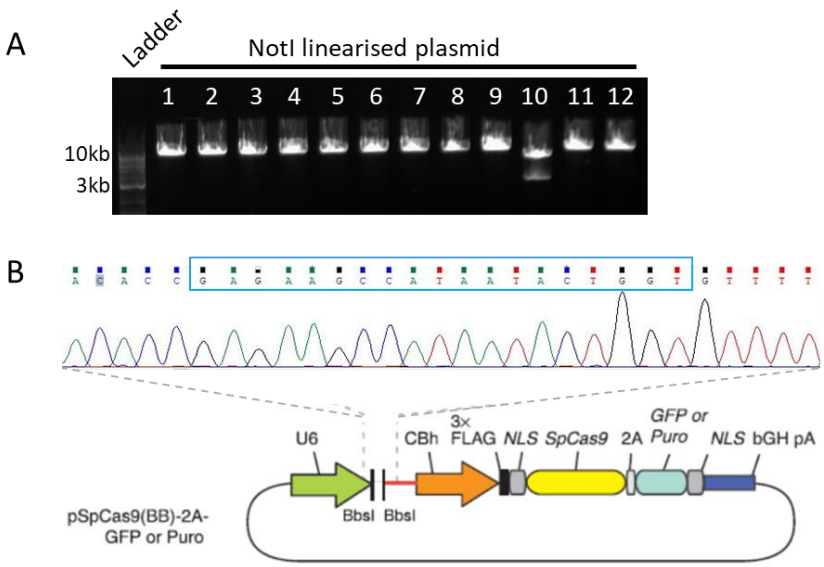

Figure 5-13. pSpCas9-2A-GFP-gRNA construct for c.2396C>T (p.P799L) TRPV4 mutation introduction. Screening of the gRNA insertion was performed by NotI restriction enzyme digestion (A) and sequencing result of plasmid #5 is shown in B with a blue box indicates the gRNA insertion in the pSpCas9-2A-GFP plasmid vector.

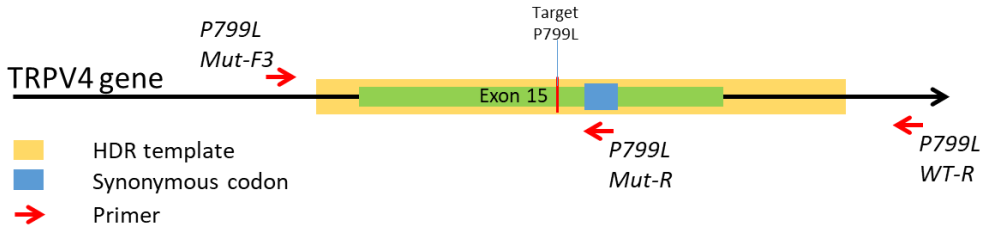

Figure 5-14. The location of the primer for TRPV4 c.2396C>T (p.P799L) heterozygous mutation screening and sequencing.

All 491 hiPSC clones were screened and 198 clones had the 286bp mutant-specific PCR band (P799L Mut-F3 + P799L Mut-R primer set) and so were very likely to have a mutant TRPV4 c.2396C>T (p.P799L) allele (Figure 5-15). To identify correctly targeted heterozygous *TRPV4* c.819C>G (p.F273L) clones, genomic DNA containing the targeted region was PCR amplified using the P799L Mut-F3 + P799L WT-R primer set (678bp) and sequenced using P799L Mut-F3. Three out of 52 clones were heterozygous mutant TRPV4 c.2396C>T (p.P799L), 5 clones were homozygous mutant TRPV4 c.2396C>T (p.P799L), and the rest of the clones had insertions and/or deletions. All the heterozygous mutants have the same sequencing results as in TRPV4-P799L-31 hiPSC clone (Figure 5-16). The heterozygous mutant clones had a heterozygous single base change from CCG to CTG at base number 2396 resulting in amino acid change from proline to leucine at amino acid number 799. They also had 5 other homozygous base

changes that were introduced into the hiPSC lines for clone screening purposes. These base changes resulted in synonymous codons encoding the same amino acids as the wild-type (Figure 5-16, blue box). TRPV4-P799L-31 was selected for further pluripotent stem cell characterisation and validation.

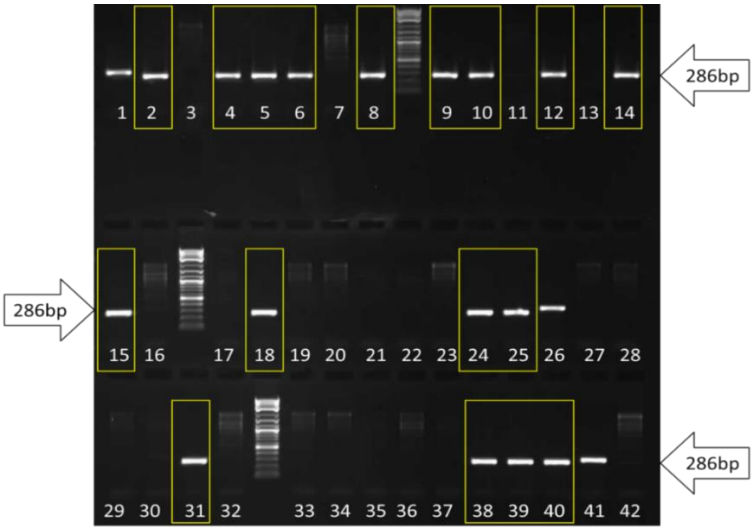

Figure 5-15. Gel electrophoresis of the mutant TRPV4 c.2396C>T (p.P799L) allele PCR screening. The first 42 clones are shown (number). The yellow boxes indicate bands that were amplified with mutant specific primer set. These clones are very likely to have a mutant TRPV4 c.2396C>T (p.P799L) allele.

While the P799L mutation was heterozygous in this clone, the 5 synonymous base changes that were also present in the HDR template were homozygous. (Figure 5-16, blue letters). These indicated that Cas9 had induced double-strand breaks in both alleles that were repaired by HDR. The repair process is illustrated in Figure 5-17.

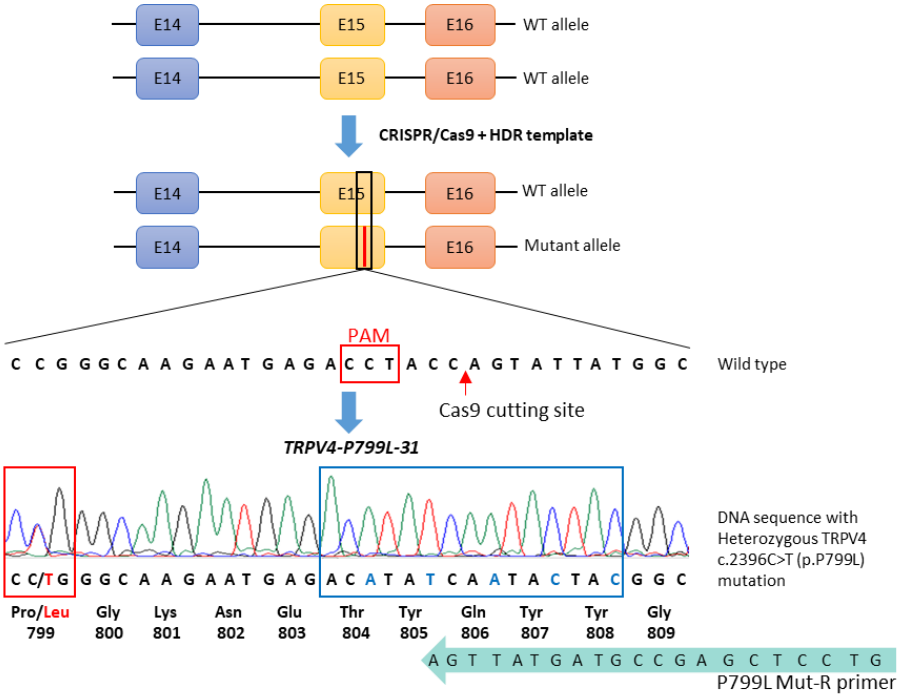

Figure 5-16. Sequencing result of TRPV4-P799L-31. Heterozygous mutation of TRPV4 c.2396C>T (p.P799L) is shown in red box & red letters and introduced base changes resulted in synonymous codon are shown in blue letters and blue box. Mut-R (a mutant specific reverse primer) sequence is shown in blue arrow. Notice that the protospacer adjacent motif (PAM) site was removed by introducing a base change in the PAM site to avoid a repeated cutting by Cas9.

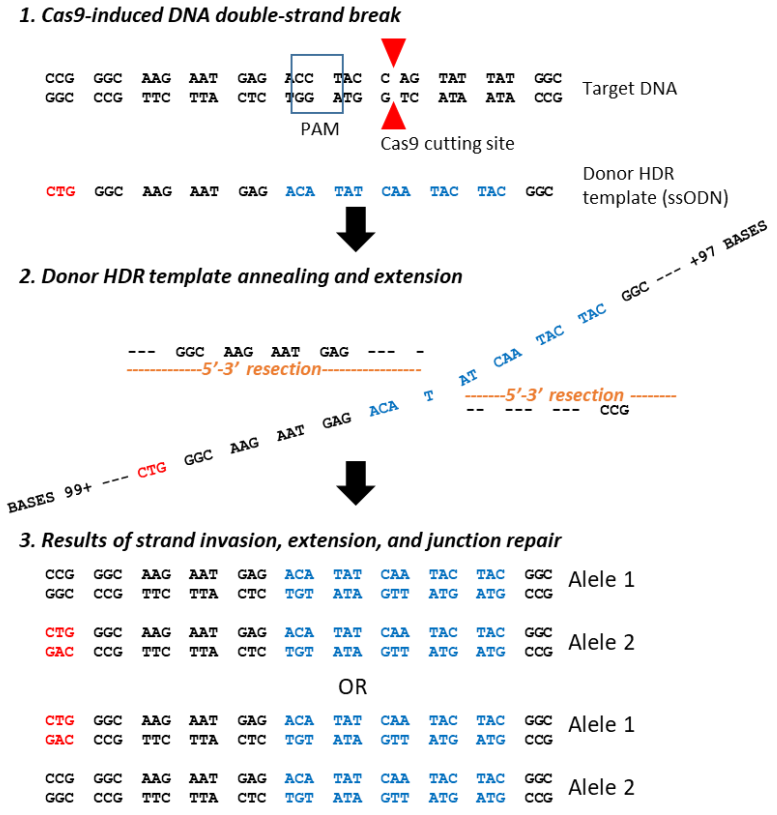

Figure 5-17. The schematic homology-directed repair process in P799L

5.3.2.3 Characterisation of TRPV4 P799L hiPSC line

Similar characterisation strategies to the TRPV4-F273L-2 were performed. The colony morphology assessment showed that the TRPV4-P799L-31 hiPSC line formed tightly packed colonies with homogenous cells and clear peripheral colony edges (Figure 5-18). Immunostaining of NANOG and OCT4 protein showed that these pluripotency markers were exclusively co-localised in the hiPSC colony (Figure 5-18).

Flow cytometry of other pluripotency markers including CD9, Ep-CAM (CD326) and SSEA-4 showed that more than 99% of cells expressed both CD9 and CD326 and around 95% of cells expressed SSEA-4 (Figure 5-19). SNP array did not detect chromosomal abnormalities and SNPduo analysis showed that TRPV4-P799L-31 had 99.9% identical genotypes to the SOX9-T2A-tdTom hiPSC line indicating that both lines were from the same individual (Appendix 7).

The TRPV4-P799L-31 hiPSCs could generate teratomas in immunocompromised mice. Histology of the teratoma showed tissues derived from the three embryonic layers (Figure 5-20), gut epithelium (endoderm), adipocytes (mesoderm) and neuroectoderm (ectoderm).

5.4 Conclusions

We have successfully generated heterozygous mutant TRPV4 c.819C>G (p.F273L) and heterozygous mutant TRPV4 c.2396C>T (p.P799L) iPSC lines. These hiPSC lines will be used to model the TRPV4 skeletal diseases in chapter 6.

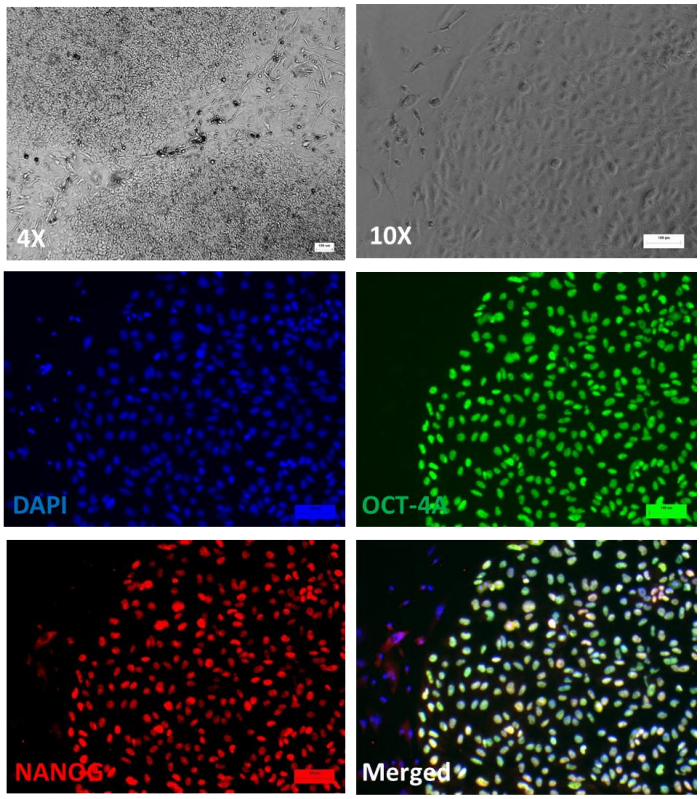

Figure 5-18. Colony morphology and pluripotency marker immunostaining of TRPV4-P799L-31 hiPSC line. Scale bar: 100µm

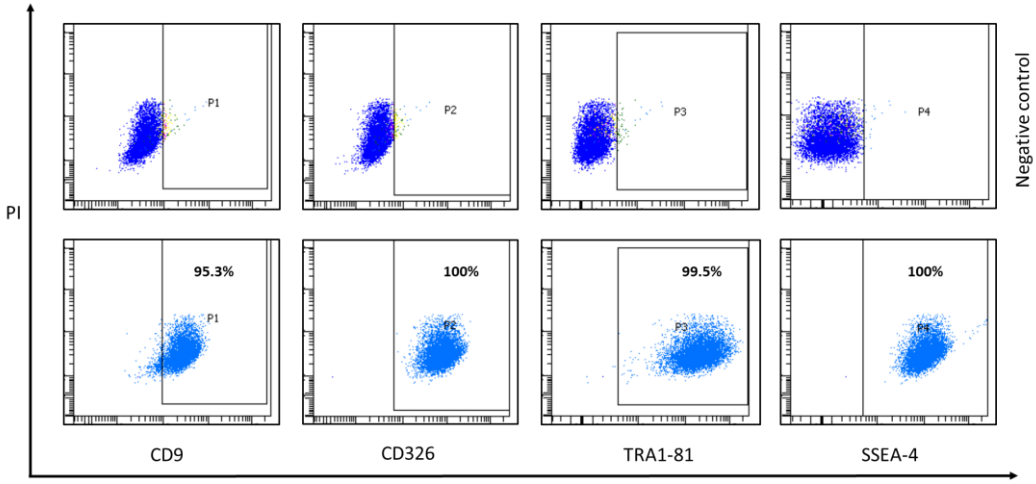

Figure 5-19. The expression of pluripotency markers assessed using flowcytometry.

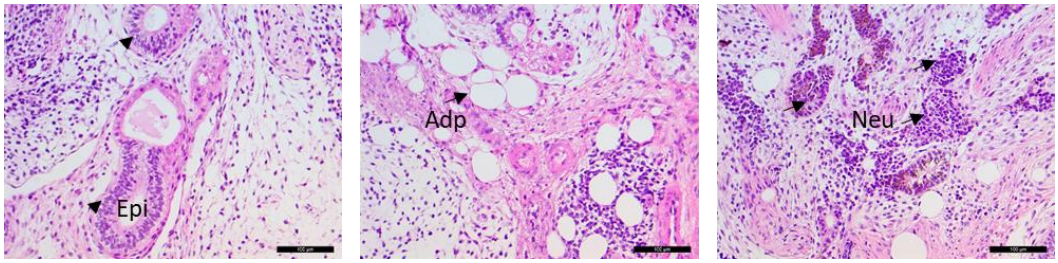

Figure 5-20. Three germ layer formation in teratoma generated from TRPV4-P799L-31 hiPSC line. Epi: gut epithelium (endoderm), Adp: adipocytes (mesoderm), Neu: Neuroectoderm (ectoderm). Scale bar: 100µm.

Chapter 6

hiPSC-disease modeling of TRPV4-inherited skeletal diseases

6.1 Introduction

TRPV4 mutations cause significant cartilage and bone malformation suggesting the importance of TRPV4 in cartilage and bone development. TRPV4 mutations cause two distinct skeletal disease phenotypes, the TRPV4 skeletal dysplasia and arthropathy. The clinical signs of TRPV4 skeletal dysplasia are absent in arthropathy phenotype, FDAB, suggesting the difference in pathogenic mechanisms. A number of studies had been performed in heterologous cell lines (7-10) and only two studies were performed in chondrocytes (8, 86). However, the pathogenesis of TRPV4 mutations in causing the two TRPV4-inherited skeletal disease phenotypes is largely undescribed.

Given the ability of hiPSCs to generate cartilage *in vitro,* the hiPSC-disease model approach has been used to model inherited skeletal diseases. Only one study has used hiPSCs to model TRPV4-inherited skeletal disease (21). However, the potential pathogenic mechanisms responsible for the disease phenotypes were not identified and some improvements are needed including the use of a more optimised chondrocyte differentiation protocol and isogenic control cell lines. Therefore, to improve the hiPSC-disease model for TRPV4-inherited skeletal disease, two hiPSC lines with heterozygous TRPV4 mutations, p.F273L and p.P799L, were generated from wild-type hiPSC line (SOX9-T2A-tdTom) hence the mutant lines and the wild-type control were isogenic (in Chapter 5). Therefore, in this chapter, the SOX9-T2A-tdTom hiPSC line is called as wild-type. These hiPSC lines were differentiated into chondrocytes and global gene expression analysis using RNA sequencing was used to explore the pathogenic mechanisms underlying the two distinct TRPV4-inherited skeletal disease phenotypes.

6.2 Results

6.2.1 The P799L mutant pellet showed a distinct morphology

The first question asked was whether TRPV4 mutations caused defects in cartilage morphology. To answer this question, the morphology of day 6+50 pellets was assessed using a transmission light microscope. The pellets derived from P799L mutant hiPSCs looked more translucent than the other two genotypes (wild-type and F273L mutant) (Figure 6-1A).

To confirm the distinct transmission light microscopy morphology, the pellet histology was assessed. The P799L pellets had relatively more non-cartilage tissues than the other two genotypes (Figure 6-1A) which could indicate a reduced capacity of the P799L mutant hiPSCs to differentiate into chondrocytes. Pellets were digested with trypsin at day 6+61 to remove the non-cartilage tissues, and after nine days of re-culturing

in chondrocyte differentiation medium, samples were collected for histology. Toluidine blue staining of day 6+70 trypsin digested pellets showed no apparent difference in cartilage tissue morphology between three genotypes (Figure 6-1B).

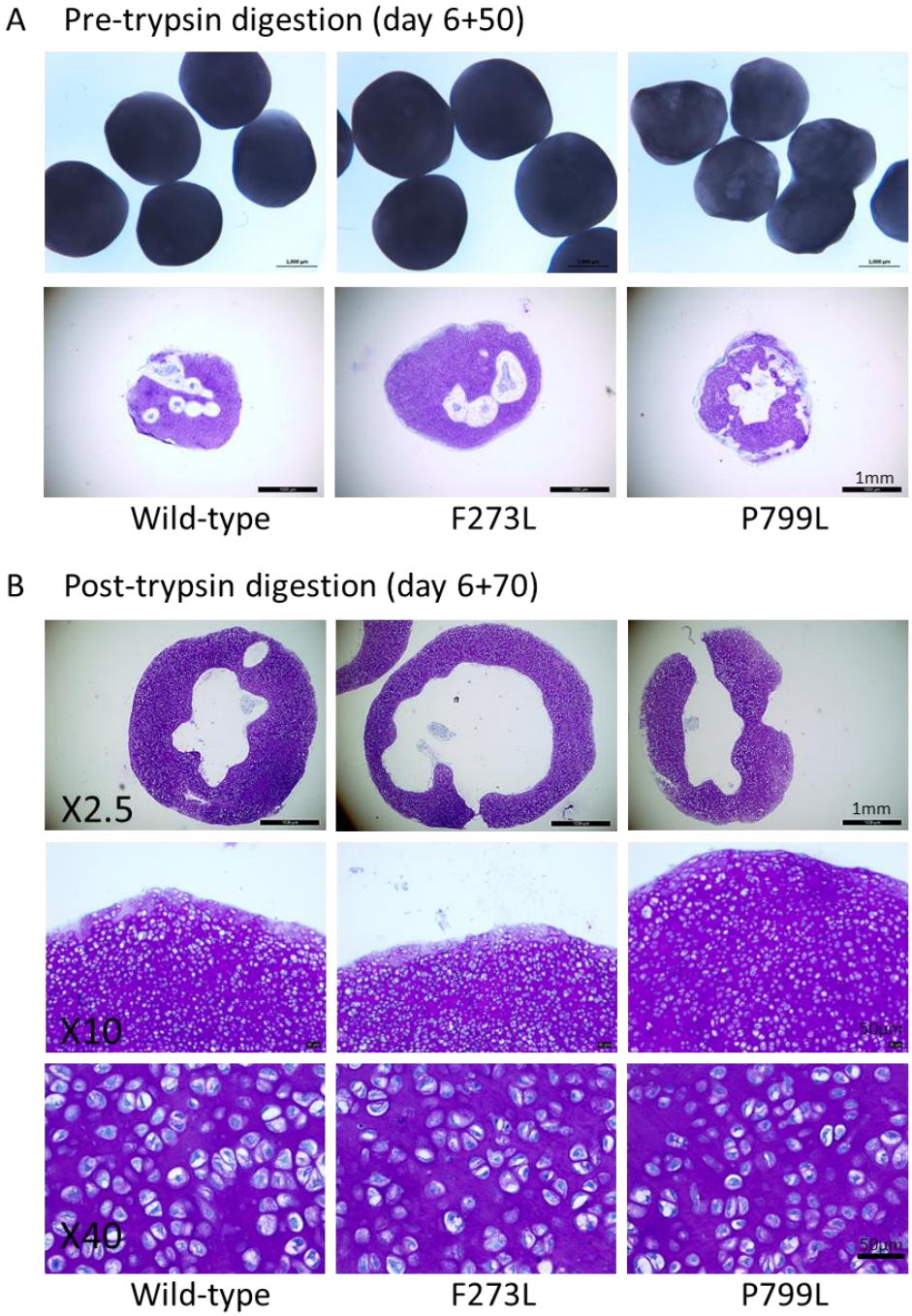

Figure 6-1. The morphology and Toluidine blue staining of pellet cartilage. The morphology of pellets before trypsin digestion is taken from day 6+50 pellets (A). The Toluidine blue staining after trypsin digestion is performed in day 6+70 pellets, and the images of each genotype are representative of 4 independent pellets, scale bar: X2.5=1mm, X10 and X40=50μM.

6.2.2 TRPV4 and COL2A1 protein expression in mutants was similar to the wild-type

The second question asked was whether TRPV4 and COL2A1 expression changed in the mutant cartilage. To answer this question, immunostaining was performed in a histology section obtained from four different pellets from each genotype (Figure 6-2A, B). We were interested in how much COL2A1 protein was deposited in the extracellular matrix hence the area of COL2A1 fluorescence was quantified (330). The COL2A1 fluorescence area was similar between wild-type and two TRPV4 mutants (Figure 6-2C).

The fluorescence intensity was used to assess TRPV4 expression as we were interested in how much SOX9 protein was expressed in the cells rather than the number of TRPV4 expressing cells (330). Immunostaining showed that the level of TRPV4 protein expression was not significantly different between wild-type and the two TRPV4 mutants (Figure 6-2D). Hence, the mutations did not have a major impact on TRPV4 protein expression or stability.

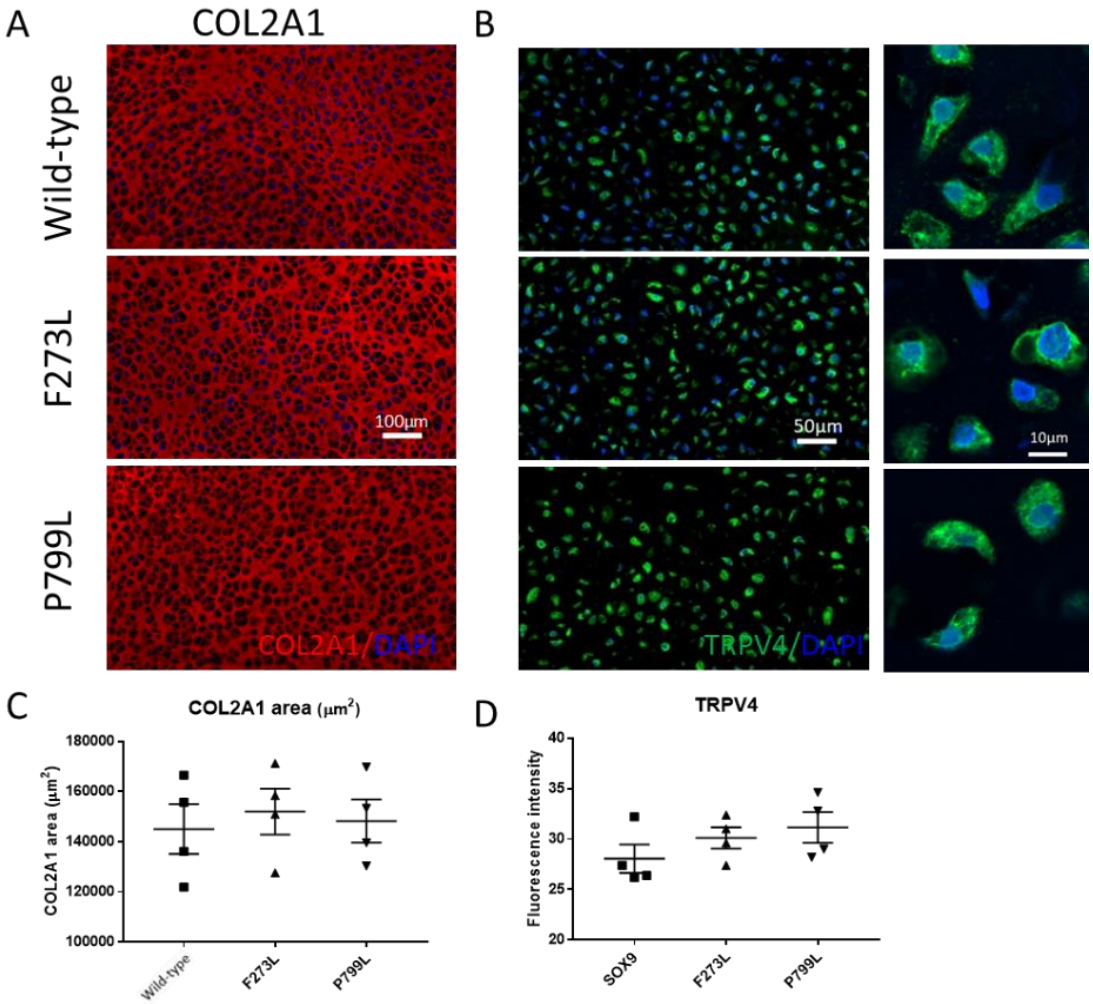

Figure 6-2. COL2A1 and TRPV4 immunostaining of day 6+70 pellets. The COL2A1 protein is shown in red fluorescence (A), and TRPV4 protein is shown in green fluorescence (B). The fluorescence area of COL2A1 (C) and fluorescence intensity of TRPV4 are calculated from fluorescence images captured from at least three randomly selected areas (at least 3 images) of a section from 4 independent pellets (n=4). The images are taken at objective magnification X10. Error bars represent SD.

6.2.3 RNA sequencing analysis of day 6+70 pellets showed differences in gene expression in the mutant cartilage

Unbiased global gene expression analysis was performed using RNA sequencing to obtain an overall picture of gene expressions downstream of TRPV4 mutations. Three different pellets per genotypes (wild-type, F273L, and P799L) were trypsin digested and after nine days of re-culturing, RNA was extracted from the pellets.

Heatmap and principle component analysis (PCA) plots were generated from the RNA sequencing data. The 1500 most variable genes between the three genotypes were used to generate the heatmap. The heatmap showed that the transcript variations among technical replicates within each genotype are minimal except for one of the wild-type technical replicates which had very distinct gene expression patterns compared to the other two technical replicates (Figure 6-3A). This might be caused by incomplete trypsin digestion thus having relatively more non-cartilage tissues than the other two replicates. The PCA plot confirmed the presence of this outlier (Figure 6-3B). The first principal component explained 31% of the variance. The outlier was discarded and only 2 wild-type technical replicates were included for further analysis.

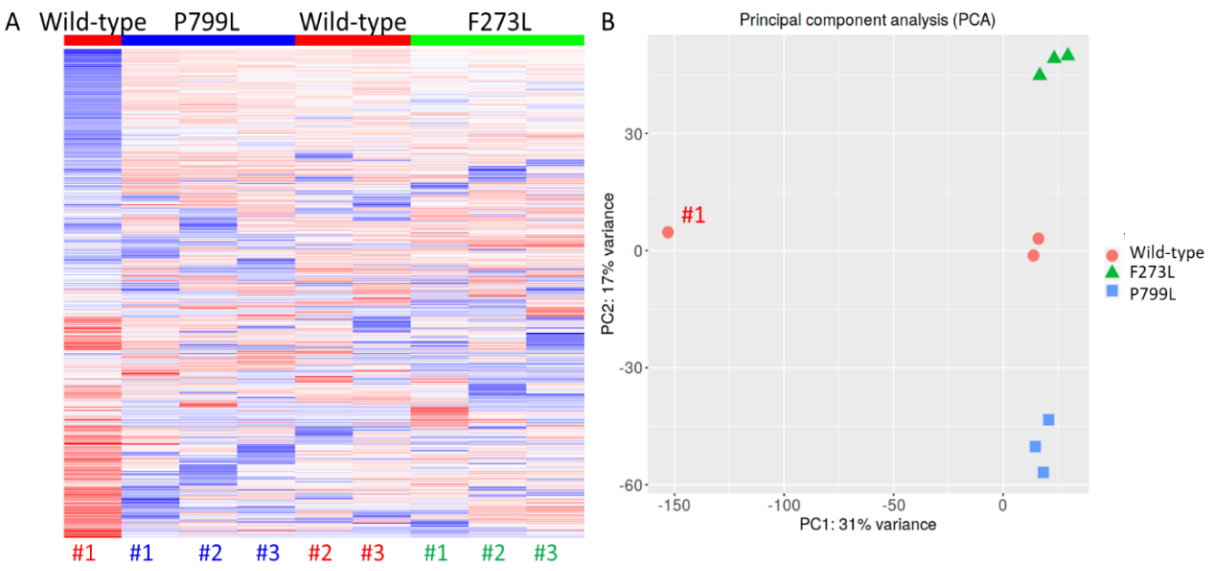

Figure 6-3. One of the three wild-type technical replicates is an outlier. Heatmap from 1500 most variable genes (A) and PCA plot (B) confirm the presence of an outlier (replicates #1) in the wild-type group.

The transcripts of the two TRPV4 mutant chondrocytes were compared to the wild-type chondrocytes. The differentially expressed transcripts with an adjusted p-value (adj.p-value) <0.05 were used for further analyses. We found 133 upregulated and 130 down-regulated genes in the F273L vs. wild-type and in the P799L vs. wild-type, we found 301 upregulated and 354 down-regulated genes (Figure 6-4C). We also found that 61 differentially expressed genes were shared between F273L and P799L. The full list of the differentially expressed genes is available in appendix 8 and 9. The scatter plot shows the differentially expressed genes in F273L vs. wild-type (Figure 6-4A) and P799L vs. wild-type (Figure 6-4B).

The heatmap of differentially expressed genes was generated to visualise the difference in gene expression patterns between the three genotypes. The heatmap showed very distinct gene expression levels and patterns between F273L and P799L indicating that the pathogenic mechanisms downstream of the two mutations were different. From the heatmap analysis, four different gene clusters were identified (Figure 6-5). To explore the function of genes in each cluster, gene ontology (GO) annotation analysis was performed using ClueGO and BiNGO bioinformatics tools. The top 10 most significant GO terms for biological processes of each gene cluster are shown in Figure 6-5. The complete list of GO terms and the genes associated with each GO term are available in Appendix 11.

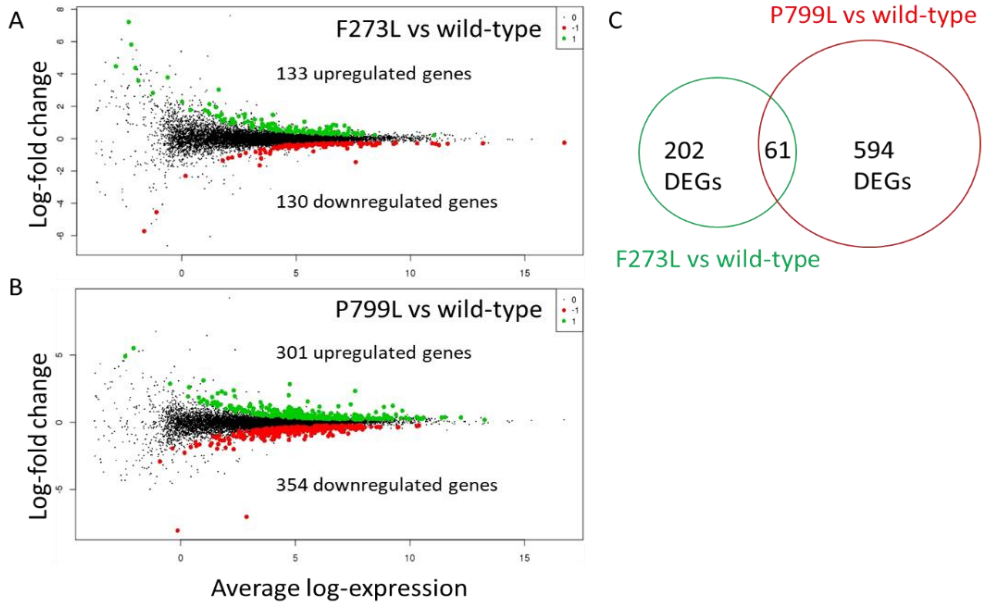

Figure 6-4. The differentially expressed genes. Scatter plots show the distribution of downregulated (red dots) and upregulated (green dots) genes in both F273L vs. wild-type (A) and P799L vs. wild-type (B). Venn diagram shows the number of differentially expressed genes (DEGs) in F273L vs. wild-type and P799L vs. wild-type, and the shared differentially expressed genes in both (C).

CLUSTER A

GO:0000278	mitotic cell cycle
GO:1903047	mitotic cell cycle process
GO:0140014	mitotic nuclear division
GO:0022402	cell cycle process
GO:0000280	nuclear division
GO:0000070	mitotic sister chromatid segregation
GO:0000819	sister chromatid segregation
GO:0010564	regulation of cell cycle process
GO:0051726	regulation of cell cycle
GO:0044770	cell cycle phase transition

CLUSTER B

GO:0019320	hexose catabolic process
GO:0019674	NAD metabolic process
GO:0006027	glycosaminoglycan catabolic process
GO:0046902	regulation of mitochondrial membrane permeability
GO:0097345	mitochondrial outer membrane permeabilisation
GO:0097178	ruffle assembly
GO:0060350	endochondral bone morphogenesis
GO:0060603	mammary gland duct morphogenesis

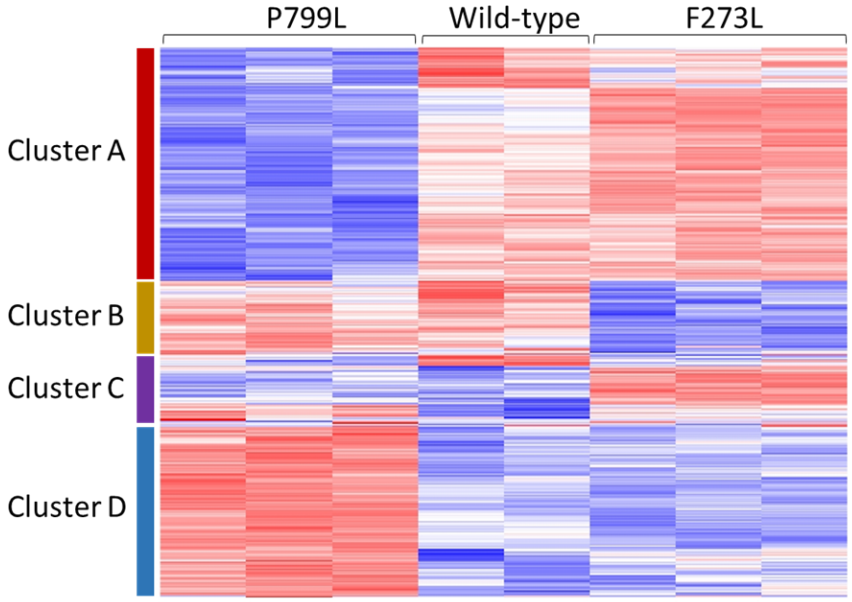

CLUSTER C

GO:0003300	Cardiac muscle hypertrophy
GO:2000725	regulation of cardiac muscle cell differentiation
GO:0048011	neurotrophin TRK receptor signaling pathway
GO:1904705	regulation of vascular smooth muscle cell proliferation
GO:0031110	regulation of microtubule polymerisation or depolymerisation
GO:0010613	positive regulation of cardiac muscle hypertrophy

CLUSTER D

GO:0051272	positive regulation of cellular component movement
GO:0030335	positive regulation of cell migration
GO:0043062	extracellular structure organisation
GO:0030198	extracellular matrix organisation
GO:0045047	protein targeting to ER
GO:0070972	protein localisation to endoplasmic reticulum
GO:0019080	viral gene expression
GO:0070848	response to growth factor
GO:0000184	nuclear-transcribed mRNA catabolic process, nonsense-mediated decay
GO:0071363	cellular response to growth factor stimulus

Figure 6-5. The four gene clusters identified from heatmap analysis and the top 10 most significant GO terms for biological processes associated with each gene cluster. GO annotation analysis was performed using ClueGO.

6.2.4 P799L and F273L showed opposite regulation of genes related to cell adhesion and skeletal development

Given that there were 61 differentially expressed genes shared between F273L and P799L, there might be common biological process regulation changes caused by the two mutants. Out of 61 genes, 32 genes were downregulated in P799L but upregulated in F273L, 16 genes were upregulated in P799L but downregulated in F273L, 7 genes were downregulated in both P799L and F273L, and 6 genes were upregulated in both P799L and F273L. To find out what biological processes were regulated by the 61 genes, gene ontology (GO) annotation analysis was performed in 61 genes using BiNGO bioinformatics tools in a default setting. Twenty three GO terms were generated with adj.p-value < 0.05 (Table 6-1). Cell adhesion and skeletal development-related GO terms were enriched in the analysis. The complete information on the generated GO terms is available in appendix 10.

Table 6-1. The GO terms for biological processes obtained from BiNGO

GO Id	GO terms	Number of genes	Adj. p-value
GO:0007155	cell adhesion	12	4.57E-03
GO:0022610	biological adhesion	12	4.57E-03
GO:0006564	L-serine biosynthetic process	2	1.43E-02
GO:0048731	system development	21	1.65E-02
GO:0048856	anatomical structure development	22	1.65E-02
GO:0016337	cell-cell adhesion	7	1.65E-02
GO:0060348	bone development	5	1.84E-02
GO:0046942	carboxylic acid transport	5	1.95E-02
GO:0015849	organic acid transport	5	1.95E-02
GO:0030154	cell differentiation	16	2.49E-02
GO:0006865	amino acid transport	4	2.49E-02
GO:0034383	low-density lipoprotein particle clearance	2	2.49E-02
GO:0048869	cellular developmental process	16	2.67E-02
GO:0006563	L-serine metabolic process	2	2.83E-02
GO:0009987	cellular process	46	3.00E-02
GO:0007275	multicellular organismal development	22	3.25E-02
GO:0009070	serine family amino acid biosynthetic process	2	4.30E-02
GO:0015837	amine transport	4	4.30E-02
GO:0048638	regulation of developmental growth	3	4.30E-02
GO:0048640	negative regulation of developmental growth	2	4.30E-02
GO:0008652	cellular amino acid biosynthetic process	3	4.30E-02
GO:0001503	ossification	4	4.30E-02
GO:0034599	cellular response to oxidative stress	3	4.84E-02

Interestingly, genes related to cell adhesion including *PTPRT, SPON1, CADM3, MMRN1, PTPRO, ITGB8, CD36, CELSR2, NTN1,* were downregulated in P799L whereas in the F273L they were upregulated (Figure 6-6A). On the other hand, genes related to skeletal development such as *WISP3, CILP2, SPP1,* and *BMP8B* were upregulated in P799L but downregulated in F273L (Figure 6-6B). These findings suggested that the two mutations had very distinct pathogenic mechanisms. *BMP3, SOX8,* and *PAX1* gene expressions were downregulated in both mutants (Figure 6-6).

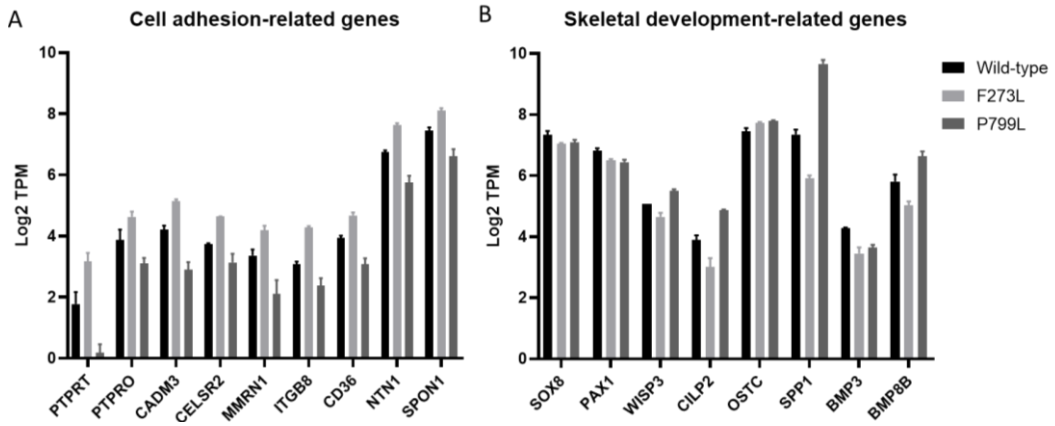

Figure 6-6. The differentially expressed genes related to cell adhesion and skeletal development that are shared between F273L vs. wild-type and P799L vs. wild-type. All these genes are differentially expressed with adj. p-value <0.05. The transcript level of each group is presented in the actual log2 transcript per million (log2TPM) value from 3 technical replicates. Error bars represent SD.

6.2.5 F273L showed a reduction in cartilage gene expression

From the heatmap (Figure 6-5), genes in cluster B were downregulated in F273L compared to the wild-type. GO annotation of this gene cluster identified terms related to glycosaminoglycan catabolic process and endochondral bone morphogenesis (Table 6-2) (see Appendix 11 for complete GO term information). The genes listed in these GO terms, *BGN, CSPG4, GPC1, SGSH, COL27A1, COL2A1, INPPL1, THBS3,* were downregulated (Figure 6-7). Moreover, cartilage-related genes such as *BMP3, COL9A2, CILP2,* and *PAX1* were also reduced in F273L. These indicated that the F273L mutation cause defects in cartilage development.

SHH was upregulated four-fold suggesting that the cartilage was less mature than the wild-type cartilage. SHH is downregulated in the post-natal nucleus pulposus of the vertebral discs compared to day 12.5 embryo (331) and a continuous SHH signalling inhibits chondrocyte differentiation in transgenic mice overexpressing human SHH (332). Downregulation of the hypertrophic maturation marker *SPP1* in F273L is also consistent with delayed cartilage maturity.

Table 6-2. The GO terms for biological processes obtained from ClueGO.

GO Id	GO Term	Number of genes	Adj. p-value
Cluster B			
GO:0019320	hexose catabolic process	6	6.79E-05
GO:0019674	NAD metabolic process	6	6.85E-04
GO:0006027	glycosaminoglycan catabolic process	5	0.001061
GO:0046902	regulation of mitochondrial membrane permeability	5	0.003843
GO:0097345	mitochondrial outer membrane permeabilisation	4	0.006406
GO:0097178	ruffle assembly	3	0.006990
GO:0060350	endochondral bone morphogenesis	4	0.007405
GO:0060603	mammary gland duct morphogenesis	3	0.010188
Cluster C			
GO:0003300	cardiac muscle hypertrophy	5	0.001698
GO:2000725	regulation of cardiac muscle cell differentiation	3	0.003504
GO:0048011	neurotrophin TRK receptor signaling pathway	3	0.004945
GO:1904705	regulation of vascular smooth muscle cell proliferation	3	0.005761
GO:0031110	regulation of microtubule polymerisation or depolymerisation	4	0.006245
GO:0010613	positive regulation of cardiac muscle hypertrophy	3	0.007264

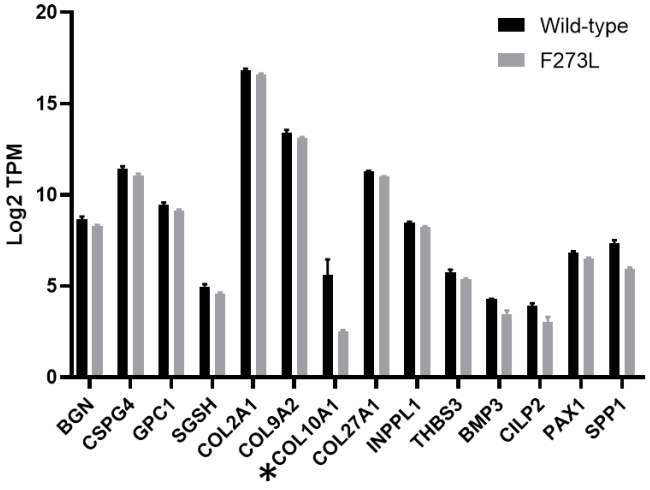

Figure 6-7. The expression of genes related to glycosaminoglycan catabolic process and skeletal development in F273L and wild-type. All these genes are differentially expressed with adj. p-value <0.05 except the ones with (*). The transcript level of each group is presented in the actual log2 transcript per million (log2TPM) value from 3 technical replicates. Error bars represent SD.

6.2.6 P799L showed accelerated chondrocyte hypertrophy

6.2.6.1 P799L showed an increased expression of genes related to cartilage and bone development

Based on the heatmap, genes in cluster D were upregulated in P799L cartilage. Clustering analysis of the GO terms resulted in 13 clusters indicated by different colour highlight (Table 6-3). The complete information on the GO terms is available in appendix 10.

Table 6-3. GO terms obtained from GO annotation analysis of genes in cluster D

GO Id	GO Terms	Number of genes	Adj. p-value
GO:0009266	response to temperature stimulus	16	0.004085
GO:0043405	regulation of MAP kinase activity	22	5.36E-04
GO:0072593	reactive oxygen species metabolic process	19	2.89E-04
GO:0030212	hyaluronan metabolic process	7	0.001704
GO:1903510	mucopolysaccharide metabolic process	10	0.006811
GO:0031960	response to corticosteroid	16	1.82E-04
GO:0048545	response to steroid hormone	25	2.02E-04
GO:0051384	response to glucocorticoid	14	0.001663
GO:1901654	response to ketone	15	0.00221
GO:0010715	regulation of extracellular matrix disassembly	6	5.67E-04
GO:0022617	extracellular matrix disassembly	9	0.006828
GO:0030198	extracellular matrix organisation	27	4.63E-08
GO:0043062	extracellular structure organisation	30	2.76E-08
GO:0030335	positive regulation of cell migration	34	1.47E-08
GO:0070848	response to growth factor	38	7.56E-07
GO:0071363	cellular response to growth factor stimulus	36	2.97E-06
GO:0044344	cellular response to fibroblast growth factor stimulus	11	0.009797
GO:0010035	response to inorganic substance	31	5.19E-05
GO:0010038	response to metal ion	25	1.95E-05
GO:0031668	cellular response to extracellular stimulus	17	0.006291
GO:0033273	response to vitamin	10	0.009736
GO:0034599	cellular response to oxidative stress	18	0.005901
GO:0071496	cellular response to external stimulus	20	0.002259
GO:0001501	skeletal system development	26	5.73E-04
GO:0001649	osteoblast differentiation	14	0.007096
GO:0030278	regulation of ossification	14	0.002110
GO:0031214	biomineral tissue development	13	0.002157
GO:0051216	cartilage development	15	0.001434
GO:0061448	connective tissue development	18	4.87E-04
GO:0001558	regulation of cell growth	23	0.001070
GO:0030308	negative regulation of cell growth	14	0.003473
GO:0045926	negative regulation of growth	17	0.004321
GO:0048588	developmental cell growth	16	0.001667
GO:0048638	regulation of developmental growth	19	0.003071
GO:0060560	developmental growth involved in morphogenesis	18	1.77E-04
GO:0000184	nuclear-transcribed mRNA catabolic process, nonsense-mediated decay	15	2.45E-06
GO:0000956	nuclear-transcribed mRNA catabolic process	17	9.25E-05
GO:0006402	mRNA catabolic process	21	0.001013
GO:0006612	protein targeting to membrane	17	4.56E-05
GO:0045047	protein targeting to ER	16	4.83E-08
GO:0070972	protein localisation to endoplasmic reticulum	17	1.18E-07
GO:0090150	establishment of protein localisation to membrane	20	0.001503

GO:0004866	endopeptidase inhibitor activity	15	3.39E-04
GO:0008236	serine-type peptidase activity	18	0.001740
GO:0010951	negative regulation of endopeptidase activity	20	1.25E-05
GO:0045861	negative regulation of proteolysis	24	1.14E-05
GO:0051346	negative regulation of hydrolase activity	27	2.86E-05
GO:0052548	regulation of endopeptidase activity	27	5.61E-06
GO:0010595	positive regulation of endothelial cell migration	11	0.001423
GO:0010631	epithelial cell migration	17	0.008979
GO:0010632	regulation of epithelial cell migration	15	0.005463
GO:0010634	positive regulation of epithelial cell migration	13	0.001078
GO:0032103	positive regulation of response to external stimulus	18	0.006077
GO:0045765	regulation of angiogenesis	18	0.002300
GO:0051272	positive regulation of cellular component movement	36	3.58E-09
GO:1901342	regulation of vasculature development	20	6.31E-04

Extracellular matrix, cartilage, and bone development related GO terms were enriched in P799L. Plotting the differentially expressed genes listed in these GO terms and other known hypertrophic chondrocyte markers showed the upregulation of genes related to cartilage and bone development. Cartilage selective genes, genes that are more abundantly expressed in cartilage tissues (40), including *CILP2*, *COMP*, *MATN3*, *HPLN1*, *PODNL1*, *COL25A1*, *SERPINE2*, *SERPINA3*, *BMP6*, and *WISP3* were upregulated in P799L (Figure 6-8A). This might suggest that P799L cartilage was more mature than the wild-type cartilage. In addition, chondrocyte hypertrophic change-related genes (48, 137, 333, 334) including *MEF2C*, *RUNX2*, *PTH1R*, and *SPP1* or osteopontin, were upregulated by 1.3, 1.43, 1.33, and 5.00 fold respectively (Figure 6-8A, red box) suggesting an accelerated in hypertrophic maturation.

In addition, terms associated with vascular development and osteoblast development were also enriched (Table 6-3) supporting the idea of accelerated chondrocyte hypertrophic maturation and endochondral ossification in P799L. The genes associated with vascular development that were upregulated including *HIF1A* (1.44 fold), *FGF2* (1.28 fold), *HMOX1* (1.89 fold), and *THBS1* (1.2 fold) (Figure 6-8B). Also, genes related to osteoblast differentiation including *RUNX2* (1.3 fold), *SP7* or *OSX* (2.22 fold), *TNFRSF11B* or *OPG* (osteoprotegerin) (1.59 fold), *NELL1* (1.38 fold), *SPP1* (5.00 fold), were upregulated (Figure 6-8B).

To know what signalling pathways involved, the Kyoto Encyclopedia of Genes and Genomes (KEGG) pathway analysis was performed using ClueGO. KEGG pathway analysis identified several signalling pathways including MAPK, PI3K-Akt, FoxO, and P53 (Table 6-4).

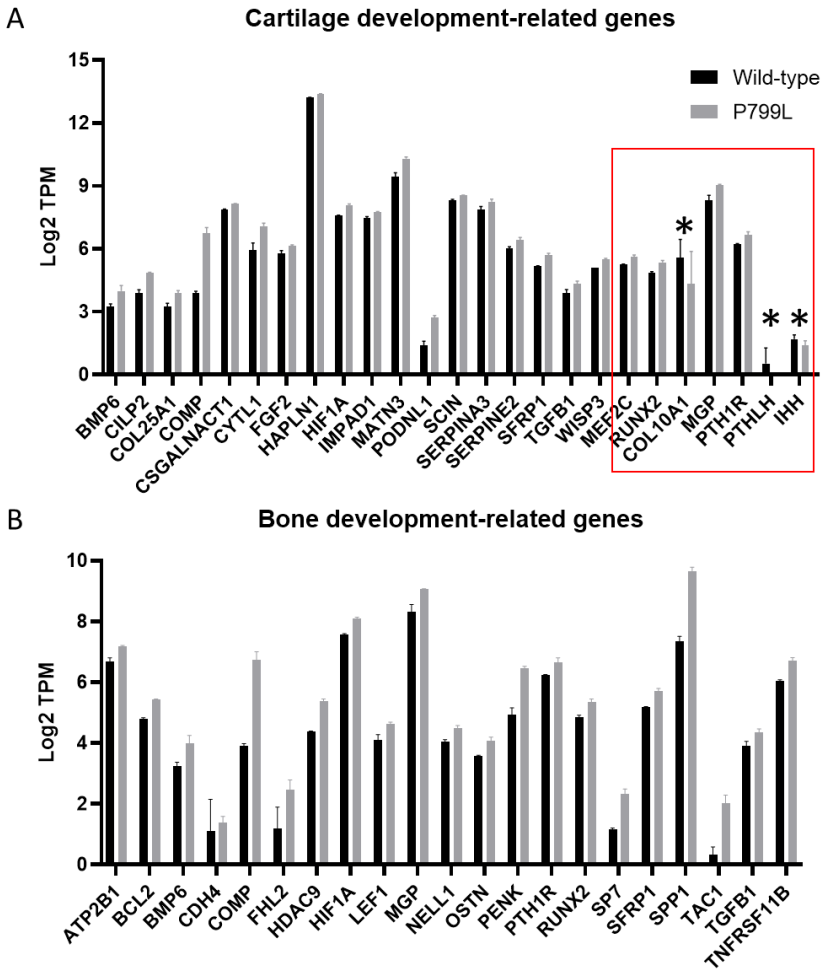

Figure 6-8. The differentially expressed genes related to cartilage and bone development in P799L vs. wild-type control. Red box: hypertrophic chondrocyte markers. All these genes are differentially expressed with adj. p-value <0.05 except the ones with (*). The transcript level of each group is presented in the actual log2 transcript per million (log2TPM) value from 3 technical replicates. Error bars represent SD.

Table 6-4. Signalling pathways identified from KEGG pathway analysis of genes in cluster D

Signalling	**Adj. p-value**	**Differentially expressed genes found in P799L vs. wild-type**
Ribosome	3.93E-06	*RPL10A, RPL14, RPL17, RPL18A, RPL27A, RPL29, RPL6, RPL7, RPS13, RPS17, RPS18, RPS19, RPS5, RPS6*
MAPK signalling pathway	0.07	*DUSP1, DUSP6, FGF2, HSPA1A, HSPA6, IL1R1, KIT, MAP3K8, NR4A1, RPS6KA3, TGFA, TGFB1*
FoxO signalling pathway	0.03	*ATM, BCL6, CDKN1A, IL6, MDM2, SETD7, SOD2, TGFB1*
p53 signalling pathway	0.03	*ATM, BCL2, CDKN1A, MDM2, PMAIP1, THBS1*
PI3K-Akt signalling pathway	0.01	*BCL2, CDKN1A, COMP, FGF2, IL6, KIT, MCL1, MDM2, NR4A1, OSMR, RPS6, SPP1, TGFA, THBS1, THBS2*
Malaria	0.03	*COMP, IL6, TGFB1, THBS1, THBS2*
Transcriptional misregulation in cancer	0.08	*ATM, BCL6, BIRC3, CDKN1A, DUSP6, ERG, IL6, MDM2, RUNX2*
Colorectal cancer	0.01	*BCL2, CDKN1A, DCC, LEF1, PMAIP1, TGFA, TGFB1*

Plotting the differentially expressed genes listed in GO term: regulation of MAP kinase activity obtained from GO annotation analysis and MAPK signalling pathway obtained from KEGG analysis showed that P799L had increased MAPK signalling. Transcription factors downstream of *MAPK14* (p38) (335), such as *MEF2C, ETS1*, and *STAT1* were detected in RNA sequencing. *MEF2C,* the master regulator of chondrocyte hypertrophy, and *ETS1* were upregulated 1.3 and 1.36 fold, respectively (Figure 6-9, red box). *OSTN* or osteocrin, a direct target of *MEF2C* (336), was upregulated 1.42 fold suggesting increased MEF2C activity. *MAP3K8*, the upstream regulator to *MAPK14* expression (337), was upregulated 2 fold. *MAPK14* (p38) and *STAT1* were not changed however since their activity is regulated by post-translational phosphorylation (335), measuring the protein activity of MAPK signalling pathways is needed to validate the increase in MAPK signalling in P799L.

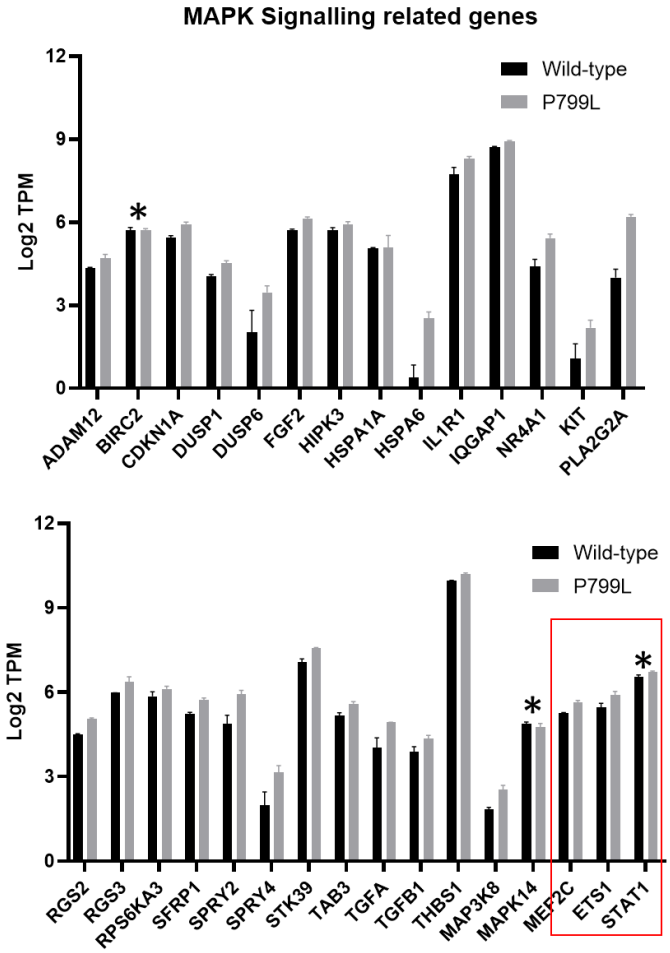

Figure 6-9. The expression of genes related to MAPK signalling. All these genes are differentially expressed with adj. p-value <0.05 except the ones with (*). Red box: downstream genes of MAPK14 signalling. The transcript level of each group is presented in the actual log2 transcript per million (log2TPM) value from 3 technical replicates. Error bars: SD.

6.2.6.2 P799L showed reduced cell proliferation and increased apoptosis

Based on the heatmap analysis, genes in cluster A were downregulated in P799L cartilage. Fifteen GO clusters were identified (indicated by different colour highlights) with cell cycle-related GO terms dominating (Table 6-5). The complete information on the GO terms is available in Appendix 11. KEGG pathway analysis confirmed the GO annotation analysis results in which cell cycle-related terms including cell cycle, DNA replication, oocyte maturation, and meiosis were enriched (Table 6-6).

Table 6-5. GO terms obtained from GO annotation analysis of genes in cluster A

GO Id	GO terms	Number of genes	Adj. p-value
GO:0007264	small GTPase mediated signal transduction	33	0.002562
GO:0051640	organelle localisation	37	0.005007
GO:0014855	striated muscle cell proliferation	10	0.005294
GO:0048145	regulation of fibroblast proliferation	12	0.002342
GO:0000226	microtubule cytoskeleton organization	42	2.39E-08
GO:0007010	cytoskeleton organisation	76	4.26E-10
GO:0030036	actin cytoskeleton organisation	38	9.83E-04
GO:0003333	amino acid transmembrane transport	12	0.003202
GO:0006865	amino acid transport	15	0.003951
GO:0015175	neutral amino acid transmembrane transporter activity	8	0.003084
GO:0050807	regulation of synapse organisation	20	7.94E-04
GO:0051962	positive regulation of nervous system development	37	3.02E-05
GO:0050808	synapse organisation	32	1.33E-05
GO:0008608	attachment of spindle microtubules to kinetochore	9	4.01E-05
GO:0045841	negative regulation of mitotic metaphase/anaphase transition	9	2.73E-04
GO:0051983	regulation of chromosome segregation	20	1.03E-09
GO:0051988	regulation of attachment of spindle microtubules to kinetochore	5	0.001788
GO:0007051	spindle organisation	20	3.02E-06
GO:0007052	mitotic spindle organisation	15	1.60E-05
GO:1902850	microtubule cytoskeleton organisation involved in mitosis	17	7.93E-06
GO:0051276	chromosome organisation	72	1.32E-09
GO:0071103	DNA conformation change	27	2.75E-06
GO:0006323	DNA packaging	23	3.56E-07
GO:0007076	mitotic chromosome condensation	8	3.20E-06
GO:0010032	meiotic chromosome condensation	5	4.50E-04
GO:0030261	chromosome condensation	13	1.27E-08
GO:0000910	Cytokinesis	21	1.99E-06
GO:0090068	positive regulation of cell cycle process	30	1.94E-07
GO:0000915	actomyosin contractile ring assembly	6	3.30E-05
GO:0032465	regulation of cytokinesis	12	0.001417
GO:0032506	cytokinetic process	9	5.18E-04
GO:0051302	regulation of cell division	17	7.77E-04
GO:0061640	cytoskeleton-dependent cytokinesis	16	3.49E-06
GO:0000070	mitotic sister chromatid segregation	31	1.62E-16
GO:0000280	nuclear division	50	3.89E-17
GO:0000819	sister chromatid segregation	33	1.27E-15
GO:0033044	regulation of chromosome organisation	26	8.22E-04
GO:0098813	nuclear chromosome segregation	35	4.14E-13
GO:0140014	mitotic nuclear division	46	7.35E-21
GO:0010720	positive regulation of cell development	32	0.007542

GO:0045664	regulation of neuron differentiation	38	9.68E-04
GO:0045666	positive regulation of neuron differentiation	26	0.002621
GO:0050767	regulation of neurogenesis	46	1.47E-04
GO:0051960	regulation of nervous system development	52	1.59E-05
GO:0060284	regulation of cell development	49	4.35E-04
GO:0010948	negative regulation of cell cycle process	27	9.31E-04
GO:0031570	DNA integrity checkpoint	18	1.98E-04
GO:0044770	cell cycle phase transition	55	1.73E-13
GO:0044843	cell cycle G1/S phase transition	23	2.50E-04
GO:1901988	negative regulation of cell cycle phase transition	22	6.44E-04
GO:1901991	negative regulation of mitotic cell cycle phase transition	19	0.008593
GO:0000083	regulation of transcription involved in G1/S transition of mitotic cell cycle	7	0.002419
GO:0006260	DNA replication	21	0.007466
GO:0000075	cell cycle checkpoint	27	2.82E-08
GO:0000086	G2/M transition of mitotic cell cycle	25	8.60E-06
GO:0000278	mitotic cell cycle	97	1.47E-28
GO:0007088	regulation of mitotic nuclear division	27	4.08E-10
GO:0007091	metaphase/anaphase transition of mitotic cell cycle	13	8.19E-07
GO:0007093	mitotic cell cycle checkpoint	19	5.11E-05
GO:0007346	regulation of mitotic cell cycle	58	2.43E-13
GO:0010389	regulation of G2/M transition of mitotic cell cycle	17	0.009579
GO:0010564	regulation of cell cycle process	65	7.50E-14
GO:0010639	negative regulation of organelle organisation	26	0.007537
GO:0022402	cell cycle process	97	5.22E-19
GO:0033043	regulation of organelle organisation	72	4.37E-08
GO:0033045	regulation of sister chromatid segregation	15	2.33E-06
GO:0033046	negative regulation of sister chromatid segregation	10	4.77E-04
GO:0044839	cell cycle G2/M phase transition	27	1.74E-06
GO:0045786	negative regulation of cell cycle	41	6.53E-05
GO:0045787	positive regulation of cell cycle	36	1.05E-07
GO:0045930	negative regulation of mitotic cell cycle	28	2.90E-05
GO:0045931	positive regulation of mitotic cell cycle	15	0.008581
GO:0051129	negative regulation of cellular component organization	41	9.30E-04
GO:0051304	chromosome separation	17	9.36E-08
GO:0051306	mitotic sister chromatid separation	14	4.77E-07
GO:0051726	regulation of cell cycle	82	1.07E-13
GO:0051783	regulation of nuclear division	29	2.17E-10
GO:0051784	negative regulation of nuclear division	10	0.006373
GO:0051984	positive regulation of chromosome segregation	7	0.002013
GO:1901990	regulation of mitotic cell cycle phase transition	36	4.28E-07
GO:1902749	regulation of cell cycle G2/M phase transition	19	0.002056
GO:1903047	mitotic cell cycle process	87	1.75E-26
GO:2001251	negative regulation of chromosome organisation	16	0.001707

Table 6-6. Signalling pathways identified from KEGG pathway analysis of genes in cluster A

Signalling	Adj. p-value	Differentially expressed genes found in P799L vs. wild-type
Cell cycle	1.58E-12	*BUB1, CCNA2, CCNB1, CCNB2, CDC20, CDC25C, CDC45, CDC6, CDK1, CDKN2C, E2F1, E2F2, ESPL1, FZR1, MCM3, MCM4, MCM5, MCM7, PCNA, PKMYT1, RAD21*
Progesterone-mediated oocyte maturation	2.55E-05	*ADCY2, BUB1, CCNA2, CCNB1, CCNB2, CDC25C, CDK1, FZR1, GNAI1, KIF22, PIK3R2, PKMYT1*
Gap junction	3.94E-04	*ADCY2, CDK1, GNAI1, PDGFC, PDGFD, PDGFRB, TUBA1B, TUBB, TUBB2B, TUBB4B*
Oocyte meiosis	0.002	*ADCY2, BUB1, CALM1, CCNB1, CCNB2, CDC20, CDC25C, CDK1, ESPL1, FBXO43, PKMYT1*
MicroRNAs in cancer	0.006	*CDC25C, CDCA5, DDIT4, DNMT1, E2F1, E2F2, ERBB3, EZH2, KIF23, MARCKS, NOTCH1, PDGFRB, PIK3R2, SLC7A1, STMN1, ZEB2, ZFPM2*
DNA replication	0.025	*MCM3, MCM4, MCM5, MCM7, PCNA*
Cellular senescence	0.050	*CALM1, CCNA2, CCNB1, CCNB2, CDK1, E2F1, E2F2, FOXM1, MYBL2, PIK3R2*
Aminoacyl-tRNA biosynthesis	0.069	*AARS, CARS, GARS, MARS, TARS, YARS*

The 46 differentially expressed genes listed in GO term: mitotic nuclear division were downregulated (Figure 6-10). Included in the gene list is a marker of cell proliferation (338), *MKI67*, which was downregulated 1.5 fold. Another cell proliferation marker (not in the list), *PCNA*, was also downregulated 1.25 fold. These indicated that P799L chondrocytes showed reduced cell proliferation. Reduced cell proliferation is a characteristic of hypertrophic zone chondrocytes (5) hence these findings also support the idea that P799L chondrocytes show accelerated hypertrophy. To validate the reduction in cell proliferation, Ki67 immunostaining was performed in day 6+70 pellets (Figure 6-11A). The Ki67 protein expression in the P799L mutant was significantly reduced compared to the wild-type (Figure 6-11B) ($p=0.035$).

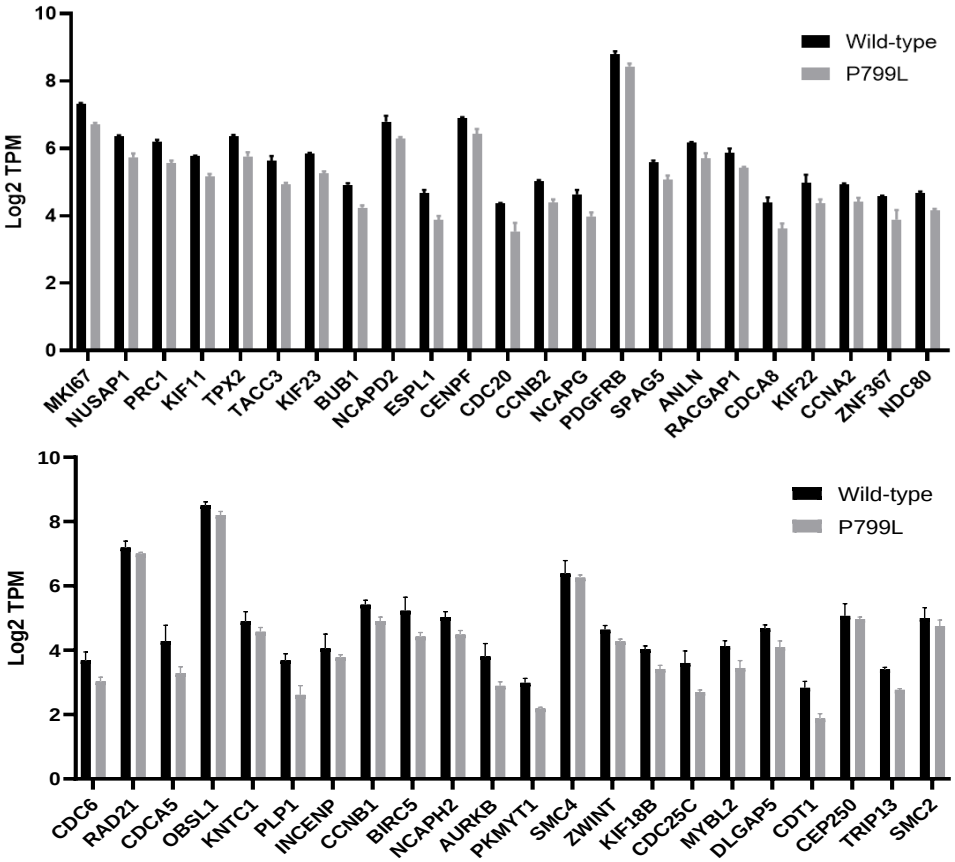

Figure 6-10. The expression of genes listed in the GO term: mitotic nuclear division. All these genes are differentially expressed with adj. p-value <0.05. The transcript level of each group is presented in the actual log2 transcript per million (log2TPM) value from 3 technical replicates. Error bars represent SD.

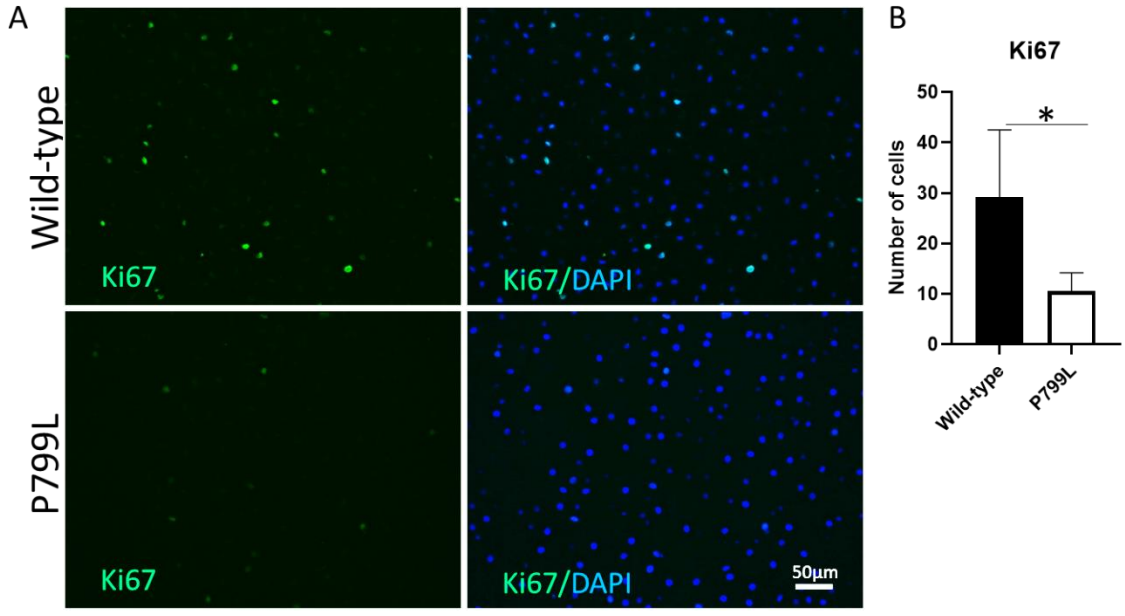

Figure 6-11. Ki67 immunostaining in P799L and wild-type cartilage. P799L cartilage shows reduced the number of cells expressing Ki67 (A). Quantification of the number of cells expressing Ki67 is obtained from a randomly selected area (3 images) of a section from 4 independent pellets (n=4) (B). Error bars represent SD. *p<0.05).

During endochondral ossification, hypertrophic chondrocytes undergo apoptosis (339, 340). Apoptosis in the pellet cartilage was detected with TUNEL staining (Figure 6-12A) and TUNEL staining showed that P799L cartilage had more TUNEL positive cells than wild-type, however it was not statistically significant (p=0.08) Figure 6-12B). The increased apoptosis in P799L cartilage was supported by the 1.18 fold upregulation of *ANXA5*, an early apoptosis marker (341) and cellular senescence (342).

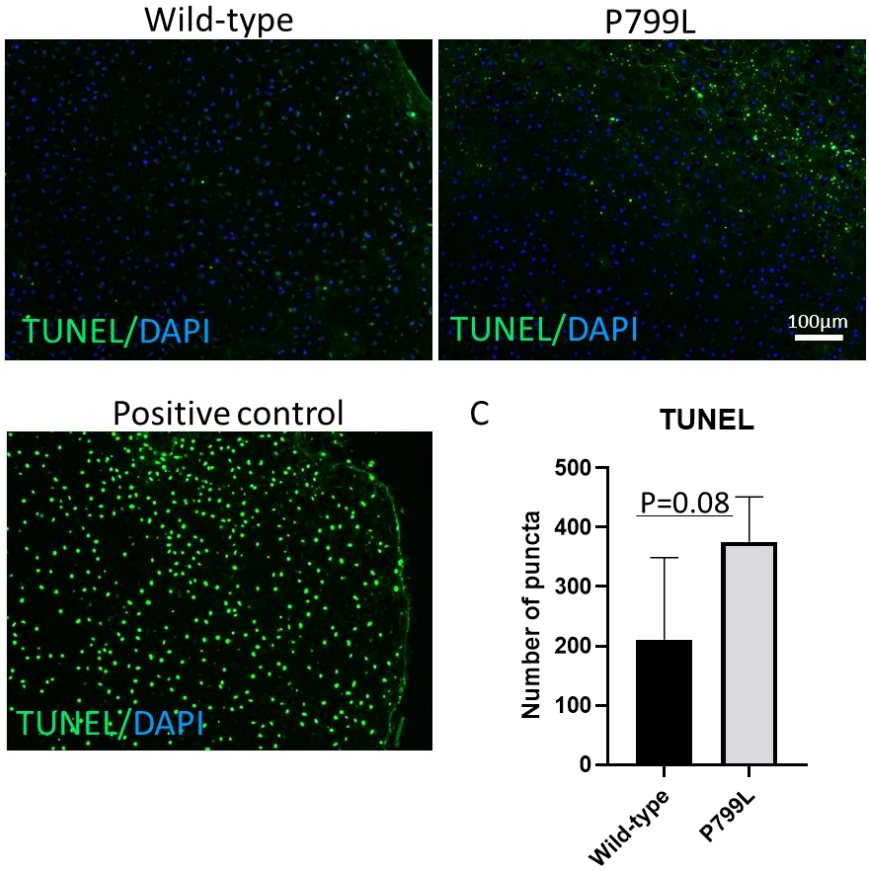

Figure 6-12. TUNEL staining of P799L cartilage shows increased apoptosis. TUNEL staining which is shown in green fluorescence shows increased apoptosis in P799L(A). Quantification of the TUNEL fluorescence area obtained from a randomly selected area (3-4 images) of a section from 4 independent pellets (n=4) indicates that P799L has increased apoptosis (B). Error bars represent SD.

6.3 Discussions

In this chapter, control and mutant TRPV4 hiPSC lines were first differentiated into cartilage and their global gene expression profiles were then compared to explore the potential pathogenic mechanisms underlying the TRPV4-inherited skeletal diseases. The two mutant lines differentiated into cartilage that was similar histologically to the isogenic control cartilage. Gene expression analyses identified 263 differentially expressed genes in F273L vs. wild-type and 655 differentially expressed genes in P799L vs. wild-type. The notable difference in the number of differentially expressed genes provides an initial impression that the mutations have different effects on cartilage. The fewer gene expression changes in F273L than in P799L suggest that the F273L is more similar to the wild-type which might partly explain the milder disease phenotype found in F273L patients.

Gene expression analyses also identified 61 differentially expressed genes shared between F273L and P799L. Gene ontology annotation analysis of these shared differentially expressed genes shows opposite regulation of genes related to cell adhesion and cartilage/bone development between P799L and F273L. P799L shows downregulation of genes related to cell adhesion and upregulation of genes related to cartilage and bone development whereas F273L shows the opposite. Collectively, these findings highlight the distinct pathogenic mechanisms in the two mutant cartilage models.

The difference between F273L and P799L mutant cartilage is also highlighted by the opposite direction of cartilage extracellular matrix expression. F273L cartilage shows downregulation of cartilage extracellular matrix genes including *COL2A1*, *CSPG4*, *BGN*, and *CILP2* whereas P799L shows increased expression of cartilage extracellular matrix genes including *CILP2, HPLN1*, *PODNL1*, *COL25A1,* and *COMP*. Given that TRPV4 plays a role in fibrosis, increased collagen and other extracellular protein production (343, 344), deregulation of cartilage extracellular matrix production could have occurred in TRPV4 mutant cartilage. Studies show that increasing TRPV4 channel activity through various stimuli including hypotonicity, synthetic agonists (4α-PDD, GSK100), and mechanical compression promotes cartilage matrix production (26, 345-347) therefore changes in TRPV4 channel activity might contribute to the different regulation of cartilage extracellular matrix production between F273L and P799L. Given that F273L mutation shows reduced TRPV4 channel activity upon hypotonic stimulation in HEK-293 cells (39), the reduced TRPV4 channel activity might cause downregulation of some cartilage extracellular matrix genes in F273L cartilage. In contrast, p.P799L TRPV4

mutation causes an over-activity of the TRPV4 channels in both fibroblasts and chondrocytes (86) hence the increased TRPV4 channel activity might result in increased cartilage matrix production in P799L cartilage. This finding is supported by a recent study that demonstrates an accelerated chondrocyte differentiation of dental pulp stem cells collected from metatropic dysplasia patients having a gain of function TRPV4 mutation, L619F (126).

Differential gene expression analysis shows that *SHH* expression is upregulated in F273L. Previous studies have shown that *SHH* expression is downregulated in the post-natal nucleus pulposus of the vertebral discs compared to day 12.5 embryo (331) suggesting that *SHH* downregulation marks cartilage maturation. Downregulation of SHH expression is also observed in our extended pellet culture where the pellet cartilage is maturing over time (see Chapter 5). Moreover, continuous SHH signalling inhibits chondrocyte differentiation in transgenic mice overexpressing human SHH (332). Therefore, the upregulation of *SHH* in F273L might suggest that F273L cartilage is less mature than the wild-type cartilage.

SHH signaling plays critical roles in cell fate determination during embryogenesis (204) and limb development (348-350). The main components of SHH signaling are concentrated in primary cilia (351), a microtubule-based cellular projection that is important for sensory and motility functions (352-354). TRPV4 is also expressed in primary cilia (31, 355, 356) suggesting a potential relationship between SHH and TRPV4 in chondrocytes. Ca^{2+} mediates SHH signaling in neurons (357) and mesenchymal stem cells (358). Binding of SHH to its receptor PATCH at primary cilia causes Ca^{2+} spikes that are mediated by the release of Ca^{2+} from intracellular storage and Ca^{2+} influx via membrane calcium channels such as VGCC and TRPC1 (357). TRPV4 in chondrocytes might have a similar role to TRPC1 in the neuron in modulating SHH signalling. Hypothetically, since the F273L mutation causes reduced TRPV4 channel activity upon stimulations (39), SHH signaling could be disrupted in F273L cartilage leading to the downregulation of cartilage genes. The cartilage gene downregulation could disturb cartilage integrity and homeostasis making it less resilient to physical forces. Consistent with this, familial digital arthropathy with brachydactyly (FDAB), the disorder caused by the F273L mutation, is characterised by early-onset cartilage degeneration of the metacarpophalangeal joints and brachydactyly (39). However, further study on TRPV4 channel activity and its relationship with SHH signalling is needed to validate this hypothesis.

Different to F273L cartilage, gene expression analysis of P799L vs. wild-type cartilage reveals that P799L cartilage shows accelerated chondrocyte hypertrophy indicated by the increased hypertrophic chondrocyte marker expression such as *MEF2C*, *RUNX2*, *PTH1R*, and *SPP1* (48, 137, 333, 334, 359). Given that hypertrophic maturation of growth plate chondrocytes is regulated by a change in basal intracellular calcium levels (360) and hypertrophic chondrocytes tend to have higher basal intracellular calcium (361), the increase in basal intracellular calcium level due to channel over-activity could have led to accelerated chondrocyte hypertrophy in P799L. The premature hypertrophic changes caused by p.P799L TRPV4 mutation could disrupt growth plate development and architecture and leads to systemic defects in bone formation and skeletal dysplasia phenotypes. Premature hypertrophic maturation can lead to early fusion of the growth plate, premature bone-growth cessation, and dwarfism (362, 363). This might explain the severe phenotypes found in patients with p.P799L TRPV4 mutations where clinical signs of skeletal dysplasias including systemic bone malformation, disproportionately short stature, short appendicular bones, progressive kyphoscoliosis, and joint contracture (111) are obvious at birth.

Hypertrophic chondrocytes have reduced cell proliferation and many terminal hypertrophic chondrocytes undergo apoptosis prior to bone matrix deposition by osteoblasts and bone matrix mineralisation during endochondral ossification (6, 339). This is consistent with our findings that chondrocytes in P799L show significant downregulation of genes related to cell cycle regulation and cell proliferation as well as an increase in apoptosis. MAPK signalling could mediate these processes as it is overrepresented in GO annotation analysis of the differentially expressed genes in P799L vs. the wild-type and it is known to play important roles in many cellular processes including chondrocyte hypertrophic changes (364, 365), cell cycle, cell proliferation, cell differentiation, and apoptosis (335, 366-369).

Study shows that MAPK signalling can be modulated by TRPV4 (370, 371). Applying osmotic stress into equine chondrocytes results in TRPV4-mediated intracellular Ca^{2+} influx which activates MAPK signalling indicated by increased ERK1/2 and p38 (MAPK14) phosphorylation (372). Since the p.P799L TRPV4 mutation causes an over-activity of TRPV4 channel (86), the higher intracellular Ca^{2+} results in the upregulation of MAPK signalling in the P799L chondrocytes. Furthermore, MAPK signalling regulates *MEF2C* expression (365, 373, 374), the main regulator of chondrocyte hypertrophic changes (359, 375). *MAPK14* (p38) upregulates *MEF2C*

expression (365, 373) which in turn upregulates *RUNX2* and other hypertrophic chondrocyte markers to promote chondrocyte maturity towards hypertrophy (359, 375, 376). Therefore, we hypothesise that an over-activated TRPV4 channel-mediated increase in MAPK signalling could upregulate MEF2C activity leading to premature hypertrophic changes in P799L mutant chondrocytes.

TRPV4 channel-mediated increase in MAPK signalling could also mediate the increased apoptosis in P799L. Studies show that elevated intracellular Ca^{2+} due to TRPV4 activation triggers MAPK signalling mediated apoptosis in neurons, astrocytes (377-379) and retinal ganglion cells (380). Transcription factors downstream to MAPK14 (p38) cascades such as *MEF2C, ETS1,* and *STAT1* (335) are upregulated in P799L cartilage as well as *ANXA5,* an early apoptotic and cellular senescence marker. However, MAPK14 was not upregulated in P799L, and because this pathway is regulated by post-translational modifications, a proteomic study is needed to validate this hypothesis (335).

P799L cartilage also shows downregulation of many cell adhesion molecules including *ITGB8, CADM3, CELSR2, MMRN1,* thrombospondin receptor (*CD36*), *SPON1,* and *NTN1*. Focal adhesion molecules such as integrins and N-cadherins is essential in transmitting mechanical signals from the ECM to the chondrocytes. This interaction plays an important role in regulating many cellular processes including cell growth, cell differentiation, cell proliferation, and cell attachment (55). Synergistic actions between integrins and growth factors facilitate many cellular processes mediated by MAPK signalling (381, 382). Integrin activation promotes MAPK14 signalling which in turn activates MEF2C to induce chondrocyte hypertrophy (383, 384) however it has also been shown that blocking integrin decreases *COL10A1* expression and inhibits hypertrophy (383, 385). Therefore, the roles of cell adhesion molecules in chondrocyte hypertrophy remains unclear. Given the essential roles of TRPV4 and cell adhesion molecules in mechanotransduction in chondrocytes (26, 30, 31, 86, 98-100), downregulation of many cell adhesion molecules in P799L might contribute to the pathogenesis of TRPV4 skeletal dysplasia. Further study is needed to examine the roles of cell adhesion molecules in chondrocyte hypertrophy.

Collectively, our findings suggest that the TRPV4 P799L skeletal dysplasia is caused by premature hypertrophic maturation of the chondrocytes. This is different from previous studies in humans (116) and transgenic mice (11). Histology of human cartilage and bone tissues obtained from two lethal skeletal dysplasias (I604M and L618P) showed minimal bone formation, cartilage overgrowth, and disorganised and a narrow

hypertrophic zone of growth plate (116). The study proposed that delayed chondrocyte maturation is responsible for the disease phenotype. Delayed chondrocyte maturation should be determined by multiple criteria including the increase in distance between the articular surface and the beginning of the hypertrophic zone, the increase in the resting or proliferative zone length, and the decrease in hypertrophic zone length (363, 386). Decrease in hypertrophic zone length should not be the only criteria to determine delayed chondrocyte maturation since increased apoptosis in the hypertrophic zone could also reduce hypertrophic zone length (363, 386). Most importantly, since there was no quantitative measurement on the growth plate characteristics in the TRPV4 I604M and L618P mutant cartilage or gene/protein expression data, further studies on human cartilage are needed to determine the causative mechanisms.

The two mutations, p.I604M and p.L618P, showed a gain of function similar to p.P799L mutation (9). Increased TRPV4 channel activity promotes SOX9 expression in a chondrogenic cell line (145, 387) and promotes osteoblast (388) and osteoclast differentiation (12). Since TRPV4 is also expressed in osteoblasts (389) and osteoclasts (13), TRPV4 mutation could also alter the physiological function of these cells in regulating skeletal development and bone homeostasis. For instance, TRPV4 knock out mice have been shown to have increased bone mass due to reduced osteoclast activity (13) and mice with gain of function TRPV4 mutations have decreased bone volume due to increased osteoclast bone resorption (12). Hence, the increased activity of both I604M and L618P mutant channel can increase osteoclast activity resulting in less bone mass as observed in the histology. On the other hand, our study is designed to only focus on chondrocytes and to rule out the influence of other cellular components hence becoming the strength of this present study.

Similar to the human study, a study on transgenic mouse line overexpressing the human p.R594H TRPV4 skeletal dysplasia mutation (11) also concluded that delayed chondrocyte maturity is responsible for the skeletal phenotype. The study finds the widening of the reserve and proliferative zones and narrowing of the hypertrophic zone with a lack of well-defined boundaries between the zones. However, the mutant mice are generated by fusing human mutant *TRPV4* cDNA downstream of a *Col2a1* promoter, resulting in an inappropriate location of mutant TRPV4 expression in the growth plate. The mutant TRPV4 is highly expressed in the proliferative and hypertrophic zones of the growth plate, however, endogenous TRPV4 expression is downregulated more than 6-fold in the hypertrophic zone (39). Moreover, the mutant TRPV4 is expressed in addition

to the endogenous wild-type mouse TRPV4 resulting in TRPV4 over-expression and the study shows that even an excess of wild-type TRPV4 can cause skeletal defects (11). These inappropriate spatial and levels of expression can disrupt the growth plate development and confound the observed skeletal dysplasia phenotypes. Similarly, another transgenic mouse expressing a skeletal dysplasia causing mutation, p.V620I, also has TRPV4 over-expression as the mutant TRPV4 was expressed on top of the endogenous wild-type mouse TRPV4. Interestingly, the mice have only minor defects in the skeletal system and do not have significant change in the growth-plate structure (8). This might suggest a mutation-specific phenotype as p.V620I causes a mild skeletal dysplasia phenotype, brachyolmia, in humans whereas p.R594H and p.799L mutations cause more severe skeletal dysplasia phenotypes, Spondylometaphyseal dysplasia, Kozlowski type (SMDK) and metatropic dysplasia respectively. By recognising the limitations of these transgenic animal studies, our study generates heterozygous TRPV4 mutation hiPSC line in order to generate human chondrocytes expressing endogenous levels of wild-type and mutant alleles.

On the other hand, a study on Scottish fold cats having a naturally occurring $Trpv4^{V342F}$ mutation shows that the mutant cats have increased articular cartilage mass with necrotic areas, hypertrophic chondrocytes, and many empty lacunae (130, 135). This is consistent with our data showing the P799L mutant has accelerated hypertrophic changes. Furthermore, Scottish fold cats have osseous matrices in the articular cartilage region and new bone formation (osteophytes) in the periarticular area suggesting increased osteoblast activity. Their subchondral bones were very thin with isolated cartilage nodules suggesting increased osteoclast activity similar to the findings in transgenic mice with osteoclast-targeted gain of function TRPV4 mutations (p.R616Q and p.V620I) (12). At age 16 months of age, Scottish fold cats have radial and ulnar growth plate fusion (135) which is normal according to age (390) but exostosis is observed particularly in the distal extremities (135, 391) suggesting increased endochondral bone formation. The p.V342F TRPV4 mutantion causes metatropic dysplasia phenotype in humans.

Only one study has conducted a global gene expression analysis in chondrocytes expressing mutant TRPV4. Porcine chondrocytes are transiently transfected with plasmids encoding human wild type or p.V620I mutant TRPV4 (8). Since the study uses transient gene expression system achieved via transfection, ensuring equal TRPV4 expression levels in mutant and wild-type cells is critical to accurately assess the effect

of the mutation. To minimise expression level differences, the TRPV4 constructs are tagged with a red fluorescent protein and transfected cells are FACS sorted and used for microarray and functional study. However, TRPV4 over-expression remains an important issue in this study as the mutant TRPV4 is expressed in addition to the endogenous porcine TRPV4. The study shows that V620I mutant chondrocytes have significantly higher basal intracellular calcium than wild type chondrocytes. The peak intracellular calcium level after hypotonic stimulation in V620I is higher than the wild type TRPV4 which is consistent with the increased membrane cell current in the transfected HEK-293 cells (7) and *Xenopus* oocytes (122). Microarray analysis of the transfected chondrocytes indicates that *FST* (follistatin), an inhibitor of BMP signalling (392), and 17 other genes are upregulated in the V620I mutant but information on the level of expression is not available. The study proposes that *FST* upregulation is the key pathogenic mechanism underlying the skeletal dysplasia phenotypes. However, *FST* is not upregulated in our study suggesting that differences in the study design might cause this finding discrepancy.

Interestingly, despite of the difference in study design, three other genes that are upregulated in V620I transfected porcine chondrocytes, *TAC1, EBF2,* and *EDNRB,* were differentially expressed in P799L suggesting these genes could be important in TRPV4 skeletal dysplasias. However, the expression level of *TAC1* and *EBF2* were low hence caution is needed in interpreting the upregulated expression in P799L. *TAC1* or Tachykinin Precursor 1 encodes four different types of tachykinin peptide hormone family, substance P, neurokinin A, neuropeptide K, and neuropeptide gamma (393). *TAC1* is upregulated 3.2 fold in P799L. Substance P is a neurotransmitter that mediates inflammatory pain. TRPV4 activation increases substance P secretion from the afferent nerves and induces neurogenic inflammation by recruiting inflammatory cells (394, 395). Therefore, the upregulation of *TAC1* in P799L might be due to increased activity of the mutant TRPV4 channel and may be involved in the inflammatory pain present in the patients.

EBF2 (early B cell factor-2) is upregulated 3.1 fold in P799L. EBF2 transcription factor is expressed in osteoblast progenitors and acts as a regulator of osteoclast differentiation (396). EBF2 activates the promoter of osteoprotegerin (*Opg*), a gene encoding a RANK decoy receptor, to regulate RANK-RANKL signalling responsible for osteoclast differentiation. Homozygous inactivation of Ebf2 in mice resulted in downregulated *Opg* expression leading to reduced bone mass due to an increase in the number of osteoclasts (396). Interestingly, lineage tracing showed that Ebf2 positive cells

have similar characteristics to mesenchymal progenitor cells that can develop into osteoblasts and chondrocytes (396) suggesting the essential role of Ebf2 in chondrocyte and osteoblast differentiation. Ebf2 is highly expressed in the perichondrial area of the E6 chicken embryo (397) where most of the osteoblasts are derived. Therefore, the increase in *EBF2* expression in P799L might be associated with upregulation of osteogenic genes such as *RUNX2, SP7, SPP1, TNFRSF11B* (osteoprotegerin), and *NELL1* (398).

EDNRB (endothelin receptor-B) is downregulated 2.4 fold in P799L whereas in V620I pig chondrocytes, it is upregulated 1.44 fold. The expression of its ligand, *EDN3* (endothelin-3), is upregulated 1.35 fold in P799L. The finding discrepancy in *EDNRB* expression might suggest a mutant specific phenotype as p.V620I mutation causes a milder skeletal dysplasia phenotype (brachyolmia) than p.P799L mutation (metatropic dysplasia). *EDNRB* is one of the components of endothelin signalling involved in the developmental process of various organ systems including cardiovascular, nerve and skeletal systems (399). In the skeletal system, increased endothelin signalling promotes osteoblast activity (400) and differentiation (401).

The only hiPSC disease model for TRPV4 inherited skeletal disease is performed to model p.I604M TRPV4 mutation. This mutation causes lethal metatropic dysplasia in human (21). The cartilage-like tissues generated from the patient-derived hiPSCs shows reduced chondrogenic marker expression, *SOX9*, *ACAN*, and *COL2A1*, as compared to the non-isogenic wild-type control. However, our study finds that the expression of *SOX9*, *ACAN*, and *COL2A1* does not change in TRPV4 P799L cartilage. Instead, the upregulation of other cartilage genes is observed. Since both p.I604M and p.P799L show characteristics of gain of function mutations (9) and cause skeletal dysplasia phenotypes in humans, this discrepancy might be caused by the difference in disease-relevant cells obtained from chondrocyte differentiation. In the I604M study, the chondrocyte differentiation protocol was a single-step chemically-defined micromass culture. The wild-type control produced some cartilage-like tissues, but there was also significant amount of non-cartilage tissue after 21 days of chondrocyte differentiation culture. Moreover, collagen type II immunostaining showed sporadic expression without clear organisation. Therefore, these findings indicated that the chondrocyte differentiation was not optimal.

One limitation of this study is that gene expression in the I604M study used RNA obtained from whole micromass cultures containing a mixed cell population thus the data

obtained are difficult to interpret. TRPV4 mRNA expression was also not reported therefore cannot be concluded with certainty that the heterozygous TRPV4 mutation contributed to the gene expression changes observed. In addition, a non-isogenic control was used in the study hence the differences could be influenced by the different genetic backgrounds between patient-derived mutant hiPSCs and control hiPSCs from an unrelated individual (402, 403). Our study was designed to avoid these issues. The mutant TRPV4 hiPSC lines were generated by introducing the TRPV4 point mutation into a control TRPV4 hiPSC line using CRISPR/Cas9 genomic editing making both the mutant lines and the wild-type line isogenic. Further, trypsin digestion performed in our study has been very important in removing the non-cartilage tissues thus the global gene expression analyses are less likely to be confounded by non-chondrogenic cells.

6.4 Conclusions

This study is the first study that conducts global gene expression analysis using RNA sequencing to characterise gene expression changes downstream of TRPV4 mutations in hiPSC-derived chondrocytes. The hiPSC disease model serves as a powerful strategy to model TRPV4-inherited skeletal disease in order to elucidate the potential pathogenic mechanisms underlying the diseases. We find that the TRPV4 FDAB mutation, p.F273L, and metatropic dysplasia mutation, p.P799L, show distinct pathogenic mechanisms. F273L has fewer gene expression changes than P799L when compared to control cartilage. This is consistent with the mild FDAB phenotype in patients with the F273L mutation, and the severe metatropic dysplasia phenotype caused by the P799L mutation. Reduced cartilage matrix expression could be a key pathogenic mechanism of the F273L mutation. Reduced cartilage matrix expression leading to altered cartilage matrix composition could disrupt cartilage integrity in the post-natal period where cartilage tissues are exposed to various types of mechanical stress and explain, at least partially, the early onset of cartilage degeneration in FDAB patients.

By contrast, enhanced chondrocyte maturation towards hypertrophic chondrocytes could be a key pathogenic mechanism in P799L mutant cartilage. This is indicated by the upregulation of chondrocyte hypertrophic genes. Premature chondrocyte maturation disrupts normal growth plate development resulting in systemic skeletal malformation. Premature chondrocyte maturation could lead to early fusion of the growth plate resulting in decreased length of the long bones, disproportionately short stature, abnormal bone shapes especially in the femur, pelvis, and vertebrae as observed in patients.

Chapter 7

General Discussions

7.1 hiPSC-derived chondrocytes

This present study establishes a protocol for chondrocyte differentiation from a SOX9-T2A-tdTom reporter hiPSC line. The established chondrocyte differentiation protocol involves a multiple-step chemically-defined 3-dimensional (3D) culture with swirling in an extended culture that includes FGF2 supplementation and optional subsequent TGFβ3 and GDF5 treatment. This protocol can produce *in vitro* cartilage that histologically resembles *in vivo* cartilage and expresses key chondrogenic markers. This finding is confirmed by RNA sequencing showing that the cartilage selective gene expression (40) of *in vitro* cartilage is similar to human fetal cartilage. This *in vitro* cartilage can be used for subsequent research applications including articular cartilage tissue engineering, *in vitro* skeletal system development study and cartilage disease modelling.

7.1.1 Articular vs. growth plate cartilage

Articular and growth plate-like cartilage can be generated from our optimised protocol. Cartilage generated without TGFβ3 and GDF5 treatment shows characteristics of growth plate cartilage whereas cartilage generated under TGFβ3 and GDF5 treatment has upregulated genes more abundantly expressed in articular cartilage. Articular and growth plate cartilage share a common origin but subsequently undergo different developmental paths leading to differences in structure and function (404). The growth plate cartilage serves as a centre of endochondral bone formation for bone elongation during children's growth whereas the articular cartilage provides a lubricated surface for joint movements. The molecular regulations that differentiate articular and growth plate cartilage remains elusive. Therefore, this differentiation protocol can be particularly useful to unravel the differences in developmental regulation between articular and growth plate cartilage.

Given that articular and growth plate cartilage are different in terms of structure and functions, generating a specific type of cartilage is relevant for cartilage disease model study. For instance, *in vitro* articular cartilage is more appropriate for osteoarthritis disease models (19) while *in vitro* growth plate-like cartilage is more appropriate for diseases causing defects in endochondral ossification such as TRPV4 skeletal dysplasias. Therefore, our hiPSC disease model for TRPV4-inherited disease was performed in chondrocyte differentiation protocol without TGFβ and GDF5 treatment in order to generate growth plate-like cartilage.

With regards to the developmental regulation differences between articular and growth plate cartilage, single-cell RNA sequencing could potentially be used to identify molecular pathways responsible for developmental specification. Single-cell RNA sequencing of mouse growth plate cartilage is able to identify transcriptional factor (TF) regulating growth plate maturation (405). Single-cell RNA sequencing has also been shown to be useful in identifying cellular heterogeneity in the osteoarthritic articular cartilage (406). Therefore, applying this technology onto the pellet cartilage could be a useful strategy to further characterise the differentiated chondrocytes and hopefully identify developmental pathways that regulate lineage specification during articular and growth plate development.

7.1.2 Cartilage tissue engineering

The ultimate goal of cartilage tissue engineering is to generate human-like tissue ready for therapeutic use. Enormous efforts have been conducted to generate clinical-grade *in vitro* articular cartilage having structural and functional features of *in vivo* articular cartilage for joint replacement therapy for degenerative joint diseases such as osteoarthritis.

Human MSCs are the most common type of cells being studied and used for cartilage-like tissue implantation and cellular injection therapy for cartilage repair (232, 407). However, a systematic review of 46 clinical studies on MSC concludes that there is limited evidence on the clinical benefit of mesenchymal stem cell therapy for articular cartilage diseases (408). This could be caused by the limited proliferation and differentiation potential towards osteochondroprogenitor cells hence reducing the healing outcome potential (407). Moreover, recent evidence shows that MSCs tend to differentiate into fibroblastic cartilage instead of hyaline cartilage following *in vivo* implantation (407, 409). Furthermore, MSCs from different tissue sites are heterogeneous in terms of chondrocyte differentiation capacity and gene expression signatures causing variability in the quality of the *in vitro* cartilage products (410). Additionally, MSCs also tend to lose their chondrogenic capacity following subsequent *in vitro* passaging (409) hence hampering the MSC expansion, a critical step of cartilage/bone tissue engineering, for large scale *in vitro* cartilage production for therapeutic purposes. To overcome these problems, pluripotent-stem cells (PSCs) provide an alternative cell source for generating *in vitro* cartilage due to their higher proliferative capacity and differentiation potentials (232, 411-413).

Given that we are now able to generate articular cartilage-like tissues from hiPSCs using our optimised protocol, there is an opportunity to use this cartilage tissues for articular cartilage regenerative therapy. For future works, further characterisation of this *in vitro* hiPSC-derived cartilage is required before being used for clinical applications. Since *in vivo* cartilage is exposed to repetitive mechanical stresses, biomechanical property characterisation that involves collagen, water and glycosaminoglycan contents, compression test, and tensile test should be performed in this *in vitro* articular cartilage (414). This will provide information on the structural and functional parameters of the *in vitro* cartilage which are important for the development of *in vitro* cartilage products.

Animal study should then be performed to examine the biologic plausibility of the *in vitro* cartilage (415). Although only a handful of studies have performed *in vivo* animal transplantation of pluripotent stem cell-derived cartilage into defective articular cartilage (18, 260, 261, 416, 417), they show the promising regenerative capacity of the pluripotent stem cell-derived cartilage. However, the follow-up period of the transplanted cartilage in most of the studies is very short. Thus long-term follow-up should be undertaken in future studies in order to monitor the cartilage engraftment, host-transplant tissue interaction, and the formation of unwanted teratomas.

For cartilage tissue engineering, large amount of *in vitro* cartilage with consistent quality is needed hence generating *in vitro* cartilage using bioreactors could be an option. Additionally, manipulating biophysical culture environment could also be performed as it can influence the biomechanical properties and histological structure of the *in vitro* cartilage. For instance, applying various types of mechanical forces including compression, tension and shear stress onto chondrocyte 3-dimensional culture (26, 68-70) and cartilage explants (32, 71, 72) results in changes in cartilage marker expressions and ECM composition and organisation. Furthermore, adding forskolin, a small-molecule activator of adenylyl cyclase, during chondrocyte differentiation has also been shown to increase extracellular matrix production and suppress cartilage hypertrophy (251). This strategy could be particularly useful for articular cartilage tissue engineering where cartilage hypertrophic maturation is considered as an undesired outcome. In doing so, this strategy provides promising way to improve the engraftment of the transplanted *in vitro* cartilage into the host's articular cartilage.

7.1.3 *In vitro* cartilage for skeletal development study

This present study has not shown any evidence of *in vitro* endochondral ossification however, recently, our laboratory has gone on to generate hypertrophic chondrocytes within the pellet cartilage (unpublished data obtained by Kung, Sampurno, Lamandé, Bateman (2019)) thus generating pellet cartilage that recapitulates the structure of *in vivo* growth plate. The expression of collagen type X could be observed from the pellet histology but there is no evidence of calcification suggesting that suitable microenvironment might be required for the calcification to occur. Transplanting hiPSC-derived sclerotome (17) and hiPSC-derived pellet cartilage (18, 418) into immunocompromised mice can generate growth plate structures with calcification and bone tissues below the hypertrophic zones producing an *in vivo* model for endochondral bone formation. This finding supports the idea that a suitable microenvironment is needed to induce endochondral ossification.

The existence of vascular components and the required bio-active molecules are likely to be the main driver of endochondral bone formation in the transplanted hiPSC-derived sclerotome and pellet cartilage (419). Other cellular components including osteoblasts and osteoclasts might also be required for efficient endochondral ossification. Therefore, providing the required growth factors or bio-active molecules for osteoblast differentiation may promote *in vitro* endochondral bone formation. Similarly, providing the essential growth factors for vascular development such as VEGF (420-422) may help mimic the vascular invasion process that occurs during endochondral hence creating a suitable microenvironment for *in vitro* endochondral ossification. Alternatively, co-culturing *in vitro* pellet cartilage with osteoblasts may also be very useful for the *in vitro* model of endochondral ossification.

Given that osteoblasts are derived from osteo-chondroprogenitor cells (423), *in vitro* cartilage could also be used to generate osteoblasts *in vitro*. Furthermore, it could also be useful for studying the lineage specification of osteo-chondroprogenitor towards chondrocytes and osteoblasts. Additionally, single-cell RNA sequencing could also be applied to explore cellular heterogeneity and trajectories of lineage specification during *in vitro* cartilage/bone development hence providing a tool for identifying skeletal developmental pathways (424).

7.2 hiPSC-disease model

Given the ability of our optimised chondrocyte differentiation protocol to generate fetal-looking cartilage, this optimised protocol is used for the TRPV4-inherited skeletal disease model study. The hiPSC disease model allows the observation of inherited-skeletal disease development during *in vitro* differentiation, a study which is not possible to be conducted in living human embryos. The hiPSC disease model of two TRPV4 mutations causing distinct TRPV4-inherited skeletal diseases, p.F273L mutation causing FDAB (arthropathy) and p.P799L mutation causing metatropic dysplasia (skeletal dysplasia), reveals differences in gene expression patterns. Consistent with the more severe disease phenotypes seen in patients, *in vitro* P799L cartilage has more gene expression changes than F273L cartilage. P799L cartilage shows increased chondrocyte hypertrophy which could be responsible for the pathogenesis of TRPV4 skeletal dysplasia. On the other hand, a slightly reduced cartilage gene expression in F273L might contribute to the mild disease phenotype, FDAB. These findings suggest that the hiPSC disease model is appropriate for TRPV4-inherited disease modelling as it recapitulates the TRPV4-inherited skeletal diseases in humans. This hiPSC disease model could also be useful for identifying pathogenic mechanisms underlying many other cartilage disorders.

Two aspects that are essential in TRPV4-inherited skeletal disease modelling are the use of isogenic control cell lines and the functional study of TRPV4 channels. This present study has used cell lines that are isogenic however the functional study of TRPV4 channels has not been done. Therefore, for future studies, functional study of the TRPV4 channels should be performed in the hiPSC-derived chondrocytes to validate the previous findings obtained from heterologous cell system.

7.2.1 Isogenic control for hiPSC-disease model

In the context of hiPSC-disease models, several factors including 1) the original cell type for hiPSC generation, 2) the reprogramming method for hiPSC generation, 3) single nucleotide polymorphism, mutations and copy number variations in the original cells and hiPSCs, 4) epigenetic status of the original cells and hiPSCs and 5) culture conditions, can influence hiPSC differentiation capacity towards disease-relevant cells or tissues (326). Consequently, the phenotypic differences between mutant and non-isogenic control will inaccurately be under-estimated or over-estimated when non-isogenic controls are used in the hiPSC-disease model study. Therefore, the use of isogenic controls is critical in minimising the confounding effects of genetic background

differences between independent non-isogenic cell lines, particularly for a disease that is partly heritable or phenotypically heterogeneous (271).

Building up to this idea, CRISPR/Cas9 genome editing is used in this present study to generate isogenic mutant hiPSC lines with heterozygous p.F273L and p.P799L TRPV4 mutations from a wild-type hiPSC line, SOX9-T2A-tdTom. Hence, the major strength of the present study is the use of isogenic cells to compare the observed phenotypes between the mutants and wild-type. The use of heterozygous mutant cell lines to model the disease improves the experimental design of previous studies where the mutant TRPV4 expression is achieved by transfecting the porcine chondrocytes with human mutant TRPV4 constructs producing TRPV4 over-expression in the transfected cells (8). Hence, our experimental design creates conditions that are more recapitulating patient chondrocytes than the transiently transfected cells.

7.2.2 The functional study of TRPV4 ion channel in hiPSC-disease model

Considering the anatomical location of cartilage tissues especially articular and growth plate cartilage, they are exposed to repetitive mechanical stresses including compression, tension and shear forces which are generated from skeletal movements and weight-bearing (49). The direct interaction between chondrocytes and ECMs allows the transduction of mechanical forces which eventually leads to the activation of various signalling pathways essential for maintaining the structural integrity of the cartilage tissues including TRPV4-mediated calcium signaling (55, 95, 96, 98-100). TRPV4 activation allows Ca^{2+} influx into the cells (26, 30, 31, 86) and the change in intracellular calcium channel triggers the activation of various signalling essential for cell cycle, cell proliferation, cell differentiation, and apoptosis (335, 366-369). Studies show that increasing TRPV4 channel activity through various stimuli including hypotonicity, synthetic agonists (4α-PDD, GSK100), and mechanical compression of the 3-dimensional chondrocyte culture promotes cartilage matrix production (26, 345-347). On the other hand, inhibiting TRPV4 activity results in downregulation of *ACAN* and *SOX9* expression in ATDC5 chondrogenic cell line (387), porcine articular chondrocytes (26), as well as a significant decreased in aligned fibrillar collagen formation in mesenchymal stem cells (97) and mouse fibroblasts (425). Therefore, functional study of TRPV4 channel activity is relevant to be undertaken in the hiPSC-cartilage disease modelling study to explore the effect of the mutations on calcium signalling in chondrocytes.

Given the minimal differences in cartilage tissue structure between mutants and wild-type cartilage observed in the pellet histology, this might suggest that TRPV4

channel stimulation is needed to induce major cartilage defects. Moreover, the TRPV4 immunostaining showed no significant differences in the level of TRPV4 protein expression between mutants and wild-type suggesting that the change in channel activity can be the major contributor for disease pathogenesis. Therefore, manipulating TRPV4 channel activity by introducing various stimulations and inhibitions on the mutants and wild-type hiPSC-derived cartilage is needed as part of future works of TRPV4-inherited disease modelling. Study shows that administration of TRPV4 agonists and performing mechanical compressions on the 3-dimensional chondrocyte culture are able to increase collagen content of the 3-dimensional culture (347). Hence, by applying these techniques to the pellet cartilage, we might be able to compare the biomechanical characteristics including collagen and glycosaminoglycan contents, tensile parameters and tissue stiffness, between mutants and wild-type cartilage hence providing more insights on the functional characteristics of the mutant cartilage.

Additionally, a study has shown that the HEK-293 cells transfected with the human p.F273L TRPV4 gene have reduced channel activity after hypotonic stimulation determined by the lower Ca^{2+} influx compared to the wild-type (39). The p.F273L mutation also causes a reduction in membrane cell localisation of the TRPV4 channel which may also contribute to the low Ca^{2+} influx. In contrast, P799L TRPV4 mutant channels show channel over-activity upon channel stimulation in both fibroblasts and chondrocytes (86). Hence, measuring mutant TRPV4 channel activity in the hiPSC-derived chondrocytes using intracellular Ca^{2+} assay or electrophysiology could be the next step in validating the changes in channel activity.

In line with this, our laboratory has recently successfully isolated chondrocytes from the pellet cartilage (unpublished data obtained by Kung, Sampurno, Lamandé, Bateman (2019)) hence allowing us to investigate TRPV4 channel activity in these chondrocytes. Additionally, in terms of disease modelling study, we will be able to validate the reduction in channel activity in the F273L mutant as well as the increased channel activity in the P799L mutant upon channel stimulation.

Furthermore, the isolated chondrocytes could also be used for proteomic studies to validate the activity of calcium-mediated signalling pathways downstream of the TRPV4 mutations such as MAPK signalling. We find that, through gene expression analysis, MAPK signalling is upregulated in P799L and it is positively correlated with the upregulation of chondrocyte hypertrophic markers. It has been shown that the increase in MAPK signalling regulates *MEF2C* expression (365, 373, 374), the main regulator of

chondrocyte hypertrophy (359, 375) hence investigating the MAPK signalling in the P799L can provide more understanding on its role in TRPV4 skeletal dysplasia pathogenesis. Given that MAPK signalling could be activated by the increase in intracellular calcium level (372), the over-activity of P799L TRPV4 mutant channels (86) could have facilitated the MAPK signalling-mediated MEF2C upregulation leading to premature hypertrophic changes in P799L mutant chondrocytes. To validate this hypothesis, a proteomic study is required since the MAPK signalling is regulated by post-translational modifications (335). Collectively, these will provide a complete understanding of the effects of TRPV4 mutations on cartilage tissue development.

7.3 Conclusions

Key elements that have emerged in this thesis include the establishment of a chondrocyte differentiation protocol for generating cartilage tissue that closely resembles *in vivo* cartilage and the feasibility of performing a hiPSC-disease modeling study for inherited skeletal diseases. The work presented in this thesis has contributed to our understanding of the different pathogenic mechanisms underlying two distinct TRPV4-inherited skeletal disease phenotypes. The p.P799L TRPV4 mutation appears to change the way chondrocytes mature towards hypertrophy and this may be the main contributor to the TRPV4-skeletal dysplasia phenotypes seen in patients. The established chondrocyte differentiation protocol in this present study will also be useful for other research applications including dissecting pathways regulating the development specification of articular vs. growth plate cartilage, exploring cartilage maturation pathways, developing *in vitro* model for endochondral ossification, and for cartilage tissue engineering.

References

1. Vlahos K, Sourris K, Mayberry R, McDonald P, Bruveris FF, Schiesser JV, et al. Generation of iPSC lines from peripheral blood mononuclear cells from 5 healthy adults. Stem Cell Research. 2019;34:101380.
2. White JPM, Cibelli M, Urban L, Nilius B, McGeown JG, Nagy I. TRPV4: Molecular Conductor of a Diverse Orchestra. Physiological reviews. 2016;96(3):911-73.
3. Andreucci E, Aftimos S, Alcausin M, Haan E, Hunter W, Kannu P, et al. TRPV4 related skeletal dysplasias: a phenotypic spectrum highlighted byclinical, radiographic, and molecular studies in 21 new families. Orphanet Journal Of Rare Diseases. 2011;6:37.
4. Nilius B, Voets T. The puzzle of TRPV4 channelopathies. EMBO reports. 2013;14(2):152-63.
5. Yeung Tsang K, Wa Tsang S, Chan D, Cheah KSE. The chondrocytic journey in endochondral bone growth and skeletal dysplasia. Birth Defects Research Part C: Embryo Today: Reviews. 2014;102(1):52-73.
6. Kozhemyakina E, Lassar AB, Zelzer E. A pathway to bone: signaling molecules and transcription factors involved in chondrocyte development and maturation. Development. 2015;142(5):817-31.
7. Rock MJ, Prenen J, Funari VA, Funari TL, Merriman B, Nelson SF, et al. Gain-of-function mutations in TRPV4 cause autosomal dominant brachyolmia. Nature Genetics. 2008;40(8):999-1003.
8. Leddy HA, McNulty AL, Lee SH, Rothfusz NE, Gloss B, Kirby ML, et al. Follistatin in chondrocytes: the link between TRPV4 channelopathies and skeletal malformations. The FASEB Journal. 2014;28(6):2525-37.
9. Loukin S, Su Z, Kung C. Increased basal activity is a key determinant in the severity of human skeletal dysplasia caused by TRPV4 mutations. PLoS ONE [Electronic Resource]. 2011;6(5):e19533.
10. Krakow D, Vriens J, Camacho N, Luong P, Deixler H, Funari TL, et al. Mutations in the gene encoding the calcium-permeable ion channel TRPV4 produce spondylometaphyseal dysplasia, Kozlowski type and metatropic dysplasia. American Journal of Human Genetics. 2009;84(3):307-15.
11. Weinstein MM, Tompson SW, Chen Y, Lee B, Cohn DH. Mice Expressing Mutant Trpv4 Recapitulate the Human TRPV4 Disorders. Journal of Bone and Mineral Research. 2014;29(8):1815-22.
12. Masuyama R, Mizuno A, Komori H, Kajiya H, Uekawa A, Kitaura H, et al. Calcium/calmodulin-signaling supports TRPV4 activation in osteoclasts and regulates bone mass. Journal of Bone and Mineral Research. 2012;27(8):1708-21.
13. Masuyama R, Vriens J, Voets T, Karashima Y, Owsianik G, Vennekens R, et al. TRPV4-Mediated Calcium Influx Regulates Terminal Differentiation of Osteoclasts. Cell Metabolism. 2008;8(3):257-65.
14. Liedtke W, Friedman JM. Abnormal osmotic regulation in trpv4-/- mice. Proceedings of the National Academy of Sciences of the United States of America. 2003;100(23):13698-703.
15. Soldner F, Jaenisch R. Stem Cells, Genome Editing, and the Path to Translational Medicine. Cell. 2018;175(3):615-32.
16. Takahashi K, Tanabe K, Ohnuki M, Narita M, Ichisaka T, Tomoda K, et al. Induction of pluripotent stem cells from adult human fibroblasts by defined factors. Cell. 2007;131(5):861-72.
17. Loh Kyle M, Chen A, Koh Pang W, Deng Tianda Z, Sinha R, Tsai Jonathan M, et al. Mapping the Pairwise Choices Leading from Pluripotency to Human Bone, Heart, and Other Mesoderm Cell Types. Cell. 2016;166(2):451-67.
18. Yamashita A, Morioka M, Yahara Y, Okada M, Kobayashi T, Kuriyama S, et al. Generation of Scaffoldless Hyaline Cartilaginous Tissue from Human iPSCs. Stem Cell Reports. 2015;4(3):404-18.
19. Craft AM, Rockel JS, Nartiss Y, Kandel RA, Alman BA, Keller GM. Generation of articular chondrocytes from human pluripotent stem cells. Nat Biotech. 2015;33(6):638-45.

20. Oldershaw RA, Baxter MA, Lowe ET, Bates N, Grady LM, Soncin F, et al. Directed differentiation of human embryonic stem cells toward chondrocytes. Nature Biotechnology. 2010;28(11):1187-94.
21. Saitta B, Passarini J, Sareen D, Ornelas L, Sahabian A, Argade S, et al. Patient-Derived Skeletal Dysplasia Induced Pluripotent Stem Cells Display Abnormal Chondrogenic Marker Expression and Regulation by BMP2 and TGFβ1. Stem Cells and Development. 2014;23(13):1464-78.
22. Strotmann R, Harteneck C, Nunnenmacher K, Schultz G, Plant TD. OTRPC4, a nonselective cation channel that confers sensitivity to extracellular osmolarity. Nat Cell Biol. 2000;2(10):695-702.
23. Stewart AP, Smith GD, Sandford RN, Edwardson JM. Atomic Force Microscopy Reveals the Alternating Subunit Arrangement of the TRPP2-TRPV4 Heterotetramer. Biophysical Journal. 2010;99(3):790-7.
24. Deng Z, Paknejad N, Maksaev G, Sala-Rabanal M, Nichols CG, Hite RK, et al. Cryo-EM and X-ray structures of TRPV4 reveal insight into ion permeation and gating mechanisms. Nature Structural & Molecular Biology. 2018;25(3):252-60.
25. Vangeel L, Voets T. Transient Receptor Potential Channels and Calcium Signaling. Cold Spring Harbor perspectives in biology. 2019.
26. O'Conor CJ, Leddy HA, Benefield HC, Liedtke WB, Guilak F. TRPV4-mediated mechanotransduction regulates the metabolic response of chondrocytes to dynamic loading. Proceedings of the National Academy of Sciences of the United States of America. 2014;111(4):1316-21.
27. Becker D, Blase C, Bereiter-Hahn J, Jendrach M. TRPV4 exhibits a functional role in cell-volume regulation. Journal of Cell Science. 2005;118(Pt 11):2435-40.
28. Liedtke W. TRPV4 as osmosensor: a transgenic approach. Pflugers Archiv - European Journal of Physiology. 2005;451(1):176-80.
29. Liedtke W. Transient receptor potential vanilloid channels functioning in transduction of osmotic stimuli. Journal of Endocrinology. 2006;191(3):515-23.
30. Vriens J, Watanabe H, Janssens A, Droogmans G, Voets T, Nilius B. Cell swelling, heat, and chemical agonists use distinct pathways for the activation of the cation channel TRPV4. Proceedings of the National Academy of Sciences of the United States of America. 2004;101(1):396-401.
31. Phan MN, Leddy HA, Votta BJ, Kumar S, Levy DS, Lipshutz DB, et al. Functional characterization of TRPV4 as an osmotically sensitive ion channel in porcine articular chondrocytes. Arthritis & Rheumatism. 2009;60(10):3028-37.
32. Walter BA, Purmessur D, Moon A, Occhiogrosso J, Laudier DM, Hecht AC, et al. Reduced tissue osmolarity increases TRPV4 expression and pro-inflammatory cytokines in intervertebral disc cells. Eur Cell Mater. 2016;32:123-36.
33. Watanabe H, Vriens J, Prenen J, Droogmans G, Voets T, Nilius B. Anandamide and arachidonic acid use epoxyeicosatrienoic acids to activate TRPV4 channels. Nature. 2003;424(6947):434-8.
34. Thorneloe KS, Sulpizio AC, Lin Z, Figueroa DJ, Clouse AK, McCafferty GP, et al. N-((1S)-1-{[4-((2S)-2-{[(2,4-dichlorophenyl)sulfonyl]amino}-3-hydroxypropanoyl)-1 -piperazinyl]carbonyl}-3-methylbutyl)-1-benzothiophene-2-carboxamide (GSK1016790A), a novel and potent transient receptor potential vanilloid 4 channel agonist induces urinary bladder contraction and hyperactivity: Part I. The Journal of pharmacology and experimental therapeutics. 2008;326(2):432-42.
35. Garcia-Elias A, Mrkonjic S, Pardo-Pastor C, Inada H, Hellmich UA, Rubio-Moscardo F, et al. Phosphatidylinositol-4,5-biphosphate-dependent rearrangement of TRPV4 cytosolic tails enables channel activation by physiological stimuli. Proceedings of the National Academy of Sciences of the United States of America. 2013;110(23):9553-8.
36. Darby WG, Grace MS, Baratchi S, McIntyre P. Modulation of TRPV4 by diverse mechanisms. The International Journal of Biochemistry & Cell Biology. 2016;78:217-28.
37. Somogyi CS, Matta C, Foldvari Z, Juhasz T, Katona E, Takacs AR, et al. Polymodal Transient Receptor Potential Vanilloid (TRPV) Ion Channels in Chondrogenic Cells. International Journal of Molecular Sciences. 2015;16(8):18412-38.

38. Cameron TL, Belluoccio D, Farlie PG, Brachvogel B, Bateman JF. Global comparative transcriptome analysis of cartilage formation in vivo. BMC Developmental Biology. 2009;9:20.
39. Lamande SR, Yuan Y, Gresshoff IL, Rowley L, Belluoccio D, Kaluarachchi K, et al. Mutations in TRPV4 cause an inherited arthropathy of hands and feet. Nat Genet. 2011;43(11):1142-6.
40. Li B, Balasubramanian K, Krakow D, Cohn DH. Genes uniquely expressed in human growth plate chondrocytes uncover a distinct regulatory network. BMC Genomics. 2017;18(1):983.
41. O'Conor CJ, Ramalingam S, Zelenski NA, Benefield HC, Rigo I, Little D, et al. Cartilage-Specific Knockout of the Mechanosensory Ion Channel TRPV4 Decreases Age-Related Osteoarthritis. Scientific Reports. 2016;6:29053.
42. Denadai-Souza A, Martin L, de Paula MA, de Avellar MC, Muscara MN, Vergnolle N, et al. Role of transient receptor potential vanilloid 4 in rat joint inflammation. Arthritis & Rheumatism. 2012;64(6):1848-58.
43. Lv M, Zhou Y, Polson SW, Wan LQ, Wang M, Han L, et al. Identification of Chondrocyte Genes and Signaling Pathways in Response to Acute Joint Inflammation. Scientific Reports. 2019;9(1):93.
44. Abed E, Labelle D, Martineau C, Loghin A, Moreau R. Expression of transient receptor potential (TRP) channels in human and murine osteoblast-like cells. Molecular Membrane Biology. 2009;26(3):146-58.
45. Suzuki T, Notomi T, Miyajima D, Mizoguchi F, Hayata T, Nakamoto T, et al. Osteoblastic differentiation enhances expression of TRPV4 that is required for calcium oscillation induced by mechanical force. Bone. 2013;54(1):172-8.
46. van der Eerden BC, Oei L, Roschger P, Fratzl-Zelman N, Hoenderop JG, van Schoor NM, et al. TRPV4 deficiency causes sexual dimorphism in bone metabolism and osteoporotic fracture risk. Bone. 2013;57(2):443-54.
47. Martin RB, Burr D, Sharkey N, Fyhrie D. Skeletal Biology. Skeletal Tissue Mechanics: Springer New York; 2015. p. 35-93.
48. Shapiro F. Developmental Bone Biology. Pediatric Orthopedic Deformities, Volume 1: Springer International Publishing; 2016. p. 1-158.
49. Mescher AL. Chapter 7. Cartilage. Junqueira's Basic Histology, 13e. New York, NY: The McGraw-Hill Companies; 2013.
50. Sabater González M. Skeletal Cartilage and Bone Formation, Composition, and Function in Small Mammals, Birds, and Reptiles. Veterinary Clinics of North America: Exotic Animal Practice. 2019;22(2):123-34.
51. Sophia Fox AJ, Bedi A, Rodeo SA. The Basic Science of Articular Cartilage: Structure, Composition, and Function. Sports Health: A Multidisciplinary Approach. 2009;1(6):461-8.
52. Roughley PJ. Articular cartilage and changes in Arthritis: Noncollagenous proteins and proteoglycans in the extracellular matrix of cartilage. Arthritis Research & Therapy. 2001;3(6):342.
53. Neame PJ, Tapp H, Azizan A. Noncollagenous, nonproteoglycan macromolecules of cartilage. Cellular and molecular life sciences : CMLS. 1999;55.
54. Jung CK. Articular Cartilage: Histology and Physiology. In: Shetty AA, Kim S-J, Nakamura N, Brittberg M, editors. Techniques in Cartilage Repair Surgery. Berlin, Heidelberg: Springer Berlin Heidelberg; 2014. p. 17-21.
55. Gao Y, Liu S, Huang J, Guo W, Chen J, Zhang L, et al. The ECM-Cell Interaction of Cartilage Extracellular Matrix on Chondrocytes. BioMed Research International. 2014;2014:8.
56. Aspberg A. Cartilage Proteoglycans. In: Grässel S, Aszódi A, editors. Cartilage: Volume 1: Physiology and Development. Cham: Springer International Publishing; 2016. p. 1-22.
57. Roughley PJ. The structure and function of cartilage proteoglycans. Eur Cell Mater. 2006;12:92-101.
58. Grässel S. Collagens in Hyaline Cartilage. In: Grässel S, Aszódi A, editors. Cartilage: Volume 1: Physiology and Development. Cham: Springer International Publishing; 2016. p. 23-53.
59. Bella J, Eaton M, Brodsky B, Berman HM. Crystal and molecular structure of a collagen-like peptide at 1.9 A resolution. Science. 1994;266(5182):75.

60. McAlinden A, Johnstone B, Kollar J, Kazmi N, Hering TM. Expression of two novel alternatively spliced COL2A1 isoforms during chondrocyte differentiation. Matrix Biology. 2008;27(3):254-66.
61. McAlinden A. Alternative splicing of type II procollagen: IIB or not IIB? Connective Tissue Research. 2014;55(3):165-76.
62. Sandell LJ, Morris N, Robbins JR, Goldring MB. Alternatively spliced type II procollagen mRNAs define distinct populations of cells during vertebral development: differential expression of the amino-propeptide. The Journal of cell biology. 1991;114(6):1307-19.
63. Sandell LJ, Nalin AM, Reife RA. Alternative splice form of type II procollagen mRNA (IIA) is predominant in skeletal precursors and non-cartilaginous tissues during early mouse development. Developmental Dynamics. 1994;199(2):129-40.
64. Luo Y, Sinkeviciute D, He Y, Karsdal M, Henrotin Y, Mobasheri A, et al. The minor collagens in articular cartilage. Protein & cell. 2017:1-13.
65. Zaucke F. Cartilage Glycoproteins. In: Grässel S, Aszódi A, editors. Cartilage: Volume 1: Physiology and Development. Cham: Springer International Publishing; 2016. p. 55-81.
66. O'Conor CJ, Case N, Guilak F. Mechanical regulation of chondrogenesis. Stem Cell Research and Therapy. 2013;4(4).
67. Wuest S, Caliò M, Wernas T, Tanner S, Giger-Lange C, Wyss F, et al. Influence of Mechanical Unloading on Articular Chondrocyte Dedifferentiation. International Journal of Molecular Sciences. 2018;19(5).
68. Vinardell T, Rolfe RA, Buckley CT, Meyer EG, Ahearne M, Murphy P, et al. Hydrostatic pressure acts to stabilise a chondrogenic phenotype in porcine joint tissue derived stem cells. European Cells & Materials. 2012;23:121-32; discussion 33-4.
69. Doyle AD, Yamada KM. Mechanosensing via cell-matrix adhesions in 3D microenvironments. Experimental Cell Research. 2016;343(1):60-6.
70. Wong M, Siegrist M, Goodwin K. Cyclic tensile strain and cyclic hydrostatic pressure differentially regulate expression of hypertrophic markers in primary chondrocytes. Bone. 2003;33(4):685-93.
71. Madden RJ, Han S-K, Herzog W. The effect of compressive loading magnitude on in situ chondrocyte calcium signaling. Biomech Model Mechanobiol. 2015;14(1):135-42.
72. Lv M, Zhou Y, Chen X, Han L, Wang L, Lu XL. Calcium signaling of in situ chondrocytes in articular cartilage under compressive loading: Roles of calcium sources and cell membrane ion channels. J Orthop Res. 2017.
73. Vincent TL, Wann AKT. Mechanoadaptation: articular cartilage through thick and thin. The Journal of Physiology. 2018;0(0).
74. Felsenthal N, Zelzer E. Mechanical regulation of musculoskeletal system development. Development. 2017;144(23):4271.
75. Lee H-p, Stowers R, Chaudhuri O. Volume expansion and TRPV4 activation regulate stem cell fate in three-dimensional microenvironments. Nature Communications. 2019;10(1):529.
76. He L, Ahmad M, Perrimon N. Mechanosensitive channels and their functions in stem cell differentiation. Experimental Cell Research. 2019;374(2):259-65.
77. Vining KH, Mooney DJ. Mechanical forces direct stem cell behaviour in development and regeneration. Nature Reviews Molecular Cell Biology. 2017;18:728.
78. Wagner DR, Lindsey DP, Li KW, Tummala P, Chandran SE, Smith RL, et al. Hydrostatic pressure enhances chondrogenic differentiation of human bone marrow stromal cells in osteochondrogenic medium. Annals of Biomedical Engineering. 2008;36(5):813-20.
79. Huang AH, Farrell MJ, Mauck RL. Mechanics and mechanobiology of mesenchymal stem cell-based engineered cartilage. J Biomech. 2010;43.
80. Bertram KL, Krawetz RJ. Osmolarity regulates chondrogenic differentiation potential of synovial fluid derived mesenchymal progenitor cells. Biochemical & Biophysical Research Communications. 2012;422(3):455-61.
81. Hosseini M-S, Tafazzoli-Shadpour M, Haghighipour N, Aghdami N, Goodarzi A. The synergistic effects of shear stress and cyclic hydrostatic pressure modulate chondrogenic induction of human mesenchymal stem cells. International Journal of Artificial Organs. 2015;38(10):557-64.

82. Gan Y, Tu B, Li P, Ye J, Zhao C, Luo L, et al. Low Magnitude of Compression Enhances Biosynthesis of Mesenchymal Stem Cells towards Nucleus Pulposus Cells via the TRPV4-Dependent Pathway. Stem Cells Int. 2018;2018:7061898.
83. Sanchez JC, Danks TA, Wilkins RJ. Mechanisms involved in the increase in intracellular calcium following hypotonic shock in bovine articular chondrocytes. General Physiology & Biophysics. 2003;22(4):487-500.
84. Becker D, Blase C, Bereiter-Hahn J, Jendrach M. TRPV4 exhibits a functional role in cell-volume regulation. J Cell Sci. 2005;118(Pt 11):2435-40.
85. Lewis R, Feetham CH, Barrett-Jolley R. Cell volume regulation in chondrocytes. Cellular Physiology & Biochemistry. 2011;28(6):1111-22.
86. Hurd L, Kirwin SM, Boggs M, Mackenzie WG, Bober MB, Funanage VL, et al. A mutation in TRPV4 results in altered chondrocyte calcium signaling in severe metatropic dysplasia. American Journal of Medical Genetics Part A. 2015;167A(10):2286-93.
87. Kuipers AJ, Middelbeek J, van Leeuwen FN. Mechanoregulation of cytoskeletal dynamics by TRP channels. European Journal of Cell Biology. 2012;91(11–12):834-46.
88. Goswami C, Kuhn J, Heppenstall PA, Hucho T. Importance of non-selective cation channel TRPV4 interaction with cytoskeleton and their reciprocal regulations in cultured cells. PLoS ONE [Electronic Resource]. 2010;5(7):e11654.
89. Becker D, Bereiter-Hahn J, Jendrach M. Functional interaction of the cation channel transient receptor potential vanilloid 4 (TRPV4) and actin in volume regulation. European Journal of Cell Biology. 2009;88(3):141-52.
90. Suzuki M, Hirao A, Mizuno A. Microfilament-associated Protein 7 Increases the Membrane Expression of Transient Receptor Potential Vanilloid 4 (TRPV4). Journal of Biological Chemistry. 2003;278(51):51448-53.
91. Chun J, Shin SH, Kang SS. The negative feedback regulation of TRPV4 Ca2+ ion channel function by its C-terminal cytoplasmic domain. Cellular Signalling. 2012;24(10):1918-22.
92. Stein RA. The genetics of brachyolmia: between cilia and cell volume regulation. Clinical Genetics. 2009;75(2):118-9.
93. Rocio Servin-Vences M, Moroni M, Lewin GR, Poole K. Direct measurement of TRPV4 and PIEZO1 activity reveals multiple mechanotransduction pathways in chondrocytes. eLife. 2017;6:e21074.
94. Matthews BD, Thodeti CK, Tytell JD, Mammoto A, Overby DR, Ingber DE. Ultra-rapid activation of TRPV4 ion channels by mechanical forces applied to cell surface beta1 integrins. Integrative Biology:Quantitative Biosciences from Nano to Macro. 2010;2(9):435-42.
95. Heinegård D, Saxne T. The role of the cartilage matrix in osteoarthritis. Nature Reviews Rheumatology. 2010;7:50.
96. van der Kraan PM, Buma P, van Kuppevelt T, van Den Berg WB. Interaction of chondrocytes, extracellular matrix and growth factors: relevance for articular cartilage tissue engineering. Osteoarthritis and Cartilage. 2002;10(8):631-7.
97. Gilchrist CL, Leddy HA, Kaye L, Case ND, Rothenberg KE, Little D, et al. TRPV4-mediated calcium signaling in mesenchymal stem cells regulates aligned collagen matrix formation and vinculin tension. Proceedings of the National Academy of Sciences. 2019;116(6):1992.
98. Fodor J, Matta C, Oláh T, Juhász T, Takács R, Tóth A, et al. Store-operated calcium entry and calcium influx via voltage-operated calcium channels regulate intracellular calcium oscillations in chondrogenic cells. Cell Calcium. 2013;54(1):1-16.
99. Zhou Y, Park M, Cheung E, Wang L, Lu XL. The effect of chemically defined medium on spontaneous calcium signaling of in situ chondrocytes during long-term culture. J Biomech. 2015;48(6):990-6.
100. Raizman I, De Croos JN, Pilliar R, Kandel RA. Calcium regulates cyclic compression-induced early changes in chondrocytes during in vitro cartilage tissue formation. Cell Calcium. 2010;48(4):232-42.
101. Zheng J, Zeng X, Wang S. Calcium ion as cellular messenger. Sci China Life Sci. 2015;58(1):1-5.
102. Clapham DE. Calcium Signaling. Cell. 2007;131(6):1047-58.

103. Kang SS, Shin SH, Auh C-K, Chun J. Human skeletal dysplasia caused by a constitutive activated transient receptor potential vanilloid 4 (TRPV4) cation channel mutation. Exp Mol Med. 2012;44:707-22.
104. Nilius B, Owsianik G. Channelopathies converge on TRPV4. Nature Genetics. 2010;42(2):98-100.
105. Cho TJ, Matsumoto K, Fano V, Dai J, Kim OH, Chae JH, et al. TRPV4-pathy manifesting both skeletal dysplasia and peripheral neuropathy: a report of three patients. American Journal of Medical Genetics Part A. 2012;158A(4):795-802.
106. Fiorillo C, Moro F, Brisca G, Astrea G, Nesti C, Balint Z, et al. TRPV4 mutations in children with congenital distal spinal muscular atrophy. Neurogenetics. 2012;13(3):195-203.
107. Oonk AM, Ekker MS, Huygen PL, Kunst HP, Kremer H, Schelhaas JJ, et al. Intrafamilial variable hearing loss in TRPV4 induced spinal muscular atrophy. Annals of Otology, Rhinology & Laryngology. 2014;123(12):859-65.
108. Koutsis G, Lynch D, Manole A, Karadima G, Reilly MM, Houlden H, et al. Charcot-Marie-Tooth disease type 2C and scapuloperoneal muscular atrophy overlap syndrome in a patient with the R232C TRPV4 mutation.[Erratum appears in J Neurol. 2015 Aug;262(8):1976 Note: Manone, Andreea [corrected to Manole, Andreea]; PMID: 26162716]. Journal of Neurology. 2015;262(8):1972-5.
109. Camacho N, Krakow D, Johnykutty S, Katzman PJ, Pepkowitz S, Vriens J, et al. Dominant TRPV4 mutations in nonlethal and lethal metatropic dysplasia. American Journal of Medical Genetics Part A. 2010;152A(5):1169-77.
110. Dai J, Kim OH, Cho TJ, Schmidt-Rimpler M, Tonoki H, Takikawa K, et al. Novel and recurrent TRPV4 mutations and their association with distinct phenotypes within the TRPV4 dysplasia family. Journal of Medical Genetics. 2010;47(10):704-9.
111. Nishimura G, Lausch E, Savarirayan R, Shiba M, Spranger J, Zabel B, et al. TRPV4-associated skeletal dysplasias. American Journal of Medical Genetics Part C, Seminars in Medical Genetics. 2012;160C(3):190-204.
112. Leddy HA, McNulty AL, Guilak F, Liedtke W. Unraveling the mechanism by which TRPV4 mutations cause skeletal dysplasias. Rare Diseases. 2014;2(1):e962971.
113. Nishimura G, Dai J, Lausch E, Unger S, Megarbane A, Kitoh H, et al. Spondylo-epiphyseal dysplasia, Maroteaux type (pseudo-Morquio syndrome type 2), and parastremmatic dysplasia are caused by TRPV4 mutations. American Journal of Medical Genetics Part A. 2010;152A(6):1443-9.
114. Grigelioniene G, Geiberger S, Horemuzova E, Mostrom E, Jantti N, Neumeyer L, et al. Autosomal dominant brachyolmia in a large Swedish family: phenotypic spectrum and natural course. American Journal of Medical Genetics Part A. 2014;164A(7):1635-41.
115. Guzman CM, Aaron GR. Spondylometaphyseal dysplasia (Kozlowski type): case report. Pediatric dentistry. 1993;15(1):49-52.
116. Camacho N, Krakow D, Johnykutty S, Katzman PJ, Pepkowitz S, Vriens J, et al. Dominant TRPV4 mutations in nonlethal and lethal metatropic dysplasia. American Journal of Medical Genetics Part A. 2010;152A(5):1169-77.
117. Damseh N, Stimec J, O'Brien A, Marshall C, Savarirayan R, Jawad A, et al. Thiemann disease and familial digital arthropathy – brachydactyly: two sides of the same coin? Orphanet Journal of Rare Diseases. 2019;14(1):156.
118. Mah W, Sonkusare SK, Wang T, Azeddine B, Pupavac M, Carrot-Zhang J, et al. Gain-of-function mutation in TRPV4 identified in patients with osteonecrosis of the femoral head. J Med Genet. 2016;53(10):705-9.
119. Mizuno A, Matsumoto N, Imai M, Suzuki M. Impaired osmotic sensation in mice lacking TRPV4. American Journal of Physiology - Cell Physiology. 2003;285(1):C96-101.
120. Minegishi Y, Hosokawa K, Tsumaki N. Time-lapse observation of the dedifferentiation process in mouse chondrocytes using chondrocyte-specific reporters. Osteoarthritis and Cartilage. 2013;21(12):1968-75.
121. Loukin SH, Teng J, Kung C. A channelopathy mechanism revealed by direct calmodulin activation of TrpV4. Proc Natl Acad Sci U S A. 2015;112(30):9400-5.

122. Loukin S, Zhou X, Su Z, Saimi Y, Kung C. Wild-type and brachyolmia-causing mutant TRPV4 channels respond directly to stretch force. Journal of Biological Chemistry. 2010;285(35):27176-81.
123. Inada H, Procko E, Sotomayor M, Gaudet R. Structural and Biochemical Consequences of Disease-Causing Mutations in the Ankyrin Repeat Domain of the Human TRPV4 Channel. Biochemistry. 2012;51(31):6195-206.
124. Saitta B, Passarini J, Sareen D, Ornelas L, Sahabian A, Argade S, et al. Patient-derived skeletal dysplasia induced pluripotent stem cells display abnormal chondrogenic marker expression and regulation by BMP2 and TGFbeta1. Stem Cells & Development. 2014;23(13):1464-78.
125. Klausen TK, Janssens A, Prenen J, Owsianik G, Hoffmann EK, Pedersen SF, et al. Single point mutations of aromatic residues in transmembrane helices 5 and -6 differentially affect TRPV4 activation by 4alpha-PDD and hypotonicity: implications for the role of the pore region in regulating TRPV4 activity. Cell Calcium. 2014;55(1):38-47.
126. Nonaka K, Han X, Kato H, Sato H, Yamaza H, Hirofuji Y, et al. Novel gain-of-function mutation of TRPV4 associated with accelerated chondrogenic differentiation of dental pulp stem cells derived from a patient with metatropic dysplasia. Biochemistry and Biophysics Reports. 2019;19:100648.
127. Su Z, Zhou X, Haynes WJ, Loukin SH, Anishkin A, Saimi Y, et al. Yeast gain-of-function mutations reveal structure-function relationships conserved among different subfamilies of transient receptor potential channels. Proceedings of the National Academy of Sciences of the United States of America. 2007;104(49):19607-12.
128. Zhou X, Su Z, Anishkin A, Haynes WJ, Friske EM, Loukin SH, et al. Yeast screens show aromatic residues at the end of the sixth helix anchor transient receptor potential channel gate. Proceedings of the National Academy of Sciences of the United States of America. 2007;104(39):15555-9.
129. Loukin SH, Teng J, Kung C. A channelopathy mechanism revealed by direct calmodulin activation of TrpV4. Proceedings of the National Academy of Sciences of the United States of America. 2015;112(30):9400-5.
130. Gandolfi B, Alamri S, Darby WG, Adhikari B, Lattimer JC, Malik R, et al. A dominant TRPV4 variant underlies osteochondrodysplasia in Scottish fold cats. Osteoarthritis Cartilage. 2016;24(8):1441-50.
131. O'Conor CJ, Griffin TM, Liedtke W, Guilak F. Increased susceptibility of Trpv4-deficient mice to obesity and obesity-induced osteoarthritis with very high-fat diet. Annals of the Rheumatic Diseases. 2013;72(2):300-4.
132. Clark AL, Votta BJ, Kumar S, Liedtke W, Guilak F. Chondroprotective role of the osmotically sensitive ion channel transient receptor potential vanilloid 4: Age- and sex-dependent progression of osteoarthritis in Trpv4-deficient mice. Arthritis & Rheumatism. 2010;62(10):2973-83.
133. Suzuki M, Mizuno A, Kodaira K, Imai M. Impaired pressure sensation in mice lacking TRPV4. Journal of Biological Chemistry. 2003;278(25):22664-8.
134. Tabuchi K, Suzuki M, Mizuno A, Hara A. Hearing impairment in TRPV4 knockout mice. Neuroscience Letters. 2005;382(3):304-8.
135. Malik R, Allan GS, Howlett CR, Thompson DE, James G, McWhirter C, et al. Osteochondrodysplasia in Scottish Fold cats. Australian Veterinary Journal. 1999;77(2):85-92.
136. Schoenwolf GC, Bleyl SB, Brauer PR, Francis-West PH. Larsen's Human Embryology, Fifth Edition. Philadelphia, PA: Churchill Livingstone/Elsevier; 2015.
137. Berendsen AD, Olsen BR. Bone development. Bone. 2015;80:14-8.
138. Carlson BM. Human Embryology and Developmental Biology : with STUDENT CONSULT Online Access. Saint Louis, UNITED STATES: Elsevier; 2012.
139. Webster S, de Wreede R. Embryology at a Glance. Hoboken, UNITED KINGDOM: John Wiley & Sons, Incorporated; 2016.
140. Gilbert S. Osteogenesis: The Development of Bones. 2000 16 August 2016. In: Developmental Biology [Internet]. Sunderland (MA): Sinauer Associates. 6. Available from: http://www.ncbi.nlm.nih.gov/books/NBK10056/.

141. Olsen B. Bone Embryology. In: Favus M, editor. Primer on the Metabolic Bone Diseases And Disorders of Mineral Metabolism. Washington DC: American society for bone and mineral research; 2006.
142. Tsang KY, Chan D, Cheah KSE. Fate of growth plate hypertrophic chondrocytes: Death or lineage extension? Development, Growth & Differentiation. 2015;57(2):179-92.
143. Wright E, Hargrave MR, Christiansen J, Cooper L, Kun J, Evans T, et al. The Sry-related gene Sox9 is expressed during chondrogenesis in mouse embryos. Nature Genetics. 1995;9(1):15-20.
144. Lefebvre V, de Crombrugghe B. Toward understanding SOX9 function in chondrocyte differentiation. Matrix Biology. 1998;16(9):529-40.
145. Muramatsu S, Wakabayashi M, Ohno T, Amano K, Ooishi R, Sugahara T, et al. Functional gene screening system identified TRPV4 as a regulator of chondrogenic differentiation. Journal of Biological Chemistry. 2007;282(44):32158-67.
146. Mescher AL. Bone. Junqueira's Basic Histology, 14e. New York, NY: McGraw-Hill Education; 2016.
147. Nishimura R, Hata K, Ikeda F, Matsubara T, Amano K, Ono K, et al. Regulation of transcriptional network system during bone and cartilage development. Journal of Oral Biosciences. 2015;57(4):165-70.
148. Karsenty G, Wagner EF. Reaching a Genetic and Molecular Understanding of Skeletal Development. Developmental Cell. 2002;2(4):389-406.
149. Aszódi A. The Cartilaginous Growth Plate. In: Grässel S, Aszódi A, editors. Cartilage: Volume 1: Physiology and Development. Cham: Springer International Publishing; 2016. p. 83-113.
150. von der Mark K, Zhou X. Cell Fate of Growth Plate Chondrocytes in Endochondral Ossification: Cell Death or Reprogramming into Osteogenic Lineage? In: Grässel S, Aszódi A, editors. Cartilage: Volume 1: Physiology and Development. Cham: Springer International Publishing; 2016. p. 115-42.
151. Bonafe L, Cormier-Daire V, Hall C, Lachman R, Mortier G, Mundlos S, et al. Nosology and classification of genetic skeletal disorders: 2015 revision. Am J Med Genet A. 2015;167(12):2869-92.
152. Wagner T, Wirth J, Meyer J, Zabel B, Held M, Zimmer J, et al. Autosomal sex reversal and campomelic dysplasia are caused by mutations in and around the SRY-related gene SOX9. Cell. 1994;79(6):1111-20.
153. Staffler A, Hammel M, Wahlbuhl M, Bidlingmaier C, Flemmer AW, Pagel P, et al. Heterozygous SOX9 mutations allowing for residual DNA-binding and transcriptional activation lead to the acampomelic variant of campomelic dysplasia. Human Mutation. 2010;31(6):E1436-44.
154. Bi W, Huang W, Whitworth DJ, Deng JM, Zhang Z, Behringer RR, et al. Haploinsufficiency of Sox9 results in defective cartilage primordia and premature skeletal mineralization. Proceedings of the National Academy of Sciences of the United States of America. 2001;98(12):6698-703.
155. Bi W, Deng JM, Zhang Z, Behringer RR, de Crombrugghe B. Sox9 is required for cartilage formation. Nature Genetics. 1999;22(1):85-9.
156. Tsuchiya H, Kitoh H, Sugiura F, Ishiguro N. Chondrogenesis enhanced by overexpression of sox9 gene in mouse bone marrow-derived mesenchymal stem cells. Biochemical & Biophysical Research Communications. 2002;301(2):338-43.
157. Hargus G, Kist R, Kramer J, Gerstel D, Neitz A, Scherer G, et al. Loss of Sox9 function results in defective chondrocyte differentiation of mouse embryonic stem cells in vitro. International Journal of Developmental Biology. 2008;52(4):323-32.
158. Akiyama H, Lefebvre V. Unraveling the transcriptional regulatory machinery in chondrogenesis. Journal of Bone & Mineral Metabolism. 2011;29(4):390-5.
159. Bell DM, Leung KK, Wheatley SC, Ng LJ, Zhou S, Ling KW, et al. SOX9 directly regulates the type-II collagen gene. Nature Genetics. 1997;16(2):174-8.
160. Lefebvre V, Huang W, Harley VR, Goodfellow PN, de Crombrugghe B. SOX9 is a potent activator of the chondrocyte-specific enhancer of the pro alpha1(II) collagen gene. Molecular & Cellular Biology. 1997;17(4):2336-46.
161. Takahashi I, Nuckolls GH, Takahashi K, Tanaka O, Semba I, Dashner R, et al. Compressive force promotes sox9, type II collagen and aggrecan and inhibits IL-1beta expression resulting in

chondrogenesis in mouse embryonic limb bud mesenchymal cells. Journal of Cell Science. 1998;111(Pt 14):2067-76.
162. Sekiya I, Tsuji K, Koopman P, Watanabe H, Yamada Y, Shinomiya K, et al. SOX9 enhances aggrecan gene promoter/enhancer activity and is up-regulated by retinoic acid in a cartilage-derived cell line, TC6. Journal of Biological Chemistry. 2000;275(15):10738-44.
163. Lefebvre V, Li P, de Crombrugghe B. A new long form of Sox5 (L-Sox5), Sox6 and Sox9 are coexpressed in chondrogenesis and cooperatively activate the type II collagen gene. EMBO Journal. 1998;17(19):5718-33.
164. Lefebvre V, Behringer RR, de Crombrugghe B. L-Sox5, Sox6 and Sox9 control essential steps of the chondrocyte differentiation pathway. Osteoarthritis & Cartilage. 2001;9 Suppl A:S69-75.
165. Akiyama H, Chaboissier MC, Martin JF, Schedl A, de Crombrugghe B. The transcription factor Sox9 has essential roles in successive steps of the chondrocyte differentiation pathway and is required for expression of Sox5 and Sox6. Genes & Development. 2002;16(21):2813-28.
166. Yang HN, Park JS, Woo DG, Jeon SY, Do HJ, Lim HY, et al. Chondrogenesis of mesenchymal stem cells and dedifferentiated chondrocytes by transfection with SOX Trio genes. Biomaterials. 2011;32(30):7695-704.
167. Han Y, Lefebvre V. L-Sox5 and Sox6 drive expression of the aggrecan gene in cartilage by securing binding of Sox9 to a far-upstream enhancer. Molecular & Cellular Biology. 2008;28(16):4999-5013.
168. Ikeda T, Kamekura S, Mabuchi A, Kou I, Seki S, Takato T, et al. The combination of SOX5, SOX6, and SOX9 (the SOX trio) provides signals sufficient for induction of permanent cartilage. Arthritis & Rheumatism. 2004;50(11):3561-73.
169. Eames BF, Sharpe PT, Helms JA. Hierarchy revealed in the specification of three skeletal fates by Sox9 and Runx2. Developmental Biology. 2004;274(1):188-200.
170. Fan H-C, Zhang X, McNaughton PA. Activation of the TRPV4 Ion Channel Is Enhanced by Phosphorylation. Journal of Biological Chemistry. 2009;284(41):27884-91.
171. Huang W, Zhou X, Lefebvre V, de Crombrugghe B. Phosphorylation of SOX9 by cyclic AMP-dependent protein kinase A enhances SOX9's ability to transactivate a Col2a1 chondrocyte-specific enhancer.[Erratum appears in Mol Cell Biol 2000 Oct;20(20):7838]. Molecular & Cellular Biology. 2000;20(11):4149-58.
172. Kumar D, Lassar AB. Fibroblast Growth Factor Maintains Chondrogenic Potential of Limb Bud Mesenchymal Cells by Modulating DNMT3A Recruitment. Cell Reports. 2014;8(5):1419-31.
173. Nifuji A, Noda M. Coordinated expression of noggin and bone morphogenetic proteins (BMPs) during early skeletogenesis and induction of noggin expression by BMP-7. Journal of Bone & Mineral Research. 1999;14(12):2057-66.
174. Pizette S, Niswander L. BMPs Are Required at Two Steps of Limb Chondrogenesis: Formation of Prechondrogenic Condensations and Their Differentiation into Chondrocytes. Developmental Biology. 2000;219(2):237-49.
175. Zehentner BK, Dony C, Burtscher H. The transcription factor Sox9 is involved in BMP-2 signaling. Journal of Bone & Mineral Research. 1999;14(10):1734-41.
176. Majumdar MK, Wang E, Morris EA. BMP-2 and BMP-9 promotes chondrogenic differentiation of human multipotential mesenchymal cells and overcomes the inhibitory effect of IL-1. Journal of Cellular Physiology. 2001;189(3):275-84.
177. Zhou N, Hu N, Liao JY, Lin LB, Zhao C, Si WK, et al. HIF-1α as a Regulator of BMP2-Induced Chondrogenic Differentiation, Osteogenic Differentiation, and Endochondral Ossification in Stem Cells. Cellular Physiology and Biochemistry. 2015;36(1):44-60.
178. Caron MM, Emans PJ, Cremers A, Surtel DA, Coolsen MM, van Rhijn LW, et al. Hypertrophic differentiation during chondrogenic differentiation of progenitor cells is stimulated by BMP-2 but suppressed by BMP-7. Osteoarthritis & Cartilage. 2013;21(4):604-13.
179. Jing J, Ren Y, Zong Z, Liu C, Kamiya N, Mishina Y, et al. BMP receptor 1A determines the cell fate of the postnatal growth plate. International Journal of Biological Sciences [Electronic Resource]. 2013;9(9):895-906.
180. Yoon BS, Ovchinnikov DA, Yoshii I, Mishina Y, Behringer RR, Lyons KM. Bmpr1a and Bmpr1b have overlapping functions and are essential for chondrogenesis in vivo. Proceedings of the National Academy of Sciences of the United States of America. 2005;102(14):5062-7.

181. Tsumaki N, Nakase T, Miyaji T, Kakiuchi M, Kimura T, Ochi T, et al. Bone morphogenetic protein signals are required for cartilage formation and differently regulate joint development during skeletogenesis. Journal of Bone & Mineral Research. 2002;17(5):898-906.
182. Koyama E, Shibukawa Y, Nagayama M, Sugito H, Young B, Yuasa T, et al. A distinct cohort of progenitor cells participates in synovial joint and articular cartilage formation during mouse limb skeletogenesis. Developmental Biology. 2008;316(1):62-73.
183. Hatakeyama Y, Nguyen J, Wang X, Nuckolls GH, Shum L. Smad signaling in mesenchymal and chondroprogenitor cells. Journal of Bone & Joint Surgery - American Volume. 2003;85-A Suppl 3:13-8.
184. Jin EJ, Lee SY, Choi YA, Jung JC, Bang OS, Kang SS. BMP-2-enhanced chondrogenesis involves p38 MAPK-mediated down-regulation of Wnt-7a pathway. Molecules & Cells. 2006;22(3):353-9.
185. Chimal-Monroy J, Rodriguez-Leon J, Montero JA, Ganan Y, Macias D, Merino R, et al. Analysis of the molecular cascade responsible for mesodermal limb chondrogenesis: Sox genes and BMP signaling. Developmental Biology. 2003;257(2):292-301.
186. Mara CS, Duarte AS, Sartori A, Luzo AC, Saad ST, Coimbra IB. Regulation of chondrogenesis by transforming growth factor-beta 3 and insulin-like growth factor-1 from human mesenchymal umbilical cord blood cells. Journal of Rheumatology. 2010;37(7):1519-26.
187. Bhang SH, Jeon JY, La WG, Seong JY, Hwang JW, Ryu SE, et al. Enhanced chondrogenic marker expression of human mesenchymal stem cells by interaction with both TGF-beta3 and hyaluronic acid. Biotechnology & Applied Biochemistry. 2011;58(4):271-6.
188. Wang W, Rigueur D, Lyons KM. TGF beta signaling in cartilage development and maintenance. Birth Defects Research Part C-Embryo Today-Reviews. 2014;102(1):37-51.
189. Song JJ, Aswad R, Kanaan RA, Rico MC, Owen TA, Barbe MF, et al. Connective tissue growth factor (CTGF) acts as a downstream mediator of TGF-beta1 to induce mesenchymal cell condensation. Journal of Cellular Physiology. 2007;210(2):398-410.
190. Karamboulas K, Dranse HJ, Underhill TM. Regulation of BMP-dependent chondrogenesis in early limb mesenchyme by TGFβ signals. Journal of Cell Science. 2010;123(12):2068-76.
191. Murphy MK, Huey DJ, Hu JC, Athanasiou KA. TGF-beta 1, GDF-5, and BMP-2 Stimulation Induces Chondrogenesis in Expanded Human Articular Chondrocytes and Marrow-Derived Stromal Cells. Stem cells (Dayton, Ohio). 2015;33(3):762-73.
192. Xu T, Wu M, Feng J, Lin X, Gu Z. RhoA/Rho kinase signaling regulates transforming growth factor-beta1-induced chondrogenesis and actin organization of synovium-derived mesenchymal stem cells through interaction with the Smad pathway. International Journal of Molecular Medicine. 2012;30(5):1119-25.
193. Correa D, Somoza RA, Lin P, Greenberg S, Rom E, Duesler L, et al. Sequential exposure to fibroblast growth factors (FGF) 2, 9 and 18 enhances hMSC chondrogenic differentiation. Osteoarthritis & Cartilage. 2014;23(3):443-53.
194. Shintani N, Siebenrock KA, Hunziker EB. TGF-ß1 Enhances the BMP-2-Induced Chondrogenesis of Bovine Synovial Explants and Arrests Downstream Differentiation at an Early Stage of Hypertrophy. PLoS ONE. 2013;8(1):e53086.
195. Huang X, Xu J, Huang M, Li J, Dai L, Dai K, et al. Histone deacetylase1 promotes TGF-beta 1-mediated early chondrogenesis through down-regulating canonical Wnt signaling. Biochemical and Biophysical Research Communications. 2014;453(4):810-6.
196. Kwon H, Paschos NK, Hu JC, Athanasiou K. Articular cartilage tissue engineering: the role of signaling molecules. Cellular and molecular life sciences : CMLS. 2016;73(6):1173-94.
197. Peters K, Ornitz D, Werner S, Williams L. Unique expression pattern of the FGF receptor 3 gene during mouse organogenesis. Dev Biol. 1993;155(2):423-30.
198. Henderson JE, Naski MC, Aarts MM, Wang D, Cheng L, Goltzman D, et al. Expression of FGFR3 with the G380R achondroplasia mutation inhibits proliferation and maturation of CFK2 chondrocytic cells. Journal of bone and mineral research : the official journal of the American Society for Bone and Mineral Research. 2000;15(1):155-65.
199. Shiang R, Thompson LM, Zhu Y-Z, Church DM, Fielder TJ, Bocian M, et al. Mutations in the transmembrane domain of FGFR3 cause the most common genetic form of dwarfism, achondroplasia. Cell. 1994;78(2):335-42.

200. Vajo Z, Francomano CA, Wilkin DJ. The Molecular and Genetic Basis of Fibroblast Growth Factor Receptor 3 Disorders: The Achondroplasia Family of Skeletal Dysplasias, Muenke Craniosynostosis, and Crouzon Syndrome with Acanthosis Nigricans*. Endocrine Reviews. 2000;21(1):23-39.
201. Murakami S, Kan M, McKeehan WL, de Crombrugghe B. Up-regulation of the chondrogenic Sox9 gene by fibroblast growth factors is mediated by the mitogen-activated protein kinase pathway. Proceedings of the National Academy of Sciences of the United States of America. 1999;97(3):1113-8.
202. Hoffman LM, Weston AD, Underhill TM. Molecular mechanisms regulating chondroblast differentiation. Journal of Bone & Joint Surgery - American Volume. 2003;85-A Suppl 2:124-32.
203. ten Berge D, Brugmann SA, Helms JA, Nusse R. Wnt and FGF signals interact to coordinate growth with cell fate specification during limb development. Development. 2008;135(19):3247-57.
204. Green JD, Tollemar V, Dougherty M, Yan Z, Yin L, Ye J, et al. Multifaceted signaling regulators of chondrogenesis: Implications in cartilage regeneration and tissue engineering. Genes & Diseases. 2015;2(4):307-27.
205. Daoud G, Kempf H, Kumar D, Kozhemyakina E, Holowacz T, Kim D-W, et al. BMP-mediated induction of GATA4/5/6 blocks somitic responsiveness to SHH. Development. 2014;141(20):3978-87.
206. Amarilio R, Viukov SV, Sharir A, Eshkar-Oren I, Johnson RS, Zelzer E. HIF1alpha regulation of Sox9 is necessary to maintain differentiation of hypoxic prechondrogenic cells during early skeletogenesis. Development. 2007;134(21):3917-28.
207. Das R, Timur UT, Edip S, Haak E, Wruck C, Weinans H, et al. TGF-beta2 is involved in the preservation of the chondrocyte phenotype under hypoxic conditions. Annals of Anatomy. 2014;198:1-10.
208. Duval E, Leclercq S, Elissalde JM, Demoor M, Galera P, Boumediene K. Hypoxia-inducible factor 1alpha inhibits the fibroblast-like markers type I and type III collagen during hypoxia-induced chondrocyte redifferentiation: hypoxia not only induces type II collagen and aggrecan, but it also inhibits type I and type III collagen in the hypoxia-inducible factor 1alpha-dependent redifferentiation of chondrocytes.[Erratum appears in Arthritis Rheum. 2014 May;66(5):1394]. Arthritis & Rheumatism. 2009;60(10):3038-48.
209. Kanichai M, Ferguson D, Prendergast PJ, Campbell VA. Hypoxia promotes chondrogenesis in rat mesenchymal stem cells: a role for AKT and hypoxia-inducible factor (HIF)-1alpha. Journal of Cellular Physiology. 2008;216(3):708-15.
210. Hosaka Y, Saito T, Sugita S, Hikata T, Kobayashi H, Fukai A, et al. Notch signaling in chondrocytes modulates endochondral ossification and osteoarthritis development. Proc Natl Acad Sci U S A. 2013;110(5):1875-80.
211. Kohn A, Rutkowski TP, Liu Z, Mirando AJ, Zuscik MJ, O'Keefe RJ, et al. Notch signaling controls chondrocyte hypertrophy via indirect regulation of Sox9. Bone Research. 2015;3.
212. Amano K, Densmore M, Nishimura R, Lanske B. Indian Hedgehog Signaling Regulates Transcription and Expression of Collagen Type X via Runx2/Smads Interactions. Journal of Biological Chemistry. 2014;289(36):24898-910.
213. Mak KK, Kronenberg HM, Chuang P-T, Mackem S, Yang Y. Indian hedgehog signals independently of PTHrP to promote chondrocyte hypertrophy. Development. 2008;135(11):1947.
214. Kim E-J, Cho S-W, Shin J-O, Lee M-J, Kim K-S, Jung H-S. Ihh and Runx2/Runx3 Signaling Interact to Coordinate Early Chondrogenesis: A Mouse Model. PLOS ONE. 2013;8(2):e55296.
215. Kobayashi T, Soegiarto DW, Yang Y, Lanske B, Schipani E, McMahon AP, et al. Indian hedgehog stimulates periarticular chondrocyte differentiation to regulate growth plate length independently of PTHrP. The Journal of clinical investigation. 2005;115(7):1734-42.
216. Chung U-i, Schipani E, McMahon AP, Kronenberg HM. Indian hedgehog couples chondrogenesis to osteogenesis in endochondral bone development. The Journal of Clinical Investigation. 2001;107(3):295-304.

217. de Crombrugghe B, Lefebvre V, Behringer RR, Bi W, Murakami S, Huang W. Transcriptional mechanisms of chondrocyte differentiation. Matrix Biology. 2000;19(5):389-94.
218. Kulyk WM, Franklin JL, Hoffman LM. Sox9 expression during chondrogenesis in micromass cultures of embryonic limb mesenchyme. Experimental Cell Research. 2000;255(2):327-32.
219. Guo J, Chung UI, Yang D, Karsenty G, Bringhurst FR, Kronenberg HM. PTH/PTHrP receptor delays chondrocyte hypertrophy via both Runx2-dependent and -independent pathways. Dev Biol. 2006;292(1):116-28.
220. Li TF, Dong Y, Ionescu AM, Rosier RN, Zuscik MJ, Schwarz EM, et al. Parathyroid hormone-related peptide (PTHrP) inhibits Runx2 expression through the PKA signaling pathway. Exp Cell Res. 2004;299(1):128-36.
221. Nishikawa S-I, Jakt LM, Era T. Embryonic stem-cell culture as a tool for developmental cell biology. Nat Rev Mol Cell Biol. 2007;8(6):502-7.
222. Thomson JA, Itskovitz-Eldor J, Shapiro SS, Waknitz MA, Swiergiel JJ, Marshall VS, et al. Embryonic stem cell lines derived from human blastocysts. Science. 1998;282(5391):1145-7.
223. Singh VK, Kalsan M, Kumar N, Saini A, Chandra R. Induced pluripotent stem cells: applications in regenerative medicine, disease modeling, and drug discovery. Frontiers in Cell and Developmental Biology. 2015;3:2.
224. Cheng A, Kapacee Z, Peng J, Lu S, Lucas RJ, Hardingham TE, et al. Cartilage Repair Using Human Embryonic Stem Cell-Derived Chondroprogenitors. Stem Cells Translational Medicine. 2014;3(11):1287-94.
225. Barna M, Niswander L. Visualization of cartilage formation: insight into cellular properties of skeletal progenitors and chondrodysplasia syndromes. Developmental Cell. 2007;12(6):931-41.
226. Tang S, Xie M, Cao N, Ding S. Patient-Specific Induced Pluripotent Stem Cells for Disease Modeling and Phenotypic Drug Discovery. Journal of Medicinal Chemistry. 2016;59(1):2-15.
227. Avior Y, Sagi I, Benvenisty N. Pluripotent stem cells in disease modelling and drug discovery. Nat Rev Mol Cell Biol. 2016;17(3):170-82.
228. Pomp O, Colman A. Disease modelling using induced pluripotent stem cells: Status and prospects. BioEssays. 2013;35(3):271-80.
229. Tiscornia G, Vivas EL, Belmonte JCI. Diseases in a dish: modeling human genetic disorders using induced pluripotent cells. Nat Med. 2011:1570-6.
230. Wert Gd, Mummery C. Human embryonic stem cells: research, ethics and policy. Human Reproduction. 2003;18(4):672-82.
231. Castro-Vinuelas R, Sanjurjo-Rodriguez C, Pineiro-Ramil M, Hermida-Gomez T, Fuentes-Boquete IM, de Toro-Santos FJ, et al. Induced pluripotent stem cells for cartilage repair: current status and future perspectives. Eur Cell Mater. 2018;36:96-109.
232. Nam Y, Rim YA, Lee J, Ju JH. Current Therapeutic Strategies for Stem Cell-Based Cartilage Regeneration. Stem Cells International. 2018;2018:20.
233. Driessen BJH, Logie C, Vonk LA. Cellular reprogramming for clinical cartilage repair. Cell biology and toxicology. 2017:1-21.
234. Cheng A, Hardingham TE, Kimber SJ. Generating Cartilage Repair from Pluripotent Stem Cells. Tissue Engineering Part B: Reviews. 2013;20(4):257-66.
235. Umeda K, Zhao J, Simmons P, Stanley E, Elefanty A, Nakayama N. Human chondrogenic paraxial mesoderm, directed specification and prospective isolation from pluripotent stem cells. 2012;2:455.
236. Xi H, Fujiwara W, Gonzalez K, Jan M, Liebscher S, Van Handel B, et al. In Vivo Human Somitogenesis Guides Somite Development from hPSCs. Cell Reports. 2017;18(6):1573-85.
237. Gadue P, Huber TL, Paddison PJ, Keller GM. Wnt and TGF-beta signaling are required for the induction of an in vitro model of primitive streak formation using embryonic stem cells. Proc Natl Acad Sci U S A. 2006;103(45):16806-11.
238. Sumi T, Tsuneyoshi N, Nakatsuji N, Suemori H. Defining early lineage specification of human embryonic stem cells by the orchestrated balance of canonical Wnt/beta-catenin, Activin/Nodal and BMP signaling. Development. 2008;135(17):2969-79.
239. Liu C, Peng G, Jing N. TGF-β signaling pathway in early mouse development and embryonic stem cells. Acta Biochimica et Biophysica Sinica. 2017;50(1):68-73.

240. Hwang NS, Varghese S, Zhang Z, Elisseeff J. Chondrogenic differentiation of human embryonic stem cell-derived cells in arginine-glycine-aspartate-modified hydrogels. Tissue Engineering. 2006;12(9):2695-706.
241. Yamashita A, Krawetz R, Rancourt DE. Loss of discordant cells during micro-mass differentiation of embryonic stem cells into the chondrocyte lineage. Cell Death & Differentiation. 2009;16(2):278-86.
242. Yamashita A, Liu S, Woltjen K, Thomas B, Meng G, Hotta A, et al. Cartilage tissue engineering identifies abnormal human induced pluripotent stem cells. Scientific Reports. 2013;3:1978.
243. Gibson JD, O'Sullivan MB, Alaee F, Paglia DN, Yoshida R, Guzzo RM, et al. Regeneration of Articular Cartilage by Human ESC-Derived Mesenchymal Progenitors Treated Sequentially with BMP-2 and Wnt5a. Stem Cells Transl Med. 2017;6(1):40-50.
244. Nakayama N, Duryea D, Manoukian R, Chow G, Han CY. Macroscopic cartilage formation with embryonic stem-cell-derived mesodermal progenitor cells. Journal of Cell Science. 2003;116(Pt 10):2015-28.
245. Diekman BO, Christoforou N, Willard VP, Sun H, Sanchez-Adams J, Leong KW, et al. Cartilage tissue engineering using differentiated and purified induced pluripotent stem cells. Proceedings of the National Academy of Sciences. 2012;109(47):19172-7.
246. Craft AM, Ahmed N, Rockel JS, Baht GS, Alman BA, Kandel RA, et al. Specification of chondrocytes and cartilage tissues from embryonic stem cells. Development. 2013;140(12):2597-610.
247. Phillips MD, Kuznetsov SA, Cherman N, Park K, Chen KG, McClendon BN, et al. Directed differentiation of human induced pluripotent stem cells toward bone and cartilage: in vitro versus in vivo assays. Stem Cells Translational Medicine. 2013;3(7):867-78.
248. Adkar SS, Wu C-L, Willard VP, Dicks A, Ettyreddy A, Steward N, et al. Step-Wise Chondrogenesis of Human Induced Pluripotent Stem Cells and Purification Via a Reporter Allele Generated by CRISPR-Cas9 Genome Editing. Stem cells (Dayton, Ohio). 2018;0(0).
249. Nakagawa T, Lee SY, Reddi AH. Induction of chondrogenesis from human embryonic stem cells without embryoid body formation by bone morphogenetic protein 7 and transforming growth factor beta1. Arthritis & Rheumatism. 2009;60(12):3686-92.
250. Lee PT, Li W-J. Chondrogenesis of Embryonic Stem Cell-derived Mesenchymal Stem Cells Induced by TGFβ1 and BMP7 Through Increased TGFβ Receptor Expression and Endogenous TGFβ1 Production. Journal of cellular biochemistry. 2017;118(1):172-81.
251. Lee JY, Matthias N, Pothiawala A, Ang BK, Lee M, Li J, et al. Pre-transplantational Control of the Post-transplantational Fate of Human Pluripotent Stem Cell-Derived Cartilage. Stem Cell Reports. 2018;11(2):440-53.
252. Umeda K, Oda H, Yan Q, Matthias N, Zhao J, Davis BR, et al. Long-term expandable SOX9+ chondrogenic ectomesenchymal cells from human pluripotent stem cells. Stem cell reports. 2015;4(4):712-26.
253. Ferguson GB, Van Handel B, Bay M, Fiziev P, Org T, Lee S, et al. Mapping molecular landmarks of human skeletal ontogeny and pluripotent stem cell-derived articular chondrocytes. Nature Communications. 2018;9(1):3634.
254. Zhao J, Li S, Trilok S, Tanaka M, Jokubaitis-Jameson V, Wang B, et al. Small molecule-directed specification of sclerotome-like chondroprogenitors and induction of a somitic chondrogenesis program from embryonic stem cells. Development. 2014;141(20):3848-58.
255. Bigdeli N, Karlsson C, Strehl R, Concaro S, Hyllner J, Lindahl A. Coculture of human embryonic stem cells and human articular chondrocytes results in significantly altered phenotype and improved chondrogenic differentiation. Stem cells (Dayton, Ohio). 2009;27.
256. Karlsson C, Emanuelsson K, Wessberg F, Kajic K, Axell MZ, Eriksson PS, et al. Human embryonic stem cell-derived mesenchymal progenitors--potential in regenerative medicine. Stem Cell Research. 2009;3(1):39-50.
257. Koay EJ, Athanasiou KA. Development of serum-free, chemically defined conditions for human embryonic stem cell-derived fibrochondrogenesis. Tissue engineering Part A. 2009;15(8):2249-57.

258. Jukes JM, Both SK, Leusink A, Sterk LM, van Blitterswijk CA, de Boer J. Endochondral bone tissue engineering using embryonic stem cells. Proceedings of the National Academy of Sciences of the United States of America. 2008;105(19):6840-5.
259. Koyama N, Miura M, Nakao K. Human induced pluripotent stem cells differentiated into chondrogenic lineage via generation of mesenchymal progenitor cells. Stem Cells Dev. 2013;22.
260. Ko JY, Kim KI, Park S, Im GI. In vitro chondrogenesis and in vivo repair of osteochondral defect with human induced pluripotent stem cells. Biomaterials. 2014;35(11):3571-81.
261. Nejadnik H, Diecke S, Lenkov OD, Chapelin F, Donig J, Tong X, et al. Improved Approach for Chondrogenic Differentiation of Human Induced Pluripotent Stem Cells. Stem Cell Rev and Rep. 2015;11(2):242-53.
262. Mahboudi H, Soleimani M, Enderami SE, Kehtari M, Ardeshirylajimi A, Eftekhary M, et al. Enhanced chondrogenesis differentiation of human induced pluripotent stem cells by MicroRNA-140 and transforming growth factor beta 3 (TGFβ3). Biologicals. 2018;52:30-6.
263. Matsumoto Y, Hayashi Y, Schlieve CR, Ikeya M, Kim H, Nguyen TD, et al. Induced pluripotent stem cells from patients with human fibrodysplasia ossificans progressiva show increased mineralization and cartilage formation. Orphanet Journal Of Rare Diseases. 2013;8:190.
264. Yamashita A, Morioka M, Kishi H, Kimura T, Yahara Y, Okada M, et al. Statin treatment rescues FGFR3 skeletal dysplasia phenotypes. Nature. 2014;513:507.
265. Matsumoto Y, Ikeya M, Hino K, Horigome K, Fukuta M, Watanabe M, et al. New Protocol to Optimize iPS Cells for Genome Analysis of Fibrodysplasia Ossificans Progressiva. Stem cells (Dayton, Ohio). 2015;33(6):1730-42.
266. Okada M, Ikegawa S, Morioka M, Yamashita A, Saito A, Sawai H, et al. Modeling type II collagenopathy skeletal dysplasia by directed conversion and induced pluripotent stem cells. Human Molecular Genetics. 2015;24(2):299-313.
267. Xu M, Stattin E-L, Shaw G, Heinegård D, Sullivan G, Wilmut I, et al. Chondrocytes Derived From Mesenchymal Stromal Cells and Induced Pluripotent Cells of Patients With Familial Osteochondritis Dissecans Exhibit an Endoplasmic Reticulum Stress Response and Defective Matrix Assembly. STEM CELLS Translational Medicine. 2016;5(9):1171-81.
268. Esseltine JL, Shao Q, Brooks C, Sampson J, Betts DH, Seguin CA, et al. Connexin43 Mutant Patient-Derived Induced Pluripotent Stem Cells Exhibit Altered Differentiation Potential. Journal of bone and mineral research : the official journal of the American Society for Bone and Mineral Research. 2017;32(6):1368-85.
269. Nakajima T, Shibata M, Nishio M, Nagata S, Alev C, Sakurai H, et al. Modeling human somite development and fibrodysplasia ossificans progressiva with induced pluripotent stem cells. Development. 2018;145(16).
270. Pini J, Giuliano S, Matonti J, Gannoun L, Simkin D, Rouleau M, et al. Osteogenic and Chondrogenic Master Genes Expression Is Dependent on the Kir2.1 Potassium Channel Through the Bone Morphogenetic Protein Pathway. Journal of Bone and Mineral Research. 2018;0(0).
271. Musunuru K, Sheikh F, Gupta RM, Houser SR, Maher KO, Milan DJ, et al. Induced Pluripotent Stem Cells for Cardiovascular Disease Modeling and Precision Medicine: A Scientific Statement From the American Heart Association. Circ Genom Precis Med. 2018;11(1):e000043.
272. Mojica FJM, Juez G, Rodriguez-Valera F. Transcription at different salinities of Haloferax mediterranei sequences adjacent to partially modified PstI sites. Molecular Microbiology. 1993;9(3):613-21.
273. Lander Eric S. The Heroes of CRISPR. Cell. 2016;164(1):18-28.
274. Ran FA, Hsu PD, Wright J, Agarwala V, Scott DA, Zhang F. Genome engineering using the CRISPR-Cas9 system. Nat Protocols. 2013;8(11):2281-308.
275. Bassett AR. Editing the genome of hiPSC with CRISPR/Cas9: disease models. Mammalian Genome. 2017;28(7):348-64.
276. Nishimasu H, Ran FA, Hsu PD, Konermann S, Shehata SI, Dohmae N, et al. Crystal structure of Cas9 in complex with guide RNA and target DNA. Cell. 2014;156(5):935-49.

277. Anders C, Niewoehner O, Duerst A, Jinek M. Structural basis of PAM-dependent target DNA recognition by the Cas9 endonuclease. Nature. 2014;513:569.
278. Jinek M, Jiang F, Taylor DW, Sternberg SH, Kaya E, Ma E, et al. Structures of Cas9 Endonucleases Reveal RNA-Mediated Conformational Activation. Science. 2014;343(6176).
279. Lander N, Chiurillo MA, Docampo R. Genome Editing by CRISPR/Cas9: A Game Change in the Genetic Manipulation of Protists. The Journal of eukaryotic microbiology. 2016.
280. Brogna S, Wen J. Nonsense-mediated mRNA decay (NMD) mechanisms. Nature Structural & Molecular Biology. 2009;16(2):107-13.
281. Sharpe JJ, Cooper TA. Unexpected consequences: exon skipping caused by CRISPR-generated mutations. Genome Biology. 2017;18(1):109.
282. Tuladhar R, Yeu Y, Tyler Piazza J, Tan Z, Rene Clemenceau J, Wu X, et al. CRISPR-Cas9-based mutagenesis frequently provokes on-target mRNA misregulation. Nature Communications. 2019;10(1):4056.
283. Tang X-D, Gao F, Liu M-J, Fan Q-L, Chen D-K, Ma W-T. Methods for Enhancing Clustered Regularly Interspaced Short Palindromic Repeats/Cas9-Mediated Homology-Directed Repair Efficiency. Frontiers in Genetics. 2019;10(551).
284. Costa M, Sourris K, Hatzistavrou T, Elefanty AG, Stanley EG. Expansion of Human Embryonic Stem Cells In Vitro. Current Protocols in Stem Cell Biology. 2008;5(1):1C..-C..7.
285. Kao T, Labonne T, Niclis Jonathan C, Chaurasia R, Lokmic Z, Qian E, et al. GAPTrap: A Simple Expression System for Pluripotent Stem Cells and Their Derivatives. Stem Cell Reports. 2016;7(3):518-26.
286. Gropp M, Shilo V, Vainer G, Gov M, Gil Y, Khaner H, et al. Standardization of the teratoma assay for analysis of pluripotency of human ES cells and biosafety of their differentiated progeny. PLoS One. 2012;7(9):e45532.
287. Soneson C, Love MI, Robinson MD. Differential analyses for RNA-seq: transcript-level estimates improve gene-level inferences. F1000Res. 2015;4:1521.
288. Robinson MD, Oshlack A. A scaling normalization method for differential expression analysis of RNA-seq data. Genome Biology. 2010;11(3):R25.
289. Law CW, Chen Y, Shi W, Smyth GK. voom: precision weights unlock linear model analysis tools for RNA-seq read counts. Genome Biology. 2014;15(2):R29.
290. Ritchie ME, Phipson B, Wu D, Hu Y, Law CW, Shi W, et al. limma powers differential expression analyses for RNA-sequencing and microarray studies. Nucleic Acids Res. 2015;43(7):e47.
291. Shannon P, Markiel A, Ozier O, Baliga NS, Wang JT, Ramage D, et al. Cytoscape: a software environment for integrated models of biomolecular interaction networks. Genome research. 2003;13(11):2498-504.
292. Maere S, Heymans K, Kuiper M. BiNGO: a Cytoscape plugin to assess overrepresentation of gene ontology categories in biological networks. Bioinformatics. 2005;21(16):3448-9.
293. Bindea G, Mlecnik B, Hackl H, Charoentong P, Tosolini M, Kirilovsky A, et al. ClueGO: a Cytoscape plug-in to decipher functionally grouped gene ontology and pathway annotation networks. Bioinformatics (Oxford, England). 2009;25(8):1091-3.
294. Ng ES, Davis R, Stanley EG, Elefanty AG. A protocol describing the use of a recombinant protein-based, animal product-free medium (APEL) for human embryonic stem cell differentiation as spin embryoid bodies. Nat Protoc. 2008;3(5):768-76.
295. Cameron TL, Bell KM, Tatarczuch L, Mackie EJ, Rajpar MH, McDermott BT, et al. Transcriptional Profiling of Chondrodysplasia Growth Plate Cartilage Reveals Adaptive ER-Stress Networks That Allow Survival but Disrupt Hypertrophy. PLOS ONE. 2011;6(9):e24600.
296. Schmitz N, Laverty S, Kraus VB, Aigner T. Basic methods in histopathology of joint tissues. Osteoarthritis and Cartilage. 2010;18:S113-S6.
297. Liu L, Chong S-W, Balasubramaniyan NV, Korzh V, Ge R. Platelet-derived growth factor receptor alpha (pdgfr-α) gene in zebrafish embryonic development. Mechanisms of Development. 2002;116(1):227-30.
298. Symon A, Harley V. SOX9: A genomic view of tissue specific expression and action. The International Journal of Biochemistry & Cell Biology. 2017;87:18-22.

299. Murphy MK, Huey DJ, Hu JC, Athanasiou KA. TGF-beta1, GDF-5, and BMP-2 stimulation induces chondrogenesis in expanded human articular chondrocytes and marrow-derived stromal cells. Stem cells (Dayton, Ohio). 2015;33(3):762-73.
300. Waese EY, Stanford WL. One-step generation of murine embryonic stem cell-derived mesoderm progenitors and chondrocytes in a serum-free monolayer differentiation system. Stem Cell Research. 2011;6(1):34-49.
301. Vunjak-Novakovic G, Martin I, Obradovic B, Treppo S, Grodzinsky AJ, Langer R, et al. Bioreactor cultivation conditions modulate the composition and mechanical properties of tissue-engineered cartilage. Journal of Orthopaedic Research. 1999;17(1):130-8.
302. Pazzano D, Mercier KA, Moran JM, Fong SS, DiBiasio DD, Rulfs JX, et al. Comparison of Chondrogensis in Static and Perfused Bioreactor Culture. Biotechnology Progress. 2000;16(5):893-6.
303. Gonçalves A, Costa P, Rodrigues MT, Dias IR, Reis RL, Gomes ME. Effect of flow perfusion conditions in the chondrogenic differentiation of bone marrow stromal cells cultured onto starch based biodegradable scaffolds. Acta Biomaterialia. 2011;7(4):1644-52.
304. Yamane S, Cheng E, You Z, Reddi AH. Gene Expression Profiling of Mouse Articular and Growth Plate Cartilage. Tissue Engineering. 2007;13(9):2163-73.
305. Chau M, Lui JC, Landman EBM, Späth S-S, Vortkamp A, Baron J, et al. Gene Expression Profiling Reveals Similarities between the Spatial Architectures of Postnatal Articular and Growth Plate Cartilage. PLOS ONE. 2014;9(7):e103061.
306. Bernardo BC, Belluoccio D, Rowley L, Little CB, Hansen U, Bateman JF. Cartilage Intermediate Layer Protein 2 (CILP-2) Is Expressed in Articular and Meniscal Cartilage and Down-regulated in Experimental Osteoarthritis. Journal of Biological Chemistry. 2011;286(43):37758-67.
307. Grogan SP, Duffy SF, Pauli C, Koziol JA, Su AI, D'Lima DD, et al. Zone-specific gene expression patterns in articular cartilage. Arthritis and rheumatism. 2013;65(2):418-28.
308. Belluoccio D, Etich J, Rosenbaum S, Frie C, Grskovic I, Stermann J, et al. Sorting of growth plate chondrocytes allows the isolation and characterization of cells of a defined differentiation status. Journal of bone and mineral research : the official journal of the American Society for Bone and Mineral Research. 2010;25(6):1267-81.
309. Dy P, Wang W, Bhattaram P, Wang Q, Wang L, Ballock RT, et al. Sox9 directs hypertrophic maturation and blocks osteoblast differentiation of growth plate chondrocytes. Dev Cell. 2012;22(3):597-609.
310. Kaneko N, Herranz-Pérez V, Otsuka T, Sano H, Ohno N, Omata T, et al. New neurons use Slit-Robo signaling to migrate through the glial meshwork and approach a lesion for functional regeneration. Science Advances. 2018;4(12):eaav0618.
311. Carr L, Parkinson DB, Dun X-p. Expression patterns of Slit and Robo family members in adult mouse spinal cord and peripheral nervous system. PLOS ONE. 2017;12(2):e0172736.
312. Whitford KL, Marillat V, Stein E, Goodman CS, Tessier-Lavigne M, Chédotal A, et al. Regulation of Cortical Dendrite Development by Slit-Robo Interactions. Neuron. 2002;33(1):47-61.
313. Caron MMJ, Emans PJ, Coolsen MME, Voss L, Surtel DAM, Cremers A, et al. Redifferentiation of dedifferentiated human articular chondrocytes: comparison of 2D and 3D cultures. Osteoarthritis and Cartilage. 2012;20(10):1170-8.
314. Albro MB, Cigan AD, Nims RJ, Yeroushalmi KJ, Oungoulian SR, Hung CT, et al. Shearing of synovial fluid activates latent TGF-beta. Osteoarthritis Cartilage. 2012;20(11):1374-82.
315. Lim J, Tu X, Choi K, Akiyama H, Mishina Y, Long F. BMP-Smad4 signaling is required for precartilaginous mesenchymal condensation independent of Sox9 in the mouse. Developmental Biology. 2015;400(1):132-8.
316. Shum L, Wang X, Kane AA, Nuckolls GH. BMP4 promotes chondrocyte proliferation and hypertrophy in the endochondral cranial base. International Journal of Developmental Biology. 2003;47(6):423-31.
317. Hatakeyama Y, Tuan RS, Shum L. Distinct functions of BMP4 and GDF5 in the regulation of chondrogenesis. Journal of Cellular Biochemistry. 2004;91(6):1204-17.

318. Suchorska WM, Augustyniak E, Richter M, Trzeciak T. Comparison of Four Protocols to Generate Chondrocyte-Like Cells from Human Induced Pluripotent Stem Cells (hiPSCs). Stem Cell Reviews. 2016;16:16.
319. Wu M, Chen G, Li Y-P. TGF-β and BMP signaling in osteoblast, skeletal development, and bone formation, homeostasis and disease. Bone research. 2016;4:16009-.
320. Miyanishi K, Trindade MC, Lindsey DP, Beaupre GS, Carter DR, Goodman SB, et al. Effects of hydrostatic pressure and transforming growth factor-beta 3 on adult human mesenchymal stem cell chondrogenesis in vitro. Tissue Engineering. 2006;12(6):1419-28.
321. Cicione C, Muinos-Lopez E, Hermida-Gomez T, Fuentes-Boquete I, Diaz-Prado S, Blanco FJ. Alternative protocols to induce chondrogenic differentiation: transforming growth factor-beta superfamily. Cell and Tissue Banking. 2015;16(2):195-207.
322. Yang X, Chen L, Xu X, Li C, Huang C, Deng CX. TGF-beta/Smad3 signals repress chondrocyte hypertrophic differentiation and are required for maintaining articular cartilage. J Cell Biol. 2001;153(1):35-46.
323. Ray A, Singh PNP, Sohaskey ML, Harland RM, Bandyopadhyay A. Precise spatial restriction of BMP signaling is essential for articular cartilage differentiation. Development. 2015;142(6):1169-79.
324. Tsang KY, Chan D, Bateman JF, Cheah KSE. In vivo cellular adaptation to ER stress: survival strategies with double-edged consequences. Journal of Cell Science. 2010;123(13):2145.
325. Jo A, Denduluri S, Zhang B, Wang Z, Yin L, Yan Z, et al. The versatile functions of Sox9 in development, stem cells, and human diseases. Genes & Diseases. 2014;1(2):149-61.
326. Yoshida Y, Yamanaka S. Induced Pluripotent Stem Cells 10 Years Later: For Cardiac Applications. Circ Res. 2017;120(12):1958-68.
327. Liang X, Potter J, Kumar S, Ravinder N, Chesnut JD. Enhanced CRISPR/Cas9-mediated precise genome editing by improved design and delivery of gRNA, Cas9 nuclease, and donor DNA. Journal of Biotechnology. 2017;241:136-46.
328. Richardson CD, Ray GJ, DeWitt MA, Curie GL, Corn JE. Enhancing homology-directed genome editing by catalytically active and inactive CRISPR-Cas9 using asymmetric donor DNA. Nat Biotech. 2016;34(3):339-44.
329. O'Brien AR, Wilson LOW, Burgio G, Bauer DC. Unlocking HDR-mediated nucleotide editing by identifying high-efficiency target sites using machine learning. Scientific reports. 2019;9(1):2788-.
330. Waters JC. Accuracy and precision in quantitative fluorescence microscopy. The Journal of Cell Biology. 2009;185(7):1135.
331. Peck SH, McKee KK, Tobias JW, Malhotra NR, Harfe BD, Smith LJ. Whole Transcriptome Analysis of Notochord-Derived Cells during Embryonic Formation of the Nucleus Pulposus. Scientific Reports. 2017;7(1):10504.
332. Tavella S, Biticchi R, Schito A, Minina E, Di Martino D, Pagano A, et al. Targeted Expression of SHH Affects Chondrocyte Differentiation, Growth Plate Organization, and Sox9 Expression. Journal of Bone and Mineral Research. 2004;19(10):1678-88.
333. Walzer SM, Cetin E, Grübl-Barabas R, Sulzbacher I, Rueger B, Girsch W, et al. Vascularization of primary and secondary ossification centres in the human growth plate. BMC Developmental Biology. 2014;14(1):36.
334. Chamoux E, Houde N, L'Eriger K, Roux S. Osteoprotegerin decreases human osteoclast apoptosis by inhibiting the TRAIL pathway. Journal of Cellular Physiology. 2008;216(2):536-42.
335. Plotnikov A, Zehorai E, Procaccia S, Seger R. The MAPK cascades: Signaling components, nuclear roles and mechanisms of nuclear translocation. Biochimica et Biophysica Acta (BBA) - Molecular Cell Research. 2011;1813(9):1619-33.
336. Ataman B, Boulting GL, Harmin DA, Yang MG, Baker-Salisbury M, Yap E-L, et al. Evolution of Osteocrin as an activity-regulated factor in the primate brain. Nature. 2016;539:242.
337. Das S, Cho J, Lambertz I, Kelliher MA, Eliopoulos AG, Du K, et al. Tpl2/Cot Signals Activate ERK, JNK, and NF-κB in a Cell-type and Stimulus-specific Manner. Journal of Biological Chemistry. 2005;280(25):23748-57.

338. Jurikova M, Danihel L, Polak S, Varga I. Ki67, PCNA, and MCM proteins: Markers of proliferation in the diagnosis of breast cancer. Acta histochemica. 2016;118(5):544-52.
339. Adams CS, Shapiro IM. The fate of the terminally differentiated chondrocyte: evidence for microenvironmental regulation of chondrocyte apoptosis. Critical reviews in oral biology and medicine : an official publication of the American Association of Oral Biologists. 2002;13(6):465-73.
340. Shapiro IM, Adams CS, Freeman T, Srinivas V. Fate of the hypertrophic chondrocyte: Microenvironmental perspectives on apoptosis and survival in the epiphyseal growth plate. Birth Defects Research Part C: Embryo Today: Reviews. 2005;75(4):330-9.
341. Boersma HH, Kietselaer BL, Stolk LM, Bennaghmouch A, Hofstra L, Narula J, et al. Past, present, and future of annexin A5: from protein discovery to clinical applications. Journal of nuclear medicine : official publication, Society of Nuclear Medicine. 2005;46(12):2035-50.
342. Hammad G, Legrain Y, Touat-Hamici Z, Duhieu S, Cornu D, Bulteau A-L, et al. Interplay between Selenium Levels and Replicative Senescence in WI-38 Human Fibroblasts: A Proteomic Approach. Antioxidants. 2018;7(1).
343. Zhan L, Li J. The role of TRPV4 in fibrosis. Gene. 2018;642:1-8.
344. Gombedza F, Kondeti V, Al-Azzam N, Koppes S, Duah E, Patil P, et al. Mechanosensitive transient receptor potential vanilloid 4 regulates Dermatophagoides farinae–induced airway remodeling via 2 distinct pathways modulating matrix synthesis and degradation. The FASEB Journal. 2017;31(4):1556-70.
345. Ylarinne JH, Qu C, Lammi MJ. Hypertonic conditions enhance cartilage formation in scaffold-free primary chondrocyte cultures. Cell and Tissue Research. 2014;358(2):541-50.
346. Lee JK, Gegg CA, Hu JC, Kass PH, Athanasiou KA. Promoting increased mechanical properties of tissue engineered neocartilage via the application of hyperosmolarity and 4α-phorbol 12,13-didecanoate (4αPDD). Journal of Biomechanics. 2014;47(15):3712-8.
347. Eleswarapu SV, Athanasiou KA. TRPV4 channel activation improves the tensile properties of self-assembled articular cartilage constructs. Acta Biomaterialia. 2013;9(3):5554-61.
348. Bouldin CM, Gritli-Linde A, Ahn S, Harfe BD. Shh pathway activation is present and required within the vertebrate limb bud apical ectodermal ridge for normal autopod patterning. Proceedings of the National Academy of Sciences of the United States of America. 2010;107(12):5489-94.
349. Guimond J-C, Lévesque M, Michaud P-L, Berdugo J, Finnson K, Philip A, et al. BMP-2 functions independently of SHH signaling and triggers cell condensation and apoptosis in regenerating axolotl limbs. BMC Developmental Biology. 2010;10(1):15.
350. Tickle C, Towers M. Sonic Hedgehog Signaling in Limb Development. Frontiers in cell and developmental biology. 2017;5:14-.
351. Lee RTH, Zhao Z, Ingham PW. Hedgehog signalling. Development. 2016;143(3):367.
352. Lai CK, Gupta N, Wen X, Rangell L, Chih B, Peterson AS, et al. Functional characterization of putative cilia genes by high-content analysis. Molecular biology of the cell. 2011;22(7):1104-19.
353. Allot A, Kress A, Thompson JD, Chennen K, Poidevin L, Poch O, et al. Insights into Ciliary Genes and Evolution from Multi-Level Phylogenetic Profiling. Molecular Biology and Evolution. 2017;34(8):2016-34.
354. Shi W, Ma Z, Zhang G, Wang C, Jiao Z. Novel functions of the primary cilium in bone disease and cancer. Cytoskeleton. 2019;76(3):233-42.
355. Lee K, Guevarra M, Nguyen A, Chua M, Wang Y, Jacobs C. The primary cilium functions as a mechanical and calcium signaling nexus. Cilia. 2015;4(1):1-13.
356. Corrigan MA, Johnson GP, Stavenschi E, Riffault M, Labour M-N, Hoey DA. TRPV4-mediates oscillatory fluid shear mechanotransduction in mesenchymal stem cells in part via the primary cilium. Scientific Reports. 2018;8(1):3824.
357. Belgacem YH, Borodinsky LN. Sonic hedgehog signaling is decoded by calcium spike activity in the developing spinal cord. Proceedings of the National Academy of Sciences. 2011;108(11):4482.

358. Li A, Cho J-H, Reid B, Tseng C-C, He L, Tan P, et al. Calcium oscillations coordinate feather mesenchymal cell movement by SHH dependent modulation of gap junction networks. Nature Communications. 2018;9(1):5377.
359. Nishimura R, Hata K, Nakamura E, Murakami T, Takahata Y. Transcriptional network systems in cartilage development and disease. Histochemistry and Cell Biology. 2018;149(4):353-63.
360. Zuscik MJ, D'Souza M, Gunter KK, Gunter TE, O'Keefe RJ, Schwarz EM, et al. Growth Plate Chondrocyte Maturation Is Regulated by Basal Intracellular Calcium. Experimental Cell Research. 2002;276(2):310-9.
361. Gunter TE, Zuscik MJ, Puzas JE, Gunter KK, Rosier RN. Cytosolic free calcium concentrations in avian growth plate chondrocytes. Cell Calcium. 1990;11(7):445-57.
362. Maeda Y, Nakamura E, Nguyen M-T, Suva LJ, Swain FL, Razzaque MS, et al. Indian Hedgehog produced by postnatal chondrocytes is essential for maintaining a growth plate and trabecular bone. Proceedings of the National Academy of Sciences. 2007;104(15):6382.
363. Domowicz MS, Cortes M, Henry JG, Schwartz NB. Aggrecan modulation of growth plate morphogenesis. Developmental Biology. 2009;329(2):242-57.
364. Stanton L-A, Underhill TM, Beier F. MAP kinases in chondrocyte differentiation. Developmental Biology. 2003;263(2):165-75.
365. Stanton L-A, Sabari S, Sampaio AV, Underhill TM, Beier F. p38 MAP kinase signalling is required for hypertrophic chondrocyte differentiation. The Biochemical journal. 2004;378(Pt 1):53-62.
366. Sun Y, Liu W-Z, Liu T, Feng X, Yang N, Zhou H-F. Signaling pathway of MAPK/ERK in cell proliferation, differentiation, migration, senescence and apoptosis. Journal of Receptors and Signal Transduction. 2015;35(6):600-4.
367. Sammels E, Parys JB, Missiaen L, De Smedt H, Bultynck G. Intracellular Ca2+ storage in health and disease: a dynamic equilibrium. Cell Calcium. 2010;47(4):297-314.
368. White CD, Sacks DB. Regulation of MAP Kinase Signaling by Calcium. In: Seger R, editor. MAP Kinase Signaling Protocols: Second Edition. Totowa, NJ: Humana Press; 2010. p. 151-65.
369. Morrison DK. MAP kinase pathways. Cold Spring Harbor perspectives in biology. 2012;4(11):a011254.
370. Gomes CC, Gayden T, Bajic A, Harraz OF, Pratt J, Nikbakht H, et al. TRPV4 and KRAS and FGFR1 gain-of-function mutations drive giant cell lesions of the jaw. Nature Communications. 2018;9(1):4572.
371. Vrenken KS, Jalink K, van Leeuwen FN, Middelbeek J. Beyond ion-conduction: Channel-dependent and -independent roles of TRP channels during development and tissue homeostasis. Biochimica et Biophysica Acta (BBA) - Molecular Cell Research. 2015.
372. Hdud IM, Mobasheri A, Loughna PT. Effect of osmotic stress on the expression of TRPV4 and BKCa channels and possible interaction with ERK1/2 and p38 in cultured equine chondrocytes. American Journal of Physiology-Cell Physiology. 2014;306(11):C1050-C7.
373. Thouverey C, Caverzasio J. Focus on the p38 MAPK signaling pathway in bone development and maintenance. Bonekey Rep [Internet]. 2015 2015; 4:[711 p.]. Available from: http://europepmc.org/abstract/MED/26131361.
374. Potthoff MJ, Olson EN. MEF2: a central regulator of diverse developmental programs. Development. 2007;134(23):4131.
375. Arnold MA, Kim Y, Czubryt MP, Phan D, McAnally J, Qi X, et al. MEF2C transcription factor controls chondrocyte hypertrophy and bone development. Dev Cell. 2007;12(3):377-89.
376. Kawane T, Komori H, Liu W, Moriishi T, Miyazaki T, Mori M, et al. Dlx5 and mef2 regulate a novel runx2 enhancer for osteoblast-specific expression. Journal of bone and mineral research : the official journal of the American Society for Bone and Mineral Research. 2014;29(9):1960-9.
377. Bai J-Z, Lipski J. Involvement of TRPV4 channels in Aβ40-induced hippocampal cell death and astrocytic Ca2+ signalling. NeuroToxicology. 2014;41:64-72.
378. Shen J, Tu L, Chen D, Tan T, Wang Y, Wang S. TRPV4 channels stimulate Ca2+-induced Ca2+ release in mouse neurons and trigger endoplasmic reticulum stress after intracerebral hemorrhage. Brain Research Bulletin. 2019;146:143-52.

379. Jie P, Hong Z, Tian Y, Li Y, Lin L, Zhou L, et al. Activation of transient receptor potential vanilloid 4 induces apoptosis in hippocampus through downregulating PI3K/Akt and upregulating p38 MAPK signaling pathways. Cell Death &Amp; Disease. 2015;6:e1775.
380. Ryskamp DA, Witkovsky P, Barabas P, Huang W, Koehler C, Akimov NP, et al. The Polymodal Ion Channel Transient Receptor Potential Vanilloid 4 Modulates Calcium Flux, Spiking Rate, and Apoptosis of Mouse Retinal Ganglion Cells. The Journal of Neuroscience. 2011;31(19):7089.
381. Miyamoto S, Teramoto H, Gutkind JS, Yamada KM. Integrins can collaborate with growth factors for phosphorylation of receptor tyrosine kinases and MAP kinase activation: roles of integrin aggregation and occupancy of receptors. The Journal of cell biology. 1996;135(6 Pt 1):1633-42.
382. Moreno-Layseca P, Streuli CH. Signalling pathways linking integrins with cell cycle progression. Matrix Biology. 2014;34:144-53.
383. Johnson KA, Rose DM, Terkeltaub RA. Factor XIIIA mobilizes transglutaminase 2 to induce chondrocyte hypertrophic differentiation. J Cell Sci. 2008;121(Pt 13):2256-64.
384. Tanaka K, Yokosaki Y, Higashikawa F, Saito Y, Eboshida A, Ochi M. The integrin alpha5beta1 regulates chondrocyte hypertrophic differentiation induced by GTP-bound transglutaminase 2. Matrix Biol. 2007;26(6):409-18.
385. Hirsch MS, Lunsford LE, Trinkaus-Randall V, Svoboda KK. Chondrocyte survival and differentiation in situ are integrin mediated. Dev Dyn. 1997;210(3):249-63.
386. Yoon BS, Pogue R, Ovchinnikov DA, Yoshii I, Mishina Y, Behringer RR, et al. BMPs regulate multiple aspects of growth-plate chondrogenesis through opposing actions on FGF pathways. Development. 2006;133(23):4667.
387. Ogawa Y, Takahashi N, Takemoto T, Nishiume T, Suzuki M, Ishiguro N, et al. Hyaluronan promotes TRPV4-induced chondrogenesis in ATDC5 cells. PLoS One. 2019;14(8):e0219492.
388. Aran S, Namju K, Jung Yun K, Ki Woo K, Yu-Mi Y, Dong Min S. TRPM3/TRPV4 regulates Ca2+-mediated RANKL/NFATc1 expression in osteoblasts. Journal of Molecular Endocrinology. 2018;61(4):207-18.
389. Abed E, Labelle D, Martineau C, Loghin A, Moreau R. Expression of transient receptor potential (TRP) channels in human and murine osteoblast-like cells. Mol Membr Biol. 2009;26(3):146-58.
390. Root MV, Johnston SD, Olson PN. The effect of prepuberal and postpuberal gonadectomy on radial physeal closure in male and female domestic cats. Veterinary radiology & ultrasound : the official journal of the American College of Veterinary Radiology and the International Veterinary Radiology Association. 1997;38(1):42-7.
391. Chang J, Jung J, Oh S, Lee S, Kim G, Kim H, et al. Osteochondrodysplasia in three Scottish Fold cats. J Vet Sci. 2007;8(3):307-9.
392. Chaly Y, Blair HC, Smith SM, Bushnell DS, Marinov AD, Campfield BT, et al. Follistatin-like protein 1 regulates chondrocyte proliferation and chondrogenic differentiation of mesenchymal stem cells. Annals of the Rheumatic Diseases. 2015;74(7):1467-73.
393. Goto T, Tanaka T. Tachykinins and tachykinin receptors in bone. Microscopy Research and Technique. 2002;58(2):91-7.
394. Alessandri-Haber N, Dina OA, Joseph EK, Reichling D, Levine JD. A Transient Receptor Potential Vanilloid 4-Dependent Mechanism of Hyperalgesia Is Engaged by Concerted Action of Inflammatory Mediators. The Journal of Neuroscience. 2006;26(14):3864.
395. Vergnolle N, Cenac N, Altier C, Cellars L, Chapman K, Zamponi GW, et al. A role for transient receptor potential vanilloid 4 in tonicity-induced neurogenic inflammation. Br J Pharmacol. 2010;159(5):1161-73.
396. Kieslinger M, Folberth S, Dobreva G, Dorn T, Croci L, Erben R, et al. EBF2 Regulates Osteoblast-Dependent Differentiation of Osteoclasts. Developmental Cell. 2005;9(6):757-67.
397. Mella S, Soula C, Morello D, Crozatier M, Vincent A. Expression patterns of the coe/ebf transcription factor genes during chicken and mouse limb development. Gene Expression Patterns. 2004;4(5):537-42.
398. Shen MJ, Wang GG, Wang YZ, Xie J, Ding X. Nell-1 Enhances Osteogenic Differentiation of Pre-Osteoblasts on Titanium Surfaces via the MAPK-ERK Signaling Pathway. Cellular

physiology and biochemistry : international journal of experimental cellular physiology, biochemistry, and pharmacology. 2018;50(4):1522-34.
399. Kristianto J, Johnson MG, Afzal R, Blank RD. Endothelin Signaling in Bone. Endocrinology and Metabolism Clinics of North America. 2017;46(1):51-62.
400. Johnson MG, Konicke K, Kristianto J, Gustavson A, Garbo R, Wang X, et al. Endothelin signaling regulates mineralization and posttranscriptionally regulates SOST in TMOb cells via miR 126-3p. Physiological Reports. 2017;5(4):e13088.
401. Sin A, Tang W, Wen CY, Chung SK, Chiu KY. The emerging role of endothelin-1 in the pathogenesis of subchondral bone disturbance and osteoarthritis. Osteoarthritis and Cartilage. 2015;23(4):516-24.
402. Musunuru K. Genome editing of human pluripotent stem cells to generate human cellular disease models. Disease Models & Mechanisms. 2013;6(4):896.
403. Lin J, Musunuru K. Genome engineering tools for building cellular models of disease. The FEBS journal. 2016;283(17):3222-31.
404. Decker RS, Koyama E, Pacifici M. Articular Cartilage: Structural and Developmental Intricacies and Questions. Current osteoporosis reports. 2015;13(6):407-14.
405. Li J, Luo H, Wang R, Lang J, Zhu S, Zhang Z, et al. Systematic Reconstruction of Molecular Cascades Regulating GP Development Using Single-Cell RNA-Seq. Cell Reports. 2016;15(7):1467-80.
406. Ji Q, Zheng Y, Zhang G, Hu Y, Fan X, Hou Y, et al. Single-cell RNA-seq analysis reveals the progression of human osteoarthritis. Ann Rheum Dis. 2019;78(1):100-10.
407. Lee WY-w, Wang B. Cartilage repair by mesenchymal stem cells: Clinical trial update and perspectives. Journal of Orthopaedic Translation. 2017;9:76-88.
408. Park Y-B, Ha C-W, Rhim JH, Lee H-J. Stem Cell Therapy for Articular Cartilage Repair: Review of the Entity of Cell Populations Used and the Result of the Clinical Application of Each Entity. The American Journal of Sports Medicine. 2017;46(10):2540-52.
409. Jiang T, Xu G, Wang Q, Yang L, Zheng L, Zhao J, et al. In vitro expansion impaired the stemness of early passage mesenchymal stem cells for treatment of cartilage defects. Cell Death &Amp; Disease. 2017;8:e2851.
410. Sacchetti B, Funari A, Remoli C, Giannicola G, Kogler G, Liedtke S, et al. No Identical “Mesenchymal Stem Cells” at Different Times and Sites: Human Committed Progenitors of Distinct Origin and Differentiation Potential Are Incorporated as Adventitial Cells in Microvessels. Stem Cell Reports. 2016;6(6):897-913.
411. Csobonyeiova M, Polak S, Zamborsky R, Danisovic L. iPS cell technologies and their prospect for bone regeneration and disease modeling: A mini review. Journal of Advanced Research. 2017;8(4):321-7.
412. Augustyniak E, Trzeciak T, Richter M, Kaczmarczyk J, Suchorska W. The role of growth factors in stem cell-directed chondrogenesis: a real hope for damaged cartilage regeneration. International Orthopaedics (SICOT). 2015;39(5):995-1003.
413. Kropp C, Massai D, Zweigerdt R. Progress and challenges in large-scale expansion of human pluripotent stem cells. Process Biochemistry. 2017;59:244-54.
414. Nimeskern L, van Osch GJVM, Müller R, Stok KS. Quantitative Evaluation of Mechanical Properties in Tissue-Engineered Auricular Cartilage. Tissue Engineering Part B: Reviews. 2013;20(1):17-27.
415. Masuda K, Lotz JC. New Challenges for Intervertebral Disc Treatment Using Regenerative Medicine. Tissue Engineering Part B: Reviews. 2009;16(1):147-58.
416. Zhu Y, Wu X, Liang Y, Gu H, Song K, Zou X, et al. Repair of cartilage defects in osteoarthritis rats with induced pluripotent stem cell derived chondrocytes. BMC Biotechnology. 2016;16(1):78.
417. Saito T, Yano F, Mori D, Kawata M, Hoshi K, Takato T, et al. Hyaline cartilage formation and tumorigenesis of implanted tissues derived from human induced pluripotent stem cells. Biomedical Research. 2015;36(3):179-86.
418. Kimura T, Ozaki T, Fujita K, Yamashita A, Morioka M, Ozono K, et al. Proposal of patient-specific growth plate cartilage xenograft model for FGFR3 chondrodysplasia. Osteoarthritis and Cartilage. 2018.

419. Blair HC, Larrouture QC, Li Y, Lin H, Beer-Stoltz D, Liu L, et al. Osteoblast Differentiation and Bone Matrix Formation In Vivo and In Vitro. Tissue Engineering Part B: Reviews. 2016;23(3):268-80.
420. Zelzer E, Mamluk R, Ferrara N, Johnson RS, Schipani E, Olsen BR. VEGFA is necessary for chondrocyte survival during bone development. Development. 2009;131(9):2161-71.
421. Hu K, Olsen BR. The roles of vascular endothelial growth factor in bone repair and regeneration. Bone. 2016;91:30-8.
422. Yang Y-Q, Tan Y-Y, Wong R, Wenden A, Zhang L-K, Rabie ABM. The role of vascular endothelial growth factor in ossification. International Journal of Oral Science. 2012;4(2):64-8.
423. Aghajanian P, Mohan S. The art of building bone: emerging role of chondrocyte-to-osteoblast transdifferentiation in endochondral ossification. Bone Research. 2018;6(1):19.
424. Kelly NH, Huynh NPT, Guilak F. Single cell RNA-sequencing reveals cellular heterogeneity and trajectories of lineage specification during murine embryonic limb development. bioRxiv. 2019:659656.
425. Arora PD, Di Gregorio M, He P, McCulloch CA. TRPV4 mediates the Ca(2+) influx required for the interaction between flightless-1 and non-muscle myosin, and collagen remodeling. J Cell Sci. 2017;130(13):2196-208.

Appendix

Appendix 1

The sequencing of homology-directed repair (HDR) template for generating SOX9-T2A-tdTom hiPSC line

Sequencing primer: Seq1

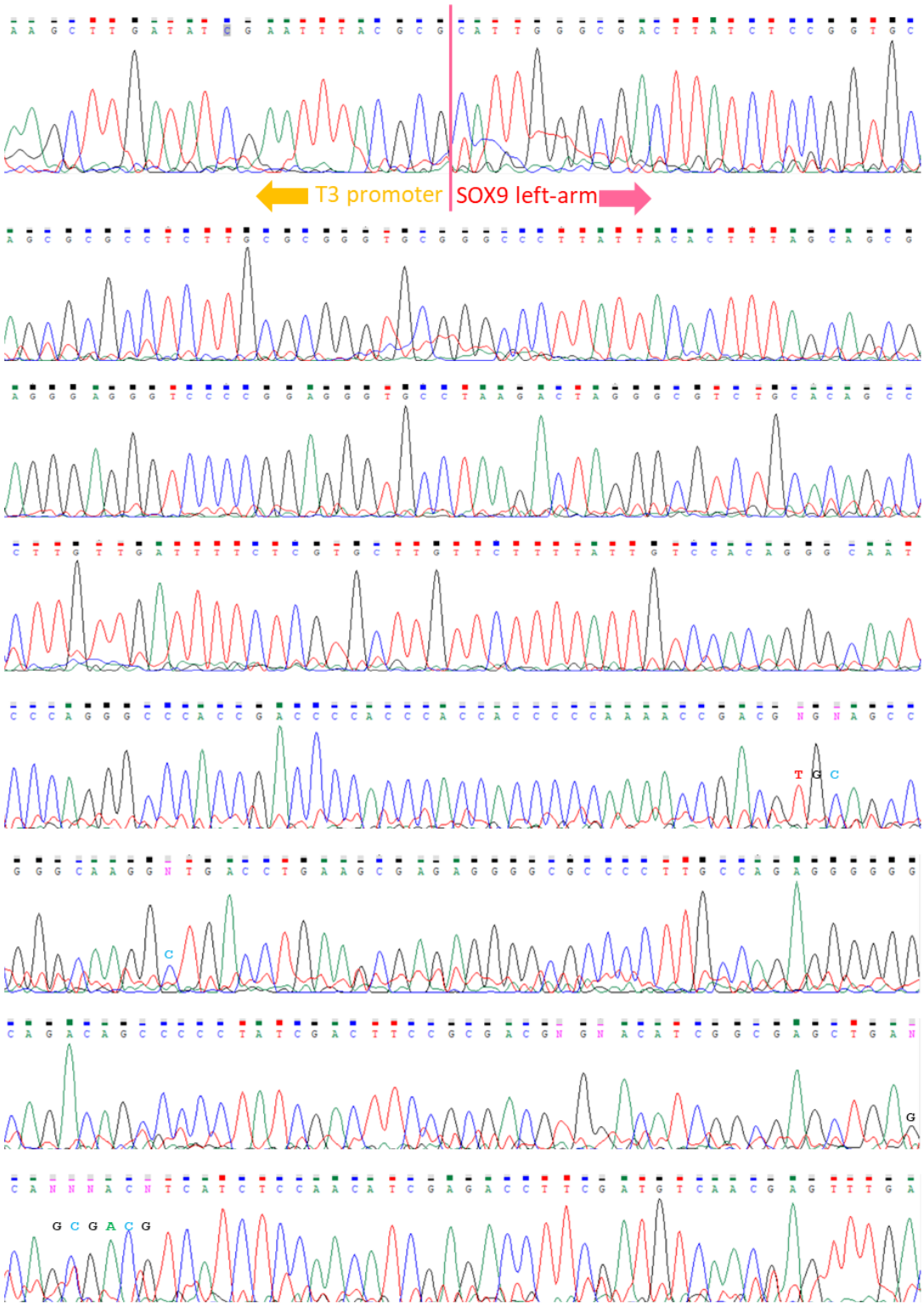

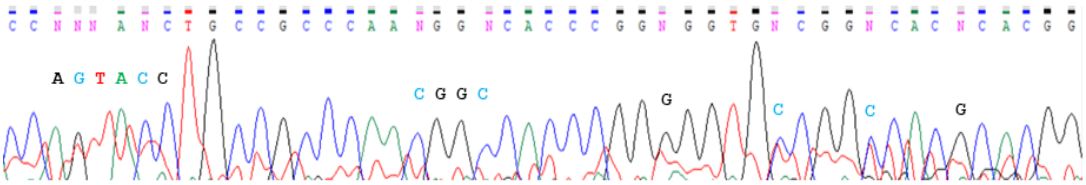

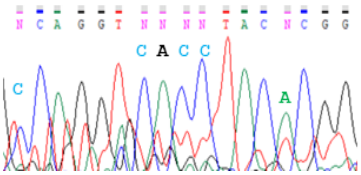

Sequencing primer: Seq2

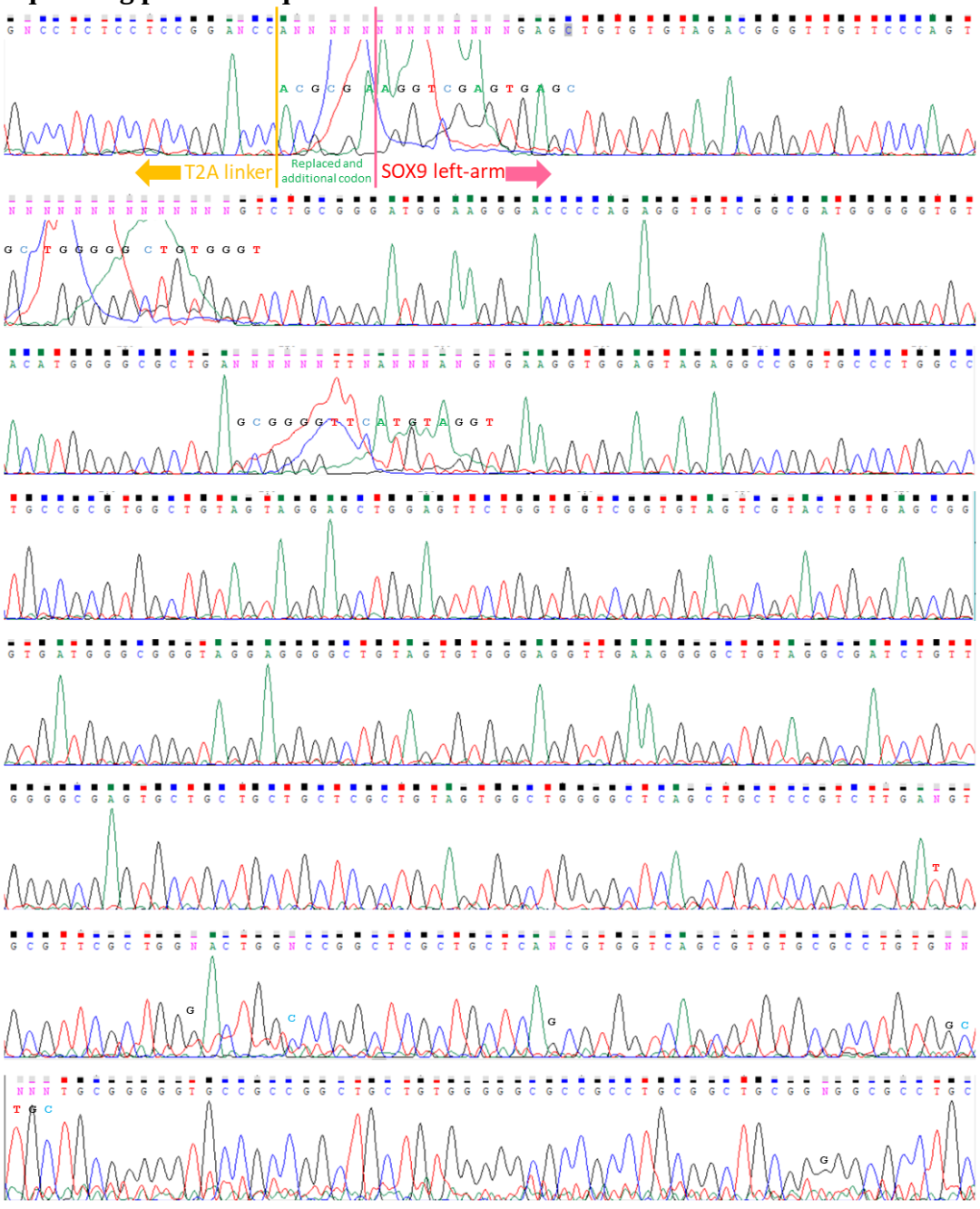

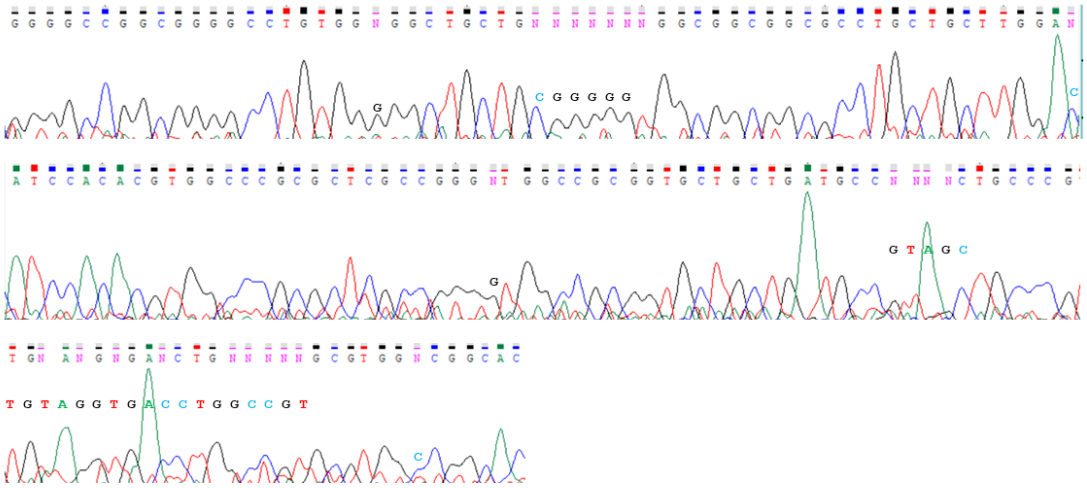

Sequencing primer: Seq3

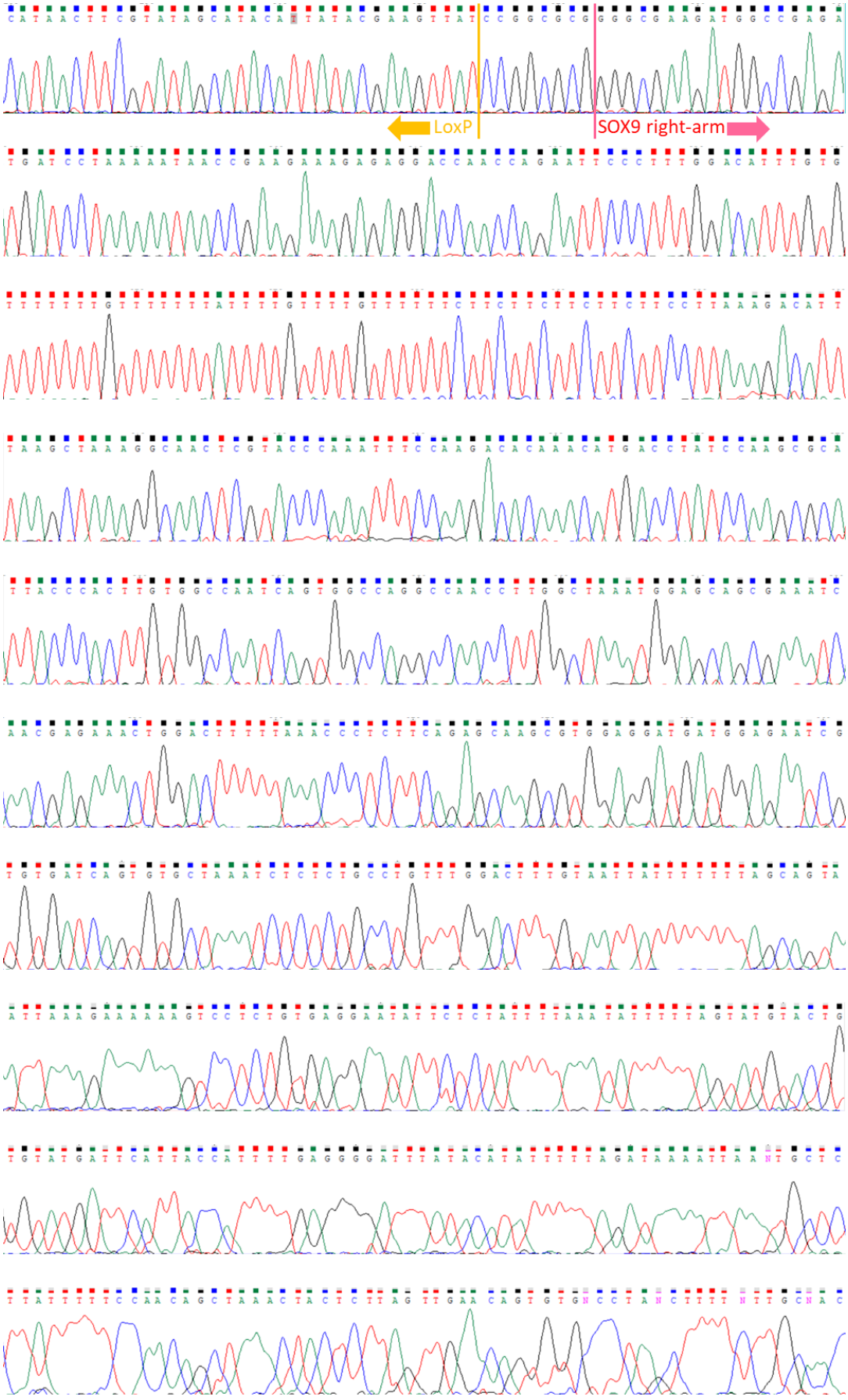

Sequencing primer: Seq4

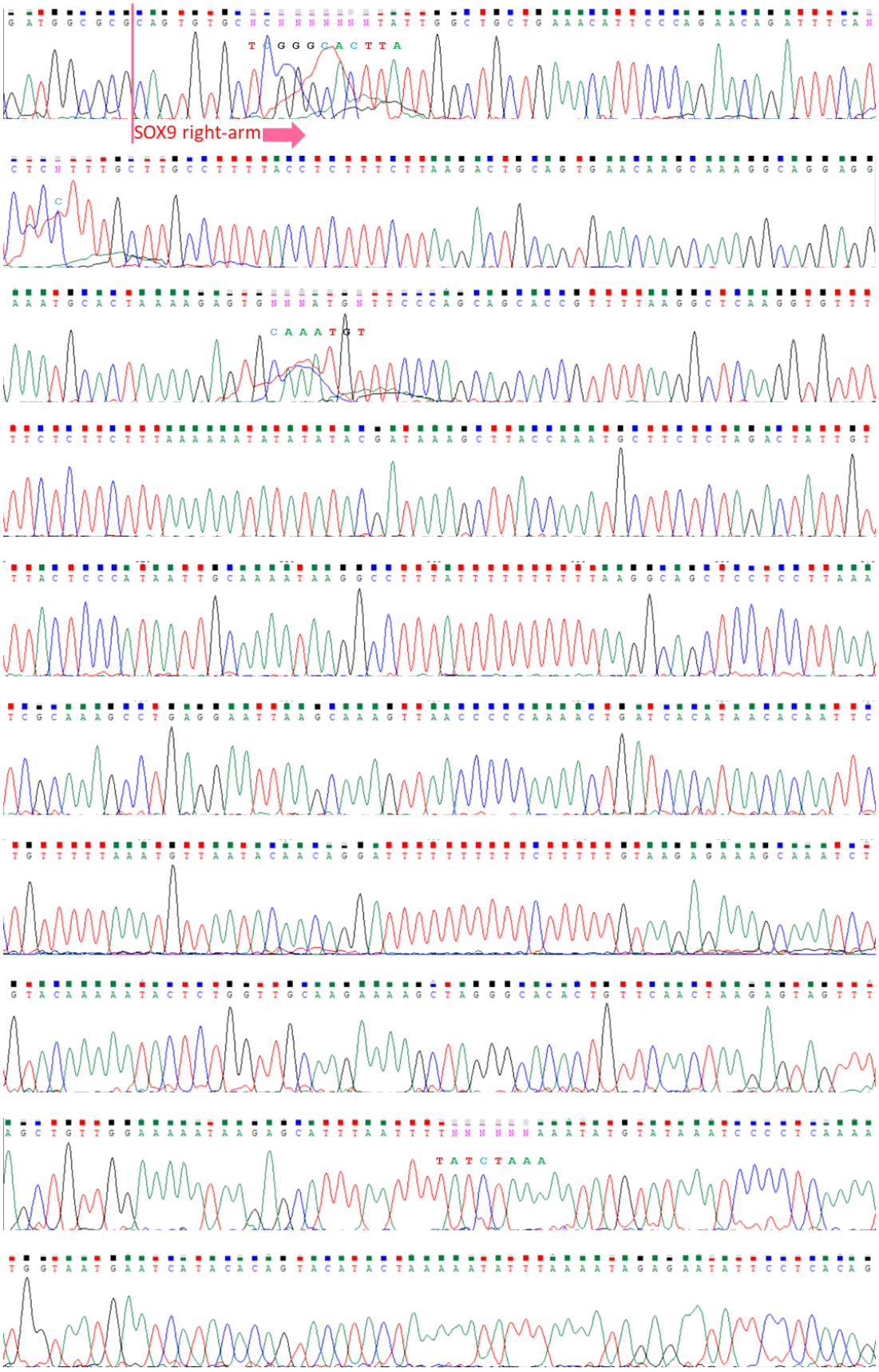

Appendix 2

Mycoplasma test result for SOX9-T2A-tdTom, F273L and P799L hiPSC lines.

SOX9-T2A-tdTom (yellow box)

Cerberus Adelaide
Unit 3 40 Holland Street
Thebarton SA 5031
Telephone: +61 8 8234 8780
Facsimile: +61 8 8234 8712
Email: cerberus@cerberus.net.au

Cerberus Sciences

Cerberus Melbourne
Unit 2 7-11 Rocco Drive
Scoresby VIC 3179
Telephone: +61 3 9763 8290
Facsimile: +61 3 9763 8290
Email: cerberus@cerberus.net.au

Submitter: Murdoch Institute - Dept of Tissue Culture

Submission No: 16/A821

Royal Childrens Hospital, Flemington Road
Parkville, VIC 3052

Your ref:

Date Submitted: 11 October 2016

Contact: Elena Fernandez

Date of issue: 14 October 2016

No.	Species	Sample Type	Sample Ref.	Test	Result
1	All Cell Lines	Cell Line	160142	Mycoplasma spp	Neg
2	All Cell Lines	Cell Line	160154	Mycoplasma spp	Neg
3	All Cell Lines	Cell Line	160155	Mycoplasma spp	Neg
4	All Cell Lines	Cell Line	2016-206	Mycoplasma spp	Neg
5	All Cell Lines	Cell Line	2016-207	Mycoplasma spp	Neg
6	All Cell Lines	Cell Line	2016-208	Mycoplasma spp	Neg
7	All Cell Lines	Cell Line	2016-209	Mycoplasma spp	Neg
8	All Cell Lines	Cell Line	2016-210	Mycoplasma spp	Neg
9	All Cell Lines	Cell Line	2016-211	Mycoplasma spp	Neg
10	All Cell Lines	Cell Line	2016-212	Mycoplasma spp	Neg
11	All Cell Lines	Cell Line	2016-213	Mycoplasma spp	Neg
12	All Cell Lines	Cell Line	2016-214	Mycoplasma spp	Neg
13	All Cell Lines	Cell Line	2016-215	Mycoplasma spp	Neg
14	All Cell Lines	Cell Line	2016-216	Mycoplasma spp	Neg
15	All Cell Lines	Cell Line	2016-217	Mycoplasma spp	Neg
16	All Cell Lines	Cell Line	2016-218	Mycoplasma spp	Neg
17	All Cell Lines	Cell Line	2016-219	Mycoplasma spp	Neg
18	All Cell Lines	Cell Line	2016-220	Mycoplasma spp	Neg
19	All Cell Lines	Cell Line	2016-221	Mycoplasma spp	Neg
20	All Cell Lines	Cell Line	2016-222	Mycoplasma spp	Neg
21	All Cell Lines	Cell Line	2016-223	Mycoplasma spp	Neg
22	All Cell Lines	Cell Line	2016-224	Mycoplasma spp	Neg
23	All Cell Lines	Cell Line	2016-225	Mycoplasma spp	Neg
24	All Cell Lines	Cell Line	2016-226	Mycoplasma spp	Neg
25	All Cell Lines	Cell Line	2016-227	Mycoplasma spp	Neg
26	All Cell Lines	Cell Line	2016-228	Mycoplasma spp	Neg
27	All Cell Lines	Cell Line	2016-229	Mycoplasma spp	Neg
28	All Cell Lines	Cell Line	2016-230	Mycoplasma spp	Neg
29	All Cell Lines	Cell Line	2016-231	Mycoplasma spp	Neg
30	All Cell Lines	Cell Line	2016-232	Mycoplasma spp	Neg
31	All Cell Lines	Cell Line	2016-233	Mycoplasma spp	Neg
32	All Cell Lines	Cell Line	2016-234	Mycoplasma spp	Neg
33	All Cell Lines	Cell Line	2016-235	Mycoplasma spp	Neg

Bob Stevenson
Managing director

F273L (blue box) and P799L (green box)

Cerberus Adelaide
Unit 3 49 Holland Street
Thebarton SA 5031
Telephone: +61 8 8234 8780
Facsimile: +61 8 8234 8712

Cerberus Sciences

Cerberus Melbourne
Unit 2 7-11 Rocco Drive
Scoresby VIC 3179
Telephone: +61 3 9763 8290
Facsimile: +61 3 9763 8290

Submitter: Murdoch Institute - Dept of Tissue Culture

Submission No: 18/A238

Royal Childrens Hospital, Flemington Road
Parkville, VIC 3052

Your ref: Mycoplasma 06/03/18

Date received: 7 March 2018

Contact: Josefina Kempster-Perez

Date of issue: 9 March 2018

No.	Species	Sample Type	Sample Ref.	Test	Result	Cell ID
1	All Cell Lines	Cell Line	01 - 160146 (CR#4)	Mycoplasma spp	Neg	
2	All Cell Lines	Cell Line	02 - 170016 (CR#13)	Mycoplasma spp	Neg	
3	All Cell Lines	Cell Line	03 - 180015	Mycoplasma spp	Neg	
4	All Cell Lines	Cell Line	04 - 180020	Mycoplasma spp	Neg	
5	All Cell Lines	Cell Line	05 - 180021	Mycoplasma spp	Neg	
6	All Cell Lines	Cell Line	06 - 180022	Mycoplasma spp	Neg	
7	All Cell Lines	Cell Line	07 - 180023	Mycoplasma spp	Neg	
8	All Cell Lines	Cell Line	08 - 180024	Mycoplasma spp	Neg	
9	All Cell Lines	Cell Line	09 - RCH-JP (CR#16)	Mycoplasma spp	Neg	
10	All Cell Lines	Cell Line	10 - 2018-43	Mycoplasma spp	Neg	
11	All Cell Lines	Cell Line	11 - 2018-44	Mycoplasma spp	Neg	
12	All Cell Lines	Cell Line	12 - 2018-45	Mycoplasma spp	Neg	
13	All Cell Lines	Cell Line	13 - 2018-46	Mycoplasma spp	Neg	
14	All Cell Lines	Cell Line	14 - 2018-47	Mycoplasma spp	Neg	
15	All Cell Lines	Cell Line	15 - 2018-48	Mycoplasma spp	Neg	
16	All Cell Lines	Cell Line	16 - 2018-49	Mycoplasma spp	Neg	
17	All Cell Lines	Cell Line	17 - 2018-50	Mycoplasma spp	Neg	
18	All Cell Lines	Cell Line	18 - 2018-51	Mycoplasma spp	Neg	
19	**All Cell Lines**	**Cell Line**	**19 - 2018-52**	**Mycoplasma spp**	**Pos**	
20	All Cell Lines	Cell Line	20 - 2018-53	Mycoplasma spp	Neg	F273L #2
21	All Cell Lines	Cell Line	21 - 2018-54	Mycoplasma spp	Neg	F273L #8
22	All Cell Lines	Cell Line	22 - 2018-55	Mycoplasma spp	Neg	F273L #126
23	All Cell Lines	Cell Line	23 - 2018-56	Mycoplasma spp	Neg	F273L #204
24	All Cell Lines	Cell Line	24 - 2018-57	Mycoplasma spp	Neg	F799L #31
25	All Cell Lines	Cell Line	25 - 2018-58	Mycoplasma spp	Neg	F799L #52
26	All Cell Lines	Cell Line	26 - 2018-59	Mycoplasma spp	Neg	F799L #64
27	All Cell Lines	Cell Line	27 - 2018-60	Mycoplasma spp	Neg	F799L #201
28	All Cell Lines	Cell Line	28 - 2018-61	Mycoplasma spp	Neg	F799L #248
29	All Cell Lines	Cell Line	29 - 2018-62	Mycoplasma spp	Neg	F799L #96
30	All Cell Lines	Cell Line	30 - 2018-63	Mycoplasma spp	Neg	F799L #113

Bob Stevenson
Managing Director

Peony Fung
Molecular Diagnostic Manager

Appendix 3

SNP array and SNPduo analysis results of SOX9-T2A-tdTom hiPSC

Victorian Clinical Genetics Services
Murdoch Childrens Research Institute
Flemington Road, Parkville, VIC 3052 Australia
P +61 3 8341 6201 F +61 3 8341 6390
W vcgs.org.au ABN 51 007 032 760

LIMS Report #: 419797

Patient: SOXG-TDTT-CRE NO.13
Soxg-Tdtt-Cre No.13

DOB: Unknown
Sex: Unknown
VCGS sample ID: 16C108606
Date collected: 01-Dec-2016
Date received: 01-Dec-2016
Date reported: 02-Mar-2018
Source: Cell Pellet
Ext. sample ID:
Ext. patient ID:

Mr. David Francis
Victorian Clinical Genetic Services
Level 4/50 Flemington Road
PARKVILLE VIC 3052

Cytogenetics Laboratory

Specimen source Cell Pellet

Molecular karyotype

Array type	Illumina Infinium CoreExome-24 v1.1
Resolution	0.50Mb
Assembly	hg19 / GRCh37 (Feb 2009)
Molecular karyotype	arr(1-22)x2,(XY)x1
Result	NO ANEUPLOIDIES DETECTED

Interpretation
Male molecular karyotype. No aneuploidies were detected in this sample.

SUPPLEMENTARY REPORT ISSUED 02-03-2018
SNPduo comparative analysis of the microarray genotyping data was performed using this sample and previous sample PB001.1 (Lab No 15C109167). Analysis has shown identical (>99.9%) genotypes for the entire genome, indicating that the two samples are from the same individual.

Molecular karyotyping is limited in its ability to detect low grade mosaicism and genomic copy number changes below the resolution stated. Balanced rearrangements will not be detected. This test does not exclude single gene disorders caused by sequence mutations or trinucleotide repeat expansions (such as fragile X syndrome, Huntington disease, some spinocerebellar ataxias, Friedreich ataxia and myotonic dystrophy) . Testing for fragile X syndrome should be considered in individuals with developmental delay/ intellectual disability. Copy number changes that do not contain genes, are well established polymorphisms, or are assessed as being of unlikely clinical significance (based on available evidence), will not be reported. Reporting of regions of homozygosity (>5Mb) is dependent on referral setting and clinical indication. Please contact the laboratory if a recessive disorder is suspected. Interpretation is based on the UCSC GRCh37/hg19 human reference sequence.

Validated: 02-Mar-2018 by Ralph Oertel

Enquiries: +61 3 8341 6258

PATHOLOGY REPORT

END OF TEST REPORT

AMENDED REPORT

Appendix 4

The list of differentially expressed genes in TG protocol vs No-TG protocol

ensembl_id	**symbol**	**gene_name**	**Chr**	**logFC**	**adj.P.Val**
ENSG00000160161	CILP2	cartilage intermediate layer protein 2	19	7.345773	3.12E-16
ENSG00000124225	PMEPA1	prostate transmembrane protein, androgen induced 1	20	4.047166	1.15E-11
ENSG00000160888	IER2	immediate early response 2	19	2.561734	4.47E-10
ENSG00000115380	EFEMP1	EGF containing fibulin extracellular matrix protein 1	2	-3.44016	4.52E-10
ENSG00000103257	SLC7A5	solute carrier family 7 member 5	16	3.409627	5.74E-10
ENSG00000186340	THBS2	thrombospondin 2	6	3.874888	9.23E-10
ENSG00000185634	SHC4	SHC adaptor protein 4	15	2.938333	9.66E-10
ENSG00000281230	SERTAD4	SERTA domain containing 4	1	3.36083	1.47E-09
ENSG00000101074	R3HDML	R3H domain containing like	20	9.624578	1.47E-09
ENSG00000105664	COMP	cartilage oligomeric matrix protein	19	8.085644	3.02E-09
ENSG00000143333	RGS16	regulator of G protein signaling 16	1	6.479781	3.02E-09
ENSG00000115414	FN1	fibronectin 1	2	3.757733	4.38E-09
ENSG00000066248	NGEF	neuronal guanine nucleotide exchange factor	2	3.473557	4.88E-09
ENSG00000134013	LOXL2	lysyl oxidase like 2	8	4.604882	4.88E-09
ENSG00000135842	FAM129A	family with sequence similarity 129 member A	1	5.11304	4.88E-09
ENSG00000107731	UNC5B	unc-5 netrin receptor B	10	3.732891	6.03E-09
ENSG00000136603	SKIL	SKI like proto-oncogene	3	3.333456	6.43E-09
ENSG00000106366	SERPINE1	serpin family E member 1	7	4.317642	6.43E-09
ENSG00000166741	NNMT	nicotinamide N-methyltransferase	11	6.125964	6.48E-09
ENSG00000111799	COL12A1	collagen type XII alpha 1 chain	6	3.741191	9.46E-09
ENSG00000179954	SSC5D	scavenger receptor cysteine rich family member with 5 domains	19	4.003558	1.18E-08
ENSG00000163453	IGFBP7	insulin like growth factor binding protein 7	4	4.199543	1.24E-08
ENSG00000143196	DPT	dermatopontin	1	3.483374	1.28E-08
ENSG00000242265	PEG10	paternally expressed 10	7	-2.55141	1.65E-08
ENSG00000074410	CA12	carbonic anhydrase 12	15	-3.03769	1.65E-08
ENSG00000164694	FNDC1	fibronectin type III domain containing 1	6	4.394575	1.65E-08
ENSG00000169436	COL22A1	collagen type XXII alpha 1 chain	8	5.361928	1.81E-08
ENSG00000162510	MATN1	matrilin 1	1	-3.83567	2.24E-08
ENSG00000198108	CHSY3	chondroitin sulfate synthase 3	5	2.531487	2.26E-08
ENSG00000171621	SPSB1	splA/ryanodine receptor domain and SOCS box containing 1	1	3.061051	2.26E-08
ENSG00000120708	TGFBI	transforming growth factor beta induced	5	4.005758	2.64E-08
ENSG00000139269	INHBE	inhibin beta E subunit	12	7.30513	2.71E-08
ENSG00000172346	CSDC2	cold shock domain containing C2	22	3.712161	4.23E-08
ENSG00000250722	SELENOP	selenoprotein P	5	-2.515	4.47E-08
ENSG00000166509	CLEC3A	C-type lectin domain family 3 member A	16	6.004771	4.76E-08
ENSG00000100234	TIMP3	TIMP metallopeptidase inhibitor 3	22	2.974908	4.76E-08
ENSG00000175264	CHST1	carbohydrate sulfotransferase 1	11	3.931051	4.83E-08
ENSG00000157554	ERG	ERG, ETS transcription factor	21	3.123152	4.96E-08
ENSG00000143768	LEFTY2	left-right determination factor 2	1	5.864635	5.06E-08
ENSG00000106688	SLC1A1	solute carrier family 1 member 1	9	-3.82025	5.94E-08
ENSG00000072682	P4HA2	prolyl 4-hydroxylase subunit alpha 2	5	3.437007	6.27E-08
ENSG00000171223	JUNB	JunB proto-oncogene, AP-1 transcription factor subunit	19	3.492207	7.94E-08
ENSG00000156219	ART3	ADP-ribosyltransferase 3	4	-3.2236	8.49E-08
ENSG00000122679	RAMP3	receptor activity modifying protein 3	7	6.244921	8.49E-08
ENSG00000073756	PTGS2	prostaglandin-endoperoxide synthase 2	1	4.376478	1.12E-07
ENSG00000177283	FZD8	frizzled class receptor 8	10	3.640712	1.26E-07
ENSG00000260428	SCX	scleraxis bHLH transcription factor	8	5.946172	1.44E-07
ENSG00000087074	PPP1R15A	protein phosphatase 1 regulatory subunit 15A	19	2.692979	1.61E-07
ENSG00000120254	MTHFD1L	methylenetetrahydrofolate dehydrogenase (NADP+ dependent) 1 like	6	2.720417	1.89E-07
ENSG00000112276	BVES	blood vessel epicardial substance	6	5.089316	1.89E-07
ENSG00000181195	PENK	proenkephalin	8	4.392486	1.89E-07
ENSG00000169174	PCSK9	proprotein convertase subtilisin/kexin type 9	1	-2.68718	2.10E-07
ENSG00000151789	ZNF385D	zinc finger protein 385D	3	3.833454	2.10E-07
ENSG00000165030	NFIL3	nuclear factor, interleukin 3 regulated	9	2.533914	2.10E-07
ENSG00000162745	OLFML2B	olfactomedin like 2B	1	3.724216	2.10E-07
ENSG00000049192	ADAMTS6	ADAM metallopeptidase with thrombospondin type 1 motif 6	5	2.22515	2.31E-07
ENSG00000162772	ATF3	activating transcription factor 3	1	3.46623	2.51E-07
ENSG00000214688	C10orf105	chromosome 10 open reading frame 105	10	2.653429	2.58E-07
ENSG00000154654	NCAM2	neural cell adhesion molecule 2	21	-2.22837	2.96E-07
ENSG00000101255	TRIB3	tribbles pseudokinase 3	20	4.693059	3.02E-07

ENSG00000166407	LMO1	LIM domain only 1	11	6.673541	3.13E-07
ENSG00000197971	MBP	myelin basic protein	18	2.992546	3.24E-07
ENSG00000230128	IER3	immediate early response 3	6	4.11118	3.32E-07
ENSG00000140092	FBLN5	fibulin 5	14	4.123238	4.44E-07
ENSG00000123243	ITIH5	inter-alpha-trypsin inhibitor heavy chain family member 5	10	3.00883	4.44E-07
ENSG00000184232	OAF	out at first homolog	11	2.565505	4.51E-07
ENSG00000065911	MTHFD2	methylenetetrahydrofolate dehydrogenase (NADP+ dependent) 2, methenyltetrahydrofolate cyclohydrolase	2	2.378044	4.51E-07
ENSG00000105329	TGFB1	transforming growth factor beta 1	19	2.499443	4.51E-07
ENSG00000179399	GPC5	glypican 5	13	-5.02767	5.07E-07
ENSG00000132000	PODNL1	podocan like 1	19	3.36801	6.54E-07
ENSG00000182752	PAPPA	pappalysin 1	9	4.125123	6.54E-07
ENSG00000148848	ADAM12	ADAM metallopeptidase domain 12	10	2.831694	6.54E-07
ENSG00000168297	PXK	PX domain containing serine/threonine kinase like	3	2.266721	6.54E-07
ENSG00000100889	PCK2	phosphoenolpyruvate carboxykinase 2, mitochondrial	14	3.190148	9.44E-07
ENSG00000171819	ANGPTL7	angiopoietin like 7	1	3.453916	9.58E-07
ENSG00000091622	PITPNM3	PITPNM family member 3	17	3.241237	9.92E-07
ENSG00000183688	RFLNB	refilin B	17	3.093033	1.07E-06
ENSG00000152785	BMP3	bone morphogenetic protein 3	4	-3.00657	1.07E-06
ENSG00000206190	ATP10A	ATPase phospholipid transporting 10A (putative)	15	3.62017	1.42E-06
ENSG00000197859	ADAMTSL2	ADAMTS like 2	9	7.491964	1.42E-06
ENSG00000099875	MKNK2	MAP kinase interacting serine/threonine kinase 2	19	2.326718	1.58E-06
ENSG00000144802	NFKBIZ	NFKB inhibitor zeta	3	3.180641	1.58E-06
ENSG00000139211	AMIGO2	adhesion molecule with Ig like domain 2	12	5.189313	1.87E-06
ENSG00000075711	DLG1	discs large MAGUK scaffold protein 1	3	2.40606	2.16E-06
ENSG00000155090	KLF10	Kruppel like factor 10	8	2.204602	2.29E-06
ENSG00000166396	SERPINB7	serpin family B member 7	18	8.318742	2.29E-06
ENSG00000108509	CAMTA2	calmodulin binding transcription activator 2	17	2.530234	2.29E-06
ENSG00000006611	USH1C	USH1 protein network component harmonin	11	7.129024	2.65E-06
ENSG00000105281	SLC1A5	solute carrier family 1 member 5	19	2.405381	2.89E-06
ENSG00000166033	HTRA1	HtrA serine peptidase 1	10	2.466934	3.25E-06
ENSG00000049323	LTBP1	latent transforming growth factor beta binding protein 1	2	2.789448	3.55E-06
ENSG00000188487	INSC	INSC, spindle orientation adaptor protein	11	6.2304	3.55E-06
ENSG00000145536	ADAMTS16	ADAM metallopeptidase with thrombospondin type 1 motif 16	5	3.707582	3.57E-06
ENSG00000157613	CREB3L1	cAMP responsive element binding protein 3 like 1	11	3.026806	3.62E-06
ENSG00000156453	PCDH1	protocadherin 1	5	3.118056	4.25E-06
ENSG00000106105	GARS	glycyl-tRNA synthetase	7	2.11131	4.75E-06
ENSG00000125740	FOSB	FosB proto-oncogene, AP-1 transcription factor subunit	19	3.961679	5.92E-06
ENSG00000131480	AOC2	amine oxidase, copper containing 2	17	3.663808	6.20E-06
ENSG00000134259	NGF	nerve growth factor	1	3.755156	7.53E-06
ENSG00000113578	FGF1	fibroblast growth factor 1	5	2.805391	1.04E-05
ENSG00000140416	TPM1	tropomyosin 1	15	3.197324	1.04E-05
ENSG00000104783	KCNN4	potassium calcium-activated channel subfamily N member 4	19	4.024156	1.08E-05
ENSG00000115107	STEAP3	STEAP3 metalloreductase	2	2.700877	1.28E-05
ENSG00000149573	MPZL2	myelin protein zero like 2	11	-2.76874	1.66E-05
ENSG00000139220	PPFIA2	PTPRF interacting protein alpha 2	12	-5.30871	1.67E-05
ENSG00000074590	NUAK1	NUAK family kinase 1	12	3.124724	1.73E-05
ENSG00000104881	PPP1R13L	protein phosphatase 1 regulatory subunit 13 like	19	3.410606	1.80E-05
ENSG00000168003	SLC3A2	solute carrier family 3 member 2	11	2.357605	1.84E-05
ENSG00000137727	ARHGAP20	Rho GTPase activating protein 20	11	-2.50486	1.98E-05
ENSG00000120129	DUSP1	dual specificity phosphatase 1	5	2.706809	1.98E-05
ENSG00000198914	POU3F3	POU class 3 homeobox 3	2	-2.36368	1.98E-05
ENSG00000100505	TRIM9	tripartite motif containing 9	14	-2.24352	1.98E-05
ENSG00000116985	BMP8B	bone morphogenetic protein 8b	1	-3.98538	1.99E-05
ENSG00000071073	MGAT4A	mannosyl (alpha-1,3-)-glycoprotein beta-1,4-N-acetylglucosaminyltransferase, isozyme A	2	-1.7024	2.04E-05
ENSG00000184144	CNTN2	contactin 2	1	2.793133	2.25E-05
ENSG00000128165	ADM2	adrenomedullin 2	22	3.286327	2.32E-05
ENSG00000180730	SHISA2	shisa family member 2	13	3.846573	2.35E-05
ENSG00000149591	TAGLN	transgelin	11	3.460467	2.41E-05
ENSG00000172216	CEBPB	CCAAT enhancer binding protein beta	20	2.516866	2.53E-05
ENSG00000115902	SLC1A4	solute carrier family 1 member 4	2	2.846737	2.57E-05
ENSG00000144655	CSRNP1	cysteine and serine rich nuclear protein 1	3	2.480294	2.58E-05

ENSG00000113070	HBEGF	heparin binding EGF like growth factor	5	4.078282	2.66E-05
ENSG00000106948	AKNA	AT-hook transcription factor	9	2.92355	2.68E-05
ENSG00000178038	ALS2CL	ALS2 C-terminal like	3	2.399796	2.71E-05
ENSG00000072110	ACTN1	actinin alpha 1	14	1.943779	3.10E-05
ENSG00000078098	FAP	fibroblast activation protein alpha	2	3.606769	3.16E-05
ENSG00000164929	BAALC	BAALC, MAP3K1 and KLF4 binding	8	2.476147	3.35E-05
ENSG00000198542	ITGBL1	integrin subunit beta like 1	13	3.940632	3.80E-05
ENSG00000135269	TES	testin LIM domain protein	7	2.867042	3.84E-05
ENSG00000153879	CEBPG	CCAAT enhancer binding protein gamma	19	2.258063	3.91E-05
ENSG00000166670	MMP10	matrix metallopeptidase 10	11	3.699898	3.95E-05
ENSG00000006652	IFRD1	interferon related developmental regulator 1	7	1.865038	3.95E-05
ENSG00000178752	ERFE	erythroferrone	2	3.773693	4.20E-05
ENSG00000124762	CDKN1A	cyclin dependent kinase inhibitor 1A	6	2.528141	4.30E-05
ENSG00000145555	MYO10	myosin X	5	2.025274	4.47E-05
ENSG00000094963	FMO2	flavin containing monooxygenase 2	1	5.570062	4.48E-05
ENSG00000283530	MGAT4C	MGAT4 family member C	12	-3.35159	5.42E-05
ENSG00000163909	HEYL	hes related family bHLH transcription factor with YRPW motif-like	1	4.006849	5.45E-05
ENSG00000006327	TNFRSF12A	TNF receptor superfamily member 12A	16	2.473097	5.52E-05
ENSG00000196611	MMP1	matrix metallopeptidase 1	11	4.850723	5.53E-05
ENSG00000114315	HES1	hes family bHLH transcription factor 1	3	2.79412	5.53E-05
ENSG00000166986	MARS	methionyl-tRNA synthetase	12	1.889495	5.54E-05
ENSG00000166147	FBN1	fibrillin 1	15	2.308278	5.59E-05
ENSG00000090776	EFNB1	ephrin B1	X	-2.0956	5.61E-05
ENSG00000049540	ELN	elastin	7	4.22701	5.76E-05
ENSG00000162998	FRZB	frizzled related protein	2	-2.31016	5.88E-05
ENSG00000105722	ERF	ETS2 repressor factor	19	1.986468	6.02E-05
ENSG00000147852	VLDLR	very low density lipoprotein receptor	9	3.193409	6.09E-05
ENSG00000137809	ITGA11	integrin subunit alpha 11	15	2.987646	6.16E-05
ENSG00000172432	GTPBP2	GTP binding protein 2	6	2.102701	7.02E-05
ENSG00000120738	EGR1	early growth response 1	5	4.199917	7.02E-05
ENSG00000130707	ASS1	argininosuccinate synthase 1	9	2.372514	7.08E-05
ENSG00000136826	KLF4	Kruppel like factor 4	9	2.542128	7.28E-05
ENSG00000128965	CHAC1	ChaC glutathione specific gamma-glutamylcyclotransferase 1	15	3.502037	7.40E-05
ENSG00000087116	ADAMTS2	ADAM metallopeptidase with thrombospondin type 1 motif 2	5	1.977637	7.53E-05
ENSG00000111199	TRPV4	transient receptor potential cation channel subfamily V member 4	12	1.873548	7.53E-05
ENSG00000215183	MSMP	microseminoprotein, prostate associated	9	-6.79122	7.53E-05
ENSG00000154856	APCDD1	APC down-regulated 1	18	-2.36317	7.98E-05
ENSG00000169508	GPR183	G protein-coupled receptor 183	13	6.019316	8.15E-05
ENSG00000143369	ECM1	extracellular matrix protein 1	1	3.02523	8.18E-05
ENSG00000119681	LTBP2	latent transforming growth factor beta binding protein 2	14	4.966012	8.29E-05
ENSG00000150051	MKX	mohawk homeobox	10	2.519064	8.35E-05
ENSG00000124212	PTGIS	prostaglandin I2 synthase	20	2.181203	8.66E-05
ENSG00000182379	NXPH4	neurexophilin 4	12	3.610852	8.66E-05
ENSG00000253276	CCDC71L	coiled-coil domain containing 71 like	7	2.262391	8.82E-05
ENSG00000135414	GDF11	growth differentiation factor 11	12	-2.33917	8.82E-05
ENSG00000122877	EGR2	early growth response 2	10	4.116684	9.53E-05
ENSG00000113083	LOX	lysyl oxidase	5	3.043235	9.89E-05
ENSG00000169136	ATF5	activating transcription factor 5	19	3.449984	0.000105
ENSG00000198517	MAFK	MAF bZIP transcription factor K	7	1.9191	0.000106
ENSG00000118785	SPP1	secreted phosphoprotein 1	4	-4.01038	0.000108
ENSG00000187735	TCEA1	transcription elongation factor A1	8	1.883565	0.000111
ENSG00000161638	ITGA5	integrin subunit alpha 5	12	2.039883	0.000114
ENSG00000105929	ATP6V0A4	ATPase H+ transporting V0 subunit a4	7	2.464261	0.000126
ENSG00000282932	PTPRD	protein tyrosine phosphatase, receptor type D	9	-2.19618	0.000126
ENSG00000169231	THBS3	thrombospondin 3	1	2.294116	0.000127
ENSG00000153823	PID1	phosphotyrosine interaction domain containing 1	2	2.970176	0.000131
ENSG00000148841	ITPRIP	inositol 1,4,5-trisphosphate receptor interacting protein	10	2.751228	0.000131
ENSG00000112309	B3GAT2	beta-1,3-glucuronyltransferase 2	6	-2.79072	0.000135
ENSG00000172061	LRRC15	leucine rich repeat containing 15	3	9.770495	0.000138
ENSG00000089327	FXYD5	FXYD domain containing ion transport regulator 5	19	2.824653	0.000148
ENSG00000118523	CTGF	connective tissue growth factor	6	4.013949	0.000153
ENSG00000187634	SAMD11	sterile alpha motif domain containing 11	1	4.700755	0.000155
ENSG00000135905	DOCK10	dedicator of cytokinesis 10	2	-3.30903	0.000159
ENSG00000076826	CAMSAP3	calmodulin regulated spectrin associated protein family member 3	19	-3.28999	0.000173

ENSG00000143878	RHOB	ras homolog family member B	2	1.915816	0.000183
ENSG00000116690	PRG4	proteoglycan 4	1	10.39334	0.000183
ENSG00000065361	ERBB3	erb-b2 receptor tyrosine kinase 3	12	-4.07819	0.000187
ENSG00000184575	XPOT	exportin for tRNA	12	2.054784	0.000187
ENSG00000187323	DCC	DCC netrin 1 receptor	18	-3.45541	0.00019
ENSG00000164530	PI16	peptidase inhibitor 16	6	-2.25288	0.000191
ENSG00000109956	B3GAT1	beta-1,3-glucuronyltransferase 1	11	-3.74747	0.000199
ENSG00000095637	SORBS1	sorbin and SH3 domain containing 1	10	-2.2277	0.0002
ENSG00000142661	MYOM3	myomesin 3	1	3.925236	0.000217
ENSG00000103522	IL21R	interleukin 21 receptor	16	4.047865	0.000226
ENSG00000009950	MLXIPL	MLX interacting protein like	7	5.139951	0.000234
ENSG00000143341	HMCN1	hemicentin 1	1	5.120327	0.000236
ENSG00000101670	LIPG	lipase G, endothelial type	18	2.613636	0.000243
ENSG00000159200	RCAN1	regulator of calcineurin 1	21	2.76348	0.000267
ENSG00000170345	FOS	Fos proto-oncogene, AP-1 transcription factor subunit	14	3.721928	0.00029
ENSG00000095752	IL11	interleukin 11	19	3.465721	0.000308
ENSG00000134198	TSPAN2	tetraspanin 2	1	2.232798	0.000325
ENSG00000215644	GCGR	glucagon receptor	17	4.42205	0.000337
ENSG00000187122	SLIT1	slit guidance ligand 1	10	-3.53335	0.000339
ENSG00000105550	FGF21	fibroblast growth factor 21	19	7.421599	0.00034
ENSG00000101230	ISM1	isthmin 1	20	2.690439	0.000361
ENSG00000189409	MMP23B	matrix metallopeptidase 23B	1	6.698383	0.000365
ENSG00000135218	CD36	CD36 molecule	7	-2.14327	0.000376
ENSG00000099860	GADD45B	growth arrest and DNA damage inducible beta	19	2.550858	0.000385
ENSG00000143512	HHIPL2	HHIP like 2	1	3.273488	0.000389
ENSG00000031698	SARS	seryl-tRNA synthetase	1	2.144119	0.000392
ENSG00000132561	MATN2	matrilin 2	8	2.74535	0.000393
ENSG00000182199	SHMT2	serine hydroxymethyltransferase 2	12	2.539703	0.000399
ENSG00000211455	STK38L	serine/threonine kinase 38 like	12	2.442363	0.000405
ENSG00000113013	HSPA9	heat shock protein family A (Hsp70) member 9	5	1.714843	0.000407
ENSG00000278843	MMP28	matrix metallopeptidase 28	17	7.353444	0.000561
ENSG00000130766	SESN2	sestrin 2	1	2.470449	0.00057
ENSG00000081277	PKP1	plakophilin 1	1	2.459385	0.000577
ENSG00000196542	SPTSSB	serine palmitoyltransferase small subunit B	3	-2.2747	0.00061
ENSG00000071282	LMCD1	LIM and cysteine rich domains 1	3	2.032656	0.000642
ENSG00000182809	CRIP2	cysteine rich protein 2	14	1.866508	0.000644
ENSG00000175906	ARL4D	ADP ribosylation factor like GTPase 4D	17	2.522818	0.000688
ENSG00000197461	PDGFA	platelet derived growth factor subunit A	7	2.719962	0.000704
ENSG00000166750	SLFN5	schlafen family member 5	17	2.857055	0.000704
ENSG00000175183	CSRP2	cysteine and glycine rich protein 2	12	2.7664	0.000706
ENSG00000156427	FGF18	fibroblast growth factor 18	5	4.019221	0.000787
ENSG00000118507	AKAP7	A-kinase anchoring protein 7	6	-2.51278	0.000816
ENSG00000167106	FAM102A	family with sequence similarity 102 member A	9	1.795768	0.000851
ENSG00000132854	KANK4	KN motif and ankyrin repeat domains 4	1	6.433967	0.000851
ENSG00000108947	EFNB3	ephrin B3	17	-2.04888	0.000851
ENSG00000146674	IGFBP3	insulin like growth factor binding protein 3	7	3.523575	0.000865
ENSG00000178860	MSC	musculin	8	6.57562	0.000902
ENSG00000178026	LRRC75B	leucine rich repeat containing 75B	22	2.444378	0.000949
ENSG00000240583	AQP1	aquaporin 1 (Colton blood group)	7	3.395557	0.000973
ENSG00000188488	SERPINA5	serpin family A member 5	14	3.47533	0.000981
ENSG00000187123	LYPD6	LY6/PLAUR domain containing 6	2	-2.73391	0.000985
ENSG00000090861	AARS	alanyl-tRNA synthetase	16	1.850246	0.001006
ENSG00000109265	KIAA1211	KIAA1211	4	2.380214	0.001006
ENSG00000063438	AHRR	aryl-hydrocarbon receptor repressor	5	-2.05682	0.001057
ENSG00000137166	FOXP4	forkhead box P4	6	1.862835	0.001057
ENSG00000167995	BEST1	bestrophin 1	11	2.820566	0.001112
ENSG00000196305	IARS	isoleucyl-tRNA synthetase	9	1.658886	0.001124
ENSG00000175197	DDIT3	DNA damage inducible transcript 3	12	2.484269	0.001126
ENSG00000186832	KRT16	keratin 16	17	3.412743	0.001156
ENSG00000134684	YARS	tyrosyl-tRNA synthetase	1	1.830348	0.001161
ENSG00000091986	CCDC80	coiled-coil domain containing 80	3	2.463823	0.001184
ENSG00000101665	SMAD7	SMAD family member 7	18	2.164893	0.001188
ENSG00000139970	RTN1	reticulon 1	14	-2.06224	0.001202
ENSG00000274619	CFD	complement factor D	19	-4.58425	0.001274
ENSG00000100219	XBP1	X-box binding protein 1	22	1.838107	0.001285
ENSG00000089199	CHGB	chromogranin B	20	-3.55094	0.001307
ENSG00000134443	GRP	gastrin releasing peptide	18	-5.97698	0.00138
ENSG00000198796	ALPK2	alpha kinase 2	18	4.554636	0.001397
ENSG00000070669	ASNS	asparagine synthetase (glutamine-hydrolyzing)	7	2.61234	0.001397
ENSG00000141526	SLC16A3	solute carrier family 16 member 3	17	2.995943	0.001445

ENSG00000110660	SLC35F2	solute carrier family 35 member F2	11	2.61629	0.001495
ENSG00000101096	NFATC2	nuclear factor of activated T cells 2	20	2.170862	0.0015
ENSG00000155465	SLC7A7	solute carrier family 7 member 7	14	3.843284	0.001515
ENSG00000171812	COL8A2	collagen type VIII alpha 2 chain	1	1.792794	0.001522
ENSG00000100346	CACNA1I	calcium voltage-gated channel subunit alpha1 I	22	3.339814	0.001554
ENSG00000048740	CELF2	CUGBP Elav-like family member 2	10	-2.56447	0.001554
ENSG00000277639	LOC105371267	p53-regulated lncRNA 1	16	-2.3624	0.001561
ENSG00000146938	NLGN4X	neuroligin 4, X-linked	X	-2.55455	0.001577
ENSG00000141485	SLC13A5	solute carrier family 13 member 5	17	3.933255	0.001577
ENSG00000185008	ROBO2	roundabout guidance receptor 2	3	-2.05331	0.001601
ENSG00000127528	KLF2	Kruppel like factor 2	19	1.704168	0.001601
ENSG00000131015	ULBP2	UL16 binding protein 2	6	3.585408	0.001627
ENSG00000140511	HAPLN3	hyaluronan and proteoglycan link protein 3	15	2.346212	0.001627
ENSG00000118508	RAB32	RAB32, member RAS oncogene family	6	1.809343	0.001643
ENSG00000196141	SPATS2L	spermatogenesis associated serine rich 2 like	2	1.544997	0.001643
ENSG00000141198	TOM1L1	target of myb1 like 1 membrane trafficking protein	17	-2.36353	0.001648
ENSG00000046653	GPM6B	glycoprotein M6B	X	-1.98795	0.001674
ENSG00000185633	NDUFA4L2	NDUFA4, mitochondrial complex associated like 2	12	4.743931	0.001759
ENSG00000196562	SULF2	sulfatase 2	20	1.949055	0.001781
ENSG00000100345	MYH9	myosin heavy chain 9	22	1.88585	0.001781
ENSG00000196878	LAMB3	laminin subunit beta 3	1	2.739322	0.001781
ENSG00000150630	VEGFC	vascular endothelial growth factor C	4	4.28547	0.001781
ENSG00000101680	LAMA1	laminin subunit alpha 1	18	2.312167	0.001781
ENSG00000118898	PPL	periplakin	16	-2.5814	0.001781
ENSG00000189320	FAM180A	family with sequence similarity 180 member A	7	2.223302	0.001781
ENSG00000106066	CPVL	carboxypeptidase, vitellogenic like	7	-3.20761	0.001802
ENSG00000175040	CHST2	carbohydrate sulfotransferase 2	3	-1.8173	0.001816
ENSG00000206527	HACD2	3-hydroxyacyl-CoA dehydratase 2	3	1.797818	0.001876
ENSG00000169302	STK32A	serine/threonine kinase 32A	5	-2.49729	0.00206
ENSG00000198889	DCAF12L1	DDB1 and CUL4 associated factor 12 like 1	X	-4.27591	0.00206
ENSG00000135069	PSAT1	phosphoserine aminotransferase 1	9	2.41809	0.00206
ENSG00000138722	MMRN1	multimerin 1	4	-2.61627	0.00211
ENSG00000075426	FOSL2	FOS like 2, AP-1 transcription factor subunit	2	2.437409	0.00211
ENSG00000196517	SLC6A9	solute carrier family 6 member 9	1	2.42209	0.002139
ENSG00000165527	ARF6	ADP ribosylation factor 6	14	1.680841	0.00222
ENSG00000144339	TMEFF2	transmembrane protein with EGF like and two follistatin like domains 2	2	-2.88773	0.002279
ENSG00000150540	HNMT	histamine N-methyltransferase	2	-1.66636	0.002392
ENSG00000066382	MPPED2	metallophosphoesterase domain containing 2	11	-1.84788	0.002404
ENSG00000168675	LDLRAD4	low density lipoprotein receptor class A domain containing 4	18	1.79184	0.002406
ENSG00000188338	SLC38A3	solute carrier family 38 member 3	3	2.372047	0.002428
ENSG00000152578	GRIA4	glutamate ionotropic receptor AMPA type subunit 4	11	-3.53669	0.002449
ENSG00000173846	PLK3	polo like kinase 3	1	2.268431	0.002794
ENSG00000244242	IFITM10	interferon induced transmembrane protein 10	11	4.86185	0.002844
ENSG00000188729	OSTN	osteocrin	3	-3.09726	0.002853
ENSG00000166123	GPT2	glutamic--pyruvic transaminase 2	16	1.965308	0.002888
ENSG00000070371	CLTCL1	clathrin heavy chain like 1	22	2.29018	0.002931
ENSG00000125848	FLRT3	fibronectin leucine rich transmembrane protein 3	20	-2.72728	0.002931
ENSG00000129009	ISLR	immunoglobulin superfamily containing leucine rich repeat	15	-1.63381	0.002942
ENSG00000128342	LIF	LIF, interleukin 6 family cytokine	22	2.596559	0.002947
ENSG00000183696	UPP1	uridine phosphorylase 1	7	2.414799	0.002998
ENSG00000188522	FAM83G	family with sequence similarity 83 member G	17	1.997128	0.003002
ENSG00000137193	PIM1	Pim-1 proto-oncogene, serine/threonine kinase	6	2.33504	0.003002
ENSG00000140873	ADAMTS18	ADAM metallopeptidase with thrombospondin type 1 motif 18	16	-3.45216	0.003002
ENSG00000011422	PLAUR	plasminogen activator, urokinase receptor	19	2.376189	0.003002
ENSG00000092421	SEMA6A	semaphorin 6A	5	-1.77136	0.003002
ENSG00000039560	RAI14	retinoic acid induced 14	5	2.521731	0.003002
ENSG00000188162	OTOG	otogelin	11	4.953832	0.003108
ENSG00000000005	TNMD	tenomodulin	X	3.540013	0.003108
ENSG00000196923	PDLIM7	PDZ and LIM domain 7	5	1.750671	0.003147
ENSG00000102755	FLT1	fms related tyrosine kinase 1	13	4.433889	0.003149
ENSG00000125148	MT2A	metallothionein 2A	16	3.348613	0.003196
ENSG00000188730	VWC2	von Willebrand factor C domain containing 2	7	-3.02336	0.003196
ENSG00000163376	KBTBD8	kelch repeat and BTB domain containing 8	3	2.660403	0.003196
ENSG00000182795	C1orf116	chromosome 1 open reading frame 116	1	-2.42268	0.003196
ENSG00000166897	ELFN2	extracellular leucine rich repeat and fibronectin type III domain containing 2	22	-3.28393	0.003338

ENSG00000152910	CNTNAP4	contactin associated protein like 4	16	-5.1882	0.003338
ENSG00000107562	CXCL12	C-X-C motif chemokine ligand 12	10	-2.12645	0.00338
ENSG00000004660	CAMKK1	calcium/calmodulin dependent protein kinase kinase 1	17	1.849529	0.003441
ENSG00000139514	SLC7A1	solute carrier family 7 member 1	13	1.796158	0.003672
ENSG00000128512	DOCK4	dedicator of cytokinesis 4	7	2.911578	0.003716
ENSG00000130635	COL5A1	collagen type V alpha 1 chain	9	2.176443	0.003721
ENSG00000175356	SCUBE2	signal peptide, CUB domain and EGF like domain containing 2	11	-2.22351	0.003756
ENSG00000197614	MFAP5	microfibril associated protein 5	12	8.968145	0.004072
ENSG00000065320	NTN1	netrin 1	17	-1.84698	0.004091
ENSG00000134253	TRIM45	tripartite motif containing 45	1	-2.00757	0.00412
ENSG00000140470	ADAMTS17	ADAM metallopeptidase with thrombospondin type 1 motif 17	15	2.593589	0.00412
ENSG00000157103	SLC6A1	solute carrier family 6 member 1	3	-3.45581	0.00412
ENSG00000163993	S100P	S100 calcium binding protein P	4	3.104712	0.00412
ENSG00000171596	NMUR1	neuromedin U receptor 1	2	2.381127	0.00412
ENSG00000048540	LMO3	LIM domain only 3	12	-3.24761	0.004294
ENSG00000078549	ADCYAP1R1	ADCYAP receptor type I	7	-3.37841	0.004294
ENSG00000177807	KCNJ10	potassium voltage-gated channel subfamily J member 10	1	-4.70347	0.004308
ENSG00000165905	LARGE2	LARGE xylosyl- and glucuronyltransferase 2	11	-2.34228	0.004313
ENSG00000106868	SUSD1	sushi domain containing 1	9	-2.19805	0.004435
ENSG00000088992	TESC	tescalcin	12	5.014287	0.004494
ENSG00000156466	GDF6	growth differentiation factor 6	8	4.265565	0.004494
ENSG00000092068	SLC7A8	solute carrier family 7 member 8	14	-1.77975	0.004712
ENSG00000176046	NUPR1	nuclear protein 1, transcriptional regulator	16	2.198523	0.004797
ENSG00000186417	GLDN	gliomedin	15	2.602689	0.004905
ENSG00000055813	CCDC85A	coiled-coil domain containing 85A	2	-3.03423	0.005048
ENSG00000184588	PDE4B	phosphodiesterase 4B	1	-2.20217	0.005245
ENSG00000179915	NRXN1	neurexin 1	2	-3.50013	0.005292
ENSG00000128578	STRIP2	striatin interacting protein 2	7	-2.16936	0.005788
ENSG00000091513	TF	transferrin	3	-2.72963	0.005844
ENSG00000272636	DOC2B	double C2 domain beta	17	7.462332	0.005844
ENSG00000153012	LGI2	leucine rich repeat LGI family member 2	4	-1.85602	0.00596
ENSG00000116679	IVNS1ABP	influenza virus NS1A binding protein	1	1.631264	0.00596
ENSG00000077063	CTTNBP2	cortactin binding protein 2	7	-2.60239	0.005966
ENSG00000153820	SPHKAP	SPHK1 interactor, AKAP domain containing	2	-5.65924	0.005966
ENSG00000136404	TM6SF1	transmembrane 6 superfamily member 1	15	5.740508	0.006362
ENSG00000132692	BCAN	brevican	1	-3.7723	0.006362
ENSG00000140941	MAP1LC3B	microtubule associated protein 1 light chain 3 beta	16	1.768841	0.006362
ENSG00000138646	HERC5	HECT and RLD domain containing E3 ubiquitin protein ligase 5	4	-3.23923	0.006362
ENSG00000164330	EBF1	early B cell factor 1	5	-1.7321	0.006554
ENSG00000156398	SFXN2	sideroflexin 2	10	-2.28901	0.006573
ENSG00000162946	DISC1	DISC1 scaffold protein	1	-2.68076	0.006619
ENSG00000076356	PLXNA2	plexin A2	1	1.906926	0.006635
ENSG00000275544	BDH1	3-hydroxybutyrate dehydrogenase 1	3	-2.20778	0.006797
ENSG00000164708	PGAM2	phosphoglycerate mutase 2	7	3.420433	0.006842
ENSG00000146006	LRRTM2	leucine rich repeat transmembrane neuronal 2	5	-2.96651	0.00695
ENSG00000120889	TNFRSF10B	TNF receptor superfamily member 10b	8	1.996404	0.00695
ENSG00000081479	LRP2	LDL receptor related protein 2	2	-2.25061	0.007092
ENSG00000166173	LARP6	La ribonucleoprotein domain family member 6	15	1.692674	0.007214
ENSG00000157514	TSC22D3	TSC22 domain family member 3	X	1.971827	0.00722
ENSG00000171885	AQP4	aquaporin 4	18	-2.03845	0.00722
ENSG00000275246	TLCD2	TLC domain containing 2	17	2.121288	0.00722
ENSG00000283154	SCHIP1	schwannomin interacting protein 1	3	3.264516	0.00731
ENSG00000180353	HCLS1	hematopoietic cell-specific Lyn substrate 1	3	3.80531	0.007749
ENSG00000074211	PPP2R2C	protein phosphatase 2 regulatory subunit Bgamma	4	-2.33556	0.007763
ENSG00000205795	CYS1	cystin 1	2	2.337757	0.007841
ENSG00000008394	MGST1	microsomal glutathione S-transferase 1	12	-2.34122	0.007915
ENSG00000198768	APCDD1L	APC down-regulated 1 like	20	3.610118	0.007915
ENSG00000185760	KCNQ5	potassium voltage-gated channel subfamily Q member 5	6	2.085402	0.007949
ENSG00000109625	CPZ	carboxypeptidase Z	4	2.767593	0.008095
ENSG00000160447	PKN3	protein kinase N3	9	2.637575	0.008119
ENSG00000081237	PTPRC	protein tyrosine phosphatase, receptor type C	1	-4.90131	0.008211
ENSG00000175161	CADM2	cell adhesion molecule 2	3	-2.34576	0.008217
ENSG00000136383	ALPK3	alpha kinase 3	15	2.426499	0.008429

ENSG00000134240	HMGCS2	3-hydroxy-3-methylglutaryl-CoA synthase 2	1	-4.20991	0.008594
ENSG00000187840	EIF4EBP1	eukaryotic translation initiation factor 4E binding protein 1	8	2.155867	0.008709
ENSG00000276644	DACH1	dachshund family transcription factor 1	13	-3.04688	0.008882
ENSG00000135298	ADGRB3	adhesion G protein-coupled receptor B3	6	-2.63691	0.008934
ENSG00000129116	PALLD	palladin, cytoskeletal associated protein	4	1.845714	0.009257
ENSG00000161642	ZNF385A	zinc finger protein 385A	12	1.785001	0.009257
ENSG00000163874	ZC3H12A	zinc finger CCCH-type containing 12A	1	2.087378	0.009475
ENSG00000081181	ARG2	arginase 2	14	2.953317	0.009611
ENSG00000149972	CNTN5	contactin 5	11	-3.87434	0.009854
ENSG00000114270	COL7A1	collagen type VII alpha 1 chain	3	2.250944	0.010689
ENSG00000120457	KCNJ5	potassium voltage-gated channel subfamily J member 5	11	3.759178	0.010856
ENSG00000162576	MXRA8	matrix remodeling associated 8	1	1.794763	0.010921
ENSG00000144645	OSBPL10	oxysterol binding protein like 10	3	1.670979	0.011079
ENSG00000166106	ADAMTS15	ADAM metallopeptidase with thrombospondin type 1 motif 15	11	-2.66707	0.011143
ENSG00000105327	BBC3	BCL2 binding component 3	19	2.313685	0.011292
ENSG00000176956	LY6H	lymphocyte antigen 6 family member H	8	-2.54199	0.011411
ENSG00000182492	BGN	biglycan	X	1.949341	0.011415
ENSG00000197959	DNM3	dynamin 3	1	2.472812	0.011626
ENSG00000062038	CDH3	cadherin 3	16	-2.9253	0.011911
ENSG00000131471	AOC3	amine oxidase, copper containing 3	17	2.927403	0.011911
ENSG00000128590	DNAJB9	DnaJ heat shock protein family (Hsp40) member B9	7	1.838445	0.012097
ENSG00000179772	FOXS1	forkhead box S1	20	4.917807	0.012168
ENSG00000113296	THBS4	thrombospondin 4	5	2.213747	0.012321
ENSG00000171243	SOSTDC1	sclerostin domain containing 1	7	-2.30346	0.012321
ENSG00000164434	FABP7	fatty acid binding protein 7	6	-1.99474	0.012635
ENSG00000168209	DDIT4	DNA damage inducible transcript 4	10	1.800716	0.012653
ENSG00000101825	MXRA5	matrix remodeling associated 5	X	2.694155	0.012919
ENSG00000113739	STC2	stanniocalcin 2	5	2.544353	0.013101
ENSG00000139318	DUSP6	dual specificity phosphatase 6	12	2.315699	0.013487
ENSG00000100647	SUSD6	sushi domain containing 6	14	1.618747	0.013487
ENSG00000139915	MDGA2	MAM domain containing glycosylphosphatidylinositol anchor 2	14	-3.08051	0.013577
ENSG00000166073	GPR176	G protein-coupled receptor 176	15	2.150567	0.013577
ENSG00000157445	CACNA2D3	calcium voltage-gated channel auxiliary subunit alpha2delta 3	3	-4.88154	0.013577
ENSG00000149380	P4HA3	prolyl 4-hydroxylase subunit alpha 3	11	2.119685	0.01396
ENSG00000070404	FSTL3	follistatin like 3	19	1.809164	0.014321
ENSG00000142449	FBN3	fibrillin 3	19	-2.79496	0.014556
ENSG00000214376	VSTM5	V-set and transmembrane domain containing 5	11	-3.17586	0.014727
ENSG00000174945	AMZ1	archaelysin family metallopeptidase 1	7	3.40641	0.015234
ENSG00000187678	SPRY4	sprouty RTK signaling antagonist 4	5	2.103408	0.015403
ENSG00000127951	FGL2	fibrinogen like 2	7	-2.88328	0.015453
ENSG00000156475	PPP2R2B	protein phosphatase 2 regulatory subunit Bbeta	5	-2.51934	0.015717
ENSG00000151012	SLC7A11	solute carrier family 7 member 11	4	2.368385	0.015758
ENSG00000187889	FYB2	FYN binding protein 2	1	-2.64452	0.015758
ENSG00000179862	CITED4	Cbp/p300 interacting transactivator with Glu/Asp rich carboxy-terminal domain 4	1	2.303319	0.015758
ENSG00000111424	VDR	vitamin D receptor	12	1.786023	0.015758
ENSG00000113594	LIFR	LIF receptor alpha	5	-2.07121	0.016091
ENSG00000028277	POU2F2	POU class 2 homeobox 2	19	3.841209	0.016091
ENSG00000165973	NELL1	neural EGFL like 1	11	-4.97637	0.016289
ENSG00000113140	SPARC	secreted protein acidic and cysteine rich	5	1.728723	0.016336
ENSG00000134258	VTCN1	V-set domain containing T cell activation inhibitor 1	1	-4.60646	0.016478
ENSG00000123685	BATF3	basic leucine zipper ATF-like transcription factor 3	1	4.087364	0.016666
ENSG00000122035	RASL11A	RAS like family 11 member A	13	4.014072	0.017021
ENSG00000198948	MFAP3L	microfibril associated protein 3 like	4	1.629164	0.017045
ENSG00000173641	HSPB7	heat shock protein family B (small) member 7	1	2.001169	0.017045
ENSG00000169860	P2RY1	purinergic receptor P2Y1	3	-2.37264	0.017045
ENSG00000198729	PPP1R14C	protein phosphatase 1 regulatory inhibitor subunit 14C	6	1.878223	0.017069
ENSG00000122861	PLAU	plasminogen activator, urokinase	10	2.785297	0.017388
ENSG00000086991	NOX4	NADPH oxidase 4	11	3.026367	0.017688
ENSG00000164690	SHH	sonic hedgehog	7	-2.90044	0.01777
ENSG00000171246	NPTX1	neuronal pentraxin 1	17	-5.39865	0.017918
ENSG00000151693	ASAP2	ArfGAP with SH3 domain, ankyrin repeat and PH domain 2	2	2.109436	0.018542
ENSG00000120053	GOT1	glutamic-oxaloacetic transaminase 1	10	1.884809	0.018651

ENSG00000139926	FRMD6	FERM domain containing 6	14	1.664297	0.01892
ENSG00000128242	GAL3ST1	galactose-3-O-sulfotransferase 1	22	-2.43707	0.01892
ENSG00000050555	LAMC3	laminin subunit gamma 3	9	1.896703	0.01892
ENSG00000128918	ALDH1A2	aldehyde dehydrogenase 1 family member A2	15	-3.19878	0.019358
ENSG00000038945	MSR1	macrophage scavenger receptor 1	8	-2.89705	0.019593
ENSG00000163328	GPR155	G protein-coupled receptor 155	2	-1.97948	0.019627
ENSG00000157388	CACNA1D	calcium voltage-gated channel subunit alpha1 D	3	2.346478	0.019857
ENSG00000120156	TEK	TEK receptor tyrosine kinase	9	3.613812	0.020452
ENSG00000167771	RCOR2	REST corepressor 2	11	2.156103	0.020561
ENSG00000130720	FIBCD1	fibrinogen C domain containing 1	9	3.382993	0.020578
ENSG00000145936	KCNMB1	potassium calcium-activated channel subfamily M regulatory beta subunit 1	5	2.144174	0.021225
ENSG00000156564	LRFN2	leucine rich repeat and fibronectin type III domain containing 2	6	-4.4226	0.021225
ENSG00000196659	TTC30B	tetratricopeptide repeat domain 30B	2	-2.09671	0.021362
ENSG00000149633	KIAA1755	KIAA1755	20	1.908944	0.021647
ENSG00000092871	RFFL	ring finger and FYVE like domain containing E3 ubiquitin protein ligase	17	1.639331	0.021783
ENSG00000086967	MYBPC2	myosin binding protein C, fast type	19	4.063496	0.021862
ENSG00000178401	DNAJC22	DnaJ heat shock protein family (Hsp40) member C22	12	2.537998	0.021999
ENSG00000168461	RAB31	RAB31, member RAS oncogene family	18	1.736015	0.022063
ENSG00000182168	UNC5C	unc-5 netrin receptor C	4	-1.78426	0.022741
ENSG00000185737	NRG3	neuregulin 3	10	-2.41994	0.022741
ENSG00000130203	APOE	apolipoprotein E	19	-2.35875	0.022741
ENSG00000181856	SLC2A4	solute carrier family 2 member 4	17	2.970092	0.023577
ENSG00000143001	TMEM61	transmembrane protein 61	1	4.329885	0.023869
ENSG00000006638	TBXA2R	thromboxane A2 receptor	19	3.177783	0.023869
ENSG00000083782	EPYC	epiphycan	12	-2.01967	0.023869
ENSG00000151490	PTPRO	protein tyrosine phosphatase, receptor type O	12	-2.05192	0.024359
ENSG00000168488	ATXN2L	ataxin 2 like	16	1.539788	0.02436
ENSG00000203883	SOX18	SRY-box 18	20	3.365738	0.02453
ENSG00000099953	MMP11	matrix metallopeptidase 11	22	2.807997	0.025069
ENSG00000206384	COL6A6	collagen type VI alpha 6 chain	3	-4.46808	0.025109
ENSG00000139197	PEX5	peroxisomal biogenesis factor 5	12	1.416173	0.025342
ENSG00000113407	TARS	threonyl-tRNA synthetase	5	1.484487	0.02584
ENSG00000176971	FIBIN	fin bud initiation factor homolog (zebrafish)	11	2.019151	0.026007
ENSG00000116455	WDR77	WD repeat domain 77	1	-1.47156	0.026223
ENSG00000168079	SCARA5	scavenger receptor class A member 5	8	-2.13929	0.02826
ENSG00000170323	FABP4	fatty acid binding protein 4	8	-4.15948	0.028554
ENSG00000114200	BCHE	butyrylcholinesterase	3	-2.22022	0.028591
ENSG00000188517	COL25A1	collagen type XXV alpha 1 chain	4	2.417723	0.0286
ENSG00000141582	CBX4	chromobox 4	17	1.791104	0.0286
ENSG00000183044	ABAT	4-aminobutyrate aminotransferase	16	-1.92589	0.028883
ENSG00000133169	BEX1	brain expressed X-linked 1	X	-2.25389	0.028886
ENSG00000164120	HPGD	15-hydroxyprostaglandin dehydrogenase	4	-3.49739	0.029066
ENSG00000173705	SUSD5	sushi domain containing 5	3	-1.50534	0.029066
ENSG00000109854	HTATIP2	HIV-1 Tat interactive protein 2	11	2.045962	0.029343
ENSG00000082641	NFE2L1	nuclear factor, erythroid 2 like 1	17	1.462458	0.0297
ENSG00000137868	STRA6	stimulated by retinoic acid 6	15	-2.79125	0.029745
ENSG00000017483	SLC38A5	solute carrier family 38 member 5	X	3.041166	0.029925
ENSG00000174951	FUT1	fucosyltransferase 1 (H blood group)	19	2.935693	0.029925
ENSG00000134548	SPX	spexin hormone	12	-3.05268	0.030581
ENSG00000196083	IL1RAP	interleukin 1 receptor accessory protein	3	1.63175	0.030605
ENSG00000100427	MLC1	megalencephalic leukoencephalopathy with subcortical cysts 1	22	-1.93693	0.030701
ENSG00000102683	SGCG	sarcoglycan gamma	13	3.950558	0.031752
ENSG00000204403	CASP12	caspase 12 (gene/pseudogene)	11	-3.29607	0.031955
ENSG00000141448	GATA6	GATA binding protein 6	18	4.460068	0.032096
ENSG00000132821	VSTM2L	V-set and transmembrane domain containing 2 like	20	-2.2173	0.032096
ENSG00000138642	HERC6	HECT and RLD domain containing E3 ubiquitin protein ligase family member 6	4	-2.14888	0.032453
ENSG00000145423	SFRP2	secreted frizzled related protein 2	4	-3.96995	0.032453
ENSG00000173926	Mar-03	membrane associated ring-CH-type finger 3	5	2.313584	0.032971
ENSG00000181790	ADGRB1	adhesion G protein-coupled receptor B1	8	-3.09604	0.033406
ENSG00000165023	DIRAS2	DIRAS family GTPase 2	9	2.794414	0.033406
ENSG00000118231	CRYGD	crystallin gamma D	2	-4.45679	0.033594
ENSG00000204262	COL5A2	collagen type V alpha 2 chain	2	2.867785	0.033831
ENSG00000075643	MOCOS	molybdenum cofactor sulfurase	18	2.68523	0.034347
ENSG00000158859	ADAMTS4	ADAM metallopeptidase with thrombospondin type 1 motif 4	1	2.441531	0.034412
ENSG00000144057	ST6GAL2	ST6 beta-galactoside alpha-2,6-sialyltransferase 2	2	1.740645	0.035271

ENSG00000136160	EDNRB	endothelin receptor type B	13	-1.88948	0.035271
ENSG00000112208	BAG2	BCL2 associated athanogene 2	6	1.802342	0.035788
ENSG00000121871	SLITRK3	SLIT and NTRK like family member 3	3	-2.93571	0.036038
ENSG00000123496	IL13RA2	interleukin 13 receptor subunit alpha 2	X	-2.6249	0.036148
ENSG00000164796	CSMD3	CUB and Sushi multiple domains 3	8	-2.26159	0.036644
ENSG00000125657	TNFSF9	TNF superfamily member 9	19	2.755717	0.036862
ENSG00000159176	CSRP1	cysteine and glycine rich protein 1	1	1.77041	0.037206
ENSG00000158292	GPR153	G protein-coupled receptor 153	1	1.696128	0.03745
ENSG00000135114	OASL	2'-5'-oligoadenylate synthetase like	12	-3.21733	0.03745
ENSG00000176438	SYNE3	spectrin repeat containing nuclear envelope family member 3	14	1.862076	0.03745
ENSG00000132639	SNAP25	synaptosome associated protein 25	20	-1.82745	0.03745
ENSG00000178235	SLITRK1	SLIT and NTRK like family member 1	13	-3.46143	0.03747
ENSG00000117472	TSPAN1	tetraspanin 1	1	2.814205	0.037495
ENSG00000112297	CRYBG1	crystallin beta-gamma domain containing 1	6	4.326423	0.037531
ENSG00000119917	IFIT3	interferon induced protein with tetratricopeptide repeats 3	10	-1.89577	0.037535
ENSG00000229998	PPP1R18	protein phosphatase 1 regulatory subunit 18	6	2.309486	0.03882
ENSG00000197565	COL4A6	collagen type IV alpha 6 chain	X	-1.9154	0.038984
ENSG00000116191	RALGPS2	Ral GEF with PH domain and SH3 binding motif 2	1	-1.68828	0.039421
ENSG00000091831	ESR1	estrogen receptor 1	6	-3.07541	0.039544
ENSG00000155304	HSPA13	heat shock protein family A (Hsp70) member 13	21	1.642901	0.03984
ENSG00000166592	RRAD	RRAD, Ras related glycolysis inhibitor and calcium channel regulator	16	3.224295	0.04019
ENSG00000163285	GABRG1	gamma-aminobutyric acid type A receptor gamma1 subunit	4	-2.99654	0.04019
ENSG00000110693	SOX6	SRY-box 6	11	-1.66854	0.040335
ENSG00000280165	PCDH20	protocadherin 20	13	-3.53934	0.04059
ENSG00000140600	SH3GL3	SH3 domain containing GRB2 like 3, endophilin A3	15	-2.56446	0.041015
ENSG00000188042	ARL4C	ADP ribosylation factor like GTPase 4C	2	2.245759	0.041356
ENSG00000277015	SALL3	spalt like transcription factor 3	18	-4.17336	0.041427
ENSG00000249992	TMEM158	transmembrane protein 158 (gene/pseudogene)	3	-2.46857	0.041894
ENSG00000153208	MERTK	MER proto-oncogene, tyrosine kinase	2	1.790734	0.041927
ENSG00000117114	ADGRL2	adhesion G protein-coupled receptor L2	1	-1.66186	0.041973
ENSG00000165553	NGB	neuroglobin	14	2.647287	0.042411
ENSG00000142871	CYR61	cysteine rich angiogenic inducer 61	1	2.153308	0.04334
ENSG00000132434	LANCL2	LanC like 2	7	-1.50838	0.043688
ENSG00000196557	CACNA1H	calcium voltage-gated channel subunit alpha1 H	16	2.196503	0.044886
ENSG00000051108	HERPUD1	homocysteine inducible ER protein with ubiquitin like domain 1	16	1.548746	0.044886
ENSG00000213316	LTC4S	leukotriene C4 synthase	5	2.213829	0.045149
ENSG00000206530	CFAP44	cilia and flagella associated protein 44	3	-2.0225	0.045605
ENSG00000103023	PRSS54	serine protease 54	16	4.003933	0.048222
ENSG00000186847	KRT14	keratin 14	17	3.179133	0.049798

Appendix 5

The base-pair sequence of homology director repair (HDR) template for generating mutant TRPV4 hiPSC lines

HDR template for TRPV4 c.819C>G (p.F273L) mutation introduction

ATGACCGTCCCCTGCCCCCAGGTCAGACAGCCCTGCACATCGCCATTGAGCGTCGC
TGCAAACACTACGTGGAACTTCTCGTGGCCCAGGGAGCTGATGTtCAtGCCCAGGCtC
GaGGaCGCTTCTTgCAGCCCAAGGATGAGGGGGGCTACTTCTACTTTGGTAAGGAGG
GGCCTGGTGGGGGCTGACAGCATGCTGGAGAAGCATGGCGGGAGATAGCATGATA
CT

HDR template for TRPV4 TRPV4 c.2396C>T (p.P799L)

TCTGAGGGGTTCCCCATGACCCTCTGCTTGGGCCCTGCCAGGGTGGATGAGGTGAA
CTGGTCTCACTGGAACCAGAACTTGGGCATCATCAACGAGGACCtCGGCAAGAATG
AGACaTAtCAaTAcTAcGGCTTCTCGCATACCGTGGGCCGCCTCCGCAGGGGTGAGTG
GAGGGGCGGGTGCGGAGGGGAGCCCCAGTCCATTCTCATCACGAATTTGCTTTGAG
CAG

Red highlight: introduced mutation

Blue highlight: synonymous codon

Lowercase: base changes

Appendix 6

SNP array and SNPduo analysis results of TRPV4-F273L-2 hiPSC line

Victorian Clinical Genetics Services
Murdoch Childrens Research Institute
Flemington Road, Parkville, VIC 3052 Australia
P +61 1300 118247 F +61 3 8341 6390
W vcgs.org.au ABN 51 007 032 760

LIMS Report #: 430998

Patient: F273L #2 F273I #2

Mr. David Francis
Victorian Clinical Genetic Services
Level 4/50 Flemington Road
PARKVILLE VIC 3052

DOB: Unknown
Sex: Unknown
VCGS sample ID: 18C101525
Date collected: 05-Mar-2018
Date received: 05-Mar-2018
Date reported: 12-Apr-2018
Source: Cell Pellet
Ext. sample ID:
Ext. patient ID:

Cytogenetics Laboratory

Specimen source Cell Pellet

Molecular karyotype

Array type	Illumina Infinium GSA-24 v1.0
Resolution	0.50Mb
Assembly	hg19 / GRCh37 (Feb 2009)
Molecular karyotype	arr(1-22)x2,(XY)x1
Result	NO ANEUPLOIDIES DETECTED

Interpretation
Male molecular karyotype. No aneuploidies were detected in this sample.

SNPduo comparative analysis of the microarray genotyping data was performed using this sample and previous sample PB001.1 (Lab No 15C109167). Analysis has shown identical (>99.9%) genotypes for the entire genome, indicating that the two samples are from the same individual.

Molecular karyotyping is limited in its ability to detect low grade mosaicism and genomic copy number changes below the resolution stated. Balanced rearrangements and Robertsonian translocations will not be detected. This test does not exclude single gene disorders caused by sequence mutations or trinucleotide repeat expansions (such as fragile X syndrome, Huntington disease, some spinocerebellar ataxias, Friedreich ataxia and myotonic dystrophy) . Testing for fragile X syndrome should be considered in individuals with developmental delay/ intellectual disability. Copy number changes that do not contain genes, are well established polymorphisms, or are assessed as being of unlikely clinical significance (based on available evidence), will not be reported. Reporting of regions of homozygosity (>5Mb) is dependent on referral setting and clinical indication. Please contact the laboratory if a recessive disorder is suspected. Interpretation is based on the UCSC GRCh37/hg19 human reference sequence.

Validated: 12-Apr-2018 by Kathy Butler

Enquiries: +61 1300 117 824

PATHOLOGY REPORT

END OF TEST REPORT

FINAL REPORT

Accredited for compliance with NPAAC Standards and ISO 15189
Accreditation number: 3171

Appendix 7

SNP array and SNPduo analysis results of TRPV4-P799L-31 hiPSC line

VCGS Leaders in Genetic Health

Victorian Clinical Genetics Services
Murdoch Childrens Research Institute
Flemington Road, Parkville, VIC 3052 Australia
P +61 1300 118247 F +61 3 8341 6390
W vcgs.org.au ABN 51 007 032 760

LIMS Report #: 431002

Patient: P799L #31 P799I #31

Mr. David Francis
Victorian Clinical Genetic Services
Level 4/50 Flemington Road
PARKVILLE VIC 3052

DOB: Unknown
Sex: Unknown
VCGS sample ID: 18C101528
Date collected: 05-Mar-2018
Date received: 05-Mar-2018
Date reported: 12-Apr-2018
Source: Cell Pellet
Ext. sample ID:
Ext. patient ID:

Cytogenetics Laboratory

Specimen source Cell Pellet

Molecular karyotype

Array type	Illumina Infinium GSA-24 v1.0
Resolution	0.50Mb
Assembly	hg19 / GRCh37 (Feb 2009)
Molecular karyotype	arr(1-22)x2,(XY)x1
Result	NO ANEUPLOIDIES DETECTED

Interpretation
Male molecular karyotype. No aneuploidies were detected in this sample.

SNPduo comparative analysis of the microarray genotyping data was performed using this sample and previous sample PB001.1 (Lab No 15C109167). Analysis has shown identical (>99.9%) genotypes for the entire genome, indicating that the two samples are from the same individual.

Molecular karyotyping is limited in its ability to detect low grade mosaicism and genomic copy number changes below the resolution stated. Balanced rearrangements and Robertsonian translocations will not be detected. This test does not exclude single gene disorders caused by sequence mutations or trinucleotide repeat expansions (such as fragile X syndrome, Huntington disease, some spinocerebellar ataxias, Friedreich ataxia and myotonic dystrophy) . Testing for fragile X syndrome should be considered in individuals with developmental delay/ intellectual disability. Copy number changes that do not contain genes, are well established polymorphisms, or are assessed as being of unlikely clinical significance (based on available evidence), will not be reported. Reporting of regions of homozygosity (>5Mb) is dependent on referral setting and clinical indication. Please contact the laboratory if a recessive disorder is suspected. Interpretation is based on the UCSC GRCh37/hg19 human reference sequence.

Validated: 12-Apr-2018 by Kathy Butler

Enquiries: +61 1300 117 824

PATHOLOGY REPORT

END OF TEST REPORT

FINAL REPORT

RCPA The Royal College of Pathologists of Australasia
NATA
Accredited for compliance with NPAAC Standards and ISO 15189
Accreditation number: 3171

Appendix 8

The list of differentially expressed genes in F273L vs wild-type

Ensembl ID	Symbol	Gene name	Chr	LogFC	adj.P.Val
ENSG00000118785	SPP1	secreted phosphoprotein 1	4	-1.44443	2.78E-06
ENSG00000135069	PSAT1	phosphoserine aminotransferase 1	9	0.797917	3.32E-06
ENSG00000070669	ASNS	asparagine synthetase (glutamine-hydrolyzing)	7	0.742666	1.82E-05
ENSG00000151012	SLC7A11	solute carrier family 7 member 11	4	1.048232	4.53E-05
ENSG00000203697	CAPN8	calpain 8	1	-1.65221	7.19E-05
ENSG00000065320	NTN1	netrin 1	17	0.870143	7.58E-05
ENSG00000120057	SFRP5	secreted frizzled related protein 5	10	-0.60813	0.000201
ENSG00000198825	INPP5F	inositol polyphosphate-5-phosphatase F	10	0.816523	0.000201
ENSG00000148053	NTRK2	neurotrophic receptor tyrosine kinase 2	9	0.725069	0.000426
ENSG00000235941	HSPA1A	heat shock protein family A (Hsp70) member 1A	6	1.477076	0.000426
ENSG00000162706	CADM3	cell adhesion molecule 3	1	0.916661	0.000446
ENSG00000139209	SLC38A4	solute carrier family 38 member 4	12	0.727258	0.000495
ENSG00000105855	ITGB8	integrin subunit beta 8	7	1.181025	0.000501
ENSG00000108947	EFNB3	ephrin B3	17	0.632078	0.000752
ENSG00000145244	CORIN	corin, serine peptidase	4	1.35916	0.001052
ENSG00000164690	SHH	sonic hedgehog	7	2.135272	0.002167
ENSG00000176046	NUPR1	nuclear protein 1, transcriptional regulator	16	0.539405	0.002167
ENSG00000180155	LYNX1	Ly6/neurotoxin 1	8	-0.91892	0.002167
ENSG00000102359	SRPX2	sushi repeat containing protein, X-linked 2	X	-0.52054	0.002167
ENSG00000167123	CERCAM	cerebral endothelial cell adhesion molecule	9	-0.48843	0.002167
ENSG00000143126	CELSR2	cadherin EGF LAG seven-pass G-type receptor 2	1	0.887965	0.002167
ENSG00000159263	SIM2	single-minded family bHLH transcription factor 2	21	-1.23383	0.003073
ENSG00000169504	CLIC4	chloride intracellular channel 4	1	0.386847	0.003221
ENSG00000065911	MTHFD2	methylenetetrahydrofolate dehydrogenase (NADP+ dependent) 2, methenyltetrahydrofolate cyclohydrolase	2	0.410314	0.004047
ENSG00000180178	FAR2P1	fatty acyl-CoA reductase 2 pseudogene 1	2	3.027276	0.0044
ENSG00000144136	SLC20A1	solute carrier family 20 member 1	2	-0.49099	0.0044
ENSG00000168209	DDIT4	DNA damage inducible transcript 4	10	0.477143	0.004404
ENSG00000152785	BMP3	bone morphogenetic protein 3	4	-0.83768	0.004404
ENSG00000128965	CHAC1	ChaC glutathione specific gamma-glutamylcyclotransferase 1	15	0.551466	0.004558
ENSG00000274671	MARVELD2	MARVEL domain containing 2	5	-5.71497	0.004887
ENSG00000253846	PCDHGA10	protocadherin gamma subfamily A, 10	5	1.513653	0.004984
ENSG00000091513	TF	transferrin	3	0.713547	0.004984
ENSG00000155849	ELMO1	engulfment and cell motility 1	7	1.175221	0.005921
ENSG00000169136	ATF5	activating transcription factor 5	19	0.545144	0.007143
ENSG00000116985	BMP8B	bone morphogenetic protein 8b	1	-0.79096	0.007143
ENSG00000135218	CD36	CD36 molecule	7	0.714443	0.007186
ENSG00000135744	AGT	angiotensinogen	1	0.575205	0.007912
ENSG00000105281	SLC1A5	solute carrier family 1 member 5	19	0.438419	0.007912
ENSG00000137558	PI15	peptidase inhibitor 15	8	0.915541	0.008314
ENSG00000052802	MSMO1	methylsterol monooxygenase 1	4	0.390545	0.008808
ENSG00000160161	CILP2	cartilage intermediate layer protein 2	19	-0.92098	0.008808
ENSG00000178209	PLEC	plectin	8	-0.40846	0.011986
ENSG00000106105	GARS	glycyl-tRNA synthetase	7	0.312976	0.011986
ENSG00000170540	ARL6IP1	ADP ribosylation factor like GTPase 6 interacting protein 1	16	0.391426	0.012298
ENSG00000149633	KIAA1755	KIAA1755	20	-1.04576	0.012729
ENSG00000153130	SCOC	short coiled-coil protein	4	0.381351	0.012729
ENSG00000185477	GPRIN3	GPRIN family member 3	4	1.564324	0.012729
ENSG00000104368	PLAT	plasminogen activator, tissue type	8	1.954512	0.012729
ENSG00000276547	PCDHGB5	protocadherin gamma subfamily B, 5	5	1.385305	0.012729
ENSG00000095713	CRTAC1	cartilage acidic protein 1	10	-0.43292	0.013219
ENSG00000160752	FDPS	farnesyl diphosphate synthase	1	0.360999	0.013726
ENSG00000010810	FYN	FYN proto-oncogene, Src family tyrosine kinase	6	0.482919	0.013726
ENSG00000162413	KLHL21	kelch like family member 21	1	-0.39556	0.013726
ENSG00000168066	SF1	splicing factor 1	11	-0.36914	0.013726
ENSG00000177106	EPS8L2	EPS8 like 2	11	-0.37102	0.015141
ENSG00000196739	COL27A1	collagen type XXVII alpha 1 chain	9	-0.32449	0.015359
ENSG00000138834	MAPK8IP3	mitogen-activated protein kinase 8 interacting protein 3	16	-0.36457	0.015359
ENSG00000196517	SLC6A9	solute carrier family 6 member 9	1	0.5944	0.015359

ENSG00000185559	DLK1	delta like non-canonical Notch ligand 1	14	-0.30653	0.015359
ENSG00000164032	H2AFZ	H2A histone family member Z	4	0.332958	0.015493
ENSG00000110328	GALNT18	polypeptide N-acetylgalactosaminyltransferase 18	11	-0.59736	0.015493
ENSG00000010282	HHATL	hedgehog acyltransferase like	3	-1.1576	0.015493
ENSG00000196090	PTPRT	protein tyrosine phosphatase, receptor type T	20	1.382301	0.015493
ENSG00000123560	PLP1	proteolipid protein 1	X	0.911158	0.015493
ENSG00000170312	CDK1	cyclin dependent kinase 1	10	0.417513	0.015931
ENSG00000109654	TRIM2	tripartite motif containing 2	4	0.334549	0.016067
ENSG00000254996	ANKHD1-EIF4EBP3	ANKHD1-EIF4EBP3 readthrough	5	-0.76744	0.016067
ENSG00000171385	KCND3	potassium voltage-gated channel subfamily D member 3	1	1.206308	0.018957
ENSG00000131747	TOP2A	DNA topoisomerase II alpha	17	0.344817	0.018957
ENSG00000077152	UBE2T	ubiquitin conjugating enzyme E2 T	1	0.652006	0.018957
ENSG00000077274	CAPN6	calpain 6	X	-0.28332	0.018987
ENSG00000272636	DOC2B	double C2 domain beta	17	7.209303	0.018987
ENSG00000109610	SOD3	superoxide dismutase 3	4	-0.62783	0.019295
ENSG00000047932	GOPC	golgi associated PDZ and coiled-coil motif containing	6	-0.36725	0.020852
ENSG00000067715	SYT1	synaptotagmin 1	12	1.065233	0.020852
ENSG00000198373	WWP2	WW domain containing E3 ubiquitin protein ligase 2	16	-0.27756	0.020852
ENSG00000197555	SIPA1L1	signal induced proliferation associated 1 like 1	14	-0.33455	0.020852
ENSG00000163536	SERPINI1	serpin family I member 1	3	-0.44408	0.020852
ENSG00000197355	UAP1L1	UDP-N-acetylglucosamine pyrophosphorylase 1 like 1	9	-0.58792	0.020852
ENSG00000103335	PIEZO1	piezo type mechanosensitive ion channel component 1	16	-0.52507	0.020852
ENSG00000081760	AACS	acetoacetyl-CoA synthetase	12	-0.41232	0.020852
ENSG00000115902	SLC1A4	solute carrier family 1 member 4	2	0.471722	0.020852
ENSG00000140983	RHOT2	ras homolog family member T2	16	-0.47278	0.021129
ENSG00000076928	ARHGEF1	Rho guanine nucleotide exchange factor 1	19	-0.36934	0.02114
ENSG00000116299	KIAA1324	KIAA1324	1	1.03157	0.021356
ENSG00000121691	CAT	catalase	11	0.602454	0.022129
ENSG00000111897	SERINC1	serine incorporator 1	6	0.277499	0.022476
ENSG00000080986	NDC80	NDC80, kinetochore complex component	18	0.448658	0.022538
ENSG00000067225	PKM	pyruvate kinase M1/2	15	-0.27715	0.023471
ENSG00000166016	ABTB2	ankyrin repeat and BTB domain containing 2	11	-0.39517	0.023905
ENSG00000117632	STMN1	stathmin 1	1	0.319594	0.024472
ENSG00000137285	TUBB2B	tubulin beta 2B class IIb	6	0.41502	0.024472
ENSG00000138722	MMRN1	multimerin 1	4	0.804152	0.024472
ENSG00000011426	ANLN	anillin actin binding protein	7	0.381818	0.024472
ENSG00000101367	MAPRE1	microtubule associated protein RP/EB family member 1	20	0.309572	0.024472
ENSG00000139044	B4GALNT3	beta-1,4-N-acetyl-galactosaminyltransferase 3	12	-0.38614	0.024552
ENSG00000114646	CSPG5	chondroitin sulfate proteoglycan 5	3	1.188431	0.024783
ENSG00000125813	PAX1	paired box 1	20	-0.3292	0.025225
ENSG00000151490	PTPRO	protein tyrosine phosphatase, receptor type O	12	0.719597	0.02548
ENSG00000196562	SULF2	sulfatase 2	20	0.620278	0.0265
ENSG00000158008	EXTL1	exostosin like glycosyltransferase 1	1	-0.32615	0.0265
ENSG00000139734	DIAPH3	diaphanous related formin 3	13	0.543629	0.0265
ENSG00000164199	ADGRV1	adhesion G protein-coupled receptor V1	5	0.648007	0.0265
ENSG00000139514	SLC7A1	solute carrier family 7 member 1	13	0.424848	0.026525
ENSG00000278091	ZNF85	zinc finger protein 85	19	-4.54216	0.026733
ENSG00000262655	SPON1	spondin 1	11	0.638645	0.027895
ENSG00000178568	ERBB4	erb-b2 receptor tyrosine kinase 4	2	1.776689	0.028789
ENSG00000137876	RSL24D1	ribosomal L24 domain containing 1	15	0.32382	0.028789
ENSG00000244560	LOC155060	AI894139 pseudogene	7	-0.87846	0.028789
ENSG00000182492	BGN	biglycan	X	-0.397	0.029223
ENSG00000163993	S100P	S100 calcium binding protein P	4	0.986474	0.029223
ENSG00000135643	KCNMB4	potassium calcium-activated channel subfamily M regulatory beta subunit 4	12	1.213498	0.029223
ENSG00000107742	SPOCK2	SPARC (osteonectin), cwcv and kazal like domains proteoglycan 2	10	0.799411	0.029471
ENSG00000123243	ITIH5	inter-alpha-trypsin inhibitor heavy chain family member 5	10	0.780651	0.029471
ENSG00000072778	ACADVL	acyl-CoA dehydrogenase very long chain	17	-0.3541	0.029471
ENSG00000119147	C2orf40	chromosome 2 open reading frame 40	2	-0.40717	0.029471
ENSG00000131016	AKAP12	A-kinase anchoring protein 12	6	0.580875	0.029471
ENSG00000115896	PLCL1	phospholipase C like 1 (inactive)	2	0.996196	0.029777
ENSG00000183036	PCP4	Purkinje cell protein 4	21	0.978609	0.029777

ENSG00000007516	BAIAP3	BAI1 associated protein 3	16	1.676397	0.029777
ENSG00000169469	SPRR1B	small proline rich protein 1B	1	4.470353	0.029777
ENSG00000114993	RTKN	rhotekin	2	-0.36898	0.029777
ENSG00000162337	LRP5	LDL receptor related protein 5	11	-0.33751	0.029777
ENSG00000148840	PPRC1	peroxisome proliferator-activated receptor gamma, coactivator-related 1	10	-0.45031	0.029777
ENSG00000244486	SCARF2	scavenger receptor class F member 2	22	-0.39358	0.029777
ENSG00000169288	MRPL1	mitochondrial ribosomal protein L1	4	0.571831	0.029777
ENSG00000143061	IGSF3	immunoglobulin superfamily member 3	1	0.470208	0.029777
ENSG00000128944	KNSTRN	kinetochore localized astrin (SPAG5) binding protein	15	0.489839	0.029777
ENSG00000174611	KY	kyphoscoliosis peptidase	3	-0.54363	0.030022
ENSG00000198734	F5	coagulation factor V	1	2.286286	0.030617
ENSG00000266714	MYO15B	myosin XVB	17	-0.48616	0.031191
ENSG00000138413	IDH1	isocitrate dehydrogenase (NADP(+)) 1, cytosolic	2	0.288909	0.031353
ENSG00000107281	NPDC1	neural proliferation, differentiation and control 1	9	-0.46483	0.03223
ENSG00000178605	GTPBP6	GTP binding protein 6 (putative)	X	-0.43644	0.03223
ENSG00000019582	CD74	CD74 molecule	5	-0.47781	0.03223
ENSG00000184005	ST6GALNAC 3	ST6 N-acetylgalactosaminide alpha-2,6-sialyltransferase 3	1	1.163247	0.03223
ENSG00000136158	SPRY2	sprouty RTK signaling antagonist 2	13	-0.53507	0.032735
ENSG00000273993	PTPRK	protein tyrosine phosphatase, receptor type K	6	0.449559	0.032735
ENSG00000197774	EME2	essential meiotic structure-specific endonuclease subunit 2	16	-0.6975	0.032735
ENSG00000165271	NOL6	nucleolar protein 6	9	-0.46809	0.032735
ENSG00000124743	KLHL31	kelch like family member 31	6	-0.54981	0.033555
ENSG00000129566	TEP1	telomerase associated protein 1	14	-0.45076	0.033555
ENSG00000067064	IDI1	isopentenyl-diphosphate delta isomerase 1	10	0.289174	0.033555
ENSG00000123146	ADGRE5	adhesion G protein-coupled receptor E5	19	-0.54027	0.033758
ENSG00000168546	GFRA2	GDNF family receptor alpha 2	8	0.658736	0.033758
ENSG00000112761	WISP3	WNT1 inducible signaling pathway protein 3	6	-0.43391	0.033758
ENSG00000005513	SOX8	SRY-box 8	16	-0.31161	0.033758
ENSG00000171992	SYNPO	synaptopodin	5	-0.30031	0.03456
ENSG00000115946	PNO1	partner of NOB1 homolog	2	-0.64623	0.035025
ENSG00000063660	GPC1	glypican 1	2	-0.32598	0.036064
ENSG00000165458	INPPL1	inositol polyphosphate phosphatase like 1	11	-0.2647	0.036064
ENSG00000081842	PCDHA6	protocadherin alpha 6	5	-2.30429	0.036064
ENSG00000166225	FRS2	fibroblast growth factor receptor substrate 2	12	0.335538	0.036544
ENSG00000135924	DNAJB2	DnaJ heat shock protein family (Hsp40) member B2	2	-0.30015	0.036544
ENSG00000196549	MME	membrane metalloendopeptidase	3	0.869475	0.036544
ENSG00000163590	PPM1L	protein phosphatase, Mg2+/Mn2+ dependent 1L	3	0.549801	0.036544
ENSG00000128159	TUBGCP6	tubulin gamma complex associated protein 6	22	-0.37449	0.036544
ENSG00000165792	METTL17	methyltransferase like 17	14	-0.43279	0.036544
ENSG00000068654	POLR1A	RNA polymerase I subunit A	2	-0.39762	0.037419
ENSG00000173546	CSPG4	chondroitin sulfate proteoglycan 4	15	-0.40053	0.039433
ENSG00000120341	SEC16B	SEC16 homolog B, endoplasmic reticulum export factor	1	-0.36873	0.039433
ENSG00000134352	IL6ST	interleukin 6 signal transducer	5	0.258731	0.039433
ENSG00000084774	CAD	carbamoyl-phosphate synthetase 2, aspartate transcarbamylase, and dihydroorotase	2	-0.33014	0.039433
ENSG00000283158	MUC5AC	mucin 5AC, oligomeric mucus/gel-forming	11	2.826277	0.039433
ENSG00000168056	LTBP3	latent transforming growth factor beta binding protein 3	11	-0.32249	0.039433
ENSG00000155304	HSPA13	heat shock protein family A (Hsp70) member 13	21	0.355754	0.039433
ENSG00000113716	HMGXB3	HMG-box containing 3	5	-0.35694	0.039484
ENSG00000088756	ARHGAP28	Rho GTPase activating protein 28	18	0.612112	0.039484
ENSG00000159399	HK2	hexokinase 2	2	-0.48471	0.039484
ENSG00000261509	TP53TG3B	TP53 target 3B	16	5.823076	0.03949
ENSG00000169231	THBS3	thrombospondin 3	1	-0.35536	0.040647
ENSG00000169604	ANTXR1	anthrax toxin receptor 1	2	0.273313	0.040886
ENSG00000177707	NECTIN3	nectin cell adhesion molecule 3	3	0.749733	0.041292
ENSG00000160111	CPAMD8	C3 and PZP like, alpha-2-macroglobulin domain containing 8	19	-0.31379	0.041292
ENSG00000011028	MRC2	mannose receptor C type 2	17	-0.29083	0.041489
ENSG00000134201	GSTM5	glutathione S-transferase mu 5	1	0.585199	0.041489
ENSG00000158467	AHCYL2	adenosylhomocysteinase like 2	7	0.318198	0.041495
ENSG00000138073	PREB	prolactin regulatory element binding	2	-0.43243	0.041495
ENSG00000089199	CHGB	chromogranin B	20	0.40967	0.041761
ENSG00000196187	TMEM63A	transmembrane protein 63A	1	-0.31633	0.042117
ENSG00000164574	GALNT10	polypeptide N-acetylgalactosaminyltransferase 10	5	-0.27532	0.042788

ENSG00000163623	NKX6-1	NK6 homeobox 1	4	0.899182	0.042788
ENSG00000182087	TMEM259	transmembrane protein 259	19	-0.30644	0.042842
ENSG00000162909	CAPN2	calpain 2	1	-0.3137	0.043133
ENSG00000092621	PHGDH	phosphoglycerate dehydrogenase	1	0.301936	0.043133
ENSG00000173281	PPP1R3B	protein phosphatase 1 regulatory subunit 3B	8	0.345269	0.043133
ENSG00000147724	FAM135B	family with sequence similarity 135 member B	8	1.765657	0.043133
ENSG00000273749	CYFIP1	cytoplasmic FMR1 interacting protein 1	15	-0.39323	0.043133
ENSG00000282458	WASH5P	WAS protein family homolog 5 pseudogene	19	-0.35762	0.043133
ENSG00000078596	ITM2A	integral membrane protein 2A	X	0.212988	0.043133
ENSG00000100292	HMOX1	heme oxygenase 1	22	-0.62591	0.043873
ENSG00000119938	PPP1R3C	protein phosphatase 1 regulatory subunit 3C	10	0.374183	0.044413
ENSG00000137804	NUSAP1	nucleolar and spindle associated protein 1	15	0.293821	0.044413
ENSG00000115310	RTN4	reticulon 4	2	0.275141	0.044413
ENSG00000100889	PCK2	phosphoenolpyruvate carboxykinase 2, mitochondrial	14	0.49939	0.044413
ENSG00000153446	C16orf89	chromosome 16 open reading frame 89	16	-0.67983	0.044413
ENSG00000197119	SLC25A29	solute carrier family 25 member 29	14	-0.37441	0.044413
ENSG00000112531	QKI	QKI, KH domain containing RNA binding	6	0.265813	0.044413
ENSG00000154309	DISP1	dispatched RND transporter family member 1	1	-0.28394	0.045186
ENSG00000101003	GINS1	GINS complex subunit 1	20	0.783205	0.045186
ENSG00000116106	EPHA4	EPH receptor A4	2	0.580423	0.045303
ENSG00000105220	GPI	glucose-6-phosphate isomerase	19	-0.37	0.045303
ENSG00000110237	ARHGEF17	Rho guanine nucleotide exchange factor 17	11	-0.29022	0.045303
ENSG00000138623	SEMA7A	semaphorin 7A (John Milton Hagen blood group)	15	-0.39219	0.045303
ENSG00000101199	ARFGAP1	ADP ribosylation factor GTPase activating protein 1	20	-0.28665	0.045489
ENSG00000064300	NGFR	nerve growth factor receptor	17	-1.33708	0.045489
ENSG00000144677	CTDSPL	CTD small phosphatase like	3	-0.32001	0.045489
ENSG00000274810	NPHP3-ACAD11	NPHP3-ACAD11 readthrough (NMD candidate)	3	1.406088	0.045489
ENSG00000165905	LARGE2	LARGE xylosyl- and glucuronyltransferase 2	11	-0.43277	0.045489
ENSG00000100599	RIN3	Ras and Rab interactor 3	14	-0.42692	0.045489
ENSG00000139219	COL2A1	collagen type II alpha 1 chain	12	-0.25744	0.045489
ENSG00000048740	CELF2	CUGBP Elav-like family member 2	10	0.465527	0.045489
ENSG00000138669	PRKG2	protein kinase, cGMP-dependent, type II	4	0.562031	0.045568
ENSG00000169432	SCN9A	sodium voltage-gated channel alpha subunit 9	2	1.536523	0.045569
ENSG00000115252	PDE1A	phosphodiesterase 1A	2	1.138871	0.045569
ENSG00000272398	CD24	CD24 molecule	6	0.613106	0.045569
ENSG00000076604	TRAF4	TNF receptor associated factor 4	17	-0.34125	0.045569
ENSG00000108773	KAT2A	lysine acetyltransferase 2A	17	-0.4442	0.045569
ENSG00000144668	ITGA9	integrin subunit alpha 9	3	-0.39679	0.045796
ENSG00000114853	ZBTB47	zinc finger and BTB domain containing 47	3	-0.41916	0.045854
ENSG00000005249	PRKAR2B	protein kinase cAMP-dependent type II regulatory subunit beta	7	0.507221	0.045854
ENSG00000198856	OSTC	oligosaccharyltransferase complex non-catalytic subunit	4	0.255192	0.045854
ENSG00000128536	CDHR3	cadherin related family member 3	7	1.139931	0.045854
ENSG00000164932	CTHRC1	collagen triple helix repeat containing 1	8	-0.28419	0.045854
ENSG00000134333	LDHA	lactate dehydrogenase A	11	-0.33817	0.045854
ENSG00000163710	PCOLCE2	procollagen C-endopeptidase enhancer 2	3	0.229223	0.045982
ENSG00000090861	AARS	alanyl-tRNA synthetase	16	0.256759	0.04605
ENSG00000117308	GALE	UDP-galactose-4-epimerase	1	-0.41006	0.04605
ENSG00000119900	OGFRL1	opioid growth factor receptor like 1	6	0.249079	0.04605
ENSG00000118733	OLFM3	olfactomedin 3	1	3.581759	0.04605
ENSG00000127418	FGFRL1	fibroblast growth factor receptor like 1	4	-0.29244	0.04605
ENSG00000183963	SMTN	smoothelin	22	-0.30969	0.04605
ENSG00000171840	NINJ2	ninjurin 2	12	-1.21092	0.04605
ENSG00000183323	CCDC125	coiled-coil domain containing 125	5	1.093204	0.04605
ENSG00000197976	AKAP17A	A-kinase anchoring protein 17A	X	-0.36814	0.04605
ENSG00000103888	CEMIP	cell migration inducing hyaluronidase 1	15	-0.55222	0.04605
ENSG00000008710	PKD1	polycystin 1, transient receptor potential channel interacting	16	-0.25794	0.04605
ENSG00000125912	NCLN	nicalin	19	-0.37921	0.04605
ENSG00000049089	COL9A2	collagen type IX alpha 2 chain	1	-0.29367	0.04605
ENSG00000162734	PEA15	proliferation and apoptosis adaptor protein 15	1	0.308623	0.04605
ENSG00000137266	SLC22A23	solute carrier family 22 member 23	6	0.674057	0.046612
ENSG00000156515	HK1	hexokinase 1	10	-0.3041	0.046612
ENSG00000114771	AADAC	arylacetamide deacetylase	3	4.377156	0.046612
ENSG00000123064	DDX54	DEAD-box helicase 54	12	-0.44049	0.047115
ENSG00000111077	TNS2	tensin 2	12	-0.27706	0.047115
ENSG00000113407	TARS	threonyl-tRNA synthetase	5	0.305164	0.047115

ENSG00000138449	SLC40A1	solute carrier family 40 member 1	2	-0.28611	0.047239
ENSG00000196604	POTEF	POTE ankyrin domain family member F	2	3.786354	0.047239
ENSG00000198026	ZNF335	zinc finger protein 335	20	-0.40662	0.047239
ENSG00000143933	CALM2	calmodulin 2	2	0.225419	0.047239
ENSG00000174233	ADCY6	adenylate cyclase 6	12	-0.31457	0.047239
ENSG00000139324	TMTC3	transmembrane and tetratricopeptide repeat containing 3	12	0.348921	0.047239
ENSG00000181523	SGSH	N-sulfoglucosamine sulfohydrolase	17	-0.41374	0.047239
ENSG00000115594	IL1R1	interleukin 1 receptor type 1	2	-0.27254	0.047239
ENSG00000058453	CROCC	ciliary rootlet coiled-coil, rootletin	1	-0.50255	0.047239
ENSG00000134443	GRP	gastrin releasing peptide	18	-0.82431	0.047239
ENSG00000182628	SKA2	spindle and kinetochore associated complex subunit 2	17	0.382825	0.047239
ENSG00000163235	TGFA	transforming growth factor alpha	2	-0.45832	0.047239
ENSG00000277443	MARCKS	myristoylated alanine rich protein kinase C substrate	6	0.598585	0.047492
ENSG00000104852	SNRNP70	small nuclear ribonucleoprotein U1 subunit 70	19	-0.27579	0.047492
ENSG00000143127	ITGA10	integrin subunit alpha 10	1	-0.24908	0.047492
ENSG00000051009	FAM160A2	family with sequence similarity 160 member A2	11	-0.38924	0.049932
ENSG00000065357	DGKA	diacylglycerol kinase alpha	12	-0.4109	0.049932

Appendix 9

The list of differentially expressed genes in P799L vs wild-type

Ensembl ID	Symbol	Gene name	Chr	LogFC	adj.P.Val
ENSG00000118785	SPP1	secreted phosphoprotein 1	4	2.32233	8.68E-10
ENSG00000188257	PLA2G2A	phospholipase A2 group IIA	1	2.0022	5.57E-08
ENSG00000135678	CPM	carboxypeptidase M	12	1.19992	2.25E-07
ENSG00000181195	PENK	proenkephalin	8	1.542273	3.35E-07
ENSG00000106153	CHCHD2	coiled-coil-helix-coiled-coil-helix domain containing 2	7	-7.02335	3.82E-06
ENSG00000132031	MATN3	matrilin 3	2	0.862075	5.79E-06
ENSG00000149090	PAMR1	peptidase domain containing associated with muscle regeneration 1	11	1.137822	5.79E-06
ENSG00000108947	EFNB3	ephrin B3	17	-1.01608	1.14E-05
ENSG00000070669	ASNS	asparagine synthetase (glutamine-hydrolyzing)	7	-0.79053	1.14E-05
ENSG00000135069	PSAT1	phosphoserine aminotransferase 1	9	-0.69691	1.24E-05
ENSG00000137441	FGFBP2	fibroblast growth factor binding protein 2	4	1.140302	1.33E-05
ENSG00000168079	SCARA5	scavenger receptor class A member 5	8	1.03205	1.33E-05
ENSG00000157240	FZD1	frizzled class receptor 1	7	-0.78624	1.76E-05
ENSG00000134602	STK26	serine/threonine kinase 26	X	0.571512	1.76E-05
ENSG00000018625	ATP1A2	ATPase Na+/K+ transporting subunit alpha 2	1	-0.99399	1.76E-05
ENSG00000109158	GABRA4	gamma-aminobutyric acid type A receptor alpha4 subunit	4	2.367923	2.01E-05
ENSG00000065320	NTN1	netrin 1	17	-0.98812	2.44E-05
ENSG00000148773	MKI67	marker of proliferation Ki-67	10	-0.59033	3.41E-05
ENSG00000282908	FAT3	FAT atypical cadherin 3	11	1.006442	3.41E-05
ENSG00000048052	HDAC9	histone deacetylase 9	7	0.996754	3.43E-05
ENSG00000168209	DDIT4	DNA damage inducible transcript 4	10	-0.81183	3.74E-05
ENSG00000083857	FAT1	FAT atypical cadherin 1	4	0.574317	4.47E-05
ENSG00000100644	HIF1A	hypoxia inducible factor 1 alpha subunit	14	0.526271	6.62E-05
ENSG00000046653	GPM6B	glycoprotein M6B	X	-0.63894	6.91E-05
ENSG00000136158	SPRY2	sprouty RTK signaling antagonist 2	13	0.927679	7.49E-05
ENSG00000110328	GALNT18	polypeptide N-acetylgalactosaminyltransferase 18	11	0.875996	7.49E-05
ENSG00000265972	TXNIP	thioredoxin interacting protein	1	-0.70386	7.49E-05
ENSG00000175899	A2M	alpha-2-macroglobulin	12	1.217683	7.92E-05
ENSG00000102313	ITIH6	inter-alpha-trypsin inhibitor heavy chain family member 6	X	0.521965	8.39E-05
ENSG00000105664	COMP	cartilage oligomeric matrix protein	19	2.838419	8.76E-05
ENSG00000128965	CHAC1	ChaC glutathione specific gamma-glutamylcyclotransferase 1	15	-0.91394	9.76E-05
ENSG00000149294	NCAM1	neural cell adhesion molecule 1	11	-0.69754	0.000101
ENSG00000198648	STK39	serine/threonine kinase 39	2	0.534004	0.000101
ENSG00000109610	SOD3	superoxide dismutase 3	4	0.914988	0.000103
ENSG00000018236	CNTN1	contactin 1	12	0.813204	0.000106
ENSG00000164761	TNFRSF11B	TNF receptor superfamily member 11b	8	0.665478	0.000106
ENSG00000162706	CADM3	cell adhesion molecule 3	1	-1.29326	0.000116
ENSG00000155850	SLC26A2	solute carrier family 26 member 2	5	0.498571	0.000127
ENSG00000175161	CADM2	cell adhesion molecule 2	3	-0.86976	0.000128
ENSG00000137804	NUSAP1	nucleolar and spindle associated protein 1	15	-0.61084	0.00016
ENSG00000091129	NRCAM	neuronal cell adhesion molecule	7	0.569146	0.000172
ENSG00000131747	TOP2A	DNA topoisomerase II alpha	17	-0.5432	0.000184
ENSG00000198901	PRC1	protein regulator of cytokinesis 1	15	-0.62763	0.000216
ENSG00000140479	PCSK6	proprotein convertase subtilisin/kexin type 6	15	1.234488	0.00022
ENSG00000139970	RTN1	reticulon 1	14	-0.87659	0.000235
ENSG00000176890	TYMS	thymidylate synthetase	18	-0.61771	0.000235
ENSG00000092621	PHGDH	phosphoglycerate dehydrogenase	1	-0.55913	0.000243
ENSG00000141682	PMAIP1	phorbol-12-myristate-13-acetate-induced protein 1	18	1.94171	0.000272
ENSG00000196104	SPOCK3	SPARC (osteonectin), cwcv and kazal like domains proteoglycan 3	4	-1.1083	0.000272
ENSG00000182752	PAPPA	pappalysin 1	9	2.140732	0.000275
ENSG00000160161	CILP2	cartilage intermediate layer protein 2	19	0.973936	0.000343
ENSG00000138160	KIF11	kinesin family member 11	10	-0.59259	0.000348
ENSG00000070961	ATP2B1	ATPase plasma membrane Ca2+ transporting 1	12	0.501665	0.000349
ENSG00000166165	CKB	creatine kinase B	14	-0.96147	0.000389
ENSG00000088325	TPX2	TPX2, microtubule nucleation factor	20	-0.58182	0.000447
ENSG00000134802	SLC43A3	solute carrier family 43 member 3	11	0.620841	0.000452
ENSG00000171617	ENC1	ectodermal-neural cortex 1	5	-0.82267	0.000458

ENSG00000115380	EFEMP1	EGF containing fibulin extracellular matrix protein 1	2	-0.48166	0.000458
ENSG00000100292	HMOX1	heme oxygenase 1	22	0.919566	0.000458
ENSG00000077274	CAPN6	calpain 6	X	0.395182	0.000458
ENSG00000136160	EDNRB	endothelin receptor type B	13	-1.27062	0.000458
ENSG00000171848	RRM2	ribonucleotide reductase regulatory subunit M2	2	-0.69621	0.000458
ENSG00000164032	H2AFZ	H2A histone family member Z	4	-0.47247	0.000458
ENSG00000115594	IL1R1	interleukin 1 receptor type 1	2	0.475274	0.000468
ENSG00000159307	SCUBE1	signal peptide, CUB domain and EGF like domain containing 1	22	0.766309	0.000521
ENSG00000164161	HHIP	hedgehog interacting protein	4	-1.04745	0.000521
ENSG00000150051	MKX	mohawk homeobox	10	0.710355	0.000521
ENSG00000163110	PDLIM5	PDZ and LIM domain 5	4	0.47425	0.000521
ENSG00000116985	BMP8B	bone morphogenetic protein 8b	1	0.848564	0.000521
ENSG00000168952	STXBP6	syntaxin binding protein 6	14	1.201585	0.000551
ENSG00000006576	PHTF2	putative homeodomain transcription factor 2	7	0.425324	0.000602
ENSG00000013810	TACC3	transforming acidic coiled-coil containing protein 3	4	-0.67703	0.00062
ENSG00000171791	BCL2	BCL2, apoptosis regulator	18	0.646574	0.00063
ENSG00000164796	CSMD3	CUB and Sushi multiple domains 3	8	-1.36815	0.000654
ENSG00000135476	ESPL1	extra spindle pole bodies like 1, separase	12	-0.7735	0.000661
ENSG00000137807	KIF23	kinesin family member 23	15	-0.57064	0.000661
ENSG00000130766	SESN2	sestrin 2	1	-0.60958	0.000661
ENSG00000197769	MAP1LC3C	microtubule associated protein 1 light chain 3 gamma	1	-1.99552	0.000683
ENSG00000171819	ANGPTL7	angiopoietin like 7	1	-0.62937	0.000683
ENSG00000276043	UHRF1	ubiquitin like with PHD and ring finger domains 1	19	-0.80711	0.000683
ENSG00000138131	LOXL4	lysyl oxidase like 4	10	0.70397	0.000738
ENSG00000163453	IGFBP7	insulin like growth factor binding protein 7	4	1.27442	0.000746
ENSG00000020577	SAMD4A	sterile alpha motif domain containing 4A	14	0.519185	0.000821
ENSG00000156265	MAP3K7CL	MAP3K7 C-terminal like	21	0.925567	0.000867
ENSG00000174938	SEZ6L2	seizure related 6 homolog like 2	16	0.744517	0.000894
ENSG00000131620	ANO1	anoctamin 1	11	1.352199	0.000971
ENSG00000113657	DPYSL3	dihydropyrimidinase like 3	5	-0.5132	0.000989
ENSG00000170891	CYTL1	cytokine like 1	4	1.163283	0.001013
ENSG00000102174	PHEX	phosphate regulating endopeptidase homolog X-linked	X	0.767861	0.001022
ENSG00000130203	APOE	apolipoprotein E	19	-0.40818	0.001052
ENSG00000122176	FMOD	fibromodulin	1	0.362692	0.001052
ENSG00000163235	TGFA	transforming growth factor alpha	2	0.664603	0.001055
ENSG00000166508	MCM7	minichromosome maintenance complex component 7	7	-0.5839	0.001055
ENSG00000145623	OSMR	oncostatin M receptor	5	0.662607	0.001056
ENSG00000146197	SCUBE3	signal peptide, CUB domain and EGF like domain containing 3	6	-0.55204	0.001102
ENSG00000106537	TSPAN13	tetraspanin 13	7	0.603933	0.001102
ENSG00000105696	TMEM59L	transmembrane protein 59 like	19	-1.26683	0.00113
ENSG00000213347	MXD3	MAX dimerization protein 3	5	-0.79587	0.001244
ENSG00000151725	CENPU	centromere protein U	4	-0.67779	0.001265
ENSG00000049860	HEXB	hexosaminidase subunit beta	5	0.386285	0.001283
ENSG00000117632	STMN1	stathmin 1	1	-0.42056	0.001371
ENSG00000111371	SLC38A1	solute carrier family 38 member 1	12	-0.48889	0.001388
ENSG00000123485	HJURP	Holliday junction recognition protein	2	-0.69739	0.001411
ENSG00000120594	PLXDC2	plexin domain containing 2	10	0.439441	0.001411
ENSG00000129521	EGLN3	egl-9 family hypoxia inducible factor 3	14	-1.89038	0.001411
ENSG00000136153	LMO7	LIM domain 7	13	0.606534	0.00142
ENSG00000169679	BUB1	BUB1 mitotic checkpoint serine/threonine kinase	2	-0.65835	0.001443
ENSG00000164104	HMGB2	high mobility group box 2	4	-0.36622	0.001496
ENSG00000129244	ATP1B2	ATPase Na+/K+ transporting subunit beta 2	17	0.473098	0.00166
ENSG00000134684	YARS	tyrosyl-tRNA synthetase	1	-0.45511	0.00166
ENSG00000260916	CCPG1	cell cycle progression 1	15	0.41555	0.00166
ENSG00000198786	ND5	NADH dehydrogenase, subunit 5 (complex I)	MT	0.380786	0.00166
ENSG00000103888	CEMIP	cell migration inducing hyaluronidase 1	15	0.731019	0.00166
ENSG00000124762	CDKN1A	cyclin dependent kinase inhibitor 1A	6	0.525023	0.00166
ENSG00000146918	NCAPG2	non-SMC condensin II complex subunit G2	7	-0.59211	0.00166
ENSG00000173376	NDNF	neuron derived neurotrophic factor	4	-0.76845	0.001712
ENSG00000127863	TNFRSF19	TNF receptor superfamily member 19	13	-0.82676	0.001722
ENSG00000152377	SPOCK1	SPARC (osteonectin), cwcv and kazal like domains proteoglycan 1	5	1.075925	0.001764
ENSG00000280610	KIF15	kinesin family member 15	3	-0.57764	0.001764
ENSG00000100600	LGMN	legumain	14	0.581322	0.001835
ENSG00000169902	TPST1	tyrosylprotein sulfotransferase 1	7	0.47879	0.001835

ENSG00000140525	FANCI	Fanconi anemia complementation group I	15	-0.6446	0.001835
ENSG00000010292	NCAPD2	non-SMC condensin I complex subunit D2	12	-0.4921	0.001835
ENSG00000180354	MTURN	maturin, neural progenitor differentiation regulator homolog	7	-0.54078	0.001991
ENSG00000176619	LMNB2	lamin B2	19	-0.46536	0.002112
ENSG00000049323	LTBP1	latent transforming growth factor beta binding protein 1	2	0.393658	0.002195
ENSG00000082196	C1QTNF3	C1q and TNF related 3	5	0.307681	0.002303
ENSG00000077942	FBLN1	fibulin 1	22	-0.59352	0.002303
ENSG00000198948	MFAP3L	microfibril associated protein 3 like	4	0.470959	0.002303
ENSG00000135048	CEMIP2	cell migration inducing hyaluronidase 2	9	0.509642	0.002303
ENSG00000133112	TPT1	tumor protein, translationally-controlled 1	13	0.352366	0.002303
ENSG00000117724	CENPF	centromere protein F	1	-0.45229	0.002303
ENSG00000103257	SLC7A5	solute carrier family 7 member 5	16	-0.57094	0.002338
ENSG00000162591	MEGF6	multiple EGF like domains 6	1	-0.55554	0.002386
ENSG00000074410	CA12	carbonic anhydrase 12	15	0.333241	0.002399
ENSG00000123080	CDKN2C	cyclin dependent kinase inhibitor 2C	1	-0.68723	0.002456
ENSG00000232575	TUBB	tubulin beta class I	6	-0.35831	0.002484
ENSG00000135842	FAM129A	family with sequence similarity 129 member A	1	0.918066	0.002484
ENSG00000139220	PPFIA2	PTPRF interacting protein alpha 2	12	-1.07936	0.00258
ENSG00000104738	MCM4	minichromosome maintenance complex component 4	8	-0.45118	0.00258
ENSG00000183856	IQGAP3	IQ motif containing GTPase activating protein 3	1	-0.51575	0.002602
ENSG00000177732	SOX12	SRY-box 12	20	-0.51089	0.002655
ENSG00000116741	RGS2	regulator of G protein signaling 2	1	0.557553	0.002749
ENSG00000104332	SFRP1	secreted frizzled related protein 1	8	0.528599	0.002793
ENSG00000250722	SELENOP	selenoprotein P	5	-0.4213	0.002858
ENSG00000142089	IFITM3	interferon induced transmembrane protein 3	11	0.761141	0.002858
ENSG00000122966	CIT	citron rho-interacting serine/threonine kinase	12	-0.52751	0.002909
ENSG00000221818	EBF2	early B cell factor 2	8	3.115452	0.002965
ENSG00000117399	CDC20	cell division cycle 20	1	-0.81065	0.00305
ENSG00000215425	DDX39B	DExD-box helicase 39B	6	-0.41772	0.003053
ENSG00000156110	ADK	adenosine kinase	10	0.472964	0.003053
ENSG00000157456	CCNB2	cyclin B2	15	-0.60282	0.003174
ENSG00000109805	NCAPG	non-SMC condensin I complex subunit G	4	-0.64519	0.003421
ENSG00000135451	TROAP	trophinin associated protein	12	-0.70525	0.003446
ENSG00000135218	CD36	CD36 molecule	7	-0.85028	0.003448
ENSG00000113721	PDGFRB	platelet derived growth factor receptor beta	5	-0.35737	0.003448
ENSG00000276644	DACH1	dachshund family transcription factor 1	13	-0.99028	0.003448
ENSG00000088882	CPXM1	carboxypeptidase X, M14 family member 1	20	-0.35587	0.003448
ENSG00000081479	LRP2	LDL receptor related protein 2	2	-1.20723	0.003448
ENSG00000278191	CARS	cysteinyl-tRNA synthetase	11	-0.41977	0.003448
ENSG00000262655	SPON1	spondin 1	11	-0.83646	0.003448
ENSG00000095713	CRTAC1	cartilage acidic protein 1	10	-0.4517	0.003448
ENSG00000101439	CST3	cystatin C	20	0.656363	0.003448
ENSG00000102804	TSC22D1	TSC22 domain family member 1	13	0.301267	0.003448
ENSG00000274487	LOC440434	aminopeptidase puromycin sensitive pseudogene	17	-8.04509	0.003506
ENSG00000170540	ARL6IP1	ADP ribosylation factor like GTPase 6 interacting protein 1	16	-0.41293	0.003511
ENSG00000026559	KCNG1	potassium voltage-gated channel modifier subfamily G member 1	20	-0.84384	0.003559
ENSG00000011201	ANOS1	anosmin 1	X	0.568061	0.003582
ENSG00000123358	NR4A1	nuclear receptor subfamily 4 group A member 1	12	0.730355	0.003593
ENSG00000065911	MTHFD2	methylenetetrahydrofolate dehydrogenase (NADP+ dependent) 2, methenyltetrahydrofolate cyclohydrolase	2	-0.365	0.003799
ENSG00000198856	OSTC	oligosaccharyltransferase complex non-catalytic subunit	4	0.338677	0.003835
ENSG00000198825	INPP5F	inositol polyphosphate-5-phosphatase F	10	0.503111	0.003866
ENSG00000106829	TLE4	transducin like enhancer of split 4	9	-0.6133	0.00387
ENSG00000101412	E2F1	E2F transcription factor 1	20	-0.73273	0.003971
ENSG00000205978	NYNRIN	NYN domain and retroviral integrase containing	14	-0.38152	0.004037
ENSG00000129422	MTUS1	microtubule associated scaffold protein 1	8	0.519509	0.004054
ENSG00000100427	MLC1	megalencephalic leukoencephalopathy with subcortical cysts 1	22	-0.69587	0.004225
ENSG00000076382	SPAG5	sperm associated antigen 5	17	-0.49166	0.004321
ENSG00000180155	LYNX1	Ly6/neurotoxin 1	8	-0.71788	0.004321
ENSG00000123416	TUBA1B	tubulin alpha 1b	12	-0.37059	0.004349
ENSG00000100297	MCM5	minichromosome maintenance complex component 5	22	-0.65004	0.004386
ENSG00000145431	PDGFC	platelet derived growth factor C	4	-0.64526	0.004459
ENSG00000152990	ADGRA3	adhesion G protein-coupled receptor A3	4	0.308161	0.00456

ENSG00000161800	RACGAP1	Rac GTPase activating protein 1	12	-0.44082	0.00456
ENSG00000112118	MCM3	minichromosome maintenance complex component 3	6	-0.42347	0.004745
ENSG00000218336	TENM3	teneurin transmembrane protein 3	4	-0.37389	0.004747
ENSG00000011426	ANLN	anillin actin binding protein	7	-0.45408	0.004789
ENSG00000013619	MAMLD1	mastermind like domain containing 1	X	-0.6219	0.004789
ENSG00000166986	MARS	methionyl-tRNA synthetase	12	-0.39277	0.004977
ENSG00000166123	GPT2	glutamic--pyruvic transaminase 2	16	-0.37031	0.004977
ENSG00000125813	PAX1	paired box 1	20	-0.36848	0.005003
ENSG00000138722	MMRN1	multimerin 1	4	-1.24132	0.005138
ENSG00000034677	RNF19A	ring finger protein 19A, RBR E3 ubiquitin protein ligase	8	-0.52306	0.005576
ENSG00000139329	LUM	lumican	12	-0.27862	0.005674
ENSG00000156103	MMP16	matrix metallopeptidase 16	8	0.304121	0.005674
ENSG00000134690	CDCA8	cell division cycle associated 8	1	-0.74056	0.005722
ENSG00000175216	CKAP5	cytoskeleton associated protein 5	11	-0.29883	0.005722
ENSG00000132000	PODNL1	podocan like 1	19	1.336433	0.005781
ENSG00000176956	LY6H	lymphocyte antigen 6 family member H	8	-1.24999	0.005797
ENSG00000138092	CENPO	centromere protein O	2	-0.71229	0.005841
ENSG00000117151	CTBS	chitobiase	1	0.399948	0.005847
ENSG00000143476	DTL	denticleless E3 ubiquitin protein ligase homolog	1	-0.65574	0.005885
ENSG00000169607	CKAP2L	cytoskeleton associated protein 2 like	2	-0.55053	0.005968
ENSG00000111341	MGP	matrix Gla protein	12	0.754233	0.006047
ENSG00000079616	KIF22	kinesin family member 22	16	-0.59787	0.006047
ENSG00000115392	FANCL	Fanconi anemia complementation group L	2	0.608851	0.006101
ENSG00000100979	PLTP	phospholipid transfer protein	20	-0.78611	0.006304
ENSG00000206560	ANKRD28	ankyrin repeat domain 28	3	0.368924	0.006304
ENSG00000178031	ADAMTSL1	ADAMTS like 1	9	-1.02343	0.006318
ENSG00000153234	NR4A2	nuclear receptor subfamily 4 group A member 2	2	0.989063	0.006396
ENSG00000132670	PTPRA	protein tyrosine phosphatase, receptor type A	20	-0.34325	0.006433
ENSG00000211448	DIO2	iodothyronine deiodinase 2	14	-0.56911	0.006518
ENSG00000125740	FOSB	FosB proto-oncogene, AP-1 transcription factor subunit	19	1.489284	0.006564
ENSG00000156535	CD109	CD109 molecule	6	0.297069	0.006564
ENSG00000196136	SERPINA3	serpin family A member 3	14	0.3958	0.006564
ENSG00000156253	RWDD2B	RWD domain containing 2B	21	-0.79827	0.006564
ENSG00000050628	PTGER3	prostaglandin E receptor 3	1	1.215031	0.006658
ENSG00000162493	PDPN	podoplanin	1	0.291942	0.006667
ENSG00000164106	SCRG1	stimulator of chondrogenesis 1	4	0.383242	0.006713
ENSG00000121753	ADGRB2	adhesion G protein-coupled receptor B2	1	-0.53067	0.006936
ENSG00000082153	BZW1	basic leucine zipper and W2 domains 1	2	0.288218	0.006936
ENSG00000145386	CCNA2	cyclin A2	4	-0.50535	0.006946
ENSG00000126878	AIF1L	allograft inflammatory factor 1 like	9	-0.46167	0.007094
ENSG00000156218	ADAMTSL3	ADAMTS like 3	15	0.55964	0.007165
ENSG00000135535	CD164	CD164 molecule	6	0.298067	0.007182
ENSG00000280641	CDH4	cadherin 4	20	2.297072	0.007212
ENSG00000253305	PCDHGB6	protocadherin gamma subfamily B, 6	5	-0.54462	0.007214
ENSG00000013573	DDX11	DEAD/H-box helicase 11	12	-0.64072	0.007368
ENSG00000060709	RIMBP2	RIMS binding protein 2	12	0.575924	0.0074
ENSG00000167325	RRM1	ribonucleotide reductase catalytic subunit M1	11	-0.34793	0.007476
ENSG00000112096	SOD2	superoxide dismutase 2	6	0.32828	0.007476
ENSG00000171241	SHCBP1	SHC binding and spindle associated 1	16	-0.65054	0.00775
ENSG00000003096	KLHL13	kelch like family member 13	X	0.613902	0.00775
ENSG00000158258	CLSTN2	calsyntenin 2	3	-0.82823	0.007778
ENSG00000168481	LGI3	leucine rich repeat LGI family member 3	8	-1.05784	0.007848
ENSG00000154864	PIEZO2	piezo type mechanosensitive ion channel component 2	18	-0.34703	0.007976
ENSG00000187678	SPRY4	sprouty RTK signaling antagonist 4	5	1.238924	0.007987
ENSG00000139209	SLC38A4	solute carrier family 38 member 4	12	-0.52023	0.008169
ENSG00000111206	FOXM1	forkhead box M1	12	-0.56428	0.008169
ENSG00000160801	PTH1R	parathyroid hormone 1 receptor	3	0.41383	0.008193
ENSG00000134258	VTCN1	V-set domain containing T cell activation inhibitor 1	1	0.90733	0.008231
ENSG00000171714	ANO5	anoctamin 5	11	1.505424	0.008231
ENSG00000106688	SLC1A1	solute carrier family 1 member 1	9	-0.37529	0.008652
ENSG00000165244	ZNF367	zinc finger protein 367	9	-0.68878	0.00874
ENSG00000153446	C16orf89	chromosome 16 open reading frame 89	16	0.686747	0.008765
ENSG00000100196	KDELR3	KDEL endoplasmic reticulum protein retention receptor 3	22	0.323844	0.008892
ENSG00000164530	PI16	peptidase inhibitor 16	6	-1.25627	0.008954

ENSG00000137801	THBS1	thrombospondin 1	15	0.261826	0.008954
ENSG00000257315	ZC3H11A	zinc finger CCCH-type containing 11A	1	0.32046	0.00901
ENSG00000182836	PLCXD3	phosphatidylinositol specific phospholipase C X domain containing 3	5	-1.0272	0.0091
ENSG00000119147	C2orf40	chromosome 2 open reading frame 40	2	0.416551	0.0091
ENSG00000188486	H2AFX	H2A histone family member X	11	-0.47606	0.009362
ENSG00000180332	KCTD4	potassium channel tetramerization domain containing 4	13	0.511752	0.009388
ENSG00000065361	ERBB3	erb-b2 receptor tyrosine kinase 3	12	-0.48062	0.009466
ENSG00000073910	FRY	FRY microtubule binding protein	13	0.276088	0.009712
ENSG00000146555	SDK1	sidekick cell adhesion molecule 1	7	-1.29977	0.009712
ENSG00000198898	CAPZA2	capping actin protein of muscle Z-line alpha subunit 2	7	0.359944	0.009784
ENSG00000120708	TGFBI	transforming growth factor beta induced	5	-0.55393	0.010016
ENSG00000152818	UTRN	utrophin	6	0.306733	0.010091
ENSG00000080986	NDC80	NDC80, kinetochore complex component	18	-0.50146	0.010091
ENSG00000169946	ZFPM2	zinc finger protein, FOG family member 2	8	-0.47499	0.010201
ENSG00000181019	NQO1	NAD(P)H quinone dehydrogenase 1	16	0.48961	0.010201
ENSG00000090861	AARS	alanyl-tRNA synthetase	16	-0.30657	0.010201
ENSG00000139318	DUSP6	dual specificity phosphatase 6	12	1.141225	0.010274
ENSG00000137941	TTLL7	tubulin tyrosine ligase like 7	1	0.794076	0.010274
ENSG00000078295	ADCY2	adenylate cyclase 2	5	-0.27487	0.010274
ENSG00000094804	CDC6	cell division cycle 6	17	-0.77409	0.010274
ENSG00000051108	HERPUD1	homocysteine inducible ER protein with ubiquitin like domain 1	16	-0.35267	0.010327
ENSG00000149451	ADAM33	ADAM metallopeptidase domain 33	20	-0.51889	0.010447
ENSG00000183576	SETD3	SET domain containing 3	14	-0.30612	0.010447
ENSG00000141314	RHBDL3	rhomboid like 3	17	-0.60263	0.010447
ENSG00000135919	SERPINE2	serpin family E member 2	2	0.417067	0.010607
ENSG00000111665	CDCA3	cell division cycle associated 3	12	-0.64489	0.010663
ENSG00000144136	SLC20A1	solute carrier family 20 member 1	2	0.344929	0.010789
ENSG00000196549	MME	membrane metalloendopeptidase	3	0.945656	0.011164
ENSG00000112761	WISP3	WNT1 inducible signaling pathway protein 3	6	0.42802	0.011164
ENSG00000162738	VANGL2	VANGL planar cell polarity protein 2	1	-0.74347	0.011164
ENSG00000110700	RPS13	ribosomal protein S13	11	0.320982	0.011164
ENSG00000147408	CSGALNACT1	chondroitin sulfate N-acetylgalactosaminyltransferase 1	8	0.26837	0.011229
ENSG00000197329	PELI1	pellino E3 ubiquitin protein ligase 1	2	0.395982	0.011397
ENSG00000164754	RAD21	RAD21 cohesin complex component	8	-0.29422	0.011437
ENSG00000051341	POLQ	DNA polymerase theta	3	-0.87261	0.011714
ENSG00000146670	CDCA5	cell division cycle associated 5	11	-0.70528	0.011756
ENSG00000152785	BMP3	bone morphogenetic protein 3	4	-0.62098	0.011943
ENSG00000109458	GAB1	GRB2 associated binding protein 1	4	0.352922	0.011943
ENSG00000241978	AKAP2	A-kinase anchoring protein 2	9	0.481247	0.011943
ENSG00000179604	CDC42EP4	CDC42 effector protein 4	17	-0.42691	0.01207
ENSG00000069020	MAST4	microtubule associated serine/threonine kinase family member 4	5	-0.44777	0.01213
ENSG00000005189	REXO5	RNA exonuclease 5	16	-0.72158	0.01213
ENSG00000182175	RGMA	repulsive guidance molecule BMP co-receptor a	15	-0.39956	0.01213
ENSG00000206455	TCF19	transcription factor 19	6	-0.5571	0.012135
ENSG00000165238	WNK2	WNK lysine deficient protein kinase 2	9	-0.42428	0.012165
ENSG00000137166	FOXP4	forkhead box P4	6	0.606766	0.012165
ENSG00000134954	ETS1	ETS proto-oncogene 1, transcription factor	11	0.444802	0.012165
ENSG00000113583	C5orf15	chromosome 5 open reading frame 15	5	0.275933	0.012234
ENSG00000164199	ADGRV1	adhesion G protein-coupled receptor V1	5	-0.77433	0.012267
ENSG00000114115	RBP1	retinol binding protein 1	3	-1.58539	0.012267
ENSG00000124813	RUNX2	runt related transcription factor 2	6	0.516312	0.012267
ENSG00000173110	HSPA6	heat shock protein family A (Hsp70) member 6	1	1.535759	0.012267
ENSG00000129514	FOXA1	forkhead box A1	14	-1.12912	0.012267
ENSG00000138768	USO1	USO1 vesicle transport factor	4	0.285139	0.012267
ENSG00000173705	SUSD5	sushi domain containing 5	3	-0.34208	0.012741
ENSG00000124006	OBSL1	obscurin like 1	2	-0.33674	0.01324
ENSG00000105325	FZR1	fizzy and cell division cycle 20 related 1	19	-0.46337	0.01324
ENSG00000184445	KNTC1	kinetochore associated 1	12	-0.49168	0.013678
ENSG00000119403	PHF19	PHD finger protein 19	9	-0.39983	0.013777
ENSG00000135114	OASL	2'-5'-oligoadenylate synthetase like	12	1.91395	0.013826
ENSG00000160949	TONSL	tonsoku like, DNA repair protein	8	-0.80979	0.013855
ENSG00000067113	PLPP1	phospholipid phosphatase 1	5	-0.54404	0.014023
ENSG00000170312	CDK1	cyclin dependent kinase 1	10	-0.39446	0.014129
ENSG00000168461	RAB31	RAB31, member RAS oncogene family	18	0.610282	0.014178
ENSG00000153012	LGI2	leucine rich repeat LGI family member 2	4	0.483726	0.014336
ENSG00000130816	DNMT1	DNA methyltransferase 1	19	-0.36598	0.014453

ENSG00000144485	HES6	hes family bHLH transcription factor 6	2	-1.33126	0.014487
ENSG00000143061	IGSF3	immunoglobulin superfamily member 3	1	-0.51625	0.014487
ENSG00000164309	CMYA5	cardiomyopathy associated 5	5	0.391581	0.014549
ENSG00000130035	KCNA6	potassium voltage-gated channel subfamily A member 6	12	-0.37027	0.014761
ENSG00000235941	HSPA1A	heat shock protein family A (Hsp70) member 1A	6	0.852968	0.014785
ENSG00000081189	MEF2C	myocyte enhancer factor 2C	5	0.375024	0.014914
ENSG00000121691	CAT	catalase	11	0.563873	0.015042
ENSG00000164346	NSA2	NSA2, ribosome biogenesis homolog	5	0.295542	0.015144
ENSG00000197381	ADARB1	adenosine deaminase, RNA specific B1	21	0.466203	0.015353
ENSG00000118523	CTGF	connective tissue growth factor	6	0.663036	0.015399
ENSG00000188517	COL25A1	collagen type XXV alpha 1 chain	4	0.666625	0.015399
ENSG00000197249	SERPINA1	serpin family A member 1	14	1.333376	0.015472
ENSG00000145244	CORIN	corin, serine peptidase	4	-1.19669	0.015472
ENSG00000112699	GMDS	GDP-mannose 4,6-dehydratase	6	0.413767	0.01566
ENSG00000100842	EFS	embryonal Fyn-associated substrate	14	-0.28679	0.015725
ENSG00000204103	MAFB	MAF bZIP transcription factor B	20	-0.90745	0.015848
ENSG00000170801	HTRA3	HtrA serine peptidase 3	4	-0.52522	0.015956
ENSG00000137135	ARHGEF39	Rho guanine nucleotide exchange factor 39	9	-0.77221	0.016515
ENSG00000157554	ERG	ERG, ETS transcription factor	21	0.666292	0.016515
ENSG00000123131	PRDX4	peroxiredoxin 4	X	0.30612	0.016515
ENSG00000074047	GLI2	GLI family zinc finger 2	2	-0.42546	0.016813
ENSG00000105939	ZC3HAV1	zinc finger CCCH-type containing, antiviral 1	7	0.565048	0.016829
ENSG00000104331	IMPAD1	inositol monophosphatase domain containing 1	8	0.267649	0.016971
ENSG00000136244	IL6	interleukin 6	7	4.909451	0.016971
ENSG00000020181	ADGRA2	adhesion G protein-coupled receptor A2	8	-0.3024	0.016987
ENSG00000157625	TAB3	TGF-beta activated kinase 1 (MAP3K7) binding protein 3	X	0.365793	0.017133
ENSG00000134049	IER3IP1	immediate early response 3 interacting protein 1	18	0.334378	0.017261
ENSG00000180178	FAR2P1	fatty acyl-CoA reductase 2 pseudogene 1	2	2.164407	0.017504
ENSG00000025770	NCAPH2	non-SMC condensin II complex subunit H2	22	-0.44399	0.017504
ENSG00000156113	KCNMA1	potassium calcium-activated channel subfamily M alpha 1	10	0.258612	0.01777
ENSG00000167670	CHAF1A	chromatin assembly factor 1 subunit A	19	-0.72756	0.017805
ENSG00000149503	INCENP	inner centromere protein	11	-0.53047	0.017809
ENSG00000120129	DUSP1	dual specificity phosphatase 1	5	0.589143	0.018086
ENSG00000164096	C4orf3	chromosome 4 open reading frame 3	4	0.295075	0.018279
ENSG00000158813	EDA	ectodysplasin A	X	-0.71303	0.018279
ENSG00000148848	ADAM12	ADAM metallopeptidase domain 12	10	0.584718	0.018279
ENSG00000110042	DTX4	deltex E3 ubiquitin ligase 4	11	-0.74537	0.018279
ENSG00000169174	PCSK9	proprotein convertase subtilisin/kexin type 9	1	-0.43812	0.018282
ENSG00000138119	MYOF	myoferlin	10	0.468971	0.018402
ENSG00000144895	EIF2A	eukaryotic translation initiation factor 2A	3	0.278782	0.018402
ENSG00000138835	RGS3	regulator of G protein signaling 3	9	0.401957	0.018512
ENSG00000124785	NRN1	neuritin 1	6	1.55789	0.018537
ENSG00000112984	KIF20A	kinesin family member 20A	5	-0.47594	0.018701
ENSG00000120802	TMPO	thymopoietin	12	-0.30122	0.01872
ENSG00000102359	SRPX2	sushi repeat containing protein, X-linked 2	X	0.312275	0.018855
ENSG00000006128	TAC1	tachykinin precursor 1	7	1.676127	0.018855
ENSG00000162599	NFIA	nuclear factor I A	1	-0.33571	0.019041
ENSG00000126860	EVI2A	ecotropic viral integration site 2A	17	2.877085	0.019284
ENSG00000138685	FGF2	fibroblast growth factor 2	4	0.353198	0.019307
ENSG00000196517	SLC6A9	solute carrier family 6 member 9	1	-0.5764	0.019473
ENSG00000138795	LEF1	lymphoid enhancer binding factor 1	4	0.556805	0.019485
ENSG00000148400	NOTCH1	notch 1	9	-0.36504	0.019554
ENSG00000123560	PLP1	proteolipid protein 1	X	-0.99367	0.019645
ENSG00000082293	COL19A1	collagen type XIX alpha 1 chain	6	0.978911	0.019731
ENSG00000134057	CCNB1	cyclin B1	5	-0.41771	0.020046
ENSG00000164300	SERINC5	serine incorporator 5	5	0.345449	0.020046
ENSG00000183087	GAS6	growth arrest specific 6	13	0.396057	0.020053
ENSG00000163590	PPM1L	protein phosphatase, Mg2+/Mn2+ dependent 1L	3	-0.63898	0.020073
ENSG00000189060	H1F0	H1 histone family member 0	22	-0.30048	0.020085
ENSG00000128918	ALDH1A2	aldehyde dehydrogenase 1 family member A2	15	1.103444	0.02014
ENSG00000171885	AQP4	aquaporin 4	18	-0.76684	0.02014
ENSG00000143816	WNT9A	Wnt family member 9A	1	-1.64615	0.02014
ENSG00000187741	FANCA	Fanconi anemia complementation group A	16	-0.54881	0.020402
ENSG00000006459	KDM7A	lysine demethylase 7A	7	0.527748	0.020596
ENSG00000138650	PCDH10	protocadherin 10	4	-0.3176	0.020881
ENSG00000164111	ANXA5	annexin A5	4	0.244536	0.020881
ENSG00000023445	BIRC3	baculoviral IAP repeat containing 3	11	1.320544	0.020881
ENSG00000255302	EID1	EP300 interacting inhibitor of differentiation 1	15	0.243546	0.020881
ENSG00000163171	CDC42EP3	CDC42 effector protein 3	2	0.324522	0.020881

ENSG00000273841	TAF9	TATA-box binding protein associated factor 9	5	5.51757	0.020881
ENSG00000175745	NR2F1	nuclear receptor subfamily 2 group F member 1	5	-0.76567	0.020881
ENSG00000100889	PCK2	phosphoenolpyruvate carboxykinase 2, mitochondrial	14	-0.59238	0.020881
ENSG00000198668	CALM1	calmodulin 1	14	-0.26021	0.020881
ENSG00000149311	ATM	ATM serine/threonine kinase	11	0.310057	0.020881
ENSG00000187134	AKR1C1	aldo-keto reductase family 1 member C1	10	1.174019	0.020974
ENSG00000089685	BIRC5	baculoviral IAP repeat containing 5	17	-0.5694	0.021126
ENSG00000111602	TIMELESS	timeless circadian regulator	12	-0.52589	0.021135
ENSG00000153162	BMP6	bone morphogenetic protein 6	6	0.746148	0.021176
ENSG00000181744	C3orf58	chromosome 3 open reading frame 58	3	-0.41722	0.021457
ENSG00000075223	SEMA3C	semaphorin 3C	7	0.363027	0.021457
ENSG00000110422	HIPK3	homeodomain interacting protein kinase 3	11	0.353805	0.021487
ENSG00000188157	AGRN	agrin	1	-0.30784	0.021666
ENSG00000140993	TIGD7	tigger transposable element derived 7	16	-0.61001	0.021772
ENSG00000135679	MDM2	MDM2 proto-oncogene	12	0.388979	0.021772
ENSG00000143384	MCL1	MCL1, BCL2 family apoptosis regulator	1	0.251214	0.021803
ENSG00000152910	CNTNAP4	contactin associated protein like 4	16	2.605471	0.021897
ENSG00000114270	COL7A1	collagen type VII alpha 1 chain	3	-0.74793	0.021938
ENSG00000121671	CRY2	cryptochrome circadian regulator 2	11	-0.31504	0.022135
ENSG00000140044	JDP2	Jun dimerization protein 2	14	-0.4483	0.022161
ENSG00000178999	AURKB	aurora kinase B	17	-0.67565	0.022495
ENSG00000079931	MOXD1	monooxygenase DBH like 1	6	0.346711	0.022495
ENSG00000108001	EBF3	early B cell factor 3	10	0.670718	0.022513
ENSG00000115419	GLS	glutaminase	2	0.264193	0.022605
ENSG00000110841	PPFIBP1	PPFIA binding protein 1	12	0.254078	0.022605
ENSG00000156011	PSD3	pleckstrin and Sec7 domain containing 3	8	0.318089	0.022779
ENSG00000137726	FXYD6	FXYD domain containing ion transport regulator 6	11	-0.24139	0.022894
ENSG00000040608	RTN4R	reticulon 4 receptor	22	-0.46894	0.023024
ENSG00000081842	PCDHA6	protocadherin alpha 6	5	-2.26477	0.023024
ENSG00000135074	ADAM19	ADAM metallopeptidase domain 19	5	-0.36581	0.023024
ENSG00000283530	MGAT4C	MGAT4 family member C	12	-1.15037	0.023068
ENSG00000151490	PTPRO	protein tyrosine phosphatase, receptor type O	12	-0.78132	0.023171
ENSG00000197780	TAF13	TATA-box binding protein associated factor 13	1	0.551304	0.023304
ENSG00000109685	NSD2	nuclear receptor binding SET domain protein 2	4	-0.29982	0.023394
ENSG00000173166	RAPH1	Ras association (RalGDS/AF-6) and pleckstrin homology domains 1	2	0.29976	0.023394
ENSG00000254996	ANKHD1-EIF4EBP3	ANKHD1-EIF4EBP3 readthrough	5	-0.62216	0.023477
ENSG00000134533	RERG	RAS like estrogen regulated growth inhibitor	12	-0.78673	0.023726
ENSG00000128594	LRRC4	leucine rich repeat containing 4	7	-1.30884	0.023726
ENSG00000278229	RPS17	ribosomal protein S17	15	0.342585	0.023863
ENSG00000154640	BTG3	BTG anti-proliferation factor 3	21	-0.35393	0.02419
ENSG00000132821	VSTM2L	V-set and transmembrane domain containing 2 like	20	-0.7624	0.024229
ENSG00000188229	TUBB4B	tubulin beta 4B class IVb	9	-0.39156	0.024479
ENSG00000127564	PKMYT1	protein kinase, membrane associated tyrosine/threonine 1	16	-0.79217	0.024674
ENSG00000168488	ATXN2L	ataxin 2 like	16	-0.29796	0.02471
ENSG00000170365	SMAD1	SMAD family member 1	4	-0.4975	0.024723
ENSG00000175155	YPEL2	yippee like 2	17	0.317694	0.024723
ENSG00000137285	TUBB2B	tubulin beta 2B class IIb	6	-0.36021	0.024858
ENSG00000169908	TM4SF1	transmembrane 4 L six family member 1	3	0.361004	0.025021
ENSG00000113810	SMC4	structural maintenance of chromosomes 4	3	-0.35287	0.025183
ENSG00000122952	ZWINT	ZW10 interacting kinetochore protein	10	-0.4222	0.025183
ENSG00000162368	CMPK1	cytidine/uridine monophosphate kinase 1	1	0.262235	0.025237
ENSG00000283391	EEF1B2	eukaryotic translation elongation factor 1 beta 2	2	0.24894	0.025247
ENSG00000186185	KIF18B	kinesin family member 18B	17	-0.62829	0.025247
ENSG00000055732	MCOLN3	mucolipin 3	1	0.56888	0.025344
ENSG00000006747	SCIN	scinderin	7	0.246456	0.025344
ENSG00000065485	PDIA5	protein disulfide isomerase family A member 5	3	0.288342	0.025344
ENSG00000111275	ALDH2	aldehyde dehydrogenase 2 family member	12	-0.33894	0.02539
ENSG00000106462	EZH2	enhancer of zeste 2 polycomb repressive complex 2 subunit	7	-0.51326	0.026005
ENSG00000147655	RSPO2	R-spondin 2	8	-0.74136	0.026108
ENSG00000166881	NEMP1	nuclear envelope integral membrane protein 1	12	-0.36397	0.026108
ENSG00000105372	RPS19	ribosomal protein S19	19	0.383422	0.026108
ENSG00000109062	SLC9A3R1	SLC9A3 regulator 1	17	-0.46837	0.026108
ENSG00000105281	SLC1A5	solute carrier family 1 member 5	19	-0.31841	0.026108
ENSG00000163328	GPR155	G protein-coupled receptor 155	2	-0.43068	0.026108
ENSG00000065154	OAT	ornithine aminotransferase	10	0.2479	0.026108
ENSG00000102226	USP11	ubiquitin specific peptidase 11	X	-0.25106	0.026108
ENSG00000147804	SLC39A4	solute carrier family 39 member 4	8	0.889451	0.02612

ENSG00000139915	MDGA2	MAM domain containing glycosylphosphatidylinositol anchor 2	14	-0.67981	0.026216
ENSG00000198168	SVIP	small VCP interacting protein	11	0.831421	0.026216
ENSG00000138180	CEP55	centrosomal protein 55	10	-0.61731	0.026236
ENSG00000158402	CDC25C	cell division cycle 25C	5	-0.67763	0.026725
ENSG00000064961	HMG20B	high mobility group 20B	19	-0.37086	0.026838
ENSG00000070159	PTPN3	protein tyrosine phosphatase, non-receptor type 3	9	0.502086	0.026966
ENSG00000161888	SPC24	SPC24, NDC80 kinetochore complex component	19	-0.59382	0.027729
ENSG00000138207	RBP4	retinol binding protein 4	10	0.743752	0.027803
ENSG00000152484	USP12	ubiquitin specific peptidase 12	13	0.364611	0.027999
ENSG00000154736	ADAMTS5	ADAM metallopeptidase with thrombospondin type 1 motif 5	21	-1.08499	0.028004
ENSG00000168374	ARF4	ADP ribosylation factor 4	3	0.232364	0.028011
ENSG00000188846	RPL14	ribosomal protein L14	3	0.252709	0.028086
ENSG00000115520	COQ10B	coenzyme Q10B	2	0.502766	0.028152
ENSG00000198914	POU3F3	POU class 3 homeobox 3	2	-0.39028	0.028411
ENSG00000149591	TAGLN	transgelin	11	1.027337	0.028456
ENSG00000100505	TRIM9	tripartite motif containing 9	14	-0.31512	0.029049
ENSG00000162244	RPL29	ribosomal protein L29	3	0.265077	0.02921
ENSG00000136108	CKAP2	cytoskeleton associated protein 2	13	-0.38205	0.02921
ENSG00000147130	ZMYM3	zinc finger MYM-type containing 3	X	-0.29333	0.029735
ENSG00000144824	PHLDB2	pleckstrin homology like domain family B member 2	3	-1.16629	0.02976
ENSG00000106511	MEOX2	mesenchyme homeobox 2	7	0.97241	0.029775
ENSG00000115339	GALNT3	polypeptide N-acetylgalactosaminyltransferase 3	2	-1.05919	0.030138
ENSG00000116117	PARD3B	par-3 family cell polarity regulator beta	2	-0.78153	0.030457
ENSG00000169554	ZEB2	zinc finger E-box binding homeobox 2	2	-0.66673	0.031294
ENSG00000184860	SDR42E1	short chain dehydrogenase/reductase family 42E, member 1	16	-1.93795	0.031299
ENSG00000157404	KIT	KIT proto-oncogene receptor tyrosine kinase	4	1.346993	0.031299
ENSG00000111728	ST8SIA1	ST8 alpha-N-acetyl-neuraminide alpha-2,8-sialyltransferase 1	12	-0.4366	0.031299
ENSG00000162909	CAPN2	calpain 2	1	0.29063	0.031299
ENSG00000197140	ADAM32	ADAM metallopeptidase domain 32	8	-1.7131	0.031304
ENSG00000112837	TBX18	T-box 18	6	-0.48137	0.031304
ENSG00000105443	CYTH2	cytohesin 2	19	-0.36899	0.031335
ENSG00000189171	S100A13	S100 calcium binding protein A13	1	0.32257	0.031434
ENSG00000164764	SBSPON	somatomedin B and thrombospondin type 1 domain containing	8	-0.96943	0.031463
ENSG00000142864	SERBP1	SERPINE1 mRNA binding protein 1	1	0.217677	0.03205
ENSG00000180440	SERTM1	serine rich and transmembrane domain containing 1	13	-0.85172	0.03205
ENSG00000027644	INSRR	insulin receptor related receptor	1	-2.90648	0.032231
ENSG00000259024	TVP23C-CDRT4	TVP23C-CDRT4 readthrough	17	-0.41948	0.032324
ENSG00000184916	JAG2	jagged 2	14	0.6169	0.032324
ENSG00000091137	SLC26A4	solute carrier family 26 member 4	7	0.775272	0.032693
ENSG00000177409	SAMD9L	sterile alpha motif domain containing 9 like	7	0.689476	0.032828
ENSG00000164742	ADCY1	adenylate cyclase 1	7	0.484613	0.033059
ENSG00000102547	CAB39L	calcium binding protein 39 like	13	0.50327	0.033363
ENSG00000105866	SP4	Sp4 transcription factor	7	0.520563	0.03363
ENSG00000165801	ARHGEF40	Rho guanine nucleotide exchange factor 40	14	-0.26362	0.033714
ENSG00000141338	ABCA8	ATP binding cassette subfamily A member 8	17	-0.89112	0.033714
ENSG00000137154	RPS6	ribosomal protein S6	9	0.258564	0.033714
ENSG00000127955	GNAI1	G protein subunit alpha i1	7	-0.41804	0.033782
ENSG00000128791	TWSG1	twisted gastrulation BMP signaling modulator 1	18	0.249499	0.033882
ENSG00000155016	CYP2U1	cytochrome P450 family 2 subfamily U member 1	4	0.521301	0.033882
ENSG00000115902	SLC1A4	solute carrier family 1 member 4	2	-0.41946	0.033882
ENSG00000158321	AUTS2	AUTS2, activator of transcription and developmental regulator	7	-0.24344	0.033882
ENSG00000155111	CDK19	cyclin dependent kinase 19	6	-0.47537	0.033882
ENSG00000105968	H2AFV	H2A histone family member V	7	-0.28876	0.033882
ENSG00000205726	ITSN1	intersectin 1	21	-0.37269	0.033882
ENSG00000050165	DKK3	dickkopf WNT signaling pathway inhibitor 3	11	-0.38597	0.033882
ENSG00000169288	MRPL1	mitochondrial ribosomal protein L1	4	0.498582	0.033882
ENSG00000119711	ALDH6A1	aldehyde dehydrogenase 6 family member A1	14	0.308267	0.033882
ENSG00000163683	SMIM14	small integral membrane protein 14	4	0.30772	0.033882
ENSG00000170374	SP7	Sp7 transcription factor	12	1.148703	0.033882
ENSG00000107796	ACTA2	actin, alpha 2, smooth muscle, aorta	10	0.801959	0.033882
ENSG00000166012	TAF1D	TATA-box binding protein associated factor, RNA polymerase I subunit D	11	0.254726	0.033993
ENSG00000127084	FGD3	FYVE, RhoGEF and PH domain containing 3	9	1.035653	0.03413

ENSG00000140600	SH3GL3	SH3 domain containing GRB2 like 3, endophilin A3	15	-0.8662	0.03413
ENSG00000005108	THSD7A	thrombospondin type 1 domain containing 7A	7	-0.62566	0.034253
ENSG00000182968	SOX1	SRY-box 1	13	-1.75879	0.034305
ENSG00000198892	SHISA4	shisa family member 4	1	-0.33475	0.034371
ENSG00000139289	PHLDA1	pleckstrin homology like domain family A member 1	12	0.484738	0.034396
ENSG00000114346	ECT2	epithelial cell transforming 2	3	-0.45336	0.034489
ENSG00000172765	TMCC1	transmembrane and coiled-coil domain family 1	3	0.34829	0.034779
ENSG00000144674	GOLGA4	golgin A4	3	0.279233	0.035068
ENSG00000132646	PCNA	proliferating cell nuclear antigen	20	-0.32513	0.035068
ENSG00000112245	PTP4A1	protein tyrosine phosphatase type IVA, member 1	6	0.422492	0.035141
ENSG00000138759	FRAS1	Fraser extracellular matrix complex subunit 1	4	1.843059	0.035184
ENSG00000265681	RPL17	ribosomal protein L17	18	0.312338	0.035184
ENSG00000101057	MYBL2	MYB proto-oncogene like 2	20	-0.61506	0.035302
ENSG00000170962	PDGFD	platelet derived growth factor D	11	-0.52936	0.035371
ENSG00000196611	MMP1	matrix metallopeptidase 1	11	1.871986	0.035668
ENSG00000168702	LRP1B	LDL receptor related protein 1B	2	-0.58762	0.035668
ENSG00000147604	RPL7	ribosomal protein L7	8	0.247179	0.035741
ENSG00000187323	DCC	DCC netrin 1 receptor	18	0.387532	0.035747
ENSG00000278053	DDX52	DExD-box helicase 52	17	1.090326	0.035747
ENSG00000223367	RPS18	ribosomal protein S18	6	0.338093	0.035747
ENSG00000140575	IQGAP1	IQ motif containing GTPase activating protein 1	15	0.227624	0.035912
ENSG00000138796	HADH	hydroxyacyl-CoA dehydrogenase	4	0.364368	0.035912
ENSG00000137727	ARHGAP20	Rho GTPase activating protein 20	11	-0.5548	0.035937
ENSG00000196090	PTPRT	protein tyrosine phosphatase, receptor type T	20	-1.61671	0.035991
ENSG00000116991	SIPA1L2	signal induced proliferation associated 1 like 2	1	-0.96874	0.035991
ENSG00000225151	GOLGA2P7	golgin A2 pseudogene 7	15	-0.42757	0.036052
ENSG00000115556	PLCD4	phospholipase C delta 4	2	0.404526	0.036343
ENSG00000164330	EBF1	early B cell factor 1	5	-0.28722	0.036494
ENSG00000105640	RPL18A	ribosomal protein L18a	19	0.300163	0.036669
ENSG00000116574	RHOU	ras homolog family member U	1	-1.16024	0.036682
ENSG00000133138	TBC1D8B	TBC1 domain family member 8B	X	0.318866	0.037153
ENSG00000071539	TRIP13	thyroid hormone receptor interactor 13	5	-0.62373	0.037345
ENSG00000124440	HIF3A	hypoxia inducible factor 3 alpha subunit	19	-0.56091	0.037345
ENSG00000239672	NME1	NME/NM23 nucleoside diphosphate kinase 1	17	0.371548	0.037407
ENSG00000090097	PCBP4	poly(rC) binding protein 4	3	-0.43634	0.037407
ENSG00000235217	TSPY26P	testis specific protein, Y-linked 26, pseudogene	20	-0.61807	0.037407
ENSG00000135541	AHI1	Abelson helper integration site 1	6	0.324595	0.037575
ENSG00000166441	RPL27A	ribosomal protein L27a	11	0.309796	0.037575
ENSG00000107968	MAP3K8	mitogen-activated protein kinase kinase kinase 8	10	0.994708	0.037896
ENSG00000089009	RPL6	ribosomal protein L6	12	0.227057	0.037896
ENSG00000113739	STC2	stanniocalcin 2	5	-1.15426	0.037896
ENSG00000249915	PDCD6	programmed cell death 6	5	0.222059	0.037996
ENSG00000164023	SGMS2	sphingomyelin synthase 2	4	0.586204	0.038042
ENSG00000105011	ASF1B	anti-silencing function 1B histone chaperone	19	-0.69469	0.038042
ENSG00000175567	UCP2	uncoupling protein 2	11	-1.01062	0.038055
ENSG00000121064	SCPEP1	serine carboxypeptidase 1	17	0.259023	0.038307
ENSG00000145681	HAPLN1	hyaluronan and proteoglycan link protein 1	5	0.184807	0.038423
ENSG00000005243	COPZ2	coatomer protein complex subunit zeta 2	17	0.288213	0.038519
ENSG00000139330	KERA	keratocan	12	-0.9652	0.038519
ENSG00000153815	CMIP	c-Maf inducing protein	16	-0.41168	0.038727
ENSG00000177189	RPS6KA3	ribosomal protein S6 kinase A3	X	0.314938	0.038769
ENSG00000137812	KNL1	kinetochore scaffold 1	15	-0.51134	0.039388
ENSG00000186340	THBS2	thrombospondin 2	6	0.789716	0.039437
ENSG00000168137	SETD5	SET domain containing 5	3	-0.24659	0.039457
ENSG00000126787	DLGAP5	DLG associated protein 5	14	-0.54305	0.039457
ENSG00000143126	CELSR2	cadherin EGF LAG seven-pass G-type receptor 2	1	-0.59731	0.039593
ENSG00000165973	NELL1	neural EGFL like 1	11	0.466856	0.040175
ENSG00000198755	RPL10A	ribosomal protein L10a	6	0.239504	0.040571
ENSG00000167513	CDT1	chromatin licensing and DNA replication factor 1	16	-0.87859	0.040571
ENSG00000113916	BCL6	B cell CLL/lymphoma 6	3	0.36791	0.040571
ENSG00000134318	ROCK2	Rho associated coiled-coil containing protein kinase 2	2	0.260769	0.040571
ENSG00000082458	DLG3	discs large MAGUK scaffold protein 3	X	-0.4084	0.040571
ENSG00000102683	SGCG	sarcoglycan gamma	13	1.45656	0.040627
ENSG00000182481	KPNA2	karyopherin subunit alpha 2	17	-0.53417	0.040627
ENSG00000188729	OSTN	osteocrin	3	0.504998	0.040676
ENSG00000187554	TLR5	toll like receptor 5	1	0.991974	0.041053
ENSG00000139865	TTC6	tetratricopeptide repeat domain 6	14	-1.55975	0.041053

ENSG00000083845	RPS5	ribosomal protein S5	19	0.258303	0.041255
ENSG00000188211	NCR3LG1	natural killer cell cytotoxicity receptor 3 ligand 1	11	1.34765	0.041255
ENSG00000115641	FHL2	four and a half LIM domains 2	2	1.318429	0.04128
ENSG00000163521	GLB1L	galactosidase beta 1 like	2	-0.43805	0.04128
ENSG00000145391	SETD7	SET domain containing lysine methyltransferase 7	4	0.249211	0.04128
ENSG00000197969	VPS13A	vacuolar protein sorting 13 homolog A	9	0.444125	0.041584
ENSG00000125885	MCM8	minichromosome maintenance 8 homologous recombination repair factor	20	-0.42078	0.041584
ENSG00000093009	CDC45	cell division cycle 45	22	-0.65583	0.041584
ENSG00000151632	AKR1C2	aldo-keto reductase family 1 member C2	10	1.480502	0.041715
ENSG00000080493	SLC4A4	solute carrier family 4 member 4	4	0.81809	0.041781
ENSG00000102287	GABRE	gamma-aminobutyric acid type A receptor epsilon subunit	X	-0.65807	0.042239
ENSG00000122584	NXPH1	neurexophilin 1	7	-1.96773	0.042405
ENSG00000274137	MYOM2	myomesin 2	8	1.455939	0.042405
ENSG00000118965	WDR35	WD repeat domain 35	2	0.296936	0.042525
ENSG00000118855	MFSD1	major facilitator superfamily domain containing 1	3	0.378895	0.042576
ENSG00000148120	C9orf3	chromosome 9 open reading frame 3	9	-0.39303	0.042737
ENSG00000187955	COL14A1	collagen type XIV alpha 1 chain	8	-0.22536	0.042737
ENSG00000163710	PCOLCE2	procollagen C-endopeptidase enhancer 2	3	-0.20796	0.042737
ENSG00000123349	PFDN5	prefoldin subunit 5	12	0.258056	0.042737
ENSG00000135596	MICAL1	microtubule associated monooxygenase, calponin and LIM domain containing 1	6	-0.38266	0.04274
ENSG00000125730	C3	complement C3	19	-1.31258	0.042912
ENSG00000129195	PIMREG	PICALM interacting mitotic regulator	17	-0.60719	0.043801
ENSG00000136824	SMC2	structural maintenance of chromosomes 2	9	-0.41497	0.043951
ENSG00000163660	CCNL1	cyclin L1	3	0.240127	0.043951
ENSG00000258289	CHURC1	churchill domain containing 1	14	0.286709	0.043951
ENSG00000118707	TGIF2	TGFB induced factor homeobox 2	20	-0.4489	0.043951
ENSG00000094631	HDAC6	histone deacetylase 6	X	-0.26265	0.04463
ENSG00000186897	C1QL4	complement C1q like 4	12	-0.40922	0.044685
ENSG00000266714	MYO15B	myosin XVB	17	-0.39867	0.044956
ENSG00000240184	PCDHGC3	protocadherin gamma subfamily C, 3	5	-0.29364	0.044956
ENSG00000169764	UGP2	UDP-glucose pyrophosphorylase 2	2	0.218042	0.045105
ENSG00000156509	FBXO43	F-box protein 43	8	-1.10503	0.045105
ENSG00000105647	PIK3R2	phosphoinositide-3-kinase regulatory subunit 2	19	-0.25399	0.045105
ENSG00000111452	ADGRD1	adhesion G protein-coupled receptor D1	12	-0.60839	0.045496
ENSG00000111678	C12orf57	chromosome 12 open reading frame 57	12	0.336485	0.045508
ENSG00000162734	PEA15	proliferation and apoptosis adaptor protein 15	1	-0.29279	0.045891
ENSG00000172175	MALT1	MALT1 paracaspase	18	0.311626	0.045996
ENSG00000213064	SFT2D2	SFT2 domain containing 2	1	0.300022	0.045996
ENSG00000125848	FLRT3	fibronectin leucine rich transmembrane protein 3	20	-0.5291	0.046088
ENSG00000164949	GEM	GTP binding protein overexpressed in skeletal muscle	8	0.678366	0.046088
ENSG00000276910	GTF2H2	general transcription factor IIH subunit 2	5	0.81495	0.046088
ENSG00000165304	MELK	maternal embryonic leucine zipper kinase	9	-0.55149	0.046088
ENSG00000074211	PPP2R2C	protein phosphatase 2 regulatory subunit Bgamma	4	-0.42842	0.046177
ENSG00000074219	TEAD2	TEA domain transcription factor 2	19	-0.72973	0.046278
ENSG00000126709	IFI6	interferon alpha inducible protein 6	1	0.450508	0.0465
ENSG00000116285	ERRFI1	ERBB receptor feedback inhibitor 1	1	0.319557	0.0465
ENSG00000161996	WDR90	WD repeat domain 90	16	-0.52333	0.046592
ENSG00000184194	GPR173	G protein-coupled receptor 173	X	-0.56961	0.047041
ENSG00000085185	BCORL1	BCL6 corepressor like 1	X	-0.43271	0.047239
ENSG00000152128	TMEM163	transmembrane protein 163	2	-0.70549	0.047239
ENSG00000011405	PIK3C2A	phosphatidylinositol-4-phosphate 3-kinase catalytic subunit type 2 alpha	11	0.260934	0.04725
ENSG00000198743	SLC5A3	solute carrier family 5 member 3	21	0.28722	0.047557
ENSG00000074964	ARHGEF10L	Rho guanine nucleotide exchange factor 10 like	1	-0.4763	0.047677
ENSG00000120742	SERP1	stress associated endoplasmic reticulum protein 1	3	0.234324	0.047681
ENSG00000174564	IL20RB	interleukin 20 receptor subunit beta	3	-0.6955	0.04777
ENSG00000136848	DAB2IP	DAB2 interacting protein	9	-0.39881	0.04804
ENSG00000075239	ACAT1	acetyl-CoA acetyltransferase 1	11	0.376949	0.048119
ENSG00000189221	MAOA	monoamine oxidase A	X	-1.33307	0.048225
ENSG00000119812	FAM98A	family with sequence similarity 98 member A	2	0.264285	0.048225
ENSG00000005513	SOX8	SRY-box 8	16	-0.25374	0.048225
ENSG00000159263	SIM2	single-minded family bHLH transcription factor 2	21	0.532939	0.048225
ENSG00000141668	CBLN2	cerebellin 2 precursor	18	-1.84198	0.048225
ENSG00000036448	MYOM2	myomesin 2	8	-1.46395	0.048225
ENSG00000282899	E2F2	E2F transcription factor 2	1	-1.0744	0.048369
ENSG00000183092	BEGAIN	brain enriched guanylate kinase associated	14	-0.5729	0.048458
ENSG00000165084	C8orf34	chromosome 8 open reading frame 34	8	-0.65935	0.04862

ENSG00000105855	ITGB8	integrin subunit beta 8	7	-0.69147	0.048739
ENSG00000134285	FKBP11	FK506 binding protein 11	12	0.371368	0.048935
ENSG00000126001	CEP250	centrosomal protein 250	20	-0.31159	0.049025
ENSG00000105329	TGFB1	transforming growth factor beta 1	19	0.456507	0.049062
ENSG00000162572	SCNN1D	sodium channel epithelial 1 delta subunit	1	-0.65995	0.04926
ENSG00000067533	RRP15	ribosomal RNA processing 15 homolog	1	0.454774	0.049274
ENSG00000183580	FBXL7	F-box and leucine rich repeat protein 7	5	-0.23964	0.049274
ENSG00000137563	GGH	gamma-glutamyl hydrolase	8	-0.35808	0.049274
ENSG00000021300	PLEKHB1	pleckstrin homology domain containing B1	11	0.483184	0.049668
ENSG00000273780	ARHGAP23	Rho GTPase activating protein 23	17	-0.48127	0.049834
ENSG00000127586	CHTF18	chromosome transmission fidelity factor 18	16	-0.62029	0.049834

Appendix 10

The list of GO terms for biological processes generated from 61 differentially expressed genes which are shared between F273L and P799L

GO ID	Description	Number of genes	Adj. p-value	Associated genes found
GO:0007155	cell adhesion	12	4.57E-03	PTPRT, SPON1, CADM3, SRPX2, MMRN1, PTPRO, SPP1, ITGB8, CD36, CELSR2, NTN1, PCDHA6
GO:0022610	biological adhesion	12	4.57E-03	PTPRT, SPON1, CADM3, SRPX2, MMRN1, PTPRO, SPP1, ITGB8, CD36, CELSR2, NTN1, PCDHA6
GO:0006564	L-serine biosynthetic process	2	1.43E-02	PSAT1, PHGDH
GO:0048731	system development	21	1.65E-02	PTPRO, ASNS, BMP8B, CELSR2, NTN1, PAX1, BMP3, TUBB2B, EFNB3, SRPX2, STMN1, SPP1, CDK1, PLP1, ITGB8, HMOX1, SPRY2, PHGDH, SOX8, SIM2, PCDHA6
GO:0048856	anatomical structure development	22	1.65E-02	PTPRO, ASNS, BMP8B, CELSR2, NTN1, PAX1, BMP3, TUBB2B, EFNB3, SRPX2, STMN1, CAPN2, SPP1, CDK1, PLP1, ITGB8, HMOX1, SPRY2, PHGDH, SOX8, SIM2, PCDHA6
GO:0016337	cell-cell adhesion	7	1.65E-02	PTPRT, CADM3, SRPX2, PTPRO, CELSR2, NTN1, PCDHA6
GO:0060348	bone development	5	1.84E-02	BMP3, SPP1, BMP8B, SOX8, PAX1
GO:0046942	carboxylic acid transport	5	1.95E-02	SLC6A9, SLC1A4, D36, SLC1A5, SLC38A4
GO:0015849	organic acid transport	5	1.95E-02	SLC6A9, SLC1A4, CD36, SLC1A5, SLC38A4
GO:0030154	cell differentiation	16	2.49E-02	PTPRO, BMP8B, CELSR2, NTN1, PAX1, BMP3, TUBB2B, EFNB3, STMN1, CAPN2, SPP1, CDK1, PLP1, SPRY2, SOX8, SIM2
GO:0006865	amino acid transport	4	2.49E-02	SLC6A9, SLC1A4, SLC1A5, SLC38A4
GO:0034383	low-density lipoprotein particle clearance	2	2.49E-02	HMOX1, CD36
GO:0048869	cellular developmental process	16	2.67E-02	PTPRO, BMP8B, CELSR2, NTN1, PAX1, BMP3, TUBB2B, EFNB3, STMN1, CAPN2, SPP1, CDK1, PLP1, SPRY2, SOX8, SIM2
GO:0006563	L-serine metabolic process	2	2.83E-02	PSAT1, PHGDH
GO:0009987	cellular process	46	3.00E-02	PTPRT, TOP2A, SPON1, ARL6IP1, PPM1L, SLC20A1, PTPRO, WISP3, TGFA, SLC1A4, CELSR2, NTN1, MRPL1, EFNB3, SRPX2, INPP5F, STMN1, CAPN2, SPP1, ITGB8, HMOX1, PHGDH, SOX8, CD36, CHAC1, PCDHA6, PCK2, CADM3, MME, H2AFZ, ASNS, BMP8B, SOD3, PAX1, ANLN, BMP3, TUBB2B,

				MMRN1, PSAT1, OSTC, CAT, CDK1, PLP1, SPRY2, SIM2, AARS
GO:0007275	multicellular organismal development	22	3.25E-02	PTPRO, ASNS, BMP8B, CELSR2, NTN1, PAX1, BMP3, TUBB2B, EFNB3, SRPX2, STMN1, CAPN2, SPP1, CDK1, PLP1, ITGB8, HMOX1, SPRY2, PHGDH, SOX8, SIM2, PCDHA6
GO:0009070	serine family amino acid biosynthetic process	2	4.30E-02	PSAT1, PHGDH
GO:0015837	amine transport	4	4.30E-02	SLC6A9, SLC1A4, SLC1A5, SLC38A4
GO:0048638	regulation of developmental growth	3	4.30E-02	SPP1, CDK1, NTN1
GO:0048640	negative regulation of developmental growth	2	4.30E-02	SPP1, NTN1
GO:0008652	cellular amino acid biosynthetic process	3	4.30E-02	PSAT1, ASNS, PHGDH
GO:0001503	ossification	4	4.30E-02	BMP3, SPP1, BMP8B, SOX8
GO:0034599	cellular response to oxidative stress	3	4.84E-02	CAT, CDK1, HMOX1

Appendix 11

The list of GO terms for biological processes generated from each gene cluster

CLUSTER A

GO ID	GO Terms	Group	Number of Genes	Associated Genes (%)	Adj. p-value	Associated Genes Found
GO:0007264	small GTPase mediated signal transduction	[Group00]	33	4.6	0.002562	[APOE, ARHGAP20, ARHGAP23, ARHGAP28, ARHGEF10L, ARHGEF39, ARHGEF40, ARL6IP1, CCNA2, CDC25C, CDC42EP4, CEP250, CYFIP1, CYTH2, DAB2IP, DNMT1, ECT2, ELMO1, FOXM1, IQGAP3, ITSN1, NOTCH1, NTN1, PDGFRB, PIK3R2, RACGAP1, RERG, RHOU, RTN4R, SIPA1L2, STMN1, TIMELESS, VANGL2]
GO:0051640	organelle localization	[Group01]	37	4.2	0.005007	[ARL6IP1, C3, CALM1, CCNB1, CDC42EP4, CDCA5, CDCA8, CDK1, CDT1, CENPF, CEP250, CKAP5, COL7A1, CSPG5, DAB2IP, DKK3, DLGAP5, ESPL1, F5, FDPS, HDAC6, KIF22, KIF23, NCAPD2, NDC80, NTN1, NUSAP1, NXPH1, PARD3B, PPFIA2, PRKAR2B, SLC9A3R1, SPAG5, SYT1, TRIM9, TUBB, TUBB4B]
GO:0014855	striated muscle cell proliferation	[Group02]	10	10.8	0.005294	[CCNB1, CDK1, DIPK2A, ERBB4, GARS, HERPUD1, NOTCH1, SHH, SMAD1, ZFPM2]
GO:0048145	regulation of fibroblast proliferation	[Group03]	12	9.7	0.002342	[ARL6IP1, C1QL4, CCNA2, CCNB1, CDC6, DAB2IP, DACH1, E2F1, NUPR1, PDGFC, PDGFD, PDGFRB]
GO:0000226	microtubule cytoskeleton organization	[Group04, Group08]	42	6.2	2.39E-08	[ARL6IP1, AURKB, BIRC5, CCNB1, CDC20, CDC42EP4, CDK1, CEP250, CKAP2, CKAP5, DAB2IP, ESPL1, FDPS, FYN, GNAI1, HDAC6, KIF11, KIF18B, KIF20A, KIF23, KNSTRN, MYBL2, NCAPD2, NDC80, NUSAP1, OBSL1, PARD3B, PHLDB2, PRC1, PTPRA, RACGAP1, RNF19A, SPAG5, STMN1, SYT1, TACC3, TPX2, TUBA1B, TUBB, TUBB2B, TUBB4B, ZNF367]
GO:0007010	cytoskeleton organization	[Group04, Group08]	76	4.7	4.26E-10	[AGRN, AIF1L, ANLN, APOE, ARHGAP28, ARHGEF10L, ARL6IP1, AURKB, BIRC5, CCNB1, CD36, CDC20, CDC42EP4, CDK1, CEP250, CIT, CKAP2, CKAP5, CYFIP1, CYTH2, DAB2IP, DIAPH3, DPYSL3, ECT2, EFS, ELMO1, ESPL1, FDPS, FYN, GNAI1, GPM6B, HDAC6, INSRR, KIF11, KIF18B, KIF20A, KIF23, KNSTRN, MARCKS, MAST4, MICAL1, MYBL2, MYOM2, NCAPD2, NCAPG, NDC80, NUSAP1, NXPH1, OBSL1, PARD3B, PDGFRB, PHLDB2, PLP1, PRC1, PTPRA, RACGAP1, RHOU, RNF19A, SETD3, SHH, SLC9A3R1, SPAG5, STMN1, SYT1, TACC3, THSD7A, TIMELESS, TMPO, TPX2, TUBA1B, TUBB, TUBB2B, TUBB4B, VANGL2, ZMYM3, ZNF367]

GO:0030036	actin cytoskeleton organization	[Group04]	38	4.5	9.83E-04	[AIF1L, ANLN, ARHGAP28, ARHGEF10L, ARL6IP1, CD36, CDC42EP4, CEP250, CIT, CYFIP1, CYTH2, DAB2IP, DIAPH3, DPYSL3, ECT2, EFS, ELMO1, FDPS, GPM6B, INSRR, KIF23, MARCKS, MICAL1, MYOM2, NCAPG, NXPH1, OBSL1, PDGFRB, PHLDB2, PLP1, RACGAP1, RHOU, SETD3, SLC9A3R1, STMN1, THSD7A, TIMELESS, VANGL2]
GO:0003333	amino acid transmembrane transport	[Group05]	12	9.4	0.003202	[ARL6IP1, ATP1A2, DDX39B, SLC1A1, SLC1A4, SLC1A5, SLC38A1, SLC38A4, SLC6A9, SLC7A1, SLC7A11, SLC7A5]
GO:0006865	amino acid transport	[Group05]	15	7.5	0.003951	[ARL6IP1, ATP1A2, DDX39B, PPFIA2, RBP1, SLC1A1, SLC1A4, SLC1A5, SLC38A1, SLC38A4, SLC6A9, SLC7A1, SLC7A11, SLC7A5, SYT1]
GO:0015175	neutral amino acid transmembrane transporter activity	[Group05]	8	15.1	0.003084	[DDX39B, SLC1A1, SLC1A4, SLC1A5, SLC38A1, SLC6A9, SLC7A11, SLC7A5]
GO:0050807	regulation of synapse organization	[Group06, Group12]	20	6.7	7.94E-04	[ADGRB2, AGRN, APOE, ARL6IP1, CALM1, CBLN2, CDC20, CLSTN2, CYFIP1, DAB2IP, EPHA4, FLRT3, FYN, FZD1, LRRC4, NTN1, PTPRO, PTPRT, SLC7A11, TUBB]
GO:0051962	positive regulation of nervous system development	[Group06, Group12]	37	5.2	3.02E-05	[ADGRB2, AGRN, APOE, ARL6IP1, C3, CALM1, CBLN2, CDC20, CLSTN2, CYFIP1, DAB2IP, DPYSL3, E2F1, ECT2, ENC1, EPHA4, EZH2, FDPS, FLRT3, FOXA1, FYN, FZD1, HMG20B, LRP2, NDNF, NKX6-1, NOTCH1, NTN1, OBSL1, RGMA, SH3GL3, SHH, SYT1, TENM3, TGIF2, TUBB2B, ZEB2]
GO:0050808	synapse organization	[Group06]	32	6.0	1.33E-05	[ADGRB2, AGRN, APOE, ARL6IP1, C3, CALM1, CBLN2, CDC20, CLSTN2, CYFIP1, DAB2IP, DLG3, EPHA4, ERBB4, FLRT3, FOXM1, FYN, FZD1, FZR1, HDAC6, LMNB2, LRRC4, NFIA, NTN1, PCDHGC3, PPFIA2, PTPRO, PTPRT, SDK1, SLC7A11, SPOCK2, TUBB]
GO:0008608	attachment of spindle microtubules to kinetochore	[Group07, Group14]	9	21.4	4.01E-05	[AURKB, CCNB1, CDT1, ECT2, KNL1, KNSTRN, NDC80, RACGAP1, SPAG5]
GO:0045841	negative regulation of mitotic metaphase/anaphase transition	[Group07, Group14]	9	17.3	2.73E-04	[AURKB, BUB1, CCNB1, CDC20, CDT1, CENPF, NDC80, RAD21, TRIP13]
GO:0051983	regulation of chromosome segregation	[Group07, Group14]	20	14.8	1.03E-09	[AURKB, BUB1, CCNB1, CDC20, CDC6, CDCA5, CDT1, CENPF, DDX11, DLGAP5, ECT2, ESPL1, KNSTRN, MKI67, NDC80, RACGAP1, RAD21, SPAG5, TACC3, TRIP13]

GO:0051988	regulation of attachment of spindle microtubules to kinetochore	[Group07]	5	35.7	0.001788	[CCNB1, ECT2, KNSTRN, RACGAP1, SPAG5]
GO:0007051	spindle organization	[Group08]	20	9.5	3.02E-06	[AURKB, BIRC5, CCNB1, CDC20, CKAP5, ESPL1, GNAI1, KIF11, KIF23, KNSTRN, MYBL2, NDC80, PRC1, PTPRA, RACGAP1, SPAG5, STMN1, TACC3, TPX2, TUBB]
GO:0007052	mitotic spindle organization	[Group08]	15	11.6	1.60E-05	[AURKB, BIRC5, CCNB1, CDC20, GNAI1, KIF11, KIF23, MYBL2, NDC80, PRC1, PTPRA, RACGAP1, STMN1, TACC3, TPX2]
GO:1902850	microtubule cytoskeleton organization involved in mitosis	[Group08]	17	10.6	7.93E-06	[AURKB, BIRC5, CCNB1, CDC20, ESPL1, GNAI1, KIF11, KIF23, MYBL2, NDC80, NUSAP1, PRC1, PTPRA, RACGAP1, STMN1, TACC3, TPX2]
GO:0051276	chromosome organization	[Group09, Group11, Group14]	72	4.7	1.32E-09	[ASF1B, AURKB, BCORL1, BUB1, C3, CCNA2, CCNB1, CDC20, CDC45, CDC6, CDCA5, CDCA8, CDK1, CDT1, CENPF, CENPO, CENPU, CEP250, CHAF1A, DDX11, DLGAP5, DNMT1, ESPL1, EZH2, FBXL7, FOXA1, H1F0, H2AFV, H2AFX, H2AFZ, HDAC6, HJURP, HMG20B, HMGB2, INCENP, JDP2, KIF18B, KIF22, KIF23, KNL1, KNSTRN, MCM4, MCM7, MKI67, NCAPD2, NCAPG, NCAPG2, NCAPH2, NDC80, NSD2, NUSAP1, PCBP4, PCNA, PEA15, PHF19, PRC1, RACGAP1, RAD21, RBP1, SETD3, SETD5, SMC2, SMC4, SOX1, SOX12, SPAG5, TACC3, TOP2A, TRIP13, TSPY26P, UHRF1, ZWINT]
GO:0071103	DNA conformation change	[Group09, Group11]	27	7.3	2.75E-06	[ASF1B, CCNB1, CDC45, CDCA5, CDK1, CENPO, CENPU, CEP250, CHAF1A, DDX11, H1F0, H2AFX, HJURP, HMGB2, KNL1, MCM4, MCM7, NCAPD2, NCAPG, NCAPG2, NCAPH2, NUSAP1, PEA15, SMC2, SMC4, TOP2A, TSPY26P]
GO:0006323	DNA packaging	[Group09]	23	9.3	3.56E-07	[ASF1B, CCNB1, CDCA5, CDK1, CENPO, CENPU, CEP250, CHAF1A, H1F0, H2AFX, HJURP, HMGB2, KNL1, MCM7, NCAPD2, NCAPG, NCAPG2, NCAPH2, NUSAP1, SMC2, SMC4, TOP2A, TSPY26P]
GO:0007076	mitotic chromosome condensation	[Group09]	8	34.8	3.20E-06	[CDCA5, CEP250, NCAPD2, NCAPG, NCAPH2, NUSAP1, SMC2, SMC4]
GO:0010032	meiotic chromosome condensation	[Group09]	5	45.5	4.50E-04	[CEP250, NCAPD2, NCAPH2, SMC2, SMC4]
GO:0030261	chromosome condensation	[Group09]	13	24.1	1.27E-08	[CCNB1, CDCA5, CDK1, CEP250, H1F0, NCAPD2, NCAPG, NCAPG2, NCAPH2, NUSAP1, SMC2, SMC4, TOP2A]
GO:0000910	cytokinesis	[Group10, Group14]	21	9.3	1.99E-06	[ANLN, ARL6IP1, AURKB, CALM1, CDC6, CDT1, CEP55, CIT, CKAP2, DAB2IP, ECT2, ESPL1, INCENP, KIF20A, KIF23, NUSAP1, PLP1, PRC1, RACGAP1, STMN1, ZNF367]

GO:0090068	positive regulation of cell cycle process	[Group10, Group14]	30	7.5	1.94E-07	[ARL6IP1, AURKB, CCNB1, CDC25C, CDC45, CDC6, CDCA5, CDK1, CDT1, CHAF1A, CIT, DAB2IP, DDX11, DLGAP5, DTL, E2F1, ECT2, ESPL1, EZH2, KIF23, NDC80, NUSAP1, PCBP4, PCNA, PDGFRB, RACGAP1, RAD21, SOX12, SPAG5, ZNF367]
GO:0000915	actomyosin contractile ring assembly	[Group10]	6	46.2	3.30E-05	[ANLN, ARL6IP1, DAB2IP, ECT2, KIF23, RACGAP1]
GO:0032465	regulation of cytokinesis	[Group10]	12	10.2	0.001417	[AURKB, CALM1, CDC6, CIT, ECT2, INCENP, KIF20A, KIF23, PLP1, PRC1, RACGAP1, ZNF367]
GO:0032506	cytokinetic process	[Group10]	9	16.1	5.18E-04	[ANLN, ARL6IP1, AURKB, CEP55, DAB2IP, ECT2, KIF20A, KIF23, RACGAP1]
GO:0051302	regulation of cell division	[Group10]	17	7.7	7.77E-04	[AURKB, CALM1, CDC6, CIT, ECT2, INCENP, KIF18B, KIF20A, KIF23, PDGFC, PDGFD, PLP1, PRC1, RACGAP1, SHH, TXNIP, ZNF367]
GO:0061640	cytoskeleton-dependent cytokinesis	[Group10]	16	12.0	3.49E-06	[ANLN, ARL6IP1, AURKB, CDT1, CEP55, CIT, CKAP2, DAB2IP, ECT2, ESPL1, INCENP, KIF20A, KIF23, NUSAP1, RACGAP1, STMN1]
GO:0000070	mitotic sister chromatid segregation	[Group11, Group14]	31	15.7	1.62E-16	[AURKB, BUB1, CCNB1, CDC20, CDC6, CDCA5, CDCA8, CDT1, CENPF, CEP250, DLGAP5, ESPL1, INCENP, KIF18B, KIF22, KIF23, KNSTRN, NCAPD2, NCAPG, NCAPH2, NDC80, NUSAP1, PRC1, RACGAP1, RAD21, SMC2, SMC4, SPAG5, TACC3, TRIP13, ZWINT]
GO:0000280	nuclear division	[Group11, Group14]	50	9.2	3.89E-17	[ANLN, AURKB, BIRC5, BUB1, CCNA2, CCNB1, CCNB2, CDC20, CDC25C, CDC6, CDCA5, CDCA8, CDT1, CENPF, CEP250, DLGAP5, ESPL1, FANCA, FBXO43, FZR1, INCENP, KIF11, KIF18B, KIF22, KIF23, KNSTRN, KNTC1, MKI67, MYBL2, NCAPD2, NCAPG, NCAPH2, NDC80, NUSAP1, OBSL1, PDGFRB, PKMYT1, PLP1, PRC1, RACGAP1, RAD21, SMC2, SMC4, SPAG5, TACC3, TOP2A, TPX2, TRIP13, ZNF367, ZWINT]
GO:0000819	sister chromatid segregation	[Group11, Group14]	33	13.5	1.27E-15	[AURKB, BUB1, CCNB1, CDC20, CDC6, CDCA5, CDCA8, CDT1, CENPF, CEP250, DDX11, DLGAP5, ESPL1, INCENP, KIF18B, KIF22, KIF23, KNSTRN, NCAPD2, NCAPG, NCAPH2, NDC80, NUSAP1, PRC1, RACGAP1, RAD21, SMC2, SMC4, SPAG5, TACC3, TOP2A, TRIP13, ZWINT]
GO:0033044	regulation of chromosome organization	[Group11, Group14]	26	5.6	8.22E-04	[AURKB, BUB1, C3, CCNB1, CDC20, CDC45, CDC6, CDCA5, CDT1, CENPF, DDX11, DLGAP5, DNMT1, ESPL1, H1F0, JDP2, MCM7, MKI67, NDC80, PEA15, PHF19, RAD21, SETD5, TACC3, TOP2A, TRIP13]
GO:0098813	nuclear chromosome segregation	[Group11, Group14]	35	10.4	4.14E-13	[AURKB, BUB1, CCNB1, CDC20, CDC6, CDCA5, CDCA8, CDT1, CENPF, CEP250, DDX11, DLGAP5, ECT2, ESPL1, INCENP, KIF18B, KIF22, KIF23, KNL1, KNSTRN, NCAPD2, NCAPG, NCAPH2, NDC80, NUSAP1, PRC1, RACGAP1, RAD21, SMC2, SMC4, SPAG5, TACC3, TOP2A, TRIP13, ZWINT]
GO:0140014	mitotic nuclear division	[Group11, Group14]	46	12.4	7.35E-21	[ANLN, AURKB, BIRC5, BUB1, CCNA2, CCNB1, CCNB2, CDC20, CDC25C, CDC6, CDCA5, CDCA8, CDT1, CENPF, CEP250, DLGAP5, ESPL1, INCENP,

						KIF11, KIF18B, KIF22, KIF23, KNSTRN, KNTC1, MKI67, MYBL2, NCAPD2, NCAPG, NCAPH2, NDC80, NUSAP1, OBSL1, PDGFRB, PKMYT1, PLP1, PRC1, RACGAP1, RAD21, SMC2, SMC4, SPAG5, TACC3, TPX2, TRIP13, ZNF367, ZWINT]
GO:0010720	positive regulation of cell development	[Group12]	32	4.5	0.007542	[APOE, ARL6IP1, C3, CALM1, CYFIP1, DAB2IP, DDX39B, DPYSL3, E2F1, ECT2, ENC1, EPHA4, EZH2, FDPS, FOXA1, FYN, FZD1, HMG20B, LRP2, NDNF, NKX6-1, NOTCH1, NTN1, OBSL1, RGMA, SH3GL3, SHH, SYT1, TENM3, TGIF2, TUBB2B, ZEB2]
GO:0045664	regulation of neuron differentiation	[Group12]	38	4.5	9.68E-04	[APOE, ARL6IP1, CALM1, CDC20, CSMD3, CYFIP1, DAB2IP, DPYSL3, ECT2, EDNRB, EFNB3, ENC1, EPHA4, EZH2, FDPS, FOXA1, FYN, FZD1, HERPUD1, HMG20B, NDNF, NKX6-1, NOTCH1, NR2F1, NTN1, OBSL1, PLP1, PTPRO, RGMA, RTN4R, SDK1, SH3GL3, SHH, SYT1, TENM3, TGIF2, TUBB2B, ZEB2]
GO:0045666	positive regulation of neuron differentiation	[Group12]	26	5.2	0.002621	[APOE, ARL6IP1, CALM1, CYFIP1, DAB2IP, DPYSL3, ECT2, ENC1, EPHA4, EZH2, FDPS, FOXA1, FYN, FZD1, HMG20B, NDNF, NKX6-1, NTN1, OBSL1, RGMA, SH3GL3, SYT1, TENM3, TGIF2, TUBB2B, ZEB2]
GO:0050767	regulation of neurogenesis	[Group12]	46	4.4	1.47E-04	[APOE, ARL6IP1, C3, CALM1, CDC20, CDK1, CSMD3, CYFIP1, DAB2IP, DPYSL3, E2F1, ECT2, EDNRB, EFNB3, ENC1, EPHA4, ERBB4, EZH2, FDPS, FOXA1, FYN, FZD1, GPR173, HERPUD1, HES6, HMG20B, HMGB2, LRP2, NDNF, NKX6-1, NOTCH1, NR2F1, NTN1, OBSL1, PLP1, PTPRO, RGMA, RTN4R, SDK1, SH3GL3, SHH, SYT1, TENM3, TGIF2, TUBB2B, ZEB2]
GO:0051960	regulation of nervous system development	[Group12]	52	4.5	1.59E-05	[ADGRB2, AGRN, APOE, ARL6IP1, C3, CALM1, CBLN2, CDC20, CDK1, CLSTN2, CSMD3, CYFIP1, DAB2IP, DPYSL3, E2F1, ECT2, EDNRB, EFNB3, ENC1, EPHA4, ERBB4, EZH2, FDPS, FLRT3, FOXA1, FYN, FZD1, GPR173, HERPUD1, HES6, HMG20B, HMGB2, LRP2, NDNF, NKX6-1, NOTCH1, NR2F1, NTN1, OBSL1, PLP1, PTPRO, RGMA, RTN4R, SDK1, SH3GL3, SHH, SYT1, TENM3, TGIF2, TUBB2B, VANGL2, ZEB2]
GO:0060284	regulation of cell development	[Group12]	49	4.2	4.35E-04	[ADGRA2, APOE, ARL6IP1, C3, CALM1, CDC20, CDK1, CSMD3, CYFIP1, DAB2IP, DDX39B, DPYSL3, E2F1, ECT2, EDNRB, EFNB3, ENC1, EPHA4, ERBB4, EZH2, FBLN1, FDPS, FOXA1, FYN, FZD1, GPR173, HERPUD1, HES6, HMG20B, HMGB2, LRP2, NDNF, NKX6-1, NOTCH1, NR2F1, NTN1, OBSL1, PLP1, PTPRO, RGMA, RTN4R, SDK1, SH3GL3, SHH, SYT1, TENM3, TGIF2, TUBB2B, ZEB2]
GO:0010948	negative regulation of cell cycle process	[Group13, Group14]	27	5.4	9.31E-04	[ARL6IP1, AURKB, BUB1, CCNB1, CDC20, CDC25C, CDC6, CDK1, CDKN2C, CDT1, CENPF, CHAF1A, DAB2IP, DTL, E2F1, ESPL1, EZH2, FBXL7, FBXO43, FZR1, NDC80, PCBP4, PCNA, RAD21, RRM2, TRIP13, ZNF367]

GO:0031570	DNA integrity checkpoint	[Group13, Group14]	18	8.1	1.98E-04	[CCNB1, CDC25C, CDC45, CDC6, CDK1, CDT1, CHAF1A, DDX39B, DTL, E2F1, FZR1, H2AFX, PCBP4, PCNA, PEA15, TIMELESS, TOP2A, ZNF367]
GO:0044770	cell cycle phase transition	[Group13, Group14]	55	6.9	1.73E-13	[ANLN, AURKB, BUB1, CALM1, CCNA2, CCNB1, CCNB2, CDC20, CDC25C, CDC42EP4, CDC45, CDC6, CDCA5, CDK1, CDKN2C, CDT1, CENPF, CEP250, CHAF1A, CIT, CKAP5, DLGAP5, DTL, E2F1, ESPL1, EZH2, FBXL7, FOXM1, FZR1, IQGAP3, KNTC1, MCM3, MCM4, MCM5, MCM7, MCM8, MELK, NCAPD2, NDC80, PCBP4, PCNA, PEA15, PKMYT1, PRKAR2B, RAD21, RHOU, RRM2, TACC3, TIMELESS, TPX2, TRIP13, TUBB, TUBB4B, TYMS, ZNF367]
GO:0044843	cell cycle G1/S phase transition	[Group13, Group14]	23	6.5	2.50E-04	[CCNA2, CCNB1, CDC25C, CDC45, CDC6, CDK1, CDKN2C, CDT1, CHAF1A, E2F1, EZH2, IQGAP3, MCM3, MCM4, MCM5, MCM7, MCM8, PCBP4, PCNA, PEA15, RHOU, RRM2, TYMS]
GO:1901988	negative regulation of cell cycle phase transition	[Group13, Group14]	22	6.4	6.44E-04	[AURKB, BUB1, CCNB1, CDC20, CDC25C, CDC6, CDK1, CDKN2C, CDT1, CENPF, CHAF1A, DTL, E2F1, EZH2, FBXL7, FZR1, NDC80, PCBP4, PCNA, RAD21, TRIP13, ZNF367]
GO:1901991	negative regulation of mitotic cell cycle phase transition	[Group13, Group14]	19	5.9	0.008593	[AURKB, BUB1, CCNB1, CDC20, CDC25C, CDC6, CDK1, CDKN2C, CDT1, CENPF, CHAF1A, E2F1, EZH2, FBXL7, NDC80, PCBP4, PCNA, RAD21, TRIP13]
GO:0000083	regulation of transcription involved in G1/S transition of mitotic cell cycle	[Group13]	7	18.9	0.002419	[CDC45, CDC6, CDT1, E2F1, PCNA, RRM2, TYMS]
GO:0006260	DNA replication	[Group13]	21	5.6	0.007466	[CCNA2, CDC45, CDC6, CDK1, CDT1, CHAF1A, DACH1, DDX11, DTL, MCM3, MCM4, MCM5, MCM7, MCM8, NFIA, PCNA, POLQ, RRM1, RRM2, TIMELESS, TONSL]
GO:0000075	cell cycle checkpoint	[Group14]	27	9.0	2.82E-08	[AURKB, BUB1, CCNB1, CDC20, CDC25C, CDC45, CDC6, CDK1, CDT1, CENPF, CHAF1A, DDX39B, DTL, E2F1, FZR1, H2AFX, KNTC1, NDC80, PCBP4, PCNA, PEA15, TIMELESS, TOP2A, TRIP13, WNT9A, ZNF367, ZWINT]
GO:0000086	G2/M transition of mitotic cell cycle	[Group14]	25	7.3	8.60E-06	[AURKB, CALM1, CCNA2, CCNB1, CCNB2, CDC25C, CDC42EP4, CDC6, CDK1, CENPF, CEP250, CIT, CKAP5, DTL, FBXL7, FOXM1, MELK, NCAPD2, PEA15, PKMYT1, PRKAR2B, RAD21, TPX2, TUBB, TUBB4B]
GO:0000278	mitotic cell cycle	[Group14]	97	7.5	1.47E-28	[ANLN, ARL6IP1, ASNS, AURKB, BIRC5, BTG3, BUB1, CALM1, CCNA2, CCNB1, CCNB2, CDC20, CDC25C, CDC42EP4, CDC45, CDC6, CDCA5, CDCA8, CDK1, CDK19, CDKN2C, CDT1, CENPF, CEP250, CEP55, CHAF1A, CIT, CKAP2, CKAP5, DAB2IP, DLGAP5, DTL, E2F1, ECT2, ESPL1, EZH2, FBXL7, FOXA1, FOXM1, FZR1, GNAI1, INCENP, IQGAP3, KIF11, KIF15, KIF18B, KIF20A, KIF22, KIF23, KNSTRN, KNTC1, MCM3, MCM4, MCM5, MCM7,

						MCM8, MELK, MKI67, MYBL2, NCAPD2, NCAPG, NCAPH2, NDC80, NUSAP1, OBSL1, PCBP4, PCNA, PDGFRB, PEA15, PKMYT1, PLP1, PPP2R2C, PRC1, PRKAR2B, PTPRA, RACGAP1, RAD21, RHOU, RRM1, RRM2, SLC9A3R1, SMC2, SMC4, SPAG5, STMN1, TACC3, TOP2A, TPX2, TRIP13, TUBA1B, TUBB, TUBB2B, TUBB4B, TYMS, WNT9A, ZNF367, ZWINT]
GO:0007088	regulation of mitotic nuclear division	[Group14]	27	10.8	4.08E-10	[ANLN, AURKB, BUB1, CCNA2, CCNB1, CCNB2, CDC20, CDC25C, CDC6, CDCA5, CDT1, CENPF, DLGAP5, ESPL1, KIF11, KNTC1, MKI67, NDC80, NUSAP1, OBSL1, PDGFRB, PKMYT1, PLP1, RAD21, TACC3, TRIP13, ZNF367]
GO:0007091	metaphase/anaphase transition of mitotic cell cycle	[Group14]	13	17.6	8.19E-07	[AURKB, BUB1, CCNB1, CDC20, CDC6, CDT1, CENPF, DLGAP5, ESPL1, NDC80, RAD21, TACC3, TRIP13]
GO:0007093	mitotic cell cycle checkpoint	[Group14]	19	8.4	5.11E-05	[AURKB, BUB1, CCNB1, CDC20, CDC25C, CDC6, CDK1, CDT1, CENPF, CHAF1A, E2F1, KNTC1, NDC80, PCBP4, PCNA, TOP2A, TRIP13, WNT9A, ZWINT]
GO:0007346	regulation of mitotic cell cycle	[Group14]	58	6.6	2.43E-13	[ANLN, ARL6IP1, ASNS, AURKB, BIRC5, BTG3, BUB1, CCNA2, CCNB1, CCNB2, CDC20, CDC25C, CDC42EP4, CDC45, CDC6, CDCA5, CDK1, CDKN2C, CDT1, CENPF, CEP250, CHAF1A, CKAP5, DAB2IP, DLGAP5, DTL, E2F1, ESPL1, EZH2, FBXL7, FOXA1, FZR1, GNAI1, INCENP, KIF11, KNTC1, MKI67, NCAPD2, NDC80, NUSAP1, OBSL1, PCBP4, PCNA, PDGFRB, PKMYT1, PLP1, PRKAR2B, RAD21, SLC9A3R1, TACC3, TOP2A, TPX2, TRIP13, TUBB, TUBB4B, WNT9A, ZNF367, ZWINT]
GO:0010389	regulation of G2/M transition of mitotic cell cycle	[Group14]	17	6.3	0.009579	[AURKB, CCNB1, CDC25C, CDC42EP4, CDC6, CDK1, CENPF, CEP250, CKAP5, DTL, FBXL7, NCAPD2, PRKAR2B, RAD21, TPX2, TUBB, TUBB4B]
GO:0010564	regulation of cell cycle process	[Group14]	65	6.2	7.50E-14	[ANLN, ARL6IP1, AURKB, BUB1, CALM1, CCNA2, CCNB1, CCNB2, CDC20, CDC25C, CDC42EP4, CDC45, CDC6, CDCA5, CDK1, CDKN2C, CDT1, CENPF, CEP250, CHAF1A, CIT, CKAP5, DAB2IP, DACH1, DDX11, DLGAP5, DTL, E2F1, ECT2, ESPL1, EZH2, FBXL7, FBXO43, FOXM1, FZR1, GNAI1, INCENP, KIF11, KIF20A, KIF23, KNSTRN, KNTC1, MKI67, NCAPD2, NDC80, NUSAP1, OBSL1, PCBP4, PCNA, PDGFRB, PKMYT1, PLP1, PRC1, PRKAR2B, RACGAP1, RAD21, RRM2, SOX12, SPAG5, TACC3, TPX2, TRIP13, TUBB, TUBB4B, ZNF367]
GO:0010639	negative regulation of organelle organization	[Group14]	26	4.9	0.007537	[ARHGAP28, AURKB, BUB1, C3, CCNB1, CDC20, CDT1, CENPF, CKAP2, DNMT1, ESPL1, FBXO43, H1F0, HDAC6, MCM7, NCAPG, NDC80, NUPR1, PEA15, PHLDB2, RAD21, STMN1, TOP2A, TRIM9, TRIP13, TUBB]
GO:0022402	cell cycle process	[Group14]	97	5.6	5.22E-19	[ANLN, ARL6IP1, AURKB, BIRC5, BUB1, CALM1, CCNA2, CCNB1, CCNB2, CDC20, CDC25C, CDC42EP4, CDC45, CDC6, CDCA5, CDCA8, CDK1, CDKN2C,

						CDT1, CENPF, CEP250, CEP55, CHAF1A, CIT, CKAP2, CKAP5, DAB2IP, DACH1, DDX11, DLGAP5, DTL, E2F1, ECT2, ESPL1, EZH2, FANCA, FBXL7, FBXO43, FDPS, FOXM1, FZR1, GNAI1, INCENP, IQGAP3, KIF11, KIF18B, KIF20A, KIF22, KIF23, KNL1, KNSTRN, KNTC1, MCM3, MCM4, MCM5, MCM7, MCM8, MELK, MKI67, MYBL2, NCAPD2, NCAPG, NCAPH2, NDC80, NOTCH1, NUSAP1, OBSL1, PCBP4, PCNA, PDGFRB, PEA15, PHGDH, PKMYT1, PLP1, PRC1, PRKAR2B, PTPRA, RACGAP1, RAD21, RHOU, RRM2, SMC2, SMC4, SOX12, SPAG5, STMN1, TACC3, TIMELESS, TOP2A, TPX2, TRIP13, TUBB, TUBB4B, TYMS, WNT9A, ZNF367, ZWINT]
GO:0033043	regulation of organelle organization	[Group14]	72	4.4	4.37E-08	[ANLN, ARHGAP28, ARHGEF10L, ARL6IP1, ATXN2L, AURKB, BUB1, C3, CCNA2, CCNB1, CCNB2, CDC20, CDC25C, CDC42EP4, CDC45, CDC6, CDCA5, CDT1, CENPF, CEP250, CIT, CKAP2, CYFIP1, DAB2IP, DDX11, DLGAP5, DNMT1, E2F1, ECT2, ESPL1, FBXO43, FDPS, FZR1, GNAI1, GPM6B, H1F0, HDAC6, JDP2, KIAA1324, KIF11, KNTC1, MCM7, MKI67, NCAPD2, NCAPG, NDC80, NUPR1, NUSAP1, OBSL1, PDGFRB, PEA15, PHF19, PHLDB2, PKMYT1, PLP1, PSAT1, RAD21, RHOU, SETD5, SPAG5, STMN1, SYT1, TACC3, TIMELESS, TOP2A, TPX2, TRIM9, TRIP13, TUBB, VANGL2, ZEB2, ZNF367]
GO:0033045	regulation of sister chromatid segregation	[Group14]	15	13.4	2.33E-06	[AURKB, BUB1, CCNB1, CDC20, CDC6, CDCA5, CDT1, CENPF, DDX11, DLGAP5, ESPL1, NDC80, RAD21, TACC3, TRIP13]
GO:0033046	negative regulation of sister chromatid segregation	[Group14]	10	14.1	4.77E-04	[AURKB, BUB1, CCNB1, CDC20, CDT1, CENPF, ESPL1, NDC80, RAD21, TRIP13]
GO:0044839	cell cycle G2/M phase transition	[Group14]	27	7.4	1.74E-06	[AURKB, CALM1, CCNA2, CCNB1, CCNB2, CDC25C, CDC42EP4, CDC6, CDK1, CENPF, CEP250, CIT, CKAP5, DTL, FBXL7, FOXM1, FZR1, MELK, NCAPD2, PEA15, PKMYT1, PRKAR2B, RAD21, TPX2, TUBB, TUBB4B, ZNF367]
GO:0045786	negative regulation of cell cycle	[Group14]	41	4.8	6.53E-05	[ARL6IP1, AURKB, BTG3, BUB1, CCNB1, CDC20, CDC25C, CDC45, CDC6, CDK1, CDKN2C, CDT1, CENPF, CHAF1A, DAB2IP, DDX39B, DTL, E2F1, ESPL1, EZH2, FBXL7, FBXO43, FOXM1, FZR1, H2AFX, KNTC1, NDC80, NOTCH1, NUPR1, PCBP4, PCNA, PEA15, RAD21, RRM2, SLC9A3R1, TIMELESS, TOP2A, TRIP13, WNT9A, ZNF367, ZWINT]
GO:0045787	positive regulation of cell cycle	[Group14]	36	6.6	1.05E-07	[ARL6IP1, ASNS, AURKB, CCNA2, CCNB1, CCNB2, CDC25C, CDC45, CDC6, CDCA5, CDK1, CDT1, CHAF1A, CIT, DAB2IP, DDX11, DDX39B, DLGAP5, DTL, E2F1, ECT2, ESPL1, EZH2, FOXA1, KIF23, NDC80, NUSAP1, PCBP4, PCNA, PDGFRB, PEA15, RACGAP1, RAD21, SOX12, SPAG5, ZNF367]

GO:0045930	negative regulation of mitotic cell cycle	[Group14]	28	6.3	2.90E-05	[ARL6IP1, AURKB, BTG3, BUB1, CCNB1, CDC20, CDC25C, CDC6, CDK1, CDKN2C, CDT1, CENPF, CHAF1A, DAB2IP, E2F1, EZH2, FBXL7, KNTC1, NDC80, PCBP4, PCNA, RAD21, SLC9A3R1, TOP2A, TRIP13, WNT9A, ZNF367, ZWINT]
GO:0045931	positive regulation of mitotic cell cycle	[Group14]	15	7.0	0.008581	[ASNS, CCNB1, CDC25C, CDC45, CDC6, CDCA5, CDK1, CDT1, DLGAP5, DTL, ESPL1, FOXA1, NDC80, NUSAP1, PDGFRB]
GO:0051129	negative regulation of cellular component organization	[Group14]	41	4.4	9.30E-04	[APOE, ARHGAP28, AURKB, BUB1, C3, CCNB1, CDC20, CDT1, CENPF, CKAP2, DNMT1, DPYSL3, EFNB3, EPHA4, ESPL1, FBLN1, FBXO43, FYN, H1F0, HDAC6, MCM7, NCAPG, NDC80, NOTCH1, NR2F1, NTN1, NUPR1, PCSK9, PEA15, PHLDB2, PLP1, PTPRO, RAD21, RGMA, RTN4R, SH3GL3, STMN1, TOP2A, TRIM9, TRIP13, TUBB]
GO:0051304	chromosome separation	[Group14]	17	14.2	9.36E-08	[AURKB, BUB1, CCNB1, CDC20, CDC6, CDT1, CENPF, CEP250, DLGAP5, ESPL1, NCAPD2, NCAPH2, NDC80, RAD21, TACC3, TOP2A, TRIP13]
GO:0051306	mitotic sister chromatid separation	[Group14]	14	16.5	4.77E-07	[AURKB, BUB1, CCNB1, CDC20, CDC6, CDT1, CENPF, DLGAP5, ESPL1, NCAPH2, NDC80, RAD21, TACC3, TRIP13]
GO:0051726	regulation of cell cycle	[Group14]	82	5.2	1.07E-13	[ANLN, ARL6IP1, ASNS, AURKB, BIRC5, BTG3, BUB1, CALM1, CCNA2, CCNB1, CCNB2, CDC20, CDC25C, CDC42EP4, CDC45, CDC6, CDCA5, CDK1, CDK19, CDKN2C, CDT1, CENPF, CEP250, CHAF1A, CIT, CKAP5, DAB2IP, DACH1, DDX11, DDX39B, DLGAP5, DTL, E2F1, E2F2, ECT2, ESPL1, EZH2, FBXL7, FBXO43, FOXA1, FOXM1, FZR1, GNAI1, H2AFX, INCENP, KIF11, KIF20A, KIF23, KNSTRN, KNTC1, MKI67, MYBL2, NCAPD2, NDC80, NOTCH1, NUPR1, NUSAP1, OBSL1, PCBP4, PCNA, PDGFRB, PEA15, PKMYT1, PLP1, PRC1, PRKAR2B, RACGAP1, RAD21, RRM2, SLC9A3R1, SOX12, SPAG5, TACC3, TIMELESS, TOP2A, TPX2, TRIP13, TUBB, TUBB4B, WNT9A, ZNF367, ZWINT]
GO:0051783	regulation of nuclear division	[Group14]	29	10.2	2.17E-10	[ANLN, AURKB, BUB1, CCNA2, CCNB1, CCNB2, CDC20, CDC25C, CDC6, CDCA5, CDT1, CENPF, DLGAP5, ESPL1, FBXO43, FZR1, KIF11, KNTC1, MKI67, NDC80, NUSAP1, OBSL1, PDGFRB, PKMYT1, PLP1, RAD21, TACC3, TRIP13, ZNF367]
GO:0051784	negative regulation of nuclear division	[Group14]	10	10.5	0.006373	[AURKB, BUB1, CCNB1, CDC20, CDT1, CENPF, FBXO43, NDC80, RAD21, TRIP13]
GO:0051984	positive regulation of chromosome segregation	[Group14]	7	19.4	0.002013	[CCNB1, CDC6, CDT1, DDX11, DLGAP5, ESPL1, RAD21]
GO:1901990	regulation of mitotic cell cycle phase transition	[Group14]	36	6.3	4.28E-07	[ANLN, AURKB, BUB1, CCNB1, CDC20, CDC25C, CDC42EP4, CDC45, CDC6, CDCA5, CDK1, CDKN2C, CDT1, CENPF, CEP250, CHAF1A, CKAP5, DLGAP5,

						DTL, E2F1, ESPL1, EZH2, FBXL7, FZR1, KNTC1, NCAPD2, NDC80, PCBP4, PCNA, PRKAR2B, RAD21, TPX2, TRIP13, TUBB, TUBB4B, ZNF367]
GO:1902749	regulation of cell cycle G2/M phase transition	[Group14]	19	6.6	0.002056	[AURKB, CCNB1, CDC25C, CDC42EP4, CDC6, CDK1, CENPF, CEP250, CKAP5, DTL, FBXL7, FZR1, NCAPD2, PRKAR2B, RAD21, TPX2, TUBB, TUBB4B, ZNF367]
GO:1903047	mitotic cell cycle process	[Group14]	87	7.8	1.75E-26	[ANLN, ARL6IP1, AURKB, BIRC5, BUB1, CALM1, CCNA2, CCNB1, CCNB2, CDC20, CDC25C, CDC42EP4, CDC45, CDC6, CDCA5, CDCA8, CDK1, CDKN2C, CDT1, CENPF, CEP250, CEP55, CHAF1A, CIT, CKAP2, CKAP5, DAB2IP, DLGAP5, DTL, E2F1, ECT2, ESPL1, EZH2, FBXL7, FOXM1, FZR1, GNAI1, INCENP, IQGAP3, KIF11, KIF18B, KIF20A, KIF22, KIF23, KNSTRN, KNTC1, MCM3, MCM4, MCM5, MCM7, MCM8, MELK, MKI67, MYBL2, NCAPD2, NCAPG, NCAPH2, NDC80, NUSAP1, OBSL1, PCBP4, PCNA, PDGFRB, PEA15, PKMYT1, PLP1, PRC1, PRKAR2B, PTPRA, RACGAP1, RAD21, RHOU, RRM2, SMC2, SMC4, SPAG5, STMN1, TACC3, TOP2A, TPX2, TRIP13, TUBB, TUBB4B, TYMS, WNT9A, ZNF367, ZWINT]
GO:2001251	negative regulation of chromosome organization	[Group14]	16	7.6	0.001707	[AURKB, BUB1, C3, CCNB1, CDC20, CDT1, CENPF, DNMT1, ESPL1, H1F0, MCM7, NDC80, PEA15, RAD21, TOP2A, TRIP13]

CLUSTER B

GO ID	GO Term	Group	Number of Genes	Associated Genes (%)	Adj. p-value	Associated Genes Found
GO:0019320	hexose catabolic process	[Group4]	6	8.7	6.79E-05	[GALE, GPI, HK1, HK2, LRP5, PKM]
GO:0019674	NAD metabolic process	[Group4]	6	5.7	6.85E-04	[FAM160A2, GPI, HK1, HK2, LDHA, PKM]
GO:0006027	glycosaminoglycan catabolic process	[Group0]	5	6.7	0.001061	[BGN, CSPG4, GPC1, KERA, SGSH]
GO:0046902	regulation of mitochondrial membrane permeability	[Group5]	5	4.9	0.003843	[HK2, HSPA1A, KERA, RHOT2, SF1]
GO:0097345	mitochondrial outer membrane permeabilization	[Group5]	4	5.6	0.006406	[HSPA1A, KERA, RHOT2, SF1]
GO:0097178	ruffle assembly	[Group3]	3	5.4	0.00699	[CYFIP1, EPS8L2, INPPL1]
GO:0060350	endochondral bone morphogenesis	[Group1]	4	4.9	0.007405	[COL27A1, COL2A1, INPPL1, THBS3]
GO:0060603	mammary gland duct morphogenesis	[Group2]	3	6.0	0.010188	[GLI2, LRP5, PKD1]

CLUSTER C

GO ID	GO Term	Group	Number of Genes	Associated Genes (%)	Adj. p-value	Associated Genes Found
GO:0003300	cardiac muscle hypertrophy	[Group2]	5	4.3	0.001698	[AGT, DDX39B, IL6ST, INPP5F, MEF2C]
GO:2000725	regulation of cardiac muscle cell differentiation	[Group2]	3	6.3	0.003504	[DDX39B, FRS2, MEF2C]
GO:0048011	neurotrophin TRK receptor signaling pathway	[Group1]	3	6.4	0.004945	[AGT, FRS2, NTRK2]
GO:1904705	regulation of vascular smooth muscle cell proliferation	[Group2]	3	4.1	0.005761	[AGT, DDX39B, MEF2C]
GO:0031110	regulation of microtubule polymerization or depolymerization	[Group0]	4	4.0	0.006245	[HSPA1A, MAPRE1, SKA2, TUBB]
GO:0010613	positive regulation of cardiac muscle hypertrophy	[Group2]	3	6.7	0.007264	[AGT, DDX39B, IL6ST]

CLUSTER D

GO ID	GO Term	Group	Number of Genes	Associated Genes (%)	Adj. p-value	Associated Genes Found
GO:0009266	response to temperature stimulus	[Group00]	16	5.0	0.004085	[ADARB1, ANO1, ATM, ATP2B1, CDKN1A, EIF2A, HMOX1, HSPA1A, HSPA6, IGFBP7, MTUS1, MYOF, PDCD6, SCARA5, SFRP1, THBS1]
GO:0043405	regulation of MAP kinase activity	[Group01]	22	4.6	5.36E-04	[ADAM12, BIRC3, CDKN1A, DUSP1, DUSP6, FGF2, HIPK3, IL6, IQGAP1, KIT, MAP3K8, PLA2G2A, RGS2, RGS3, SFRP1, SPRY2, SPRY4, STK39, TAB3, TGFA, TGFB1, THBS1]
GO:0072593	reactive oxygen species metabolic process	[Group02]	19	5.3	2.89E-04	[AKR1C1, ARF4, BCL2, CCN2, CCN6, CDKN1A, HIF1A, IFI6, MEOX2, NQO1, PMAIP1, PRDX4, ROCK2, SOD2, SOD3, TGFB1, THBS1, TLR5, WDR35]
GO:0030212	hyaluronan metabolic process	[Group03]	7	14.3	0.001704	[CEMIP, CEMIP2, FGF2, HEXB, IL6, ITIH6, TGFB1]
GO:1903510	mucopolysaccharide metabolic process	[Group03]	10	7.4	0.006811	[CEMIP, CEMIP2, CSGALNACT1, FGF2, FMOD, HEXB, IL6, IMPAD1, ITIH6, TGFB1]
GO:0031960	response to corticosteroid	[Group04]	16	6.5	1.82E-04	[ADAM12, AKR1C1, ATP2B1, BCL2, BMP6, CCN2, CDKN1A, DUSP1, ERRFI1, FOSB, IGFBP7, IL1R1, IL6, PAPPA, RAPH1, TGFB1]
GO:0048545	response to steroid hormone	[Group04]	25	4.4	2.02E-04	[ADAM12, AKR1C1, ATP2B1, BCL2, BMP6, CCN2, CDH4, CDKN1A, DUSP1, ERRFI1, FHL2, FOSB, IGFBP7, IL1R1, IL6, LEF1, MDM2, NR4A1, NR4A2, PAPPA, RAPH1, SFRP1, SPP1, TGFB1, THBS1]
GO:0051384	response to glucocorticoid	[Group04]	14	6.1	0.001663	[ADAM12, ATP2B1, BCL2, BMP6, CDKN1A, DUSP1, ERRFI1, FOSB, IGFBP7, IL1R1, IL6, PAPPA, RAPH1, TGFB1]
GO:1901654	response to ketone	[Group04]	15	5.6	0.00221	[ADCY1, AKR1C1, AKR1C2, ATP2B1, CDKN1A, DUSP1, ERRFI1, FOSB, IGFBP7, NME1, ROCK2, SFRP1, SPP1, TGFB1, THBS1]
GO:0010715	regulation of extracellular matrix disassembly	[Group05]	6	22.2	5.67E-04	[CST3, ETS1, IL6, PDPN, PMAIP1, TGFB1]
GO:0022617	extracellular matrix disassembly	[Group05]	9	8.3	0.006828	[A2M, CST3, ETS1, IL6, MMP1, PDPN, PMAIP1, SCUBE1, TGFB1]
GO:0030198	extracellular matrix organization	[Group05]	27	6.2	4.63E-08	[A2M, ADAM12, CCN2, COL19A1, COL25A1, COMP, CSGALNACT1, CST3, ETS1, FGF2, FMOD, GAS6, HAPLN1, IL6, LOXL4, MATN3, MMP1, PDPN, PMAIP1, PRDX4, RUNX2, SCUBE1, SGCG, SPP1, TGFB1, THBS1, TNFRSF11B]
GO:0043062	extracellular structure organization	[Group05]	30	5.8	2.76E-08	[A2M, ACAT1, ADAM12, BIRC3, CCN2, COL19A1, COL25A1, COMP, CSGALNACT1, CST3, ETS1, FGF2, FMOD, GAS6, HAPLN1, IL6, LOXL4, MATN3,

						MMP1, PDPN, PLA2G2A, PMAIP1, PRDX4, RUNX2, SCUBE1, SGCG, SPP1, TGFB1, THBS1, TNFRSF11B]
GO:0030335	positive regulation of cell migration	[Group06, Group12]	34	5.3	1.47E-08	[ADAM12, ATM, BCL2, BIRC3, CEMIP, CNTN1, ETS1, FGF2, GAS6, HDAC9, HIF1A, HMOX1, IL1R1, IL6, IQGAP1, KIT, LEF1, LGMN, MDM2, NELL1, PDCD6, PDPN, PMAIP1, PTP4A1, ROCK2, RUNX2, SEMA3C, SGCG, SOD2, SPRY2, STK39, TAC1, TGFB1, THBS1]
GO:0070848	response to growth factor	[Group06, Group12]	38	4.2	7.56E-07	[ADAM12, ANOS1, ATM, BIRC3, BMP6, CCN2, CD109, COMP, DUSP6, ERRFI1, FGF2, FMOD, GAS6, HIF1A, HSPA1A, IL6, IQGAP1, LEF1, LGMN, LTBP1, MDM2, MYOF, NELL1, NR4A1, PCSK6, PDCD6, PENK, ROCK2, RPL29, RUNX2, SFRP1, SGCG, SPP1, SPRY2, SPRY4, TAC1, TGFB1, THBS1]
GO:0071363	cellular response to growth factor stimulus	[Group06, Group12]	36	4.1	2.97E-06	[ADAM12, ANOS1, ATM, BIRC3, BMP6, CCN2, CD109, COMP, ERRFI1, FGF2, FMOD, GAS6, HIF1A, HSPA1A, IL6, IQGAP1, LEF1, LGMN, LTBP1, MDM2, MYOF, NELL1, NR4A1, PCSK6, PDCD6, PENK, RPL29, RUNX2, SFRP1, SGCG, SPP1, SPRY2, SPRY4, TAC1, TGFB1, THBS1]
GO:0044344	cellular response to fibroblast growth factor stimulus	[Group06]	11	6.4	0.009797	[ANOS1, CCN2, FGF2, IQGAP1, NR4A1, RPL29, RUNX2, SFRP1, SPRY2, SPRY4, THBS1]
GO:0010035	response to inorganic substance	[Group07]	31	4.1	5.19E-05	[ADAM12, ADCY1, AKR1C1, ANXA5, BCL2, BMP6, CDKN1A, DUSP1, EIF2A, ETS1, FOSB, HIF1A, HMOX1, IL6, IQGAP1, KIT, LGMN, MDM2, ND5, NQO1, PDCD6, PENK, PHEX, PPFIBP1, S100A13, SGCG, SOD2, SOD3, STK26, THBS1, TNFRSF11B]
GO:0010038	response to metal ion	[Group07]	25	5.0	1.95E-05	[ADAM12, ADCY1, AKR1C1, ANXA5, BCL2, BMP6, CDKN1A, DUSP1, EIF2A, FOSB, HIF1A, HMOX1, IQGAP1, KIT, LGMN, MDM2, NQO1, PDCD6, PENK, PPFIBP1, S100A13, SGCG, SOD3, THBS1, TNFRSF11B]
GO:0031668	cellular response to extracellular stimulus	[Group07]	17	4.6	0.006291	[AKR1C1, ATP2B1, BCL2, CDKN1A, EIF2A, GAS6, HMOX1, MDM2, NR4A2, PENK, PHEX, PMAIP1, RUNX2, SFRP1, SLC39A4, STK26, UTRN]
GO:0033273	response to vitamin	[Group07]	10	7.1	0.009736	[ALDH1A2, ATP2B1, GAS6, MDM2, PENK, PHEX, RUNX2, SFRP1, SPP1, TGFB1]
GO:0034599	cellular response to oxidative stress	[Group07]	18	4.5	0.005901	[AKR1C1, BCL2, CDKN1A, EIF2A, ETS1, HIF1A, HMOX1, HSPA1A, IGFBP7, IL6, MCL1, MDM2, NQO1, NR4A2, PENK, SOD2, SOD3, STK26]
GO:0071496	cellular response to external stimulus	[Group07]	20	4.4	0.002259	[AKR1C1, ATP2B1, BCL2, BMP6, CDKN1A, EIF2A, GAS6, HMOX1, MDM2, NR4A2, PENK, PHEX, PMAIP1, RUNX2, SFRP1, SLC39A4, STK26, TGFB1, TLR5, UTRN]
GO:0001501	skeletal system development	[Group08]	26	4.0	5.73E-04	[BMP6, CCN2, COL19A1, COMP, CSGALNACT1, CYTL1, FGF2, HAPLN1, HEXB, HIF1A, IMPAD1, JAG2, KIT, MATN3, MGP, PHEX, PTH1R, RBP4, RPL29, RPS6KA3, RUNX2, SCIN, SERP1, SFRP1, TGFB1, TNFRSF11B]

GO:0001649	osteoblast differentiation	[Group08]	14	5.3	0.007096	[BMP6, CDH4, FHL2, HDAC9, IL6, LEF1, NELL1, OSTN, PENK, PTH1R, RUNX2, SFRP1, SP7, SPP1]
GO:0030278	regulation of ossification	[Group08]	14	6.0	0.00211	[ATP2B1, BCL2, BMP6, COMP, HDAC9, HIF1A, IL6, MGP, NELL1, OSTN, RUNX2, SFRP1, TAC1, TGFB1]
GO:0031214	biomineral tissue development	[Group08]	13	6.4	0.002157	[ATP2B1, BMP6, COMP, GAS6, HIF1A, MGP, NELL1, PHEX, PLA2G2A, PTH1R, ROCK2, SPP1, TGFB1]
GO:0051216	cartilage development	[Group08]	15	5.8	0.001434	[BMP6, CCN2, COMP, CSGALNACT1, CYTL1, FGF2, HIF1A, IMPAD1, MATN3, MGP, PTH1R, RUNX2, SCIN, SFRP1, TGFB1]
GO:0061448	connective tissue development	[Group08]	18	5.4	4.87E-04	[ACAT1, ACTA2, BMP6, CCN2, COMP, CSGALNACT1, CYTL1, EBF2, FGF2, HIF1A, IMPAD1, MATN3, MGP, PTH1R, RUNX2, SCIN, SFRP1, TGFB1]
GO:0001558	regulation of cell growth	[Group09]	23	4.2	0.00107	[BCL2, BCL6, CDH4, CDKN1A, DCC, GOLGA4, HSPA1A, IGFBP7, LEF1, NELL1, NRCAM, OSTN, PMAIP1, RGS2, RPS6KA3, SEMA3C, SERPINE2, SFRP1, SLC43A3, SPOCK1, SPP1, TAF9, TGFB1]
GO:0030308	negative regulation of cell growth	[Group09]	14	5.7	0.003473	[BCL2, BCL6, CDKN1A, DCC, HSPA1A, NELL1, OSTN, RGS2, SEMA3C, SERPINE2, SFRP1, SLC43A3, SPP1, TGFB1]
GO:0045926	negative regulation of growth	[Group09]	17	4.8	0.004321	[BCL2, BCL6, CDKN1A, DCC, HIF1A, HSPA1A, LGMN, NELL1, OSTN, RBP4, RGS2, SEMA3C, SERPINE2, SFRP1, SLC43A3, SPP1, TGFB1]
GO:0048588	developmental cell growth	[Group09]	16	5.4	0.001667	[CDH4, DCC, GOLGA4, IQGAP1, NELL1, NRCAM, NRN1, OSTN, PDLIM5, PMAIP1, RAPH1, RGS2, RUNX2, SEMA3C, SGCG, SPP1]
GO:0048638	regulation of developmental growth	[Group09]	19	4.5	0.003071	[BCL2, CDH4, CDKN1A, DCC, DUSP6, FGF2, GOLGA4, LGMN, NELL1, NRCAM, OSTN, PMAIP1, RBP4, RGS2, SEMA3C, SERP1, SFRP1, SGCG, SPP1]
GO:0060560	developmental growth involved in morphogenesis	[Group09]	18	5.8	1.77E-04	[BIRC3, CDH4, DCC, GOLGA4, IQGAP1, NELL1, NRCAM, NRN1, OSTN, PMAIP1, RAPH1, RUNX2, SEMA3C, SFRP1, SGCG, SPP1, SPRY2, TGFB1]
GO:0000184	nuclear-transcribed mRNA catabolic process, nonsense-mediated decay	[Group10]	15	9.6	2.45E-06	[ERRFI1, RPL10A, RPL14, RPL17, RPL18A, RPL27A, RPL29, RPL6, RPL7, RPS13, RPS17, RPS18, RPS19, RPS5, RPS6]
GO:0000956	nuclear-transcribed mRNA catabolic process	[Group10]	17	6.4	9.25E-05	[ATM, ERRFI1, RPL10A, RPL14, RPL17, RPL18A, RPL27A, RPL29, RPL6, RPL7, RPS13, RPS17, RPS18, RPS19, RPS5, RPS6, SAMD4A]
GO:0006402	mRNA catabolic process	[Group10]	21	4.5	0.001013	[ATM, ERRFI1, HSPA1A, ROCK2, RPL10A, RPL14, RPL17, RPL18A, RPL27A, RPL29, RPL6, RPL7, RPS13, RPS17, RPS18, RPS19, RPS5, RPS6, SAMD4A, SERBP1, ZC3HAV1]
GO:0006612	protein targeting to membrane	[Group10]	17	6.7	4.56E-05	[CEMIP, ERRFI1, PPFIBP1, RPL10A, RPL14, RPL17, RPL18A, RPL27A, RPL29, RPL6, RPL7, RPS13, RPS17, RPS18, RPS19, RPS5, RPS6]

GO:0019080	viral gene expression	[Group10]	20	8.0	1.77E-07	[ADARB1, ERRFI1, IFITM3, LEF1, MTUS1, RPL10A, RPL14, RPL17, RPL18A, RPL27A, RPL29, RPL6, RPL7, RPS13, RPS17, RPS18, RPS19, RPS5, RPS6, UTRN]
GO:0045047	protein targeting to ER	[Group10]	16	11.5	4.83E-08	[ERRFI1, PPFIBP1, RPL10A, RPL14, RPL17, RPL18A, RPL27A, RPL29, RPL6, RPL7, RPS13, RPS17, RPS18, RPS19, RPS5, RPS6]
GO:0070972	protein localization to endoplasmic reticulum	[Group10]	17	10.0	1.18E-07	[ERRFI1, KDELR3, PPFIBP1, RPL10A, RPL14, RPL17, RPL18A, RPL27A, RPL29, RPL6, RPL7, RPS13, RPS17, RPS18, RPS19, RPS5, RPS6]
GO:0090150	establishment of protein localization to membrane	[Group10]	20	4.6	0.001503	[BCL2, CEMIP, ERRFI1, GOLGA4, PMAIP1, PPFIBP1, RPL10A, RPL14, RPL17, RPL18A, RPL27A, RPL29, RPL6, RPL7, RPS13, RPS17, RPS18, RPS19, RPS5, RPS6]
GO:0004252	serine-type endopeptidase activity	[Group11]	16	4.7	0.008048	[A2M, ANOS1, CD109, CNTN1, IL6, ITIH6, MMP1, PAMR1, PCSK6, SERPINA1, SERPINA3, SERPINE2, SERPINI1, SGCG, SPOCK1, THBS1]
GO:0004857	enzyme inhibitor activity	[Group11]	21	4.2	0.003496	[A2M, ANOS1, ANXA5, BIRC3, CD109, CDKN1A, CST3, FRY, GAS6, IQGAP1, ITIH6, LEF1, RPL17, RPS6KA3, SERPINA1, SERPINA3, SERPINE2, SERPINI1, SGCG, SPOCK1, SPRY2]
GO:0004866	endopeptidase inhibitor activity	[Group11]	15	6.6	3.39E-04	[A2M, ANOS1, BIRC3, CD109, CST3, GAS6, ITIH6, LEF1, RPS6KA3, SERPINA1, SERPINA3, SERPINE2, SERPINI1, SGCG, SPOCK1]
GO:0004867	serine-type endopeptidase inhibitor activity	[Group11]	10	8.1	0.00334	[A2M, ANOS1, CD109, ITIH6, SERPINA1, SERPINA3, SERPINE2, SERPINI1, SGCG, SPOCK1]
GO:0008236	serine-type peptidase activity	[Group11]	18	4.9	0.00174	[A2M, ADARB1, ANOS1, CD109, CNTN1, IL6, ITIH6, MMP1, PAMR1, PCSK6, SCPEP1, SERPINA1, SERPINA3, SERPINE2, SERPINI1, SGCG, SPOCK1, THBS1]
GO:0010951	negative regulation of endopeptidase activity	[Group11]	20	6.2	1.25E-05	[A2M, ANOS1, BIRC3, CD109, CST3, GAS6, IFI6, IL6, ITIH6, LEF1, MDM2, NR4A1, RPS6KA3, SERPINA1, SERPINA3, SERPINE2, SERPINI1, SGCG, SPOCK1, THBS1]
GO:0045861	negative regulation of proteolysis	[Group11]	24	5.3	1.14E-05	[A2M, ANOS1, BIRC3, CD109, CST3, GAS6, IFI6, IL6, ITIH6, LEF1, MDM2, NR4A1, PTPN3, RPL17, RPS6KA3, SERPINA1, SERPINA3, SERPINE2, SERPINI1, SGCG, SPOCK1, SVIP, TAF9, THBS1]
GO:0051346	negative regulation of hydrolase activity	[Group11]	27	4.6	2.86E-05	[A2M, ANOS1, BIRC3, CCNL1, CD109, CST3, GAS6, HDAC9, IFI6, IL6, IQGAP1, ITIH6, LEF1, MDM2, NR4A1, RGS2, RIMBP2, ROCK2, RPS6KA3, SERPINA1, SERPINA3, SERPINE2, SERPINI1, SGCG, SPOCK1, SPRY2, THBS1]
GO:0052548	regulation of endopeptidase activity	[Group11]	27	5.0	5.61E-06	[A2M, ANOS1, BIRC3, CCN2, CD109, CNTN1, CST3, GAS6, IFI6, IL6, ITIH6, LEF1, LGMN, MDM2, NR4A1, PDCD6, PMAIP1, ROCK2, RPS6KA3, SERPINA1, SERPINA3, SERPINE2, SERPINI1, SGCG, SPOCK1, THBS1, WDR35]

GO:0010595	positive regulation of endothelial cell migration	[Group12]	11	8.0	0.001423	[ETS1, FGF2, HDAC9, HIF1A, HMOX1, LGMN, NELL1, PDCD6, ROCK2, TGFB1, THBS1]
GO:0010631	epithelial cell migration	[Group12]	17	4.5	0.008979	[ADAM12, BIRC3, ETS1, FGF2, HDAC9, HIF1A, HMOX1, KIT, LGMN, MEOX2, NELL1, NR4A1, PDCD6, ROCK2, TAC1, TGFB1, THBS1]
GO:0010632	regulation of epithelial cell migration	[Group12]	15	5.2	0.005463	[ADAM12, BIRC3, ETS1, FGF2, HDAC9, HIF1A, HMOX1, LGMN, MEOX2, NELL1, PDCD6, ROCK2, TAC1, TGFB1, THBS1]
GO:0010634	positive regulation of epithelial cell migration	[Group12]	13	6.8	0.001078	[ADAM12, ETS1, FGF2, HDAC9, HIF1A, HMOX1, LGMN, NELL1, PDCD6, ROCK2, TAC1, TGFB1, THBS1]
GO:0032103	positive regulation of response to external stimulus	[Group12]	18	4.5	0.006077	[BMP6, CNTN1, ETS1, FGF2, GAS6, IL6, LGMN, NELL1, OSMR, PLA2G2A, PMAIP1, PTGER3, RPS19, SGCG, STK39, TAC1, TGFB1, THBS1]
GO:0045765	regulation of angiogenesis	[Group12]	18	4.8	0.0023	[ADAM12, BIRC3, CEMIP2, CNTN1, ETS1, FGF2, HDAC9, HIF1A, HMOX1, IL6, MEOX2, NELL1, PDCD6, ROCK2, SFRP1, SPRY2, THBS1, THBS2]
GO:0051272	positive regulation of cellular component movement	[Group12]	36	5.3	3.58E-09	[ADAM12, ATM, BCL2, BCL6, BIRC3, CEMIP, CNTN1, ETS1, FGF2, GAS6, HDAC9, HIF1A, HMOX1, IL1R1, IL6, IQGAP1, KIT, LEF1, LGMN, MDM2, NELL1, PDCD6, PDPN, PMAIP1, PTP4A1, ROCK2, RPS19, RUNX2, SEMA3C, SGCG, SOD2, SPRY2, STK39, TAC1, TGFB1, THBS1]
GO:1901342	regulation of vasculature development	[Group12]	20	4.9	6.31E-04	[ADAM12, BIRC3, CEMIP2, CNTN1, ETS1, FGF2, HDAC9, HIF1A, HMOX1, IL6, KIT, MEOX2, NELL1, PDCD6, ROCK2, SFRP1, SOD2, SPRY2, THBS1, THBS2]